CAMBRIDGE PLANETARY SCIENCE

The Surface of Mars

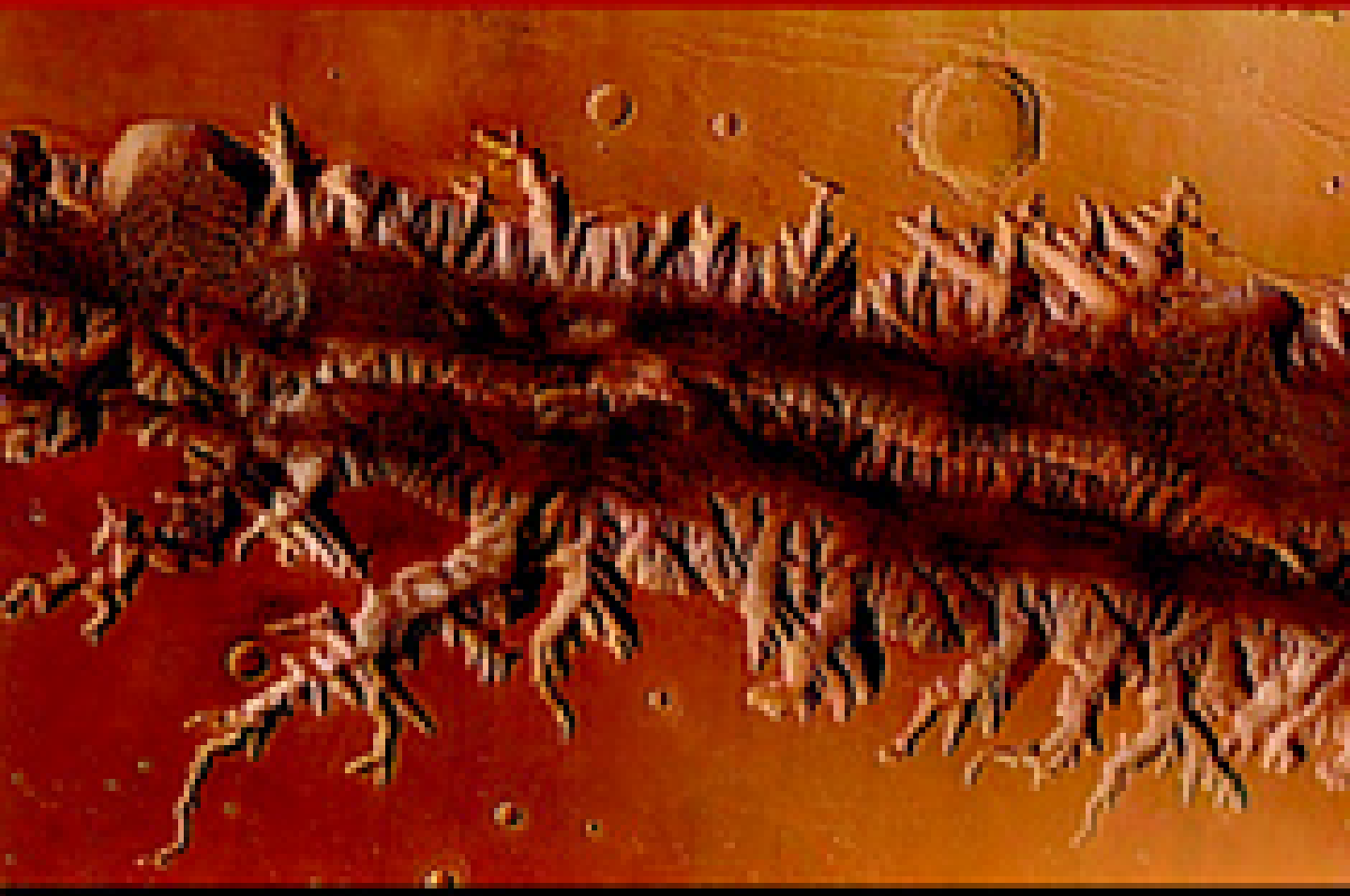

Michael Carr

CAMBRIDGE www.cambridge.org/9780521872010

The Surface of Mars

Our knowledge of Mars has grown enormously over the last decade as a result of the Mars Global Surveyor, Mars Odyssey, Mars Express, and the two Mars Rover missions. This book is a systematic summary of what we have learnt about the geological evolution of Mars as a result of these missions, and builds on the themes of the author's previous book on this topic.

The surface of Mars has many geological features that have recognizable counterparts on Earth. Many are huge in comparison to those on Earth, including volcanoes, canyons and river channels that are ten times larger than their terrestrial equivalents. The book describes the diverse Martian surface features and summarizes current ideas as to how, when, and under what conditions they formed. It explores how Earth and Mars differ and why the two planets evolved so differently. While the author's main focus is on geology, he also discusses possible implications of the geological history for the origin and survival of indigenous Martian life.

Up-to-date and richly illustrated with over two hundred figures, the book will be a principal reference for researchers and students in planetary science. The comprehensive list of references will also assist readers in pursuing further information on the subject.

MICHAEL CARR is a Geologist Emeritus at the U.S. Geological Survey, and has over 40 years' experience of planetary science research. In the early 1970s Dr. Carr was a member of the Mariner 9 team and leader of the Viking Orbiter Imaging team. He was co-investigator on the Mars Global Surveyor, the Mars Exploration Rovers, and the High Resolution Stereo Camera on Mars Express. He is a Fellow of the Geological Society of America, the American Geophysical Union, and the American Association for the Advancement of Science, and was awarded the 1994 National Air and Space Museum Lifetime Achievement Award for his work on Mars. He is also the author of *The Surface of Mars* (1981) and *Water on Mars* (1996).

Cambridge Planetary Science Series

Books in the series

Jupiter: The Planet, Satellites and Magnetosphere F. Bagenal, T. E. Dowling and W. B. McKinnon
Meteorites: A Petrologic, Chemical and Isotopic Synthesis R. Hutchinson
The Origin of Chondrules and Chondrites D. W. G. Sears
Planetary Rings L. Esposito
The Geology of Mars: Evidence from Earth-Based Analogs M. Chapman
The Surface of Mars M. Carr

The Surface of Mars

MICHAEL H. CARR

U.S. Geological Survey
Menlo Park, CA

CAMBRIDGE
UNIVERSITY PRESS

CAMBRIDGE UNIVERSITY PRESS
Cambridge, New York, Melbourne, Madrid, Cape Town, Singapore, São Paulo

Cambridge University Press
The Edinburgh Building, Cambridge CB2 8RU, UK

Published in the United States of America by Cambridge University Press, New York

www.cambridge.org
Information on this title: www.cambridge.org/9780521872010

First published in print format 2006

ISBN-13 978-0-511-27041-3 eBook (NetLibrary)
ISBN-10 0-511-27041-0 eBook (NetLibrary)

ISBN-13 978-0-521-87201-0 hardback
ISBN-10 0-521-87201-4 hardback

Contents

Preface

This book summarizes our knowledge of the morphology of the martian surface and speculates on how the surface evolved to its present state. During the last three decades our knowledge of Mars has increased dramatically. A succession of orbiting spacecraft (Table I) have observed the planet at ever-increasing resolution, rovers have traversed the surface, analyzing and scrutinizing rocks along the way, and ever more sophisticated techniques are being used to analyze increasing numbers of martian meteorites. The planet has had a complicated history. The aim of the book is to summarize our understanding of the nature and sequence of the processes that led to the present configuration of the surface. While the book is intended for the serious student or researcher, technical jargon is avoided to the extent that it is possible without compromising precision. It is hoped that the book will be readable to informed non-Mars specialists as well as those active in the field. Sufficient documentation is provided to enable the reader to dig more deeply wherever he or she wishes. Heavy reliance is placed on imaging data. Other evidence is referred to where available, but at the present time, imaging is by far the most comprehensive global data set that we have in terms of areal coverage and resolution range.

Exploration of Mars has captured world-wide interest. Mars is an alien planet yet not so alien as to be incomprehensible. The landscape is foreign yet we can still recognize familiar features such as volcanoes and river channels. We can transport ourselves through our surrogate rovers to a surface both strange and familiar and readily imagine some future explorers following in their paths. While past speculations about martian civilization may now seem absurd, the possibility that Mars may at one time have hosted some form of life remains plausible. It remains the strongest scientific driver of the Mars Exploration program. The life

Table I. *Mars missions*

Mariner 4	US	11/28/1964	Flew by 7/15/1965; first S/C images
Mariner 6	US	2/24/1969	Flew by 7/31/1969; imaging and other data
Mariner 7	US	3/27/1969	Flew by 8/5/1969; imaging and other data
Mars 2	USSR	5/19/1971	Crash landed; no surface data
Mars 3	USSR	5/28/1971	Crash landed; no surface data
Mariner 8	US	5/8/1971	Fell into Atlantic Ocean
Mariner 9	US	5/30/1971	Into orbit 11/3/1971; mapped planet
Mars 4	USSR	7/21/1973	Failed to achieve Mars orbit
Mars 5	USSR	7/25/1973	Into orbit 2/12/1975; imaging and other data
Mars 6	USSR	8/5/1973	Crash landed
Mars 7	USSR	8/9/1973	Flew by Mars
Viking 1	US	8/20/1975	Landed on surface 7/20/1976; orbiter mapping
Viking 2	US	9/9/1975	Landed on surface 9/3/1976; orbiter mapping
Phobos 1	USSR	7/7/1988	Lost 9/2/1988
Phobos 2	USSR	7/12/1988	Mars and Phobos remote sensing
Mars Observer	US	9/22/1992	Failed Mars orbit insertion
Pathfinder	US	12/4/1996	Landed 7/4/1997; lander and rover
Global Surveyor	US	11/7/1996	Into orbit 9/11/1997; imaging and other data
Odyssey	US	4/7/2001	Into orbit 10/24/2001: imaging, remote sensing
Spirit Rover	US	6/10/2003	Landed in Gusev 1/3/2004
Opportunity Rover	US	7/7/2003	Landed in Meridiani 1/24/2004
Mars Express	Europe	6/2/2003	In orbit 12/25/2003; imaging, remote sensing
Reconnaissance Orbiter	US	8/12/2005	In orbit 3/10/2006; imaging, remote sensing

theme is constantly in the background throughout the book. Impacts have implications for survival of any early life, and may have resulted in cross-fertilization of Mars and Earth. Large floods may have temporarily affected global climates and provided temporary refuges in the resulting lakes and seas. Volcanic activity may have created hydrothermal systems in which life could thrive. Conditions on early Mars may have been very similar to those on early Earth, at a time when life had already taken hold. Thus, while the book is not explicitly about life, almost every chapter has implications for the topic.

The book is intended as a replacement for an earlier book (Carr, 1981) that summarized our understanding of the planet as it was shortly after completion of the Viking missions. This book is different from the original in several ways. The field was much less mature when the first book was written. I was able to read most of the literature and examine most of the imaging data. Neither of these tasks is possible any longer. Approximately 500 papers are published on Mars each year and the number is increasing. One can no more write a book about Mars and reference all the relevant papers, than one can about the Earth. Similarly, the book has been written without seeing most of the available imaging.

Over 200,000 images have been taken just with the Mars Orbiter Camera on Mars Global Surveyor, and a comparable amount of imaging data has been acquired by THEMIS on Mars Odyssey, the High Resolution Stereo Camera on Mars Express, and the Mars rovers. In addition to the imaging there are vast amounts of other remote sensing data, as well as analytical data from the surface and from meteorites. Clearly, summarizing all this data has involved a great deal of simplification.

The book is a snapshot of a moving picture. Following Viking there was almost a twenty-year drought during which barely any data was returned from the planet. But since the landing of Mars Pathfinder in 1996 and the insertion of Mars Global Surveyor into orbit in 1997, we have been receiving a steady stream. Along with the new data have come new ideas as to how the planet has evolved. The pace of change is rapid because our knowledge of the planet is still rudimentary and the data flux is high. It could be argued that the time is inopportune for a summary because of the rate of change. But change will continue. After two decades, new interpretations of the Viking data were still forthcoming. It will likely also take decades to digest the data currently being returned. I hope that there will never be a time when the field stabilizes and a good time to write a summary arrives.

The book was written in 2005 and 2006. I had just retired after having participated in almost every mission to Mars since the late 1960s, including several months of Mars Exploration Rovers (MER) operations at Jet Propulsion Laboratory (JPL). The book has benefited significantly from the continuous informal science discussions that are part of participating in missions. The Mars Rover end-of-day discussions, when the scientists would gather and exchange ideas about any topic that had intrigued them, were particularly stimulating. The Mars Orbiter Laser Altimeter (MOLA) team on Mars Global Surveyor held regular meetings on different science topics that were always fun. Of course, the book has benefited mostly from the engineers who have built and operated the spacecraft that have flown all the science instruments to Mars in recent years. Without sound engineering there is no science. The engineers do most of the hard work acquiring the data. The scientists have the fun of interpreting it all.

Two people deserve special mention for the help they provided. Phil Christensen, of Arizona State University, the THEMIS Principal Investigator, offered to make mosaics of areas of interest for illustrations. Some of the most spectacular images in the book are these THEMIS mosaics. Jim Head of Brown University is also a major contributor to the book. Jim has unusually broad expertise in planetary science, and is possibly the most prolific author in the field of planetary geology. He agreed to review all the chapters as they were written and provided numerous insightful comments that added greatly to the accuracy and comprehensiveness of the final product. Above all he provided encouragement to keep at it.

Michael H. Carr
U. S. Geological Survey
Menlo Park, CA 94025, USA

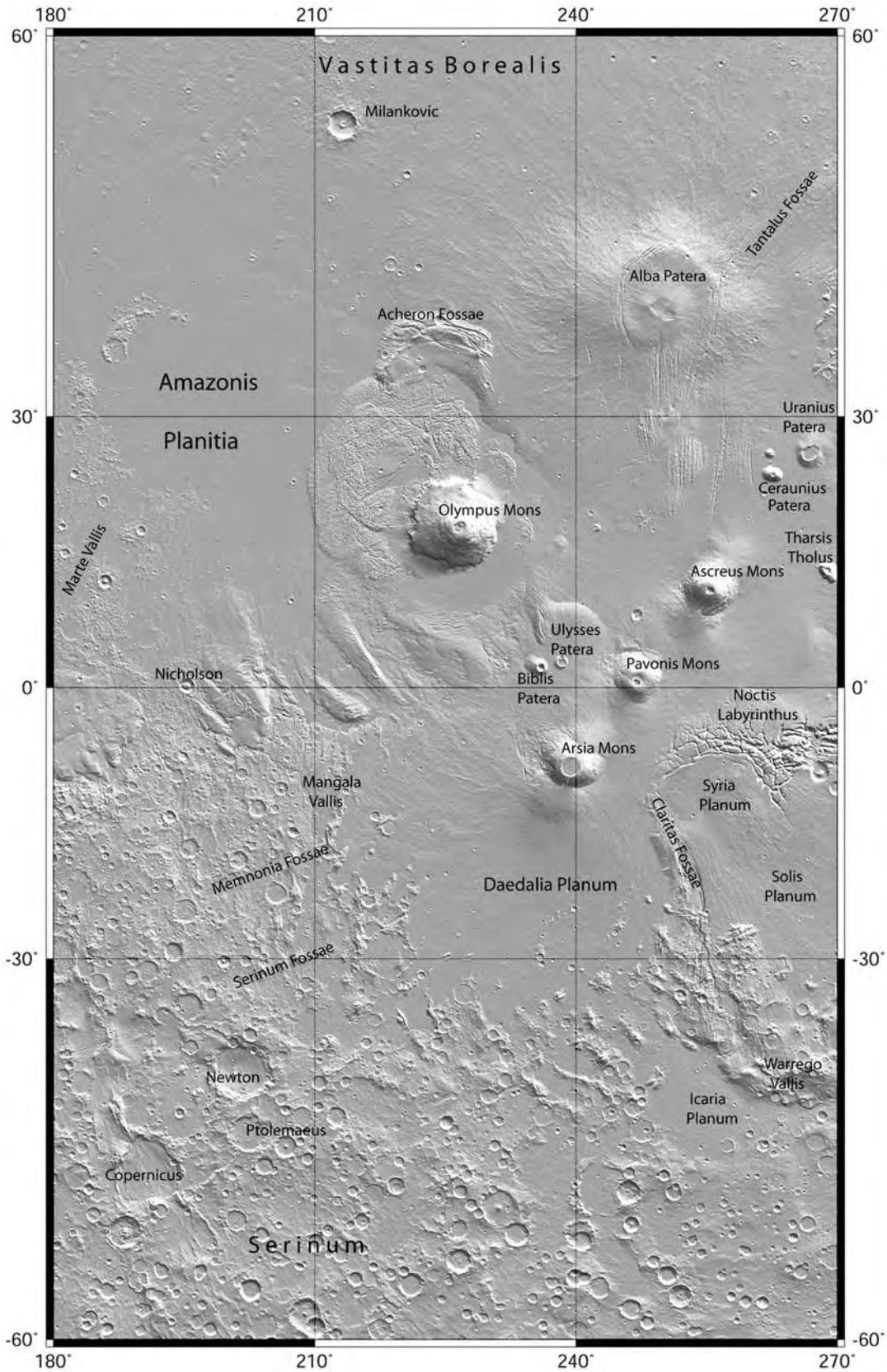
180°
210°
240°
270°
60°
30°
0°
-30°
-60°
Vastitas Borealis
Milankovic
Tantalus Fossae
Alba Patera
Acheron Fossae
Amazonis
Planitia
Uranius
Patera
Ceraunius
Patera
Olympus Mons
Marte Vallis
Tharsis
Tholus
Ascreus Mons
Ulysses
Patera
Pavonis Mons
Nicholson
Biblis
Patera
Noctis
Labyrinthus
Arsia Mons
Mangala
Vallis
Syria
Planum
Claritas Fossae
Memnonia Fossae
Daedalia Planum
Solis
Planum
Serinum Fossae
Warrego
Vallis
Newton
Icaria
Planum
Ptolemaeus
Copernicus
Serinum

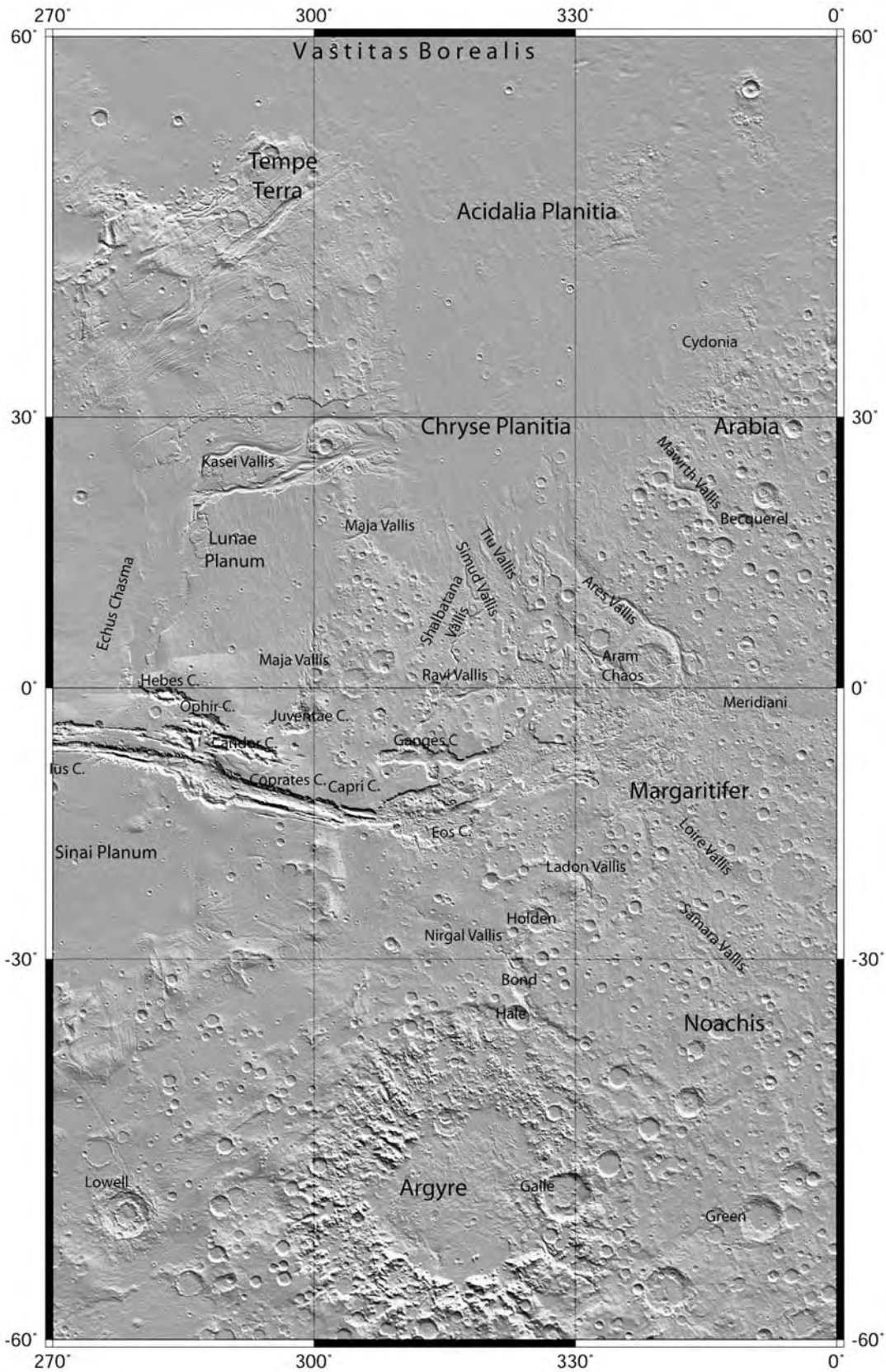
270°
300°
330°
0°
60°
30°
0°
-30°
-60°
Vastitas Borealis
Tempe Terra
Acidalia Planitia
Cydonia
Chryse Planitia
Arabia
Kasei Vallis
Mawrth Vallis
Becquerel
Maja Vallis
Tiu Vallis
Simud Vallis
Lunae Planum
Echus Chasma
Shalbatana Vallis
Ares Vallis
Aram Chaos
Maja Vallis
Hebes C.
Ophir C.
Juventae C.
Candor C.
Ganges C.
Ius C.
Coprates C.
Capri C.
Meridiani
Margaritifer
Eos C.
Sinai Planum
Loire Vallis
Ladon Vallis
Holden
Nirgal Vallis
Samara Vallis
Bond
Hale
Noachis
Lowell
Argyre
Galle
Green

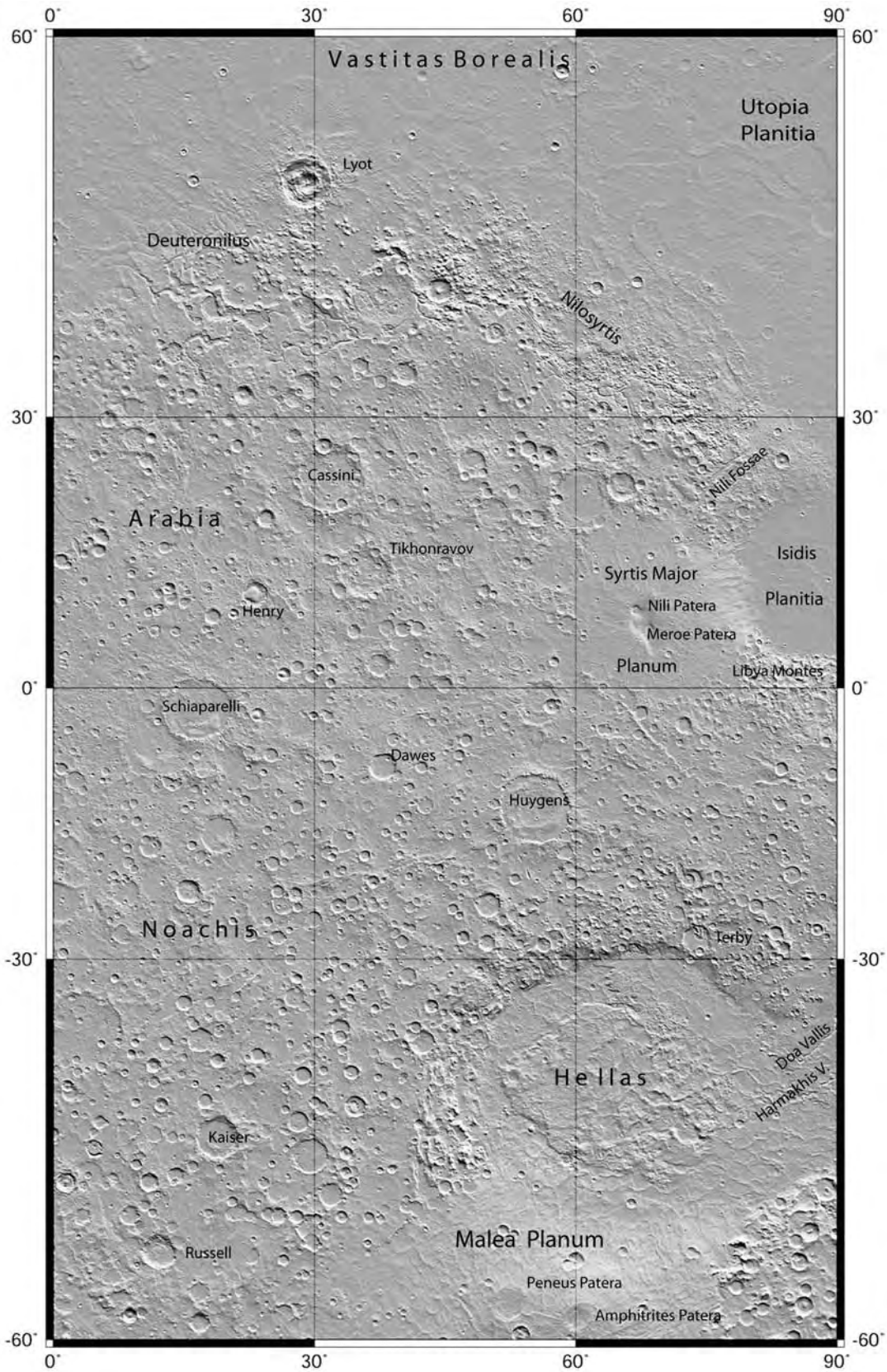
0°
30°
60°
90°
60°
30°
0°
-30°
-60°
Vastitas Borealis
Utopia Planitia
Lyot
Deuteronilus
Nilosyrtis
Cassini
Nili Fossae
Arabia
Tikhonravov
Isidis Planitia
Syrtis Major
Nili Patera
Henry
Meroe Patera
Planum
Libya Montes
Schiaparelli
Dawes
Huygens
Noachis
Terby
Hellas
Dao Vallis
Harmakhis V.
Kaiser
Malea Planum
Russell
Peneus Patera
Amphitrites Patera

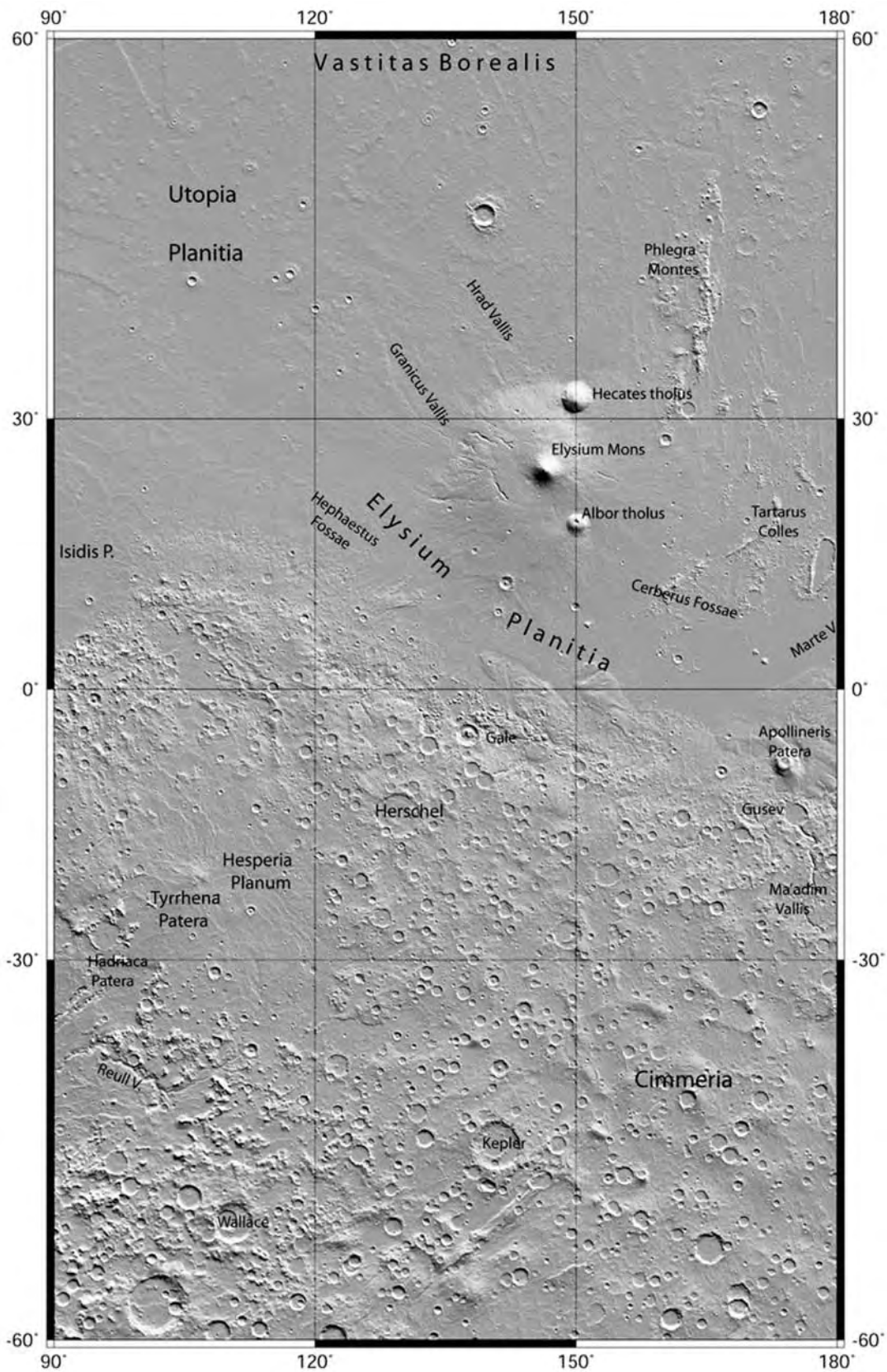
90°
120°
150°
180°
60°
30°
0°
-30°
-60°
Vastitas Borealis
Utopia
Planitia
Phlegra
Montes
Hrad Vallis
Granicus Vallis
Hecates tholus
Elysium Mons
Albor tholus
Tartarus
Colles
Hephaestus
Fossae
Elysium
Planitia
Isidis P.
Cerberus Fossae
Marte V.
Gale
Apollinaris
Patera
Herschel
Gusev
Hesperia
Planum
Tyrrhena
Patera
Ma'adim
Vallis
Hadriaca
Patera
Reull V.
Cimmeria
Kepler
Wallace

1 Overview

This chapter has several goals. The first is to provide some general historical background on how Mars was perceived before spacecraft exploration started with the launch of Mariner 4 in 1964. The second goal is to provide an overview of what conditions are like on Mars today. Most of the book concerns the record of past events as preserved in the landscape and in the rocks at the surface. Although conditions may have been different in the past, those that prevail today provide strong constraints on how we interpret that past record. A third purpose is to give a brief overview of topics that are important for our understanding of the planet, but which are a little off the main theme of the book, which is to describe the major geological features of the planet and their origin. A brief description of the present atmosphere is included here, for example. We also include a section on martian meteorites. These are both huge topics with a vast literature, and no attempt is made in the book to treat them comprehensively. A fourth aim of the chapter is to provide a short geological overview so that the subsequent, more detailed chapters can be read in light of a general knowledge of the planet's geology. Most geological topics are just touched upon here and referenced to later chapters.

Telescopic observations

Mars is the fourth planet from the Sun. With a mean radius of 3389.5 km, it is intermediate in size between the Earth (6378 km) and the Moon (1738 km). As Earth and Mars move in their orbits around the Sun, telescopic viewing conditions change. When Earth and Mars are on opposite sides of the Solar System, they are close to 400 million km apart and Mars subtends an angle of only 3.5 arcsec. At closest approach (opposition) the distance between the two planets may be as small as 55 million km, and the planet subtends an angle of 25 arcsec. Telescopic viewing is thus best at opposition when features as small as 150 km across can be distinguished with the best ground-based telescopes. Oppositions are spaced roughly 780 days apart. The exact spacing varies because Mars' orbit, unlike the the Earth's, is distinctly eccentric. This results in an orbital velocity that changes according to where the planet is in its orbit. The spacing between oppositions therefore changes according to where Mars is at opposition. Eccentricity also affects the quality of the oppositions, the best being when Mars is at perihelion. This has caused a bias of telescopic observations toward the southern hemisphere, since at perihelion Mars' southern hemisphere is tilted toward the Sun and hence toward Earth.

No topography can be seen from Earth-based telescopes (Figure 1.1). What are seen are variations in the reflectivity (albedo) of the surface, including the polar caps, and changes in the opacity of the atmosphere. Although the surface markings may change in detail from opposition to opposition or over decadal time scales, the gross pattern has remained constant for the entire period of telescopic observation. The most prominent features outside the poles are dark markings in the 0–40°S latitude belt, although the most prominent dark feature on the planet, Syrtis Major, is outside this belt. The dark areas were originally thought to be seas and so were called maria. They are mostly areas that have been swept partly clean of the bright dust that covers much of the surface. Most dark markings do not correspond to topographic features, although some do. Some bright markings, such as Hellas and Nix Olympica, noted on some early maps, also correspond to topographic features, probably because of persistent clouds in these areas. The most famous features of the planet from the telescopic era, the canals, were portrayed on almost all twentieth-century maps until the mid 1960s. They are largely illusions on the part of observers straining to see markings at or below the limits of telescopic observation.

Transient brightenings of part, or all, of the telescopic image of the planet were correctly attributed to clouds, of which two types were identified: yellow clouds interpreted as dust storms, and white clouds interpreted as condensate clouds. The yellow dust clouds were observed to occur mostly in the southern hemisphere in southern spring and summer. In some years such as 1956 and 1971 the dust storms became truly global. The classical markings disappeared and

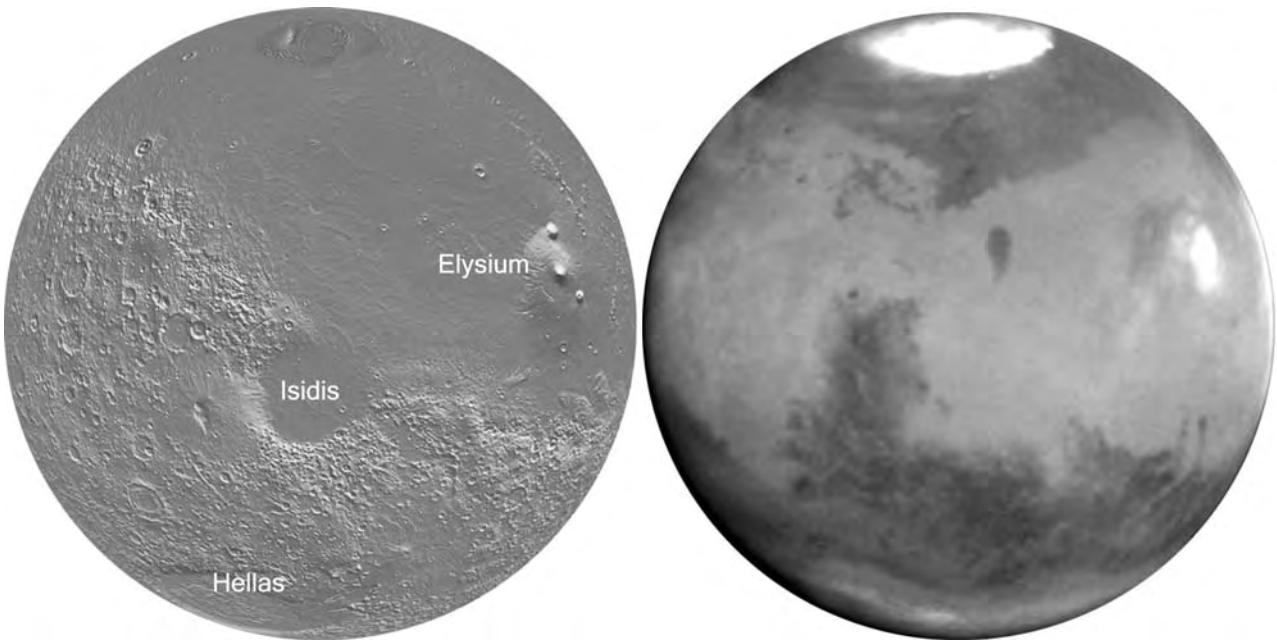

Figure 1.1. Comparison of martian terrain with what is seen in a telescopic image. The view on the left is a MOLA reconstruction of martian terrain from the same perspective as the telescopic image on the right. The MOLA image is of surface relief. The telescopic image was taken by Hubble Space Telescope in late northern spring when the planet was 103×10^6 km from Earth. It shows variations in the reflectivity of the ground and the atmosphere. Bright clouds are present in Hellas and Elysium, and the seasonal CO_2 cap in the north has almost completely dissipated. The dark and light surface markings are only poorly correlated with the relief.

became re-established only after several months. White clouds were observed at places, such as Olympus Mons, Alba, Patera, and Sinai Planum, where we now know from spacecraft observation that water ice clouds are common. Two other phenomena deserve mention. The first is the wave of darkening, a progressive darkening of the dark markings that proceeded from pole to equator as the polar caps receded. It was variously interpreted as growing vegetation, release of water from the receding cap, and sweeping of dust from the area around the receding cap by strong off-pole winds. The second phenomenon was the appearance of blue clearings, times when the dark markings appear particularly crisp and clear. Neither phenomenon has been confirmed by spacecraft observations. For a comprehensive summary of Mars as viewed from the telescope see Martin *et al.* (1992).

Orbital and rotational motions

The orbital and rotational motions of the planet (Figure 1.2) affect how much insolation falls on the planet and how the amount changes with time of year and latitude. The motions, therefore, affect surface temperatures, atmospheric circulation, and climatic conditions in general. Variations in obliquity (the angle between the spin axis and the orbit normal) are particularly important for Mars since the changes are large and can cause significant variations in atmospheric pressure and transfer of water between the poles and lower latitudes

The Mars day is 24 hr 39.6 min and the year is 687 Earth days or 669 Mars days (sols). Instead of months, the areocentric longitude of the Sun (L_s) is used to denote time of year. This is the equivalent of the Sun-centered angle between the position of Mars in its orbit and the position of the northern spring equinox. At the start of northern spring $L_s = 0°$, at northern summer solstice $L_s = 90°$ and so on. Mars' rotation axis is tilted 25° with respect to the orbit plane so that the planet has seasons like the Earth. The orbit of Mars is, however, distinctly elliptical (eccentricity of 0.093), in contrast to the near-circular orbit of the Earth (eccentricity of 0.017), and this affects the length and intensity of the seasons. At closest approach to the Sun (perihelion), the Mars–Sun distance is 1.381 AU (One Astronomical Unit or AU is the mean Earth–Sun distance or 149.5×10^6 km.) At its furthest distance from the Sun aphelion, the Mars–Sun distance is 1.666 AU. Since the solar flux varies with the

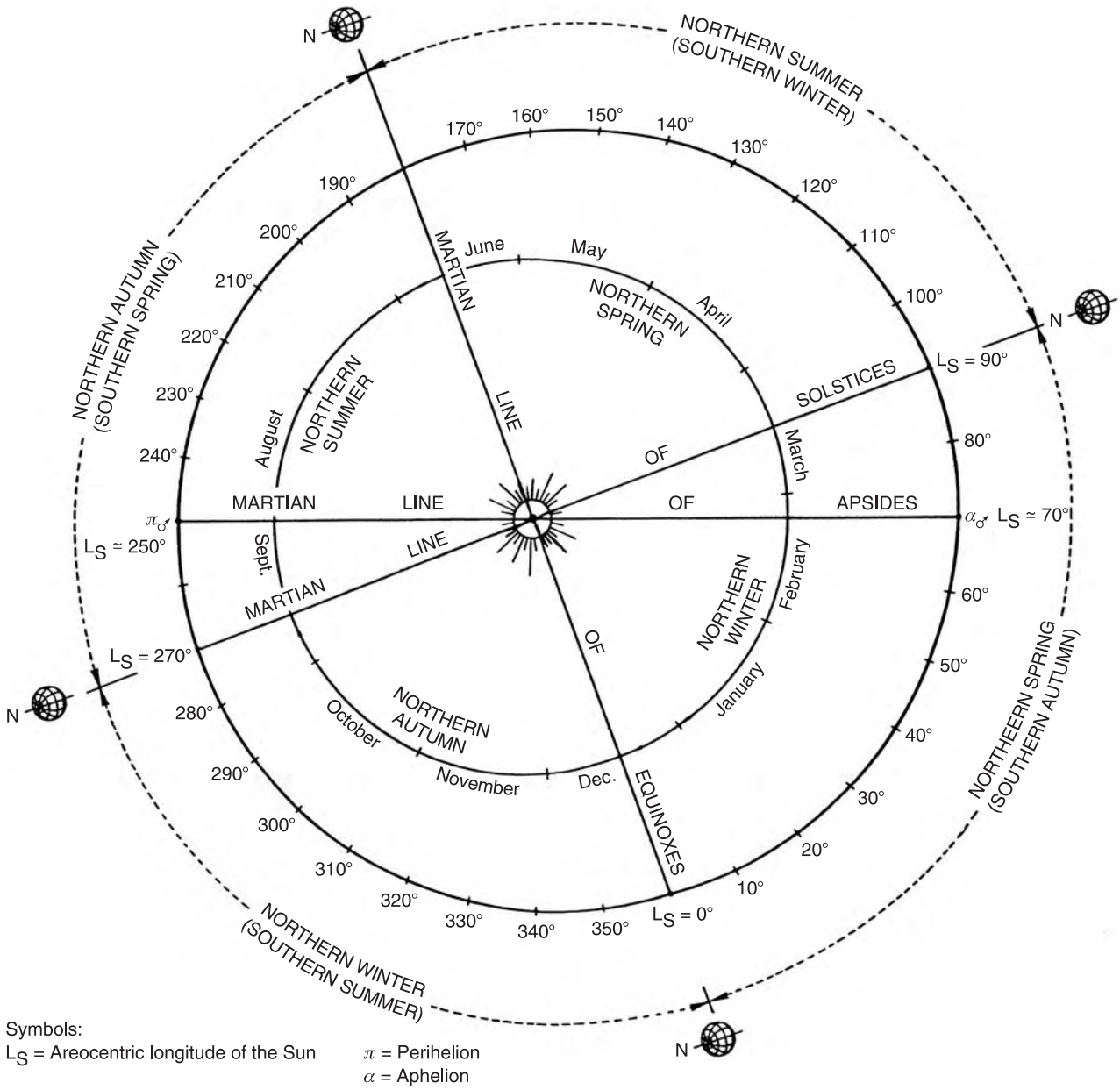

Figure 1.2. The orbits of Mars and the Earth compared. The Earth's orbit is circular whereas Mars' orbit is distinctly eccentric. The areocentric longitude of the Sun, L_S, denotes the martian time of year as shown. (Adapted from Michaux and Newburn, 1972, NASA/JPL.)

square of the distance from the Sun, 45 percent more sunlight falls on the planet at perihelion than at aphelion. At present, perihelion occurs at the end of southern spring, so southern springs and summers are hotter than the same seasons in the north. They are also shorter because of the higher orbital velocity closer to perihelion. The eccentricity changes with time, mostly between values of 0 and 0.12, although over geological time values may have been as high as 0.15 (Laskar *et al.*, 2004) The oscillation has two periods, a 95,000–99,000 yr period with an amplitude of 0.04, and a 2.4 Myr period with an amplitude of 0.1 (Figure 1.3). These oscillations, coupled with precessional motions that control the timing of perihelion, cause the length and intensity of the seasons to change on time scales of 10^4 to 10^6 yrs.

Precession is the slow conical motion of an axis of rotation such as observed with a spinning top.

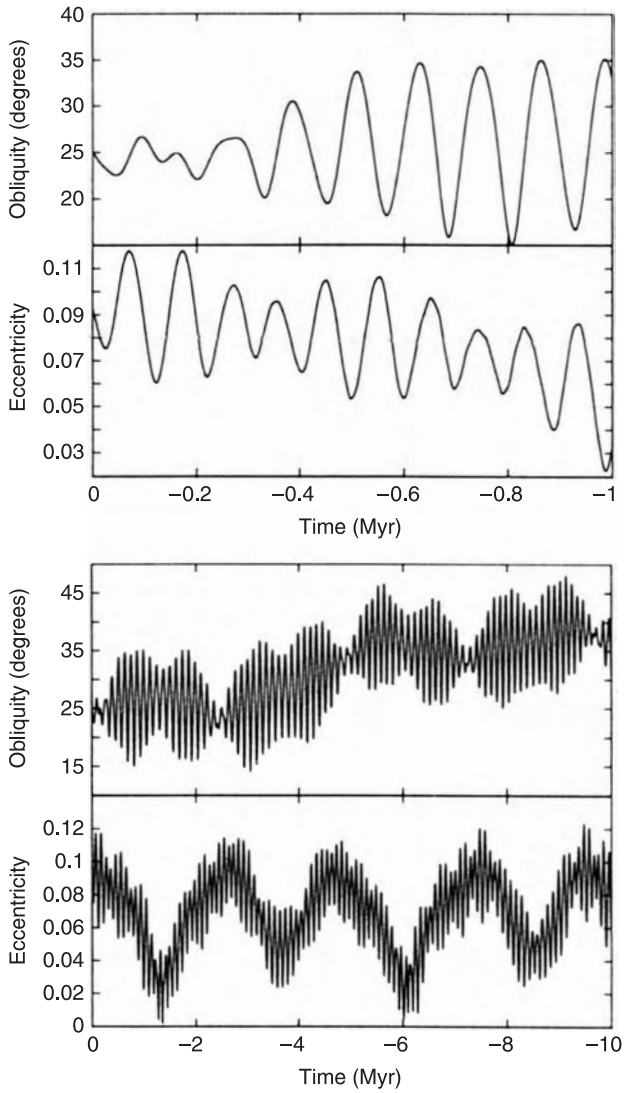

Figure 1.3. Changes in eccentricity and obliquity projected back in time. The upper two panels show projections back 1 Myr. The lower two panels show projections back 10 Myr. Modulation of the 1.2×10^5 yr obliquity cycle has been modest for the last 0.4 Myr. From 0.4 to 4 Myr ago, obliquities ranged from 15° to 35° about a mean of 25°. From 4 to 10 Myr ago the mean was close to 35°. Prior to 10 Myr obliquities are chaotic and cannot be definitively predicted. Obliquity may affect a wide range of phenomena such as atmospheric pressure, the stability of water ice at the surface and in the ground, and the incidence of dust storms. The effects are most marked at the poles (Chapter 10). (From Laskar *et al.*, 2002, copyright © Nature Publishing Group.)

Precession causes a slow rotation of the line of equinoxes – the intersection of the equatorial plane and the orbit plane – with a 175,000 yr period and a rotation of the line of apsides – the line joining perihelion and aphelion – with a period of 72,000 yrs. The net result is that the longitude of perihelion, the angle between equinox and perihelion passage, changes with a period of 51,000 yrs. Thus, while today perihelion occurs in southern spring causing southern springs and summers to be short and hot, 25,000 yrs from now it will be the northern springs and summers that are short and hot.

Changes in obliquity are likely to have much larger climatic effects than changes in eccentricity and the timing of perihelion. The present obliquity is 25.19° but it undergoes large changes (Figure 1.3). During the current epoch, it is thought to oscillate between 15° and 35°, about a mean of 24° (Laskar *et al.*, 2004). The oscillations have a period of 1.2×10^5 yrs with an amplitude that is modulated on a 2 Myr cycle. Variations in obliquity have a particularly strong effect in the polar regions. At obliquities higher than 54° the average solar flux is higher at the poles than at the equator. Moreover, during polar summers at high obliquities, the pole is constantly illuminated, leading to high sublimation rates of any ice that may be present and deep penetration of a large annual thermal wave. During these periods water ice may be driven from the poles and accumulate at low to mid latitudes (Chapters 8 and 10).

There are considerable uncertainties as to what past obliquities were (Ward, 1992; Laskar and Robutel, 1993; Touma and Wisdom, 1993; Laskar *et al.*, 2004). Minute differences in the starting values for the calculations of past motions lead to large differences in the solutions when projected backward (or forward) in time, such that projections larger than 10 Myr are uncertain. Part of the problem concerns resonances. If the period of precession of the spin is commensurate with one of the periods of variation of the orbit, then spin-orbit resonances can occur. Excursions in obliquity significantly larger than are suspected from the current oscillations are then possible. These variations cause the obliquity to be chaotic, at least on time scales greater than 10 Myr. Laskar *et al.* (2004) ran a large number of simulations in order to estimate the distribution of obliquities over geological time. They found that the average obliquity is close to 40°, that there is a 63 percent probability of reaching 60° in the next 1 Gyr and >5 percent probability of exceeding 70° in 3 Gyr. In this respect Mars differs from the other terrestrial planets. The obliquities of Mercury and Venus have been stabilized by dissipation of solar tides, and that of the Earth by the presence of the Moon. Although the obliquity variations are chaotic on time scales longer than 10 Myr, calculations on the time scale of fewer than 10 Myr are reproducible (Laskar *et al.*, 2004).

They indicate that obliquities were significantly higher prior to 3 Myr ago. Between 3 Myr and 10 Myr ago they oscillated between 25° and 46°, instead of the present 15–35°. Possible geological and climatic effects of the obliquity cycle are discussed in Chapters 8 and 10.

Global structure and topography

Mars, like the Earth, is differentiated into a crust, mantle, and core (Chapter 4). Because we have no seismic data, the size of the core is poorly defined but the radius is estimated to be between 1300 and 1500 km. From the partitioning and depletion of core-forming elements in the mantle, as indicated by the composition of martian meteorites, the core appears to be more sulfur-rich than the Earth's (Treiman *et al.*, 1986; Wänke and Dreibus, 1988). Present-day Mars has no magnetic field so that the core is probably solid, but large remanent crustal magnetic anomalies indicate that the core was molten early in the planet's history (Acuna *et al.*, 1999). From relations between gravity and topography, the crust is estimated to range in thickness from 5 to 100 km, with a thicker crust in the southern hemisphere than in the north (Chapter 4). The crust is basaltic in composition. No crust analogous to terrestrial "granitic" continental crust has been detected. Two crustal compositions have been identified from Thermal Emission Spectrometer (TES) data (Bandfield, 2002). At low latitudes ($< 30°$), where not dust covered, the surface has a basaltic spectrum. Higher latitudes have a different spectrum that was initially interpreted as that of basaltic andesite. Subsequently, Wyatt *et al.* (2004) suggested that the spectrum was more likely that of weathered basalt, the weathering having preferentially occurred at high latitudes because ice is stable at these latitudes.

Although Mars has only 28 percent of the surface area of the Earth, it has much larger variations in surface relief. The range is 29.429 km, from −8.200 km in the floor of Hellas to 21.229 km at the summit of Olympus Mons (Figures 1.4, 1.5). Since Mars has no sea level, elevations have to be referenced to some artificial datum. During the Mariner 9 mission it was decided to use the elevation at which the atmospheric pressure is 6.1 mbar, the triple point of water. This surface was approximated by a triaxial ellipsoid with radii defined by occultation measurements and shape defined by a fourth-order representation of the gravity field (Wu, 1978). With the acquisition of direct measurements of radii by the Mars Orbiter Laser Altimeter (MOLA) (Smith *et al.*, 2001) and a vastly improved gravity field from Mars Global Surveyor (Lemoine *et al.*, 2001), the elevations are now referenced to an equipotential surface whose average radius at the equator is 3396 km. The precision of the elevation measurements is close to 1 m.

A fundamental feature of Mars' topography is the so-called global dichotomy. Much of the northern hemisphere is at elevations well below the reference surface, while much of the southern hemisphere stands above the reference. One result is a south polar radius of 3382.5 km as compared with 3376.2 for the north, a 6.3 km difference. Other results are a center of mass/center of figure offset of 2.99 km, and a distinctly bimodal distribution of elevations with maxima at 1.5 km above the mean and 4 km below the mean (Smith *et al.*, 2001). The north–south dichotomy is also expressed as differences in crater density and differences in the thickness of the crust (Chapter 4).

Other than the dichotomy the largest positive topographic feature on the planet is the Tharsis bulge, 10 km high and 5000 km across centered on the equator at 265°E. The bulge formed very early in the history of the planet and has been a focus of volcanic activity ever since. A much smaller bulge is centered in Elysium at 25°N, 147°E. The largest negative topographic feature is the impact basin Hellas at 47°S, 67°E, which has a floor that is mostly 9 km below the rim. The rim itself forms a broad annulus around the basin that includes most of the highest terrain in the eastern part of the southern hemisphere. A second large impact basin, Argyre, at 50°S, 318°E is much shallower, with a floor that is mostly only 1–2 km below the datum.

Atmosphere

The Mars atmosphere is thin and composed largely of CO_2 (Tables 1.2 and 1.3). At the Viking 1 landing site, at an elevation of −2 km, the pressure ranged from 6.9 to 9 mbar (Figure 1.6), less than one-hundredth of the atmospheric pressure at sea level on Earth. The pressure varies with the seasons as up to 25 percent of the atmosphere condenses on the winter pole. The cycle is dominated by growth and dissipation of the south polar cap, it being more extensive than that in the north because of the longer, colder winters in the south. The pressure cycle is highly repeatable from year to year. The scale height of the atmosphere (the height over which the pressure declines to 1/e or 0.3678 of its original value) is roughly 10 km. This implies that for a pressure of 7.5 mbar at the −2 km elevation of the Viking 1 landing site, the pressure at the surface ranges from 0.7 mbar at the summit of Olympus Mons to 14 mbar in the deepest part of Hellas.

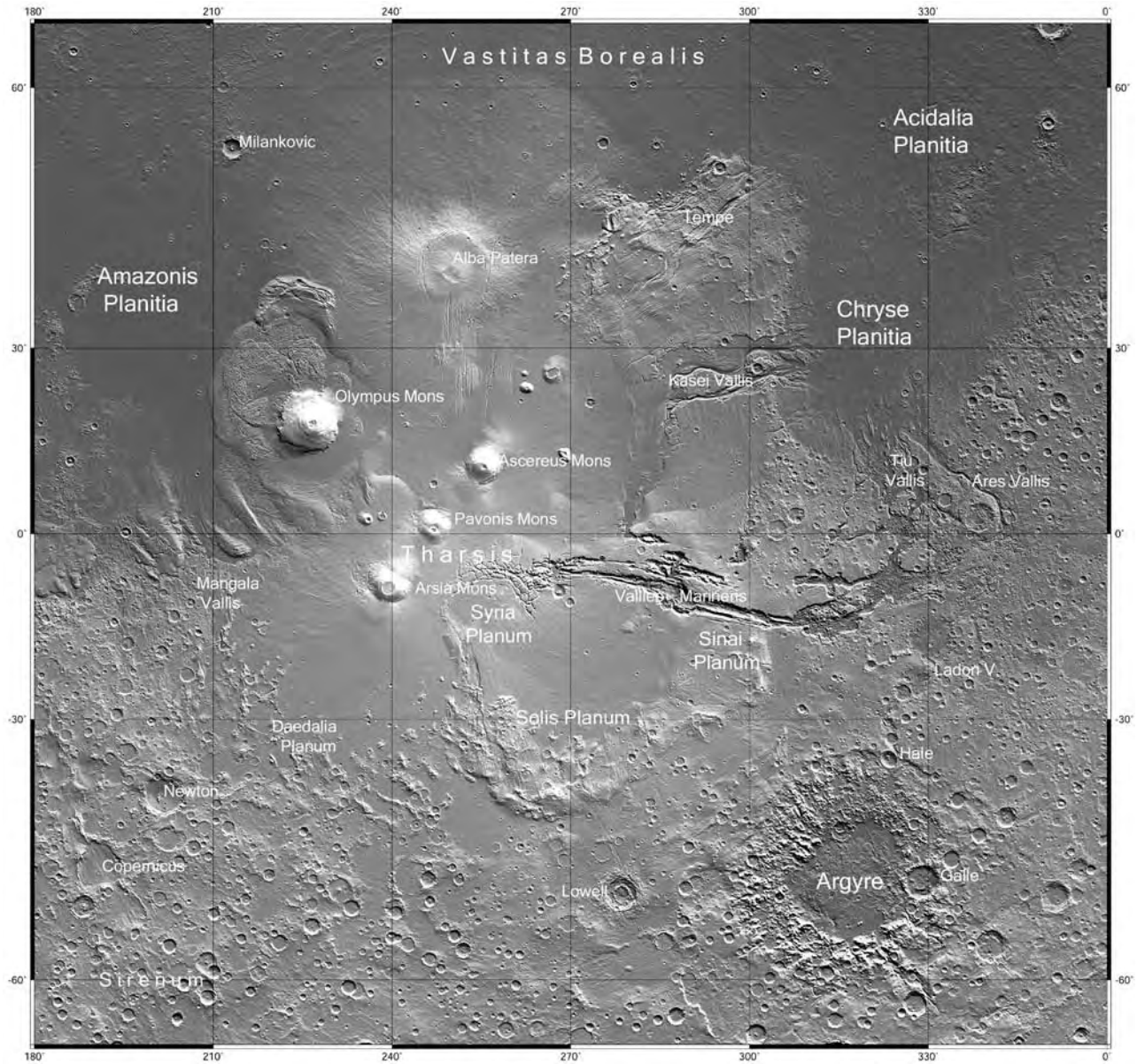

Figure 1.4. The western hemisphere of Mars. Higher areas have lighter tones. The hemisphere is dominated by the Tharsis bulge, centered on the equator at 260° E. The bulge straddles the boundary between the low-lying, sparsely cratered plains to the north and the high-standing cratered terrain to the south (MOLA).

The vertical temperature profile of the martian atmosphere is quite different from the Earth's, partly because of the lack of ozone to create a stable stratosphere, and partly because of the effects of dust (Zurek, 1992). In the lowest part of the Earth's atmosphere, the troposphere, temperatures decline with elevation and are controlled largely by radiative and conductive heat exchange with the surface, and release of latent heat from the condensation of water vapor. In the stratosphere, above the tropopause, temperatures increase with elevation as a consequence of adsorption of ultraviolet radiation by ozone. Because of the reversed temperature gradient, there is very little vertical mixing. Above the Earth's stratosphere, in the mesosphere, the temperature gradient reverses again and temperatures decline with elevation, being controlled by radiative emission and absorption by CO_2. Finally, at the mesopause, the temperatures again start to increase with elevation, as heating is by conduction from above

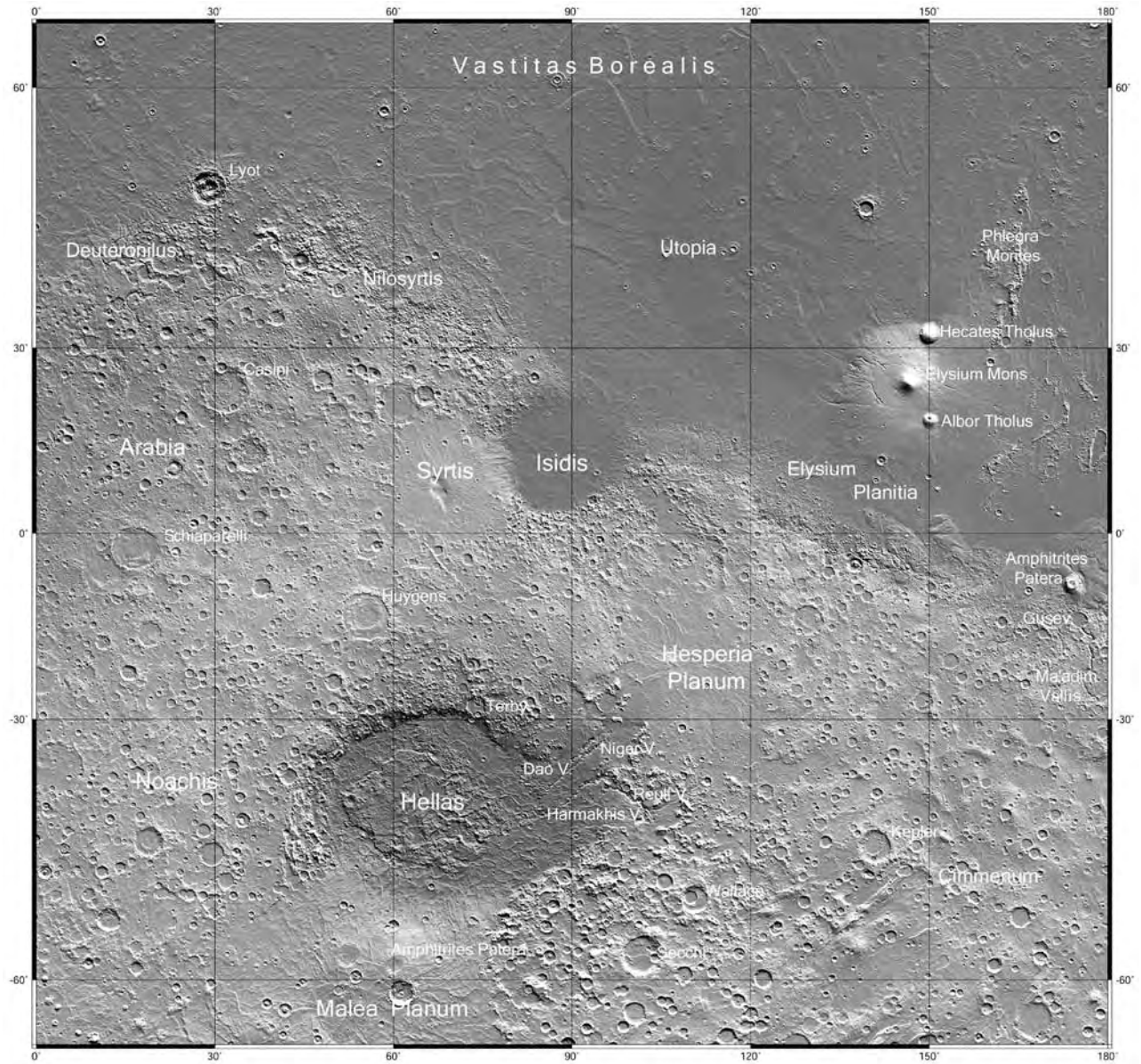

Figure 1.5. The eastern hemisphere of Mars. The most prominent features of this hemisphere are the two impact basins Hellas and Isidis and the volcanic province of Elysium. The north–south dichotomy boundary is more obvious in this hemisphere than in the west where it is buried by Tharsis (MOLA).

where the Sun's extreme ultraviolet radiation is absorbed.

When clear, temperatures in the lower part of the martian atmosphere decline with elevation as in the Earth's troposphere, but there is no gradient reversal due to ozone as in the Earth's atmosphere. Up to an elevation of about 45 km, temperatures are controlled largely by exchange of heat with the ground. With the small amounts of water present, latent heating is negligible. From 45 to 110 km elevations, temperatures continue to fall but radiative emission and absorption by CO_2 dominate. Above the mesopause, at 110 km, the temperature gradient reverses, like on Earth, as the effects of absorption of extreme ultraviolet radiation high in the atmosphere becomes important. Just above the mesopause, at 125 km, is the homopause, above which atmospheric gases begin to separate diffusively. At still higher elevations is the exosphere where the atmosphere is so thin that atoms and molecules are on ballistic trajectories and can escape. Diffusive separation of atmospheric components above the homopause and escape from the exosphere

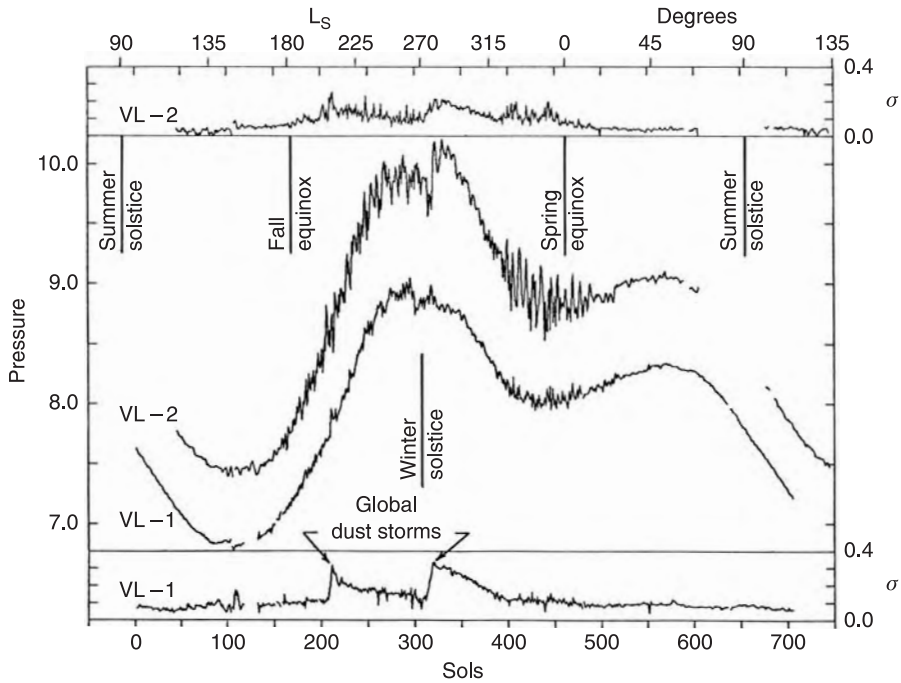

Figure 1.6. Variation in surface pressure at the two Viking landing sites. The origin is at the northern summer solstice when the southern seasonal cap is approaching its maximum extent, and the atmospheric pressure is near its lowest. The second minimum, at the end of northern winter, is much shallower than the first because of the smaller seasonal cap in the north. The upper and lower panels show the standard deviation of the pressure within a sol. These increase substantially when the atmosphere is dusty because of heating throughout the atmosphere rather than from the surface (Hess *et al.*, 1980, copyright 1980, American Geophysical Union, reproduced by permission of the America Geophysical Union).

have resulted in a substantial enrichment of the atmosphere in deuterium and other, heavier, isotopes.

The conditions just described are for a clear atmosphere. The martian atmosphere holds at least a small fraction of dust at all times. Because the dust directly absorbs the Sun's radiation, heat transfer from the surface becomes less important in controlling the temperature. The more dust that is present, the more isothermal is the vertical profile. Diurnal temperature variations at the surface are also suppressed.

The circulation of the atmosphere has several components (Zurek *et al.*, 1992). A north–south (meridional) flow results from seasonal exchange of CO_2 between the two poles, as 10–15 percent of the atmosphere condenses on the northern polar cap in northern winter and 25 percent on the southern polar cap in southern winter. Heating of the atmosphere at low to mid latitudes in the summer hemisphere causes air to rise there, promoting a seasonal meridional overturning (Hadley cell) that extends across the equator, thereby facilitating exchange of water vapor between the two hemispheres. The north–south flow and strong latitudinal thermal gradients in the winter hemisphere cause instabilities (eddies) at mid latitudes. As a result, eastward-propagating planetary waves develop, accompanied by strong westerly winds, high-altitude jet streams and traveling storm systems. While the Viking landers were on the surface, the storms passed regularly on a roughly 3-day cycle. Modeling suggest that the northern storms are more intense than those in the southern mid latitudes. Other elements of the circulation include low-latitude, westward-propagating thermal tides, driven by the diurnal heating cycle, and quasi-stationary waves caused by the large-scale topography and large-scale variations in albedo.

At the Viking landing sites, outside the dust storm season, winds were typically a few meters per second with daily maxima of $8–10\,m\,s^{-1}$. During the dust storm period, and at the times of the winter storms in the north, where the landing sites were, winds at the Viking sites were in excess of $10\,m\,s^{-1}$ 10 percent of the time and gusts reached almost $40\,m\,s^{-1}$. The wind sensor was 1.6 m above the ground. At this elevation, winds of $20–60\,m\,s^{-1}$ are needed to cause saltation of surface grains, the exact value depending on the size of the grains and the surface roughness (Greeley *et al.*, 1992). Dust is commonly

raised by dust devils which have left criss-crossing tracks in many areas of the planet (Chapter 9).

When the atmosphere is clear, it is heated mostly from below, with the result that a convective boundary layer expands to a few kilometers thick during the day then collapses at night. Most of the daily temperature variations damp out within 2 km of elevation above the surface. Because the atmosphere is so dry, latent heat effects are negligible and the vertical profile is close to the dry adiabat. The thermal stability of the base of the atmosphere at night, caused by the extremely cold surface temperatures, decouples the atmosphere from surface friction and a strong nocturnal jet may develop, particularly at those places and at those times when the general circulation has a strong north–south component.

During southern spring and summer, dust storms tend to start at low latitudes wherever there are large slopes and/or large gradients in surface albedo or thermal inertia. They also may start along the edge of the seasonal caps. Areas where dust storms have historically been initiated are the northwest rim of Hellas, the Claritas Fossae region, and low-lying parts of Isidis Planitia (Gierasch, 1974). Dust storms may be local, or they may grow to global proportions as they did in 1971, at the start of the Mariner 9 mission and in 1977 during the Viking mission. Global dust storms can spread to encompass almost the whole planet in several weeks. The storms are most common in southern spring and summer, close to perihelion, when summer temperatures are at their highest. During the 1977 dust storm the optical depth at the Viking 1 landing site, far from the initiation site of the dust storm, rose from a value of 0.5 just before the storm to a high of 5 during the peak of the storm. The total amount of dust elevated into the atmosphere in the global storms is small, equivalent to a few micrometers spread over the whole planet (Kahn *et al.*, 1992). At present, the storms appear to be causing a net transfer of dust from the southern hemisphere to bright low-thermal inertia regions at low northern latitudes.

Surface temperatures

Because the atmosphere is dry and thin, it has a low heat capacity and absorbs little of the Sun's incoming short-wave radiation or the outgoing long-wave radiation, at least when it is clear. As a result, for most of the year, surface temperatures have a wide range and are close to those expected from a simple balance between the solar radiation adsorbed at the surface, the emitted infrared radiation, and heat conducted into or out of the ground (Figure 1.7). Mean diurnal temperatures range from close to 150 K (−123°C) at the poles to 240 K (−33°C) at the warmest locations at mid summer in the southern hemisphere (Kieffer *et al.*, 1977). Daily maxima can reach 300 K (27°C) during summer at mid southern latitudes, but this is somewhat deceiving since the high temperatures are reached only where the thermal inertia (see below) is low. At such locations, the daily fluctuations damp out rapidly with depth (Figure 1.8) so that the above freezing temperatures are reached only within the upper centimeter of the soil.

Surface temperatures depend on latitude and season, and on the albedo and thermal inertia of the surface. They are also affected by the slope of the ground and the configuration of the surrounding terrain. The radiometric albedo is the fraction of the total incident solar radiation not adsorbed by the surface. Albedos of unfrosted ground range from 0.095 to 0.415, with preferred values at 0.135 and 0.275 (Kieffer *et al.*, 1977). The thermal inertia (I) is a measure of the responsiveness of a material to changes in the thermal regime. It is defined as $(K\rho c)^{1/2}$ where K is the thermal conductivity, ρ is the density, and c is the specific heat of the material. Because the density and specific heat of rock materials do not vary greatly, most of the variations in thermal inertia are caused by variations in the thermal conductivity. Solid rocks have high thermal inertias; loose granular materials with abundant void spaces have low thermal inertia, conduction of heat through them being largely restricted to the contact points between grains. Thermal inertias have historically been measured in units of cal cm^{-2} $s^{-1/2}$, but are normally referred to in units (sometimes informally referred to as Kieffers) where the actual values have been multiplied by 10^3. One thermal inertia unit = 10^{-3} cal cm^{-2} $s^{1/2}$ = 41.84 J m^{-2} $s^{-1/2}$. Thermal inertias of the martian surface range from 1 (41.84 J m^{-2} $s^{-1/2}$ to 15 (627.6 J m^{-2} $s^{-1/2}$) (Kieffer *et al.*, 1977; Palluconi and Kieffer, 1981). Bare rocks typically have thermal inertias in excess of 30 (1255 J m^{-2} $s^{-1/2}$), so all the martian surface is at least partly covered with loose materials. The thermal inertias of the martian surface cluster around two values, 6 and 2.5, corresponding respectively to the preferred albedo values of 0.135 and 0.275 (Kieffer *et al.*, 1977). Figure 1.7 shows how surface temperatures change during the day as a function of latitude for typical martian values for albedo and thermal inertia.

At high latitudes in winter, surface temperatures are controlled mainly by condensation and sublimation of CO_2. In the fall, temperatures fall until they reach 150 K, the frost point for CO_2, at which point CO_2 starts to condense. The 150 K temperatures are

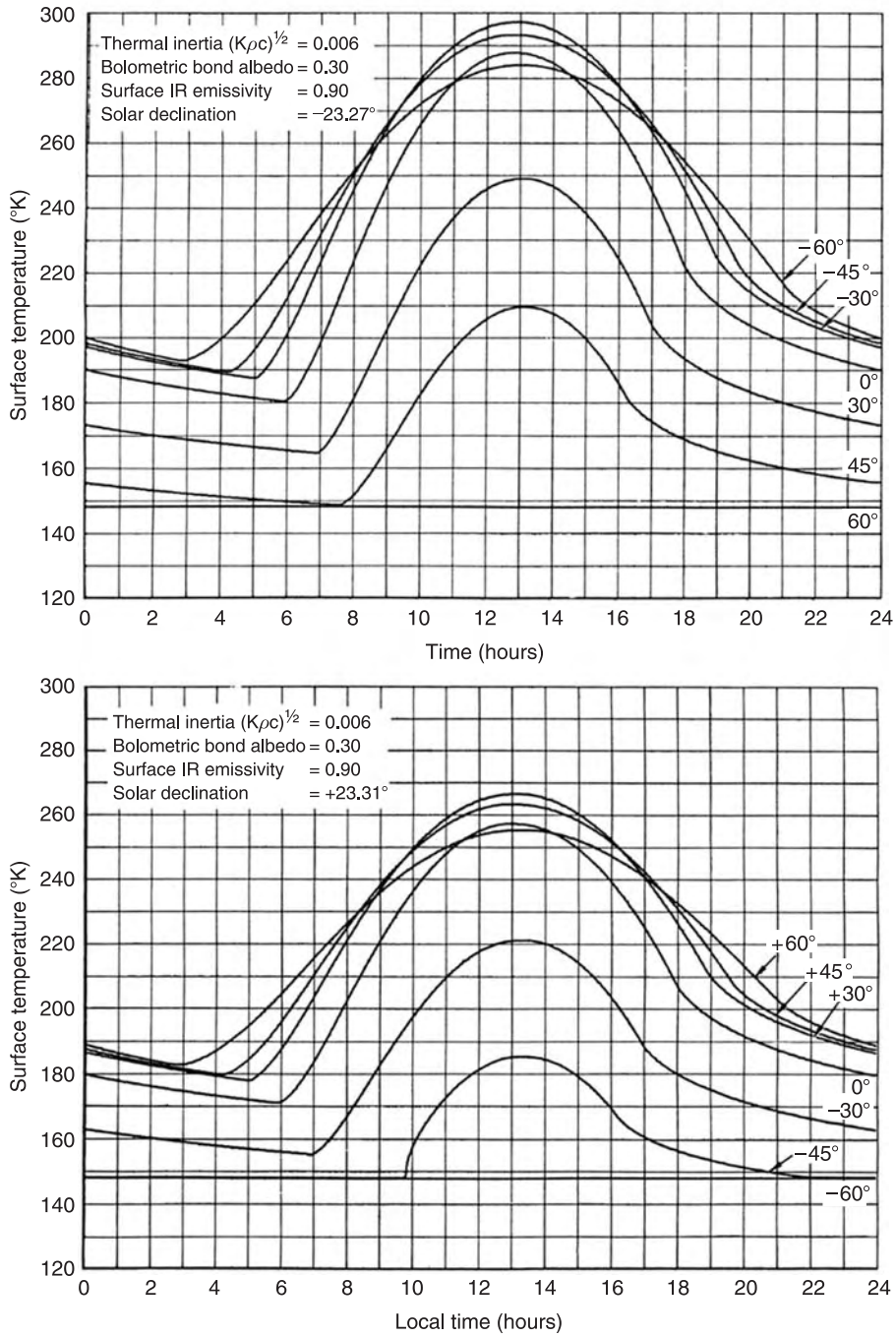

Figure 1.7. Models of the daily temperature fluctuations at the martian surface as a function of latitude. The upper diagram is for perihelion, when it is summer in the south. The lower diagram is for aphelion, when it is summer in the north. Because of the effect of eccentricity, peak summer temperatures in the south are significantly higher than those in the north. Temperatures rise rapidly at dawn, peak just after noon, then decline steadily to their pre-dawn lows (Michaux and Newburn, 1972, NASA/JPL).

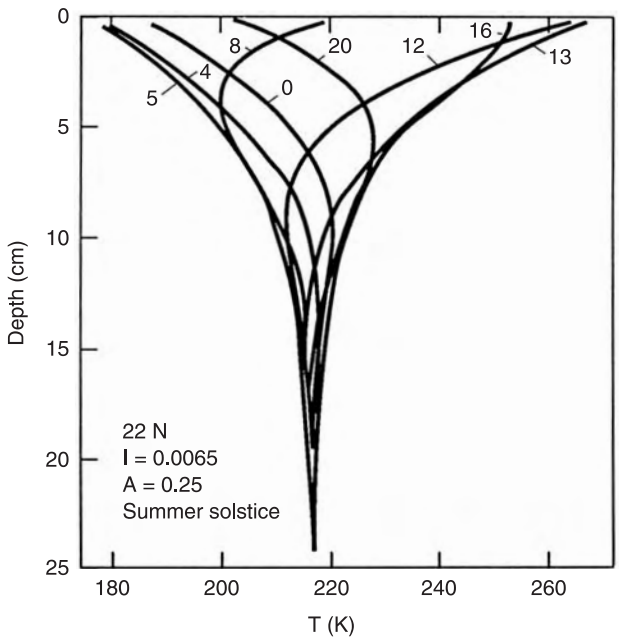

Figure 1.8. Temperatures as a function of depth below the surface at different times of day for the conditions shown at northern summer solstice. Excursions from the mean damp out rapidly with depth. The temperatures shown here are for dark areas that have a thermal inertia of 242 J m^{-2} $s^{-1/2}$. For the bright low thermal inertia areas the damping with depth is even more rapid. Temperatures exceed 273 K only in the upper few millimeters.

maintained until the CO_2 sublimates in spring. During northern summers, retreat of the CO_2 cap exposes a water ice cap and the temperatures at the pole rise to close to 200 K, the frost point of water. At the south pole, the seasonal CO_2 cap does not completely sublime but temperatures rise locally within the residual cap as small areas of water ice are exposed (Byrne and Ingersoll, (2003a,b).

The above discussion applies to conditions today. At high obliquities, temperatures well in excess of freezing can be reached on pole-facing slopes at high latitudes. Costard *et al.* (2002) calculate, for example, that at the present obliquity of 25° the maximum temperature reached on a 20° southward facing slope at 70°S is 235°K, whereas temperatures reach 305°K on the same slope at 50° obliquity. Moreover, because of the sustained summer illumination at high latitudes, these high temperatures penetrate much more deeply into the ground than the highest equatorial temperatures.

Stability of water

The stability of liquid water is of special interest because of its biological implications. Liquid water is essential for life. If liquid water is present near the surface, then the probability of life surviving at the surface is considerably enhanced. The stability of water is also of considerable geological interest. We have compelling evidence of water-eroded valleys in the distant past, and somewhat less compelling evidence that liquid water has recently carved gullies on steep slopes (Chapter 6). Both these observations appear to be at odds with conditions today. Figure 1.9 shows the phase diagram for water. Liquid water is stable only where the temperature is over 273 K and the partial pressure of water exceeds 6.1 mbar. We have just seen that temperatures can exceed 273 K in the upper centimeter of a soil, so that if the partial pressure of water reached 6.1 mbar, then liquid water would be stable. Such conditions are very unlikely, however, in the present epoch. The water content of the martian atmosphere was measured as a function of location and season for a full martian year by the Mars Atmospheric Water Detector on the Viking orbiters (Farmer *et al.*, 1977). They found that the water content of the atmosphere ranged from less than 1 pr μm (i.e. if all the water precipated out of the atmosphere it would form a layer 1 μm deep) over the CO_2 caps to 100 pr μm over the residual northern summer ice cap. If the atmosphere is well mixed, these numbers imply partial pressures of water at the surface that range from 10^{-6} to 10^{-5} bars, 2–3 orders of magnitude short of the 6.1 mbars needed to stabilize liquid water. For average conditions, liquid water is unstable everywhere at the surface and in the atmosphere. Rainfall is not possible. Any precipitation that occurs must be as ice.

Despite its thermodynamic instability, liquid water could occur transiently near the surface today under certain conditions. Over most of the planet, the total atmospheric pressure is less than 6.1 mbar. In these areas any water brought to the surface would rapidly boil and freeze. Any ice present would, on heating, sublimate without any intervening liquid phase. In low areas, however, where the atmospheric pressure exceeds 6.1 mbar, liquid water brought to the surface or produced by the melting of ice would not boil. It would remain until consumed by evaporation and freezing. Similarly, liquid water could form in ice-rich soil that is heated if the heating rate were high enough and the permeability of the soil low enough that the vapor pressure of water in the pores of the soil could build to over 6.1 mbar. Under these conditions, liquid water would form transiently if temperatures got above freezing. With soils containing salts, brines might be formed at temperature significantly lower than 273 K (Brass, 1980). The required temperatures

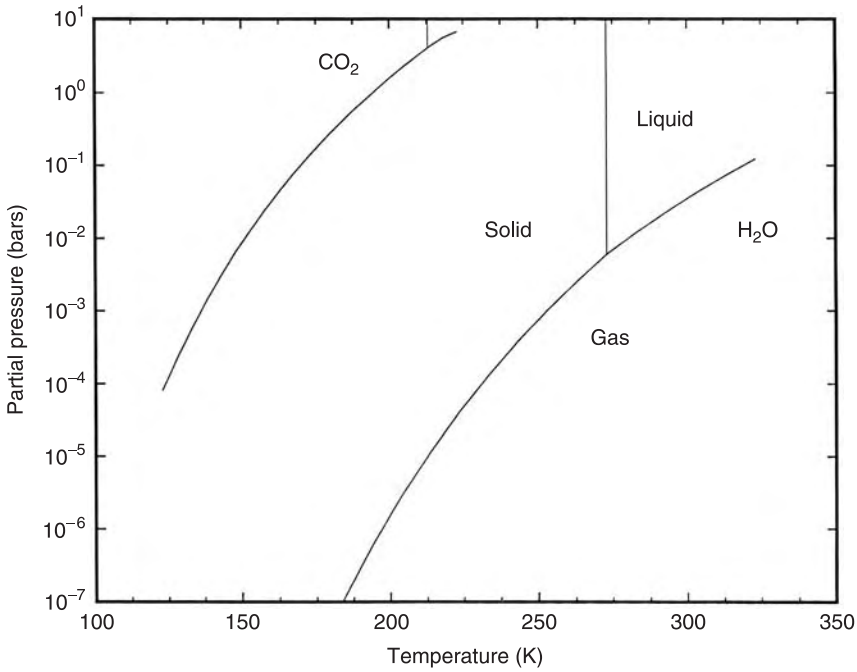

Figure 1.9. Phase diagrams for water and carbon dioxide. Liquid water is stable only where temperatures are above 273 K and partial pressures are over 6.1 mbar. As shown in the previous diagram, temperatures typically exceed 273 K only in the upper millimeters of a soil. The partial pressure of water at the surface is typically in the 10^{-6} mbar range to give a frost point temperature of close to 200 K. Above this temperature, any ice or liquid will sublimate; below this temperature, ice will condense out of the atmosphere. For the present atmospheric pressure of 7 mbar the frost point temperature for CO_2 is 148 K, so that below this temperature CO_2 ice condenses.

would occur only temporarily, however, close to noon, and only in the upper centimeter of the soil because of the rapid decline of daytime temperatures with depth (Figure 1.8). Situations where liquid water might transiently exist may occur more commonly at mid to high latitudes because of the presence of ice in the soil and greater penetration of the diurnal thermal wave in summer, although the temperature requirements would be more difficult to meet. Liquid water at mid to high latitudes is more likely at high obliquities for the reasons given in the previous section, and because at high obliquities the atmosphere may contain significantly more water than it does at present.

After the Viking mission, Farmer and Doms (1979) showed that, under present conditions, water ice is stable just below the surface at high latitudes but is unstable at all depths at low latitudes. The key to this stability is the frost point temperature. The measured amounts of water present in the atmosphere imply that the frost point temperature is close to 200 K if the atmosphere is well mixed. The exact temperature depends on the local variations in water content. If the atmosphere is cooled to the frost point temperature, ice condenses out. Conversely, if ice is heated to the frost point temperature, it starts to sublimate. At latitudes lower than about 40°, mean temperatures are higher than 200 K at all depths so that any ice present in the ground should have sublimated. Unless there is some process of renewal, the ground should be dehydrated. At latitudes higher than 40°, frost point temperatures are exceeded in summer in the upper few tens of centimeters, so they should be free of ice, but below this depth temperatures never reach the frost point so ice is stable, and remains stable down to kilometer depths where geothermal gradient causes melting or sublimation. Water ice caps survive at the poles because sublimation losses in summer are replaced by condensation in winter. These predictions have been largely confirmed by measurements (Figure 1.10). The gamma-ray and neutron spectrometers on Mars Odyssey show that at high latitudes a desiccated layer tens of centimeters thick at the surface overlies materials that may contain as much as 100 percent ice (Prettyman *et al.*, 2004). A surprise is that at low latitudes the near surface materials contain several percent water. This may be chemically bound water or water ice inherited from an

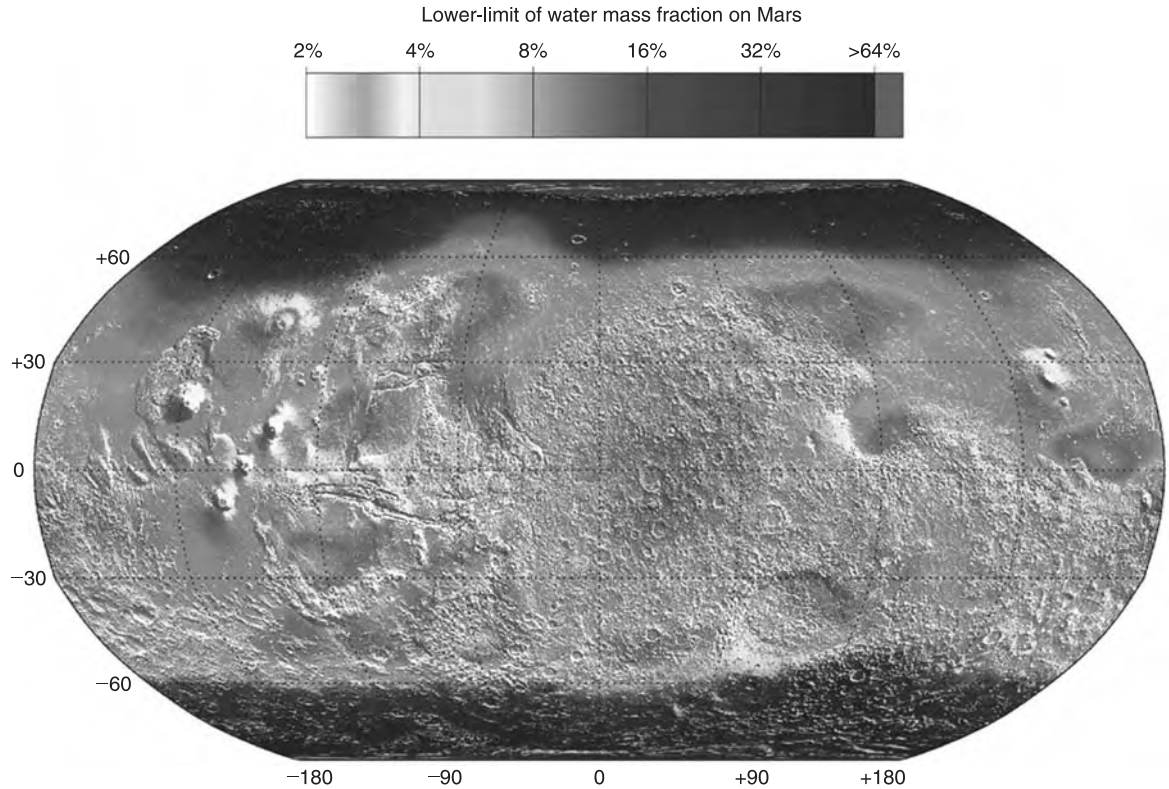

Figure 1.10. The distribution of near-surface water. At high latitudes several tens of percent of water ice is present in the ground below a centimeters-thick dehydrated layer. The depth to which the ice-rich layer extends is unknown but it could be large (kilometers). At low latitudes several percent water ice may be present, even though it is unstable. The ice could have been inherited from an earlier era when stability conditions were different, as discussed in the text (Feldman *et al*., 2004). (For a color version go to http://photojournal.jpl.nasa.gov/catalog/PIAO4907.)

earlier era when stability conditions were different from today's. It should be emphasized that the stability conditions just outlined are equilibrium conditions. Any number of processes from volcanic activity to obliquity changes could result in a disequilbrium distribution.

The stability relations are somewhat different at different obliquities (Mellon and Jakosky, 1995). At obliquities lower than today's, polar temperatures fall, equatorial temperatures rise, and the amount of water in the atmosphere probably decreases because of the cold polar temperatures. As a result, the latitude belt over which ice is unstable at all depths widens. At higher obliquities than today's, the reverse occurs. Equatorial temperatures fall, polar temperatures rise, and the amount of water present in the atmosphere increases and with it the frost point temperature. Ice may then be stable at shallow depths below the surface even at the equator (Chapter 8).

Because mean annual temperatures are well below freezing over the entire planet, the ground is everywhere frozen to considerable depths, except for the seasonal near-surface effects discussed above (Figure 1.11). The term "cryosphere" has been used to refer to the zone where, if water is present, it would be ice. The thickness of the cryosphere depends on the mean annual surface temperature, the thermal conductivity of the crustal materials, the salinity of the groundwater, and the heat flow. A major uncertainty is the heat flow for which we have no measurements and for which estimates vary considerably. Clifford (1993) estimated that for a heat flow of $30\,\mathrm{mW\,m^{-2}}$, and plausible values for salinity and thermal conductivity, the cryosphere thickness ranged from 2.3 km at the equator to 6.5 km at the poles. For a more likely $15\,\mathrm{mW\,m^{-2}}$ heat flow (Chapter 4), and no freezing point depression by salts, he estimated the thickness to range from 11 to 24 km. Heat flows have declined with time so that other factors being equal, the cryosphere has probably increased in thickness with time. However, the thickness is very dependent on surface temperatures. If there have been warmer surface

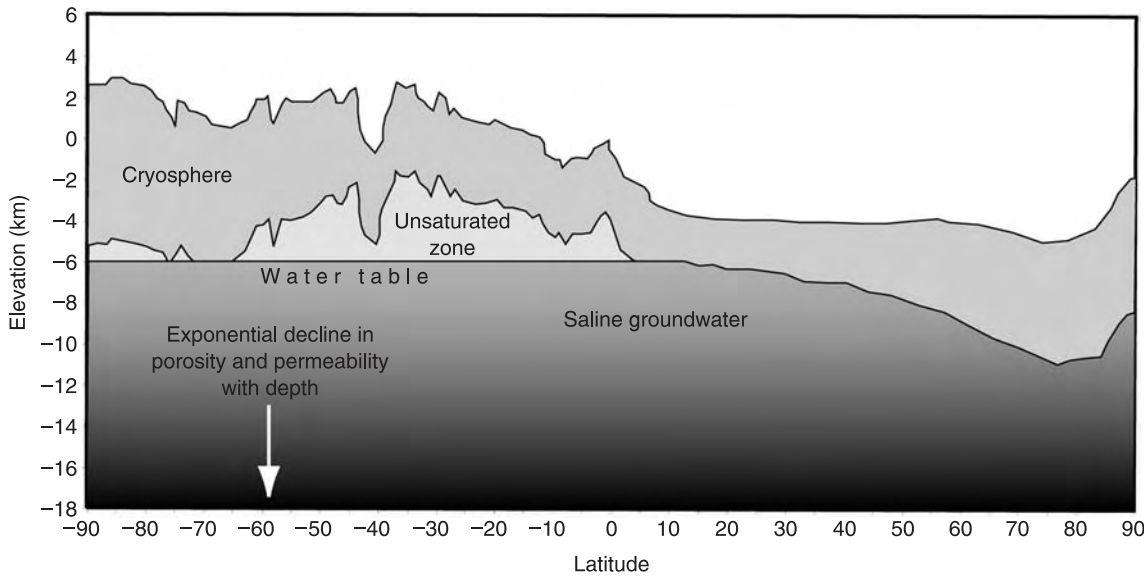

Figure 1.11. Hypothetical cross-section of the martian cryosphere and hydrosphere as a function of latitude. The upper surface of the cryosphere is the present surface as determined by MOLA. The thickness of the cryosphere, where any water present would be frozen, is controlled mainly by mean annual surface temperature and the heat flow, which is poorly known. Groundwater probably exists below the cryosphere but the amount present is unknown. Between the water table and the base of the cryosphere may be an unsaturated zone across which water vapor may diffuse (adapted from Clifford and Parker, 2001).

conditions in the past, as is suggested by the valley networks and evaporites, then the cryosphere may have been at times non-existent. The cryosphere is a large potential sink for water. Its holding capacity depends on the rock porosities which are thought to decrease with depth. Clifford (1993) estimated that it could contain as much as the equivalent of several hundred meters spread evenly over the whole planet.

The cryosphere is underlain by the hydrosphere, that part of the crust where, if water were present, it would be liquid. It extends from the base of the cryosphere to depths where the porosity is negligible. The amount of water, if any, that is present in the hydrosphere is unknown but any water present could move through the host rock if it is permeable and a hydraulic gradient exists. Over time scales of millions of year the global water table would assume an equipotential surface unless there is some mechanism for perturbing the equilibrium such as recharge from above. For a review of the capacity of the hydrosphere and possibilities for recharge, see Clifford (1993) and Clifford and Parker (2001).

Global geology

Geologists attempt to reconstruct the history of a solid planet from the fragmentary record left at the surface. The main concerns are age and process, from which the sequence and nature of the events that led to the present configuration of the planet can be determined. With Mars the most extensive record we have is the morphology of the surface. Normally a geologist will interpret the geology of a region, armed with knowledge of the lithology, chemistry, mineralogy, and three-dimensional configuration of its rocks. Unfortunately, for most of Mars we have knowledge only of properties that can be determined remotely, such as morphology, elevation, and gravity. While interpretation of surface morphology can be unambiguous, as in the case of the large volcanoes, it more often is not, so that many aspects of the geological history are poorly understood. The purpose of this section is to provide the reader an overview of the planet's geology so that subsequent chapters that deal with different topics in detail can be read with some contextual background knowledge

One of a geologist's prime concerns is age. Although we have datable samples in the SNC meteorites (see p. 20), we do not know where on Mars they came from, so they are of little help in dating the features that we see. We are forced to extract age information from the morphology of the surface. Relative ages are determined from remote sensing mainly in two ways, from intersection relations and

from the number of superimposed impact craters. Clearly, if a channel cuts a lava flow, it is either the same age as or younger than the flow. But intersection relations are often ambiguous and other dating methods have to be used. Crater counting is the most commonly used way of determining relative ages. Older surfaces have more superimposed impact craters. While this is a simple relationship, the method is in practice often difficult to apply, particularly for younger surfaces where smaller craters must be counted, which are more vulnerable to erosion and for which there might be confusion distinguishing primary craters from secondary craters.

A stratigraphic system for assigning ages to different parts of the martian surface has been devised that is calibrated against the numbers of superimposed impact craters (Tanaka, 1986). The relative ages so derived apply, of course, to the sculpting of the surface not to the rocks themselves, although these are often identical, as with the formation of a lava flow. The geological record has been divided into three time stratigraphic systems. Surfaces of Noachian age date back to the time of heavy bombardment, when impact rates were much higher than they were for the rest of the planet's history (Figure 1.12). A 10^6 km^2 area of the surface that has survived from the top of the Noachian will have accumulated 200 impact craters with diameters larger than 5 km, and 25 larger than 16 km (Table 1.1). The base of the Noachian has not been defined, but most of the visible large impact basins are thought to have formed after 4.1 Gyr ago (Nimmo and Tanaka, 2005). The period before this time is informally referred to as the pre-Noachian. A second system, the Hesperian system, refers to the oldest surfaces that postdate the end of heavy bombardment. A 10^6 km^2 area of the surface dating from the top of the Hesperian will have accumulated 67 impact craters with diameters larger than 5 km and 400 larger than 2 km. It will have accumulated too few 16 km diameter craters for meaningful counts. The youngest system is called the Amazonian system, and obviously has lower numbers of craters than those just given for the Hesperian. The three terms Noachian, Hesperian, and Amazonian are used throughout the book.

The absolute ages represented by these three systems have been estimated by comparisons with the Moon. The cratering history of the Moon is reasonably well known from crater counts and absolute dating of samples (see, for example, Wilhelms, 1987). Prior to 3.5 Gyr ago, the cratering rate was declining very rapidly (Figure 1.12), so much so that surfaces that date from 3.85 Gyr ago appear to be heavily cratered, almost saturated, whereas the maria from the

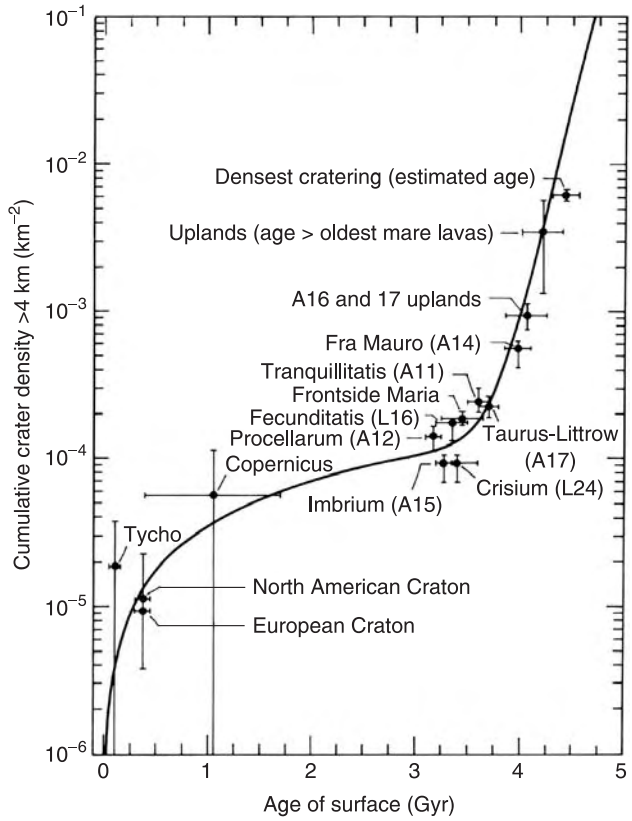

Figure 1.12. The cumulative lunar crater density as a function of age. A similar array of objects that produced this record also impacted Mars (Chyba, 1991, reproduced by permission from Elsevier).

Apollo 11 and 17 sites, with dates that range mostly between 3.6 and 3.75 Gyr ago, are only sparsely cratered. The time before about 3.8 Gyr is referred to as the era of heavy bombardment. After the heavy bombardment tailed off, a uniformly low cratering rate was maintained. Assuming that a similar population of objects cratered the Moon and Mars, and making the appropriate corrections for how this population might differentially crater the two objects, Hartmann and Neukum (2001) estimate that the Noachian ended 3.7 Gyr ago and that the Hesperian ended 2.9–3.1 Gyr ago. There are, however, considerable uncertainties associated with converting crater frequencies to absolute ages as discussed in Chapter 2.

While Mars is much smaller than the Earth, the two planets have comparable land areas. Roughly two-thirds of the martian surface, including almost all the southern hemisphere, is high-standing and heavily cratered. The surface clearly dates back to prior to 3.7 billion years ago, when impact rates were much higher than they were subsequently. It has survived mostly with only modest modification since the end of

Table 1.1. *Some useful Mars numbers*

Astronomical unit (A.U.)		1.49597870×10^8 km
Orbit semimajor axis		1.52366 A.U.
Sun–Mars distance at perihelion		1.3815 A.U.
Sun–Mars distance at aphelion		1.6660 A.U.
Eccentricity		0.0934
Obliquity		25.19°
Mean orbital period		686.98 Earth days
		669.60 Mars solar days (sols)
Mean solar day		88775.2 s (24 h 39 m in 35.2 s)
Mass		6.4185×10^{23} kg
Mean radius		3389.508 km
Mean equatorial radius		3396.200 km
North polar radius		3376.189 km
South polar radius		3382.580 km
Center of mass/figure offset		2.986 km
Surface area		1.4441×10^8 km^2
Ratio of surface area to Earth's		0.2825
Ratio of surface area to Earth's land area		0.976
Gravitation acceleration (equator)		3.711 m s^{-2}
Mean atmospheric pressure at surface		5.6 mbar or 560 Pa
Average mass of atmosphere		2.17×10^{16} kg
Mean atmospheric scale height		10.8 km
Solar constant at mean Mars–Sun distance		598.98 W m^{-2}
Average surface temperature		210 K
Range of surface temperatures		140–300 K
Mars seasons		
Northern spring	$L_s = 0–90°$	199 Earth days
Northern summer	$L_s = 90–180°$	183 Earth days
Northern fall	$L_s = 180–270°$	147 Earth days
Northern winter	$L_s = 270–360°$	158 Earth days
Time-stratigraphic system		
Noachian–Hesperian boundary		
Crater densities	200 > 5 km in diameter/10^6 km^2	
	25 > 16 km in diameter/10^6 km^2	
Absolute age	3.5–3.7 Gyr[a]	
Hesperian–Amazonian boundary		
Crater densities	400 > 2 km in diameter/10^6 km^2	
	67 > 5 km in diameter/10^6 km^2	
Absolute age	2.9–3.3 Gyr[a]	

[a]Estimates from Hartmann and Neukum (2001)

heavy bombardment. The martian highlands are probably stratigraphically complex. While impact craters are the dominant landforms, intercrater plains appear to be volcanic as implied by the occasional flow. Branching valleys indicate that fluvial erosion was widespread. Termination of valleys within local lows suggest that lakes were common. Many areas are clearly layered and have an etched appearance as though the upper layers had been partly stripped away. Layered deposits also partly fill many of the large craters. Stripping away of the upper layers commonly exhumes older craters that predate the layers. The cratered uplands thus appear to be composed of a mixture of materials of diverse origin, which are probably commonly separated by unconformities and weathering horizons. Included are impact ejecta, volcanic rocks, and deposits that result from mass-wasting, fluvial, lacustrine, and eolian processes. The diverse mixture of rocks, some aqueously altered, found by the Spirit rover in the Columbia Hills (Chapter 12) may be

Table 1.2. *Chemical composition of the atmosphere (Kieffer* et al., *1992)*

Species	Abundance
CO_2	0.9532
N_2	0.027
Ar	0.016
O_2	0.0013
CO	0.0007
H_2O	0.0003
Ne	2.5 ppm
Kr	0.3 ppm
Xe	0.08 ppm
O_3	0.04 to 0.2 ppm

Table 1.3. *Isotopic composition of the atmosphere compared with Earth (Kieffer* et al., *1992)*

Ratio	Earth	Mars
$^{12}C/^{13}C$	89	90 ± 5
$^{14}N/^{15}N$	272	170 ± 15
$^{16}O/^{18}O$	489	490 ± 25
$^{36}Ar/^{38}Ar$	5.3	5.5 ± 1.5
$^{40}Ar/^{36}Ar$	296	3000 ± 500
$^{129}Xe/^{132}Xe$	0.97	2.5
D/H	1.6×10^{-4}	$9 \pm 4 \times 10^{-4}$

typical of what is present in these ancient terrains. Cratering continued as the materials accumulated, as did erosion, so that craters are present in various states of preservation. How far back in time we are seeing in the uplands is unclear. Because smaller craters are more easily destroyed than larger craters, the mean age of the 20 km diameter craters is almost certainly less than the mean age of the 200 km diameter craters. The oldest features of all are large basins, such as Hellas, and large circular depressions, which are almost completely destroyed and detectable only in the altimetry (Chapter 2).

Martian craters differ significantly in appearance from those on the Moon. On Mars, the ejecta around craters 2–50 km in diameter is commonly arrayed in discrete lobes, each outlined by a low ridge. This is true of almost all well-preserved martian impact craters in this size range, irrespective of location. In contrast, on the Moon the ejecta typically forms a disorganized, hummocky accumulation on the rim. Two reasons have been suggested for the characteristic martian ejecta patterns. The first is that impact craters above a certain size eject water-laden or ice-laden materials that flow across the ground after ballistic deposition. The second suggestion is that interaction between the ejecta and the atmosphere causes the flow-like patterns (Schultz and Gault, 1984). Another difference between craters in the lunar and martian uplands is their state of preservation. Most of the craters in the martian uplands are highly degraded. This has been taken as one indication of high erosion rates and climatic conditions very different from the present during the early epoch represented by the cratered uplands.

The one-third of the planet not covered by heavily cratered uplands is mostly covered by plains. The most extensive are in the northern hemisphere. The number of superimposed craters on these plains varies substantially, indicating that the plains continued to form throughout much of the history of the planet. The plains are diverse in origin. The most unambiguous in origin are those on which numerous flow fronts are visible. They are clearly formed from lava flows superimposed one on another, and are most common around the volcanic centers of Tharsis and Elysium. On other plains, such as Lunae Planum and Hesperia Planum, flows are rare but wrinkle ridges like those on the lunar maria are common. These are also assumed to be volcanic, although evidence for a volcanic origin is weak. The lowest-lying plains are at high northern latitudes, away from the volcanic centers. They mostly lack obvious volcanic features. Instead they are curiously textured and fractured. Many of their characteristics have been attributed to the action of ground ice, or to their location at the ends of large flood features, where large lakes must have formed and sediments deposited. In some areas particularly around the north pole, enormous dune fields are present. In yet other areas, are features that have been attributed to the interaction of volcanism and ground ice. Thus the plains appear to be complex in origin, having variously formed by volcanism and different forms of sedimentation, and then been subsequently modified by tectonic forces and by wind, water, and ice.

The two most prominent volcanic provinces are Tharsis and Elysium. Three large volcanoes are close to the summit of the Tharsis bulge. Olympus Mons, the tallest volcano on the planet, is on the northwest flank. All these volcanoes are enormous by terrestrial standards. Olympus Mons is 550 km across and 21 km high, and the three others have comparable dimensions. To the north of Tharsis, Alba Patera, the largest volcano on the planet in areal extent, is roughly 2000 km across but only a few kilometers high.

Lava flows and lava channels are clearly visible on the flanks of all the volcanoes and each has a large complex summit caldera. The large sizes of the volcanoes have been attributed to the lack of plate tectonics on Mars, the long life of the magma sources, and the buoyancy of the martian magmas with respect to the edifices they build (Wilson and Head, 1994). The small number of superimposed impact craters on the flanks of the large Tharsis volcanoes indicates that their surfaces are young. The large Tharsis volcanoes have, however, probably been growing throughout much of Mars' history.

Elysium Mons, the largest volcano in the Elysium province, appears to be a shield volcano formed largely of fluid lava. However, huge channels start at the periphery of the volcano and extend northwest, down the regional slope for hundreds of kilometers. The channels have streamlined forms, enclose teardrop-shaped islands, and have other characteristics of large floods. They are thought to have formed by massive flows of water and mud following injection of hot magma into ice-rich ground on the volcano flanks.

The rates of volcanism on Mars are much lower than those on Earth. Greeley and Schneid (1991) estimated that roughly $6 \times 10^7\,km^3$ of lava have accumulated on the martian surface since the end of heavy bombardment and that the average extrusion rate was $0.016\,km^3\,yr^{-1}$. Taking into account intrusive rocks, the average magma production rate is likely to be about ten times this figure. For comparison, the Earth has produced roughly $30\,km^3\,yr^{-1}$ for the last 180 Myr (Sclater *et al.*, 1980). The rate of volcanism on Mars per unit mass of the planet is about 0.05 times that on the Earth.

Despite suggestions that plate tectonics may have formed the northern lowlands (Sleep, 1994), Mars lacks obvious manifestations of plate tectonics such as linear mountain chains, subduction zones, large transcurrent faults, and an interconnected system of ridges. The most widespread indicators of surface deformation are normal faults, indicating extension, and wrinkle ridges indicating compression. The most obvious deformational features are those associated with the Tharsis bulge. Around the bulge is a vast system of radial grabens that affects about a third of the planet's surface. Circumferential wrinkle ridges are also present in places, particularly on the east side of the bulge in Lunae Planum. Both the fractures and the compressional ridges are believed to be the result of stresses in the lithosphere caused by the presence of the Tharsis bulge. No comparably extensive system of deformational features occurs around Elysium, but fractures occur in other places where the crust has been differentially loaded, as around large impact basins, such as Hellas and Isidis, or around large volcanoes, such as Elysium Mons and Pavonis Mons.

The vast canyons on the eastern flanks of the Tharsis bulge are the most spectacular result of crustal deformation. The canyons extend from the summit of the Tharsis bulge, eastward for 4000 km until they merge with chaotic terrain and large channels south of the Chryse basin. In the central section, where several canyons merge, they form a depression 600 km across and several kilometers deep. Although the origin of the canyons is poorly understood, faulting clearly played a major role. The canyons are aligned along the Tharsis radial faults, and many of the canyon walls are straight cliffs, or have triangular faceted spurs, clearly indicating faulting. Other processes were also involved in shaping the canyons. Parts of the walls have collapsed in huge landslides, other sections of the walls are deeply gullied. Fluvial sculpture is particularly common in the eastern sections. Faulting may have created most of the initial relief, which then enabled other processes such as mass wasting and fluvial action to occur. Creation of massive fault scarps may also have exposed aquifers in the canyon walls and allowed groundwater to leak into the canyons, thereby creating lakes, as suggested by thick sequences of layered, sulfate-rich sediments.

One of the attributes that Mars shares with the Earth is that water has played a key role in its evolution. Channels tens of kilometers across and hundreds to thousands of kilometers long appear to have formed by large floods. They occur in just a few locations, mainly around the Chryse basin and in Elysium and Hellas. The amount of water involved in their formation is controversial, but, if formed by water, all must have left behind large bodies of water when the floods were over. Branching valley networks are another class of seemingly water-worn features. In plan they resemble terrestrial river systems. They are found mainly, but not exclusively, in the Noachian cratered uplands, and are thought to have formed when surface conditions were warmer and wetter than they are today. A third type of probably water-worn feature, called a gully, occurs on steep slopes and appears to be forming in the present epoch. Finding of evaporites by the Opportunity rover in Meridiani, and in several other locations by the OMEGA instrument on Mars Express, provides further support for the supposition that water flowed across and pooled on the suface at times in the past. As discussed in Chapter 12, however, what climatic conditions are

implied by the different types of water-worn features, and how such conditions came about, remain puzzling.

The poles are distinctively different from the rest of the planet. At each pole, and extending outward to about the 80° latitude circle, are thick stacks of layered sediments, roughly 3 km thick. The layering is best seen as a fine horizontal banding on defrosted slopes. The deposits are believed to be composed of layers with different proportions of dust and ice. The scarcity of impact craters indicates a relatively young age, those in the north being possibly as young as 10^5 years. The cyclic sedimentation implied by the layering, and the young age, suggest that the origin of the deposits may result in some way with changes in obliquity (Chapter 10).

Meteorites

Meteorites are important for our understanding of Mars for two main reasons. First, some of them, the carbonaceous chondrites, are almost certainly samples of the materials from which the planets formed 4.55 Gyr ago. They therefore provide a geochemical reference against which the composition of various components of a planet can be compared in order to better understand the processes and changes that occurred during a planet's formation and its subsequent evolution. Second, among the thousands of known meteorites, there are approximately thirty that have come directly from Mars. They were ejected from the surface during large impact events, went into orbit around the Sun, and ultimately fell on the Earth. These meteorites have been analyzed in great detail and provide clues about the history of Mars that could only be acquired by analysis of samples here on Earth.

Carbonaceous chondrites and chemical fractionation

Meteorites can be classified into two large groups: undifferentiated and differentiated (Wood, 1979; Lipschutz and Schultz, 1999). Undifferentiated meteorites are those that consist of the primitive materials from which the planets formed. Their most characteristic attribute is the presence of spherical chondrules, millimeters in diameter and composed of olivine and pyroxene with minor amounts of Fe–Ni metal and troilite (FeS). They are droplets of rocky material that condensed out of the high temperature, (500–1000°C) reducing cloud that surrounded the protosun by processes that are poorly understood. Differentiated meteorites are parts of larger objects that had accreted from the condensed material around the early Sun, then differentiated before being broken up, presumably by collisions with one another. Included in this group are irons, achondrites, and stony irons. Irons are pieces of cores from larger bodies. Achondrites are igneous rocks or breccias from the silicate portion of a larger body. Stony irons are mixtures of the two components.

Chondrites can be divided into two broad groups: ordinary chondrites and carbonaceous chondrites. In ordinary chondrites, the chondrules are embedded in a high-temperature matrix that has a composition similar to that of the chondrules. In contrast, carbonaceous chondrites are a disequilibrium mixture of a high-temperature component similar in composition to chondrules, and a low-temperature component of clay-like minerals, magnetite, Fe/Ni sulfides, and small amounts of carbonate and sulfate. Carbonaceous chondrites also contain up to 5 percent of a tarry mixture of complex organic compounds. Irregular rock fragments, called Ca/Al-rich inclusions, that are composed of minerals that condense only at very high (>1000°C) temperatures, may also be present. Different types of carbonaceous chondrites are recognized mainly according to their different proportions of the high-temperature, refractory components and the low-temperature, volatile components. Because of their 4.56 Gyr age and their composition, which is almost identical to that of the photosphere of the Sun, carbonaceous chondrites are believed to be representative of the materials in the early Solar System from which the planets formed. Of all the different types of carbonaceous chondrites, type C1 is the best match for the Sun's photosphere so, it is thought to be best representative of the composition of the solar nebula, the disk-like cloud of gas and dust that surrounded the early Sun, and so best representative of the material from which the planets accumulated.

The temperature at which a given element condenses from a gas of nebular composition at a pressure of 10^{-4} bars is generally used as a measure of the element's volatility (Ringwood, 1970). As materials condensed from the nebula and aggregated into larger bodies the condensed solid phases were fractionated against uncondensed gaseous phases. As a result, elements of like volatility followed one another and the condensed materials developed different compositions according to the mix of materials of different volatility materials that they incorporated. Differences in the bulk composition of terrestrial planets can thus be modeled as mixes of materials of different volatilities, on the assumption that during accretion elements of like volatility were incorporated into planets in like proportions with respect to the solar nebula composition, as represented by C1 chondrites.

Once materials became incorporated into planets, volatility was no longer an important factor in fractionation, except for the highly volatile components such as H_2O and CO_2 and the noble gases. Fractionation within hot planetary interiors depends more on chemical affinity and mineralogical compatibility. Three main chemical affinities are recognized. In coexisting silicate, metal, and sulfide melts, lithophile elements (e.g. Mg, Al, U, Th) preferentially partition into the silicate melts, siderophile elements (e.g. Ni, Co, Ir) preferentially partition into the metal melts, and chalcophile elements (e.g. As, Cu, Sb) preferentially partition into the sulfide melts. Thus formation of the Earth's core preferentially scavenged siderophile elements from the mantle to leave it depleted in siderophiles with respect to C1 carbonaceous chondrites. Analyses of martian meteorites indicates that the martian mantle is more depleted in chalcophile elements than is the Earth's, probably because of incorporation of more sulfur into the core (Wänke, 1981).

Compatibility is another property that affects composition. Compatibility is a measure of the ability of a particular element to be accommodated in the major mineral phases in the mantle. In partial melting, incompatible elements preferentially enter the melts and during crystallization they tend to concentrate in the remaining melts. On Earth, incompatible elements, such as U, Th, and K, tend to be preferentially concentrated in the crust. Although not an element, water acts as if it were incompatible, remaining largely in the residual liquids in a crystallizing basalt.

Martian meteorites

A small group of differentiated meteorites are now known to have come from Mars. They were originally suspected of being martian because they are igneous rocks with crystallization ages as young as 150 Myr, more than 4 Gyr younger than any other meteorites. They had to have come from a planet large enough to be volcanically active that recently (Wood and Ashwal, 1981). They could not come from the Earth or the Moon because they all have oxygen isotope patterns that, while similar to each other, are distinctively different from those of Earth–Moon rocks (Clayton and Mayeda, 1983). An asteroid source was considered unlikely because no asteroid is large enough to have been volcanically active 150 Myr ago. Planets other than Mars were considered unlikely because of difficulties of escape and transportation to Earth. Mars was the only likely source. A martian origin was finally determined unambiguously when it was found that gases trapped in the meteorites had isotopic and chemical compositions identical to the martian atmosphere, as determined by the Viking landers (Bogard and Johnson, 1983; Becker and Pepin, 1984; Bogard *et al*., 1984). The gases were probably implanted in the rocks during the impacts that launched the meteorites into space. Three types of meteorites were recognized in the original group and named after Shergotty, Nakhla, and Chassigny, representative meteorites of each type. The group was originally known as SNC meteorites, but the term is falling into disuse as more examples are found. They are now usually referred to simply as martian meteorites.

The rocks are believed to have been ejected by spallation from the near surface during impact events as rarefaction waves caused by the impact were reflected from the surface. Ejection was around the periphery of the impact point and could have occurred even though the rocks experienced only modest peak shock pressures (Melosh, 1984). Some of the meteorites show evidence of high shock pressures and shock melting, but others show only limited shock effects. Once the rocks were ejected from Mars they went into orbit around the Sun. Radioactivity induced by cosmic ray exposure while in orbit around the Sun enables ejection times to be estimated. Dates of ejection cluster around 11 Myr, 3 Myr, and 1 Myr (McSween, 2002). Numerical integrations indicate that a few percent of the material ejected from Mars during an impact would be captured by the Earth within 10 Myr (Gladman *et al*., 1996), which is consistent with the cosmic ray exposure ages.

All the martian meteorites except the 4.5 Gyr orthopyroxenite ALH84001 are volcanic rocks with ages ranging from 0.15 to 1.3 Gyr (McSween and Treiman, 1998; Nyquist *et al*., 2001). Shergottites are named for several stones that fell in Shergotty, India, in l865. Some are medium-grained basalts or diabases, consisting mostly of clinopyroxene and maskelynite, a shock metamorphosed plagioclase. Olivine is a significant phase in only one shergottite, EETA79001. Minor amounts of Fe–Ti oxides, amphibole, chromites, sulfates, and phosphates may also be present. Other shergottites are lherzolites that have medium-grained olivine and chromite enclosed in large orthopyroxenes. Nakhlites are named for a shower of about forty stones that fell in El Nakhla, Egypt, in 1911. They are pyroxenites with minor amounts of olivine. Interstitial minerals are similar to those in the shergottites. The one Chassigny known, fell in France in 1815. It is a dunite, consisting mostly of olivine with minor amounts of ortho- and clinopyroxenes. All the martian meteorites have cumulate textures, that is, they formed

as a result of concentration of crystals derived by fractional crystallization from a melt. Post-cumulus minerals are found in the interstices between the larger crystals. The modest crystal grain sizes indicate that the SNC parent magmas were emplaced at shallow depths within the crust or extruded onto the surface as phenocryst-rich lavas. All the martian meteorites fall within the basalt field. The basalts on the floor of Gusev crater are somewhat more mafic than the meteorites (McSween *et al.*, 2004); the rocks at the Pathfinder site appear to be more silicic, although this may be partly the result of surface alteration

The source of the martian meteorites is unknown. Clusters at three separate ejection ages indicate that three separate impact events delivered the meteorites to Earth. The young crystallization ages suggest that, except for the 4.5 Gyr ALH84001, the meteorites originated from the one-third of the planet's surface that is covered mainly by post-Noachian plains. Thus, there appears to have been a bias in favor of young terrains, possibly because spallation is favored by the presence of coherent rocks at the surface. A poor match between the TES spectra of the meteorites and those from martian plains, where not masked by dust, suggested to McSween (2001) that the rocks may be from Tharsis or Elysium where we have no TES rock spectra because of the dust.

The availability of the martian meteorites has enabled a wide range of constraints to be placed on the evolution of the planet (summarized, for example, in McSween (1994, 2001). The following are some salient points. The materials from which Mars accreted were enriched in volatile and moderately volatile elements with respect to the Earth. The planet differentiated into crust, mantle, and core very early, within 30 Myr of the formation of the Solar System. The crust had solidified by 4.5 Gyr ago, the age of ALH84001. The core of Mars is more sulfur-rich than the Earth's. The mantle composition has been modeled and among other characteristics it has a higher Fe/Mg ratio and lower Mg/Si and Al/Si than the Earth's. The meteorites are derived from mantle sources that differentiated early and then remained largely inert for most of the planet's history. Vigorous mantle convection and crustal recycling have been minor or were very short-lived. The planet was volcanically active as recently as 165 Myr ago, and is probably still active today. Other points are discussed in other chapters, particularly Chapter 4.

2 Impact craters

Impact craters are the most distinctive landforms on solid planetary bodies other than the Earth. Almost every solid surface on every planet and satellite observed so far is cratered to some degree. Craters form as a result of high-velocity collisions between planetary bodies and comets and asteroids in orbit around the Sun. Impact velocities range from ten to a few tens of kilometers per second. The cratering rate today on all planetary bodies is very low. From the terrestrial crater record, Grieve and Shoemaker (1994) estimated that, on the Earth, the rate of formation of craters 20 km or larger is $5.6 \times 10^{-15}\,\mathrm{km}^{-2}\,\mathrm{yr}^{-1}$ and that the rate is proportional to $D^{-1.8}$ where D is the diameter of the crater. This implies that a 10 km diameter crater forms in the United States (10 million km^2) every 5 Myr and a 1 km diameter crater forms every 80 kyr. Comparably low rates occur today on other planetary bodies of the inner Solar System. The present low rates are thought to have been typical for the last 3 Gyr (Neukum *et al.*, 2001). The lunar record shows, however, that early in the history of the Solar System, prior to 3.5 Gyr ago, the rate of crater formation was dramatically higher. The rate 4 Gyr ago was 500 times higher than the roughly constant rate of the last 3 Gyr. The rapid decrease in the cratering rates between 4 and 3 Gyr ago resulted in the striking contrast between the heavily cratered lunar highlands, with large, 3.8–4.0-Gyr-old impact basins, and the much more sparsely cratered maria, even though the ages are only a few hundred million years apart (Stöffler and Ryder, 2001). Mars, Moon, and the Earth likely had similar cratering records (Neukum *et al.*, 2001). Much of the cratering record on the Earth has, of course, been lost because of the higher rates of erosion and other geological processes, although approximately 160 impact craters, or their remains, have been identified, most being on the old continental cratons (Grieve, 2001). The martian record is similar to that of the Moon. We have heavily cratered terrains that have survived since the heavy bombardment ended roughly 3.8 billion years ago, and more sparsely cratered terrains, mostly plains, where the older surfaces have been buried by younger deposits.

Craters on Mars look much like craters elsewhere in the Solar System. They follow the same transitions to more complex forms with increasing size. However, the patterns of ejecta around martian craters are very different from those around most craters elsewhere. Fresh-appearing craters on the Moon and Mercury have a coarse, hummocky texture close to the crater rim, which changes to a radial texture and, in the case of larger craters, strings of small secondary craters, further out. In contrast, the ejecta around most fresh-appearing martian craters is arrayed in discrete lobes, each outlined by a low ridge or an outward-facing slope. Suggested causes of the distinctiveness of martian craters include fluidization of the ejecta because of the presence of volatiles, particularly water, in the martian surface, and entrainment of the ejecta in Mars' thin atmosphere. Because of their unique ejecta patterns, martian craters are commonly referred to as fluidized ejecta craters. Martian craters also undergo modification after their formation to produce forms rarely seen elsewhere in the Solar System.

In this chapter we first discuss the array of objects that a planet might encounter on its path around the Sun. We then examine the morphology of craters and how it changes with crater size. We also discuss the process of crater formation and how it varies with the size of the event. This discussion draws on comparisons with lunar and terrestrial craters, and with those produced experimentally, as well as on the results of computer modeling. We then discuss the unique ejecta patterns of martian craters and how they might have formed. Finally we have an extended discussion on crater dating. Craters provide a way of getting relative dates on different surfaces. Older surfaces are normally more cratered. While this is a simple relationship, there are many pitfalls in deriving relative ages, because of effects such as erosion, burial, and exhumation. Obtaining reliable absolute ages is much more difficult.

Crater-forming objects

The size-frequency distribution (SFD) of craters produced on a planetary body is a reflection mostly

of the size-frequency distribution of the impacting objects. The SFD of objects within the Solar System has been determined over a wide range of sizes from 10^{-20} kg dust particles to asteroids over 10^{20} kg. Over this huge range the flux of objects in Earth–Moon space is roughly proportional to $D^{-2.5}$, although the slope of the distribution curve, that is, the value of the exponent of D, varies according to the size of the object. The techniques used to determine the fluxes depend on particle size. Fluxes of dust-sized particles (10^{-20} to 10^{-2} kg) have been estimated from micro-craters on the Moon, scattering of sunlight by particles around the Sun (zodiacal light), various detectors on spacecraft, upper atmosphere collections, and detection of meteors in the Earth's upper atmosphere by radio and visual techniques (Grun, 1999). The fluxes of intermediate size objects, up to 10^{15} kg, have been estimated from the statistics of meteorite infall and observations of meteors (Dohnanyi, 1972). The numbers and orbits of the largest objects have been determined from sky surveys (e.g. Shoemaker and Wolfe, 1982). With respect to craters on Mars we are interested mainly in the larger objects, the comets and asteroids.

The term "comet" initially referred to prominent objects that appeared episodically in the night sky with a bright head or coma and a long tail. The term now encompasses all ice-rich bodies with eccentric orbits irrespective of whether the coma and tail are present. A comet's nucleus is an ice-rich conglomerate, consisting of frozen gases, organics, and silicate dust. When a comet enters the inner Solar System it is heated by the Sun and the ices sublimate, producing a diffuse atmosphere or coma and releasing dust that forms the tail. Comets are classified according to their orbits. Conventionally, if their orbital period is over 200 years they are referred to as long-period comets. Long-period comets move in highly elliptical, almost parabolic orbits with random inclinations to the ecliptic (the plane of the Earth's orbit). They spend most of their time in the Oort cloud, a vast, spherical cloud of 10^{12} to 10^{13} comets that surrounds the Solar System, extending out to distances of tens of thousands of Astronomical Units from the Sun. Sudden comet showers may result when comets in the Oort cloud are perturbed by passing stars, molecular clouds, or galactic tides. Being on highly elliptical orbits, long-period comets move rapidly through the inner Solar System and typically have impact velocities at Mars of a few tens of kilometers per second (Hartmann, 1977). Short-period comets are divided into two groups. Halley-type comets have orbital periods of 20–200 years and random inclinations like the long-term comets. Jupiter-family comets have periods less than 20 years and orbit inclinations that are close to the plane of the ecliptic. Impact velocities at Mars for short-period comets are around 10 km s^{-1}. For a summary of comets and their orbits see Boice and Huebner (1999) and Fernandez (1999).

Asteroids are rocky objects in orbit around the Sun. Many may be dead comets that no longer display a coma and tail when within 4 AU of the Sun, as active comets normally do. Most meteorites are samples of asteroids, although it has proven difficult to correlate the different types of meteorites with the different spectral types of asteroids. The largest known asteroid is Ceres, which is 940 km in diameter; the 20 largest are all over 220 km in diameter. There are over 8500 known asteroids, and new ones are being discovered at a rate of over 30 per month. Most are in the asteroid belt between 1.8 and 4.0 AU. Among the asteroids, the size and numbers of Earth-crossers are best known because of observational bias. Like the rest of the smaller objects in the Solar System, Earth-crossers follow a size-distribution curve of the form $N = kD^{-b}$, where N is the number of asteroids larger than diameter D. The exponent b varies according to diameter between 2 and 5 but averages 2.5 for objects larger than 100 m (Rabinowitz *et al.*, 1994). Most workers assume that most of the craters on Mars are produced by asteroids. This is partly because of difficulty in reconciling the estimated cometary flux with the terrestrial cratering record, possibly because the coma prevents an accurate measure of the diameter of a comet nucleus (Shoemaker and Wolfe, 1982), and partly because the size-frequency distribution of craters best corresponds to that which would be produced by asteroids (Neukum *et al.*, 2001).

Crater morphology

Simple craters

Fresh-appearing Martian craters smaller than approximately 5 km in diameter are mostly bowl-shaped with a depth/diameter ratio close to 0.2 (Pike, 1980a,b). Horizontally layered bedrock usually crops out at the top of the crater walls just below the crater rim (Figures 2.1 and 2.2). Below the bedrock ledges, talus slopes with a strong radial fabric either converge toward the center of the crater or terminate against a flat floor. In some areas dark streaks, common on the talus slopes, appear to be forming today. In the highest resolution images of the freshest craters, blocks may be seen on the rim and within the crater, particularly toward its center. Bright or dark radial streaks, or rays, occur around some craters, but they are much less common than on the Moon, presumably because of

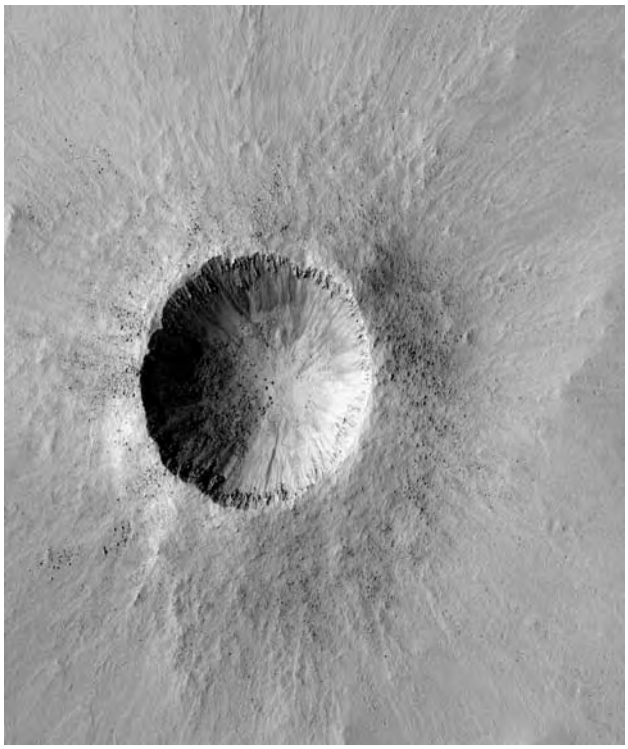

Figure 2.1. 1 km diameter simple crater at 4.8°N, 46.1°E. The crater is almost the same size as Meteor Crater, Arizona, which it strongly resembles. Its interior also resembles simple lunar craters. A bouldery, smooth to hummocky rim transitions outward, at about one crater radius from the rim, to terrain with a strong radial fabric (MOC R1502146).

higher rates of erosion and burial on Mars. Detailed characteristics of a prominent 10 km diameter ray crater are described by McEwen *et al.* (2005).

Meteor Crater, Arizona, 1.1 km in diameter, is a familiar example of a simple terrestrial impact crater. It is thought to have formed 50,000 years ago by the impact of a 30 m diameter object moving at 20 km s^{-1} (Melosh, 1989). A geological cross-section of the crater (Figure 2.3) gives an indication of what might underlie simple martian craters. The impact was into a horizontally layered sequence of sedimentary rocks. The crater has a raised rim. Roughly one-quarter to one-half of the rim height is the result of uplift and tilting outward of the wall rocks. The remainder of the rim height results from material ejected from the crater, some of which forms an overturned flap in which the local stratigraphy is inverted. Although much of the ejecta has been eroded away, the remains still form hummocky topography as far out as 1.3 crater radii from the crater center. Drilling reveals the presence of a 150 m thick breccia lens of crushed sandstone, glass, and meteorite spherules beneath the crater.

Complex craters

At a diameter of roughly 5–8 km, martian craters change from simple bowl-shaped types to complex types (Figure 2.4). Complex craters have one or more of the following interior features: (1) a broad, generally level floor interrupted by hills and mounds; (2) a central peak complex; (3) single or multiple blocks or slices of material slumped from the walls; and (4) continuous terraces on the wall indicating wholesale circumferential failure of the rim. With increasing crater size the central peaks become more complex and the number and size of the terraces on the walls increase. All complex craters are proportionately shallower than their simple counterparts (Figure 2.5). The depth to diameter ratio varies with size, falling from 0.2 at the 5–8 km transition diameter to 0.03 for a 100 km diameter crater. The transition diameter from simple to complex craters varies according to the size of the target body. On the Moon, it is in the 15–25 km range, on Mars in the 5–8 km range, and on Earth in the 2–5 km range (Pike, 1980a,b).

Examination of experimental impact craters and complex terrestrial impact craters gives an indication of what might underlie martian complex craters and how they might have formed. Figure 2.6B shows a cross-section through a 108 m diameter crater (Snowball) made by a 500-ton hemispherical charge of TNT lying on a horizontal sequence of poorly consolidated sediments (Roddy, 1977). While not an impact crater, the phenomenology of large surface explosions and impact craters is very similar (Melosh, 1989). The Snowball explosion produced a shallow crater with a central peak surrounded by an almost flat floor. Marker cans buried before the event indicate that movement was downward and slightly inward at the rim, horizontally inward under the flat floor, and diagonally upward under the central peak. An overturned flap near the rim crest merged outward with a continuous ejecta blanket that extended to 130 m from the rim, beyond which were rays and secondary craters.

The cross-section across the Snowball crater is similar to that inferred for complex terrestrial impact craters. Figure 2.6A is an idealized section across a complex terrestrial crater based on the 3.6 km diameter Steinheim basin (von Engelhardt *et al.*, 1967), the 13 km Sierra Madera structure (Wilshire *et al.*, 1972), the 22 km Gosses Bluff (Milton *et al.*, 1972), and the 3.8 km Flynn Creek structure (Roddy, 1979). The lowest units (A and B) are exposed as steeply dipping beds within the central peak, in which unit A is 1 km above its true stratigraphic position for the larger craters. The uppermost of the original units (F) is largely missing

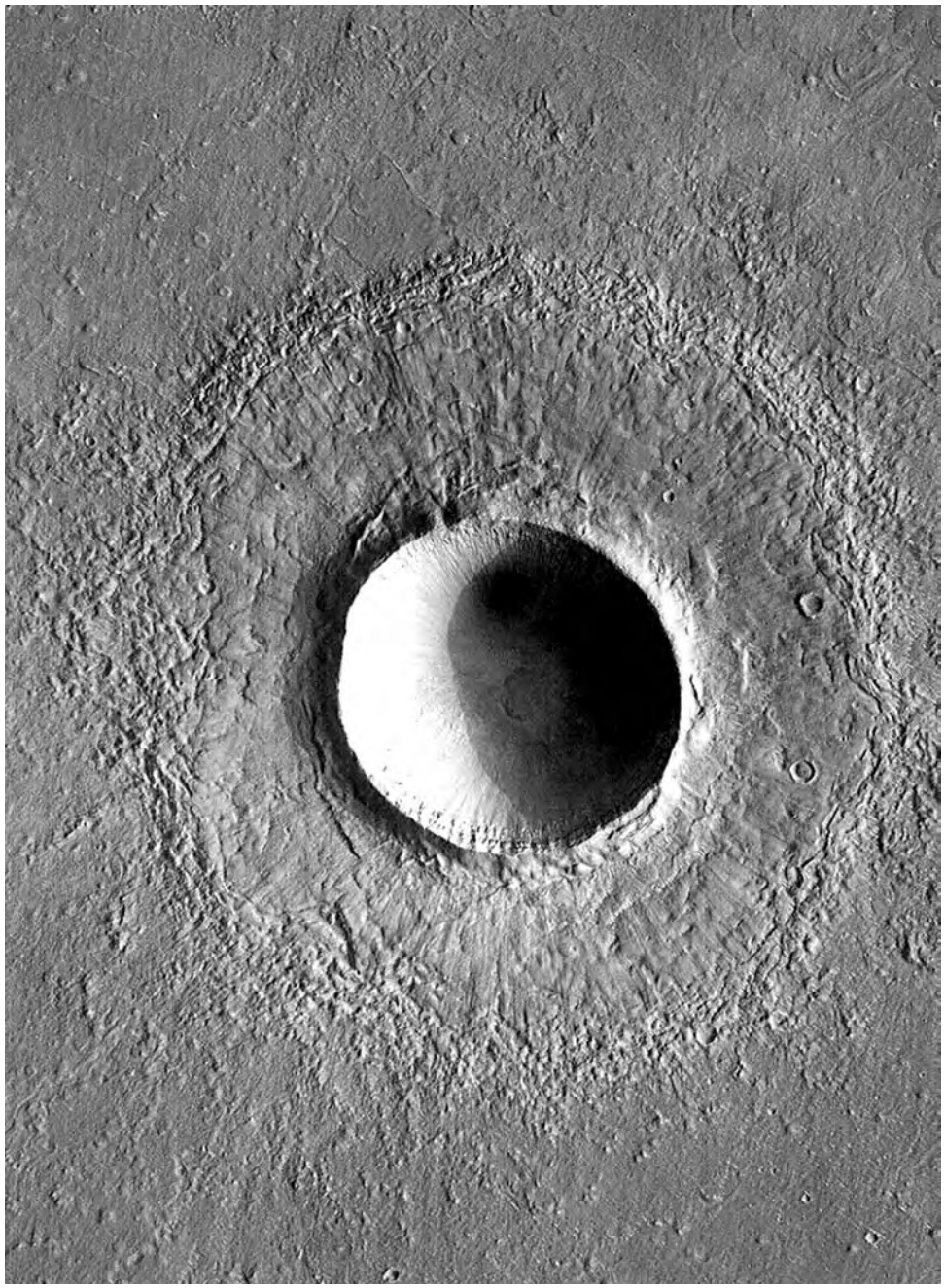

Figure 2.2. A 2.5 km diameter simple crater at 33°N, 122°E in Elysium Planitia. The crater size is below the 5 km transition diameter for simple to complex, but is larger than the onset diameter for fluidized ejecta patterns in this area. The crater is surrounded by circular platform of ejecta, with a strong radial fabric on its surface (MOC SP2-43704).

within the crater, having been either ejected or, in the very center of the crater, vaporized during the event. Ejecta covers the rim and floor. Faults around the periphery have formed in response to the inward movement of the floor toward the central peak uplift. Although based on terrestrial craters, the cross-section is likely representative also of martian craters in the 8–130 km diameter range.

Multi-ringed basins

Another transition occurs at around 130 km in diameter. Instead of, or in addition to, a central peak,

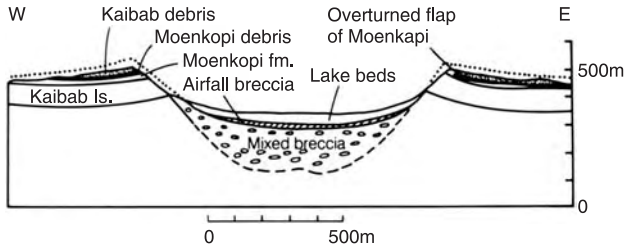

Figure 2.3. Cross-section through Meteor Crater, Arizona, gives an indication as to what may underlie simple craters on Mars (from Melosh, 1989, reproduced by permission from Oxford University Press).

craters larger than this have a ring of hills on the floor, within the crater rim. The Orientale basin on the Moon is the best-preserved multi-ring basin in the Solar System. Its outer escarpment, the Montes Cordillera, is 2–7 km high and 930 km across. Within this escarpment are two rings of hills, the Montes Rook, 480 and 620 km across. Basins with comparable, clearly defined, multiple rings of hills and inward-facing escarpments, such as occur around Mare Orientale, do not occur on Mars, although indistinct, multiple-ring structures can be traced around some of the larger basins and shallow circular depressions. Most martian basins have just one ring of hills inside the basin rim. The 225 km diameter basin Lyot is the youngest and best-preserved ring structure on Mars (Figure 2.7). It has a rugged inner ring and minor central peak. Lobes of ejecta extend radially away from the rim, and further out are dense fields of secondary craters, some forming radial strings. There is little ambiguity as to what is the true basin rim. This has been an issue with Orientale, where the Cordillera and two Rook rings have variously been proposed as the rim of the transient cavity that formed during the impact (Head, 1974; Wilhelms, 1987; Melosh, 1989).

The two largest basins on Mars are Argyre and Hellas. Argyre most resembles Orientale (Heisinger and Head, 2002). It has an inner, circular, 700 km diameter plain that is surrounded by an annulus of massifs with an outer diameter of 1800 km. Although vague circular structures can be traced through the massifs in the annulus, distinct circular mountain ranges comparable to the Montes Rook are not present. Hellas is even less like Orientale. At its center is a roughly circular plateau surrounded by plains. There are no traces of inner, circular mountain ranges. Similarly, the 1500 km diameter Isidis basin has no inner ring, although there are several discontinuous circular faults surrounding the basin. All the large basins are underlain by a thinner than normal crust (Zuber *et al.*, 2000).

The readily visible basins constitute only a fraction of the impact basins that formed on Mars. MOLA data has revealed the presence of numerous large circular depressions, not readily visible in images. Some of these, the Utopia basin, for example, had been suspected before acquisition of the MOLA data (Wilhelms and Squyres, 1984; McGill, 1989; Schultz and Frey, 1990), but the MOLA data has revealed many more (Frey *et al.*, 2002a). Frey *et al.* called them "quasi-circular depressions" or QCDs. The Utopia basin, centered at 40°N, 105°E, is among the largest. Like the Utopia basin, many of these newly discovered basins are buried beneath the younger deposits of the northern plains.

Crater formation

Experimental high-velocity impact experiments, large nuclear and explosion craters, theoretical modeling, and large terrestrial impact structures have all contributed to our understanding of what happens during a high-velocity impact (see summaries in Roddy *et al.*, 1977; Melosh, 1989). Formation of a crater by a high-velocity impact can be thought of as a three-stage process: compression, excavation, and modification (Gault *et al.*, 1968; Melosh, 1989). The compression stage starts with contact between the target and projectile (Figure 2.8). The projectile pushes the target material out of its path, compressing and accelerating it to a large fraction of the impact velocity. At the same time the leading part of the projectile is compressed and decelerated. Shock waves are generated at the contact point. One shock wave travels back into the projectile, another down and into the target. Pressures within the compressed region between the shock waves may reach hundreds of GPa, greatly exceeding the strength of the materials, and causing them to behave like fluids. In this early stage, some of the highly compressed material between upgoing and downgoing shock waves is squirted out laterally to form jets.

The compression stage can be thought of as ending and the excavation stage starting when the shock wave moving back into the projectile reaches the rear of the projectile. The compression stage is very short. For typical impact velocities of a few tens of kilometers per second, shock wave velocities are in the $10-20\,\mathrm{km\,s^{-1}}$ range so that a 1 km diameter impactor would be engulfed in one-tenth of a second or less. At the start of the excavation stage a rarefaction wave begins to move from the back of the projectile into the highly compressed and fluidized materials around the impact point, causing their decompression, expansion, and ejection. At the same time, a roughly hemispherical shock wave continues to move into the

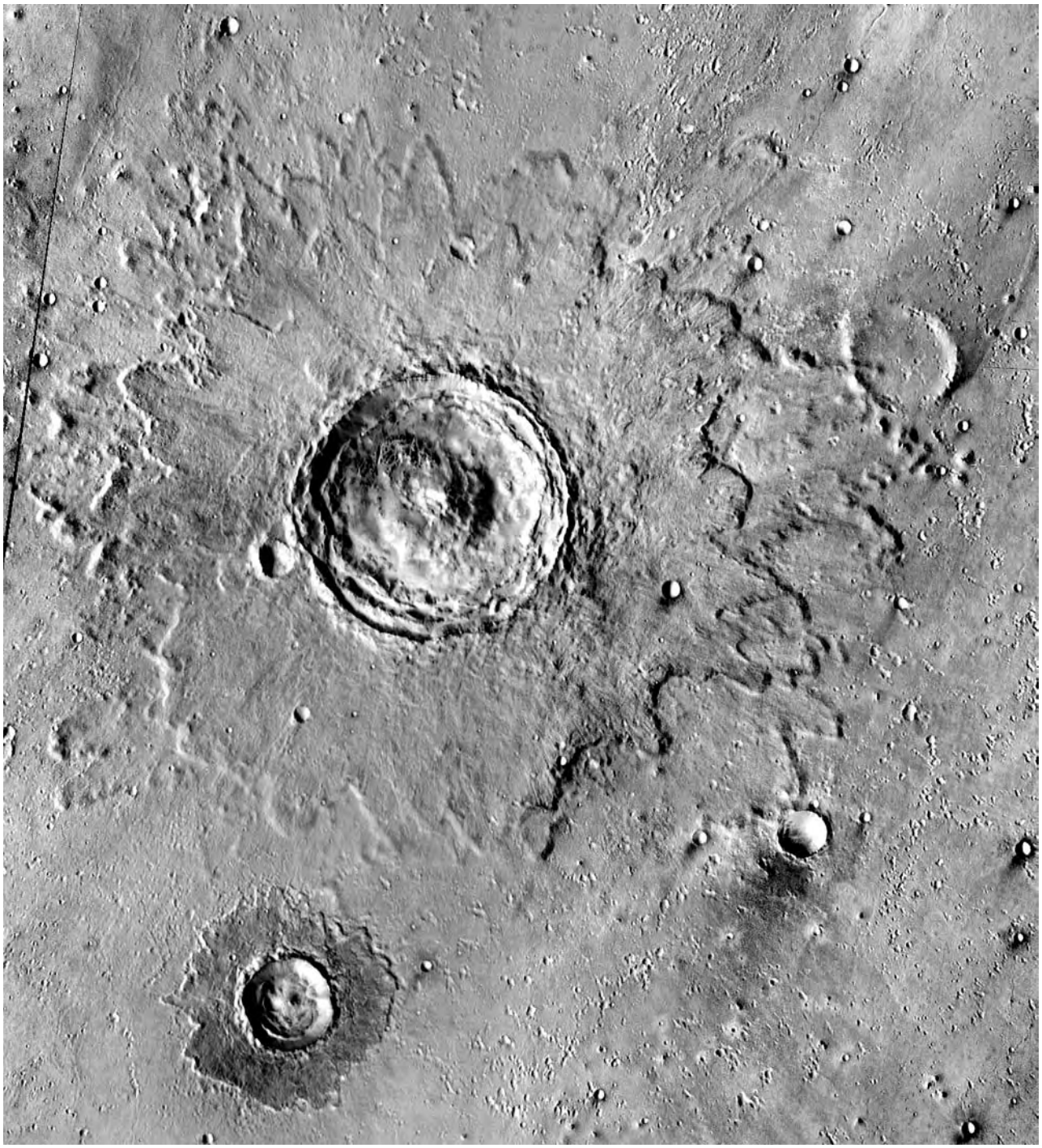

Figure 2.4. A 31 km diameter complex crater at 26°N, 321°E with the full array of complex crater features. The central peak encompasses almost the entire floor, the walls have partly collapsed to form a complex array of circumferential terraces, and lobes of ejecta extend to two crater radii beyond the crater rim. Further out are numerous secondary craters (THEMIS mosaic).

target. Particle motions in the compressed material immediately behind the shock wave are radial to the impact point, but rarefaction waves from the surface add an upward component to the flow causing the flow lines to curl up toward the surface (Figure 2.9). Expansion of the compressed material behind the shock wave toward the surface causes their ejection, thereby enlarging the crater. The ejecta forms an outward-moving curtain in which the individual pieces are on independent ballistic trajectories. As the shock wave moves outward, the peak pressures behind it fall. Ultimately the peak pressures are so low that the rarefaction waves fail to disrupt and eject the target materials and growth of the crater ceases. The crater that has formed at this stage is generally referred to as the transient cavity.

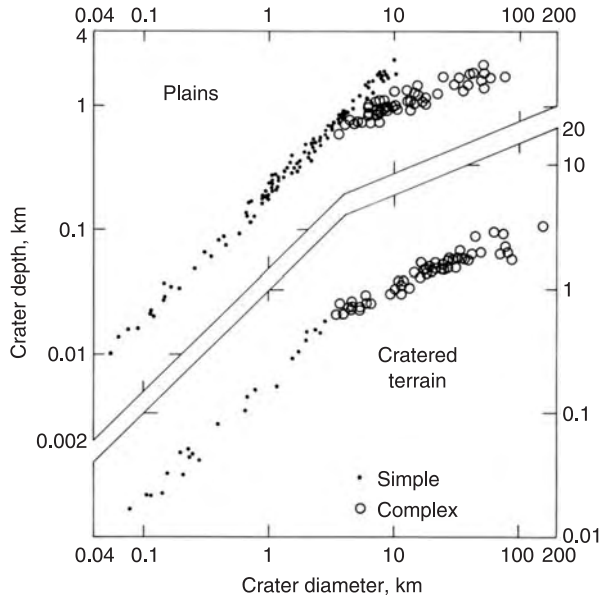

Figure 2.5. Crater diameter versus crater depth for martian craters. Simple craters maintain a roughly constant depth/diameter ratio, whereas complex craters are proportionately shallower with increasing size (from Pike, 1980).

Modification of simple craters subsequent to the formation of the transient cavity is relatively minor. During the growth stage the cavity is lined with breccia and melt that is flowing up and out of the crater. When growth stops, the steep walls of the transient crater collapse toward the center so that the original crater floor becomes buried under a lens of breccia and melt derived from the walls.

The first stages of formation of complex craters are similar to those for simple craters. However, according to Melosh (1989), although breccia and melt may be found in a stratigraphic position that suggests that they lined the original transient cavity, thick breccia lenses, such as form in simple craters by centripetal flow of material from the walls of the transient cavity, are not observed. This implies that

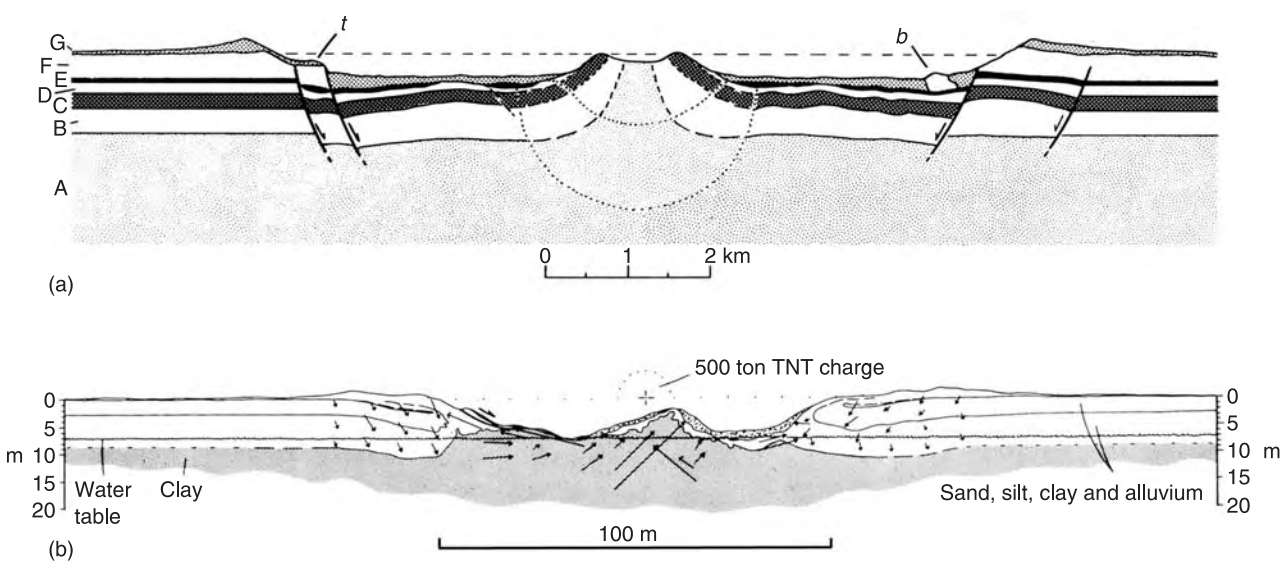

Figure 2.6. (a) Schematic cross-section across a complex impact crater based on four terrestrial impact craters, ranging in size from 3.6 km to 22 km in diameter. All are in horizontal sedimentary rocks. The larger semicircle shows the approximate location of the transient cavity, subsequently filled by flow inward and upward to form the central peak. For further details see the text (Pike, 1980). (b) Cross-section through a 108 m diameter crater produced by a 500-ton surface charge of TNT. The crater has a central uplift, terraced walls, and exterior concentric fractures. Buried markers showed that movement was down and in around the crater edge and up under the central peak (Roddy, 1977).

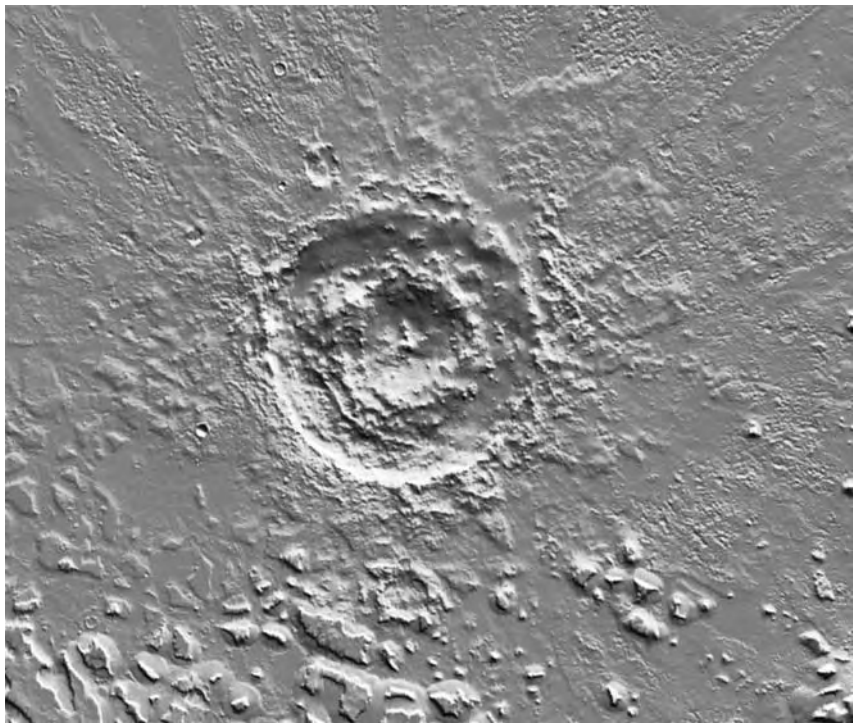

Figure 2.7. The 220 km diameter, multi-ringed basin Lyot located at 50°N, 29°E. This is the freshest appearing impact basin on Mars. Within the basin is a prominent ring and minor central peak. Outside the basin are lobes of ejecta and dense fields of secondary craters (MOLA).

both the formation of the central peak and the collapse of the transient cavity to form circumferential terraces took place quickly before centripetal flow of the transient cavity lining could occur. This is consistent with observations of experimental craters in low-strength targets, in which the central peak starts to form as soon as the crater stops growing in depth. It is also consistent with observations of large lunar craters, which suggests that impact melt is draped over the terraces, that is, the terraces formed before the impact melt was deposited. Central peak formation has been likened to formation of the central jet that forms when a water droplet falls into water. If the analogy is appropriate, it implies that the rock materials behave like a liquid for a short period of time during an impact, but that the material "freezes" part way through the process so that the peak is preserved. Fluidization cannot be due to melting, because only a small amount of melt is produced. Water in the target may facilitate fluidization and formation of complex craters, as suggested by some large experimental craters (Roddy, 1977), but water cannot be invoked to explain the complex craters on the Moon, which is very dry. A third possibility is acoustic fluidization. Melosh (1983) suggested that the fragmented rock beneath the transient cavity could temporarily behave as a fluid as acoustic vibrations generated by the impact and passage of the shock waves causes separation of the constituent rock particles. As the acoustic energy decays, the fluidized material would revert to its solid state and freeze. In the case of the larger multi-ringed basins, fluidization was maintained until later in the process, by which time the central peak had completely or partly collapsed to form an outward-moving wave that froze to form a ring, much like the rings that form when a water droplet falls into water.

Material ejected from a crater during its formation may form secondary craters. McEwen *et al.* (2005) estimate, for example, that the fresh 10 km diameter crater Zunil created around 10^7 secondary craters 10–200 m in diameter, many concentrated in radial streaks or rays that extend up to 1600 km from the parent crater. Dense fields of shoulder-to-shoulder secondaries also occur around the impact basin Lyot (Figure 2.7). Secondary craters close to the parent crater commonly form irregularly shaped craters, but ejecta that is thrown distances of hundreds of kilometers impacts at high velocities and forms

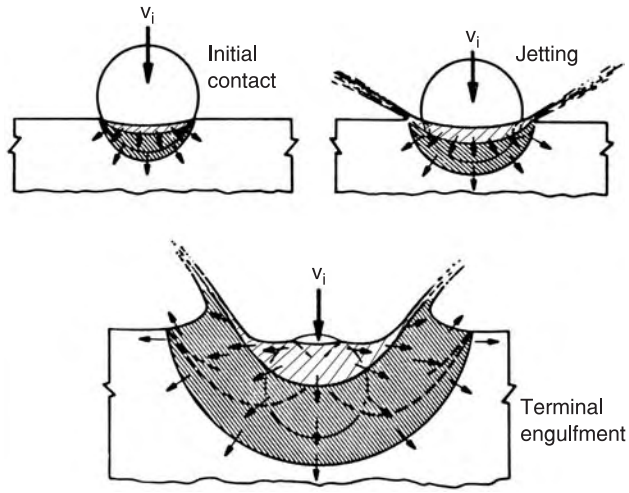

Figure 2.8. A schematic of the initial compressional stage of a high-velocity impact. At contact, shock waves start moving into the target and back into the projectile. Although the shock wave moves back into the target at a velocity of several kilometers per second, it still moves downward with respect to the original target because of the higher initial velocity of the projectile. The shaded region is shocked target material. The lightly hatched region is the shocked part of the projectile. In the second stage, the highly compressed target and projectile material is jetted out laterally around the contact point. In the third stage, the shock wave moving back into the projectile has almost reached the rear of the projectile. Flow of the compressed materials is initially radially away from the contact point, but rarefaction waves reflecting off the free surface behind the shock wave cause the flow to be deflected toward the surface (adapted from Gault *et al.*, 1968)

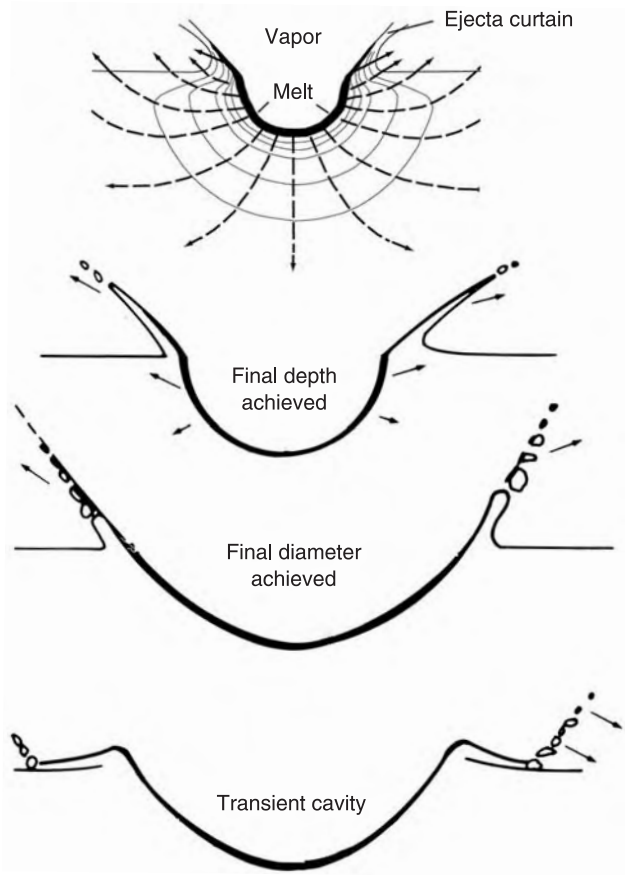

Figure 2.9. The expansion stage. In the upper diagram, solid lines show the peak pressure contours, dashed lines show the flow directions. Vaporized materials around the contact point expand into the space above the growing crater which becomes lined with melt. The other diagrams show successive stages in forming the crater (adapted from Melosh, 1989).

circular craters, generally indistinguishable from primary craters, except possibly for a shallower depth. This may present problems in dating surfaces by counting craters in the size range (< 50m) where secondary craters may be common (see below).

Ejecta morphology

The feature that most distinguishes martian craters from craters on other planets is the configuration of their ejecta. Lunar craters are surrounded by a continuous blanket of ejecta that merges outward with the surrounding terrain. Within half a crater radius of the rim, the ejecta surface is smooth or has a gentle hummocky surface. Just outside the near-rim deposits, and extending out to about one crater radius from the rim, there may be radial ridges and grooves or arrays of low concentric ridges or dune-like forms. This zone merges outward into a zone of secondary craters that are normally arrayed in loops or radial chains. A braided or herringbone pattern may develop in association with the secondary craters. The pattern is created by faint ridges that extend outward from secondary craters at a small angle to the radial direction to produce V-shaped ridges that point toward the primary crater. Further out and extending large distances are linear, bright markings or rays, in which secondary craters are normally concentrated. The various ejecta facies are deposited from the ejecta curtain as it expands away from the crater (Figure 2.10). The materials within the curtain are on ballistic trajectories. The ejecta that lands close to the crater is launched at low velocity so it lands at low velocity, barely disturbing the surface. The ejecta that lands further out, however, does so at higher velocities. As a consequence it disturbs the surface and becomes mixed with local materials.

The ejecta patterns around martian craters are generally very different, and vary considerably. The

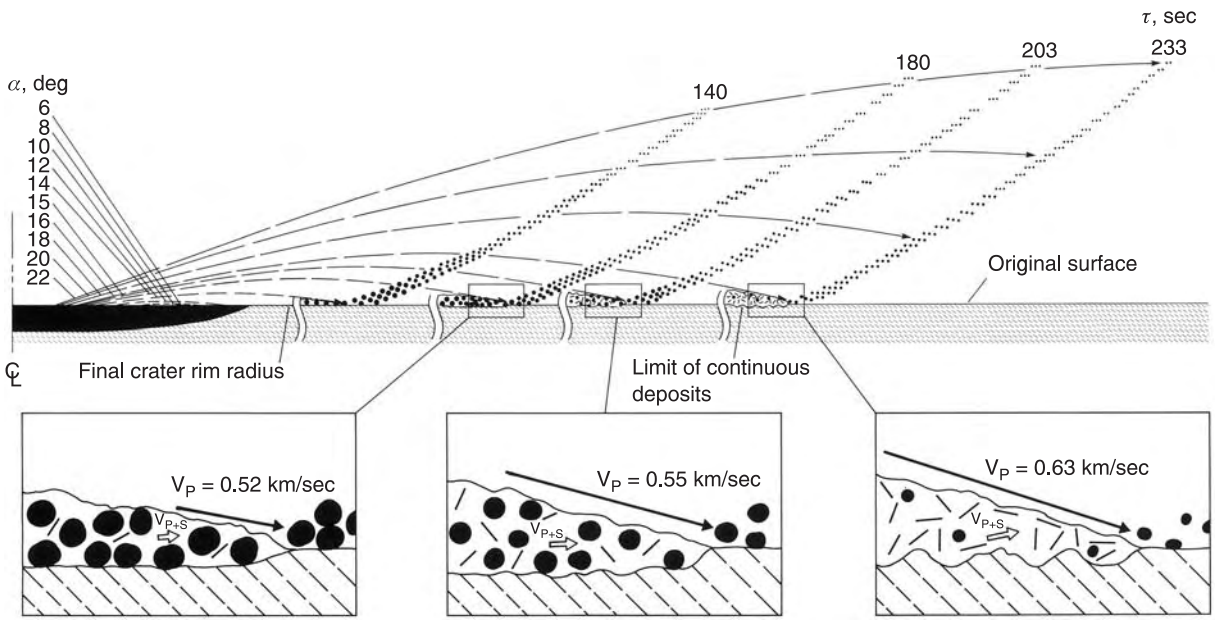

Figure 2.10. Deposition of ejecta on the Moon in the absence of an atmosphere. Formation of the crater results in an outward-moving curtain of debris (see Figure 2.9). With decreasing height within the curtain the debris is coarser and moving at lower velocities. Ejecta falling close to the rim has a low velocity and forms a continuous deposit that barely disturbs the surface. Further out the ejecta lands at a higher velocity and stirs up and mixes with the surface materials. In the presence of an atmosphere the finer components of the curtain will tend to be decelerated and entrained in the atmosphere to form turbulent clouds, and possibly ground-hugging density currents (from Oberbeck, 1975).

pattern around some simple craters, particularly those smaller than about 2–3 km in diameter, resembles that around lunar craters (Figure 2.1). Hummocky ejecta near the rim crest transitions outward into ejecta with a distinct radial fabric. Secondary craters, herringbone patterns, and rays may also be present beyond the transition zone. Other simple craters have unique martian ejecta patterns. Outside the sharply raised rim, there may be a single annulus of ejecta, roughly one crater radius wide. The surface of the annulus typically has a marked radial striation (Figure 2.11), a pattern similar to that on many landslides within the canyons (see Chapter 5). At its outer edge, the annulus terminates fairly abruptly with only a narrow transition zone between it and the more distal parts of the ejecta field. The annulus is normally outlined by a convex upward slope, but there may be a low ridge. Beyond the annulus the surface around fresh simple craters typically has faint radial ridges, lines of secondary craters, and rays, much like the more distant parts of the ejecta around lunar craters.

The patterns around complex craters are more complicated. Immediately adjacent to the rim there may be coarse, hummocky topography. This zone is typically very narrow ($< 0.1R$) around craters that have the fluidized ejecta patterns, but with the rarer craters that have more lunar-like patterns this zone extends much further out. Two types of fluidized ejecta components are observed. The first is an annulus of strongly striated ejecta like that around simple craters. As with simple craters, it may be outlined by a low ridge or an outward-facing slope. The annulus typically extends out about one crater radius from the rim forming a crudely circular platform around the crater. The second component is an array of radially elongate lobes of ejecta, each lobe being outlined by a low ridge. The lobes may extend as far as three crater radii from the rim. In general, the larger the crater, the more lobes there are present. Smaller craters may have just a single, circular rampart (Figure 2.12), but in larger craters many elongate lobes are superimposed one on another (Figure 2.4). Many of the lobes have radial striations, but the striations are much less marked than on the inner annulus. The lobes also appear to be very thin except for the outer rampart, for subtle underlying topography commonly shows through. Around the freshest craters, secondary craters can be seen beyond the ejecta lobes. Where both an annulus and lobes are present, the annulus appears to be uppermost. The prominence of the two components appears to depend

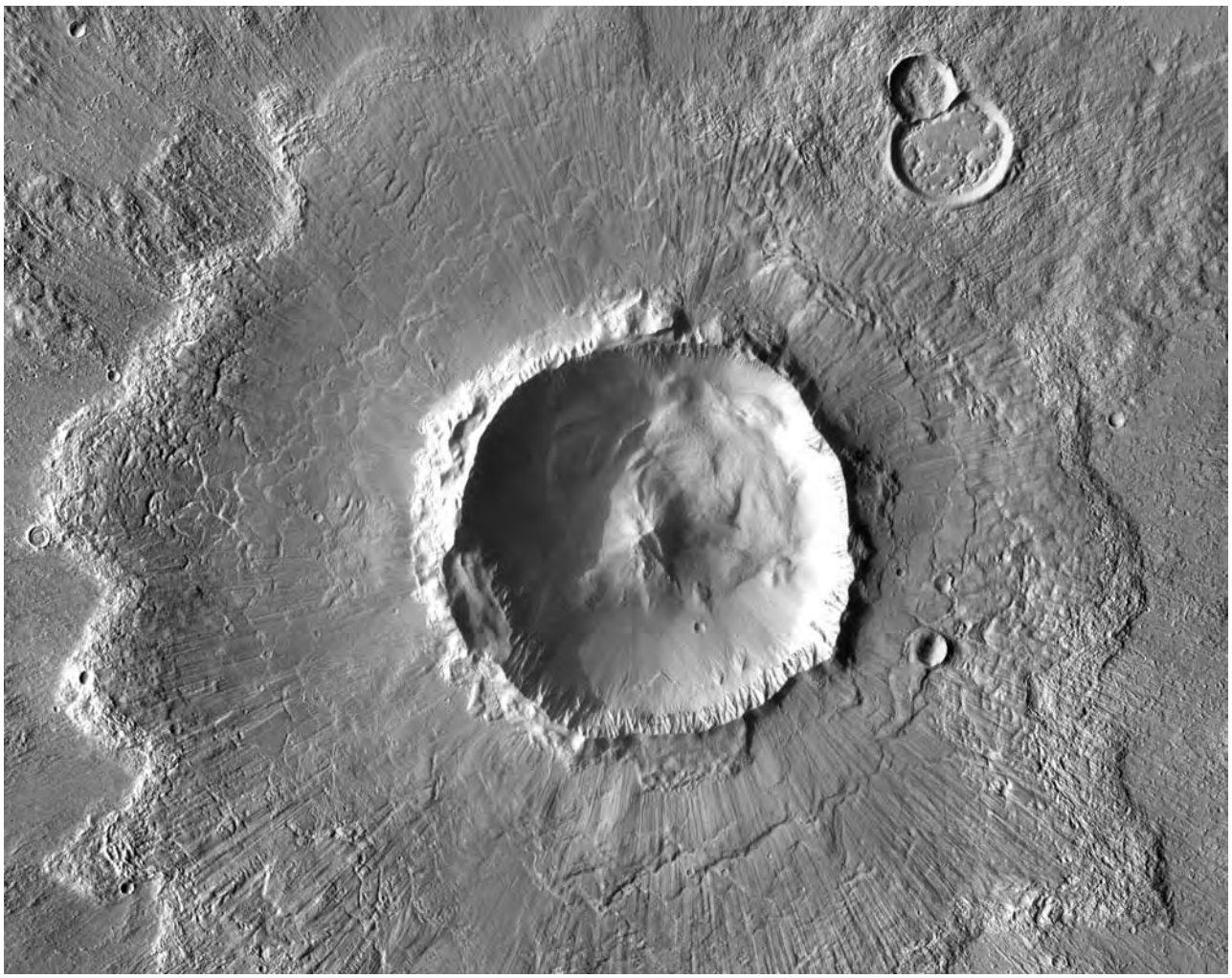

Figure 2.11. 20 km diameter crater at 33°N, 118°E. As is typical of craters in this general area, the crater has a distinct platform of ejecta around the rim (see Figure 2.13). Beyond the platform are radially elongate ejecta lobes. The surface of the platform is sculpted by strong radial striae. In the center of the image the striae cross a small crater, indicating that the crater was present before the impact, yet was not buried by ejecta (THEMIS mosaic).

on location. In Lunae Planum and most of Tharsis, for example, the inner annulus is generally inconspicuous, whereas in Utopia Planitia almost every crater has a distinct platform around the crater rim (Figure 2.13).

The terminology used in the literature can be confusing. Craters with a prominent annulus have been referred to as pancake, pedestal, and mound craters. Those with prominent lobes or ramparts have been referred to as petal, flower, or rampart craters. All are referred to as fluidized ejecta craters, because of their inferred mode of origin. Barlow *et al.* (2000) proposed a standardized terminology based on the number and types of ejecta layers. They propose that non-genetic, self-explanatory terms should be used such as single-layer pancake, and single-, double-, and multiple-layer rampart craters. The term ''pedestal'' should not be used to describe primary impact features but should be reserved for craters that have been modified subsequent to their formation such that a crater and its ejecta are left perched above the surrounding terrain (see below under Crater modification).

The unique martian ejecta patterns have been attributed to two causes: volatiles in the surface or entrainment of ejecta in the atmosphere. Shortly after the patterns were first observed during the Viking mission, Carr *et al.* (1977) proposed that material ejected from martian craters, instead of mostly forming a hummocky deposit close to the rim as on the Moon (and Earth), continued to flow outward as a thin, ground-hugging flow. The evidence was deflection

Figure 2.12. 17 km diameter crater at 21°S, 285°E. The ejecta is surrounded by a prominent ridge or rampart. A platform, as seen in the Figure 2.11, is almost completely absent (THEMIS V11200040, V05808002).

of the ejecta around obstacles and the much greater radial distance that continuous ejecta is found around martian craters, as compared to lunar craters. They proposed that the greater mobility of martian ejecta was due to incorporation of water, or some other volatile, into the ejecta. Martian ejecta was thus likened to terrestrial mudflows. Subsequently, Gault and Greeley (1978) were able to reproduce the martian patterns by firing Pyrex spheres into viscous targets. Unfortunately, there are problems with this simple explanation. The onset diameter for the flow patterns is about 3 km, which would require liquid water to be present at depth of 400–600 m almost everywhere on the planet. While ice may be present almost everywhere on Mars at these depths, liquid water is unlikely because of the low surface temperatures and the low heat flow. Melting of ice during the impact would likely be only minor, and unlikely to alter the rheological properties of the bulk of the ejecta (Melosh, 1989). Moreover, if the patterns are due to presence of water or ice, one might expect a strong dependence of the type of ejecta patterns on latitude. While there may be some dependence on latitude (see references in Barlow and Perez, 2003), what patterns have been identified are rather subtle and difficult to separate from effects of size, modification, and detectability of the fluidized patterns in different kinds of terrain.

Schultz and Gault (1979), mainly on the basis of theoretical calculations, and observations of dust-laden, ground-hugging clouds, or base surges, around large experimental explosion craters, alternatively suggested that the martian ejecta patterns could have been produced by interaction of the ejecta curtain with the thin martian atmosphere. The interaction results in sorting of the ejecta. The coarser debris maintains its ballistic trajectory and forms secondary craters, but the finer debris is decelerated and becomes part of a complex cloud that mixes with the just-formed secondary crater products to form a basal ejecta flow. Somewhat similar lobate ejecta patterns around Venusian craters support the supposition that the atmosphere can have a significant influence on ejecta configuration (Schultz, 1992). The relative effects of target properties and the atmosphere are unlikely to be resolved soon. The target clearly influences ejecta geometry, as indicated by the contrast between the patterns in Lunae Planum and Utopia Planitia (Figure 2.13), but the Venusian craters indicate that at least a thick atmosphere can have a strong influence too.

Crater modification

Once craters form and are exposed to conditions on the martian surface they are vulnerable to modification by a wide range of processes such as mass wasting, erosion by impacts, wind, water, and ice, and burial by eolian deposits, volcanics, and so forth. The extent to which the primary impact features are preserved depends on location. On most Hesperian and Amazonian volcanic plains situated at low latitudes, impact craters have undergone very little modification despite being exposed to the surface conditions for billions of years. Delicate details of the ejecta are preserved and filling of the craters is mostly negligible (Figure 2.13A), although of course the occasional crater is seen that is partly filled with lava. The excellent preservation in these terrains is consistent with the very low erosion rates estimated for the post-Noachian period (Golombek and Bridges, 2000; Carr, 1992). Preservation is more difficult to assess in the heavily cratered uplands because the fine textures on the ejecta are

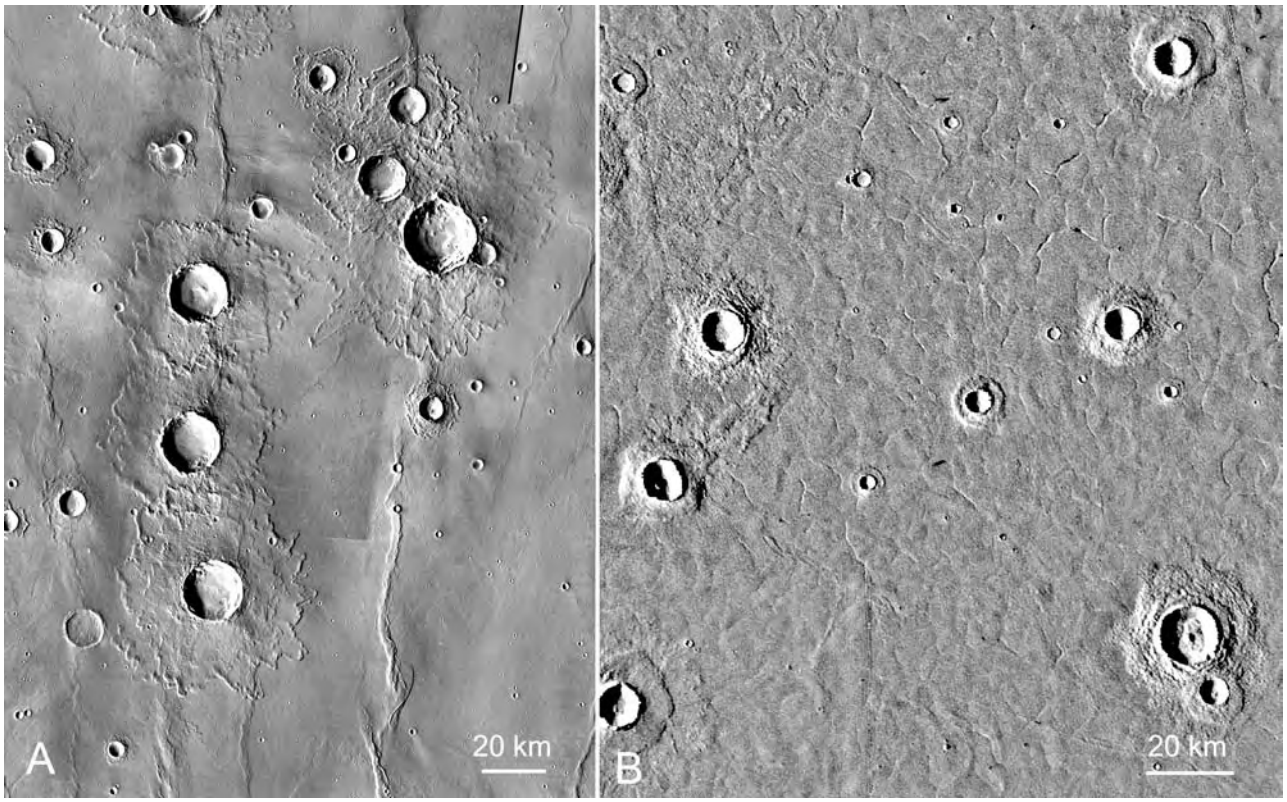

Figure 2.13. The ejecta patterns around craters depend on location. The left image is of a cluster of craters around 8°N, 287°E in Lunae Planum. All the craters have well-developed rampart ejecta patterns but no platform such as shown in Figure 2.11 (THEMIS mosaic). The right image is of a crater cluster around 33°N, 103°E. Each has a prominent annulus of ejecta around the rim, but rampart patterns further out are poorly developed (MDIM2).

more difficult to discern in this more complicated terrain, but low-latitude erosion rates are likely to be low in these terrains also (Craddock and Maxwell, 1993). There are, however, exceptions. The Amazonian-aged Medusae Fossae Formation, for example, is an easily erodible airfall deposit that straddles the plains–upland boundary between 140°E and 220°E. It buries craters, and where partly removed leaves behind pedestal craters (see below). But, in general, most low-latitude, post-Noachian craters are well preserved.

Post-Noachian craters are more modified at high latitudes. Pedestal craters are common over much of the northern plains (Figure 2.14). These are craters that are surrounded by a platform that is at an elevation well above the surrounding terrain. Commonly the primary ejecta textures can be seen on the surface of the platform. The platforms or pedestals have been attributed to removal of a near-surface layer of material by the wind (Arvidson *et al.*, 1976). The layer is retained only around craters where the surface was armored by ejecta. With smaller craters the platform is proportionately narrower so that small impact craters are left atop low hills and may be confused with volcanic craters.

Pedestal craters also form at low latitudes where a near-surface layer has been partly removed. The Medusae Fossae Formation has already been mentioned, but throughout the cratered uplands there is evidence of deposition and removal of layers of near-surface materials (Malin and Edgett, 2001). Removal of the layers exhumes craters that formed before the layers were deposited, and leaves pedestals around craters that formed after the layers were deposited (Figures 2.15 and 2.16). Irregular escarpments outline the areas where the layers are retained, giving these locations an etched appearance.

In contrast to those in younger terrains, most of the craters in the Noachian terrains are highly degraded. With increasing degradation and presumably age, complex craters progressively lose the ejecta patterns around the crater, the individual terraces on the walls, and the central peak. The trend is toward shallow, flat-floored craters, with steep gullied walls. The rim crest typically remains sharply defined and may be slightly raised. The process of crater filling was

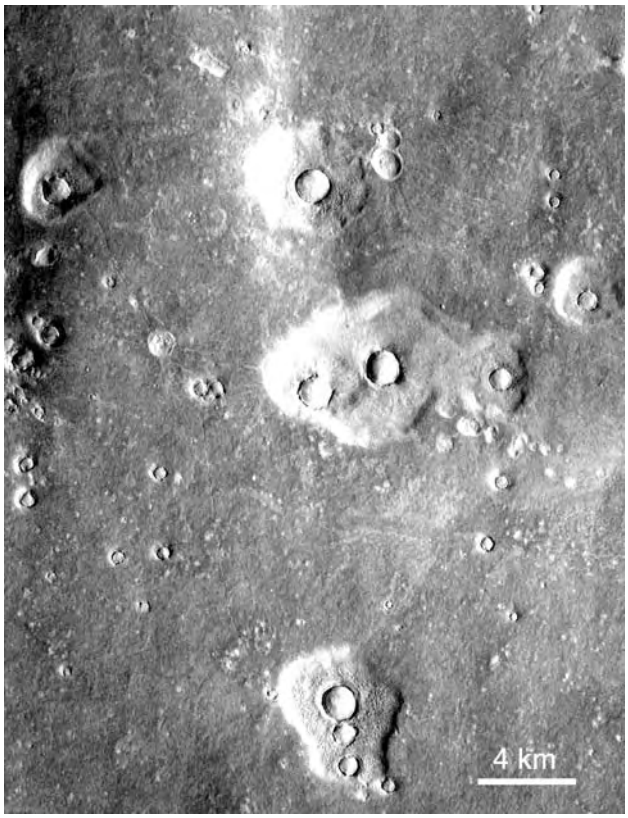

Figure 2.14. Pedestal craters in the northern plains at 47°N, 10°E. Each crater is inset into a platform that stands above the surrounding plain. This area was likely covered formerly by a layer of debris that has now been removed except around craters where the surface was armored by ejecta. The ejecta patterns can be seen around some of the craters. The scene is 19 km across (THEMIS V04993017).

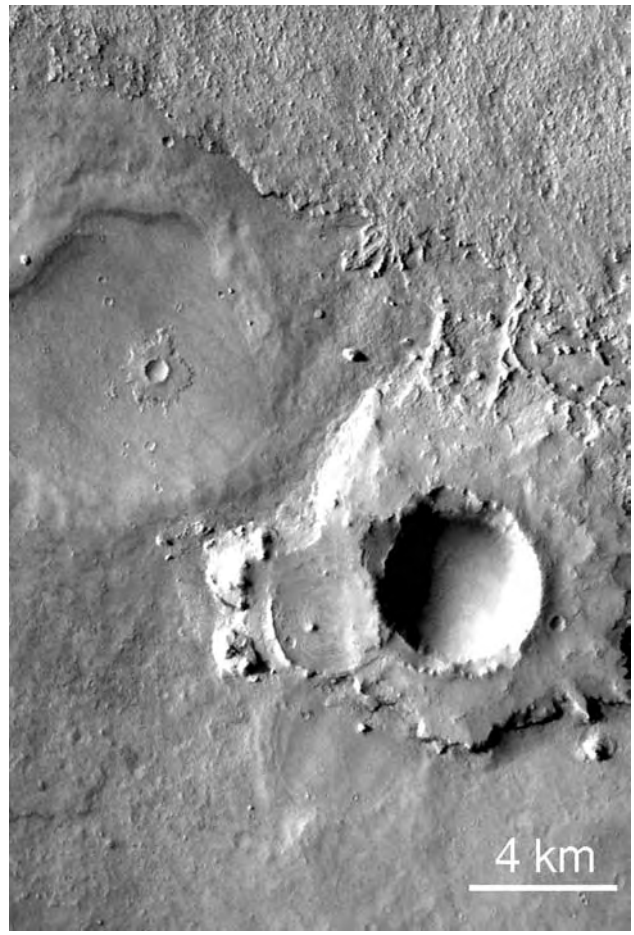

Figure 2.15. Pedestal craters in the cratered upland at 6°N, 358°E. A small pedestal crater in the left of the image has been left behind as the material in the upper right corner of the image has been stripped back. The larger pedestal crater is inset into a platform that is much thicker than the stripped back area and suggests that the area was, in addition, once covered by a much thicker blanket that has also been largely removed. The scene is 19 km across (THEMIS V04756006).

slow because ghost craters, common on the crater floors, indicate that significant numbers of impact craters formed while the larger crater was being filled. What processes contributed to filling of the craters is unclear. We know that volcanism contributed at Gusev crater (Chapter 11), but other processes, such as direct eolian deposition, or trapping of atmospheric debris by intracrater lakes, likely operated also (Chapter 7).

Crater size frequencies and ages

The main interest in size-frequency distributions of craters on planetary surfaces stems from their potential for revealing information about the history of the surface and its age. Counting craters to determine the relative age of a surface is a technique that is widely used, and the literature is replete with estimates of ages of martian surfaces derived from craters. But before discussing ages we will briefly examine how a crater population evolves with time. Shoemaker (1966) showed that for the Moon a plot of the cumulative number of craters against diameter has a change in slope around 1 km in diameter. For craters larger than 1 km the slope is close to −2; for craters smaller than 1 km the slope is significantly higher. Shoemaker attributed the change in slope to an increasing number of secondary craters with decreasing crater size. This interpretation was subsequently challenged by Neukum *et al.* (1975), who found similar crater size distributions by counting only circular, well-shaped craters in areas away from rays. They concluded that the slope change was a reflection of the primary distribution and not due to the contribution of

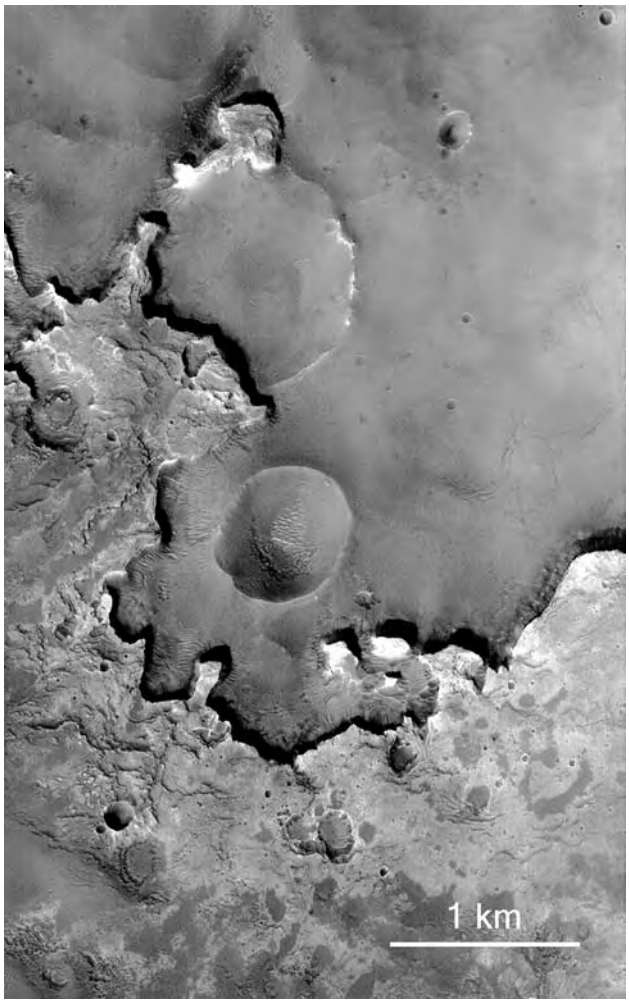

Figure 2.16. Ghost craters being exhumed at 37°N, 359°E. Several craters have been partly buried by the material that formed the plains in the upper right section of the image. The plain in turn was buried by the material in the lower part of the image, which was subsequently partly removed to exhume the ghost craters (MOC R1003225).

secondaries. Irrespective of whether the smaller craters are primary or secondary, as a surface ages the number of superposed craters increases until an equilibrium is reached between crater production and crater destruction, at which point the crater size-frequency curve rolls over to a lower slope. Smaller craters are more easily destroyed than larger craters, so that the rollover diameter starts out small but with increasing age of the surface it moves to larger sizes. The approach to equilibrium with increasing age and the move of the rollover diameter to larger sizes applies also to Mars, as shown by figures in Hartmann and Neukum (2001) in which crater frequency curves of increasing age intersect the equilibrium curve at larger and larger diameters. A cartoon of the Shoemaker *et al.* lunar model is shown in Figure 2.17. If cratering rates were high enough and cratering was the only process leading to destruction of other craters, then given enough time, the entire crater frequency curve would approach the equilibrium curve, in other words, the point c_2 in Figure 2.17 would approach the x-axis. Although this has happened on the 4.5 Gyr surface of Mars' moon, Phobos, as a result of destruction of old craters by new craters, it has not happened for 0.5–30 km diameter craters on the oldest parts of Mars because processes other than mutual destruction by impact craters have led to elimination of a significant fraction of craters of this size in these old terrains.

The size-frequency distribution of craters can be displayed in different ways (Figure 2.18). The most widely used format is the cumulative plot in which the log of the number of craters larger than diameter D is plotted against log D. This is the format that Neukum and co-workers use, and one of the formats recommended by the Crater Analysis Techniques Working Group (CATWG, 1979). The technique has the advantage of producing smooth, clean curves, but has the disadvantage that slope variations tend to be masked. The other plots that are used are incremental plots in which the number of craters in some size increment is plotted against some measure of the size increment or bin. The simplest incremental plot is one in which the number of craters N in a bin is plotted against $D_a - D_b$, where D_a and D_b are the diameter limits of the bin, but this is rarely used. More commonly the R-incremental plot is used in which the D^{-3} slope of the typical incremental plot is factored out. The plot has the advantage of displaying well deviations in slope, which are commonly masked in simple incremental plots, but the plots tend to be noisy. The third incremental plot is one used by Hartmann and co-workers. In this plot the number of craters in a size increment is plotted against fixed logarithmic increments in D. This has the advantage over simple incremental plots in that the slope of the distribution is lower by a factor of 1, and is the same as the cumulative plots. It is less noisy than the R plot, yet shows slope variations better than the cumulative plot. For details on how to transpose crater counts into these plots see CATWG (1979).

In most of the early literature, ages were presented as "crater ages" in which the number of craters larger than a specific size was given. The size-distribution curve of craters has a steep slope so that many more small craters form than large craters. The younger the surface, the smaller the size of the craters that must be counted to get meaningful numbers.

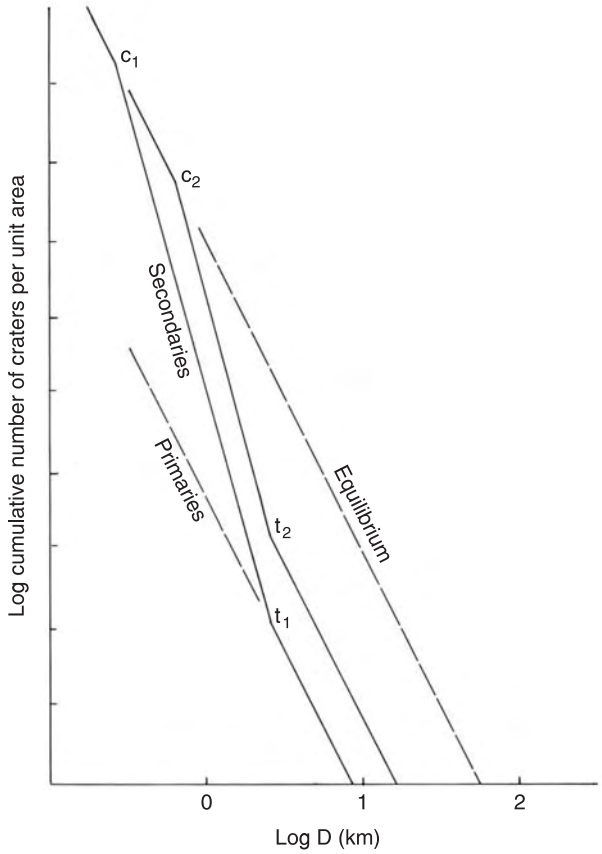

Figure 2.17. The Shoemaker (1966) model of the accumulation of craters on lunar maria. The production curve consists of two parts, craters that are mainly secondary in origin below 2–3 km in diameter and those that are mainly primary above. The equilibrium curve represents a limiting distribution, along which destruction of old craters and creation of new ones just balance one another. As the surface ages from t_1 to t_2, the crater diameter at which the production and equilibrium curves intersect moves from c_1 to c_2. The diagram is schematic. Values on the y-axis will depend on the age of the surface.

Thus, Scott and Tanaka (1986) and Greeley and Guest (1987) had to use different-sized craters to define ages on their geological maps. They used 16 km diameter craters to define Noachian ages and 2 km diameter craters for Amazonian ages. Acquisition of higher resolution photography is now enabling smaller craters to be identified and is thus opening the way to dating younger surfaces. While this is fortunate, use of smaller craters for dating can lead to complications because small craters are more vulnerable to destruction by erosion and burial, and are more likely to be secondaries, and thus may be less reliable indicators of age.

Recently, renewed attempts have been made to translate crater ages into absolute ages (Hartmann and Neukum, 2001; Ivanov, 2001; Neukum *et al.*, 2001), which has led to more crater ages being given as absolute ages. The ages are derived by comparing Mars with the Moon where the cratering rate has been determined from absolute ages on samples returned from different cratered units on the Moon (Figure 2.19). The first step in the estimation of martian ages from crater counts is to derive a lunar crater production function. It was recognized early that the size-frequency distribution of lunar craters roughly follows a power law of the form $N = kD^{-b}$. The values of the constants k and b depend on the age of the surface and on whether the N is cumulative or incremental and, if incremental, what type of increment. Detailed crater counts soon revealed, however, that b is not constant over all size ranges. Hartmann (1999) divided the lunar crater production function into three segments. For craters smaller than 1.41 km in diameter the value of b is 3.82, between 1.41 km and 64 km in diameter b is 1.80, and for craters larger than 64 km b is 2.2. Neukum (1983), using similar data (Figure 2.20), expressed the lunar curve as a polynomial. In compiling the lunar curve, care was taken to avoid secondary craters. Mare areas distant from large craters were chosen, and shallow irregularly shaped craters were not counted. Nevertheless, secondary craters may have influenced the curve, particularly at diameters less than 100 m.

The second step is to derive the size-frequency distribution of the projectiles that resulted in the lunar craters. Over decades of research, scaling laws have been developed that relate the diameter of a crater to the diameter of the transient cavity, and the diameter of the transient cavity to the projectile diameter, the densities of the target and projectile, the impact velocity, gravity, and so forth. The scaling law most commonly used is that of Schmidt and Housen (1987). Using these laws and the radiometric ages, and the size-frequency distribution of the craters, the impact rate of different-sized objects on the Moon can then be calculated.

The next step is to compare the impact rates for the same-size projectiles on Mars and the Moon, which is done by comparing the numbers of Mars-crossing and Earth-crossing asteroids, on the assumption that most of the craters on Moon and Mars were caused by asteroids. The best estimate is that the rate of impact per unit area of Mars is 2.04 times the rate for the Moon for the same-size projectiles (Ivanov, 2001). Knowing the impact rates and the size-frequency distribution of projectiles, the cratering

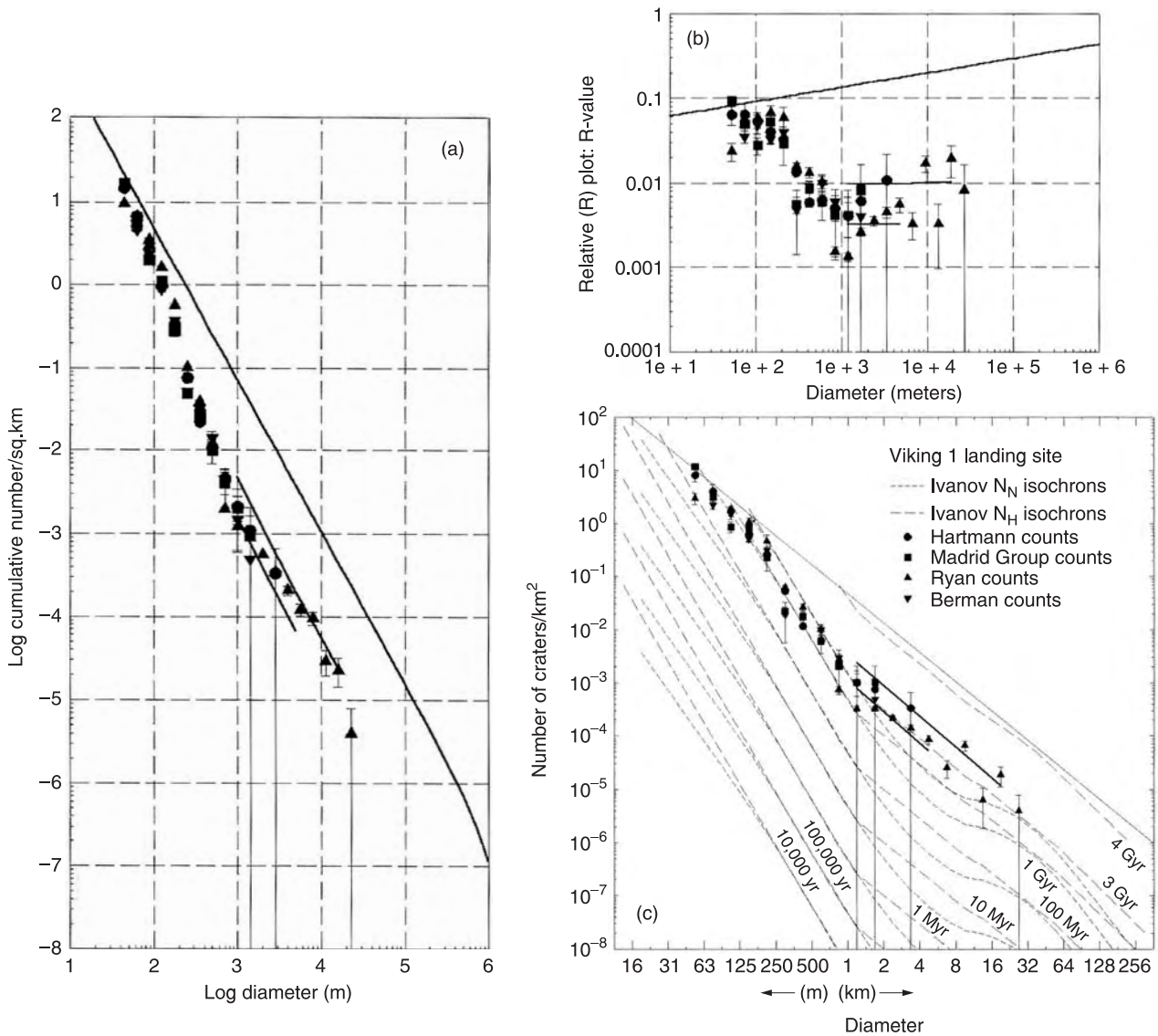

Figure 2.18. Different ways of plotting size-frequency distributions. (a) is a cumulative plot. The upper solid line is the saturation-equilibrium line. The two short solid lines show the size frequencies at the Noachian–Hesperian boundary and the Hesperian–Amazonian boundary. (b) is an R–incremental plot in which the steep −3 slope typical of incremental plots has been subtracted out. (c) is an incremental plot in which the D_u/D_l is a constant ratio, in this case 2, where the D_u and D_l are the upper and lower diameters of the counting interval. The dashed lines are crater production functions for the Hartmann and Neukum models. If a surface is exposed at the surface for the length of time indicated by the labels in the curves, and not subject to complications due to erosion and burial, then all points on the crater frequency curve should fall on the line. See text for fuller explanation (Hartmann and Neukum, 2001, reproduced with permission from Kluwer Academic Publishers).

rate as a function of diameter can be derived for Mars using the same scaling laws used for the Moon, on the assumption that the size-frequency distribution of the crater-forming projectiles was the same for the two bodies, and taking into account the different impact velocity and gravity on Mars.

Using the procedure just outlined, the Neukum (1983) polynomial production function for craters on the Moon has been translated into a polynomial crater production function for Mars (Ivanov, 2001). Ages are determined from the following expression, which relates the cumulative number of craters larger than 1 km in diameter $N(1)$ to time T in Gyr:

$$N(1) = 2.68\times10^{-14}\,[\exp(6.93T) - 1] + 4.13 \times 10^{-4}T$$

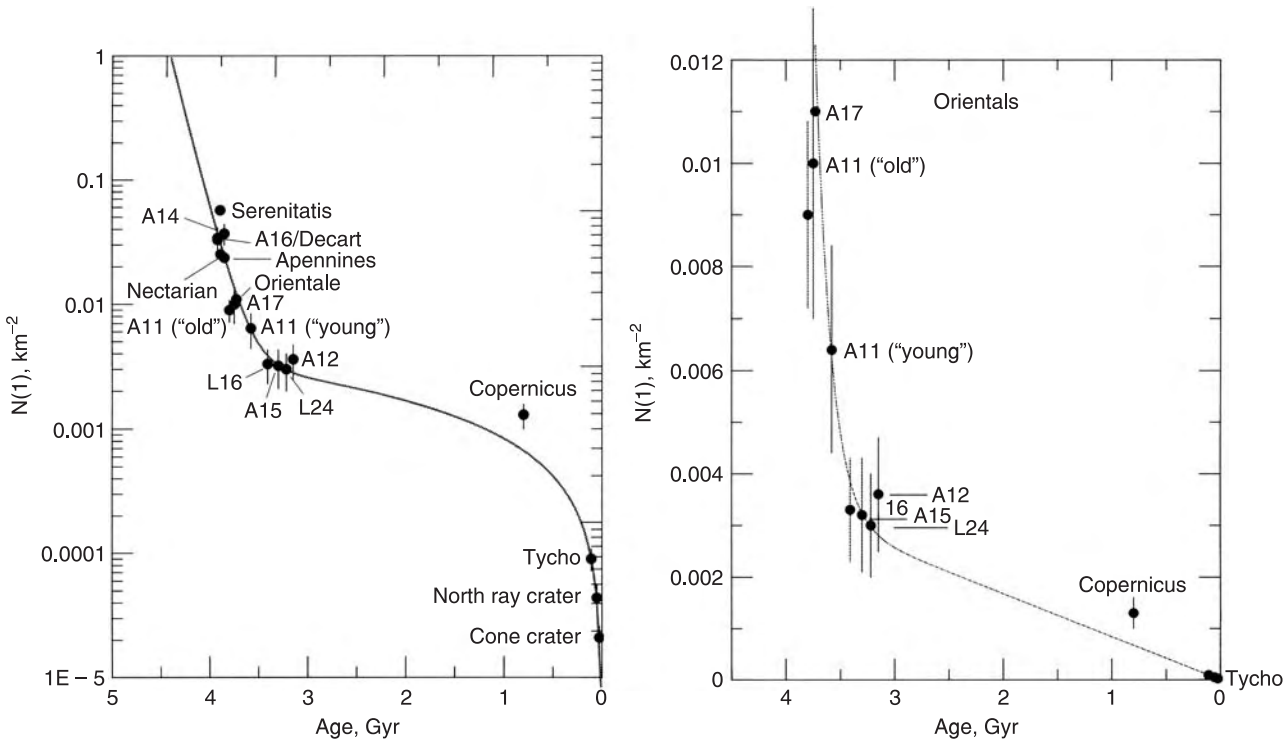

Figure 2.19. Comparison of a semi-log plot (left) and linear plot (right) of the cratering history of the Moon. The number of craters larger than 1 km in diameter is plotted against the age of the surface. Points on the curves are shown where radiometric dates have been obtained for a cratered surface (Neukum *et al*., 2001, reproduced with permission from Kluwer Academic Publishers).

The function is shown in Figure 2.21. The three-part Hartmann (1999) lunar crater production function can be similarly transposed into a three-part martian crater production function.

In practice, Neukum and Hartmann and their co-workers derive crater ages in a slightly different way. Neukum and his co-workers make a cumulative plot of the craters on the surface to be dated. They then find the best fit between the plot and the Neukum standard size-distribution curve by moving the standard curve vertically on the cumulative plot. The cumulative number of craters larger than 1 km, $N(1)$, is read off the plot and the age determined from the equation above. Problems may arise because of a poor fit between the standard curve and the curve from the surface to be dated. Poor fits can result from a variety of causes, such as partial burial of an older population of craters. In such a case, Neukum fits more than one curve to the distribution, one for the younger population and others for the older, partly preserved populations, and derives multiple ages. Hartmann and his co-workers plot their data incrementally on plots on which "isochrons" are plotted. These are simply plots of the Hartmann standard size-frequency curves for different ages. The surface is then dated according to which isochron best fits the crater count on the surface. The unknown counts may cross isochrons for the same reasons that not all counts fit the standard Neukum curve. The surface has had a history of resurfacing. Hartmann and Neukum (2001) estimate that these ages are valid to within a factor of two, but this may be optimistic for very young ages partly because of problems caused by secondary craters, as discussed below.

As discussed in Chapter 1, three major time periods on Mars have been defined according to the number of superimposed craters of different sizes. Crater ages, particularly absolute ages, should be viewed with some skepticism. The meaning of crater ages is often ambiguous and dependent on the scale of observation. The cratered uplands, for example, at a coarse scale are Noachian in age. The major elements of the topography, the large crater rims, large basins and central peaks, have survived from the period of heavy bombardment prior to 3.7 Gyr ago. However, many of the smaller-scale features, such as

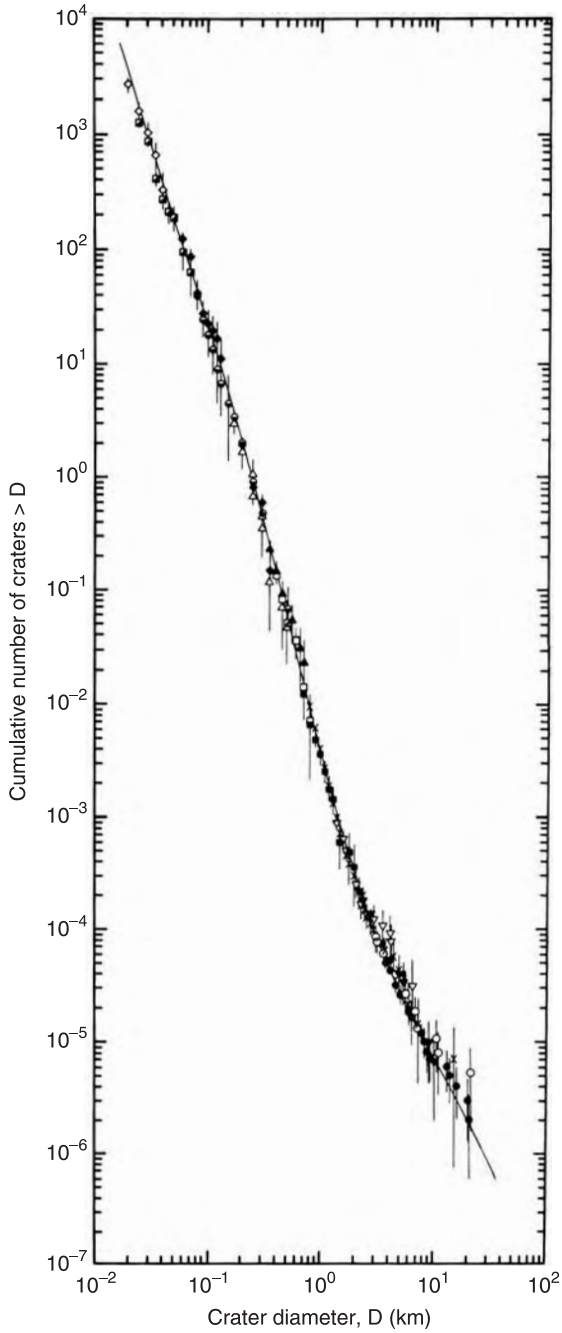

Figure 2.20. Normalized size-frequency distribution of craters on the Moon. To construct the curve, crater counts from several areas have been normalized to an arbitrary age. As a surface ages the curve will be displaced vertically on the graph but the shape will remain unchanged. According to the Neukum model, the curve for Mars has the same shape but is displaced laterally according to scaling laws and vertically according to the age of the surface (from Neukum and Ivanov, 1994, reproduced with permission from Kluwer Academic Publishers).

the flat floors of craters, may be younger. The uplands have had a complex history. Many parts have been resurfaced and exhumed since the end of the Noachian. The same areas that have a Noachian age when viewed at a global scale, may be mostly younger when viewed more closely. Craters larger than 50 km may give an old age, craters in the 10–50 km size range may give a somewhat younger age, and craters less than 10 km may give a still younger age, all on the same unit. While such complications should be evident from the crater distributions – they will deviate from the production function on the Neukum plots and from the isochrons on the Hartmann plots – designating a single age to a piece of terrain can lead to misunderstandings.

Secondary craters may create a more severe problem when small areas and small craters are used to date young surfaces. As demonstrated by McEwen *et al.* (2005), large numbers of secondary craters in the 10–200 m size range form from primary craters larger than 10 km in diameter. At large distances from the crater these are indistinguishable from primary craters. If the secondaries were uniformly distributed around the planet, they would not create a problem since they could be treated as part of the crater production function. We know from observations on the Moon, Mars, and other bodies, however, that secondary craters are distributed very unevenly, being mostly concentrated in rays. If the crater production function includes secondaries, as it likely does, then the number of small (< 100m) primaries is likely overestimated, as would be the primary cratering rate. As a consequence, counting small craters on sparsely cratered areas (away from rays) would result in derived ages that are too young.

Concern is not just for young ages. Neukum and Hartmann suggest that the crater ages could be off by a factor or two. Their best estimate of the age of the Hesperian/Amazonian boundary is 3 Gyr. If the proposed age is too old by a factor of two, then the boundary could be as young as 1.5 Gyr. It cannot be older than 3.7 Gyr since the Hesperian surfaces are not heavily cratered. Thus, the age of the boundary is probably in the 1.5–3.7 Gyr range, and the evolution of Mars would be very different at the upper and lower limits of this range. Clearly, we need to get radiometric dates on samples of units that have well-documented numbers of superimposed craters.

Summary

Craters are the most common landform on planetary surfaces. On Mars they form mostly by high-velocity impacts between the planet and asteroids.

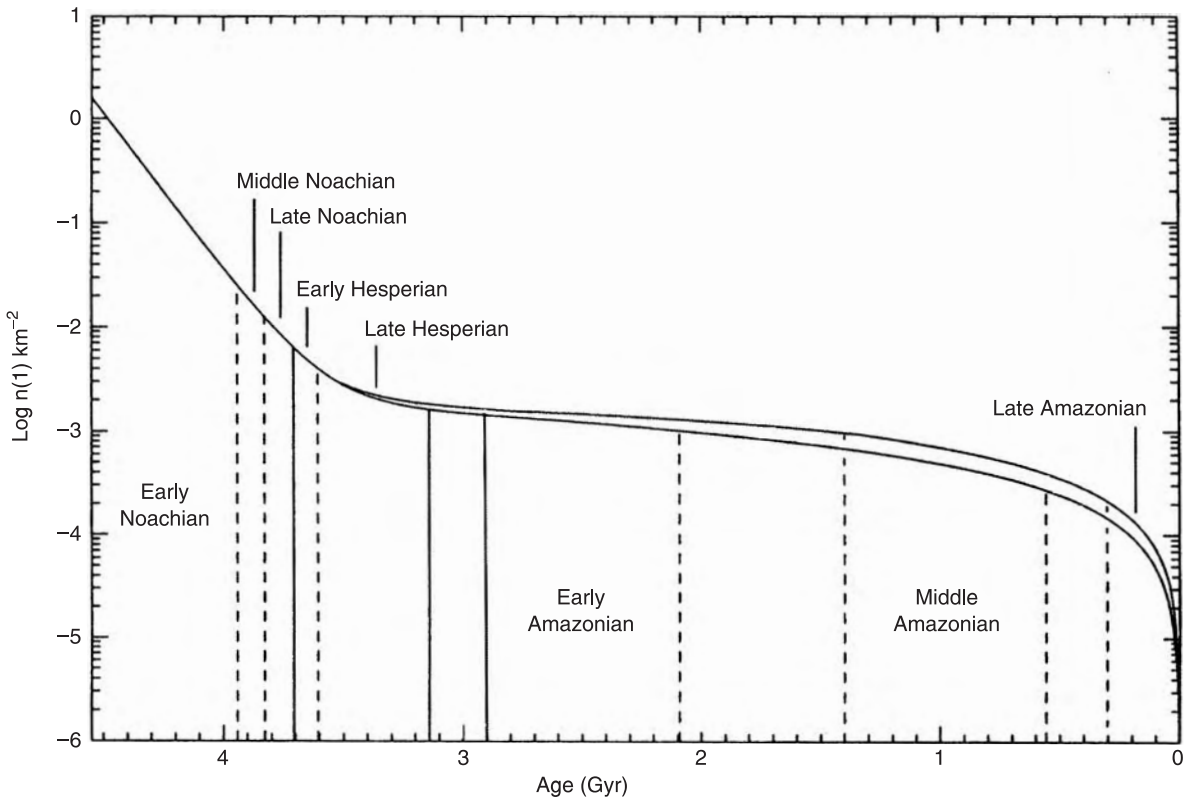

Figure 2.21. Martian chronology. The number of craters larger than 1 km in diameter is plotted against age for the Hartmann model and the Neukum models. Vertical lines show the ages of the different stratigraphic units defined by Tanaka (1986) on the basis of the number of superimposed craters. The Neukum model gives somewhat older ages than the Hartmann model (from Hartmann and Neukum, 2001, reproduced with permission from Kluwer Academic Publishers).

Craters change appearance with increasing size. Those smaller than 3 km have a simple bowl shape; in the roughly 3–130 km size range most craters are complex, having a central peak and terraced walls; in the 130–1000 km size range they have an inner ring instead of, or in addition to, a central peak; and the very largest basins have no inner ring. The most distinctive characteristic of martian craters is their ejecta pattern. In fresh craters two basic patterns are observed: (1) the crater may be surrounded by a radially striated annulus of ejecta roughly one crater radius wide, surrounded by a ridge or outward-facing escarpment; (2) an array of radially elongate lobes of ejecta may be present, each lobe being surrounded by a low ridge. One or another or both components may be present. The peculiar martian patterns have been attributed to fluidization of ejecta as a result of volatiles in the surface or to entrainment of the ejecta in the thin martian atmosphere. The size-frequency distribution curve of craters has a complex shape in detail but is steeper for craters smaller than 2 km in diameter than for larger ones. For small craters the slope on a cumulative log N versus log D plot is steeper than -3, implying that for every 10-fold decrease in crater diameter the number of craters increases by over 1000. Current cratering rates are very low, but they were much higher prior to around 3.5 Gyr ago. The rapid drop-off in cratering rates early in the planet's history has resulted in the striking contrast between the heavily cratered terrains that formed before the drop-off and the more sparsely cratered plains that formed after. Because an exposed surface slowly accumulates craters, they provide a means of assessing age. Craters have been used to estimate absolute ages by comparing crater frequencies on martian surfaces with crater frequencies on lunar surfaces that have been radiometrically dated. In the absence of dated samples from units with known crater densities, absolute ages derived from crater counts should be viewed with caution.

3 Volcanism

In the late 1960s the Mariner 6 and 7 spacecraft sent back images of Mars that seemed to indicate that it was a dead, cratered planet, much like the Moon. The volcanoes gave us the first indications that this was a false impression. When Mariner 9 approached Mars late in 1971, the planet was engulfed in a global dust storm. The surface in the equatorial regions could barely be seen. There were, however, four dark spots, and in the center of each spot was a complex crater. The craters resembled terrestrial summit calderas, volcanic depressions that form by collapse as a result of withdrawal of magma from below. Most calderas look very different from impact craters because they form by collapse rather than by excavation, and because they are commonly the result of multiple events rather than a single event. The craters were clearly calderas and the dark spots were clearly volcanoes poking up above the surrounding dust storm.

We now know that Mars has had a long and complex history of volcanism, and that the planet is probably still active today. The largest volcanoes and the most extensive lava plains are in and around the region of Tharsis. Volcanism probably started very early in the planet's history. By the end of the Noachian, around 3.8 billion years ago, the Tharsis bulge, a volcanic pile 10 km high and 5000 km across, had been largely built. But volcanic activity continued for the rest of the planet's history to create some of the largest volcanoes in the Solar System. Other prominent volcanic centers are in Elysium and around Hellas.

While martian and terrestrial volcanoes have many attributes in common, the tectonic context within which volcanism takes place is very different on the two planets. The Earth's crust is divided into plates that move with respect to each other. Most volcanism occurs at mid-oceanic ridges, where new crust is being formed, and at subduction zones where old crust is being consumed. The contribution of intraplate volcanism to the Earth's total is rather modest. In contrast, although linear magnetic anomalies suggest that there may have been some form of plate tectonics very early in the planet's history (Connerny *et al*., 1999), we have no evidence that there has been plate tectonics on Mars in the last ~4 Gyr. Thus, if we are to look to the Earth to try and understand the root causes of martian volcanism, we should perhaps focus on intraplate examples rather than on plate margins, for which there are no martian equivalents.

Most of the large volcanoes on Mars resemble terrestrial shield volcanoes, which form mainly by eruption of relatively fluid, basaltic lava. Shields typically have gentle ($< 10°$) slopes, a convex upward profile, and a summit caldera. The main difference between the large Tharsis volcanoes and terrestrial shields is size. The most familiar examples of shield volcanoes on Earth are those in Hawaii. The resemblance between the Hawaiian and large Tharsis shields is striking. Not only do the volcanoes have similar profiles, but the subsidiary features, such as calderas, lava channels, flow fronts, and collapse pits, are also similar, although somewhat puzzlingly the martian features are mostly far larger than their terrestrial equivalents. Other martian volcanoes termed "paterae" are of broad areal extent but have much less vertical relief than the shields. They have no known terrestrial counterparts. The most common type of volcano on Earth, the stratocone, which typically forms when large amounts of ash as well as lava are produced, is much less obvious on Mars.

Volcanism has not only reshaped the landscape, it has affected the evolution and chemistry of the atmosphere and altered the rocks and soils at the surface. The atmosphere is largely a product of the outgassing of the interior. Formation of the massive volcanic pile that is Tharsis must have been accompanied by large-scale release of volatiles, such as water, from the interior. Alteration of post-Noachian rocks at Gusev, although limited, is testament to the continued outgassing of such volatile elements as S, Cl, and Br.

Basaltic volcanism

Volcanism is the result of transport of material from within a planet to its surface. On Earth (and the Moon) most volcanism is basaltic. On Mars it almost

certainly is also. The mantles of the terrestrial planets are all thought to have a similar composition, one that resembles that of chondritic meteorites from which the planets are believed to have largely formed. Partial melting of material of chondritic composition yields basaltic magma. Narrowly defined, basalts are fine-grained igneous rocks containing roughly equal proportions of plagioclase feldspar and calcium-rich pyroxene, and less than 20 percent of other minerals such as olivine, calcium-poor pyroxenes, and iron–titanium oxides. But the term "basalt" is commonly used to denote a range of rocks derived from basaltic magma. Compositional variations may occur because of compositional differences in the mantle and differences in the degree of partial melting. Such differences are small for the major elements that form the rock-forming minerals; they are much more marked for the minor and trace elements. As the magma rises to the surface it may change in composition as a result of partial crystallization and separation of the crystals from the rest of the melt. The magma may also ingest materials from the crust through which it moves. As a consequence, the magma delivered to the surface, although basaltic, may exhibit significant variations. Only a fraction of the rising magma actually reaches the surface. On Earth, more than 80 percent stalls within the crust to form plutonic rocks (Wilson, 1995).

The dominantly basaltic nature of martian volcanism is supported by a variety of observations in addition to geochemical models. The TES data show that, on a global scale, the planet's rock surface has a fairly uniform composition. From these data, two global units were initially identified: Type 1, which is restricted mostly to low latitudes, and Type 2, which is mostly at high latitudes (Bandfield *et al.*, 2000). Initially, Type 1 was interpreted as basalt and Type 2 as andesite, a more silicic rock than basalt. Subsequently, the Type 2 material was reinterpreted as weathered basalt (Wyatt and McSween, 2002), an interpretation that seems confirmed by OMEGA data (Bibring *et al.*, 2005). The rocks at the Pathfinder site were also initially interpreted as andesites (McSween *et al.*, 1999), but this interpretation also now seems suspect. More likely the spectral and elemental observations were made of weathering rinds and the rocks are actually basalts. Basalts are the dominant rock at the Gusev site (Squyres *et al.*, 2004b). The martian meteorites are also all of the basaltic family. They are mostly basaltic cumulates, that is, they formed by the concentration of crystals that settled out of a basaltic melt (McSween, 1999).

Effect of Martian conditions

Basaltic volcanism is expected to express itself somewhat differently on Mars than on Earth because of the lower gravity, the lower atmospheric pressure, and the different structure of the crust (Wilson and Head, 1994). Magma generated within the mantle will rise buoyantly because it is less dense than the surrounding rock. It will rise through the deeper, viscous parts of the planet as diapirs and through the brittle, upper few tens of kilometers as dikes. Because the gravitational acceleration on Mars is one-third that on the Earth, the buoyant forces are correspondingly less. The viscous and strength properties of the rocks are, however, similar. As a result, diapirs need to be larger on Mars to overcome the viscous resistance in the deeper regions and dikes need to be larger to overcome the strength of the rocks in the upper regions of the crust. According to Wilson and Head, for similar magma composition and stress conditions in the crust, eruption rates should be a factor of 3 to 5 higher on Mars because of the larger dimensions of the dikes.

Rocks at the surface are porous and have a low density, but self-compaction by gravity causes their density to increase with depth. As the magma rises, the contrast in density between it and the country rock declines until ultimately the magma is no longer buoyant, and it stalls. Where it stalls it may build a dense network of dikes and spread laterally to form a magma chamber. Because of the lower martian gravity, the rate of increase in density with depth due to compaction is lower on Mars than on the Earth so that the depth of a magma chamber should be deeper for similar conditions. Wilson and Head, for example, estimated that conditions that lead to a 3 km deep magma chamber on Earth would result in a magma chamber on Mars 8–11 km deep. The actual picture is, of course, much more complicated than that just portrayed. In particular, degassing of magma as it approaches the surface has a major effect on magma density, and encountering ground ice and groundwater can lead to a range of explosive interactions.

Lava flows can be produced by direct overflow from a vent or by coalescence of hot magma clots from a fire fountain. We have just seen that effusion rates are expected to be higher on Mars than on Earth, but in addition, and somewhat counterintuitively, the lower gravity causes flows to travel farther on Mars than on Earth because, in order to move, the flows have to be thicker for given magma properties, and the cooling rates per surface area are similar. As a consequence, Wilson and Head estimate that lava flows on Mars should be typically 6 times the length of their terrestrial counterparts.

As magma approaches the surface, gases are exsolved, gas bubbles begin to nucleate, and the magma may be disrupted into a mixture of pyroclasts (clots of magma) and gas. The combination of the lower martian gravity and the lower atmospheric pressure causes both nucleation and disruption to occur at greater depths on Mars than on the Earth. Wilson and Head estimate that, for a basalt containing 1 percent water, nucleation will occur at a depth of 800 m on Earth and 2100 m on Mars, and fragmentation will occur at 110 m on Earth and 320 m on Mars. Figure 3.1 shows how interaction between the exsolved gases and the rising magma leads to different types of eruption. We will not discuss in detail all the different types of eruptions, but just mention a few aspects of the Hawaiian and Plinian types. Hawaiian eruptions have fairly high effusion rates and moderately gas-rich magmas. A typical Hawaiian eruption starts with eruption from a fissure to form a curtain of fire. Clots of lava that fall back and congeal close to the vent may form a spatter rampart. Activity normally converges rapidly on a single vent

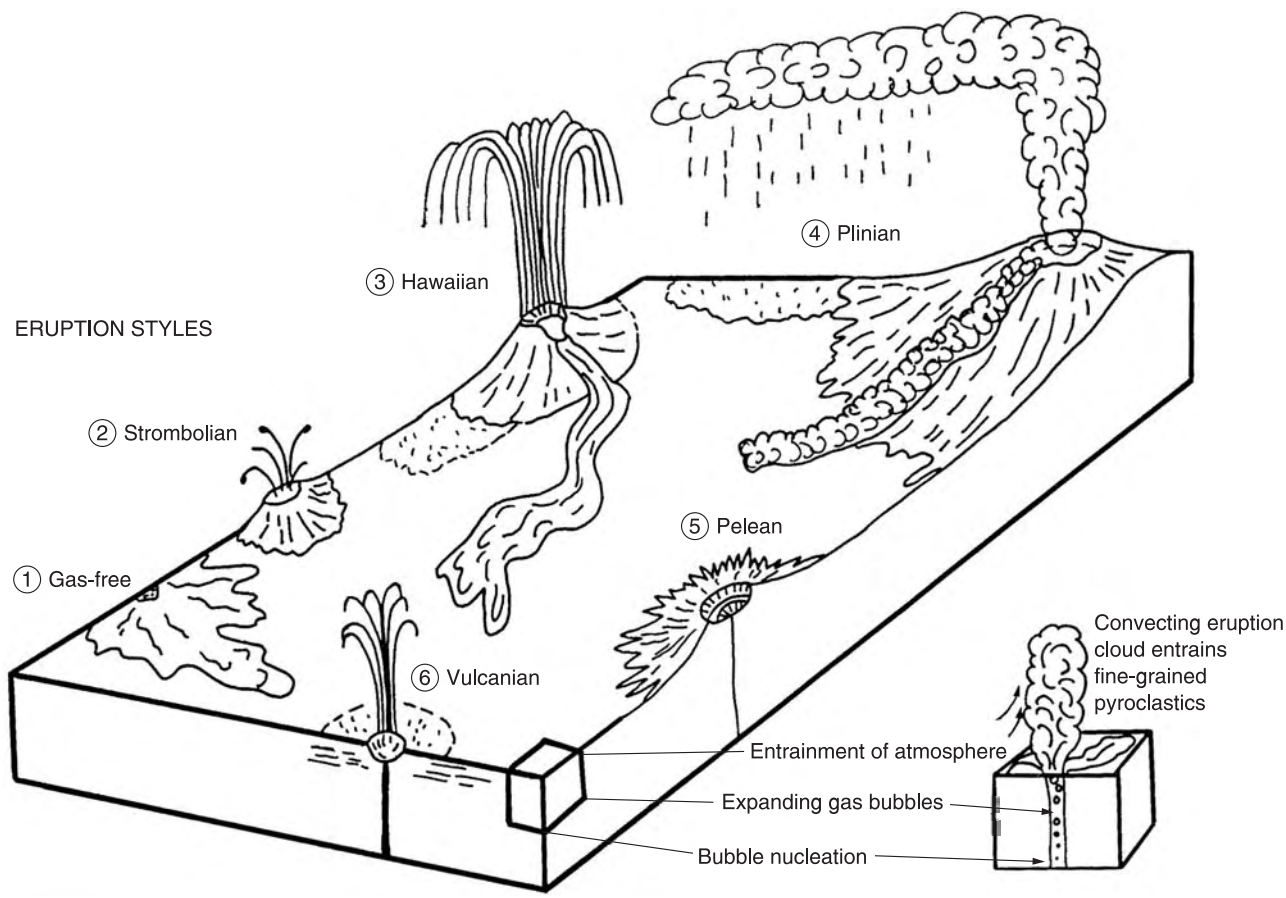

Figure 3.1. Different eruption styles. (1) Essentially gas-free magma erupts to produce a low fountain that feeds the flow. (2) Strombolian eruption: gas rise exceeds magma rise; bubbles grow and coalesce, causing intermittent disruption of the lava lake within the vent and near-vent accumulation of spatter. (3) Hawaiian eruption: steady explosive eruption creates a pyroclastic fire fountain; most clasts fall back to feed flows, some cool and create scoria, building a cone, others are convected upward and create ash deposits. (4) Plinian eruption: magma disrupts into small fragments that are carried by the gas stream. The atmosphere is incorporated and heated and rises to produce a convecting plume that can spread laterally and deposit tephra. If insufficient atmosphere is incorporated, the column will collapse to form pyroclastic flows that stream downslope. (5) Pelean eruption: low magma rise speed causes cooling and formation of a viscous dome with a solid carapace; catastrophic disruption of the carapace causes a small convecting plume and pyroclastic flows. (6) Vulcanian eruption: solidification of magma and resultant gas build-up in the near-surface conduit causes an explosive disruption of the solidified cap and country rock (from Wilson and Head, 1994, copyright 1994, American Geophysical Union, reproduced by permission of the American Geophysical Union).

to form a fire fountain. Most of the magma is erupted in large clots that fall back close to the vent to form a lava pool, which gives rise to lava flows. Smaller clots that cool more quickly and are more easily entrained in the atmosphere form cones of scoria or cinders. Because the lower gravity permits wider ballistic dispersal, the cinder cones on Mars are expected to be lower and wider than on the Earth. In a Hawaiian eruption the conditions are such that most of the clots produced are too large to be incorporated into a convective cloud and produce a Plinian eruption.

In Plinian eruptions, a mixture of volcanic gases, heated atmospheric gases, and pyroclasts form a convecting plume over the volcano. The magma must be disrupted into clots so small that they are carried along in the gas stream emerging from the vent. Because of the thinner atmosphere on Mars, the particles must be finer-grained to be entrained, 100 times more fine-grained than on Earth, but the lower atmospheric pressure on Mars also causes magma to be disrupted into finer-sized grains than on Earth. This, together with the expected higher martian effusion rates and deeper depth of fragmentation, should favor Plinian eruptions over Hawaiian-style eruptions. As a consequence, many eruptions that would be Hawaiian on Earth may be Plinian on Mars. Differences in atmospheric pressure and temperature structure would cause martian Plinian eruption clouds to rise about 5 times higher than terrestrial clouds for the same eruption rate. The Plinian cloud can remain buoyant only if sufficient atmospheric gas is incorporated into the cloud. If the mass eruption rate is too large or the volatile content of the magma too small, the cloud will collapse and form ground-hugging flows of ash and gas. Wilson and Head suggest that collapse of the convecting column to form pyroclastic flows should be more likely on Mars than on the Earth, and that such flows could travel at least a few hundred kilometers. One conclusion from the above discussion is that explosive activity and formation of Plinian columns and ash flows, which on Earth tend to be associated more with silicic volcanism, may on Mars be common phenomena of basaltic volcanism.

Tharsis

The Tharsis Montes narrowly refers to the line of three large volcanoes, Arsia Mons, Ascreus Mons, and Pavonis Mons, centered on the equator at 247°E, but the name Tharsis is commonly used in a more general sense to refer to a broad region of anomalously high elevations centered just south of the equator at roughly 265°E (Figures 3.2 and 3.3). The broad high, referred to as the Tharsis rise or the Tharsis bulge, is roughly 5000 km across and 10 km high, the exact figures depending on how one defines the edge of the bulge. The rise straddles the plains–upland boundary. The load that it represents has deformed the lithosphere (Phillips *et al.*, 2001) and caused faulting over half of the planet, as discussed in Chapter 4. Although almost the whole bulge is covered by post-Noachian lava plains, the individual volcanoes are distributed unevenly. To the southeast of the summit of the bulge, in northern Syria Planum, there are a large number of low volcanic mounds roughly 20 km across, but otherwise volcanoes are absent (Figure 3.4). In contrast, on the northwestern flank, tens of individual, significantly sized edifices have been recognized (Hodges and Moore, 1994), including some of the largest volcanoes in the Solar System. The tallest volcano of all, Olympus Mons, stands just off the northwest flank of the bulge.

The three aforementioned volcanoes together with Ceraunius Tholus and Uranius Patera form a SW–NE trending line that cuts across Tharsis. Not only are the volcanoes aligned in this direction, but the northeast and southwest flanks of the three largest volcanoes have vents from which large volumes of lava have been erupted to form shoulders adjacent to the shields. The SW–NE line is clearly a major structural feature of the planet, whose origin remains obscure.

Tharsis Montes

Arsia Mons (Figure 3.5), the southernmost of the three shields that form the Tharsis Montes, is 400 km across, has a summit elevation of 17.7 km, and a volume of $9 \times 10^5\,km^3$ (Plescia, 2004). For comparison, the largest volcano on Earth, Mauna Loa in Hawaii, is roughly 120 km across, stands 9 km above the ocean floor, and with a volume of $3 \times 10^4\,km^3$ is a factor of 30 smaller. The Arsia summit caldera is 130 km across, 1.3 km deep, and bounded by concentric faults. Crater dating suggests that the caldera floor is 150 Myr old (Neukum *et al.*, 2004). From the caldera rim the flanks slope away at roughly 5°. On the northeast and southwest flanks, numerous pits have coalesced to form rifts from which large volumes of lava have erupted. Lava flows from the rifts fan out over the adjacent plains to form broad aprons. The apron flows cut across the flows that extend down the flanks of the shield, indicating that most of the apron flows are younger than those on the shield.

Emerging from under the Arsia-derived flows 1200 km to the southwest of the volcano and extending

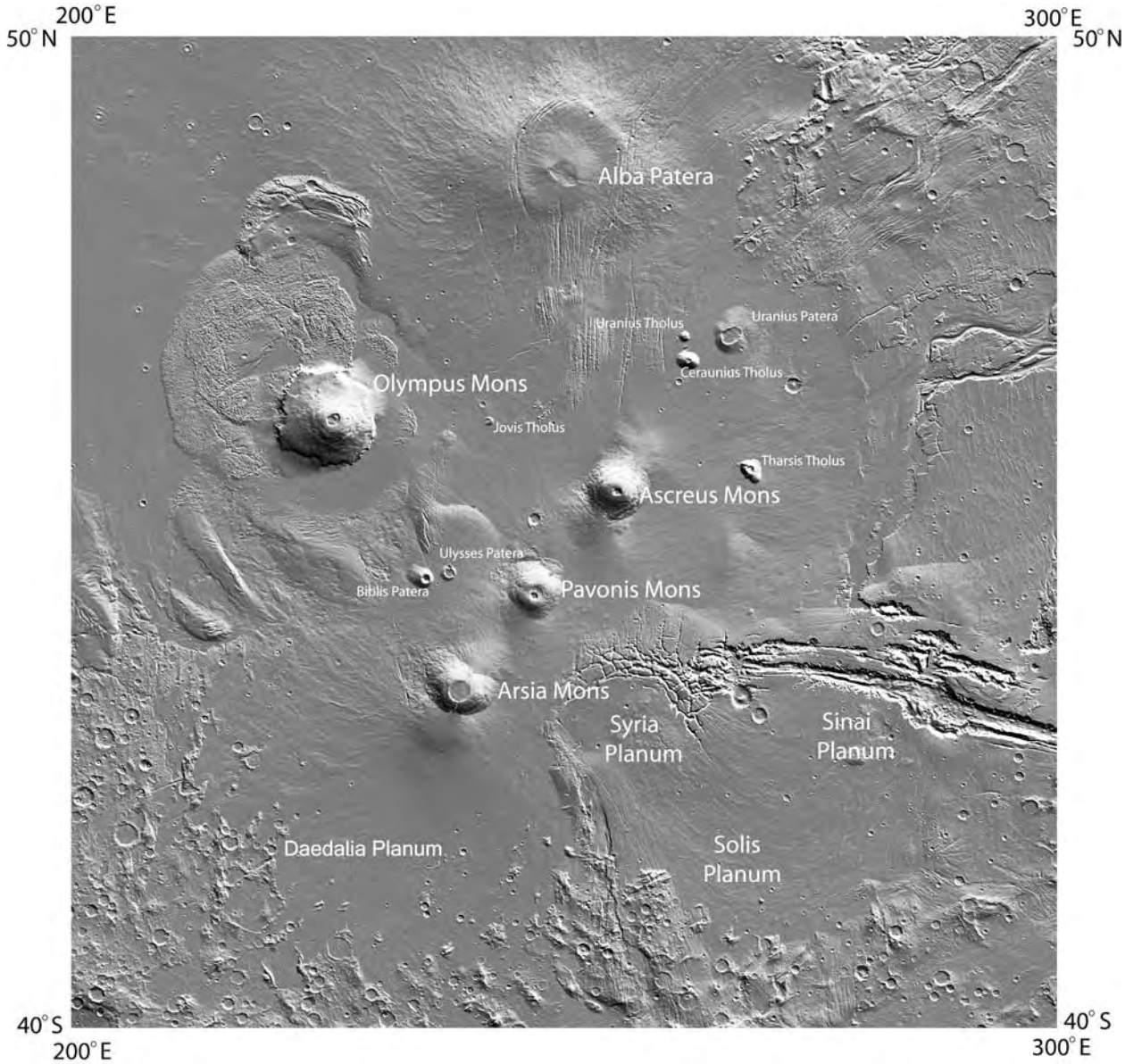

Figure 3.2. Index map of the Tharsis province.

for thousands of kilometers to the west-southwest are numerous graben roughly radial to Arsia Mons. The graben have been interpreted as surface manifestations of large dikes radial to the central magma reservoir of Arsia Mons (Wilson and Head, 2002). They are similar to Archean radial dike swarms seen on Earth and appear to represent periods in the early history of the volcano during which a near-continuous supply of magma propagated magma-filled cracks from the reservoir below the volcano to distances of several thousand kilometers away. Such dikes are important not only for understanding the nature of the magma supply, but also because their presence may have had a major effect on the global groundwater regime, causing regional impediments to flow or channeling the flow. The fracturing may also have fractured the cryosphere, thereby releasing groundwater to the surface, as discussed in Chapter 6.

The western flank of the volcano appears to have been significantly modified. It has a coarse radial texture partly caused by irregular pits, in contrast to the fine radial texture of the opposing east flank. Also present is a thin striated unit that appears to drape

Figure 3.3. Oblique view of the Tharsis province looking southeast. The cliff facing us at the base of Olympus Mons is 8 km high. The extremely low slopes on Alba Patera on the left contrast sharply with the other volcanoes. In the background is Noctis Labyrinthus (MOLA, 8× vertical exaggeration).

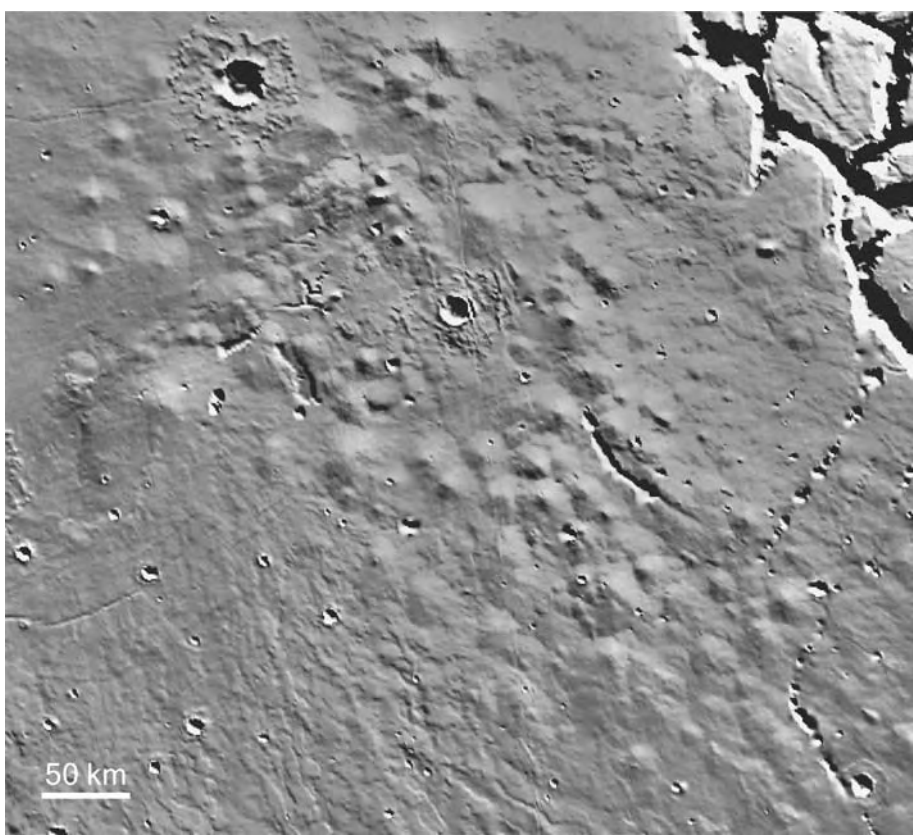

Figure 3.4. Small shield volcanoes 10–20 km across in Syria Planum, close to the summit of the Tharsis bulge. Noctis Labyrinthus is in the upper right (MOLA).

over the terrain adjacent to the shield. The unique features of the northwest part of the shield have been attributed to the former presence of glaciers (Head and Marchant, 2003; Chapter 8). Although the volcano is clearly formed of lava flows, individual flows on the flanks are difficult to identify in the available imaging. They are much more readily identifiable on the younger northeast and southwest aprons. Some of the flows from the southwest rift extend for several hundred kilometers across the adjacent plains.

Pavonis Mons (Figure 3.6), the middle volcano of the three large Tharsis Montes, is somewhat smaller

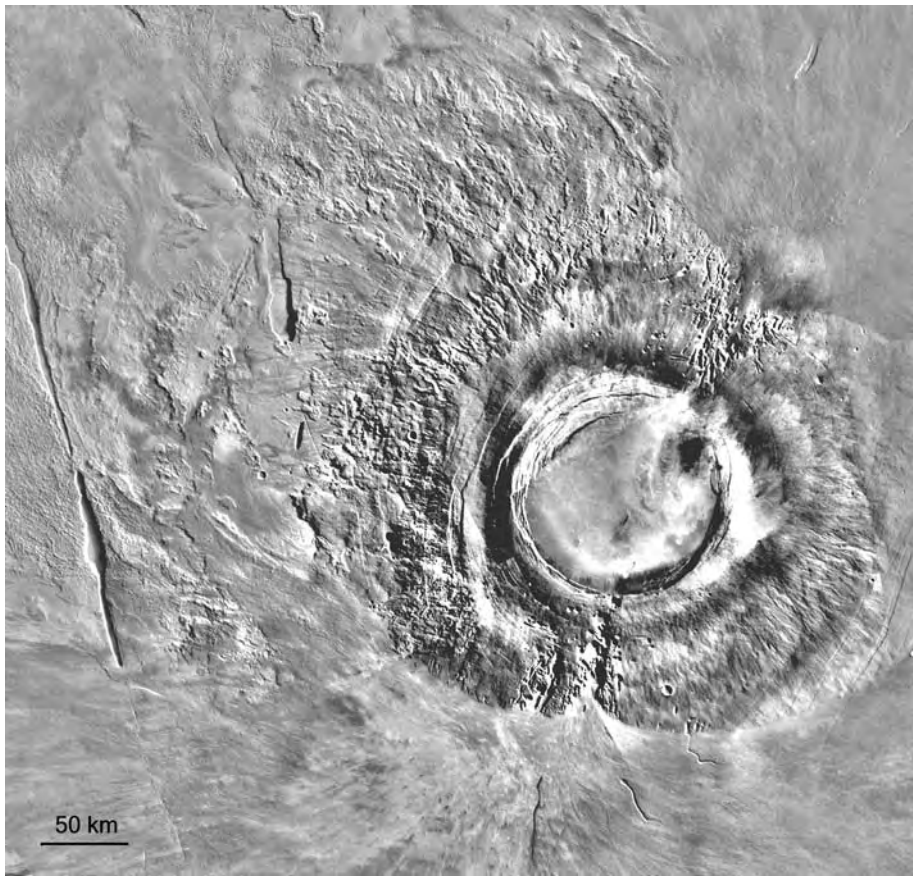

Figure 3.5. Arsia Mons. Deep rifts, formed of coalesced pits, on the northeast and southwest flanks have been the sources of flows that bury the lower parts of the shield. A chain of low mounds within the 130 km diameter summit caldera connects the two rifts. The ragged, eroded appearance of the northwest flank contrasts with the smoother, primary volcanic surface of the southeast flank (MDIM2).

than the other two, being 14 km high and having a volume of 4×10^5 km^3. Like Arsia Mons, it has gently sloping flanks. The summit caldera, almost 5 km deep, is inset into a larger older depression, now almost filled. Rifts on the northeast and southwest flanks have been the sources of flows that cover the adjacent plains. The southwest apron has two parts, an older part to the west and a younger part to the east. Flows from the eastern part of the apron, and possibly from some adjacent low shields, appear to wrap all the way around the eastern flank of the shield to bury most of the northeastern apron. As with Arsia Mons, the northwest flank has a ragged appearance and a striated unit is draped over the adjacent plains (Shean *et al.*, 2005). Circumferential fractures around the northern edge of the shield have been attributed to flexure of the lithosphere under the load of the volcano (Comer *et al.*, 1985).

Ascreus Mons, the most northerly of the three large Tharsis shields, is the tallest, being 18.2 km high and having a volume of 1.1×10^6 km^3. As with the other two shields, vents low on the northeast and southwest flanks have been the source of flows that bury nearby parts of the shield and spread over the adjacent plains. Ascreus has a complex summit caldera, with mutually intersecting floors at different levels. Neukum *et al.* (2004) give crater ages for the different parts of the caldera that range from 100 Myr for the main central caldera to 3.8 Gyr for a smaller, partly preserved depression to its southeast. If the dates are valid, it would imply that the volcano has been active for most of the planet's history. The flank vents, or fissures, on Ascreus are different from those on Arsis and Pavonis. Whereas the fissures on the latter two appear to have formed by coalescing collapse pits, those on Ascreus have formed by the merger of many narrow, sinuous, rille-like depressions, which occur not only on the shield but also out on the aprons. Narrow crevasse-like depressions and lines of pits roughly circumferential to the shield are also

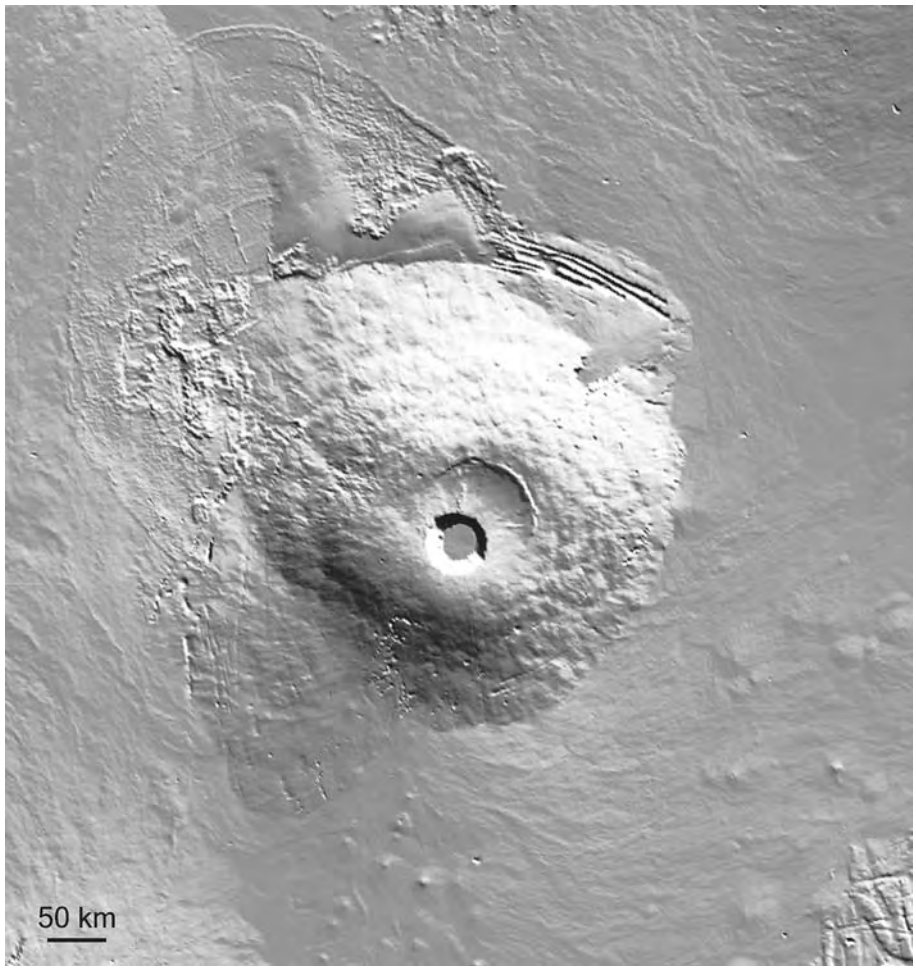

Figure 3.6. Pavonis Mons. Its summit caldera is almost 5 km deep with a rim that stands 8.4 km above the surrounding plains. Circumferential fractures have been attributed to crustal flexure caused by the load of the volcano. As with the other Tharsis shields, lava from fissures in the northeast and southwest flanks has buried the lower parts of the shield (MOLA).

common elsewhere on the shield's flanks. The flanks of Ascreus Mons, like those of Olympus Mons, step down from the summit in a succession of rounded terraces that have been attributed to thrust faults caused by compression of the edifice as the lithosphere flexes under the volcanic load (Thomas *et al*., 1990).

The Hawaiian shield volcanoes share many attributes in common with the Tharsis shields and provide clues as to how the martian shields might have formed. The Hawaiian Islands are at the end of a long chain of now inactive volcanoes, the Hawaiian–Emperor chain, which stretches 6000 km across the Pacific Ocean (see, for example, Clague and Dalrymple 1987). Extinct volcanoes 5000 km up the chain from Hawaii have Potassium–Argon ages of 60 Myr during which roughly 10^6 km^3 of lava have erupted to form the chain. Thus the entire output of the Hawaiian plume would build one of the Tharsis shields in 60 Myr. The conventional view is that a mantle plume underneath Hawaii is feeding lava to its volcanoes. Hawaii is on the Pacific plate. As motion of the plate carries the volcanoes away from the plume they become extinct, and new volcanoes start to form over the plume, thereby adding more islands to the chain.

The Hawaiian volcanoes are fed by magma rising through dikes from sources in the mantle tens of kilometers from the volcano (Ryan *et al*., 1987). The magma rises mainly by buoyancy, being less dense than the surrounding country rock. As the magma approaches the surface, the density contrast between it and the surrounding rock diminishes as a result of compositional changes and increasing porosity of the country rock near the surface. Ultimately a zone

of neutral buoyancy is reached where the density of the magma and country rock is the same. The magma stalls and spreads laterally to form a magma chamber, which is probably a dense nexus of intersecting dikes. The magma chamber is identifiable as an aseismic zone within the edifice below the summit. At Kilauea the chamber is roughly 2 km across and is 3–7 km below the summit. It is roughly the same diameter as the summit caldera. Magma is episodically erupted from the magma chamber either at the summit or onto the volcano flanks, partly driven by the pressure of gases that exsolve from the magma as it rises to shallower depths. Eruptions are generally preceded by inflation of the magma chamber. After an eruption, the summit deflates. More rarely collapse may occur at the summit, thereby modifying the summit caldera. As the volcano grows higher as a result of summit eruptions, the zone of neutral buoyancy and the magma chamber rise with it.

A similar sequence of events probably takes place with the large Tharsis volcanoes, except that there is no plate motion to carry the volcanoes away from the magma source, the magma chambers are much larger, the individual eruptions are more voluminous, and the intervals between eruptions are much longer. In addition, the Tharsis volcanoes are probably longer-lived than the Hawaiian source, although we do not know how long the plume under Hawaii has been supplying magma. All we know is that it has been active for at least 60 Myr (Clague and Dalrymple, 1987). Wilson and Head (2001) argued that the Tharsis volcanoes were built by voluminous eruptions spaced widely in time. They argue that if the volcanoes are at least 1 Gyr in age, as seems likely, then the average supply rate of magma for Arsia Mons (volume = $\sim 10^6\,km^3$) is no more than $0.001\,km^3\,yr^{-1}$. (For comparison, the average rate of supply for the Hawaiian–Emperor chain for the last 60 Myr is $0.017\,km^3\,yr^{-1}$.) The magma chambers in the large shields are likely much larger than those within the Hawaiian shields, as indicated by the size of the calderas, and the likely 2–3 times greater vertical extent because of the lower gravity. Given the large magma chamber, if magma were supplied at the meager average rate, it could not keep the magma chamber molten. It is more likely, Wilson and Head argue, that magma supply from the mantle was episodic, and that growth of the volcano was characterized by very active periods, with large lava effusion rates, as indicated by the size of many of the lava flows, separated by long periods of quiescence during which the magma chamber solidified. The exact location of the magma chamber may shift between active periods, hence the complex calderas with different centers of collapse such as we see in Ascreus Mons and Olympus Mons. Thus, it is not inconceivable that, despite their seemingly young surfaces, the large Tharsis volcanoes started being built in the Noachian and have been active ever since, albeit at very infrequent intervals.

Olympus Mons

Olympus Mons resembles the other three large Tharsis shields except that it is larger, and surrounded by a cliff and an aureole, consisting of large lobes of lineated deposits (Figure 3.7). The edifice is 840 × 640 km wide, as measured from the base of the bounding cliff, and rises to an altitude of 21 km, almost 22 km above the surrounding plain (Plescia, 2004). It is somewhat asymmetric, the northwest flanks having shallower slopes than the southeast flank. The average slope is close to 5°. On the flanks are prominent rounded terraces. With a volume of $2.4 \times 10^6\,km^3$, it is 2–3 times larger than the other Tharsis shields and the entire Hawaii–Emperor chain. However, as discussed below, the shield was likely formerly more extensive. In addition, much of its volume may be hidden because of flexing of the lithosphere under the shield's huge load, so the above volume should be considered a minimum. The summit has six nested calderas forming a depression 72 × 91 km across and up to 3.2 km deep (Figure 3.8). Crater ages on the caldera floor range from 140 to 200 Myr (Neukum *et al.*, 2004). The cliff around the edifice ranges considerably in elevation. The highest section is to the north and northwest, where the cliff is 8 km high, extending from a base level of −2 km up to an elevation of 6 km. The northeast and southwest parts of the cliff are buried by flows that form distinct aprons that extend well beyond the former position of the cliff. The cliff to the southeast is mostly around 4 km high, above a base level of 0 km. On the southeast flank, just inside the cliff, are some mesas, several kilometers across and a few hundred meters in height (Figure 3.9). The mesas are puzzling. Are they uplifted blocks, or remnants of a former higher surface? If the former, what caused the uplift? If the latter, what caused the removal or lowering of the terrain between the mesas?

The most distinctive feature of Olympus Mons is its aureole. The aureole consists of several huge lobes of terrain, each with closely spaced arcuate ridges that give the lobes a characteristic corrugated texture. Francis and Wadge (1983) identify four major lobes on the western side of the volcano, where the aureole is best developed, and there may be additional minor lobes. Several much smaller lobes are on the east side.

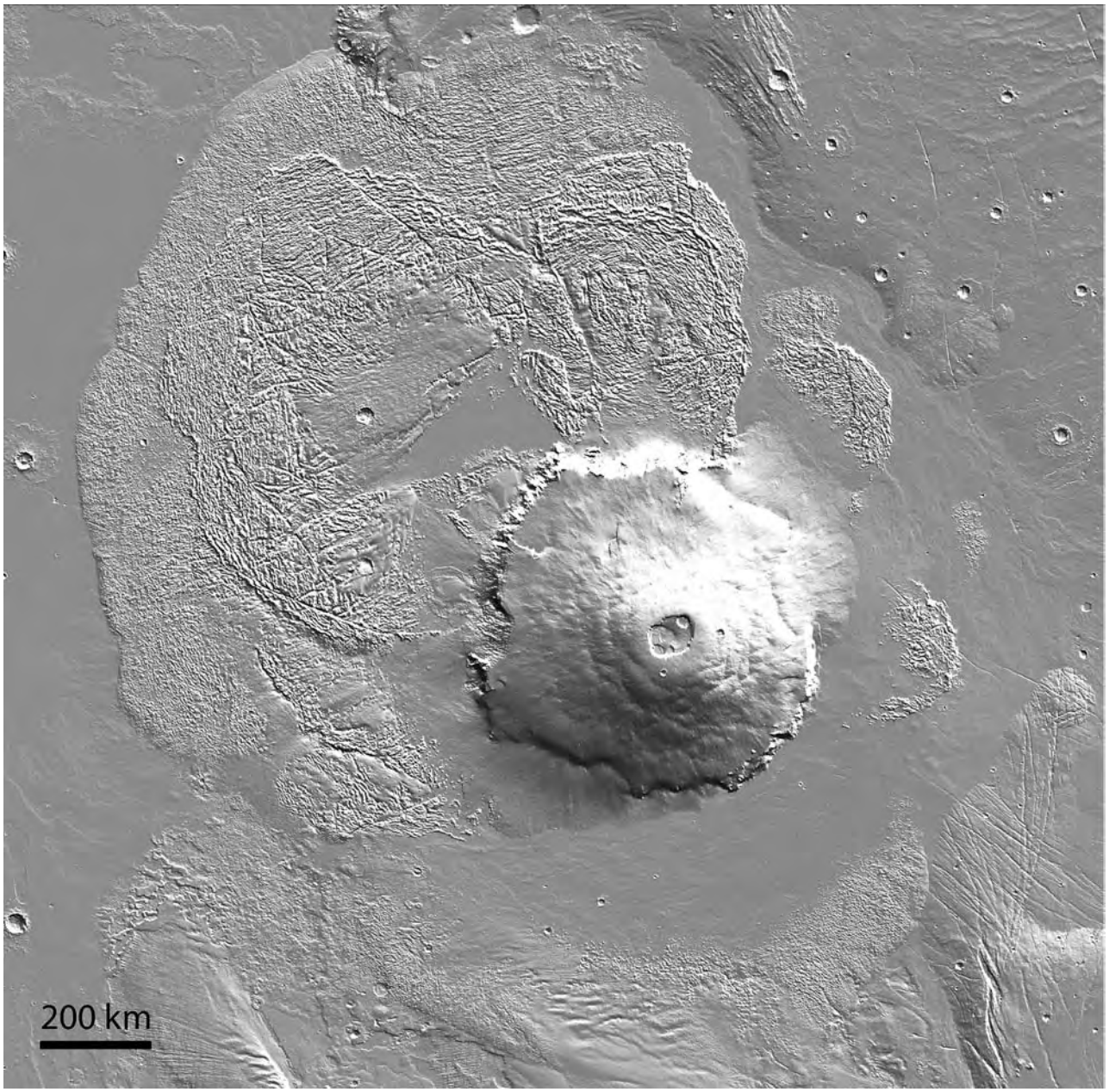

Figure 3.7. Olympus Mons and its aureole. The shield, outlined by a kilometers-high cliff, stands 22 km above the surrounding plains. Surrounding the shield are huge lobes of terrain with a characteristic ridged texture. The lobes may be caused by gravitational failure of the outer parts of a formerly more extensive shield. A partial moat around the shield, partly filled with lava flows, is the result of flexing of the underlying lithosphere under the load of the volcano (MOLA).

The largest, oldest, outer lobe extends 750 km westward from the Olympus cliff. It is now buried by younger lobes, but if it originally was connected to Olympus Mons, as are the younger lobes, then it would have covered an area of $6 \times 10^5\,km^2$, roughly the area of France ($5.5 \times 10^5\,km^2$). While the dominant structural fabric within the lobes is arcuate and parallel to the lobes' margins, numerous faults cut across the dominant grain. The inner parts of many of the lobes are buried by younger lava flows, some from Olympus Mons, others peripheral to the volcano.

The origin of the aureole has been much debated, but the consensus is that it formed in

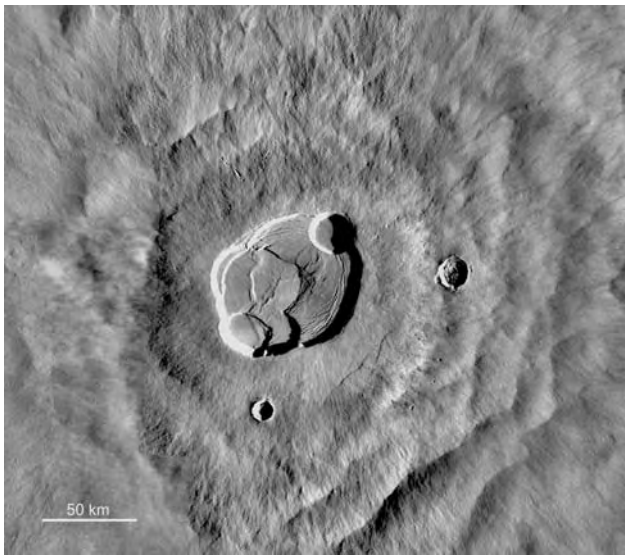

Figure 3.8. The Olympus Mons summit. The caldera formed by several episodes of collapse, probably widely spaced in time. The radial pattern is caused by flows; the sharp breaks in slope and terraces around the summit may be caused by thrust faults (Viking 890A68).

some way by gravity-induced failure around the periphery of a formerly more extensive Olympus Mons (Figure 3.10). Failure resulted also in formation of the cliff. Harris (1977) proposed, on the basis of analogy with the Bearpaw Mountains, Montana that the lobes are vast gravity-assisted thrust sheets, caused by squeezing out of material from beneath Olympus Mons along planes of weakness. Francis and Wadge (1983) also invoked thrusting, but suggested that each lobe formed as the outer parts of a formerly more extensive Olympus Mons was displaced outward along a series of shallow, concave upward fractures, which merged downward onto a decoupling surface, or zone of weakness. They point out that sliding under gravity can take place even if the sole of the thrust slopes upward, as long as the center of gravity of the moving material moves downslope. The surface of the lobes to the northwest of the volcano is mostly at an elevation of -1 to -2 km as compared to an elevation of 6 km for the top of the adjacent cliffs, so that there is considerable relief to drive the thrusts. Tanaka (1985) suggested that the aureole formed by gravity spreading of the former outer parts of the volcano at low strain rates. He suggested that movement took place along a detachment zone, with low resistance to shear because of the presence of ice. The mechanisms just discussed imply slow gravitationally induced deformation.

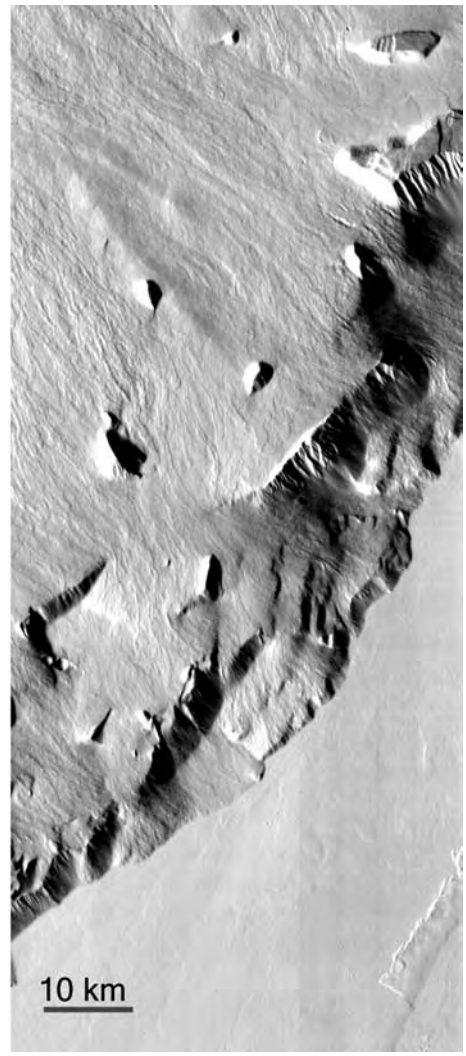

Figure 3.9. The southeast cliff of Olympus Mons showing its complicated structure. The cliff steps down to the adjacent plain in a series of terraces, partly draped with lava flows. The origin of several blocks both on the volcano flanks and the cliff is unclear (THEMIS).

In contrast, Lopes *et al*. (1980, 1982) invoked a series of catastrophic failures around the periphery of a formerly more extensive Olympus Mons. The geometry is similar to that in the Francis and Wadge mechanism. Because of the greater extent of the shield at the time of failure, the runout distance of the landslides is significantly less than the distance from the cliff to the outer margin of the lobes, but it is still substantial. They point out that failure would be aided by high pore fluid pressure. Intriguingly, water appears to have erupted from faults adjacent to the present cliff, presumably under where the shield formerly extended (Chapter 6).

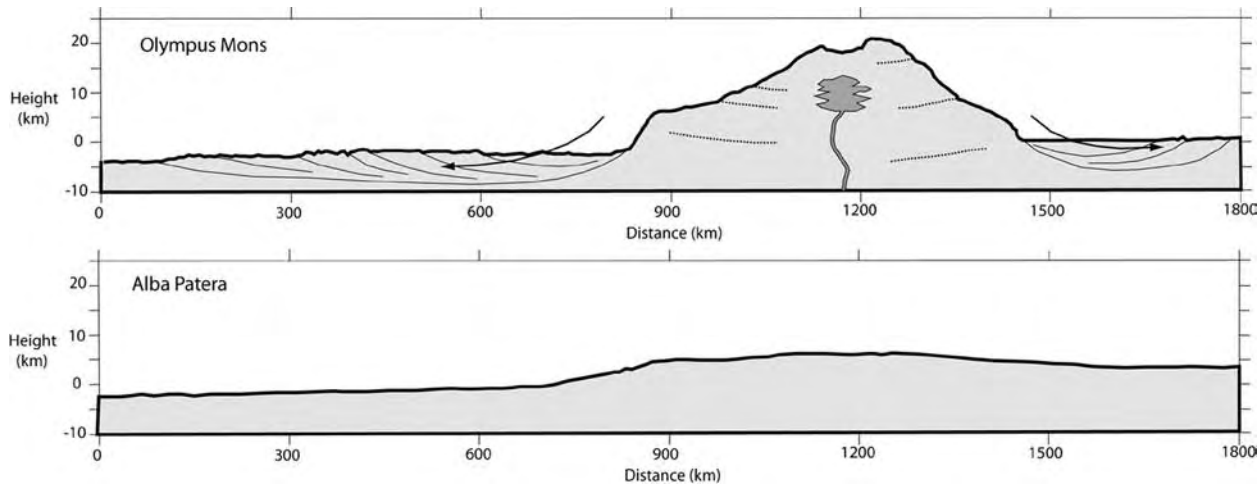

Figure 3.10. MOLA profiles across Olympus Mons and Alba Patera with 7.5× vertical exaggeration. The diagram also shows the hypothesized origin of the Olympus Mons aureole and location of the magma chamber beneath the Olympus summit.

Alba Patera

Alba Patera is very different from any terrestrial volcano and any other martian volcano (Figure 3.11). Among its unique characteristics are its size, low slopes, swarms of fractures that form an incomplete ring around its center, and extremely long lava flows on its flanks. In areal extent it is the largest volcano on the planet, Alba-derived flows can be found as far south as 26°N and as far north as 61°N, giving it a north–south span of 2000 km, roughly that of the United States. Its maximum width is close to 3000 km. The slopes are very low. From the summit at 6800 m to the edge of the volcano 1200 km to the north, where the elevation is −3000 m, the average slope is only 0.5°. The volcano can be divided into several roughly concentric units. At the center is an edifice 350 km across and 1.5 km high with gently sloping flanks and a central caldera, 200 m deep. Outside the edifice is an annulus of very low, and in places reversed slopes, outlined by an incomplete ring of fractures 500 km in diameter. Outside the fracture ring is a unit with prominent flows and ridges, which has the volcano's steepest slopes, although they are still only 1°. At the outer margin of this unit is a break in slope, outside of which the ground slopes gently away at 0.2° to the outer margin of the volcano.

One of the most striking features of the volcano is the array of fractures that cross its flanks. They are oriented mostly N–S to the south of the volcano and mostly NE–SW on the north and northeast flanks. Where the fractures cross the center of the volcano they form an incomplete ring. Deformational features, mainly graben and ridges, are common throughout the western hemisphere of the planet, mainly as a result of the Tharsis load (see Chapter 4). From the orientation of the fractures and their burial by different-aged units, Anderson *et al.* (2001) showed that the Tharsis deformation center shifted and decreased in intensity with time. They identify five centers that range in age from the Noachian to the middle Amazonian. Alba was one such center in the late Hesperian. There are at least three causes of the graben that cut Alba. The N–S and NE–SW graben appear to be controlled by regional stresses created by the Tharsis bulge. A second set appears to be related to dikes emplaced from a volcanic center well to the south of Alba (Mège and Masson, 1996), and a third cause is crustal loading, either negative or positive, by Alba Patera itself. Cailleau *et al.* (2003) were able, for example, to simulate the fracture ring by combining regional extension, presumably due to Tharsis, with local subsidence below the center of the volcano. However, McGovern *et al.* (2001) argue that in order to get tensional failure on the volcanoes flanks, buoyant subsurface loads are required. Such loading could be caused by underplating of the lithosphere, formation of sill complexes within the lithosphere, or dynamic support. They suggest a self-regulating mechanism of volcano growth in which the growing edifice compresses the upper lithosphere, thereby causing the rising magma to stall. Continual supply of magma from the mantle creates a buoyant load in the lithosphere, which then relieves the near-surface compression. This allows the magma to rise again,

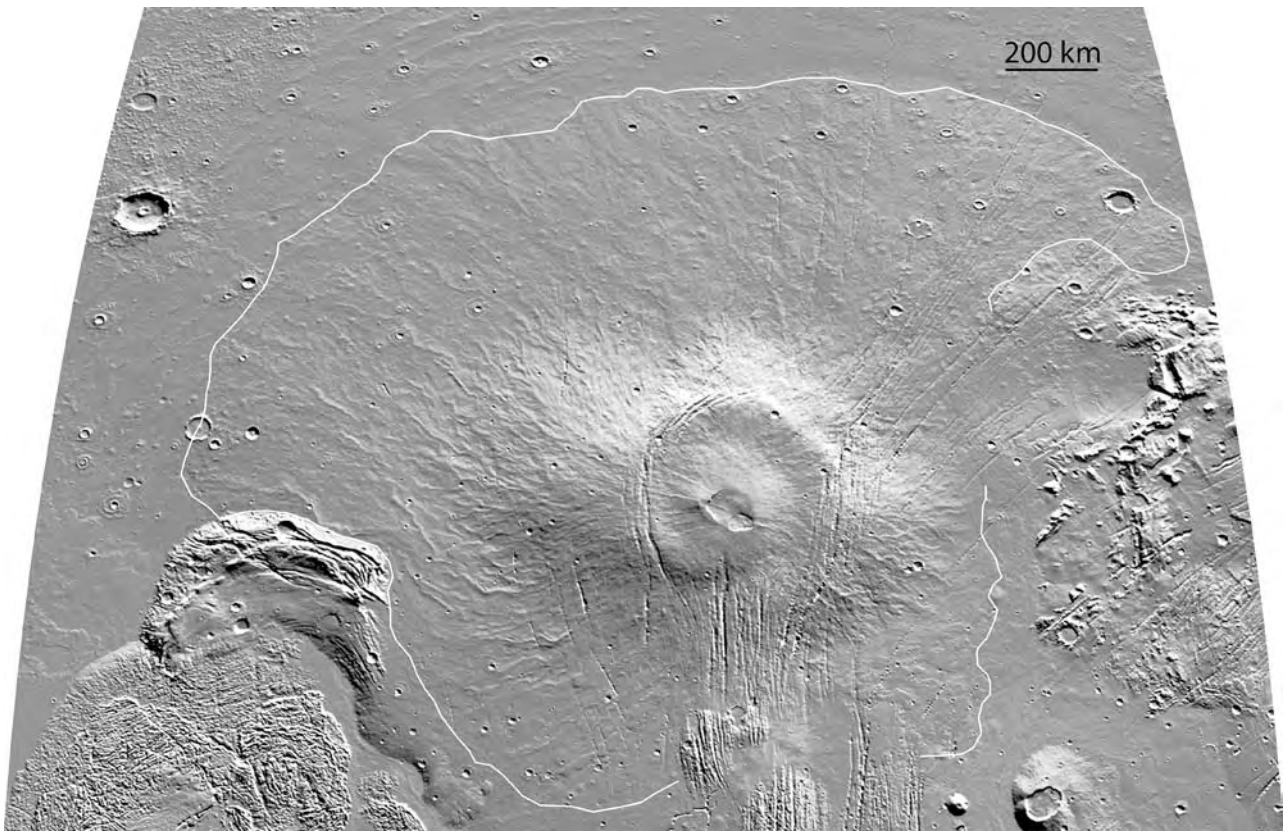

Figure 3.11. Alba Patera. The white line shows the maximum extent of Alba-related flows. A compound caldera is at the center of a low edifice within the fracture ring. The steepest slopes of the volcano and the most prominent flows are immediately outside the ring (MOLA).

adding to the edifice and increasing the near-surface compression until the magma stalls again. The growth of the volcano is thus episodic. They suggest that this does not happen with the Tharsis shields because they rest on a thicker lithosphere that provides more support for the volcano's load.

The fractures themselves may be simply manifestations of the failure of the crust in response to the local and regional tensional stresses. Alternatively, or in addition, the graben may be pathways along which magma moved laterally or vertically to create dikes. In this case, the magma would have been an active agent in causing the fractures, although their orientation would still be controlled by the crustal stresses. Lines of pit craters commonly occur within the graben or merge to form graben (Figure 3.12). Again there are different possibilities for their origin. Ferrill *et al.* (2004) suggest that the pits are caused simply by collapse of the surface materials into voids created by dilatational faults. On the other hand, Scott and Wilson (2002) argue that the origin of the pits is connected with dike emplacement. They suggest that they result either from collapse following degassing of a stalled dike or from collapse following small explosive eruptions.

The low slopes of the volcano could result from a combination of eruptive style and tectonic causes. Two main types of flows can be identified on the volcanoes flanks: sheet flows and tube-fed flows (Figures 3.13, 3.14). Sheet flows are flat-topped and outlined by a steep, lobate escarpment. They tend to broaden downstream where the larger ones may achieve widths of a few tens of kilometers. The narrower upstream portions may have a central, levéed channel, although such channels are less common on Alba than other Tharsis shields. Tube-fed flows form long, curvilinear, ridges, typically 5–10 km across, at the crest of which may be a discontinuous channel. The origin of the ridges is not entirely clear. All the ridge building may be at the end of the ridge where lava carried down the channel or tube at the crest of the ridge adds to the ridge's length. Alternatively, the channel or tube may back up, possibly as a result of surges in magma supply, so that overflows occur along

Figure 3.12. Graben and lines of pits (catenae) on the southeast flank of Alba Patera. Such graben and catenae are common on the south and east flanks of Alba, and may be several hundred kilometers in length. Some of the graben may have formed over dikes. The pits may have formed simply by collapse or by explosive eruptions, the result of interaction of the dikes with subsurface volatiles (THEMIS V10102011).

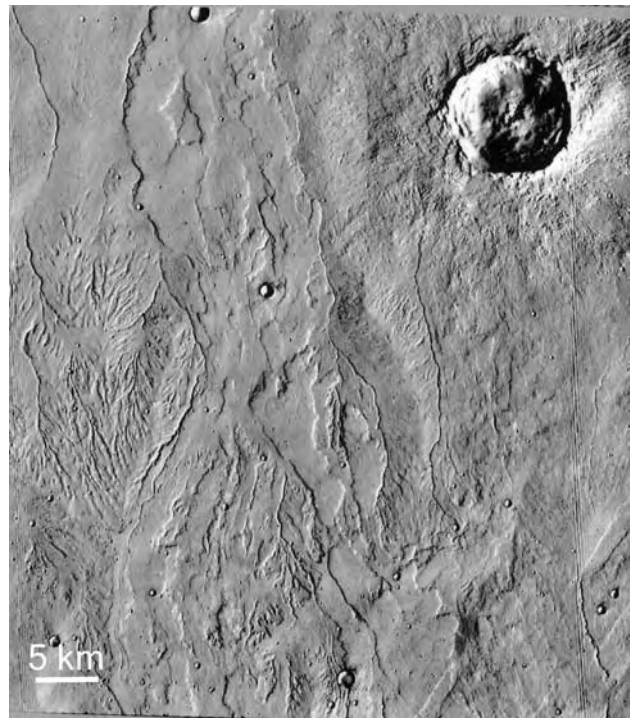

Figure 3.13. Flows and channels on the northwest flank of Alba Patera at 45.5°N, 244.6°E. Sheet flows extend north–south through the center of the image. Tube-fed flows form ridges whose sides are crudely channeled. Narrow channels are common between the ridges and flows. Distinguishing volcanic features from what might be fluvial features is challenging. The crater in the upper right is 9 km across (Viking 252S36).

the length of the ridge and add to its height. The flanks of the ridges are commonly crudely gullied. The gullies may converge downstream on narrow channels (not levéed) in the depression between adjacent ridges. Both types of flows are most common on the steeper part of the volcano just outside the fracture ring. Tube-fed flows are particularly prominent on the west flank of the volcano where individual ridges can be traced for several hundred kilometers.

In places, the volcano flanks are dissected by different types of channels. Some that have numerous tributaries that converge downstream resemble in plan terrestrial river systems and were likely cut by water. Others such as those that run along the crests of ridges are clearly lava channels. Yet others, like the gullies on the sides of the lava ridges (Figure 3.13), or single isolated narrow channels, are of ambiguous origin. The fluvial features and the mostly low slopes of the volcano suggested to Mouginis-Mark *et al.* (1988) that Alba Patera was built largely of easily erodible, volatile-rich, pyroclastic deposits. They suggested that the deposits were emplaced by long-runout, ground-hugging flows that erupted from around the central caldera. According to their model the fluvial-like valleys formed by sapping, the result of groundwater migrating through the permeable pyroclastic deposits and emerging on the volcano flanks. The new Mars Global Surveyor (MGS) and Odyssey data suggest, however, that most of the surface of Alba is composed of lava flows (Ivanov and Head, 2005). If pyroclastic flows played a large role in its construction, they must have formed very early in its history, prior to the emplacement of the extensive flows. These observations, together with the more detailed documentation of flow length, suggest that the broad, low-sloped nature of Alba may be due to the extreme length of its flows compared with other Tharsis Montes. Ivanov and Head attribute the small areas of channeling

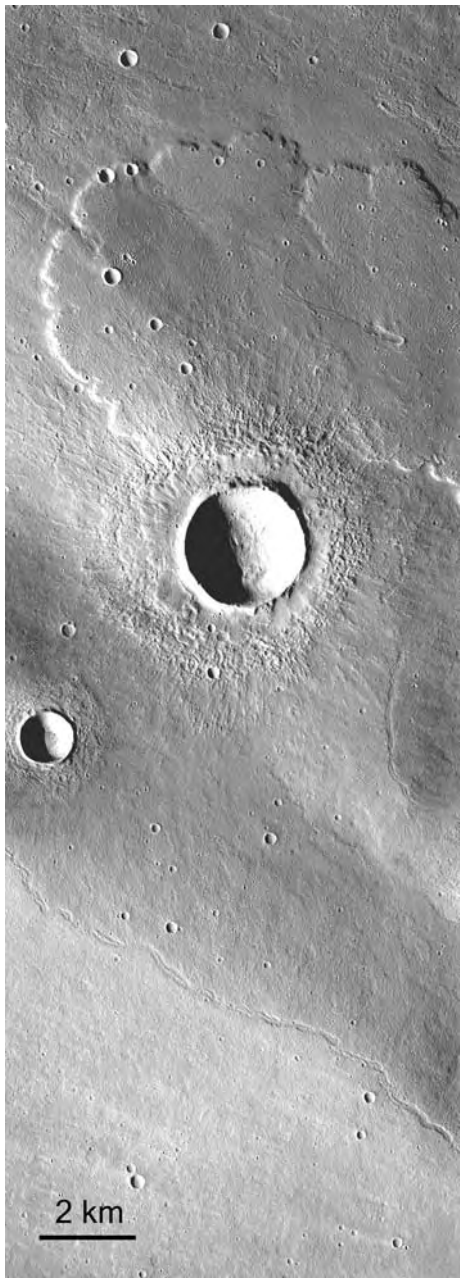

Figure 3.14. Sheet flow (top) and tube-fed flow (bottom) on the flanks of Alba Patera at 36.7°N, 236.0°E. The tube-fed flow forms a low ridge on the top of which is a discontinuous channel (THEMIS V10265007).

on the northern flanks to deposition and melting of ice-rich dust during periods of climate change.

Small Tharsis shields

Within Tharsis are several shield volcanoes that are considerably smaller than those so far discussed. They range in size from 60 km across and 1 km high (Jovis Tholus) to 300 km across and 3 km high (Uranius Patera). These smaller volcanoes all appear to have surfaces older than those of the large shields. They also have summit calderas that are large in proportion to the size of the volcano, the caldera diameters being roughly one-third the diameter of the edifices. In eastern Tharsis there are four such shields. Perhaps the most distinctive is Ceraunius Tholus (24°N, 263°E) (Figure 3.15). It is 125 × 94 km across and 6 km high. Its steeply sloping (6–11°) flanks are almost completely covered with radial channels, mostly 300–500 m wide. Most of the channels are highly degraded but some are not. A particularly large channel, over 1 km across on the northwest flank, terminates in a fan within a nearby impact crater. Identifiable lava flows are rare on the flanks, if present at all. Also rare are outcrops on crater rims and channel walls. Many impact craters on the flanks appear subdued as though buried, and the surface between and within the channels appears stippled as though the surface materials had been modified by the wind. All these characteristics suggest that an easily erodible, airfall deposit, such as ash, is at the surface. Reimers and Komar (1979) proposed that the valleys were eroded by ground-hugging ash flows or nueés ardentes, but this idea has lost favor. The prevailing view now is that the valleys were water-eroded into ash deposits (e.g. Gulick and Baker, 1990). Uranius Tholus, just to the north of Ceraunius Tholus, is similar. It is 60 km across, 3 km high, and has densely channeled flanks. The main difference is that Uranius Tholus has a multiple central caldera. A third shield, Uranius Patera, 240 × 280 km across, is the largest of the three Uranius group volcanoes. Its large central caldera is as large as the entire Ceraunius Patera. The flanks have a distinct radial pattern caused by long linear flows. There is little evidence of the blanketing and channeling seen on the two volcanoes nearby. It appears to have formed almost entirely by effusion of fluid lava. Crater counts on the three volcanoes just discussed indicate that they have ages that range from late Noachian to early Hesperian, significantly older than the surfaces of the larger shields (Plescia, 2000). A fourth shield, Tharsis Tholus, lies 800 km south of the three just discussed. This 130 × 150 km shield has a distinctly convex upward shape with a 7 km deep, 45 km diameter caldera. The flanks are almost featureless. While there is a faint radial pattern, there are no clearly identifiable flows or channels. The dominant flank features are impact craters and faults, of which some appear to disrupt the entire edifice.

Three volcanoes in western Tharsis are similar in size to those just described. Biblis Patera, 130 × 180 km

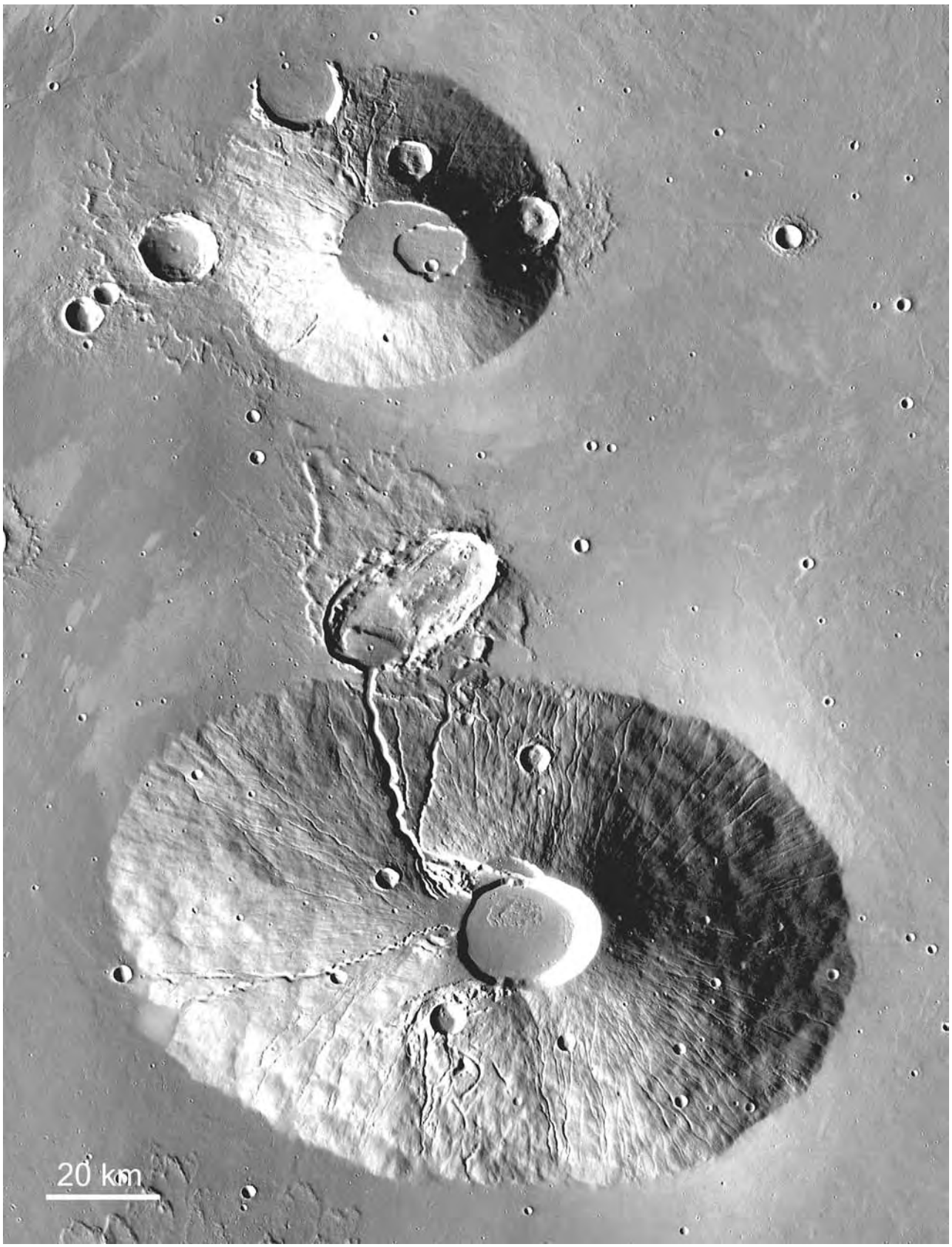

Figure 3.15. Ceraunius Tholus (bottom) and Uranius Tholus (top). The flanks of both volcanoes are densely channeled, and lava flows are rare. The channels suggest that easily erodible materials such as ash are at the surface. The number of superimposed impact craters indicates an age significantly older than the surfaces of the central Tharsis volcanoes (THEMIS mosaic).

across and 3.6 km high, has a large summit caldera, 60 km across, 4.6 km deep, with complexly faulted walls (Plescia, 2004). The faulting and the fact that the caldera is deeper than the edifice is high implies repeated collapse as a result of withdrawl of magma from a magma chamber well below the visible edifice. Two additional shields in western Tharsis, Ulysses Patera and Jovis Tholus, also have large calderas in proportion to the width of their visible edifices.

The seven volcanoes just described all have large calderas in proportion to the size of the edifices. This is somewhat puzzling in that, as we saw above, a large caldera almost certainly implies a large magma chamber, which in turn implies large eruptions. A complex caldera such as that in Biblis Patera implies many such eruptions. The geometry becomes more understandable if, with these smaller features, we are just seeing the tops of much larger volcanoes whose lower flanks are now buried. The Tharsis bulge is likely a thick accumulation of volcanic rock (Solomon and Head, 1982) that was largely built by the end of the Noachian (Phillips *et al*., 2001). The age of the exposed surfaces of these smaller volcanoes range from Noachian to lower Hesperian. But this dates only the last active period. They could have been active for extended periods of time during the Noachian, building large shields, now mostly buried, and adding to the accumulation of volcanics that is now the Tharsis bulge.

Most of the plains between the volcanoes are covered by flows (Figure 3.16). But in addition to the named volcanoes, there are, throughout Tharsis, numerous low mounds roughly 20 km across and 200 m high. They are particularly common on the southern aprons of Pavonis Mons and Ascreus Mons and between Pavonis Mons and Noctis Labyrinthus. These are unlikely to have deep mantle sources. More likely, they are some form of rootless vent, such as might form over a dike propagating from a central vent, or over a tube transporting lava from a central vent. However, in view of their size and location they are unlikely to be the type of rootless cone that forms when lava moves over volatile-rich materials such as wet sediments.

Elysium

The Elysium province is much smaller than Tharsis. Within it are only three volcanoes of significant size: Elysium Mons, Hecates Tholus, and Albor Tholus (Figures 3.17, 3.18). Elysium Mons, at the center of the province, is at the crest of a broad dome roughly 2000 km across and 5 km high, depending on how one defines the extent of the dome and the Elysium Mons edifice. Lava flows radial to the dome can be found as far as 1000 km to the southeast of the center of the dome, in the Athabasca region, discussed in the next section, and as far as 1700 km to the northwest near the center of the Utopia basin. The dome is asymmetric, with slopes of 0.6–0.9° to the northwest and 0.1–0.4° to the east and southeast. Several prominent faults cross the outer parts of the dome from ESE to WNW, including the Cerberus, Galaxia, and Elysium Fossae. Concentric graben partly surround the dome within 300 km of its center. The concentric and radial graben are particularly prominent to the northwest of Elysium Mons, where they give rise to several large channels that extend deep into the Utopia basin. The origin of these seemingly fluvial channels, and the role that volcanic and tectonic process played in their formation, present some of the most puzzling problems of this region's geology.

Elysium Mons, at the center of the dome, is 14 km high. At its base it merges gently with the surrounding plains. Plescia (2004) used a gradual break in slope around 1.3 km elevation to define the base of the volcano. By this definition the edifice is 375 km across and has a volume of 2×10^5 km^3, roughly one-fifth the volume of Arsia Mons. At the summit is a simple, shallow, 100 m deep caldera, 14 km across (Figure 3.19). Extending away from it are several lines of pits and fissures. Identifiable flows of any kind are rare on the upper flanks of the volcano, although sheet flows and tube-fed flows are common on the more gentle slopes beyond the main edifice. On the steeper upper flanks there is an indistinct radial texture caused by lines of pits, and possibly the remains of flows. The intersection of the radial fabric with the regional ESE–WNW fabric gives the flanks a hummocky texture.

Hecates Tholus is very different (Figures 3.20, 3.21). It has a sharply defined edifice 180 km across with a complex summit caldera, 13 km in diameter, 400 m deep, at an altitude of 4.8 km. The volcano's most distinctive feature is its channeled slopes, which are among the most densely dissected slopes on the planet. The larger channels, typically a few hundred meters wide, commonly start full size, having rounded alcove-like upper terminations. The vast majority of the channels, however, have no obvious source. The only part of the edifice that is not dissected is a small area around the summit, especially to the northwest. The smoothing has been attributed to the presence of pyroclastic deposits (Mouginis-Mark *et al*., 1982). Suggestions for the origin of the channels include melting of ground ice by volcanic heat (Gulick, 1998) and melting of a summit snow pack as a result of

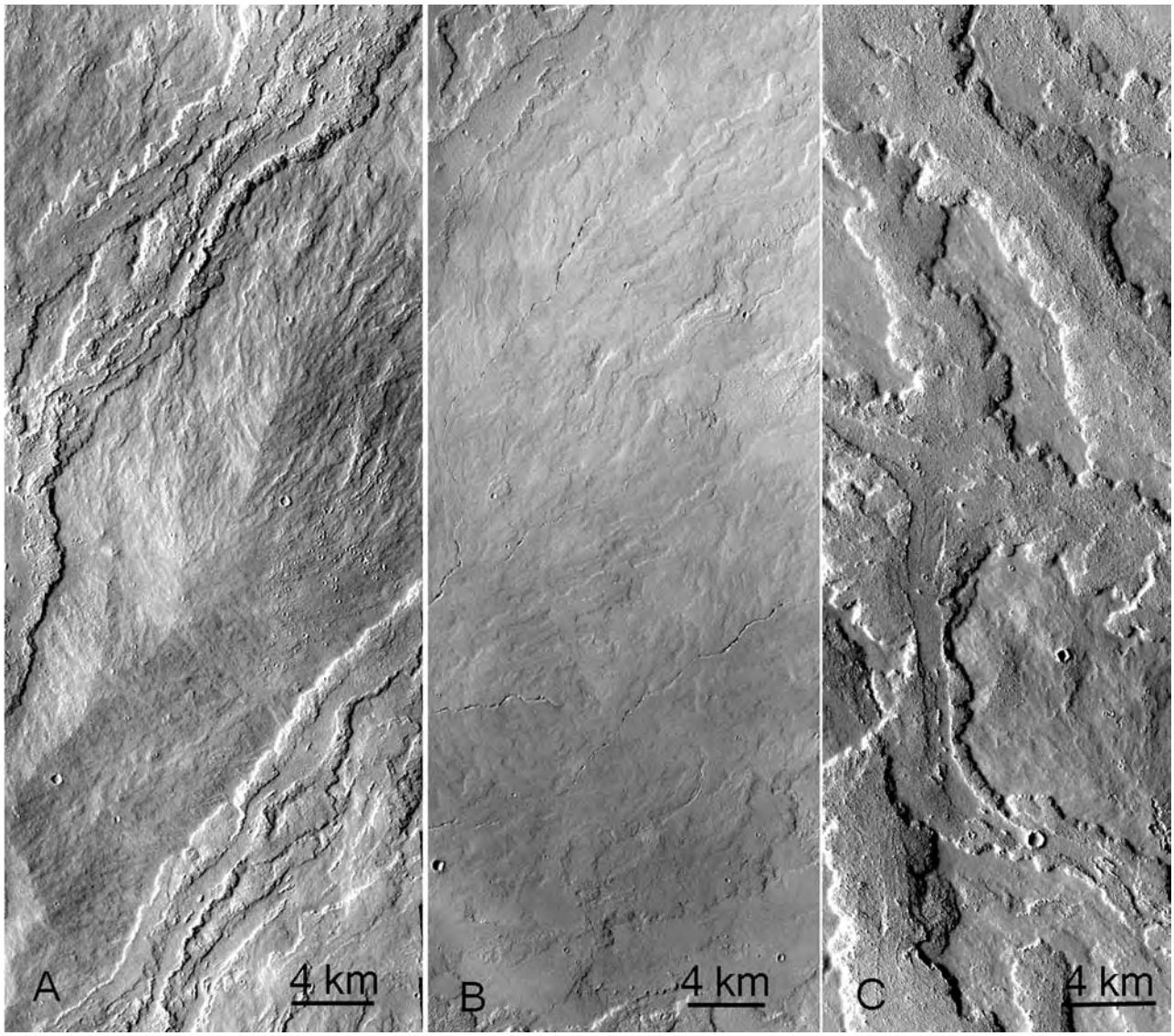

Figure 3.16. Lava flows on the Tharsis plains. (A) Flows at 15°N, 260°E on the northeast apron of Ascreus Mons. A tube-fed flow in the center is between two sheet flows. Narrow flows can be seen on the side of the ridge built by the tube-fed flow. Compare with Figure 3.14 (THEMIS V11537009). (B) Flows at 13°N, 270°E near Tharsis Tholus. Numerous discontinuous fissures trace the paths of lava tubes, although here the tube-fed flows do not build conspicuous ridges (THEMIS V11911012). (C) Sheet flows from Pavonis Mons at 0.4°N, 240°E. Some of the flows have a broad, central, flat-floored channel (THEMIS V05559022).

volcanic intrusions (Fassett and Head, 2004). A large re-entrant in the western flank of the shield could be a subsidiary caldera (Hauber *et al*., 2005b).

The third Elysium shield, Albor Tholus, is 150 km across and 4.1 km high. Its flanks are sparsely cratered and smoother than those of the other two volcanoes. As with Hecates Tholus, the smoothest area is to the northwest of the summit. Concentric faults cut the southern flanks. The smoothing of the summits of the Elysium volcanoes and the presence of numerous fluvial-like valleys on several volcanoes such as Alba Patera, Ceraunius Tholus, and Hecates Tholus have been attributed to the presence of ash.

Lahars and dikes

Several graben on the east side of the Elysium dome are the sources of narrow, simple, sinuous valleys that resemble lunar rilles. They are likely lava channels and indicate that the graben were sources of some of the lava that built the adjacent plains.

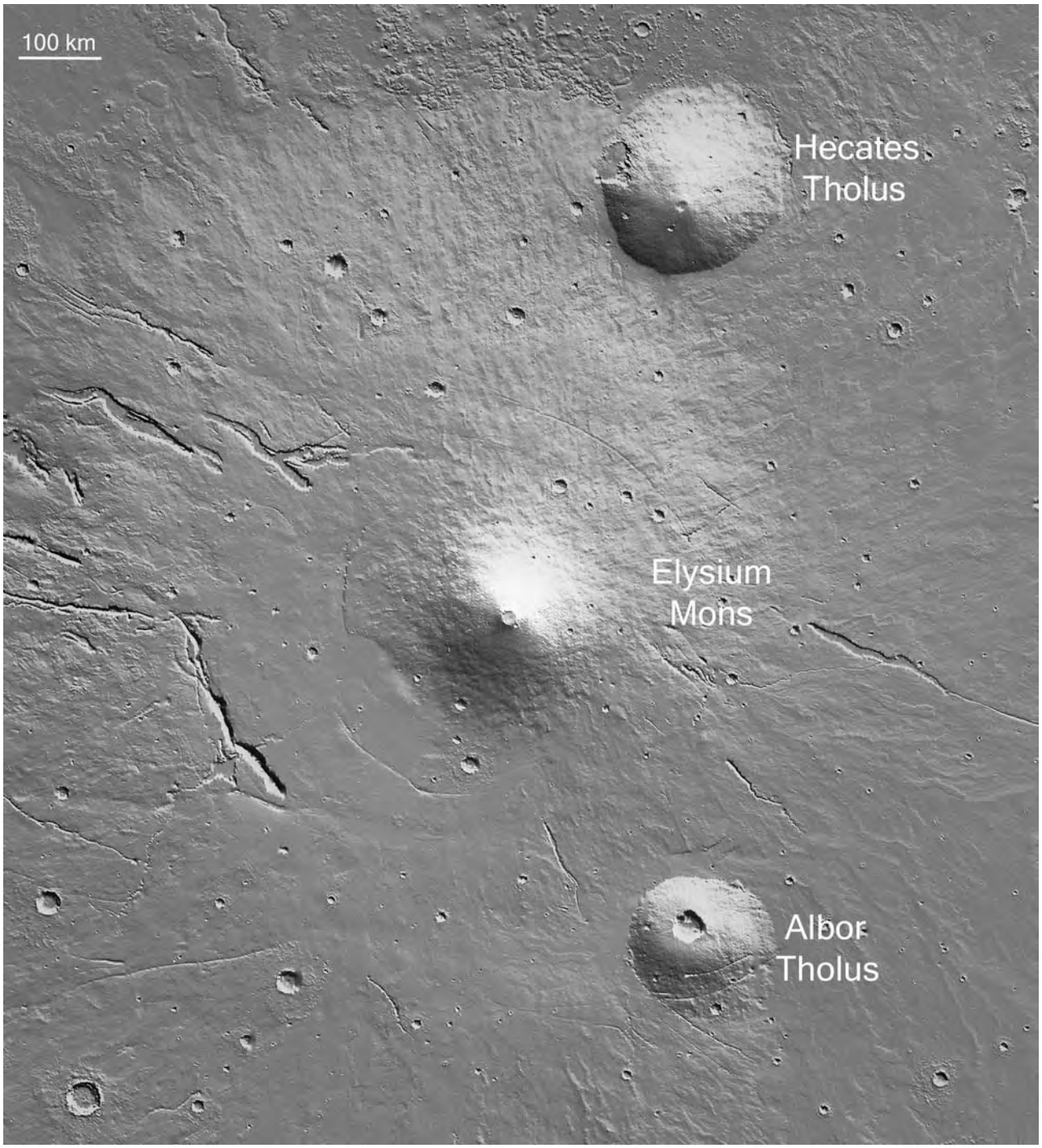

Figure 3.17. Index map of Elysium (MOLA).

The valleys that emerge from the graben on the west side of the dome are very different (Figure 3.22). They are much larger, they branch complexly, and they contain islands. The larger ones have flat, commonly striated floors. Some of the channels appear to be within flow-like deposits with lobate outer margins. Interspersed between the western channels and their associated deposits are lava flows. The entire channeled region has a complex, hummocky topography that differs markedly from the plains to the north or the lava plains on the east side of the dome. The channels are discussed briefly in Chapter 6.

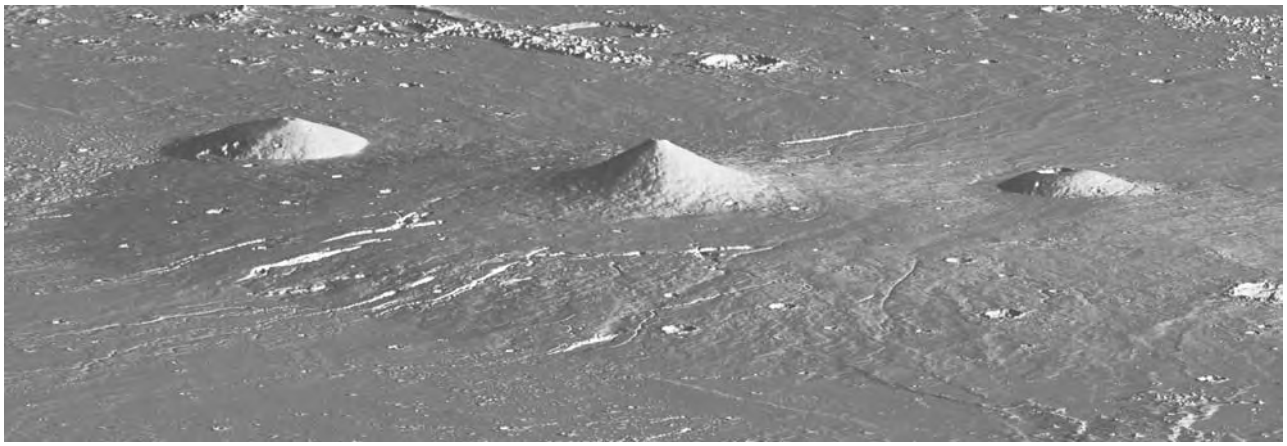

Figure 3.18. Oblique view of Elysium looking to the east over the Utopia basin in the foreground. (MOLA 8× vertical exaggeration.)

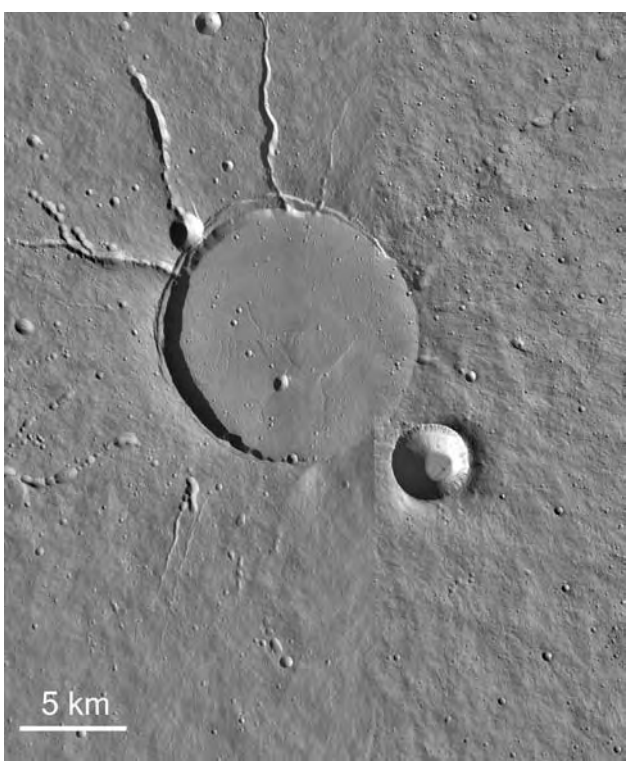

Figure 3.19. The summit caldera of Elysium Mons. The caldera is simple and shallow compared with other shields. Rifts, lines of craters, and narrow channels radiate from the caldera (THEMIS mosaic).

The discussion here focuses on the possible volcanic implications of the channels.

The peculiarity of the channels and their associated deposits has led to a variety of interpretations, mostly involving the interaction of lava with groundwater, ground ice, or surface ice (summarized in Russell and Head, 2003). As discussed above, under a volcanic complex, such as Tharsis or Elysium, magma is expected to rise from its source in the mantle through the crust, until it reaches the zone of neutral buoyancy, where it will stall and form a magma chamber. Vertical dikes will then tend to propagate laterally from the chamber in a direction at 90° to the least principal stress. The dikes will cause fracturing ahead of them, and graben will form if the dike is close enough to the surface (Mastin and Pollard, 1988; Wilson and Head, 2002). Regional-scale fractures across the Elysium region indicate that the direction of minimum stress is in the NE–SW direction, although the direction deviates locally around the Elysium dome. Russell and Head (2003) point out that lava flows emanate from several graben to the west of the Elysium center, thereby supporting the graben–dike connection. Lunar rille-like channels on the east side of the rise also originate in graben-like depressions with the same orientation. On their rise through the upper crust the dikes are likely to encounter water and ice-rich materials. As we saw in Chapter 1, Mars has a kilometers-thick cryosphere within which is likely ground ice (Clifford, 1993). Confined below the cryosphere is probably groundwater. Propagation of fractures through the cryosphere and encounters of magma with ice- and water-rich materials could have a variety of outcomes. Simply fracturing the cryosphere, unaccompanied by an intrusion, could result in release of water if the disruption took place below the local level of the water table. A propagating dike could also disrupt the cryosphere. The scale of the release would depend on the hydrostatic head at the disruption site. Russell and Head found little evidence for release of

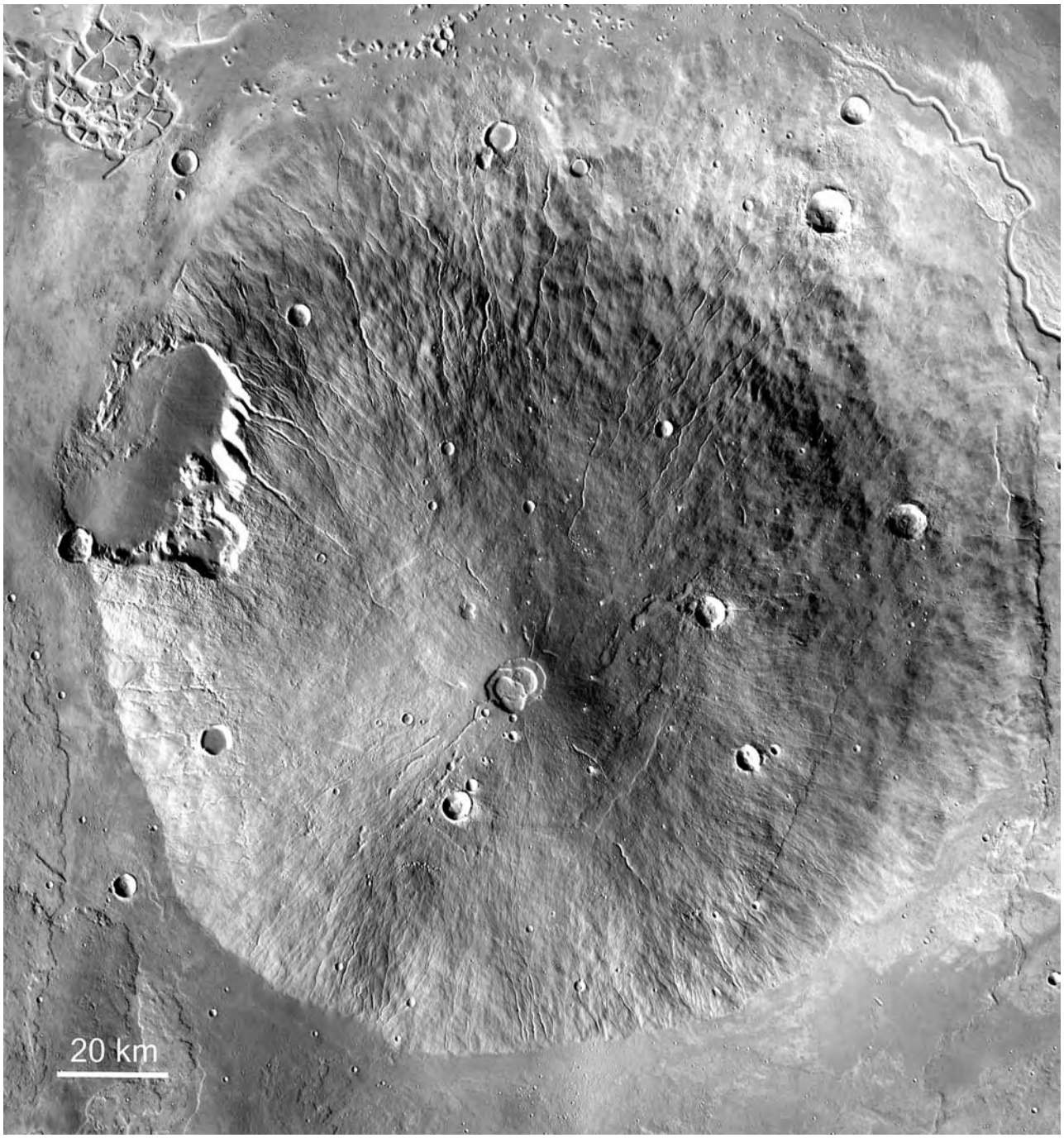

Figure 3.20. Hecates Tholus. In contrast to Elysium Mons in the previous image, the flanks are densely channeled, which suggests that flanks are composed of easily erodible ash. The origin of the channels is unclear. They have been variously interpreted as lava channels, valleys eroded by ash flows, or valleys eroded by water derived from rain or snow (THEMIS mosaic).

water from the graben west of Elysium at elevations higher than −3100 m. They concluded therefore that the water table was no higher than this during the period of active fracturing and dike emplacement. Interaction of a dike with water and ice may lead to phreatomagmatic eruptions (explosive eruptions caused by interaction of water and magma) with production of large amounts of steam and ash.

Figure 3.21. Detail of the southwest flank of Hecates Tholus centered at 30.2°N, 149.3°E. The flanks are densely channeled and lines of pits are common. The scene is 18 km across (THEMIS V12090005).

Such eruptions could send shock waves through the aquifer system, adding further to the likelihood of causing groundwater release. Finally, a dike approaching the surface would tend to melt any ground ice, if present, destabilize fragmental material on slopes, and possibly cause lahars.

Lahars are massive mudflows, normally composed of pyroclastic materials, which form on the flank of volcanoes. The morphological evidence for lahars in western Elysium are deposits, generally confined to within a few tens of kilometers of channels, which have steep, lobate outer margins (Christiansen, 1989). The deposits are interpreted as the remains of debris-rich, fluid flows that either overtopped the channels or were later incised by the channels. Formation of lahars requires a source of water and steep slopes covered with unconsolidated debris. On terrestrial volcanoes, causes of fluidization and slope failure include rainfall, melting of snow, subglacial eruptions, and disruption of crater lakes. The source of the water that lubricated the postulated Elysium lahars is unclear. Most likely it was groundwater or meltwater from ground ice, but rain or snow cannot be ruled out. The regional slopes in western Elysium are mostly only 2–4° and unlikely to result in slope failure. Slopes of the graben walls are, however, much steeper. Thus, failure of poorly consolidated materials in the graben walls, lubricated by groundwater or meltwater, and triggered by faulting or dike intrusion, appears the most likely cause of any possible lahar deposits. If some of the deposits are lahars, it implies that the region where the graben are located in western Elysium is underlain by poorly consolidated ash deposits. Wilson and Mouginis-Mark (2003) invoked lahars, in a different form, to explain some of the features associated with Hrad Vallis, the northernmost of the large Elysium channels. They suggested that injection of dikes and sills into the source areas of the channel resulted in large-scale phreatomagmatic eruptions and that the eruptions ejected ice-rich materials over a broad region. Melting of the ice created mudflows, which were subsequently eroded by water from the source region.

While the role of lahars has been emphasized in the above discussion, the role that lahars played in producing the features in western Elysium is still very uncertian. Volcanism and tectonic and fluvial processes have clearly all contributed to the complexity of the terrain, and melting of ground ice, subglacial eruptions, mass wasting, and marine processes may also have been contributors. Unraveling what role each process played will be very challenging.

Cerberus–Amazonis

2000 km to the southeast of Elysium Mons is an almost level plain between the uplands to the south and the Tartarus Colles to the north (Figure 3.23). Lava flows from the eastern flanks of the Elysium dome flow into the plains from the west and a large, shallow channel, Marte Vallis, connects the plains to Amazonis Planitia to the east. WNW–ESE trending graben, the Cerberus Fossae, cut through the northern edge of the plain and the Tartarus Colles to the north. The graben are the sources of at least two outflow

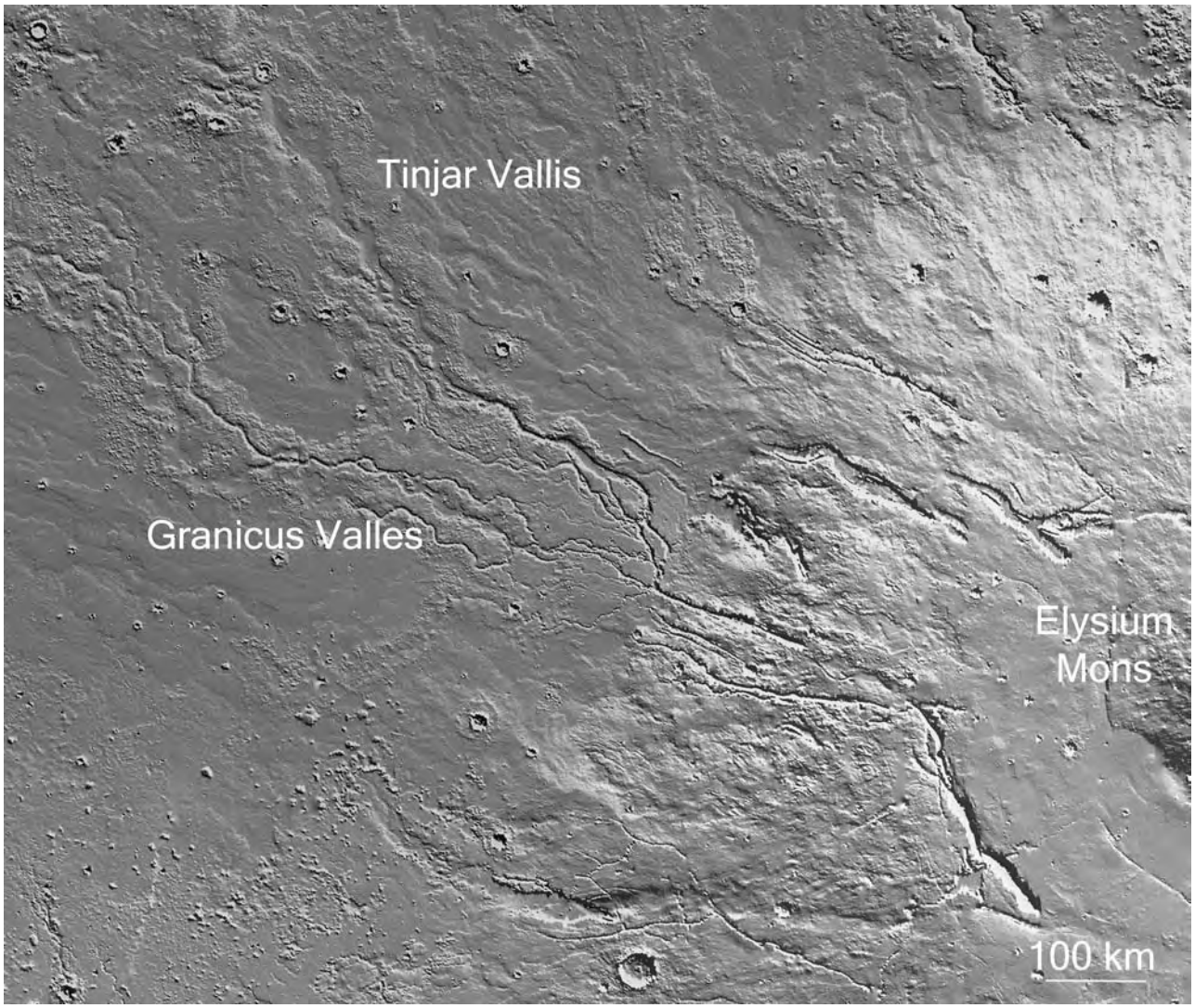

Figure 3.22. Valleys, graben, and flows to the west of Elysium Mons. Dikes radial to Elysium Mons may have caused release of groundwater to cause floods and debris flows. Granicus and Tinjar Valles both lie within a flow-like deposit that has been interpreted as the result of debris flows or lahars (MOLA).

channels, Athabasca Vallis and Grjota Vallis, and possibly more. Water from some of the outflow channels probably pooled in the Cerberus plains and exited to the west, cutting Marte Vallis. The Cerberus Fossae have also been the source of lavas that appear to have pooled in the low-lying plains. The outflow channels are discussed in Chapter 6. Here, we discuss the volcanic features.

The Cerberus plains are of interest in that they contain some of the youngest volcanic features on the planet, and are among the few locations where platey flows are found. The plains encompass the region between 0–10°N and 160–180°E. The slopes of the plains within this region are very low. Elevations range from −2900 m at 160°E to −3100 m at 180°E, giving an average slope of only one in 17,000 as compared with one in 1000 for the lower flanks of the Elysium rise. To the northwest of this area, the plains on the southeast flanks of the Elysium rise are composed mainly of lava flows, both sheet flows and sinuous ridges, indicative of tube-fed flows. Although there are also clearly identifiable flows within the Cerberus plains, most of the plains, as viewed at the MOLA scale, are characterized by long narrow ridges and depressions that trend WNW–ESE in the western part of the area, then curl to the northwest and converge on Marte Vallis to the east. The cause of the fluting, whether fluvial or volcanic or both, is unknown.

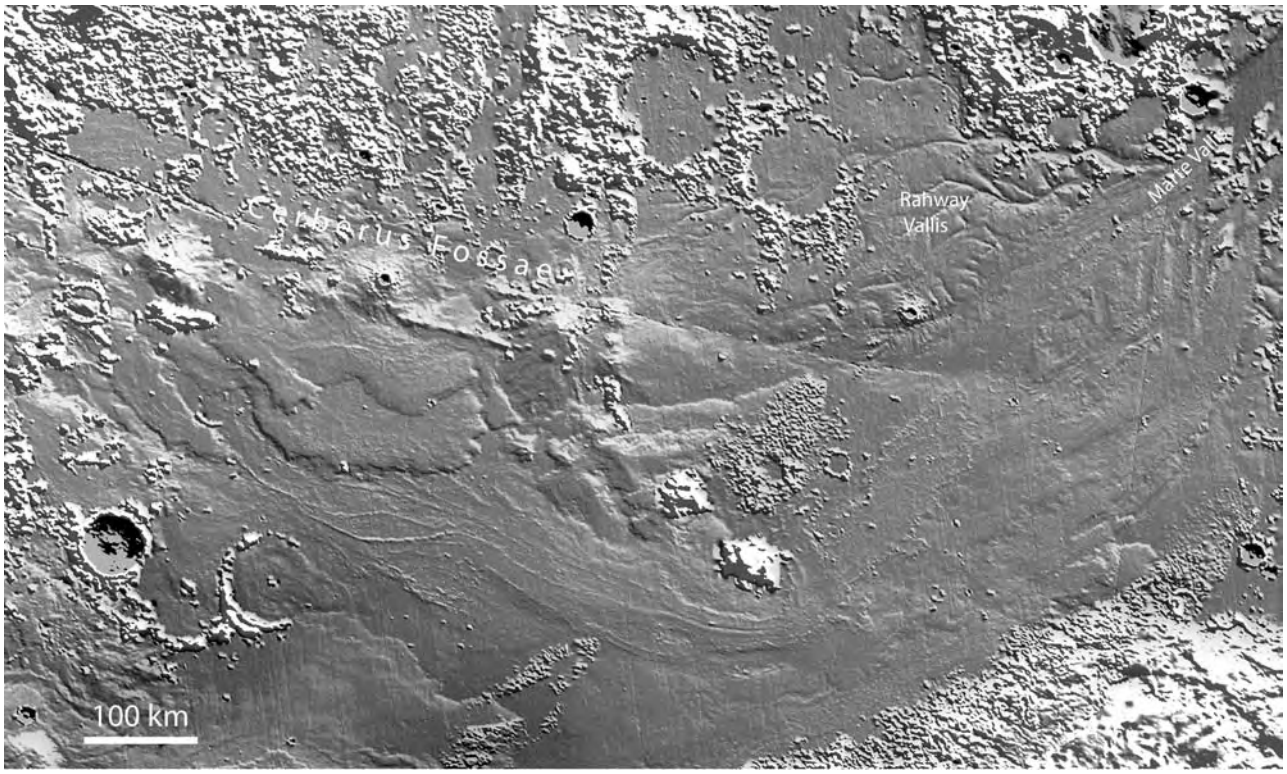

Figure 3.23. The Cerberus plains, centered at 5°N, 170°E. The image has been stretched to bring out the detail on the almost flat-lying plains. The area is a confusing mix of volcanic and fluvial features. The Cerberus Fossae have been the source of both lava flows and large floods. Large lava flows enter the area from the left and water probably entered the area through the hills to the north to cut Rahway Vallis and Marte Vallis and possibly pooled on the plains. Both water and lava may have exited the area through Marte Vallis in the upper right of the image (MOLA).

Unambiguous lava flows are common both within and around the Cerberus plains. The sources of the flows appear to be both the Cerberus Fossae and several low shields (Plescia, 2003a). A 100 km long line of spatter ramparts and low shields aligned along the trend of the Cerberus Fossae at 7°N, 167°E, for example, appears to be the source of several large flows (Figure 3.23). Head *et al.* (2003b) make the same arguments here for the role of dikes in creating the Cerberus Fossae and causing massive release of water, as were made for the graben and fluvial features northwest of Elysium (Figure 3.24). The appearance of most of the surface in the low-lying, almost level, plains is distinctively different from that of the more steeply sloping lava plains to the northwest. Some of the plains are broken into dark plates separated by lighter-toned material (Figure 3.25). In some places the plates can be reassembled like a jigsaw puzzle. In one example (Figure 3.26), a plate has moved past a crater leaving a shadow. Clearly, the plates are remnants of a crust of some kind that has been pulled apart. In other places, the surface is divided into rough and smooth areas, with the smoother areas crossed by numerous sinuous ridges that connect with each other and the rough areas to form complex patterns. Some areas combine the characteristic of the two different types of plains. These textures occur mainly, if not exclusively, on very level plains. In addition to the Cerberus plains, they are also common in northern Amazonis Planitia (Figure 3.27), where the slopes are even less than on the Cerberus plains.

The textures just described have been compared to textures found on some terrestrial lava flows, specifically the 1783–4 Laki flow in Iceland, which was subject to large surges in lava input (Keszthelyi *et al.*, 2000). By analogy, the martian textures have been attributed to rafted slabs of crusted-over lava, pressure ridges, ponded surfaces, and squeeze-ups. The textures only occur on almost level surfaces, presumably because the flow disrupted by increased inflow must be moving so slowly as to be almost a lava lake. Acceptance of the platey textures as due

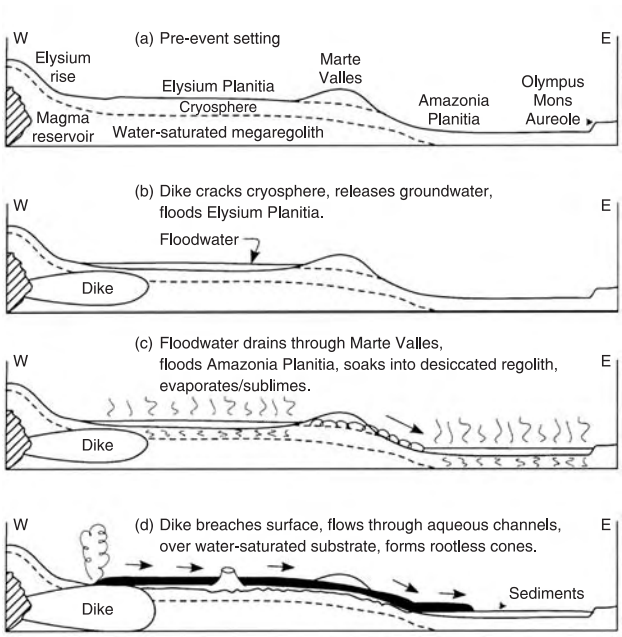

Figure 3.24. Cartoon showing a dike as the source of the lava and floods of water that have erupted from the Cerberus Fossae. Both lava and water followed the same paths across the Cerberus plains, through Marte Vallis into Amazonis Planitia (Fuller and Head, 2002b, copyright 2002, American Geophysical Union, reproduced by permission of the American Geophysical Union).

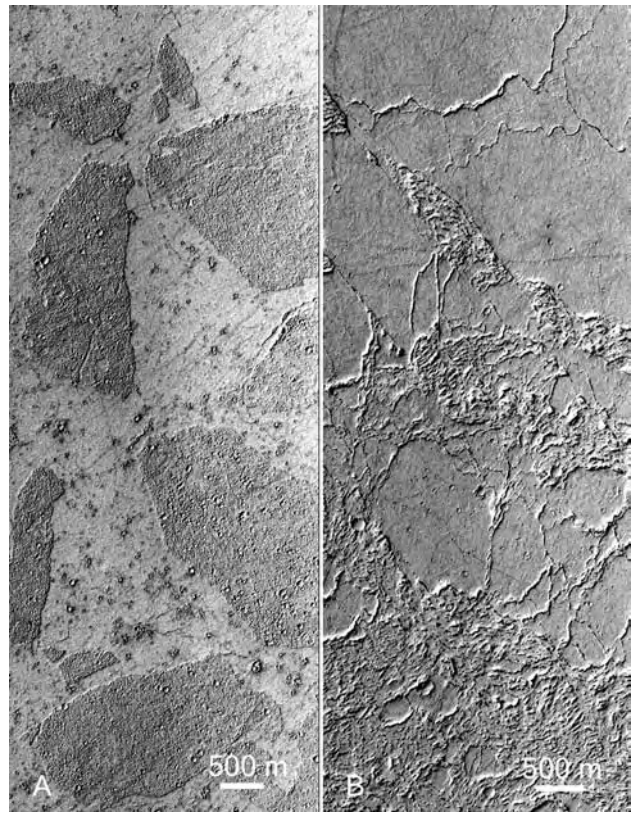

Figure 3.25. Cerberus flows. (A) The surface is composed of dark plates embedded in a lighter matrix. In places, the plates have clearly moved with respect to each other and can be fit back together (see next image). Curiously, the plates here are more heavily cratered than the matrix. The plates have been attributed to either crusted lava or to ice flows (MOC E2101678, 7.6°N, 178.3°E). (B) More typical lava flows as they appear in areas with low slopes. The surface is divided into rough and smooth units. The rough units form complex patterns connected by sinuous ridges. The patterns have been compared with similar patterns on some terrestrial lava flows (MOC E2201640, 3.2°N, 165.9°E).

to break-up of a lava crust is not unanimous. Murray *et al*. (2005) argue that water derived from the nearby Cerberus Fossae pooled and froze in the low, level Cerberus plains, and that at least some of the platey textures, and specifically that shown in Figure 3.26, are due to pack ice. Whatever their origin, the Cerberus plains are young. They yield model crater ages of no more than a few million years (Berman and Hartmann, 2002).

Marte Vallis appears to have been a conduit between the Cerberus plains and Amazonis Planitia for both water flows and lava flows. Lava flows have been observed within Marte Vallis (Figure 3.28) and several large flows are seen at the lower end of Marte Vallis where it enters Amazonis Planitia. Lava flows also enter Amazonis Planitia from the south and from under the Olympus Mons aureole to the east. The very low slopes in Amazonis Planitia have been attributed to the presence of a pre-Olympus Mons aureole flow that created a barrier along the northern edge of the plains (Fuller and Head, 2002b). Outflow channels (and possibly lava flows) were thus hindered from continuing into the lower northern plains. If the northern exit from Amazonis Planitia was indeed dammed, then the water flows and lava flows would have pooled, and the smoother, more northerly plains of Amazonis Planitia should comprise a mixture of lava flows and effluent from the outflow channels that enter from the west and south. Curiously, the textures on these plains are identical to those in the Cerberus plains so that the ambiguity between lava and ice flows is unresolved.

Most of the volcanic features of the Cerberus–Amazonis region are upper Amazonian in age. They are very young relative to the rest of the martian surface. Just south of the Cerberus plains is, however, an older volcano, Apollinaris Patera (Figure 3.29). Apollinaris is 190 km across, 5.4 km high, and has a central caldera 1.8 km deep and 80 km

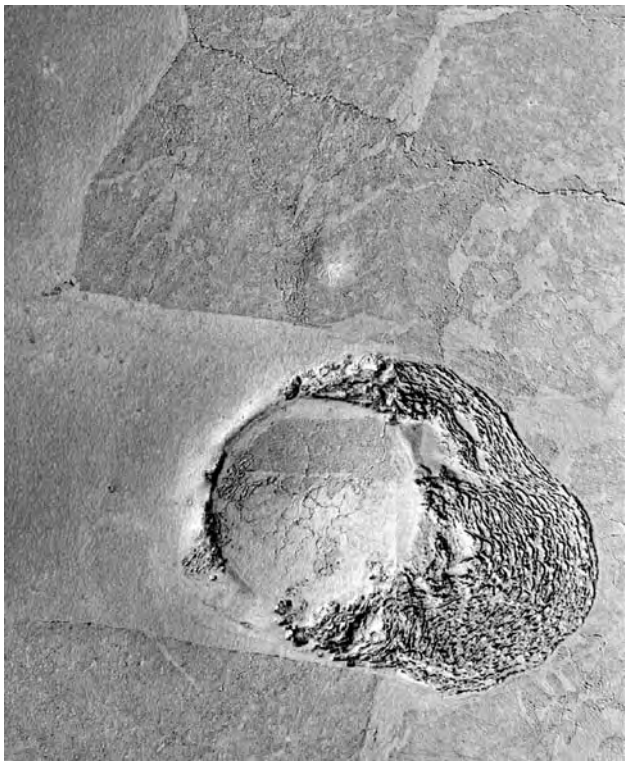

Figure 3.26. Rafted materials at 6°N, 150.5°E. The dark rafts have moved by a pre-existing crater leaving material piled up on one side of the crater and a "shadow" on the other side. At the top of the image a raft has pulled apart. The rafts have been interpreted both as ice flows and crusted lava. The crater is 2.1 km across (MOC E2100112, R0900475).

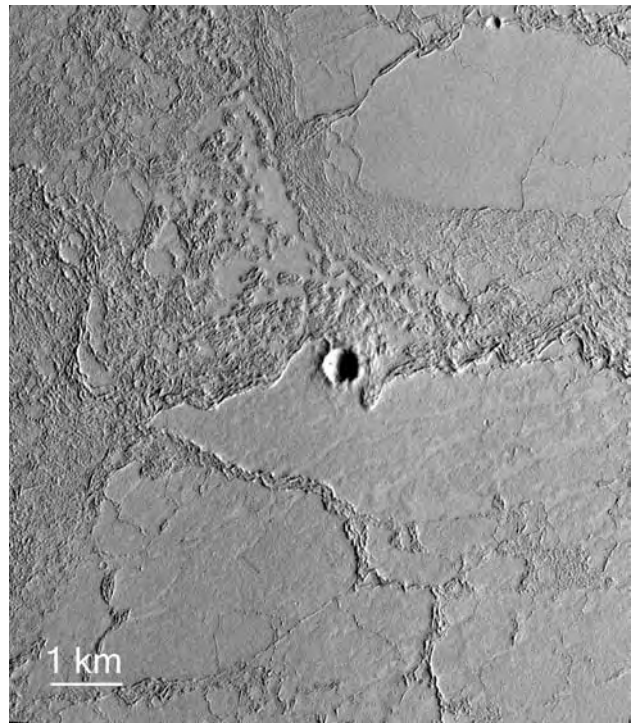

Figure 3.27. Flows in Amazonis at 25.7°N, 193°E. Lava likely pooled in Amazonis Planitia, which has very low slopes. The textures seen here are typical of lava that has pooled wherever there are low slopes. See Figure 3.24B (MOC SP242604).

across (Plescia, 2004). The flanks immediately around the caldera are densely channeled. Around the periphery of much of the volcano is a cliff, which suggests that the volcano was formerly more extensive than at present and that part of the outer margin has been removed by tectonic or erosional processes. Materials erupted from a vent on the southeast flank have formed an extensive apron that buries part of the adjacent edifice. On the apron is a fan-shaped array of ridges, but unlike on the aprons of the Tharsis shields, individual flows are difficult to see in any of the available imaging. An extensive airfall deposit, the Medusae Fossae Formation, covers much of the plains–upland boundary in this region. It partly buries the eastern part of the apron and northern flank of the volcano. Deposits within the caldera may also be of this material. The channeled flanks and eroded outer margin suggest that pyroclastic eruptions played a prominent role in the formation of the volcano.

Hellas–Hesperia

The several volcanoes in the Hellas–Hesperia region look very different from those in Tharsis and Elysium (Crown and Greeley, 1993; Plescia, 2004). All have low relief and a large central caldera; most are surrounded by ridged and furrowed terrain. Hadriaca Patera (30.1°S, 92.5°E), on the northeast rim of Hellas, is 275 km across in the east–west direction and 550 km in the north–south direction down the regional slope toward Hellas (Figure 3.30). The large channel complex of Dao and Niger Valles cuts into its southwest flank. The summit caldera is 90 km across and 700 m deep. Its height above the surrounding terrain is difficult to assess because of the regional slope into which it is set, but Crown and Greeley (1993) estimated it to be 1 km high as measured in the east–west direction, across the regional slope. The slopes are less than 1°. The most characteristic feature of the volcano is its flanks, which consist of radial, sharp-crested ridges with V-shaped valleys between. Layering is visible in some of the valley walls, and some of the valleys contain a small channel. Close to the caldera, the ridges are covered with an etched deposit, and remnants of this deposit can be seen on

Figure 3.28. Lava flow in Marte Vallis at 19.2°N, 185.4°E. Marte Vallis, a water-worn valley connecting the Cerberus plains with Amazonis Planitia, is in places occupied by younger lava flows (MOC SP240703).

the ridges well away from the caldera (Figure 3.31). It is clear that the deposit is easily erodible, was formerly more extensive, and has been mostly removed.

In Malea Planum (Figure 3.32) on the southern rim of the Hellas basin are two shallow, circular, caldera-like structures, Amphitrites Patera (59.0°S, 61.1°E), 121 km in diameter, and Pineus Patera (58.1°S, 52.5°E), 130 km in diameter. Amphitrites has radial ridges similar to those at Hadriaca, but smoother and less well pronounced. Pineus Patera, although having a well-defined caldera, has poorly developed radial structures, if any. The main structures in the vicinity are mare ridges, which are common throughout Malea Planum. Clearly identifiable volcanic features other than the calderas themselves are rare around both features. As is common at high latitudes, deposits, possibly of recent origin, mantle much of the surface and may be obscuring the fine-scale volcanic features. To the southwest of the Amphitrites and Pineus Paterae are two wide, shallow, circular depressions, roughly 300 km across and 1 km deep, one at 63.3°S, 52.0°E, the other at 67.3°S, 37.6°E. These may be calderas, although they are poorly defined and there is no evidence of extrusive activity associated with them other than the ridged plains in which they occur.

Tyrrhena Patera (22°S, 107°E), in Tyrrhena Planum, 900 km northeast of Hadriaca Patera, is possibly the most complex volcano on the planet (Figure 3.33). At the center of the structure is a 40 km diameter, 400 m deep depression that stands at 1.5 km above the surrounding plain. Around the structure at various radial distances are circumferential fractures that typically subtend arcs of only a few tens of degrees. The farthest out that the circumferential fabric can be discerned is 180 km from the center. Several large, flat-floored channels extend radially away from the volcano center. The largest, to the southwest, is 4 km across and 170 km long. The volcano appears to consist of horizontally bedded materials that have been eroded back to form radially elongate, flat-topped ridges, each outlined by a steep, irregular escarpment with deep indentations. The escarpments give the outer margins of the volcano an etched appearance.

The scarcity of lava flows, the low relief, and the seemingly easily erodible nature of the materials around Tyrrhena Patera strongly suggest that it is built largely of ash. Greeley and Crown (1990) argue that the volcano was built by gravity-driven ash flows generated either by magmatic explosive activity or hydromagmatic activity. The case for ash flows is less strong for the other volcanoes around Hellas. The ridges radial to Hadriaca Patera could, for example, be analogous to the radial, tube-fed flows on Alba Patera. However, the presence of extensive etched deposits close to the rim and remnants further out supports pyroclastic activity at Hadriaca, at least in the late stages. All these volcanoes are Noachian in age. Interaction of magma with groundwater is consistent with the evidence for warmer climatic conditions on early Mars that led to widespread fluvial erosion, and with evidence of extensive hydrous alteration of volcanic rocks at Gusev (Squyres *et al.*, 2006). The very different style of volcanoes around Hellas, as

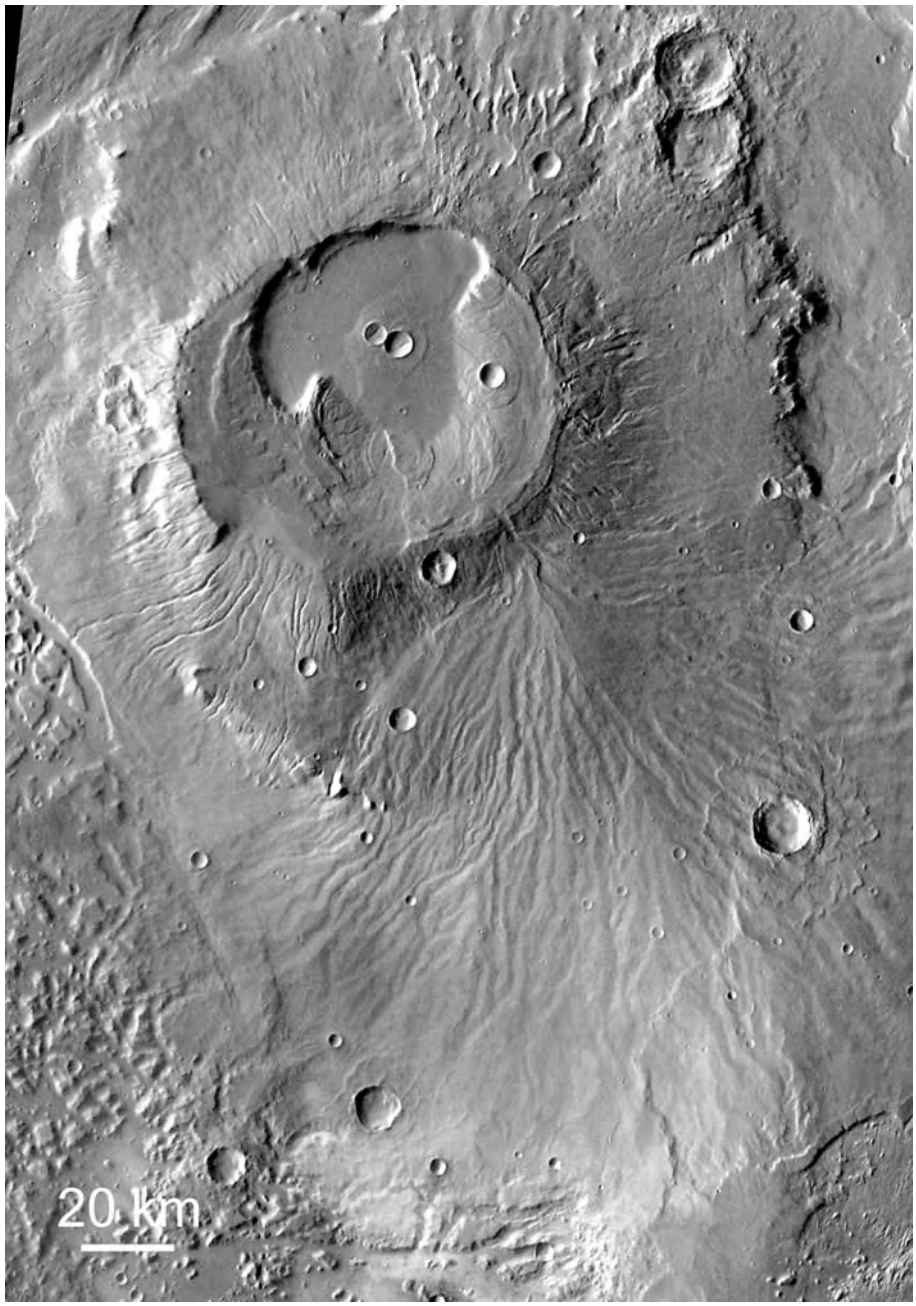

Figure 3.29. Appolinaris Patera at 8°S, 174°E. This volcano has an 80 km diameter central caldera. Around much of its circumference is a cliff, which suggests that the volcano may have been larger at one time. Narrow valleys are incised into the flanks just outside the caldera, except to the south where flows have built a ridged apron that cuts across valleys on the main shield. The number of impact craters indicates an old age (THEMIS mosaic).

compared with most of those in Tharsis and Elysium, may thus be another manifestation of changing surface conditions at the end of the Noachian.

Plains volcanism

The volcanic plains of Mars can be divided into two broad categories: those on which volcanic features are common and wrinkle ridges are rare, and those on which volcanic features are rare and wrinkle ridges are common. Plains with abundant flow features are mainly close to the center of the volcanic provinces of Tharsis and Elysium. Thus, all the plains between the volcanoes on the northwest side of the center of the Tharsis bulge are flow plains. On the southeast side

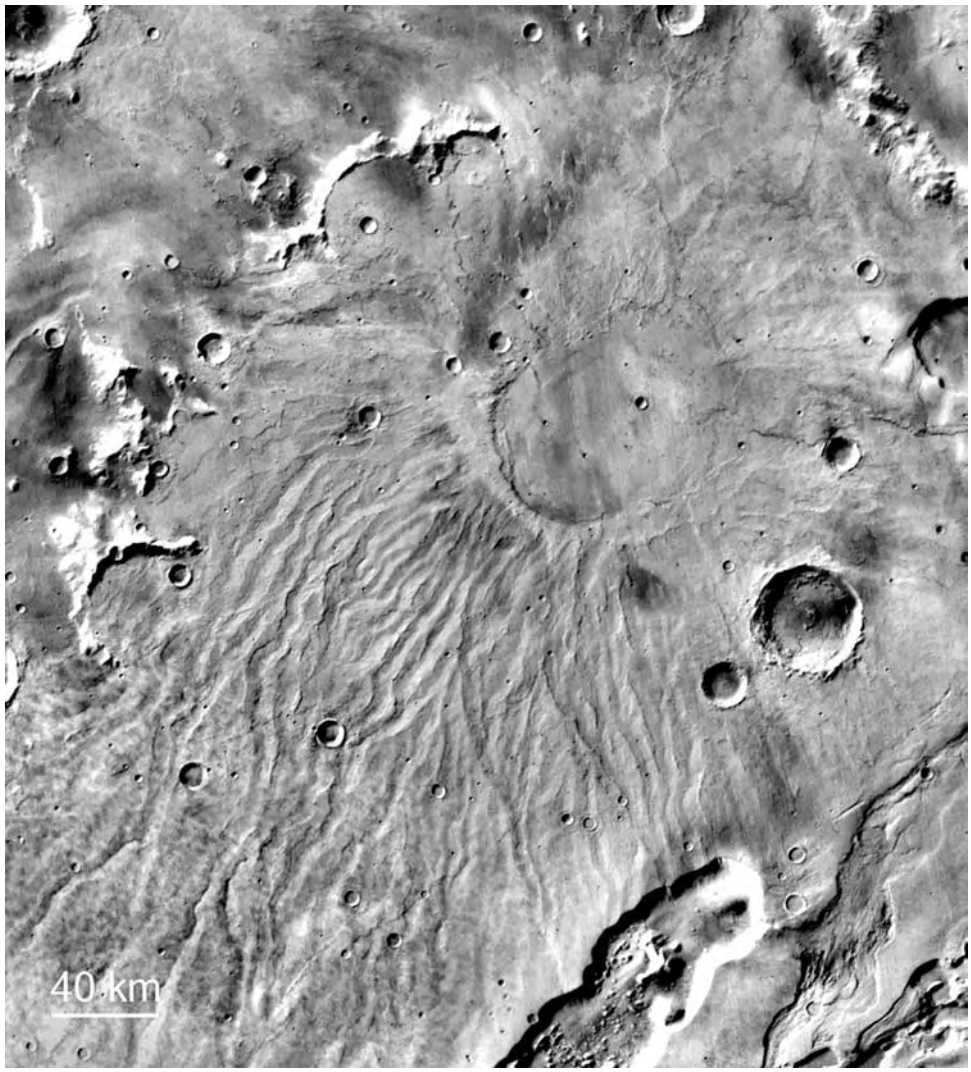

Figure 3.30. Hadriaca Patera at 30°S, 93°E. A shallow central caldera is surrounded by a low edifice marked by radial ridges. The Dao and Niger Valles cut across the periphery of the volcano in the lower right corner of the image. The area has a regional slope to the southwest (MOC WA).

of the bulge, in Syria Planum, flows can be traced 1500 km to the southeast of the center of the bulge before they transition into ridged plains. The situation is similar in Elysium. Within 1000 km of the center of the province the plains are mostly flow plains, beyond that they are ridged plains. On most of the flow plains, two different kinds of flows can be distinguished, sheet flows and tube-fed flows. A third type of flow, comprised of platey materials, occurs only in Cerberus and Amazonis.

Ridged plains occur throughout the north polar basin, Chryse Planitia, Isidis Planitia, Syrtis Major Planum, Lunae Planum, Hesperia Planum, Malea Planum, parts of the Hellas basin, in numerous local lows between craters in the southern highlands, and in many of the larger craters. They cover roughly 30 percent of the planet. Wrinkle ridges are typically 5–10 km across and a few tens of meters high. They are commonly asymmetric with a sharp sinuous contact with the undeformed plains on one side and merging with the plains on the other side. Most are compound, having narrower ridges superimposed on the broad arch. Wrinkle ridges are common on the lunar maria, so are often called mare ridges. They are deformational features that result from compression (Plescia and Golombek, 1986; Golombek *et al*., 2001). The ridged plains are thought to have been emplaced largely by effusive fissure eruptions, but in most locations flows that would support a volcanic origin are rare. The ridges, being deformational features,

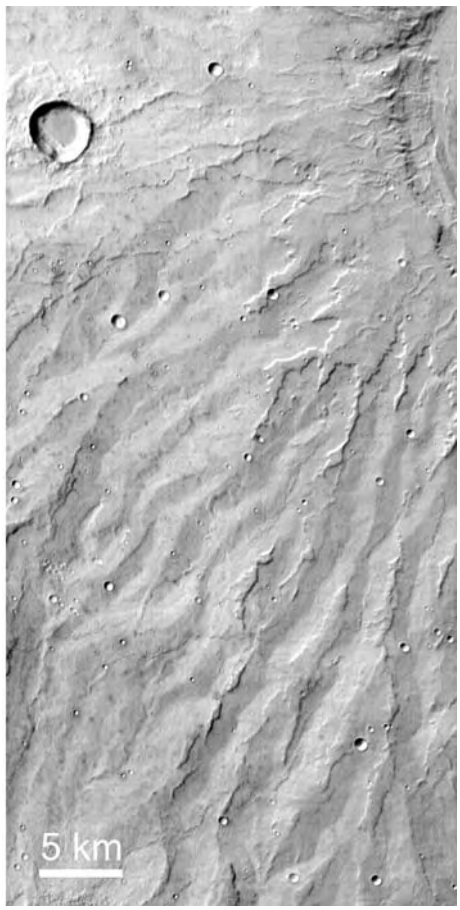

Figure 3.31. Detail of the flanks of Hadriaca Patera. An etched deposit can be seen close to the caldera in the upper right and in isolated patches elsewhere (THEMIS mosaic).

do not in themselves indicate volcanism. In addition, although the ridged plains may be volcanic, they may be covered with a veneer of other material, through which the ridges can still be seen. This is likely true of much of the northern plains (Kreslavsky and Head, 2002) and many local plains within the highlands. Almost all the ridged plains are lower Hesperian in age in contrast to the mostly Amazonian age of the flow plains. The volcanic nature of the ridged plains is supported by analogy with the Moon, what sparse spectral data we have on them (Bandfield *et al.*, 2000; Bibring *et al.*, 2005), and by the volcanic rocks found at the Viking 1 and Pathfinder landing sites on the ridged plains of Chryse Planitia, and at the Spirit landing site on the ridged plains in Gusev crater. It appears that volcanic plains were emplaced extensively in the lower Hesperian, and were subsequently deformed by wrinkle ridges. Lava flows emplaced later in the Hesperian and Amazonian are largely undeformed by wrinkle ridges.

The typical ridged plain, such as Lunae Planum, is almost featureless except for the ridges and superimposed impact craters. At the MOC scale they have a finely speckled look, possibly the result of fine-grained material filling the lows in a rough surface. Two ridged plains that look different from the others are Syrtis Major Planum and Isidis Planitia (Figure 3.34). These are two adjacent similar-sized ridged plains. Volcanic processes have played a major role in the formation of both plains, but the results are very different. In the center of Syrtis Major is an elliptical depression, which includes two calderas, Nili Patera and Meroe Patera, both 70 km in diameter. Arrayed around the depression are numerous ridges that are mostly radial in the northern half of the plain and more random in the south. Slopes over most of the plain are very low ($\ll 1°$), but along the eastern margin the slopes dip more steeply ($\sim 1°$) into Isidis Planitia, which is over 4 km lower in elevation. On the steeper slopes between the two planitiae are prominent tube-fed flows, that is, ridges with discontinuous summit channels. At the base of the slope, in Isidis, the volcanic flows appear to break up into discontinuous blocks. Ivanov and Head (2003) ascribe the break-up to interaction of the young lava flows from Syrtis Major with volatile-rich materials on the floor of Isidis Planitia.

Isidis Planitia itself is characterized by numerous cratered domes a few hundred meters across, and commonly arrayed in lines (Figure 3.35). Similar domes, found in the northern plains, have been described as pseudocraters (Frey, 1979), craters that form when lava flows over a water- or ice-rich substrate (e.g. Greeley and Fagents, 2001). However, how the cratered domes formed in Isidis is unclear. There may have been, at one time, volatile-rich materials at the surface. The surface textures within Isidis resemble those of the Vastitas Borealis Formation, which occurs extensively over the northern plains (Scott and Tanaka, 1986; Greeley and Guest, 1987). The formation may be a water-rich deposit from the large floods thought to have created the northern ocean (Chapter 7). The materials at the surface in Isidis Planitia may also be a part of the Vastitas Borealis Formation. Typically, pseudocraters form where lava flows over a volatile-rich deposit, but there is little evidence in Isidis Planitia of lavas at the surface, other than those along the western margin that flowed in from Syrtis Major Planum, so evidence that the cones in Isidis are the result of lava flowing over a volatile-rich substrate is weak. Another possibility, supported by the alignment of the cones, is that they result from injection of dikes (and sills) and the only expression of the volcanism at the surface is the presence of the cones themselves.

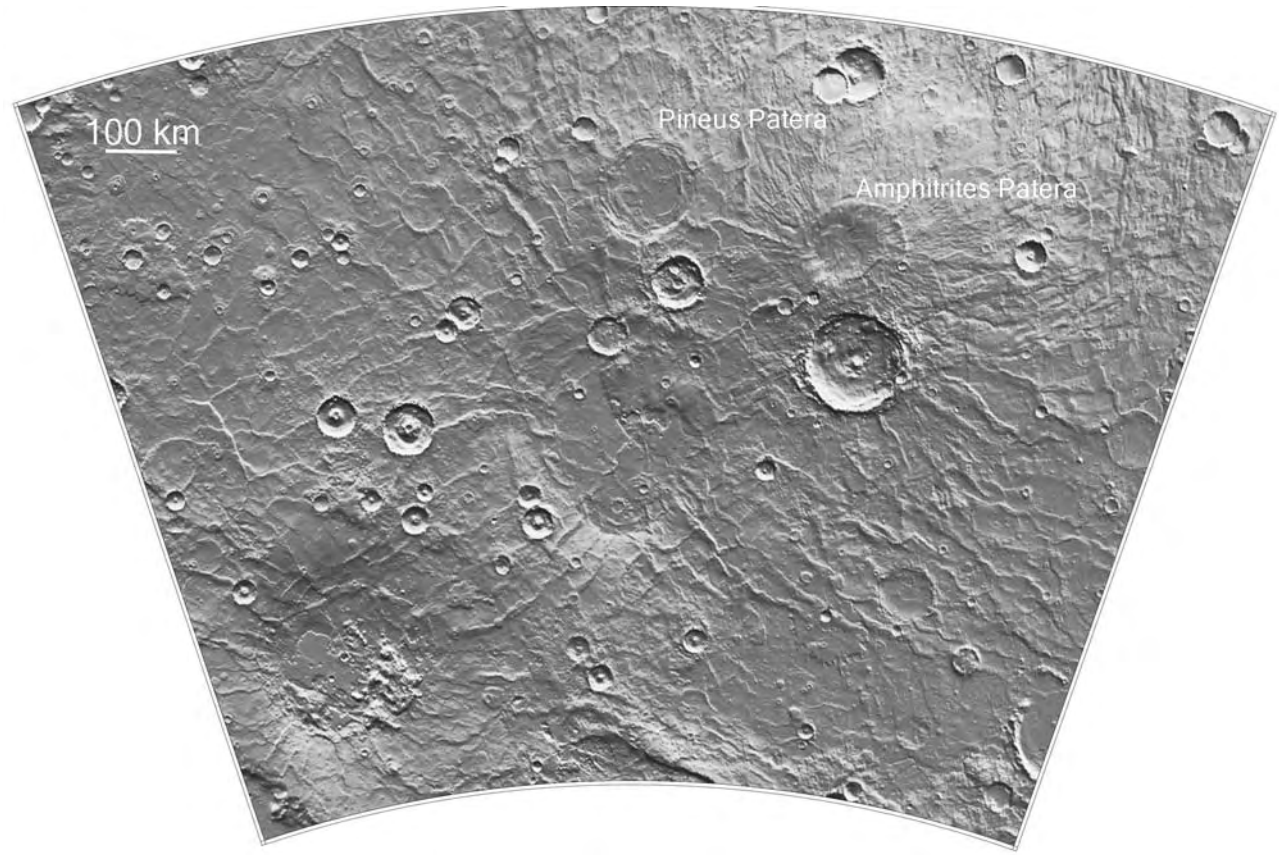

Figure 3.32. Volcanic features on the southern rim of the Hellas basin. The area shown is from 53°S to 70°S and 30°E to 75°E. The ground slopes to the north into the Hellas basin. The two named volcanoes both have shallow calderas. Around Amphitrites are numerous radial ridges, some identifiable as flows, but there is little indication of any constructional features around Pineus Patera. To the southwest of these two volcanoes are two larger vague circular depressions that could be volcanic (MOLA).

Volcano–ice interactions

We have seen that Mars has had a long and still continuing history of volcanic activity. Greeley and Schneid (1991) estimated that since the end of the Noachian the equivalent of 0.4 km of volcanics have been erupted onto the surface and another 3 km may have been intruded into the near-surface. We suspect that Mars has a kilometers-thick cryosphere in which ice is common, and that water has periodically erupted onto the surface and frozen (Chapters 1, 6). Volcano–ice interactions should, therefore, have been common, but whether such interactions have produced any distinctive landforms is unclear. We have mentioned in several places the possibility that injection of dikes into the ice-laden cryosphere would have resulted in explosive activity and the production of large amounts of ash and steam. Such eruptions could have produced ash-rich edifices of various sizes and shapes depending on the scale and conditions of the eruptions, but discriminating such edifices from those produced simply by exsolution of magmatic gases may not be possible.

Some martian landforms have been interpreted as analogs of terrestrial tuyas or table mountains (Allen, 1979; Hodges and Moore, 1979; Chapman, 2002; Head and Wilson, 2002), which in Iceland and Antarctica commonly result from eruptions under ice. Formation of a table mountain is a three-stage process. First, intrusions under the ice form pillow lavas on the floor of a subglacial lake formed by melting of the ice. Second, water enters the vent causing explosive activity and the building of an underwater edifice of pillow lava fragments, tephra, and glass. Third, when the edifice reaches the level of the lake's surface, less water gets into the vent and subaerial eruptions form flows at the surface. The result is a flat-topped mountain of fragmental debris, with a central vent and capped by lava flows. Moberg ridges form similarly but from fissure eruptions.

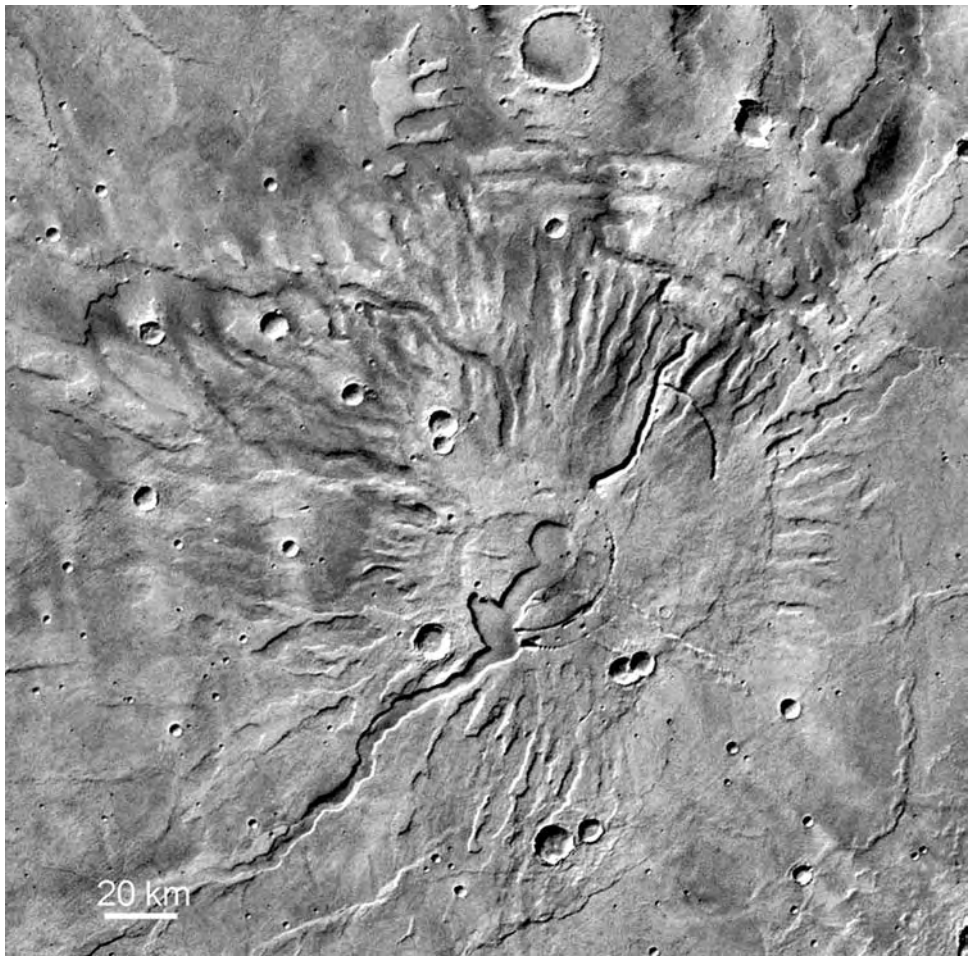

Figure 3.33. Tyrrhena Patera at 22°S, 107°E. The volcano has a 40 km diameter caldera at its center from which radiate numerous flat-floored valleys and flat-topped ridges. The volcano is thought to consist mainly of horizontally bedded ash deposits (MOC WA).

How common such mountains and ridges are on Mars is unclear. Chapman and Tanaka (2001) interpret the thick, layered deposits within the canyon as the result of subaqueous or sub-ice volcanism, but the fine, rhythmic layering of the deposits (Malin and Edgett, 2001) and the finding of sulfates within them (Gendrin *et al.*, 2005) makes this now seem less likely. Flat-topped hills with central depressions are common in the northern plains. Many have been interpreted as table mountains, but as described in the previous chapter, erosion of impact craters in the northern plains commonly leads to formation of flat-topped hills, or cones with central depressions that resemble table mountains or stratocones. Commonly, the impact origin is unambiguous because the textures of the ejecta are preserved on the surface, but the smaller the crater, the more difficult it is to discern the ejecta. So, while the numerous small table mountains and cratered domes common in the northern plains could be the result of volcanism, an impact origin seems more likely.

Other possible examples of volcano–ice interactions are the Cavi Angusti near the south pole (Ghatan *et al.*, 2003). These are irregular pits, up to tens of kilometers across and 1.5 km deep in the Dorsa Argentea Formation, which is interpreted to be a sequence of volatile-rich sediments. Lava-flow-like structures, and other features within the pits, suggest that volcanic intrusions and extrusions caused melting of the ice-rich sediments and formation of the pits.

Summary

The tectonic framework within which martian volcanism occurs is very different from that of most terrestrial volcanism because of the lack of plate tectonics on Mars. Most martian volcanism is basaltic.

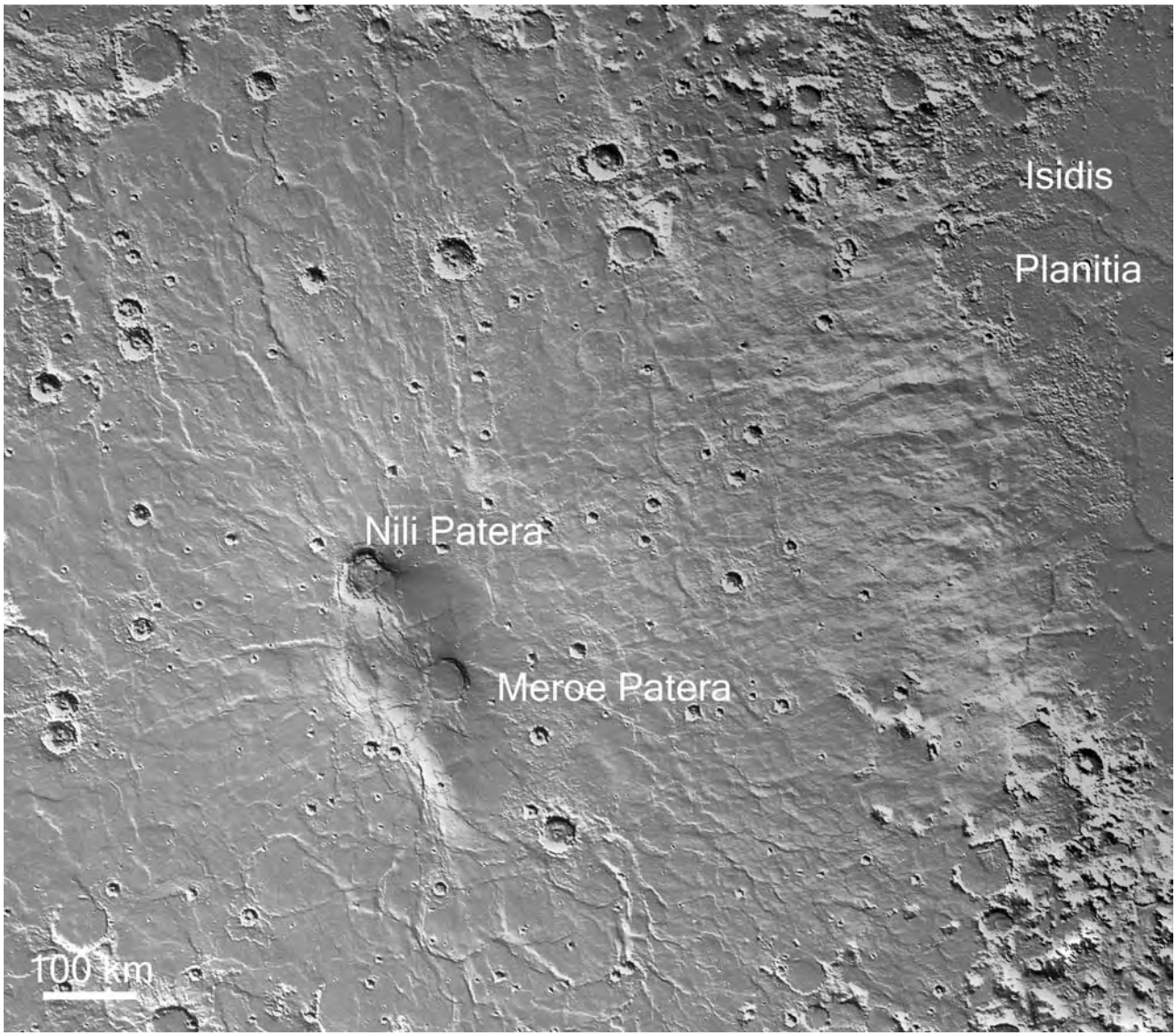

Figure 3.34. The ridged plains of Syrtis Major Planum centered at 10°N, 70°E. In the center of the plain is an elongate depression containing two caldera-like structures. The plain stands at an elevation of 4 km above Isidis Planitia to the east. Sheet flows and tube-fed flows can be seen where lava from Syrtis Major flowed down the slope between the two plains on the right-hand side of the image (MOLA).

Basaltic volcanism expresses itself somewhat differently on Mars because of the lower gravity and lower atmospheric pressure. Eruptions are expected to be larger and less frequent, more likely to produce ash, and ash clouds are more likely to collapse and produce pyroclastic flows. By the end of the Noachian, the Tharsis bulge, a volcanic pile 5000 km across and 10 km high, had been largely built. Volcanic activity continued in Tharsis, probably to the present day, building several enormous shield volcanoes, as a result of numerous, voluminous eruptions spaced widely in time. The present Olympus Mons edifice is at least 100 times larger than the largest volcano on Earth. It was formerly more extensive than at present but its outer flanks have collapsed, forming giant gravity flows, and leaving the edifice surrounded by a cliff several kilometers high. Alba Patera, while 2000–3000 km across, is only a few kilometers high. It may have been built largely by ash, although much of its present surface is covered with sheet flows and tube-fed flows. Other smaller volcanoes in Tharsis are densely channeled, suggesting that they are composed of easily erodible ash. Some small Tharsis shield volcanoes with large summit calderas may be the

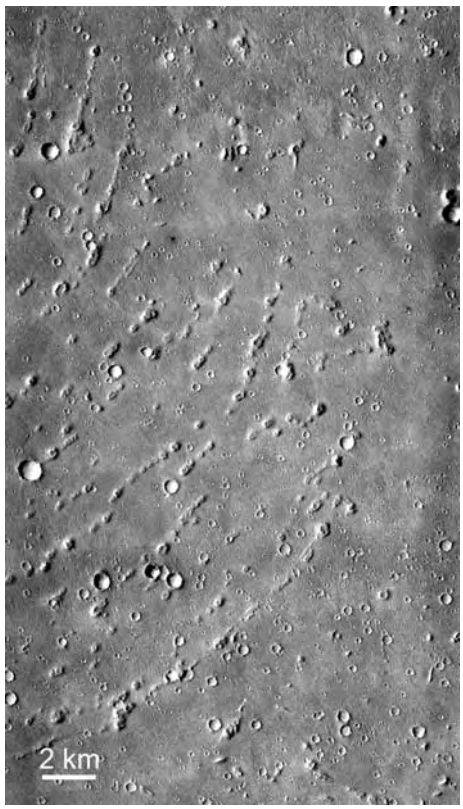

Figure 3.35. Typical Isidis plains at 15.1°N, 91.6°E. When viewed at low resolution Isidis Planitia resembles a typical ridged plain. However, when viewed at higher resolution it appears very different. Over almost all of Isidis Planitia are low, cratered cones, a few hundred meters across, such as we see here. They could be some form of rootless cone, caused by interaction of water and lava. They could alternatively be pingos, cones that form by squeeze-up of lake sediments when a lake freezes. Their origin remains obscure (THEMIS V02718003).

tops of much larger volcanoes now almost completely buried. Elysium, the second largest volcanic province, has only three shields. The most striking characteristic of the province is the presence of large channels that emerge from graben northwest of the volcanic center. The channels are thought to result from release of groundwater and melting of ground ice by injection of dikes. Collapse of the water-saturated, steep graben walls may have produced lahars or mudflows. In the center of the Elysium province, most of the surface is covered with sheet flows and tube-fed flows. 2000 km to the southeast of Elysium are the almost level, low-lying Cerberus plains. Lava erupted from the nearby Cerberus Fossae appears to have pooled in these plains. They have a surface texture that suggests that lava crusted over, and then the crust was pulled apart to form rafts. Similar textures are also seen in the low-lying, level plains of Amazonis Planitia. The volcanoes around Hellas are very different from those in Tharsis and Elysium. They are older, and most have a large central caldera and very gently sloping flanks that appear to be formed of easily erodible materials, such as ash. Lava plains cover most of the northern hemisphere. There are three kinds of plains: flow plains, on which flows are visible; ridged plains, on which flows are rarely visible; and the platey plains, described above and found only in Cerberus and Amazonis. Ridged plains are also found throughout the southern highlands, both in intercrater areas and within large craters. The ridged plains appear to have formed almost entirely in the lower Hesperian, whereas plains composed of lava flows continued to form for the rest of the planet's history. Very young crater ages, especially in Cerberus and Amazonis, and young crystallization ages of martian meteorites suggest that volcanism is continuing today.

The discussion in this chapter has focused on the major volcanic features of the planet. Many small shield-like structures within the volcanic plains, such as those close to the summit of the Tharsis bulge, were barely discussed. Ancient volcanic constructs within the uplands (Hodges and Moore, 1994; Stewart and Head, 2001) and many structures of unknown origin, but which may have involved volcanism in their formation, were ignored. In addition, morphological evidence for volcanic activity that the planet experienced before the end of the Noachian has been mostly destroyed so could not be discussed. As a consequence, the volcanic history of the planet is almost certainly more complex than portrayed and much of the volcanic activity took place before the geological record emerged around 3.8 Gyr ago.

4 Global structure and tectonics

Recent work on martian meteorites and recent acquisition of high-resolution global topography and gravity enables more constrained models to be made of Mars' internal structure and evolution than was formerly possible. The isotopic data from meteorites demonstrates unambiguously that Mars formed and differentiated into core, mantle, and crust in a remarkably short period of time, just a few tens of millions of years after the formation of the Solar System. The recent discovery of large magnetic anomalies in old terrains suggests also that for the first 0.7 Gyr the core was convecting and producing a strong magnetic field. In addition, the global dichotomy and Tharsis both appear to have formed during the same period. Thus, the first 0.7 Gyr of the planet's history, through the pre-Noachian until roughly the end of the Noachian, was one of rapid change.

The first part of this chapter concerns these early events. The evidence for the timing of global differentiation is summarized, and the global dichotomy is described, as is evidence for the early formation of Tharsis. The global north–south dichotomy is expressed in three ways: as a difference in elevation (high in the south, low in the north), as a difference in crustal thickness (thick in the south, thin in the north), and as a change in crater density (high in the south, low in the north). Its cause remains controversial. Tharsis appears to be a massive pile of volcanics that has loaded the lithosphere, causing it to flex on a global scale, thereby creating a shallow moat around the rise and causing formation of an array of deformational features that cover almost the entire western hemisphere. The bending of the lithosphere under different loads, as deduced from the relations between gravity and topography, also allows estimates to be made of lithosphere thickness. By examining different-aged features, the change in lithosphere thickness with time, and hence the heat flow, can be estimated. The second half of the chapter mostly concerns the deformational features that are observed. These are described and their distribution compared with those predicted by models of the stress fields created by surface loads, mainly that of Tharsis.

Much of the discussion in the chapter is based on detailed geophysical modeling. These models are complex and only cursorily described. All the models must make simplifying assumptions about parameters such as the density and rheological properties of the crust and mantle, and crustal thickness. The results should therefore be viewed with some skepticism. The sophistication of the techniques is no guarantee of the validity of the results.

Formation of the core

Like the Earth, Mars is differentiated into a core, mantle, and crust. The core is iron-rich, the mantle probably approximates that of chondritic meteorites from which the planet formed, and the crust is essentially a melt extract from the mantle. The Earth's core is inferred to be iron-rich from the composition of meteorites, from the core's density as deduced from the core size and the planet's moment of inertia, and from the depletion of siderophile elements in mantle-derived rocks, as compared with chondritic meteorites. (Siderophile elements preferentially dissolve in iron-rich melts rather than in co-existing silicate melts. The Earth's core formed early in the planet's history by gravitational separation of iron-rich liquids from a silicate matrix so that when the core formed, the siderophile elements preferentially entered the core and left the mantle depleted with respect to a chondritic composition.) By the same reasoning, Mars also has an iron-rich core, except that, because we have no seismic data to directly measure its size, it must be inferred from the moment of inertia of the planet and the planet's mean density (Folkner *et al.*, 1997; Stevenson, 2001). The errors are large because of uncertainties in the mantle and core temperatures and compositions, particularly the amount of sulfur present in the core. The best estimate is that the core radius is between 1300 and 1500 km (Stevenson, 2001).

The timing of the events that led to accumulation of Mars and formation of its core can be determined with considerable accuracy and precision. It formed within a few tens of millions of years of formation of the elements from which the Solar System formed. The evidence is survival of products of the

decay of short-lived isotopes, as inferred from isotope patterns in martian meteorites. ^{182}Hf decays to ^{182}W with a half-life of 9 Myr. W is a siderophile element, so would have preferentially entered the core when it formed, leaving the mantle depleted in W. Hf is not a siderophile element. Thus, if the core formed before all the ^{182}Hf had decayed, then we should expect to find an excess of ^{182}W in the mantle, and hence in the mantle-derived rocks of which we have samples in the martian meteorites. This, in fact, is what is found. The ratio of ^{182}W to other W isotopes is higher in martian meteorites than in the chondritic material from which the planet formed, so that there was still some ^{182}Hf present in the mantle after the core formed. For enough to have been present and leave a detectable signal, the core must have formed within roughly 20 Myr after the formation of the Ca–Al-rich inclusions found in carbonaceous chondrules (Kleine *et al.*, 2002), which, with an age of 4.567 Gyr, are the oldest materials in the Solar System, predating chondrules by 1–2 Myr (Amelin *et al.*, 2002). Thus, the core had likely formed by 4.54 Gyr ago. The 4.5 Gyr age of the martian meteorite ALH84001 (Nyquist *et al.*, 2001) indicates that some crust had also formed by this time. In addition, separation of a crust would fractionate Sm and Nd. The Nd isotopics indicate that some short-lived ^{146}Sm, which decays to ^{142}Nd, was still present at the time that the early crust formed, indicating that at least some crust formed within 30 Myr of planet formation. Early crust formation is also consistent with isotope systematics of Pb, Sr, and Os (Chen and Wasserburg, 1986; Borg *et al.*, 2003). It appears that accretion of the planet and differentiation to form the core and at least some of the crust, and possibly a large fraction, were both accomplished within a rather short period of time. The short accretion time likely resulted in massive heating and melting to form a global magma ocean, thereby facilitating early segregation of the core and crust.

One of the more surprising results of the Mars Global Surveyor mission was the discovery of large magnetic anomalies in the crust despite the absence of a magnetic field today (Connerny *et al.*, 1999). Their presence indicates that Mars had a magnetic field in the past, but that it switched off at some time. The size of the anomalies suggests that they must result from sources in the outer few tens to several tens of kilometers of the crust and that their magnetizations are higher by an order of magnitude than magnetizations typically encountered in terrestrial rocks (Stevenson, 2001). The anomalies probably formed when rocks, containing Fe-bearing minerals, crystallized in the presence of a magnetic field. Although there are small anomalies north of the dichotomy boundary, most of the anomalies and all the largest are in the southern uplands. They are particularly prominent in Terra Cimmeria and Terra Sirenum on either side of the 180° longitude where there are several broad, east–west stripes. One interpretation of the linear anomalies is that they result from injection of dikes or dike swarms several tens of kilometers wide and hundreds of kilometers long in the presence of a strong magnetic field (Nimmo, 2000). Anomalies are mostly absent around the youngest large impact basins, Utopia, Hellas, Isidis, and Argyre. The simplest explanation is that there was no longer a magnetic field when these basins formed, formation of the basins destroyed any pre-existing anomalies, and no new ones formed when the affected materials cooled after the basin-forming events. The ages of the basins are not known, but, by analogy with the Moon, they are likely to have formed toward the end of heavy bombardment around 3.8–4 Gyr ago. Thus, the magnetic field may have turned off by around 4 Gyr ago.

The Earth's magnetic field is generated by convection within its core. Mars' early dynamo probably had a similar cause. Core formation probably released enough energy to heat the molten core, enable convection, and start a dynamo around 4.5 Gyr ago. Possible causes for cessation of the dynamo are loss of core heat, solidification of most of the core, and/or changes in the mantle convection regime (Solomon *et al.*, 2005). Magnetization of minerals within 3.9–4.1-Gyr-old carbonates in the martian meteorite ALH84001 (Weiss *et al.*, 2002) suggests that there was still a magnetic field at this time. If true, it implies that Mars had a magnetic field for the first 500 Myr of its history and that the field turned off around 4 Gyr ago, just before formation of the youngest impact basins. However, there may be an inconsistency here between the meteorite data, which indicates the presence of a magnetic field 4 Gyr ago, and the absence of anomalies around large impact basins, which suggests the absence of a field at that time.

Global dichotomy

The global dichotomy between the heavily cratered southern uplands and the sparsely cratered, low-lying northern plains is a fundamental feature of the planet that must have also formed during the first 500 Myr of the planet's history. The boundary between the two provinces is expressed in at least three ways that are not everywhere coincident: first as a change in elevation, second as a change in crater density,

and third as a change in crustal thickness. The contact is transitional in most places, but its surface expression can readily be traced all the way around the planet except through Tharsis, where it is buried beneath younger volcanic deposits (Figure 4.1).

The dichotomy is very evident in the global hypsometry (Aharonson *et al.*, 2001). The planet's surface elevations have a strongly bimodal distribution with a peak at −4 km representing the dominant elevations of the northern plains and another peak at 1.5 km representing the dominant elevations of the southern uplands. Thus, on average, the southern uplands are 5.5 km higher than the northern plains, and the average pole-to-pole tilt is 0.036° to the north.

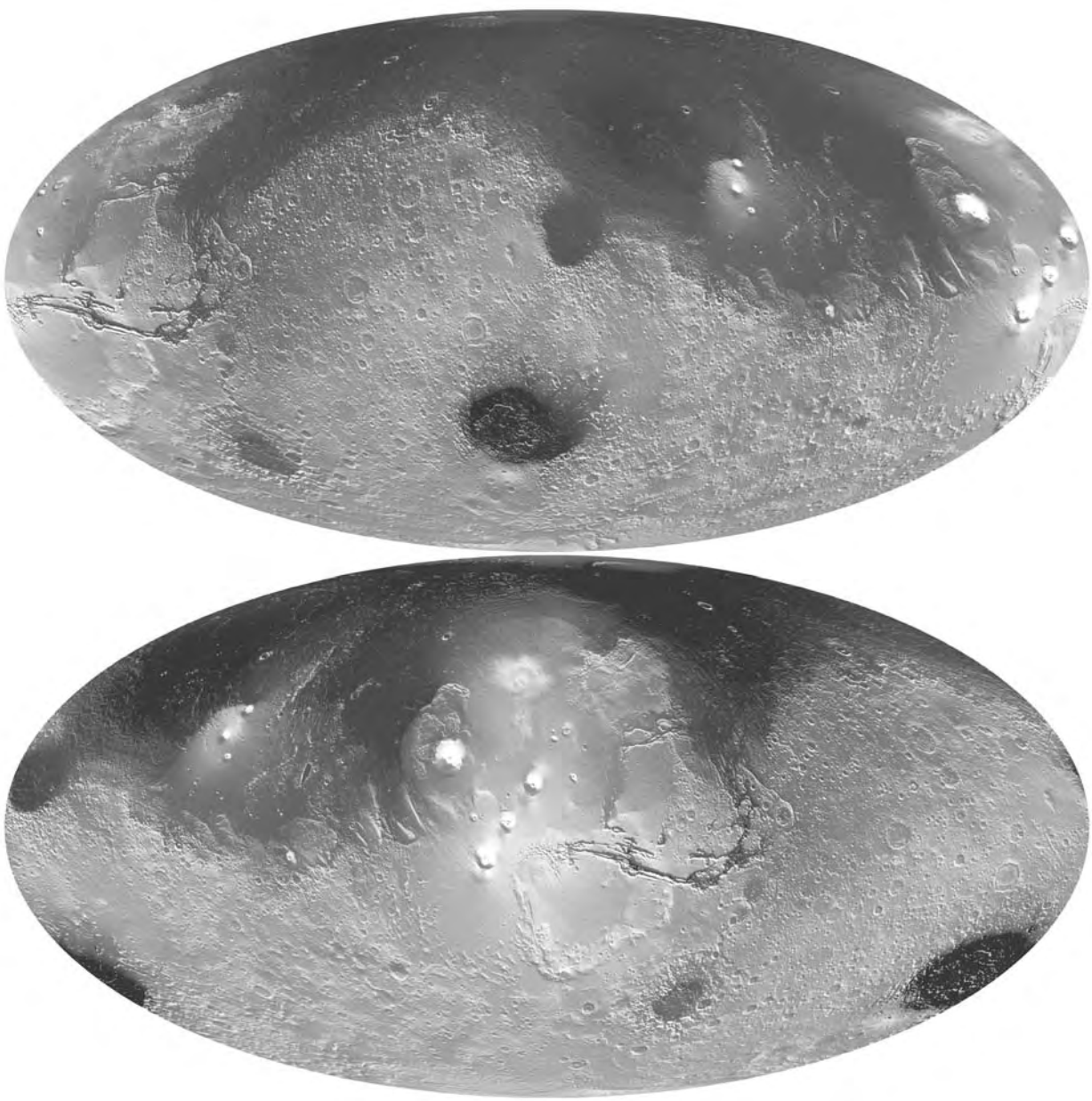

Figure 4.1. The global dichotomy. The upper view is centered on 80°E, antipodal to Tharsis. The dichotomy boundary is seen here expressed in two ways, as an elevation difference (dark vs. light) and as a difference in crater density. The lower view, centered on Tharsis at 260°E, shows the position of Tharsis astride the dichotomy boundary (MOLA).

The elevation difference between the two hemispheres offsets the planet's center of figure from its center of mass by 2.986 km as measured along the polar axis (Smith *et al.*, 1999b). The abruptness of the change from typical upland elevations to typical lowland elevations varies considerably across the boundary. In northwest Arabia, the elevation transition from uplands to plains is very gentle with elevations falling 4 km over a distance of 2500 km to give a regional slope of only 0.0016°. In contrast, around Isidis, the same elevation drop is achieved over a distance of 250 km. In most areas the drop in elevation takes place over several hundred kilometers (Figure 4.2), even though the boundary may appear abrupt in the imaging. In Tempe Terra, for example, the geomorphic boundary is very sharp and expressed as an escarpment a few hundred meters high (Figure 4.3), but the regional slope is quite shallow, such that surface elevations drop 2 km over a distance of 600 km. The highest elevations in the southern uplands are in a broad annulus around Hellas. Some of the steepest slopes along the dichotomy boundary are where this annulus intersects the boundary, as to the south and east of Isidis.

A second way that the boundary is expressed is as a change in crater densities. The uplands are heavily cratered whereas the lower-lying plains are sparsely cratered. This may, however, be a somewhat superficial attribute since a heavily cratered surface lies at a shallow depth below the surface of the plains. This has long been evident in certain areas such as between longitudes 160 and 190°E, where numerous low hills outline the remnants of large craters among the plains, but more recently, MOLA data has revealed the presence of numerous large circular depressions throughout the northern plains that are not evident in the imaging (Frey *et al.*, 2002b). They are presumably buried impact craters and basins. Their presence indicates that a heavily cratered Noachian, and possibly pre-Noachian, surface is almost everywhere at shallow depths below the younger plains. The contrast in crater density across the boundary thus appears to indicate merely preferential accumulation of post-Noachian deposits in the low areas north of the boundary.

The third way in which the dichotomy is expressed is as a change in crustal thickness. Zuber *et al.* (2000) and Neumann *et al.* (2004) derived crustal thicknesses from the relation between the global gravity field and the global topography. Different models can be used to make the derivation. Zuber *et al.* and Neumann *et al.* chose to assume uniform mantle and crustal densities and attempted to reproduce the planet's measured gravity field from the measured

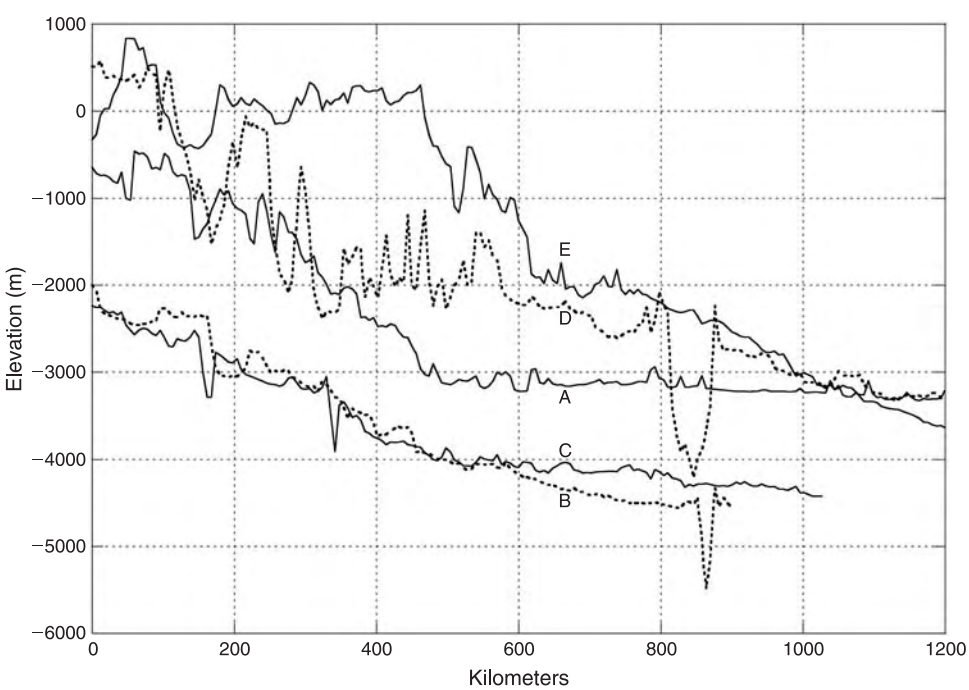

Figure 4.2. Elevation profiles across the dichotomy boundary at the five locations portrayed in Figure 4.3. Although the boundary may appear abrupt in the imaging, the elevation transition typically takes place over 1000 km.

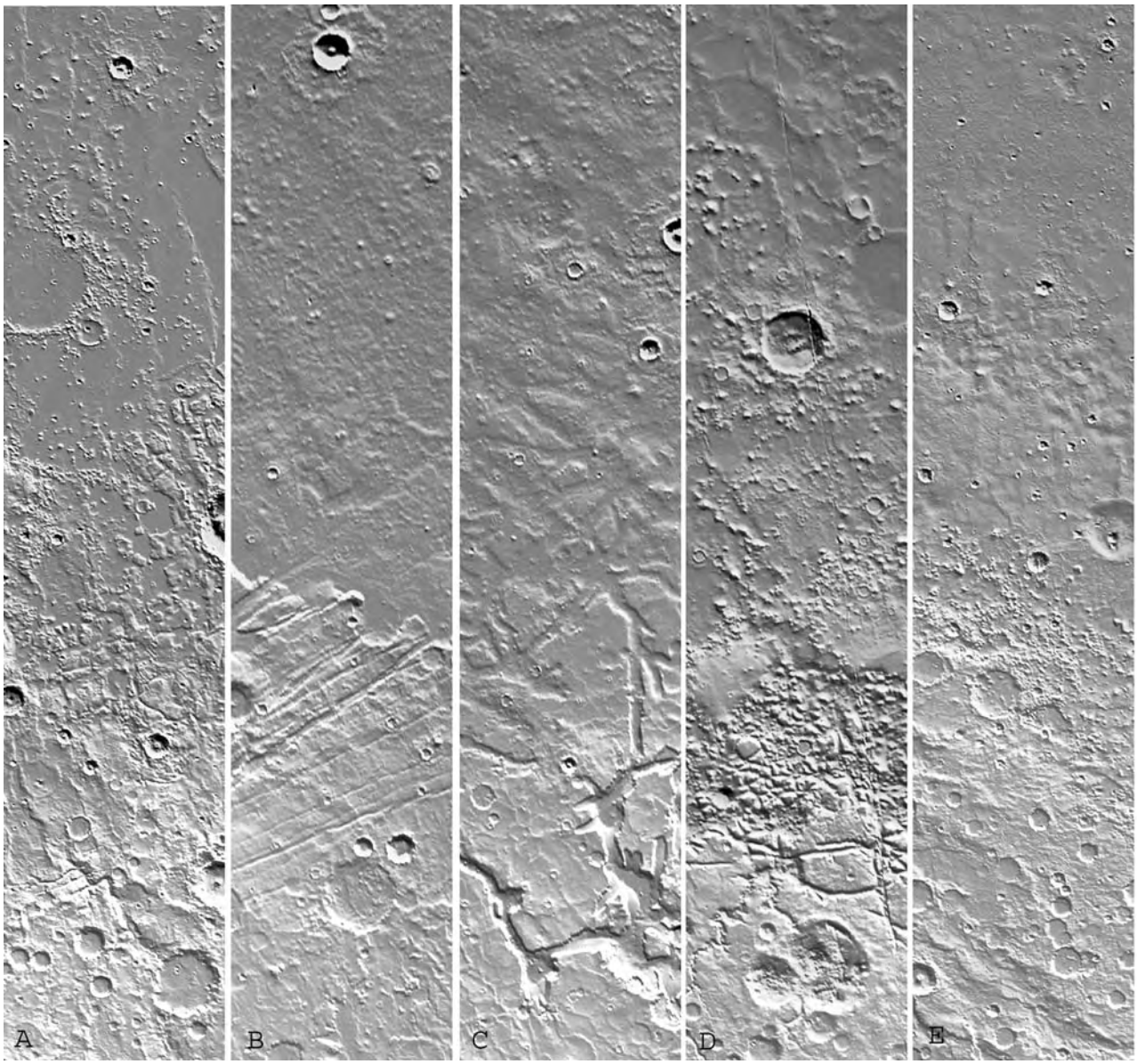

Figure 4.3. North–south strips showing the appearance of the dichotomy boundary at different locations. (A) 190–195°E at the southern boundary of Amazonis Planitia. The ground slopes steeply from the south to the center of the image then is essentially flat to the top of the image. Outlines of large craters in the plains indicate that the Noachian surface is at a shallow depth. (B) 300–305°E at the northern end of the Tempe plateau. The ground slopes gently northward across the image. The escarpment at the center is only a minor interruption of the regional slope. (C) 10–15°E in the fretted terrain of Deuteronilus. At the bottom of the image, escarpments several hundred meters high interrupt the gentle regional slope to the north. (D) 60–65°E in Nilosyrtis. The boundary here is extensively disrupted with crevasses and rubble-filled hollows 1–2 km deep (E) 110–115°E, south of Elysium. In the middle of the image a 2 km high escarpment, difficult to see, separates intact cratered uplands from the plains to the north. North of the escarpment is a low bench of unknown origin that follows the boundary through this region for roughly 2000 km (compare with Figure 8.19).

topography by varying the depth to the crust–mantle boundary. They used a crustal density of 2900 kg m^{-3} based on martian meteorites and on local correlations between gravity and topography, and a mantle density of 3500 kg m^{-3} based on martian meteorite geochemistry. An average crustal thickness must also be assumed. Neumann *et al.* chose a value of 45 km on the basis of geochemical arguments, viscous

relaxation arguments, and the necessity to maintain a finite crustal thickness where it is expected to be thin, as under Hellas. Other refinements include assumptions of non-average crustal densities for the young volcanic features in Tharsis and Elysium and for the polar layered terrains.

The Neumann *et al.* results indicate that the crust varies in thickness from 5.8 km to 102 km. In general the crust thins from south to north. The thickness is strongly bimodal with peaks at 32 km and 58 km, indicating a 26 km difference in the average crustal thickness between the northern plains and the southern highlands The thinnest crust is under the Hellas and Isidis basins, which geological evidence suggests contain a few kilometers of fill. Their assumption of an average crustal thickness of 45 km is thus consistent with the geological evidence, but a thinner average thickness would not be. The abruptness of the change in crustal thickness across the dichotomy boundary varies according to location. From 60°E to 180°E the change in crustal thickness is abrupt and is coincident with the morphological boundary between cratered uplands and plains, which roughly follows the 40 km crustal thickness contour. In northwest Arabia, however, from 330°E, eastward to 60°E, the crust thins slowly to the northwest, and much of the Noachian terrain is underlain by crust with thicknesses more typical of the northern plains than of the southern uplands. In most of the western hemisphere, changes in crustal thickness due to the dichotomy boundary cannot be discriminated from the effects of Tharsis.

The Zuber–Neumann models assume uniform crustal and mantle densities. Other models are possible. Spohn *et al.* (2001), while acknowledging the plausibility of variations in crustal thickness, point out that rather modest variations in crustal density could contribute significantly to the observed variations in the gravity field. Density variations would alleviate the necessity for large differences in crustal thickness that have to be sustained against viscous relaxation for much of the history of the planet.

The dichotomy boundary has different morphological attributes in different places. In some areas, as in southwest Chryse, the younger plains simply lap onto a largely undisturbed Noachian terrain as it slopes down under the plains. More commonly, however, the Noachian terrain is extensively disrupted and broken up into numerous closely spaced hills (Figure 4.3A, D, E). Intact cratered upland transitions into locally disrupted upland, then to massively disrupted terrain with the fragments all in contact, and then to terrain with widely spaced remnants separated by plains. The relations suggest that, before accumulation of the post-Noachian plains, much of the northern plains looked like the massively disrupted areas that we now see along the boundary. The plains with numerous closely spaced hills between 160 and 190°E may be where this disrupted surface is particularly close to the surface. In some areas, as between 100 and 130°E, a broad, sparsely cratered bench, of unknown origin, occurs between the disrupted uplands and the main body of the plains (Figure 4.3E).

Escarpments occur along some parts of the boundary; other parts of the boundary are more transitional. Escarpments are particularly common eastward of 10°E through the fretted terrain of northern Arabia to the northern rim of Isidis. Although escarpments are common, linear escarpments parallel to the boundary that might indicate fault scarps are rare. In the classic fretted terrain of northern Arabia the plateau remnants have linear outlines suggesting faulting, but scarps parallel to the boundary are not clearly dominant. Further east in the Nilosyrtis region a better case can be made for faulting along the boundary (Smrekar *et al.*, 2004), but in most areas evidence for faults parallel to the boundary is sparse.

Erosion has clearly played a role in modifying parts of the boundary, as in the fretted terrain where valleys reach deep into the uplands and erosional debris is at the base of escarpments. But erosion is clearly not the prime cause of the boundary. For erosion to occur, relief must be created. Once the relief was created, then the steeper than average slopes along some parts of the boundary probably led to enhanced erosion and possibly formation of some of the boundary escarpments by fluvial and possibly marine processes (Parker *et al.*, 1989, 1993; Craddock and Howard, 2002). Nevertheless, the effects of erosion are likely superficial.

The cause of the dichotomy remains puzzling. Wilhelms and Squyres (1984), by analogy with the South Pole–Aitken basin on the Moon, suggested that very early in the history of the planet a large impact excavated a 7700 km diameter crater, centered at 50°N, 170°E to create the northern depression. As can be seen from Figure 4.4, the proposed basin rim follows the dichotomy boundary all the way around the proposed impact point, except in Tharsis, where it is buried by younger deposits, around Chryse, which may be another impact basin (Frey and Schultz, 1988), and at the Isidis basin. Despite the good fit of the proposed basin rim to the topography, Zuber *et al.* (2000) and Neumann *et al.* (2004) expressed skepticism that the northern lowlands could be of impact origin,

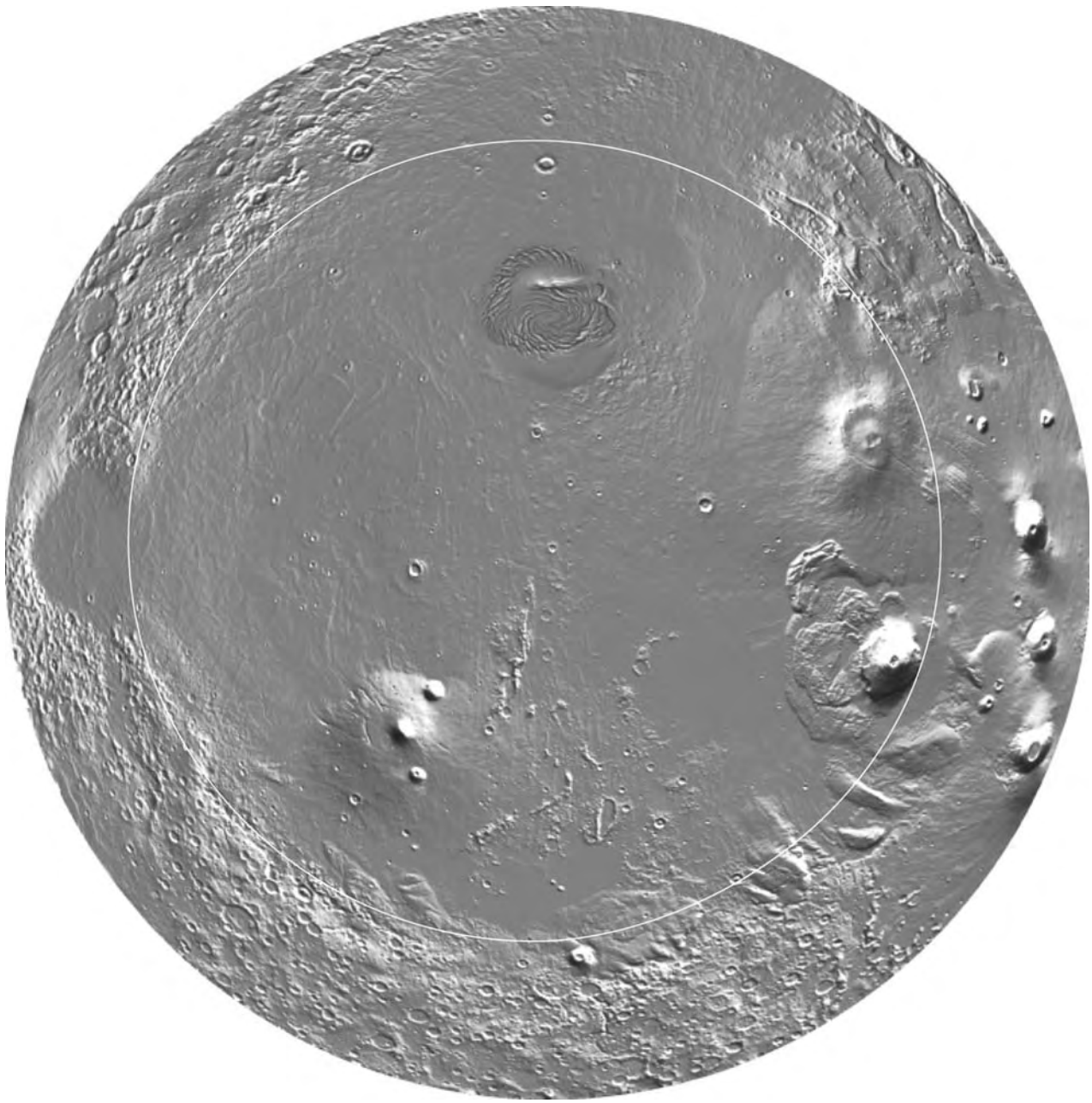

Figure 4.4. View of the Borealis impact basin proposed by Wilhelms and Squyres (1984) to explain the global dichotomy. The circle shown here is centered at 55°N, 170°E, slightly offset from the center originally proposed. The circle is a fair fit to the boundary except at the top of the image where the boundary deviates around the Chryse basin. The boundary cannot be traced through Tharsis on the right side of the image because of burial by the Tharsis volcanic pile.

pointing out that there is no thinning of the crust under the northern plains comparable to that under the younger and smaller impact basins of Isidis, Hellas, and Utopia. Massive rim deposits comparable to those around the Hellas basin are also missing. If the northern lowlands were caused by a large impact, then it must have been so early in the history of the planet that the impact signatures have been erased.

Sleep (1994) alternatively proposed that the northern plains were analogous to terrestrial ocean basins and formed as a result of generation of new crust at spreading centers. He assumed that the northern

lowlands formed after the end of the Noachian and were younger than the southern uplands. We now know that an ancient Noachian surface is at a shallow depth below the surface of the northern plains, which essentially invalidates the plate tectonic model as originally proposed. Magnetic stripes in the Mare Sirenum/Cimmerium region provide no support for the original hypothesis since they are in the upland (continental) part of the crust rather than in the lowlands (ocean basin).

A third possibility is that the dichotomy is of internal origin (Wise *et al*., 1979; Zuber *et al*., 2000; Zhong and Zuber, 2001). Crystallization of an early magma ocean may have led to gravitationally unstable mantle layering, thereby causing the mantle to overturn (Solomon *et al*., 2005). Under certain circumstances, such as presence of a very low viscosity asthenosphere, which is likely to have been met only early in the history of the planet, overturn can result in upwelling in one hemisphere and downwelling in the other. One possibility is that overturn could result in flow-induced thinning of the crust over upwellings. Alternatively, the crust could be thicker over upwellings as a result of enhanced magmatic activity. Clearly there is much uncertainly here.

In summary, most of the planet, outside Tharsis, can be divided into two provinces: sparsely cratered plains underlain by a thin crust, and heavily cratered upland underlain by a thick crust. The difference in crater density appears to be a superficial attribute, merely reflecting accumulation of post-Noachian deposits in the low-lying areas. More fundamental are the differences in elevation and crustal thickness. The cause of these differences, which appear to be inherited from very early in the planet's history, whether the result of major impact events or the consequence of internal processes, remains uncertain.

Thickness of the lithosphere

The lithosphere is the rigid outer rind of the planet that deforms elastically rather than plastically. The effective elastic thickness of the lithosphere (T_e) can be regarded as the depth to the ~650°C isotherm, beneath which the interior is too weak to support stresses over geologically long (~10^8 years) time intervals (Zuber *et al*., 2000). Prior to acquisition of MGS topography and gravity, estimates were made of the thickness of the elastic lithosphere by comparing relations between the observed gravity and topography with those predicted by models of thin elastic shells of different thicknesses deforming under topographic loads (Turcotte *et al*., 1981). A wide array of assumptions had to be made about the thickness of crust, the mantle and crust densities, and so forth. With the pre-MGS data, the spatial resolution of the gravity and topography was insufficient to discriminate regional differences, and estimates could realistically be made only of a global average. In addition, estimates were made of the lithosphere thickness under volcanoes based on the assumption that circumferential fractures around the volcanoes were located at positions of maximum lithosphere flexure (Comer *et al*., 1985).

With the much better topography and gravity from MGS, regional variations in lithosphere thickness can now be determined following procedures similar to those used by Turcotte *et al*. (1981) and McGovern *et al*. (2002), using topography and gravity up to harmonic degrees of 60, calculated admittances (the ratio of gravity to topography) as a function of harmonic degree for different-sized windows centered on different features, such as Olympus Mons. These curves were then compared with gravity/topography relations predicted by models for different lithosphere thicknesses to find the best fit. In this way, they were able to estimate the thickness of the lithosphere under features at different locations and with a wide spread of ages. The results show in general that the younger the feature, the thicker the lithosphere, as is expected from a cooling planet. The thicknesses measured are essentially those that prevailed at the time that the topography was frozen in, that is, the time at which the topography was no longer causing additional flexure of the lithosphere. The young volcanoes of Olympus Mons, Ascreus Mons, and Pavonis Mons appear to be sitting on a lithosphere 70–170 km thick. Thicknesses estimated for the somewhat older Alba Patera and Elysium Rise are in the 40–80 km range. For the much of the Noachian terrain, the derived thicknesses are less than 15 km. Given that the base of the elastic lithosphere is close to the 650°C isotherm, the thickness values can be transposed into heat flows and thermal gradients as shown in Figure 4.5. In effect, lithosphere thickness is acting as a proxy for heat flow. The heat flows derived from the admittance data are considerably less than those derived from thermal models of the evolution of the interior (Stevenson *et al*., 1983; Schubert *et al*., 1992), and somewhat less than those derived from estimates of radiogenic heat production from meteorite data (Laul *et al*., 1986; Treiman *et al*., 1986).

Formation of Tharsis

The western hemisphere of Mars is dominated by Tharsis. By the end of the Noachian the Tharsis rise had been largely built, and it became the focus for

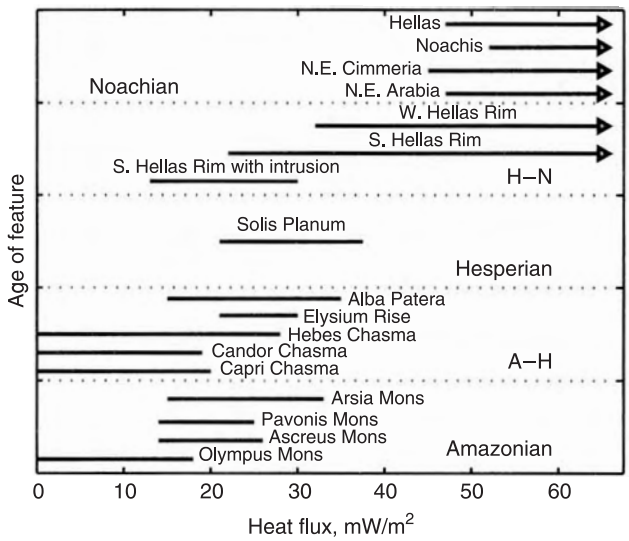

Figure 4.5. Thermal gradient and heat flux as a function of time, as derived from estimates of lithosphere thicknesses. Ages are from crater counts (Plescia and Saunders, 1979; Neukum and Hiller, 1981; Scott and Tanaka, 1986; Greeley and Guest, 1987). Lithosphere thicknesses were determined as described in the text (McGovern *et al*., 2002, copyright 2002, American Geophysical Union, reproduced by permission of the American Geophysical Union).

much of the planet's subsequent volcanic and tectonic activity. The evidence for the early formation of Tharsis is (1) the Noachian age of many of the deformational features that result from the presence of Tharsis (Anderson *et al*., 2001); (2) the consistency of flow directions of Noachian valley networks with Tharsis-induced topography (Phillips *et al*., 2001); (3) observation of kilometers-thick sequences of probably Noachian-aged volcanic rocks in the walls of the canyons on the eastern flank of the rise (McEwen *et al*., 1999); and (4) comparisons of models of lithospheric strain with deformation features, which suggest that, by the end of the Noachian, the Tharsis-induced lithospheric load was similar in scale and magnitude to that seen today (Banerdt and Golombek, 2000; Phillips *et al*., 2001).

Most recent modeling studies (Banerdt and Golombek, 2000; Phillips *et al*., 2001) support the suggestion that Tharsis is the result of voluminous extrusive and intrusive magmatic activity (Solomon and Head, 1982) rather than active uplift (Phillips *et al*., 1973). The huge volcanic load that accumulated to form Tharsis caused flexure of the lithosphere under Tharsis and widespread fracturing. How volcanic activity became focused on Tharsis is unclear (Solomon *et al*., 2005). One possibility is the presence of one or more long-lived mantle plumes beneath the province. Endothermic phase changes at the base of the mantle may have heated the lower mantle and localized convective transport from the base of the mantle into one or two local upwellings (Harder and Christensen, 1996). Modeling studies suggest that, in a compositionally stratified mantle, upper mantle plumes can develop over broad upwellings in the lower mantle. The upwellings tend to be concentrated where there is an insulating cap such as might be provided by the thicker crust of the southern highlands. This model does not work very well, however, since Tharsis straddles the plains–uplands boundary, rather than being centered in the uplands. Mantle upwelling is not necessarily required to form Tharsis. Solomon and Head (1982) suggested a feedback mechanism for sustaining volcanism in the Tharsis region. They suggested that fracturing due to local and global causes would become concentrated in areas of thin lithosphere. The fractures would provide easy access of magma to the surface, thereby localizing volcanism. The enhanced volcanism would result in heating and maintenance of a thin lithosphere in the volcanic area, thereby focusing further volcanism so that volcanic products would preferentially accumulate in specific areas. Other suggestions are that Tharsis may have been initiated by a large, impact-induced, thermal anomaly that formed during heavy bombardment (Reese *et al*., 2002), or that its formation antipodal to Hellas was somehow connected with the large impact that resulted in Hellas. Thus, although several suggestions have been made as to how Tharsis may have formed, the issue remains unresolved.

Formation of Tharsis appears to have deformed the planet's surface on a global scale. Phillips *et al*. (2001) modeled the loading of spherical elastic shell with Tharsis topography as the only load to determine how such a load would affect the topography of the rest of the planet, and the global gravity field. The model predicts a topographic low around Tharsis, which they called the Tharsis trough, and a high area antipodal to Tharsis. It also predicted a negative gravity anomaly around Tharsis. The predictions are largely consistent with the observations. The northern half of Tharsis is surrounded by the low areas of Chryse, Acidalia, the north polar basin, and Amazonis. The low areas around the southern half are less obvious, although southeast of Tharsis there is a definite low from Argyre, northward into the Chryse basin (Figure 4.1). Southwest of Tharsis, any low, if present, is very shallow. The predicted rise antipodal to Tharsis is also difficult to discern and to distinguish from the combined rims of the Hellas and Isidis

basins (Figure 4.1). The model predicts a gravity low around Tharsis that roughly follows the trough, and correspondence between the predicted and actual gravity (Smith *et al*., 1999a) is excellent. The results support the volcanic loading with lithosphere flexure model for Tharsis. Since the flow direction in Noachian valley networks is consistent with the slopes of the Tharsis trough, and because the topographic and gravity predictions were based on the present Tharsis load, the modeling also implies that Tharsis was already largely built by the end of the Noachian.

Surface indicators of stress

Extensional structures

Deformation of the surface, such as that caused by the Tharsis load, manifests itself mainly as faults and folds. There are two fundamental types of rock failure (Mandl, 1988; Ferrill and Morris, 2003). In shear failure, displacement is parallel to the fracture surface and the effective normal stress acting on the failure surface is greater than zero. In tensile failure, displacement is normal to the fracture surface and the normal stress acting on the failure surface is less than zero. In the first case, the rocks on each side of the fracture surface slide by one another. In the second case, the rocks are pulled apart along the fracture surface. In a third type of failure, termed hybrid, failure is tensile but there is lateral displacement along the fault plane to form what has been called a dilatant fault (Mandl, 1988).

In addition, three types of shear failure may occur according to the magnitude and orientation of the three principal stresses. Because the surface is stress-free, one of the three principal stresses is vertical and the other two are horizontal. If the maximum principal stress is vertical, then a normal fault results, in which the hanging wall moves down with respect to the footwall. The strike of the fault is at right angles to the least principal stress and the net result is horizontal extension in the direction of the least principal stress. If the least principal stress is vertical, then a reverse or thrust fault results in which the hanging wall moves up with respect to the footwall. The strike of the fault is at right angles to the maximum principal stress and the net result is compression in the direction of the maximum principal stress. The third case is where the maximum and minimum principal stresses are in the horizontal plane. In this case, dislocation is in a horizontal direction along a vertical plane to form a strike-slip fault. Thus, if the sense of the movement along the fault plane is known, then the orientation of the fault defines the directions of the three principal stresses. The stresses implied by the observed structures can then be compared with stresses calculated for different loads. Stresses implied by different mechanisms for the formation of Tharsis can, for example, be tested for consistency with the stresses implied by the array of structures around the province (Banerdt *et al*., 1992).

The most common extensional tectonic features on Mars are graben, long, narrow, linear depressions bound by two normal faults that enclose a downfaulted section of the crust. They characteristically have a flat floor enclosed between two fault scarps that face each other. Radial graben are common all around Tharsis, with some such as the Icaria, Sirenum, and Memnonia Fossae extending for 4000 km from the center of the rise. Perhaps the clearest development of simple graben is on the volcano Alba Patera, where numerous linear flat-floored depressions are clearly bound by faults scarps (Figure 4.6). Arrays of flat-floored graben are also common in Thaumasia, Tempe Terra, and in inliers of older terrain within Tharsis itself. Not all graben are radial to Tharsis. The Nili Fossae, for example, are circumferential to the Isidis basin and the Elysium Fossae are radial to Elysium. From modeling studies, terrestrial and lunar analogs, and observations of faults on trough walls, the dips of the bounding faults

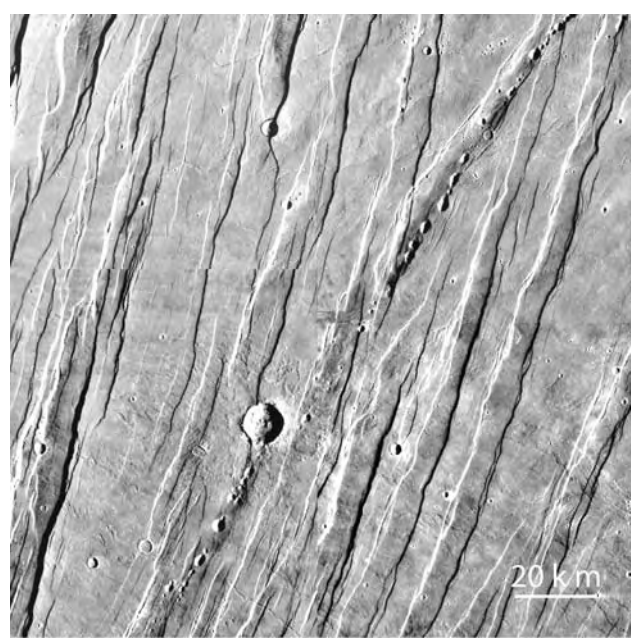

Figure 4.6. Simple graben on Alba Patera. at 39°N, 258°E. The graben have flat floors bound by walls of roughly equal height. Lines of pits suggest drainage into subsurface voids, possibly created by dilational faults (Viking MDIM).

of most graben are thought to be around 60° (Banerdt *et al*., 1992). From the distance between the bounding faults of graben in the western hemisphere, Davis and Golombek (1990) determined that 60° dipping faults would intersect at depths of 0.5 to 5 km below the surface, indicating failure of just the upper crust, not the entire lithosphere.

In the more intensely faulted areas, such as the Ceraunius Fossae (Figure 4.7), simple graben with flat floors bound by two straight walls are rare. The walls may have complex, scalloped segments, floors may be multi-leveled, and lateral offsets of both walls and floor are common. Different sets of graben may have slightly different orientations and successive generations of faults appear to have reactivated previous faults created under different stress fields so that en echelon patterns result.

In practice, graben are often difficult to distinguish from tension cracks, in which there is no downfaulted block between the crack walls. Inability to distinguish between the two may in many cases be simply a problem of resolution, or the result of talus from the graben walls covering the flat floor, but large tension cracks may also be common. The Cerberus Fossae, which can be traced for over 1000 km and which have been the sources of floods of water and lava, may be tension cracks (Chapters 3 and 6). They have deep, V-shaped profiles and walls that in detail lack straight segments (Figure 4.8). Similarly the Olympica Fossae, also flood sources, may be tension cracks. Tension cracks form in the vertical plane

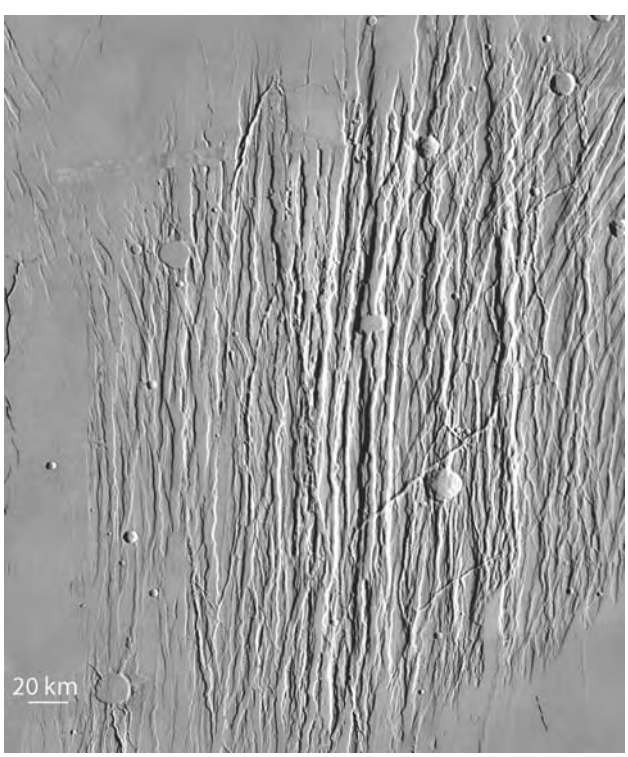

Figure 4.7. The Ceraunius Fossae centered on 25°N, 253°E. This inlier of highly fractured ground is surrounded by younger plains. Several generations of graben with different orientations are present, together with tension cracks, as along the western margin of the image (Viking MDIM).

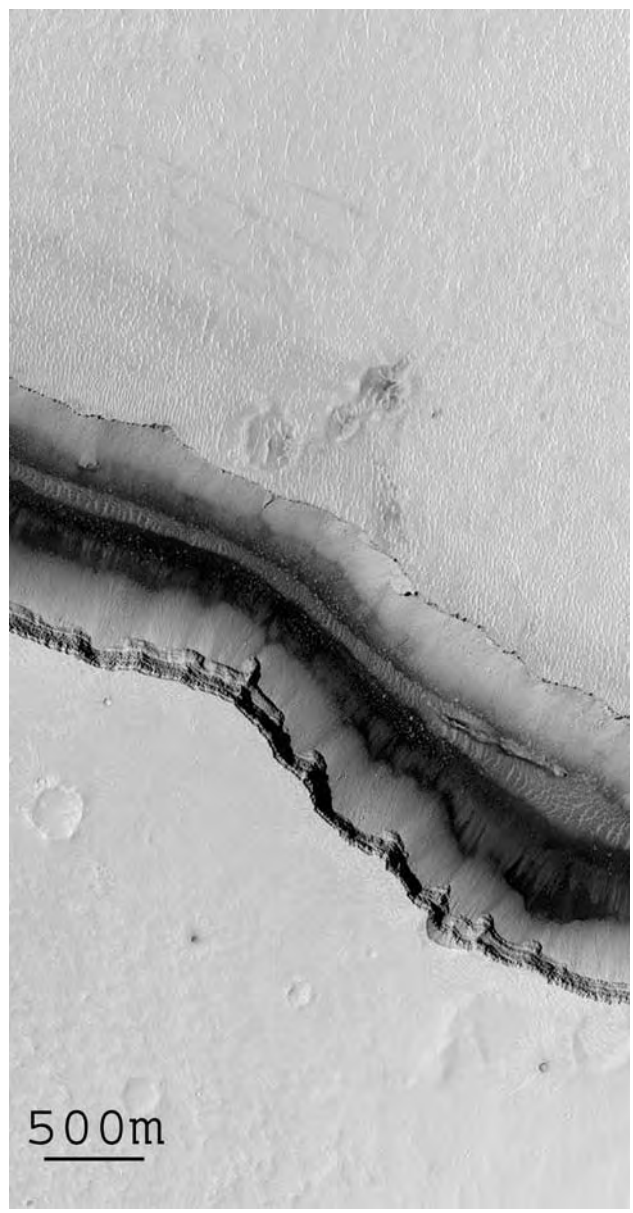

Figure 4.8. One of the Cerberus Fossae at 9.9°N, 158.1°E. Lacking a flat floor and straight walls, it appears to be a tension crack rather than a graben. It has been the source of floods of both water and lava (MOC E21000319).

normal to the least principal stress, so are not subject to the same depth limitations as the normal faults that bound graben. They may therefore extend to greater depths than graben faults, possibly enabling them to tap deep water and lava sources.

The largest tectonic features on the planet are the equatorial canyons on the east flanks of the Tharsis rise. As discussed in Chapter 5, aligned triangular facets at the base of some of the canyon walls provide compelling evidence that some of the walls, particularly those in Coprates Chasma and eastern Ophir Chasma, are fault scarps. The canyons appear to be gigantic rifts. The spacing of the faults and their probable large throw suggest that the entire lithosphere is faulted, as with some terrestrial rifts.

A common feature of many fractures, graben, and rifts is the presence of pit craters aligned along their length (Figure 4.9). The pits probably result from collapse of the near-surface materials into voids created by the faulting (Ferrill *et al*., 2004). The presence of the pits indicates, therefore, some dilation (extension and creation of a void) at depth. Since dilational faults have steeper dips than normal faults (Mandl, 1988), the calculations of the depth of origin of the faults based on a 60° dip may be invalid where pits are present.

Figure 4.9. Detail of graben and pits on the flank of Alba Patera at 36.5°N, 241.5°E (THEMIS V12299006).

The above discussion assumes that the fractures observed at the surface are purely tectonic in origin. However, some of the fractures, particularly the longer ones such as the Icaria, Sirenum (Figure 4.10), and Memnonia Fossae, may be the surface expression of dikes (Mège and Masson, 1996; McKenzie and Nimmo, 1999; Wilson and Head, 2002). As a magma diapir rises toward the surface, the density of the surrounding rocks will tend to decrease because of their increasing porosity until the diapir reaches a neutral buoyancy zone. At this point the diaper will tend to spread laterally to form vertical dikes oriented at right angles to the least principal stress. Lateral extension of the dike will follow when stress intensities at the dike's lateral tip exceed the effective fracture strength of the host rocks, and when lateral extension

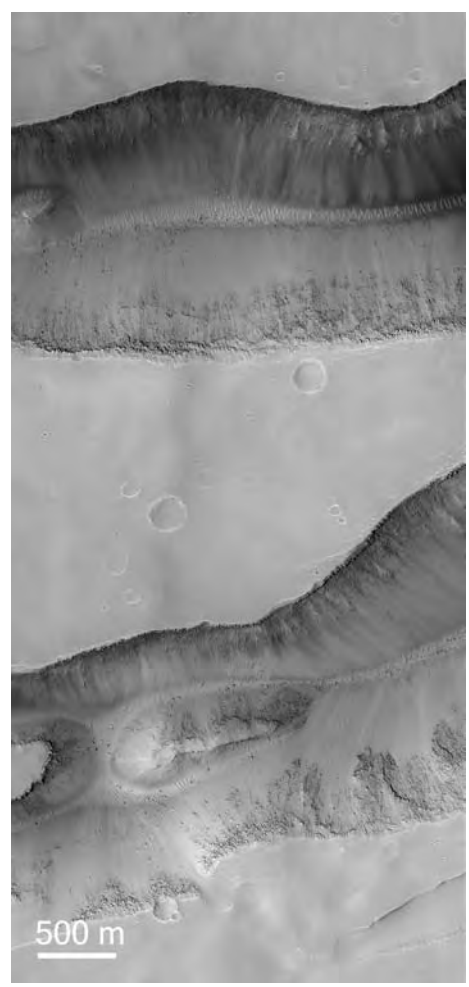

Figure 4.10. The Sirenum Fossae cutting Noachian terrain at 30°S, 212°E. These linear structures extend for thousands of kilometers southwest from the vicinity of Arsia Mons. They may indicate dikes at depth (MOC R1003514).

offers less resistance to magma pressure than vertical growth. Terrestrial dikes may be up to 2000 km long, with widths of 50–100 m and volumes of ~500 km^3. Modeling by Wilson and Head (2002) suggests that for the largest martian dikes (>3000 km long), magma volumes could be in the 20,000–60,000 km^3 range. They also suggest that the long graben to the southwest of Tharsis result from dikes that spread from two centers, one under Arsia Mons and one under Syria Planum.

Compressional structures

Wrinkle ridges, first recognized on the lunar maria, are Mars' most common compressional feature (Banerdt *et al*., 1992; Watters, 1993, and references therein). They are asymmetric linear features, many tens to hundreds of kilometers long and a few kilometers wide (Figures 4.11, 4.12). They typically consist of a broad arch, about 100–200 m high, on which is superimposed one or more narrow, discontinuous crenulations or wrinkles. They occur almost exclusively on volcanic plains. In the western hemisphere the ridges are mostly circumferential to Tharsis. They are particularly prominent to the east of Tharsis in Lunae Planum, eastern Solis Planum, and Chryse Planitia. They are also common to the north of Tharsis, in Vastitas Borealis, where they wrap around the northern margin of the Tharsis rise. They are much less common to the south and southeast of Tharsis, probably because of the dominance of Noachian uplands in these regions, but where there are intercrater plains in these areas, they generally have ridges circumferential to Tharsis also. In the eastern

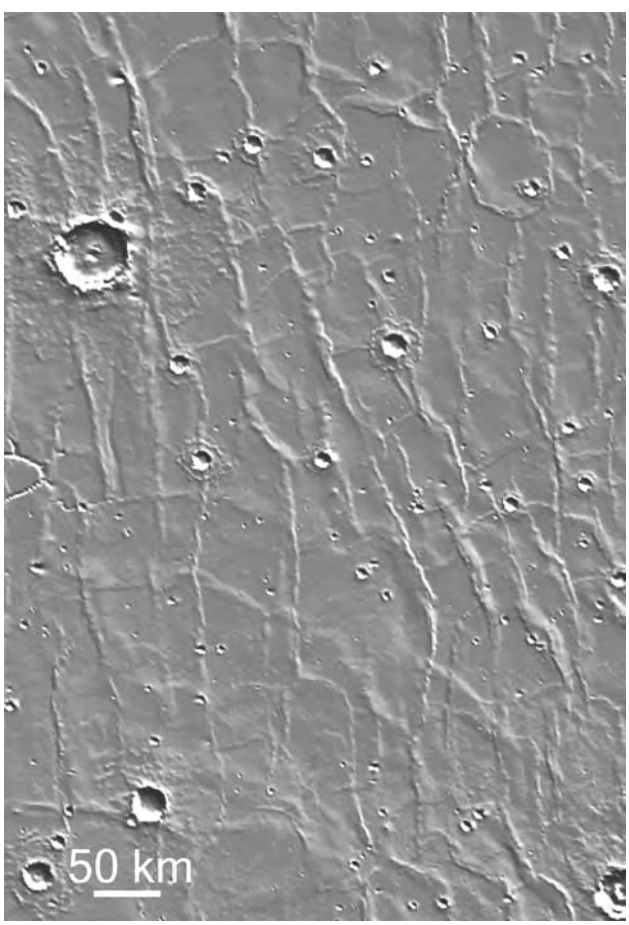

Figure 4.11. Wrinkle ridges in Lunae Planum. The Tharsis load centered to the west has caused east–west compression in the area and resulted in north–south ridges. The image is centered at 15°N, 293°E (MOLA).

Figure 4.12. Typical wrinkle ridge in Lunae Planum at 17°N, 293°E. Most ridges consist of a broad arch and a narrower wrinkle, which may be on the arch or along the margin of the arch. The plains to the southwest of the ridge are roughly 100 m higher than the plains to the northeast (THEMIS V05345013).

hemisphere, wrinkles are largely confined to the volcanic plains of Isidis Planitia, Hesperia Planum, and Malea Planum. They also occur locally on crater floors, as in Gusev, and wherever there are significant areas of intercrater plains. In this hemisphere, outside the influence of Tharsis, the orientation of the wrinkle ridges is much more random than around Tharsis.

While wrinkle ridges are common wherever sparsely cratered plains materials overlie the older, heavily cratered Noachian surface, compressional features are much more difficult to discern in the Noachian surface itself. Watters (1993) mapped a number of lobate scarps in Memnonia, and in the uplands north of Hesperia Planum, that he interpreted as compressional features. Those north of Hesperia are parallel to the dichotomy boundary and may be related in some way to stresses along that boundary (Figure 4.13). Also, numerous elongate ridges in Memnonia southwest of Tharsis and in Terra Sirenum south of Tharsis, roughly circumferential to Tharsis, could be compressional features related to Tharsis-induced stresses. But in general, analogs to wrinkle ridges in the cratered upland are rare.

Wrinkle ridges appear to be the surface expression of thrust faults (Golombek *et al*., 2001; Montesi and Zuber 2003). Where there are parallel wrinkle ridges as in Solis and Lunae Plana, the areas between the ridges, which look flat in images, are revealed in the MOLA data to be bowed upward a few tens of meters and at different elevations on either side of the ridge. For the ridges around Tharsis, the plains are typically 100 m higher on the Tharsis side of the ridges than on the distal side. The ridges therefore delineate a sequence of rounded steps, down and away from Tharsis. The consistent down to the southeast offset of the ridges in Solis and Lunae Plana suggests that the offsets are caused by thrust faults that dip to the northwest. As the faults approach the surface, they may transition to folds (Figure 4.14). While there is no direct evidence for the depth and dips of the faults, estimates of the brittle and ductile yield strength for plausible crustal thicknesses and thermal gradients suggest that there may be a weak ductile layer at a few tens of kilometers in depth (Banerdt *et al*., 1992) in which the thrust faults could root. Montesi and Zuber (2003) derived similar depth origins from the spacing of wrinkle ridges in Luna Planum. Alternatively, the deformation may be thin-skinned, extending to no more than a few kilometers, being confined to the plains materials that become decoupled from the underlying megaregolith (Watters, 1991).

Deformational features related to Tharsis

The massive volcanic pile of Tharsis caused stresses in the lithosphere, extensive enough to have

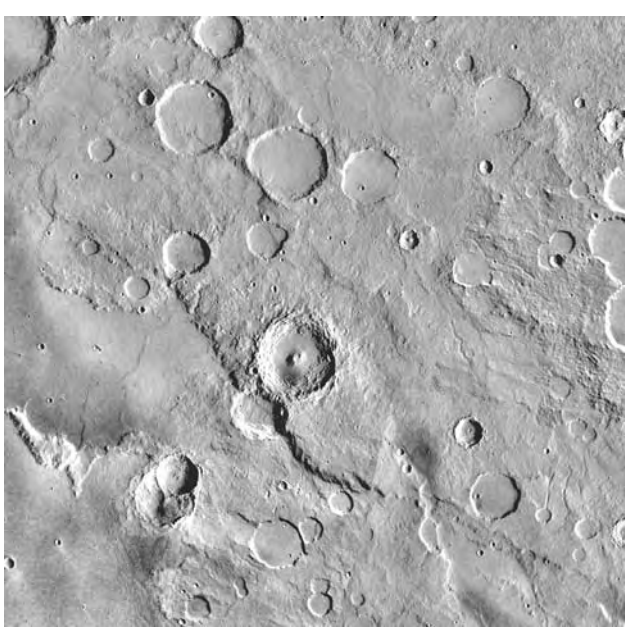

Figure 4.13. Possible thrust fault in the cratered uplands at 2°N, 110°E. The fault is parallel to the dichotomy boundary, which is just to the north of the area seen here (MDIM2).

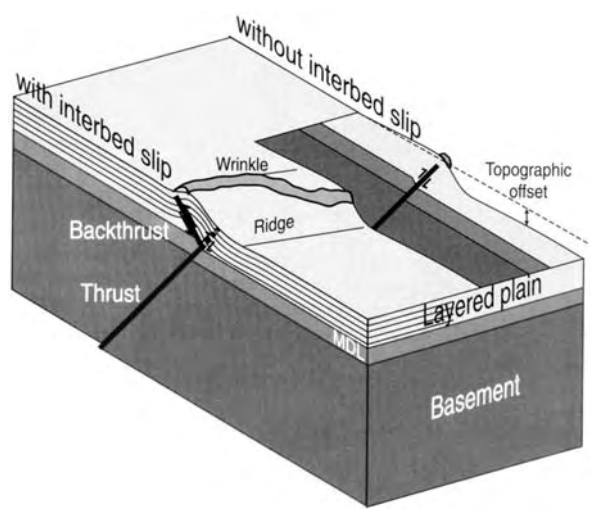

Figure 4.14. Possible structure beneath a wrinkle ridge. A thrust offsets the basement beneath a layered unit of sedimentary or volcanic origin, thereby causing an elevation offset of the plains on either side of the ridge. Folding and faulting of the layered sediments cause the wrinkle (from Montesi and Zuber, 2003, copyright 2003, American Geophysical Union, reproduced by permission of the American Geophysical Union).

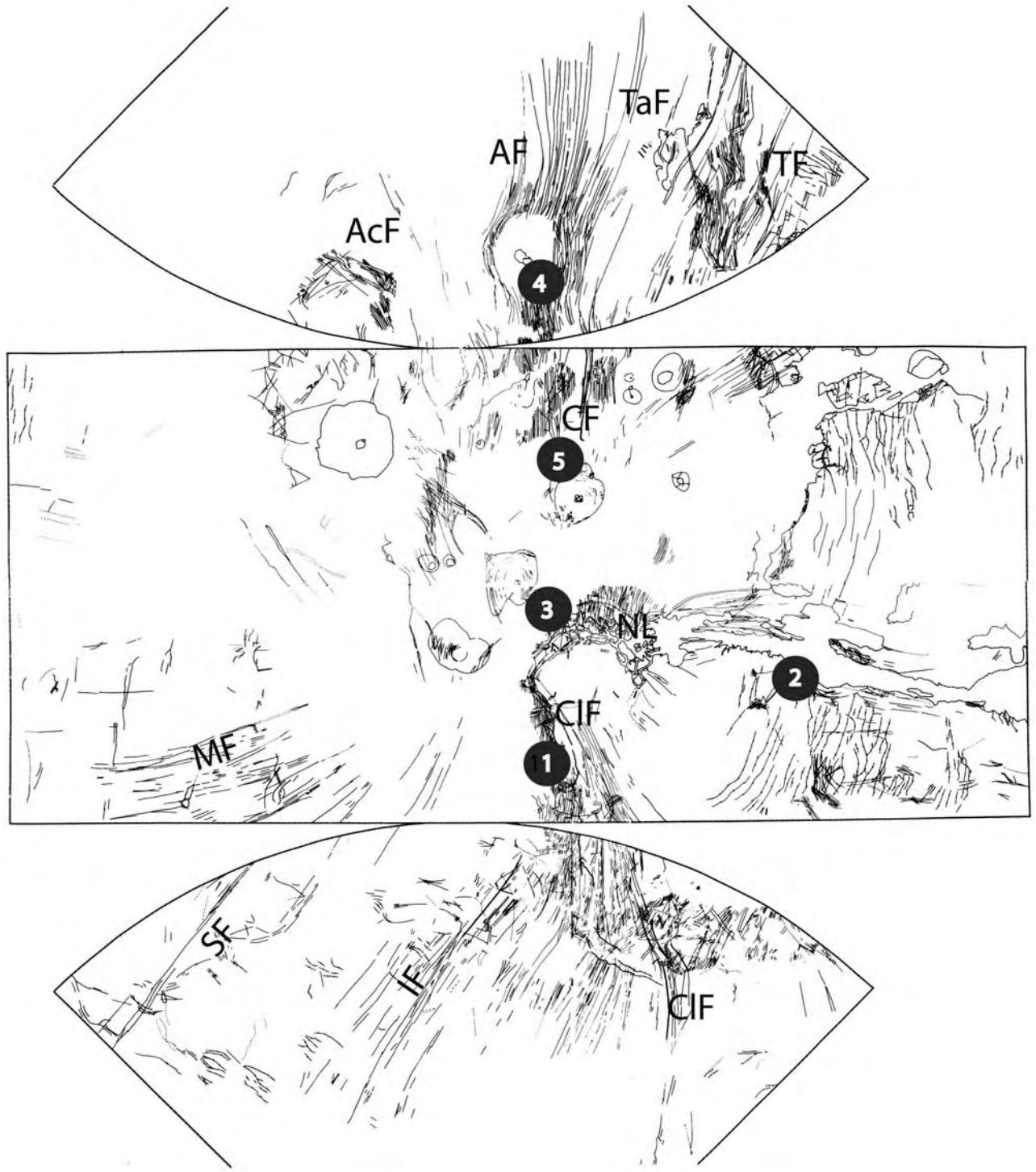

Figure 4.15. Deformational features on and around Tharsis. Numbered circles indicate the change in locations of deformation centers with time, as described in the text. AcF, Acheron Fossae; AF, Alba Fossae; TaF, Tantalus Fossae; TF, Tempe Fossae; Cf, Ceraunius Fossae; NL, Noctis Labyrinthus; ClF, Claritas Fossae; MF, Memnonia Fossae; SF, Sirenum Fossae; IF, Icaria Fossae. (Base map by J. Plescia, Applied Physics Lab.)

resulted in an array of tectonic features that covers the entire western hemisphere (Wise *et al.*, 1979; Plescia and Saunders, 1982; Tanaka *et al.*, 1991; Banerdt *et al.*, 1992; Anderson *et al.*, 2001). Included are graben, mostly radial to Tharsis, and wrinkle ridges, which are mostly circumferential. The most comprehensive analysis of the deformational features caused by Tharsis is that by Anderson *et al.* (2001), who mapped the orientation and location of 25,000 tectonic features in the western hemisphere. They also determined their relative age from their intersection relations with geological units on the western hemisphere geological map (Scott and Tanaka, 1986). Different stress centers were identified by contouring the number of intersection points on a latitude–longitude grid of great circles passing through the many graben, or in the case of compressive features, for great circles that contained the normal to the features. In this way they were able to determine the center of the stress fields at different times, that is, the points from which the extensional features radiated and around which the compressional features were arrayed (Figure 4.15).

Taking all the data, irrespective of relative age and including both compressional and extensional structures, indicates that the integrated center of the stress field is at 4°S, 253°E in western Noctis Labyrinthus, close to the highest part of the Tharsis rise. Secondary centers are in the Claritas Fossae and Tempe Terra. But the data also indicates that the stress center has changed with time. Anderson *et al.* recognize five stages. Stage 1 features are mainly extensional and found in Noachian terrain around the periphery of Tharsis and in small inliers within Tharsis. These features define a broad center in Claritas at 27°S, 254°E, although the center is poorly defined, being spread out in a north–south direction. Stage 2 extensional features of late Noachian to early Hesperian age define a center at 14°S, 282°E just south of Valles Marineris. The stage 3 (early Hesperian) extensional features radiate from a well-defined center at 4°S, 107°E, in Noctis Labyrinthus. Early Hesperian wrinkle ridges are disposed around a somewhat broader area that includes the extensional center. Stage 4 (late hesperian–early Amazonian) is centered on Alba Patera and Stage 5 (Amazonian) is centered on Ascreus Mons.

The orientation of the deformational features can be used to test models of the Tharsis rise, specifically whether Tharsis is an uplifted dome, is supported isostatically by intrusions, or whether it represents a massive surface load that has caused flexure of the lithosphere. We saw above that the gravity and topography support the surface load model. That is true also of the deformational features. Early modeling suggested that faulting on or close to the topographic rise was consistent with isostatic support, whereas more distant faulting was consistent with flexure under a surface load (Banerdt *et al.*, 1992). However, improved gravity and topography and better estimates of crust and lithosphere thicknesses now enable more sophisticated models to be developed. Banerdt and Golombek (2000) show that almost all the faulting in and around Tharsis can be explained by lithospheric flexure under the Tharsis load. Isostatic support is not needed. The main exceptions are those caused by local loads such as Alba Patera and other volcanoes. The correlation between the computed strains and the observed structures is striking. Not only are the orientations of the faults consistent with model predictions, but the major graben and rifts, such as the Memnonia, Sirenum, and Tempe Fossae, coincide with major strain concentrations. In addition, the magnitude of the calculated extensional strains is roughly similar to the circumferential strains estimated from the observed faults (Golombek *et al.*, 1996). Since a large fraction of the faults date from the Noachian (stages 1 and 2), and the modeling used in the predictions is based on current gravity and topography, their mutual consistency implies that Tharsis has

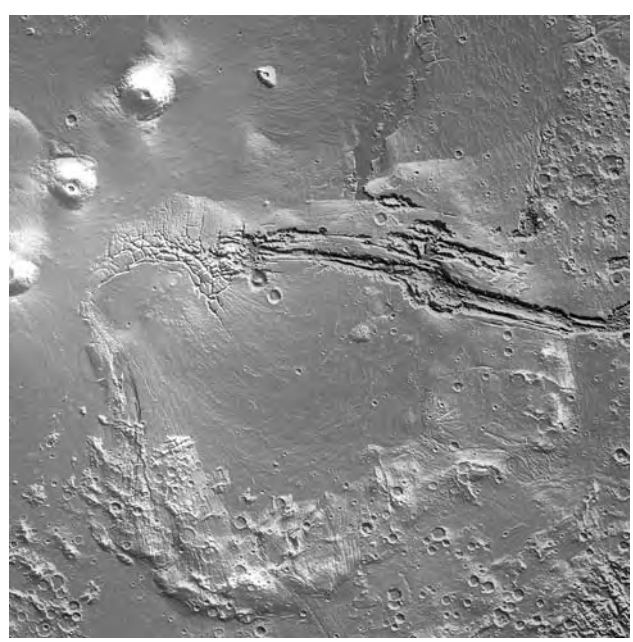

Figure 4.16. The Syria–Thaumasia block. This roughly rectangular block is outlined by high ground and an outward-facing slope. The interior of the block is a closed basin. Its origin is unknown (MOLA).

not changed significantly in the last 3 Gyr, that is, Tharsis formed very early in the planet's history.

A feature of Tharsis that has received little attention in the literature is the Syria–Thaumasia block (Figure 4.16). This roughly rectangular block of terrain, 3000 km across, is bound on all sides by high ground and outward-facing slopes. The high ground around the margin of the block encircles a closed depression containing the volcanic plains of Solis Planum. Along the western and southern margins, the high ground and steep outward-facing slopes are in Noachian terrain, but along the eastern margin of the block and especially to the north, much of the steeper-sloping, higher ground around the block is Hesperian in age, which suggests that, whatever process caused the block, it continued into the Hesperian. The block is clearly a major structural feature of the planet.

5 Canyons

Just south of the equator between longitudes 250°E and 320°E are several enormous, interconnected canyons, collectively called Valles Marineris. They extend roughly east–west for over 4000 km from Noctis Labyrinthus at the summit of the Tharsis bulge, down the crest of broad rise on the eastern flank of the bulge, to some low-lying areas of chaotic terrain in Margaritifer Terra, south of Chryse Planitia (Figure 5.1). Regional elevations drop from over 7000 m at the western end of the canyons to less than 1000 m at the eastern end. Most individual canyons range in width up to 150 km, but Melas Chasma is almost 300 km wide, and in the central part of the system three canyons merge to form a depression 600 km across. Along much of the canyon's length, depths are over 6000 m. The deepest parts, in western Coprates Chasma, are over 10,000 m below the canyon rim. By comparison, the Grand Canyon, Arizona, is 450 km long, 30 km across at its widest, and 1700 m below the north rim at its deepest.

The relief of the canyons probably results mostly from faulting. Their origin is thus fundamentally different from that of the Grand Canyon, which was produced almost entirely by erosion, and more akin to that of the African Rift Valleys. Because of the scarcity of fluvial features in the canyons, Sharp (1973a) suggested that the term "canyon," with connotations of water erosion, was inappropriate. However, we will continue to use the term with the understanding that it has no genetic implication. While faulting has clearly played a major role in the formation of the canyons, the precise way in which they arrived at their present configuration remains puzzling. One issue concerns the faulting itself. The faults that created the rifts are part of the radial system around Tharsis. The system affects much of the western hemisphere, but the huge canyon-forming rifts developed only to the west of Tharsis, and we do not know why. Mass-wasting and other erosional processes have clearly contributed to canyon formation, but what fraction of the present volume is due to faulting and what is due to other processes such as erosion or solution is unknown. Layered, sulfate-rich sediments in many places within the canyons and streamlined landforms at their eastern end suggest that the canyons formerly contained deep lakes. Whether this interpretation is true, and if so, how persistent the lakes were, whether they were ice-covered, how and when they drained, and what effect they had on the regional water table are all uncertain. Hebes Chasma is particularly puzzling, since it is a completely enclosed canyon and has no obvious outlet for any water it might have contained, nor for any of the materials that had to be removed to form the canyon. Like many of the other canyons, it contains thick stacks of sediments.

The canyons clearly played a significant role in the formation of the circum-Chryse outflow channels.

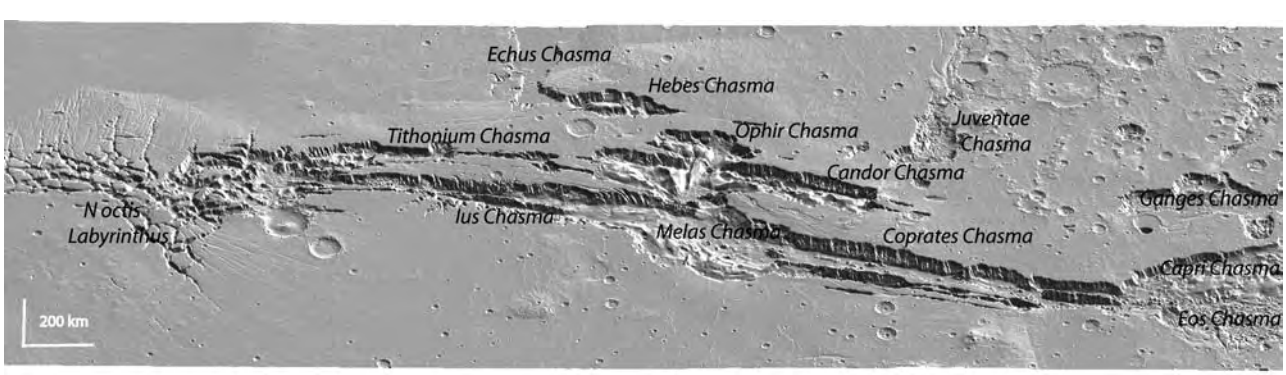

Figure 5.1. View of the canyons from the south. The scene is 3900 km across.

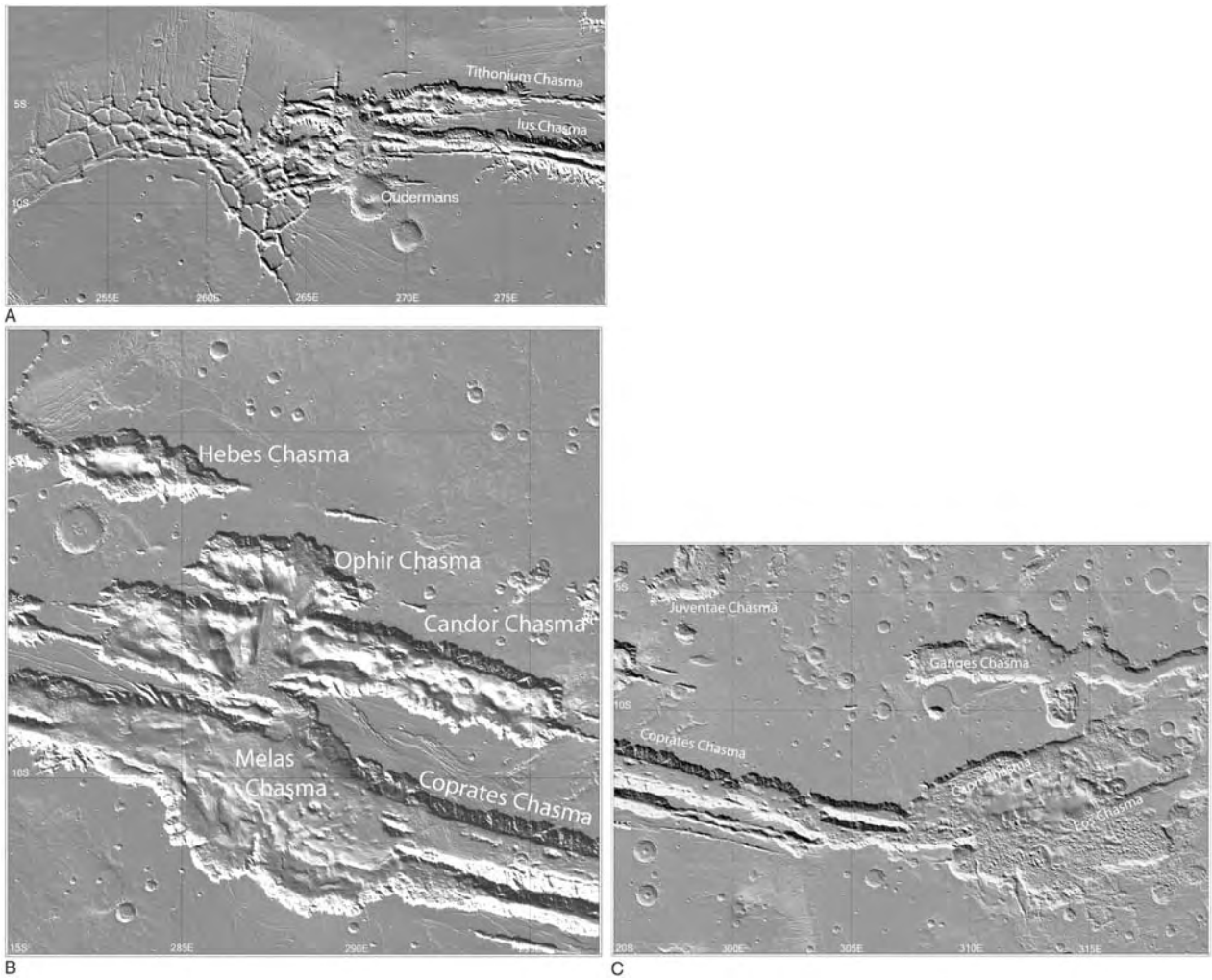

Figure 5.2. (A) The eastern end of the canyons between 250 and 280°E. The grid lines are 300 km apart. The crest of the Tharsis bulge at 9037 m is at 265°E, 7.5°S in Noctis Labyrinthus at the middle of the image. Noctis Labyrinthus merges to the west with a north–south fracture zone, the Claritas Fossae, just off the left side of the image. (B) The central section of the canyons between 280 and 297°E. Mounds of sediments occupy the centers of the Candor, Ophir, and Hebes Chasmata, mostly separated by a gap from the canyon walls. Floor deposits within Melas Chasma are more discontinuous and irregular than in the adjacent canyons. A linear fault scarp can be seen at the base of the north wall of Coprates Chasma. (C) The eastern section of the canyons between 295 and 320°E. In this section, at roughly 307°E, the canyons transition from linear depressions with high, parallel opposing walls, and level floors, to irregularly shaped depressions with rubbly floors. Fluvial channels start in two small depressions in the adjacent plains along the 10°S latitude. Other fluvial features occur locally in and next to the Ganges, Capri, and Eos Chasmata (MOLA).

The main canyons transition eastward into chaotic terrain and outflow channels. To the north of the main canyon system, Echus Chasma, Juventae Chasma, and Ravi Chasma all give rise to outflow channels, and small outflow channels start at other local sources. This chapter concerns the canyons themselves. Outflow channels are discussed in Chapter 6. The broader tectonic framework within which the canyon-forming faults fit was discussed in Chapter 4.

Physiography

The canyons can be divided into three sections: Noctis Labyrinthus in the west, the main, linear, WNW–ESE trending canyons in the center, and the more irregularly shaped canyons that merge with chaotic terrain and outflow channels to the east (Figure 5.1). Noctis Labyrinthus (Figure 5.2A) is a maze of interconnected depressions that divide the high plains around the summit of the Tharsis bulge

into a mosaic of blocks. The actual summit, at an elevation of 9000 m, is at 265°E, 7°S, in the middle of the labyrinth. Several sets of fractures, roughly radial to Tharsis, converge on the area. Most of the fracture directions are represented in the labyrinth by short canyon segments (Figure 5.3). To the west, the fractured plains of Noctis Labyrinthus curl south, around a secondary high at 14°S, 252°E, to merge with a complex, NNW–SSE trending fracture zone, the Claritas Fossae. The fractured plains extend to a few hundred kilometers north of Noctis Labyrinthus, to where they are buried by younger Tharsis lava flows. Around the periphery of Noctis Labyrinthus, lines of pits are common along the fracture directions. Within the labyrinth the pits are larger and merge to form segmented canyons, separated by septa and with floors at different levels, or they coalesce more completely to form continuous canyons. Merging of sections with different orientations forms the labyrinth. Most of the depressions in the western part of the labyrinth are disconnected and typically less than 3000 m deep. Farther east, the depressions become deeper and more continuous. Ultimately the labyrinth merges with the more or less continuous canyons to the east. There is no indication of fluvial activity or grading of the floors. Layering can be seen in places on the floor, but mounds of layered deposits, such as are seen elsewhere within the canyons, appear not to be present. The dominance of closed depressions in the eastern part of the labyrinth indicates that the negative volume is created largely by collapse, probably the result of extensional faulting. The contribution of other processes such as deflation and mass wasting appears small.

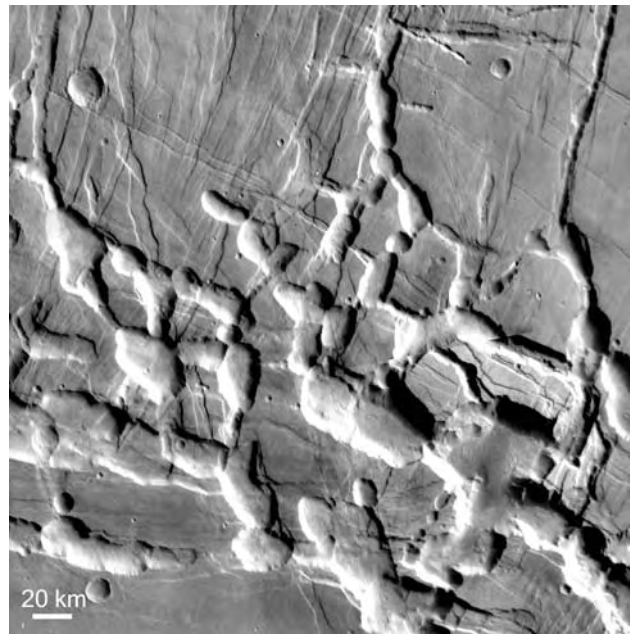

Figure 5.3. Detail of Noctis Labyrinthus centered at 5°S, 258°E. The labyrinth is made up of pits elongate in the direction of faults in the surrounding plains. The pit floors are at different levels and commonly separated by septa. The elevation of the plain ranges from 7 to 8.5 km above the datum. The floor of the pit is in places as low as 3.5 km above the datum, so that there is 5 km of relief within the image. The labyrinth appears to have formed by collapse following outward extension (Viking MDIM).

Extending eastward from Noctis Labyrinthus are two discontinuous canyons, the Tithonium Chasma and Ius Chasma. The northernmost of the pair, Tithonium Chasma, has no eastern outlet. To the east it degenerates into strings of closed depressions. Ius Chasma broadens to the east, and the elevation of its floor drops from close to 0 m where it merges with Noctis Labyrinthus to below −3000 m where it merges with Melas Chasma, 900 km to the east. Over much of its length, Ius Chasma has a central spine that appears to be a remnant of the plains material into which the canyons are cut. Branching valleys are deeply incised into the southern wall while several huge landslides have modified the northern wall and blocked the canyon north of the spine (Figure 5.4). Although the landslides block the canyon, there is little indication of deposits at the mouths of the valleys on the south wall of Ius Chasma. Between the two main canyons and to the north of Tithonium Chasma the plains are cut by numerous faults, some marked by lines of pits. Most of the faults are roughly parallel to the trend of the canyons, but deep indentations occur in the canyon walls where faults intersect the walls at an angle. In the east end of northernmost Tithonium Chasma, at 4°S, 271°E, are mounds of layered deposits, similar to those in the central Hebes, Ophir, and Candor Chasmata. Layering is also seen on all the canyon walls.

The central part of the canyon system is a broad 600 km wide depression created by the merger of the Ophir, Candor, and Melas Chasmata (Figure 5.2B). Ophir and Candor Chasmata are somewhat rectangular in shape with their blunt eastern and western ends penetrated by narrow segmented depressions or lines of pits that parallel the general WNW–ESE trend of the canyons. The south wall of Melas Chasma is broadly concave to the north, as are several faults in the plains to the south. The most distinctive characteristic of this central section is the presence of thick sequences of layered deposits (Figure 5.5). The layered deposits are over 6000 m thick in western Candor. They reach elevations of over 3000 m in western Ophir, extending

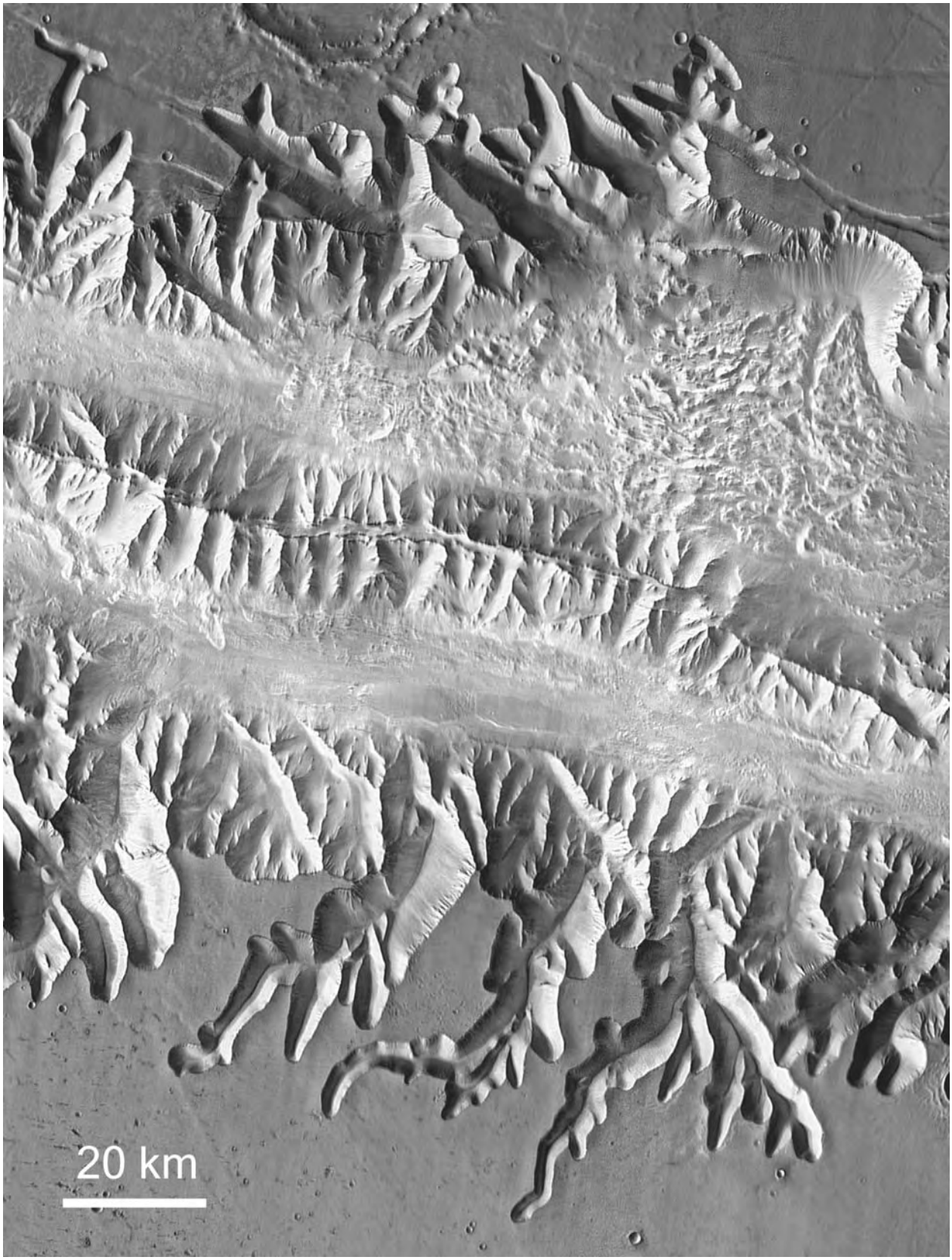

Figure 5.4. Detail of Ius Chasma centered at 8°S, 278°E. This section of Ius Chasma is 7–8 km deep. Branching tributary canyons are well developed on the south wall of the canyon. Part of the north wall has collapsed in massive landslides. The central spine and canyon walls are eroded into downward-branching spurs with intervening talus chutes, as are most of the canyon walls (THEMIS mosaic).

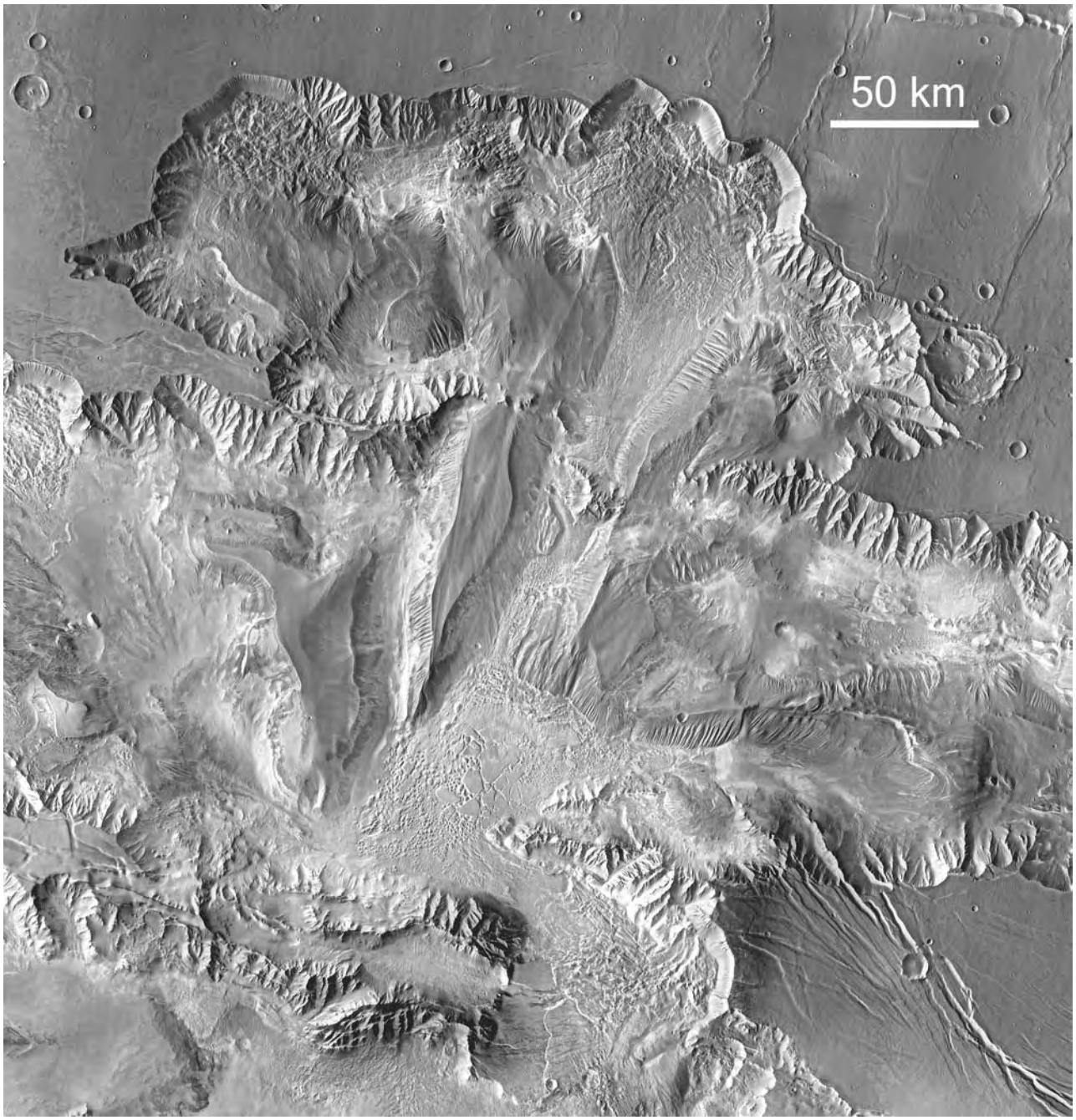

Figure 5.5. Ophir (top) and Candor (middle) Chasmata. The two canyons are separated by a narrow ridge with the typical ridge and gully topography of the canyon walls. Within both canyons and superimposed on the divide are mounds of sediments, which, in the center of the image, have been eroded into N–S ridges. Large landslides have created large alcoves in the north wall of Ophir Chasma (THEMIS).

to an elevation just below the canyon rim. The completely enclosed Hebes Chasma to the northwest of Ophir Chasma also contains thick sedimentary sequences (Figure 5.6). Juventae Chasma, to the northeast of Candor Chasma (Figure 5.7), contains layered deposits (Figure 5.8), although far fewer than Hebes Chasma. It is also almost completely enclosed, its deepest part being 4000 m below its outlet, Maja Vallis. Almost all the layered deposits are rich in sulfates (Bibring *et al*., 2006).

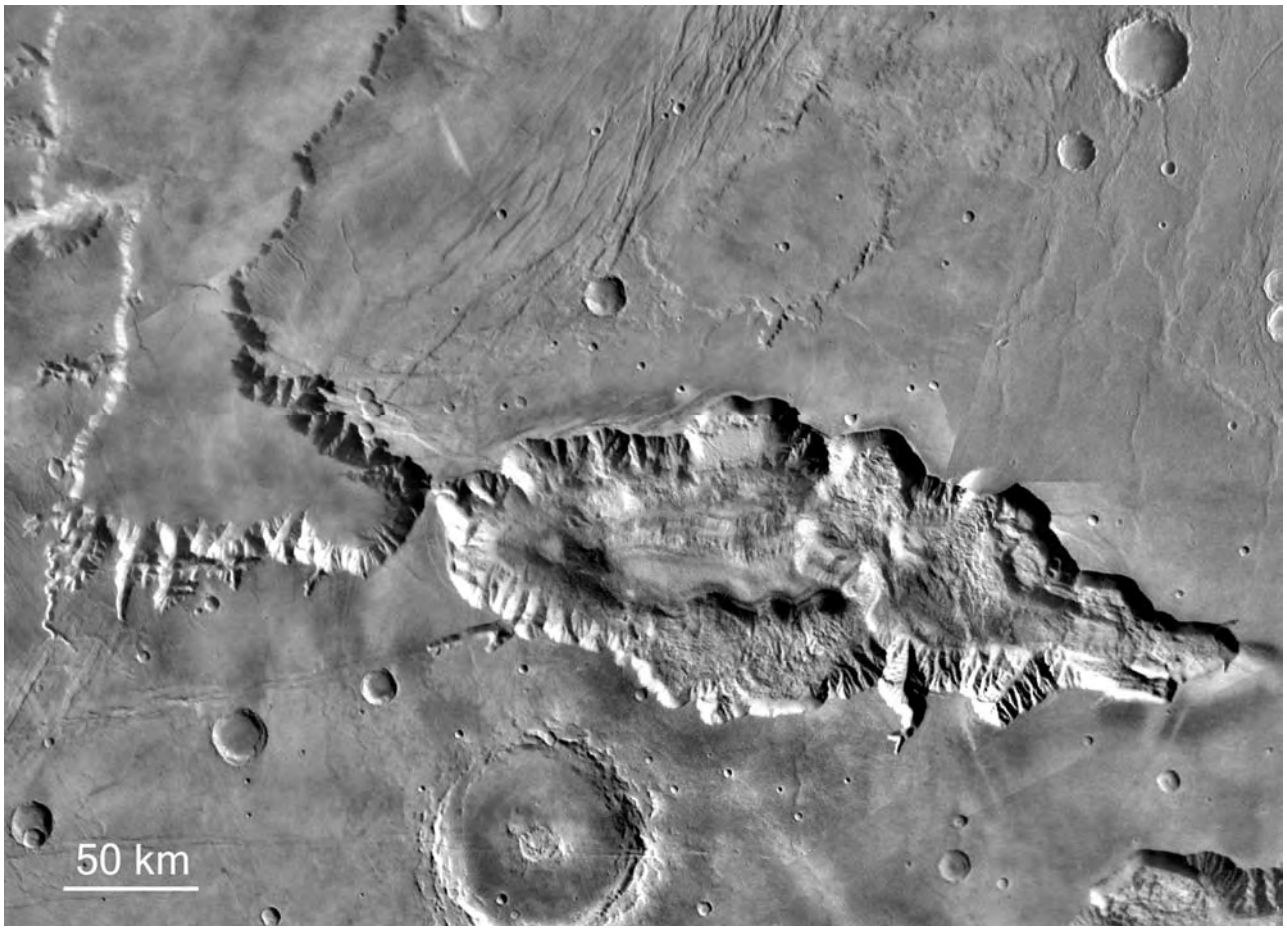

Figure 5.6. Hebes Chasma. The canyon is completely enclosed, although separated from Echus Chasma to the west by only a narrow barrier. Layered deposits in the middle of the canyon are separated from the canyon walls mostly by what appear to be landslide deposits. (Viking MDIM).

Coprates Chasma, extending east from Melas Chasma, consists of several parallel sections separated by flat-topped or sharp-crested ridges depending on the width of the divides (Figure 5.2C). The main canyon has a floor that is relatively free of landslide debris and layered sediments compared with other canyons, although it is partly blocked at its narrowest point at 301°E (Figure 5.9). The floor also has only a small regional slope, floor elevations dropping from close to −4000 m at the western end to only −4500 m 1000 km to the east. At the canyon's western end are some of the highest walls within the canyon system. They are roughly 10,000 m high, extending from under −4500 m to over 5000 m in elevation.

The canyons change significantly east of 307°E where three canyons are identified, the Ganges, Capri, and Eos Chasmata. To the west the canyons are deep, and commonly have straight walls that are clearly fault scarps (see below). To the east, the canyons become shallower and more irregular in outline and generally lack the straight wall segments. They no longer follow the WNW−ESE trend but instead curl northward toward the Chryse basin. The floors are covered with closely spaced hills except for smooth pathways with streamlined forms. Within Ganges Chasma are layered deposits similar to those in the canyons farther west (Figure 5.10). To the east and south of Ganges Chasma, channels start at depressions in the plains and extend to and over the canyon wall as though water had erupted from the depressions and flowed into the canyon. In contrast, channels on the south wall of Eos Chasma at 13°S, 322°E extend from the high-standing rim of the canyon away from the canyon to lower terrain to the south. To the northeast the irregular canyons merge with the chaotic terrain and outflow channels south of the Chryse basin, so that there is a continuous transition from the main, poorly graded, canyons with rectilinear walls, to irregular, chaos-filled

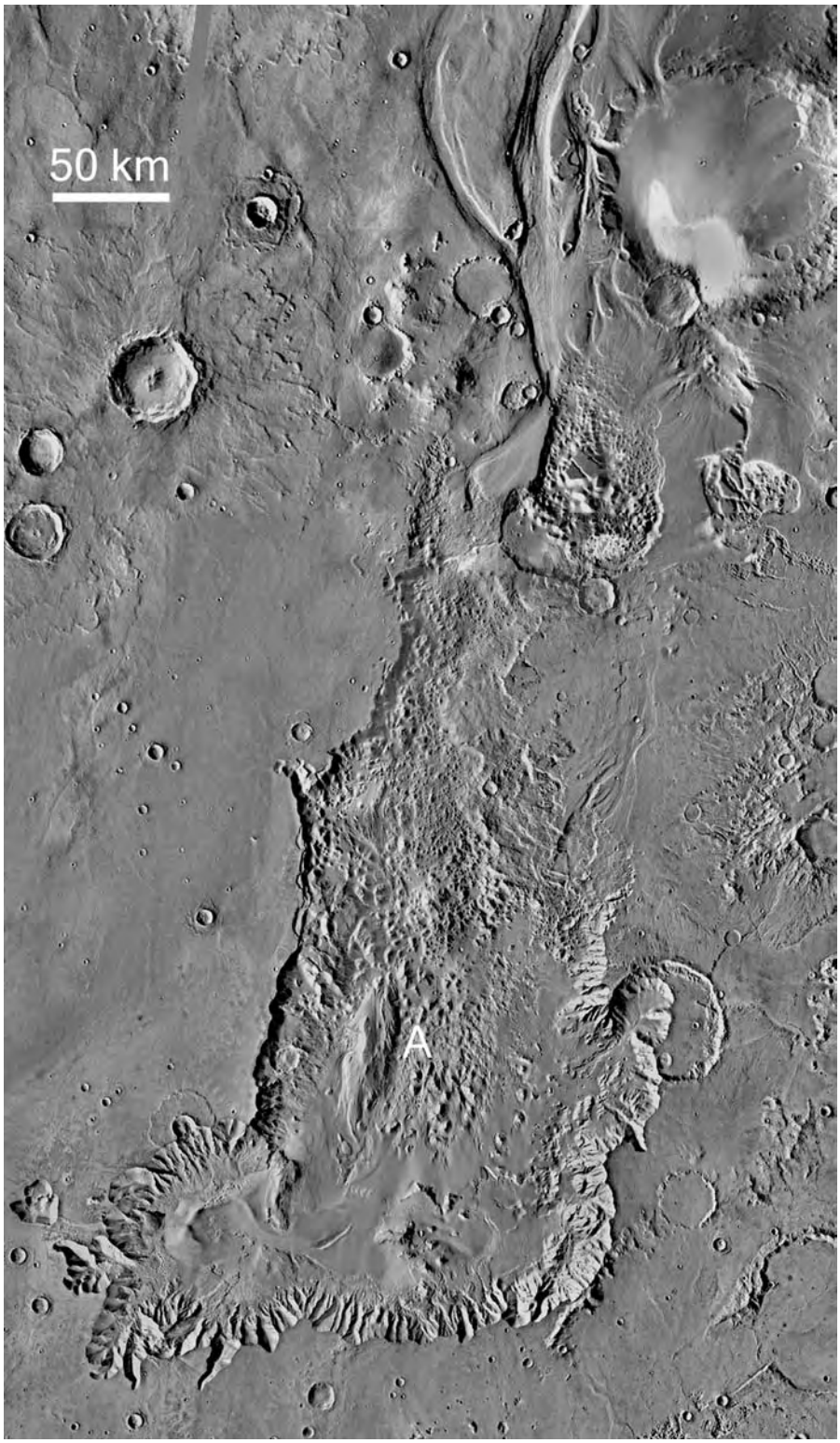

Figure 5.7. Juventae Chasma. Water seemingly pooled in the canyon and overflowed to the north to form a large outlflow channel, Maja Vallis, which is just visible at the top of the image The outlet is 4000 m higher than the bottom of the canyon, indicating that Juventae Chasma once contained a deep lake. Details of the layered sediments at A, are shown in Figure 5.8. They appear to overlie the rubbly floor of the canyon, and are sulfate-rich (Gendrin *et al*., 2005) (Viking MDIM).

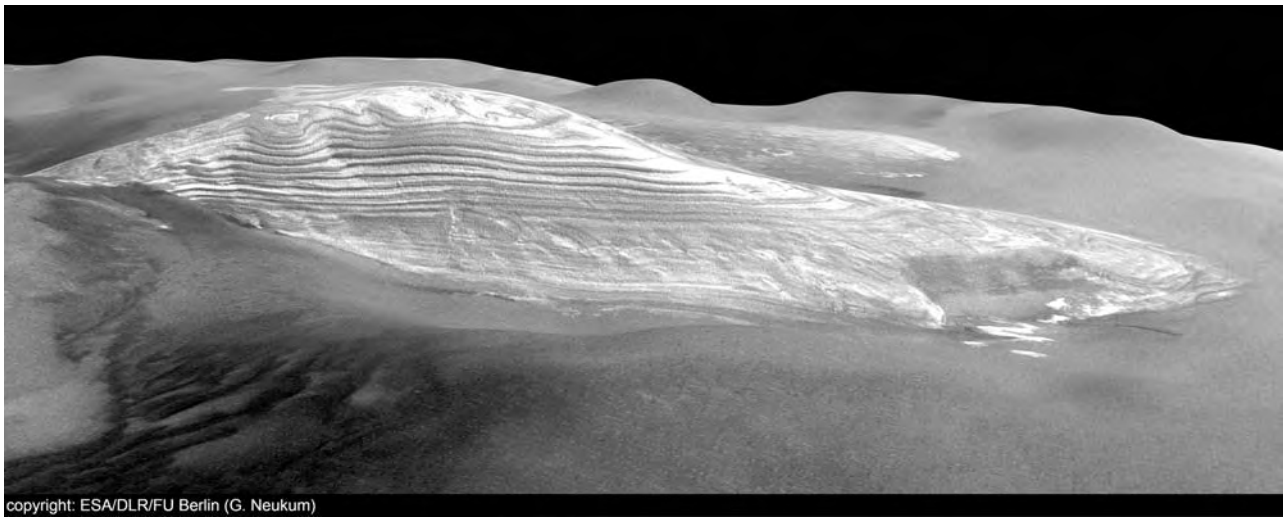

Figure 5.8. Oblique view of the sulfate-rich, layered deposits in Juventae Chasma (HRSC).

depressions, to outflow channels with graded floors and streamlined walls (Chapter 6).

Canyon walls

The canyons are incised into a sequence of finely layered rocks several kilometers thick (McEwen *et al.*, 1999; Malin and Edgett, 2000b, 2001). The layers are best seen in the upper slopes of the walls where outcrops of bedrock are common (Figure 5.11). On the lower slopes, the bedrock tends to be covered with talus. The upper layers are clearly part of the sequence of volcanic rocks that comprise the Hesperian plains adjacent to the canyons. But these Hesperian rocks must transition downward into Noachian rocks, and where this occurs is unclear. The scarcity of boulders at the base of the canyon walls suggested to Malin and Edgett (2001) that most of the walls were composed not of coherent volcanic rock but of fine-grained rocks such as sediments and impact-disturbed materials. The deeper, older rocks may also be highly altered like those in the Columbia Hills of Gusev crater, the result of weathering and/or hydrothermal alteration. However, in most places there is no obvious marker where the hypothesized transition from coherent Hesperian volcanics to the finer-grained, possibly more altered, variegated Noachian rocks occurs, unless it is close to the rim where outcrops commonly form a continuous cliff.

Most of the walls are characterized by a ridge and gully morphology consisting of sharp-crested, downward-bifurcating ridges with talus chutes between (Figure 5.4). Bedrock outcrops are common along the crests of the ridges. Downslope, the ridge-crest outcrops tend to be fewer and the talus chutes may merge to form an almost continuous talus slope. Along some of the walls, particularly the north walls of Coprates Chasma and east Candor Chasma, the downward-branching spurs are truncated near their bases to form triangular facets. Alignment of the facets results in continuous linear escarpments hundreds of kilometers long that resemble terrestrial fault scarps. Since the escarpments cut the eroded walls, they indicate that faulting continued as the walls were being eroded.

Branching side canyons are cut deeply into some of the walls. This style of degradation is best developed on the southern wall of Ius Chasma between 273 and 283°E, and around the south end of Echus Chasma (Figure 5.4). The Ius tributaries extend up to 100 km from the main east–west canyon, and are mostly oriented NW–SE or NE–SW. Most are V-shaped with steep, talus-covered walls and alcove-like terminations. Down-valley slopes are typically close to 10°. Junctions with each other and with the main canyon are mostly concordant. The side canyons at the southern end of Echus Chasma are fed by dense, branching valleys shallowly incised into the surrounding plains (Mangold *et al.*, 2004). Similar valleys are rare in the plains adjacent to Ius Chasma. Although deposits are observed at the mouths of some of the side canyons where they intersect the main canyon floor, such accumulations are rare and incommensurate in size with the volumes eroded to form the valleys. This may indicate that erosion of the valleys continued contemporaneously with the downfaulting to form the canyons, so eroded products did not accumulate

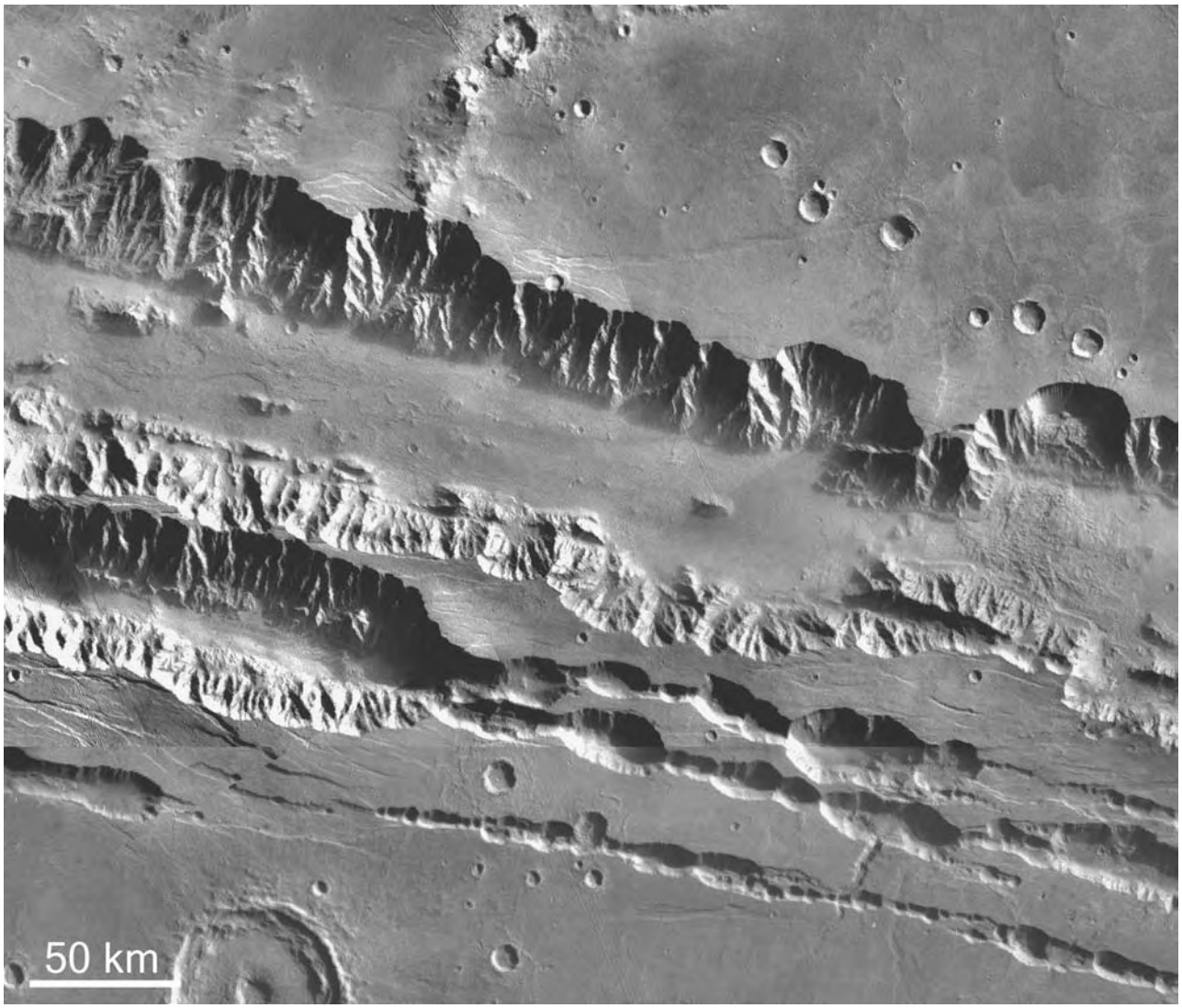

Figure 5.9. Coprates Chasma. The flat floor of the canyon is at an elevation 9 km below the surrounding plains. Spurs on the far wall are truncated at their base by a fault scarp. The canyon narrows and is partly blocked in the right side of the image. Merger of crater chains with a continuous depression south of the main canyon suggests that most of the canyon volume results from tectonic collapse (Viking MDIM).

at the mouth of the valleys, but if so, some process must have redistributed the eroded material to leave the canyon floor flat. The tributaries to Ius Chasma probably formed primarily by sapping processes acting preferentially along faults (Sharp, 1973a; Kochel *et al*., 1985). Preferential development of the side canyons on the south wall may have been aided by regional dip of the wall rocks to the north (Sharp and Malin, 1975), or it may result from better development of fractures along which erosion was concentrated (Davis and Golombek, 1990). The valley networks leading into the side canyons of Echus Chasma suggest that surface runoff contributed to their formation and that precipitation occurred after formation of Echus Chasma was well under way. A puzzling aspect of these small valleys, if they formed by precipitation, is why they formed only close to the canyon and are not on similar-aged plains more distant from the canyons.

Landslides

In many places the walls of the canyons have collapsed to form huge landslides. From Viking images, Lucchitta (1979) identified 35 such landslides ranging up to almost 100 km across, 80 km long, and

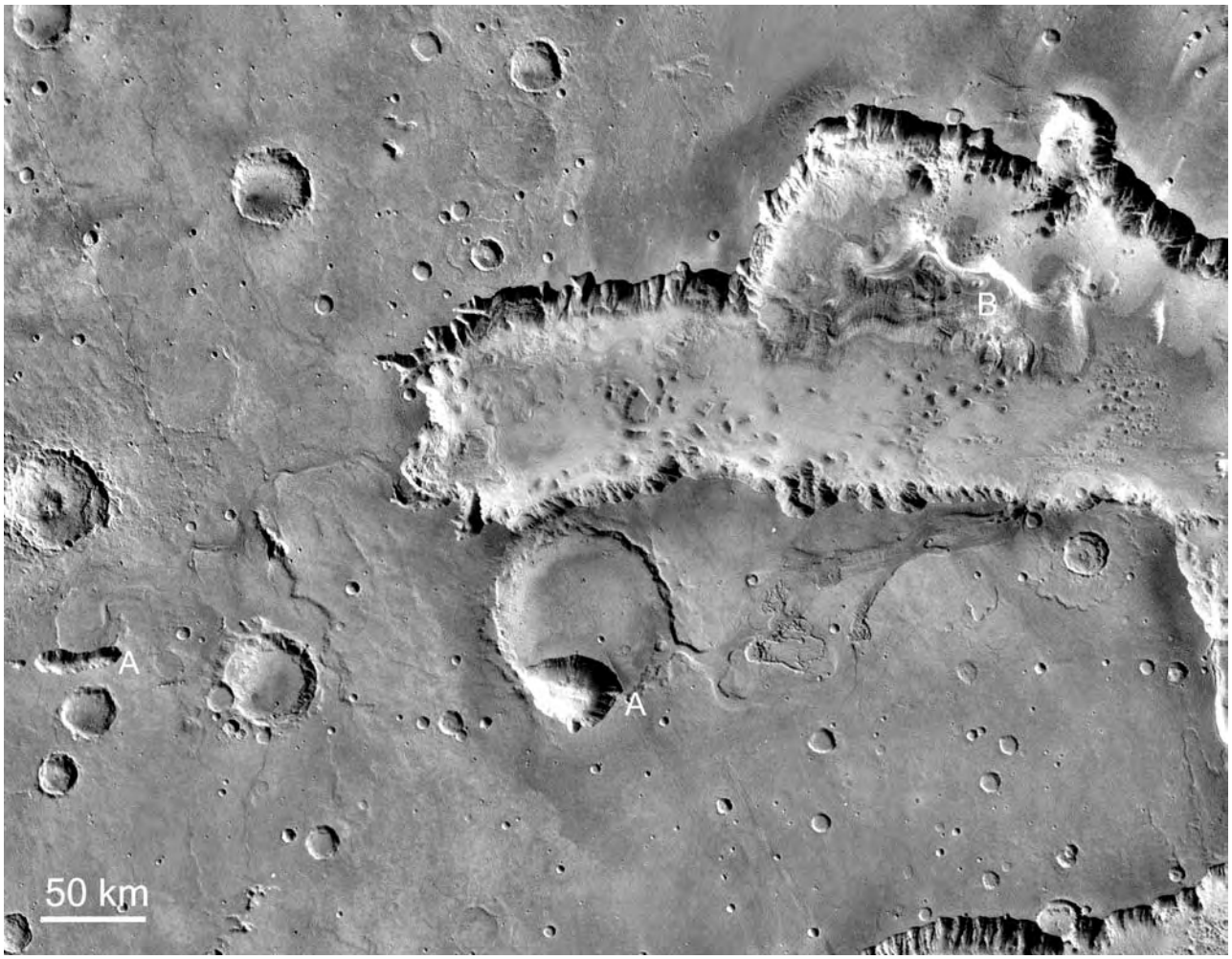

Figure 5.10. Ganges Chasma. At B is a thick sequence of layered sediments. Channels that start at two local depressions marked A and extend into the canyon suggest ground water pressure was at one time high enough to raise water to the elevation of the plains, well above the canyon floors (Viking MDIM).

10,000 km^3 in volume. She recognized two basic types: unconfined landslides that moved across the canyon floor without encountering any significant barrier, and confined types that ran into and sometimes partly up an opposing wall. The landslides leave an alcove-shaped scar in the canyon wall, typically with bedrock outcrops at the top of the wall and continuous talus slopes below (Figure 5.12A). The landslides commonly have two distinct units. The upper parts of the landslides consist of coarse, rotated, and jostled blocks in which the layering of the country rock can commonly be seen. Below this unit, in unconfined landslides, is commonly a longitudinally striated, fan-shaped debris apron extending from the blocky facies across the canyon floor. The blocky unit is mostly confined to within the scar in the wall, but the striated debris of the larger landslides may extend for tens of kilometers out into the canyon. In many places, debris aprons are superimposed one on another (Figure 5.12B). They appear to be thin since the underlying topography commonly shows through. Where a landslide encounters a barrier such as the opposing wall, the longitudinal striations are lost and transverse ridges develop. The two very different landslide units probably reflect differences in the properties of the wall rock, the blocky upper unit being of a competent, possibly volcanic, caprock and the lower unit being of less competent, finer-grained, and possibly more weathered and volatile-rich materials at greater depths. A combined crater count on several different landslides (Lucchitta, 1979) suggests that the landslides are young, with an average

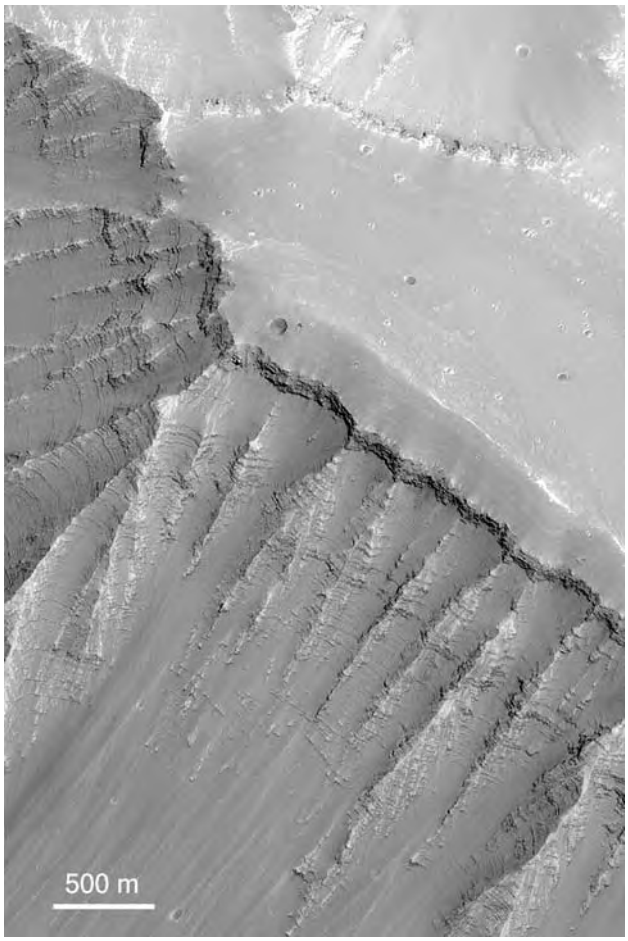

Figure 5.11. Layers exposed in the northwest wall of Melas Chasma at 7.6°S, 283.6°E. At the top of the slope is an almost continuous caprock. The image has been inverted for ease of viewing (MOC E1400415).

age of middle to late Amazonian. A young age is consistent with their remaining intact and not being cut by the canyon-forming faults. They thus appear to have formed after the branching valleys discussed above.

From comparisons with terrestrial landslides, and theoretical considerations, several workers have attempted to determine the volatile content of the landslides, that is, whether they were supported by gas or liquid. The longitudinal pattern of striae is rare in terrestrial landslides. Transverse ridges normally form as a result of compression of material within the flow as materials in the distal parts of the flow slow because of basal friction. An exception is the Sherman landslide, Alaska, which moved over glacier ice (Shreve, 1966b). This and other considerations, including observations of donut-shaped hills resembling terrestrial kettles formed by melting of ice blocks, led Lucchitta (1987) to conclude that the Valles Marineris landslides were wet. On the other hand, McEwen (1989) noted that the height of drop of the martian landslides as a function of their runout length followed a trend almost identical to terrestrial dry landslides after appropriate correction for gravity. He accordingly concluded that the martian landslides were dry. Harrison and Grimm (2003) analyzed landslides from different locations on Mars with the aid of a theoretical model (Hungr, 1995) that had been used successfully to model terrestrial landslides with a wide range of rheologies. They found that the geometries of the Valles Marineris landslides were best reproduced with models in which a supporting liquid or gas was present. They suggested that this could be liquid water below a thin cryosphere or flash sublimation of CO_2. Yet another possibility is that the landslides were subaqueous, the wall failures having occurred when lakes were formerly present in the canyons (Shaller *et al.*, 1989).

A very different and very puzzling kind of deposit found in Melas Chasma (Figure 5.13) and possibly elsewhere may also be the result of landslides (Weitz *et al.*, 2003). It consists of crudely oval-shaped blocks within a dark matrix. Most of the blocks have a smooth outline. Most, but not all, are light-toned, and some have a bright outer margin and dark core. Layering within the blocks is common. Where the blocks are closely spaced they appear to indent one another, as though they had deformed plastically. Weitz *et al.* (2003), acknowledging the puzzling nature of the deposits, tentatively suggested two possibilities for their formation: (1) subaqueous landslides that formed while a lake was formerly present in Melas Chasma, and (2) landslides of waterlogged sediments that occurred immediately after draining of the postulated former lake. The sediments could have been either from the canyon walls or from interior sediment mounds.

Interior layered deposits

Layered deposits interior to the Valles Marineris were first recognized in Mariner 9 images. They remain among the most puzzling and controversial of the canyons' features. Significant deposits occur in every chasma except possibly Coprates. The most conspicuous are in Hebes, Ophir, Candor, and Ganges, where they form thick sequences that extend from the canyon floors almost to the heights of the canyon rims. In all these canyons the layered deposits tend to form light-toned, rounded mounds or flat-topped mesas

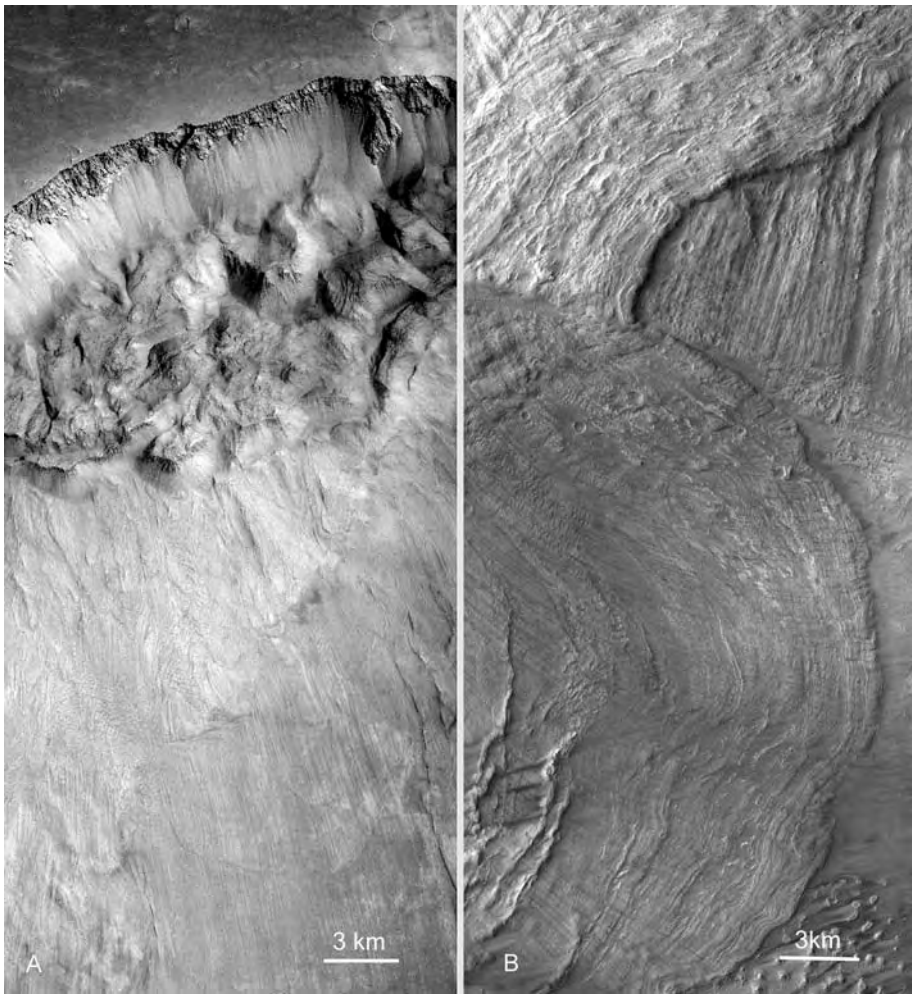

Figure 5.12. Landslides. (A) Looking north at the north wall of Ganges Chasma at 8.6°S, 315°E. The upper part of the landslide consists of rotated blocks of the former wall caprock, in which layering can be seen. Below the blocks, the landslide has longitudinal striae. The contrast between the two units suggests that the upper part of the walls is more competent than the lower (THEMIS V01001002). (B) Overlapping landslides in Melas Chasma at 8.6°S, 282.1°E. The landslide in the lower part of the frame has circumferential ridges typical of terrestrial landslides rather than the longitudinal striae typical of martian landslides (THEMIS V0255002).

toward the center of the canyons and separated from the canyon walls by an irregular depression or moat. Layering is indicated in several ways and at a wide range of scales (Figure 5.14). The layers may be seen as horizontal, alternating bright and dark markings on the sides of the sediment mounds or as swirling patterns on the upper eroded surface. The sides of the mounds may be finely terraced or they may step down to the canyon floor in a few broad, flat-topped terraces. In some places the sides of the mounds have an etched appearance and layering is barely discernible. Commonly, the sides of the mounds display different erosional styles at different levels. Some of the most convincing indications of layering are on the upper surfaces of the deposits, which may be eroded into intricate patterns of finely terraced hills and valleys. Elsewhere the upper surface may be smooth. In almost all cases the layering appears to be close to horizontal, although measurements indicate that the layers slope down toward the edges of the mounds (Hauber *et al.*, 2006). The sides of many of the sediment mounds are eroded into a characteristic pattern. Equally spaced, parallel ridges and grooves oriented at right angles to the slope give the slopes a fluted appearance (Figure 5.15) that contrasts sharply with the spur and gully style of the canyon walls. Elsewhere, the mounds appear more massive, their surface has an etched appearance, and continuous

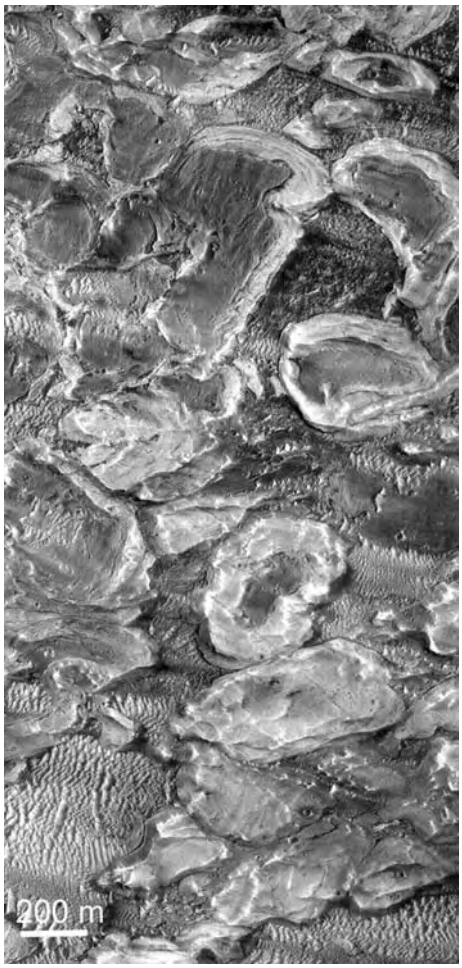

Figure 5.13. A blocky deposit of unkown origin in Melas Chasma at 8.8°S, 282.6°E. The rounded blocks are light-toned or have a dark center. Where they are in contact, some appear deformed. Dunes are present between the blocks. The scene is 1.4 km across (MOC M0904367).

layers are difficult to discern (Figure 5.16). This erosional style is similar to that of mounds of sediments elsewhere on the planet, particularly within large craters (Malin and Edgett, 2000b).

The origin of the layered deposits is very puzzling. A fundamental issue is whether the sediments are simply remnants of the rocks into which the canyons are cut or whether they are younger deposits that accumulated in the canyons after the canyons were at least partly formed. Malin and Edgett (2000b) maintain that the sediments are remnants of the country rock, which we know is layered from the 10 km sections in the walls. They argue that the wall rocks are mostly sediments. They note the presence, in places, of light-toned rocks in the canyon walls and suggest that these could be the equivalents of light-toned sediments that are common elsewhere in Noachian terrains, particularly in large craters. Erosion and retreat of the canyon walls, they argue, could leave behind the stacks of light-toned sediments that we observe. However, these arguments appear at odds with stratigraphic relations that suggest that at least some of the sediments are younger than the wall rocks. The layered sediments are, for example, clearly superimposed on the divide between the Ophir and Candor Chasmata (Carr, 1981; Lucchitta *et al*., 1992) (Figure 5.5), and in the Juventae and Ganges Chasmata they are superimposed on chaotic terrain, which must have formed after the canyons. The interior deposits also typically have an albedo and erosive style very different from the wall rocks. Considerations such as these have led most observers to conclude that most of the interior sediments accumulated after the canyon formed. Despite this, there remains the possibility, even the likelihood, that some significant fraction of the interior sediments is Noachian country rock remnants.

Although many suggestions have been made, no satisfactory hypothesis exists as to how the thick piles of sediments accumulated in the canyons or how the moats around many of the piles formed. McCauley (1978) suggested that the sediments were deposited in lakes, asserting that no other process could explain the horizontal nature and continuity of the beds, their subtle differences in reflectance and competence, and the rhythmic nature of the sequences. The former presence of deep lakes is also supported by the emergence of outflow channels from the east end of the canyons, and from the closed canyons north of the main system. Channels that start at local depressions in the plains adjacent to the canyons imply a high water table, consistent with the presence of lakes in the canyons (Figure 5.10). The lake hypothesis has been elaborated upon by numerous workers (e.g. Nedell *et al*., 1987; Lucchitta *et al*., 1992, 1994; Komatsu *et al*., 1993; Weitz and Parker, 2000). Possible additional support for the former presence of lakes within the canyons is the recent detection of significant fractions of the sulfates kieserite ($MgSO_4.H_2O$) and gypsum ($CaSO_4.2H_2O$) in the light-toned layered deposits (Gendrin *et al*., 2005). The salts are found over a wide range of elevations from −4 km to +3 km. While sulfates can form by evaporation of standing bodies of saline water, it is not the only way that they can form. They could, for example, result from alteration of previously deposited sediments by groundwater circulation. A significant problem with the lake hypothesis is that much of the layering in many of the sedimentary stacks is not

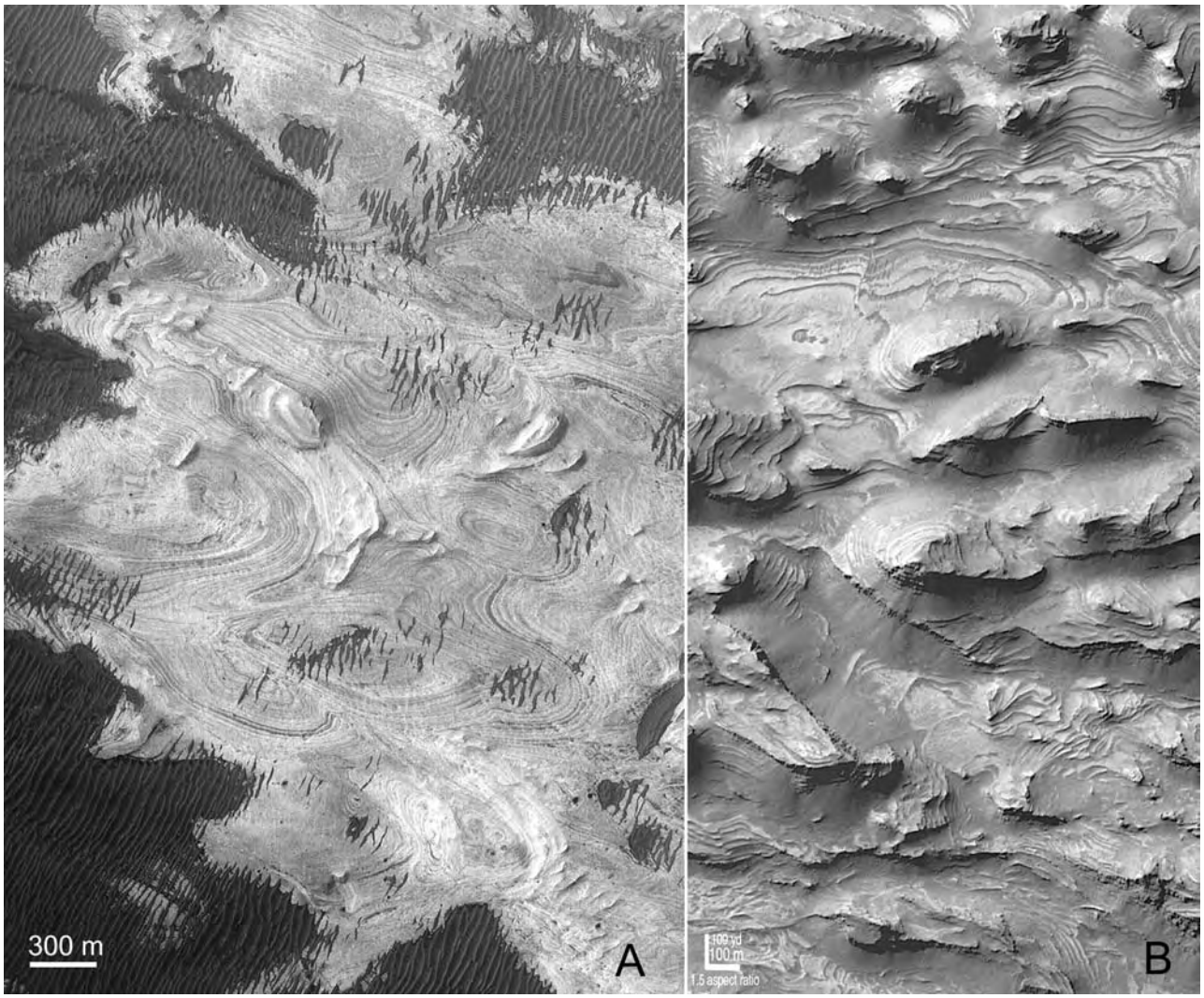

Figure 5.14. (A) Layered sediments in Melas Chsma at 9.0°S, 285.3°E. The layering is expressed both topographically and as variations in brightness. The dark areas are dunes (MOC R1401823). (B) Layered deposits on the floor of Candor Chasma at 6.3°S, 282.5°E. The location is in the low between the canyon wall and the central sediment mounds (MOC FHA01278).

horizontal. Hauber *et al*. (2006) showed, for example, that the sedimentary layers in Hebes Chasma slope up to 22°. They prefer a pyroclastic origin rather than a lacustrine origin for these and other similar deposits.

For the canyons to have contained lakes, they must at some time have been closed to the east. If the layered deposits accumulated in lakes, then they must have done so before Ophir, Candor, Melas, and Coprates merged because sediment stacks in both Ophir and Candor reach elevations of over 3000 m, well in excess of parts of the rim of eastern Coprates. How the canyons could have filled to this level is puzzling. One possibility is that they filled by rainfall, which implies a much warmer climate and no cryosphere. But if lakes filled the canyons to the 2000−3000 m level under warm conditions, how could the lakes have been sustained against losses by percolation to the surrounding low-lying areas, particularly to the north and east? Another possibility is that they formed under cold conditions, as a result of melting of thick ice deposits that may have accumulated during periods of high obliquity (Jakosky and Carr, 1985; Misehna *et al*., 2003), or melting of ground ice by injection of dikes (McKenzie and Nimmo, 1999). Water could have been introduced into the canyons from deep below the cryosphere as a direct consequence of the faults that caused the canyons (Hanna and Phillips, 2005), in a manner analogous

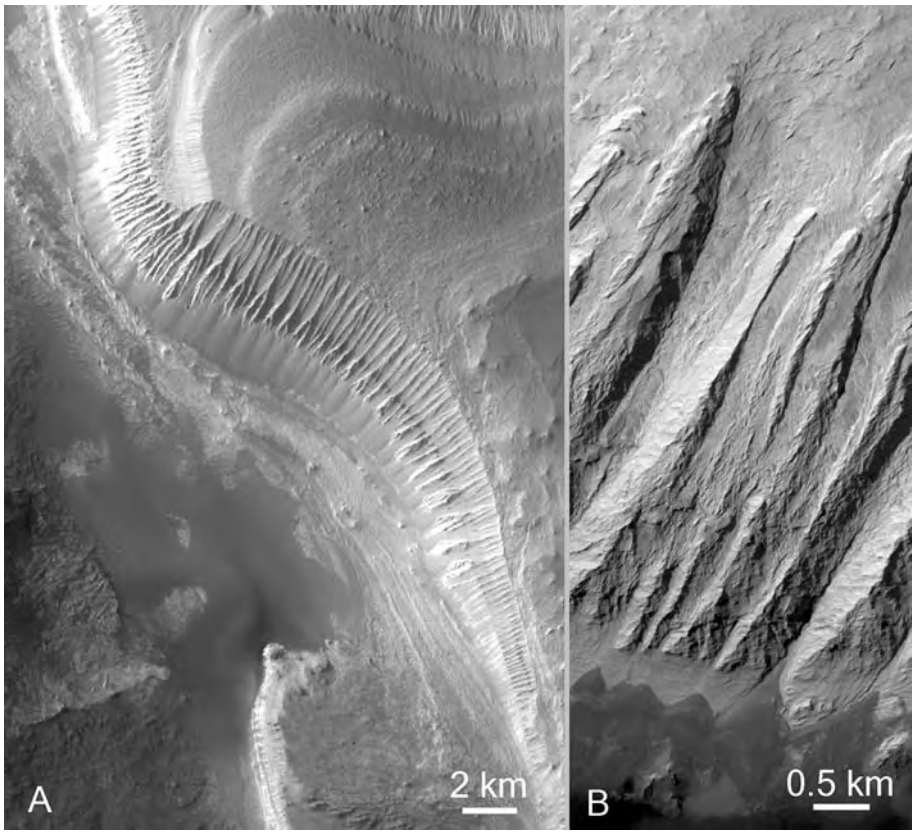

Figure 5.15. Different erosional styles in layered sediments. (A) Stacks of layered sediments in Melas Chsma at 10.4°S, 285.0°E. At the top of the image broad terraces step down to the canyon floor. In the middle of the image the slopes of the sediment pile have different erosional styles at different levels, probably the result of different lithologies (THEMIS V03948003). (B) Detail of flutes on the side of sediments in Candor Chasma at 6.8°S, 288.2°E. (MOC E1900200). The style of erosion is very different from that of the canyon walls (see Figures 5.9 and 5.11).

to formation of some large outflow channels (see Figures 6.9 and 6.10). If conditions were cold percolation losses would have then been limited by the cryosphere. Yet another possibility is that the canyons were filled during a transitional period, when there was rainfall or snowfall, but a thick cryosphere had been inherited from an earlier colder time. The lakes are not likely to have been sustained by global percolation fed by basal melting of ice at the south pole (Clifford, 1987) because the inferred lake levels are at a higher elevation than the base of the ice at the pole. Despite the difficulties in seeing how lakes could form and be sustained, their former presence remains a strong possibility. The relations at Juventae Chasma are particularly compelling (Figure 5.7). If Maja Vallis was cut by water, then Juventae Chasma had to have contained a deep lake that overflowed to the north.

Even if lakes were formerly present in the canyon, many questions regarding the sediments remain unanswered. Are the sediments locally derived materials, that is, materials that formerly occupied the voids that are now the canyons? If so, how did the local materials become disaggregated and redeposited as finely layered sequences that unconformably overlie the older deposits, as at the Ophir–Candor divide? If the sediments are of introduced materials, how were they introduced? Could the lakes have acted as traps for eolian debris, deposition perhaps being modulated by astronomically induced climate variations? Could groundwater have introduced sedimentary material into the canyons, but if so, how, and what was the source of the erosion products? Could the sediment mounds be the result of subaqeous or sub-ice volcanism, as suggested by Chapman and Tanaka (2001), or simply mounds of pyroclastic deposits as suggested by Hauber *et al.* (2006)?

The gap that typically exists between the layered deposits and the canyon walls is equally puzzling. One possibility is that Hebes, Ophir, and Candor

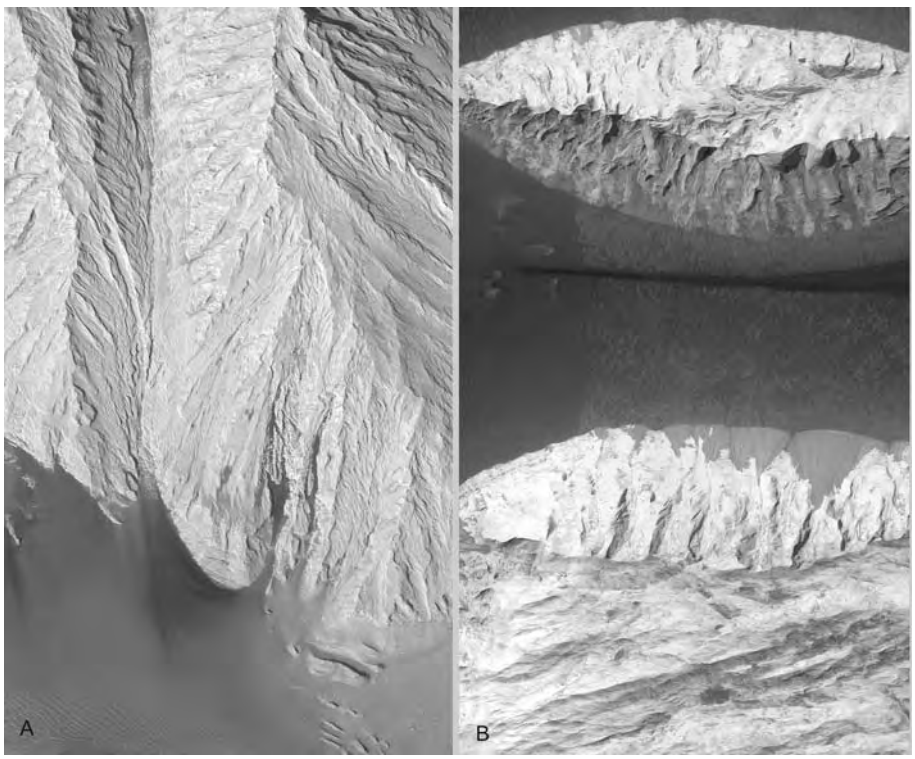

Figure 5.16. Massive, light-toned deposits in different parts of the canyons. (A) East Candor Chasma at 7.8°S, 294.7°E (MOC R1800260). (B) Ganges Chasma at 8.5°S, 310°E (MOC E170009). Both images are 3 km across.

Chasmata, those canyons most nearly filled with sediments, were at one time actually filled and that the canyons were subsequently enlarged to leave the sediments in the middle of the canyons. But what was the process of enlargement? It could have been structural, but there is little or no evidence for faulting in Hebes Chasma. If scarp retreat was erosional, how were the erosional products removed? One possibility is that catastrophic release of the lakewater within the canyons to form the outflow channels observed to the east was followed by rapid inflow of groundwater from surrounding terrain into the canyons. This resulted in preferential erosion around the periphery of the canyons to form the moats. Clearly there is much here that is not understood.

Formation of the canyons

Formation of the canyons has been variously attributed to erosion by wind and water, collapse, and faulting. Early proposals of formation by sublimation of ice and removal of material by the wind (Sharp, 1973a; McCauley,1978) appear untenable because of the difficulty of accumulating so much ground ice, particularly at the equator, the lack of indication of ground ice in the canyon walls, and difficulties in removing so much material by the wind. Other suggestions of removal of thick carbonate deposits (Spencer and Croft, 1986; Spencer and Fanale, 1990) are unsupported by any evidence, particularly spectral evidence for the presence of carbonates. Collapse as a result of opening of tension fractures at depth (Tanaka and Golombek, 1989) may have occurred, as indicated by the common association of lines of pits with graben in many places on the planet (e.g. Ferrill *et al.*, 2004), and the common merger of lines of pits to form discontinuous depression in Noctis Labyrinthus and in small canyons that parallel the main canyons. However, there is little indication of merging of collapse pits to form the main canyons.

Faulting appears to have been the dominant process of canyon formation. Although other processes may have played a role, faulting is indicated by the orientation of the canyons roughly radial to Tharsis, their graben-like form, the straight walls of many of the canyons, the triangular faceted spurs on some of the walls, the many graben in the adjacent plains parallel to the canyons, and models that indicate that the lithosphere in the canyon region should be under tension because of the presence of the Tharsis bulge (Blasius *et al.*, 1977; Masson, 1985; Schultz, 1991; Banerdt *et al.*, 1992; Lucchitta *et al.*, 1992; Mège and Masson, 1996; Anderson and Grimm, 1998;

Schultz and Lin, 2001). Some of the troughs, particularly Coprates Chasma, appear to be graben bound by normal faults with large displacements that were oriented radial to Tharsis, the result of tensional stresses circumferential to Tharsis, as described in the previous chapter. Once the relief was created, then erosional processes could operate to further enlarge the structural depressions. Faults radial to Tharsis occur all the way around the rise, albeit very unevenly and commonly in clusters of closely spaced, nearly parallel graben (see Figure 5.15). Given this crude radial symmetery, it is not clear why only the faulting east of the Tharsis summit resulted in broad structural troughs.

Early work suggested that the graben were the result of keystone-like failure on a broad arch on the eastern flank of the Tharsis bulge. The MOLA data provides some support for the presence of such an arch. The canyons cut across the northern edge of a roughly rectangular plateau incorporating much of the Syria, Sinai, and Solis Plana (Figure 5.16). The plateau is slightly lower in its center and outlined by a broad high and outward-facing slopes. The western and central sections of the canyons extend along the high that marks the northern boundary of the plateau. However, the eastern troughs are not at the crest of any significant arch, but instead cut into and across the rise at the eastern margin of the plateau.

Irrespective of the presence of an arch, the orientation of the canyons is consistent with rifting as a result of extension circumferential to Tharsis. Terrestrial rifts can form dynamically over local mantle upwellings or more slowly by passive extension of the lithosphere under tension. Rifts may be narrow, with successive extensional episodes confined to a single, weakened zone, or, more rarely, they are wide, with extension occurring in multiple zones, as in the Basin and Range province of the western United States. On the assumption that the canyons are partly compensated at depth by a thinner crust, Anderson and Grimm (1998) estimated the thickness of the crust under the canyons from the local gravity and topography and for various assumed lithosphere thicknesses. They then examined different models of crustal extension in light of these limits. They concluded that a wide rift/slow extension model best fits the data. In this model, extension causes crustal thinning, which in turn results in uplift of upper mantle materials. The process is slow enough that the materials have time to cool and strengthen between successive deformational episodes, and the site of deformation is displaced and the rift widens. From the thinning of the crust under the canyons, they estimated that there had been 10–30 percent extension across the canyons, an estimate that is independent of the observed surface features, but which is roughly consistent with estimates from those features. In a complementary study, Schultz and Lin (2001) used a 3-D mechanical model to derive characteristics of the major normal faults that created each of the troughs. They concluded that the faults had dips of 40°–50° and offsets ranging up to 12 km, and that they extended through the entire lithosphere to depths of 60–75 km. Extension may have been accompanied by intrusions to form dikes swarms beneath the canyons (Mège and Masson, 1996) or a small number of megadykes (McKenzie and Nimmo, 1999).

The troughs appear to be younger than early Hesperian since they cut Lunae Planum lavas of this age (Scott and Tanaka, 1986). If the draining of the postulated lakes in Valles Marineris contributed to the formation of fluvial features in Tiu and Simud Valles, and in the Capri and Eos Chasmata, which are all Hesperian in age, then the canyons must have formed, filled with water, and drained all within the Hesperian, which is estimated to have lasted from roughly 3.7 to 3.0 Gyr ago (Hartmann and Neukum, 2001). Crater counts on landslides (Lucchitta, 1979) indicate that enlargement of the canyons by landsliding continued well after this date. Faulting may also have continued, although continuity of the floor of Coprates Chasma with the fluvial features farther east suggests that the floor of Coprates has not been significantly downfaulted since the Hesperian when the fluvial features formed. The age of the interior layered deposits is poorly constrained. If they were deposited in lakes, or eroded as a consequence of the release of water from the lakes, then they are also Hesperian in age. But some may be the result of late-stage volcanism and be as young as late Amazonian (Lucchitta, 1989; Chapman, 2002).

Summary

In the early Hesperian a series of gigantic troughs formed on the eastern flank of the Tharsis bulge. The troughs formed primarily by faulting, the result of roughly north–south tensional stresses caused by the presence of the Tharsis bulge to the west. Why these megatroughs developed only to the east of the bulge and not elsewhere around the bulge, where similar stresses probably occurred, is unclear. The fault troughs were subsequently enlarged by fluvial and mass-wasting processes, most obviously by huge landslides. The troughs expose >10 km thick layered sequences in the walls that likely extend in age from Hesperian at the surface to deep into the

Noachian at the deepest exposures. Thick, layered, sulfate-rich deposits are also present in the canyons, but what fraction are remnants of the rock sequence into which the canyon is incised and what fraction are later deposits is not known. Lakes may have formerly occupied the canyons and drained catastrophically to the east in the late Hesperian, as indicated by merging of the canyons eastward with large fluvial channels. Possible sources of the water are rainfall, the result of warmer climatic episodes in the Hesperian, or meltwater from ice deposits that formed during periods of high obliquity. How or if the layered deposits accumulated within lakes is not known. Possible origins for these deposits include reworking of the local country rock, trapping of eolian debris, and subaqueous volcanism. The moat surrounding the sediments is also puzzling. One possibility is that draining of the lakes in the canyons was followed by flow of water into the canyons from the surrounding region as the water table was lowered, and that this resulted in preferential erosion of the internal deposits around their periphery. Activity in the canyons during the Amazonian was modest, including limited movement along some of the faults, further landsliding and fluvial activity, and possibly late-stage volcanism.

6 Channels, valleys, and gullies

The discovery of seemingly water-worn valleys during the Mariner 9 mission remains one of the most transforming events in the history of our exploration of the Solar System. Our perception of Mars as a dry, cold, sterile planet was changed forever to that of a planet that likely had experienced warm and wet surface conditions under which life could have originated and survived. When the channels and valleys were first observed, there was considerable resistance to accepting them as water-worn because of the cold conditions that prevail on Mars today. Several alternative origins were proposed, including erosion by lava, hydrocarbons, and liquid CO_2, glaciation, and mobilization of the surface materials as debris flows. However, the close resemblance of the channels and valleys to terrestrial water-worn features, the abundant presence of water ice, the finding of evaporites in Meridiani Planum and elsewhere, and the difficulties with other erosive agents, make it almost certain that the principal erosive agent that cut most of the channels and valleys was liquid water. While liquid water is likely the main agent, the source of the water and the conditions under which the channels and valleys formed are still controversial. In this chapter we explore how the channels and valleys formed and what they might imply about the abundance of water and past conditions on the planet. Climate history is discussed more fully in Chapter 12.

Valley is a general term used to describe any linear depression. Valleys can form by a variety of processes such as water erosion, glaciation, faulting, mass wasting, and volcanism, acting individually or in combination. The term ''channel'' is customarily used more restrictively. In fluvial geomorphology it normally refers to the actual conduit within which a stream is confined. Thus a stream channel is comparable in width to the stream that cut it, whereas a fluvial valley is usually substantially wider and deeper than any of the streams that contributed to its formation. For Mars, three types of linear, incised, and likely water-eroded features are generally distinguished: outflow channels, valley networks, and gullies. Outflow channels are linear swaths of scoured ground, tens to hundreds of kilometers across, that commonly contain streamlined remnants of the preexisting terrain. Most start full size and have no tributaries. They are widely, although not universally, believed to have formed by huge floods. Valley networks are much narrower. Individual valleys are typically only 1–5 km across although they may be hundreds, even thousands, of kilometers in length. They form branching networks much like terrestrial river systems. Most are believed to have formed by slow erosion of running water. Gullies are smaller still. They are restricted to steep slopes, and are only several to tens of meters wide and hundreds of meters long. Although their origin is controversial, water was probably also responsible for their formation. While three types of likely water-worn valleys are recognized, they cannot always be confidently distinguished from each other. Ma'adim Vallis, for example, has attributes of both an outflow channel and a valley network, possibly having formed by a combination of large floods and slow erosion (Irwin *et al.*, 2002). Similarly, some gullies on crater walls may merge downstream to form networks. Nor can water-worn valleys always be distinguished from non-fluvial valleys. The problem is particularly difficult on and around volcanoes where lava channels can closely mimic water-worn features.

A fourth type of valley, the so-called fretted valley, is not discussed here. They are found mainly at high to mid latitudes where abundant ground ice may be present. Mass wasting, aided by the presence of abundant ice, probably played a significant role in their formation. They are discussed, along with other ice-related topics, in Chapter 8.

Outflow channels

Outflow channels vary greatly in size. The largest, Kasei Vallis, is over 400 km across at its mouth and in places over 2.5 km deep. Other outflow channels may be less than 1 km across. After the outflow channels were discovered, a wide range of possible origins were explored (see summary in Carr, 1981). The likelihood that these features were caused by large floods was recognized early (Baker and Milton, 1974; Baker, 1982) and this is still the prevailing view. They start full size and have an

array of characteristics remarkably similar to those of large floods on Earth such as the Channeled Scablands of eastern Washington state (Baker and Nummedal, 1978). The channels have low sinuosity and high width–depth ratios. Their walls are streamlined and they contain teardrop islands around which flow has diverged and converged. On their floors are a wide range of bedforms including longitudinal striae, cataracts, plucked zones, and inner channels. These are all characteristics of large terrestrial floods. While a flood orgin is the prevailing view, other possible modes of origin, such as erosion by glaciers (Lucchitta, 1982, 2001) or lava (Leverington, 2004) or mobilization of surface materials as debris flows, either water-lubricated (Tanaka, 1999) or CO_2-supported (Hoffman, 2000), are still debated. If the channels formed by large floods, then the larger channels such as Kasei Vallis imply that enormous volumes of water episodically flowed across the martian surface. The estimated discharge rates are so high that the water that cut them could not have been provided simply by surface runoff immediately following rainfall. Some form of storage, followed by rapid release of the stored volume, is required. Also, if the channels formed by floods, then large bodies of water must have formed at the ends of the larger channels. We have little evidence that large bodies of water (ice) are present at the ends of the channels now, so what happened to the water? We also want to know what the floods imply about the climatic conditions when they formed and whether these enormous events affected the climate.

Outflow channels occur in several regions of the planet and start in several different types of geological terrain. They clearly do not all originate in the same way. In the following discussion, outflow channels in different regions are described and their possible origins examined. The emphasis is almost exclusively on the flood hypothesis, but, as we shall see, floods can be generated in a variety of ways.

Circum-Chryse channels

Description By far the most prominent outflow channels on the planet occur around the Chryse basin (Figure 6.1). At the south end of the basin several large channels emerge from the uplands and cross the southern part of Chryse Planitia where they form an 800 km wide swath clearly marked by longitudinal scour and numerous teardrop-shaped islands. Many of the islands have a crater at their upstream end and a long triangular tail pointing downstream (Figure 6.2), indicating that flow had diverged around the pre-existing crater thereby protecting the area immediately downstream of the crater from erosion. Between the islands, the flow path is marked by closely spaced, subparallel striae. More rarely, the scoured surface within the channel has a rough, etched-like appearance as though some of the surface materials had been plucked away. Channels, scour marks, and islands indicate a northward flow from the uplands, across the southern boundary of Chryse Planitia, then across the plains until about 25°N where the flow lines curl to the northeast and merge with those from Kasei Vallis to the west. Evidence for flow can be traced northeastward to roughly the 40° latitude. Although the dominant flow is to the north and then to the northeast, the flow diverges and converges around numerous obstacles, such as craters and mare ridges.

The Pathfinder spacecraft landed in an area scoured by the southern Chryse floods (Golombek *et al.*, 1997). The rocky surface on which it landed is consistent with a depositional plain. The nearby rounded and semi-rounded cobbles and boulders are similar to those observed on depositional plains of large terrestrial floods, and the imbricate placement of some of the rocks is that expected from the direction of flow inferred from the orbiter data (Chapter 11). However, the lander data in general provided little compelling evidence that the surface was indeed the result of a large flood. The characteristics of most of the individual rocks could plausibly be interpreted as simply the result of volcanism, impacts, and wind, without the intervention of fluvial processes.

The scour marks of Chryse Planitia can be traced southward into the uplands where they converge either on well-defined linear channels such as Ares Vallis and Shalbatana Vallis, or into broad, irregular, steep-walled depressions, such as the Tiu and Simud Valles. Most of the linear channels have scoured floors and contain teardrop-shaped islands; the irregular channels have blocky or smooth floors. Further upstream, in the source region of the channels, extensive areas of the uplands have seemingly collapsed to form broad depressions partly filled with rubble or blocks that range up to tens of kilometers across (Figure 6.3). These low-lying rubble-filled hollows have been called chaotic terrain or chaos. Most of the hollows are to the east of the canyons, but some such as Ravi, Juventae and Orson Welles are to the north. The hollows range widely in size. The depression in which Ravi Vallis (Figure 6.4) starts is only 40 km across whereas Iani Chaos, at the head of the much larger Ares Vallis, is 500 km across. Although several large channels exit full size from such hollows, valleys rarely feed into the hollows. The channels simply start at a hole in the ground, with no obvious catchment area.

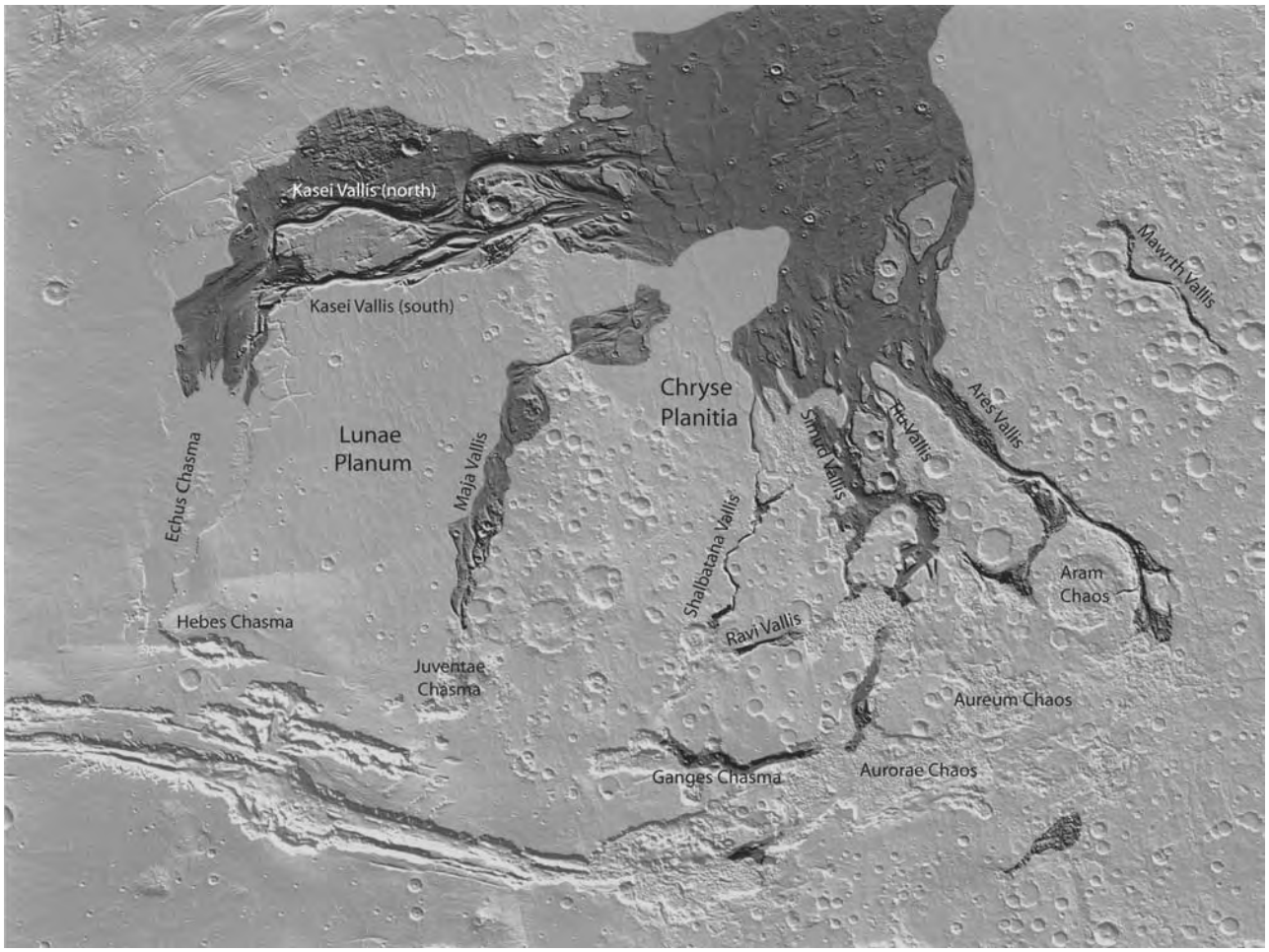

Figure 6.1. Outflow channels around the Chryse basin. Dark areas are regions of scoured ground with teardrop-shaped islands. The outflow channels start in box canyons to the north of the main east–west canyons, or in chaotic terrain to the east of the canyons. The image is 3000 km top to bottom (MOLA).

Several of the chaos-filled depressions near the upper reaches of the Chryse channels in Margaritifer Terra, such as Aureum Chaos and Arsinoes Chaos, have no outlet, and many of the individual blocks within the chaos retain on their upper surfaces the textures of the surrounding, higher, undisturbed terrain. These closed depressions have therefore not been hollowed out by erosion but have rather formed by collapse. Even where a channel emerges from the chaotic terrain, the source may still be a completely enclosed depression because the chaotic surface is at a lower elevation than the emergent valley. Parts of the floor of Ravi Chaos are, for example, over 1.5 km below the floor of its outlet channel (Figure 6.5) and parts of Juventae Chasma are over 3 km below the floor of its outlet, Maja Vallis (Figure 5.7). Any theory of origin for the channels must not only account for the sudden emergence of channels from the hollows, but for the formation of the hollows themselves.

Streamlined and scoured forms are less common in the irregular depressions of Tiu and Simud Valles. More typically they contain chaotic terrain and irregularly shaped islands. However, smooth, linear pathways through the chaos and occasional streamlined forms still indicate flow across the surface. To the south and southwest the steep walls of Tiu and Simud Valles merge with those of the canyons so that there is a continuous transition from the scoured terrain of Chryse Planitia, through chaos-filled depressions into the canyons.

The largest well-preserved outflow channel on the planet is Kasei Vallis. It probably also originally started near the main east–west canyons. It starts in Echus Chasma, a large north–south canyon that

Figure 6.2. Teardrop-shaped islands and scoured ground are common in most outflow channels. Here we see the floor of Ares Vallis at 16.0°N, 329.0°E (THEMIS V01786010).

narrows to the south and almost merges with the completely enclosed Hebes Chasma just south of the equator (Figures 5.6, 6.1). The floor of the southern part of the canyon is mostly smooth, and partly filled with young lava flows from Tharsis to the west. At about 15°N, striations and streamlined islands emerge from under the younger deposits and extend northwards. Kasei Vallis has two deeply incised branches (Figure 6.6) with a rich array of teardrop-shaped islands, scoured sections, plucked zones, and inner channels (Figure 6.7). The channel can be traced for 3500 km across the northern edge of Lunae Planum then across Chryse Planitia until it disappears at roughly 40°N in southern Acidalia Planitia. Where the channel cuts through northern Lunae Planum (Figure 6.6), the eroded swath is over 500 km wide and reaches depths of over 2.5 km below the adjacent plains.

Not all the circum-Chryse channels start in chaos or canyons. The 15 km wide Mawrth Vallis has no tributaries and no obvious source. It simply starts almost full size within the cratered terrain at 18°N, 347°E. Howard and Moore (2006) suggest that this channel had a fundamentally different origin from most other outflow channels, having formed by density currents on the floor of a former ocean.

The circum-Chryse channels are estimated to range in age from early Hesperian to early Amazonian (Scott and Tanaka, 1986; Tanaka, 1986; Rotto and Tanaka, 1995), probably from 2.0 to 3.8 Gyr ago (Hartmann and Neukum, 2001). They are therefore younger than most of the valley networks, which formed mainly in the Noachian.

Mode of formation The following discussion assumes the conventional view that the channels were cut by water. Various estimates have been made of the discharges implied by the large sizes of the outflow channels. The estimates are based on relations observed for terrestrial rivers, after correcting for the lower gravity on Mars (Komar, 1979). The basic equation is

$$Q = A\{g_m S R^{4/3}/g_e n^2\}^{1/2}$$

where A is the cross-sectional area of the flow, g_m and g_e are gravity on Mars and Earth, S is the local slope, R is the hydraulic radius (ratio of cross-sectional area to wetted perimeter, and n is the Manning roughness coefficient (Williams *et al.*, 2000). The roughness coefficient takes into account factors such as the roughness of the stream bed and the sinuosity of the channel and is determined empirically from terrestrial rivers. Applying this equation to Mars is very uncertain, in part because the relation was determined from terrestrial rivers, which are orders of magnitude smaller than the martian channels. Choosing the appropriate Manning coefficient is particularly uncertain. Wilson *et al.* (2004) suggest that previous workers had overestimated discharges by a factor of up to 25 because of inappropriate choice of the coefficient. But also we do not know the depth of the rivers that cut the martian channels, or their cross-sectional area; we only know the final result of all the

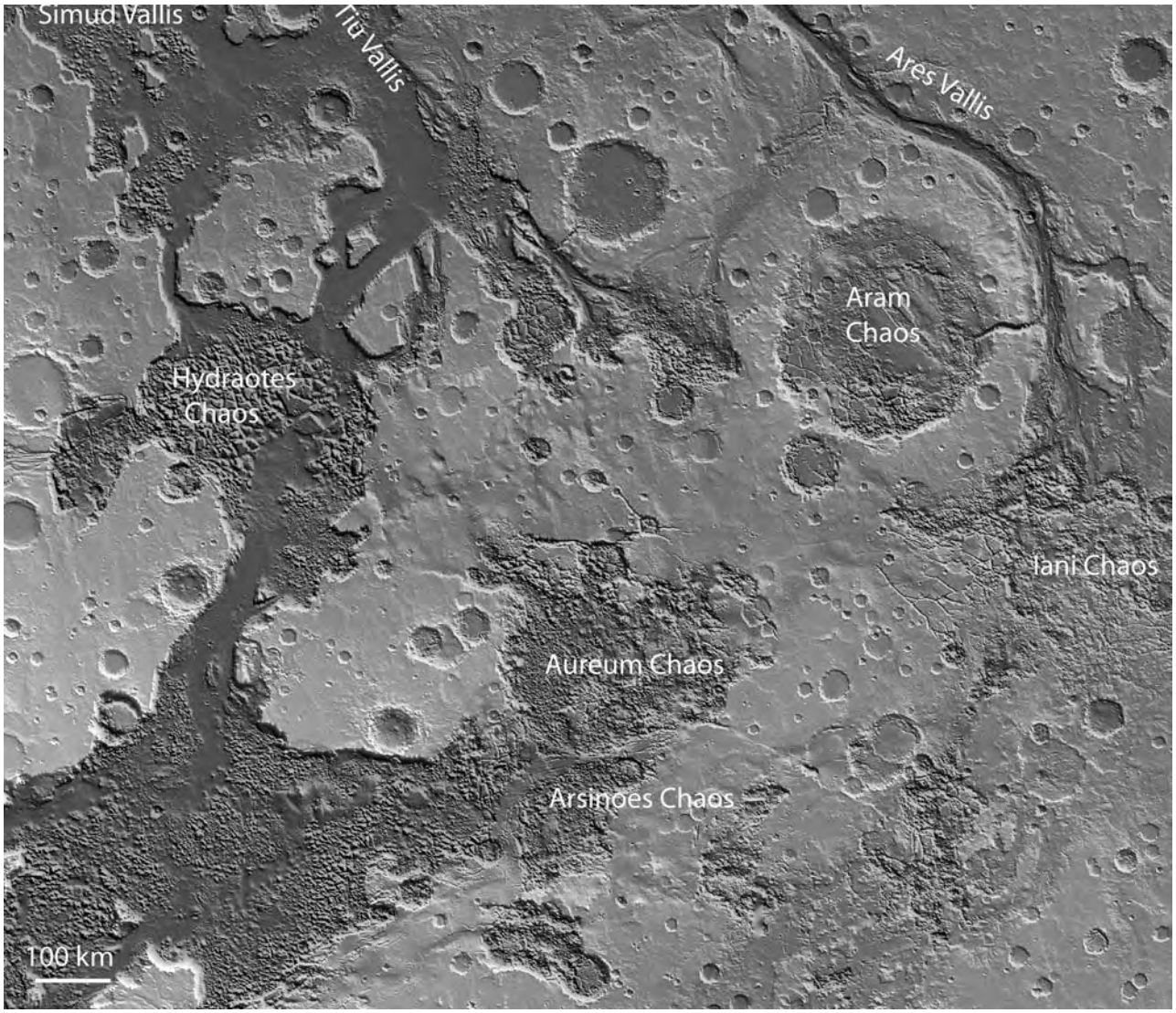

Figure 6.3. Chaos and valleys south of Chryse Planitia and east of the canyons. Darker areas are at a lower elevation. The Aureum Chaos, Arsinoes Chaos, and other small areas are depressions with no outlet. Aram Chaos and Iani Chaos are sources of Ares Vallis (MOLA).

downcutting. As a result, the discharge estimates vary widely. For Kasei Vallis, estimates for the peak discharge range from $10^4\,m^3\,s^{-1}$ (Williams *et al.*, 2000) to $10^9\,m^3\,s^{-1}$ (Robinson and Tanaka, 1990), with most estimates being in the order of $10^7\,m^3\,s^{-1}$. For comparison, the peak discharge of the Mississippi is $3 \times 10^4\,m^3\,s^{-1}$ and the discharges of the Missoula floods that created the Channeled Scablands are estimated to be of the order of $10^7\,m^3\,s^{-1}$ (Baker, 1982). Despite the uncertainties, the floods were enormous by terrestrial standards.

The observation that many of the channels start full size at rubble-filled hollows suggests that some of the floods formed as a result of massive eruptions of groundwater. Carr (1979) examined this possibility and suggested that some of the valleys formed by eruptions of groundwater trapped under high pressure beneath a thick cryosphere. The high pressures are needed to generate the large discharges. A thick cryosphere is needed to contain the high pressures within the underlying aquifer. The high pressures could have been created in several ways, such as continuity of the aquifer to high elevations in Tharsis to the west, by the trapping of the aquifer between an impermeable basement and a growing cryosphere, by volcanic eruptions into the aquifer system, and by tectonic compression. If the hydrostatic head within the aquifer exceeded the depth of burial, then any

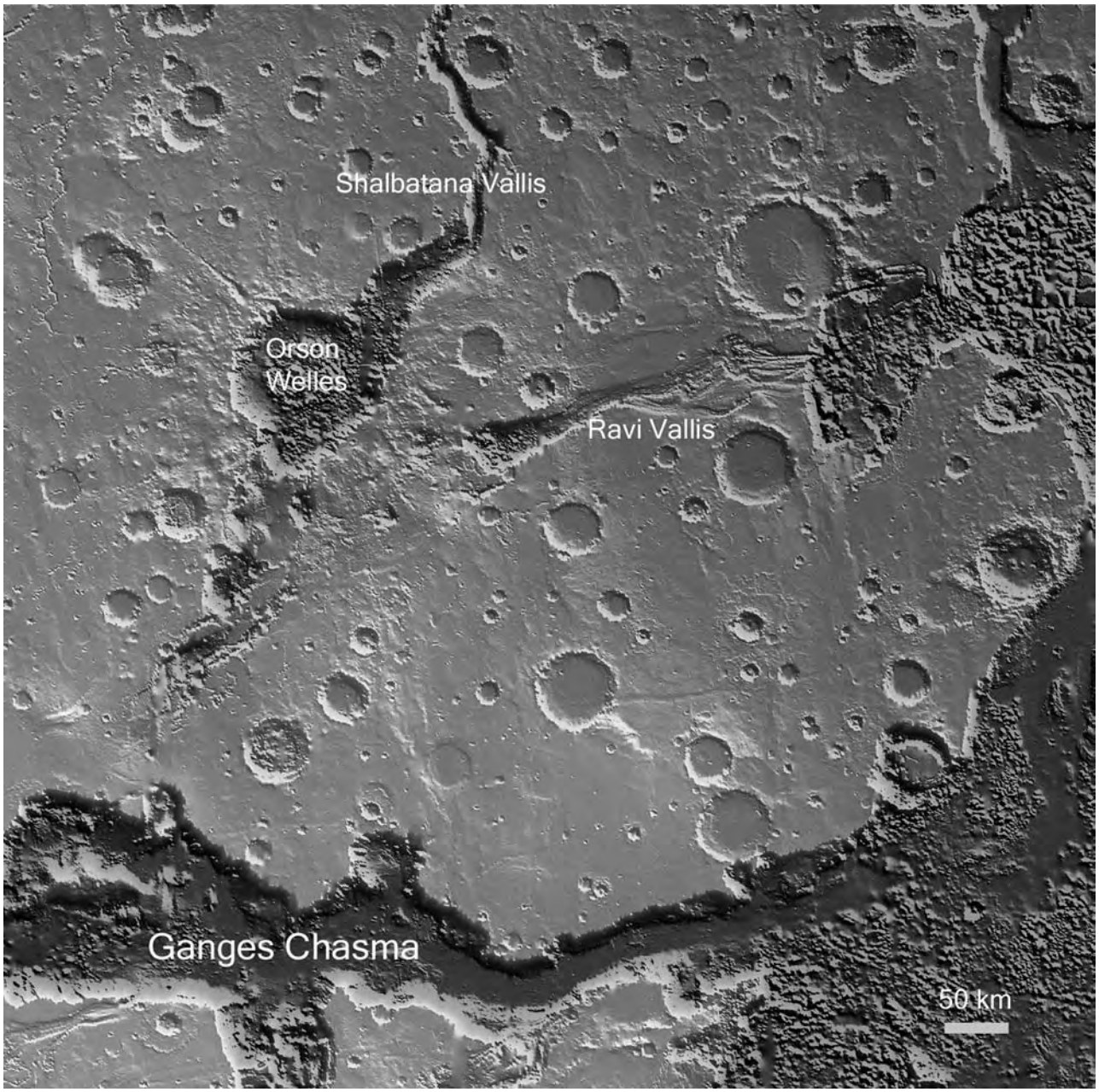

Figure 6.4. The sources of Ravi Vallis and Shalbatana Vallis. Both start in rubble-filled hollows. Extending southward from Orson Welles, the source of Shalbatana Vallis, is an ill-defined collapse depression that almost reaches Ganges Chasma. Subsurface drainage from a lake formerly present in Ganges Chasma may have caused the depression. Ultimately the lake drained catastrophically to the east. Darker areas are at a lower elevation (MOLA).

breach of the aquifer seal (the cryosphere) would result in eruption of groundwater. Eruptions could have been triggered by local or distant impacts, faulting, dike emplacement, or volcanic events.

A significant issue with this model is whether water can be drawn from the aquifer for any significant time at the high discharge rates implied by the dimensions of the channels. The rate of withdrawal of water from an aquifer is constrained by the dimensions of the conduit to the surface, the hydrostatic head, and the dimensions and permeability of the aquifer (Carr, 1979; Head *et al.*, 2003a; Manga, 2004). Because the permeability of the aquifer would restrict flow to an eruption site, any eruption of groundwater

Figure 6.5. Detail of the source of Ravi Vallis. The channel starts in a rubble-filled closed depression whose floor is at 1.5 km below its outlet. Compare with the much larger Juventae Chasma in Figure 5.7 (THEMIS).

would result in rapid drawdown of the hydrostatic head around the eruption site, with a corresponding rapid decline in the discharge rate. Manga (2004), modeling the Cerberus Fossae floods, showed, for example, that if the discharges are large, the hydrostatic head could drop by an order of magnitude within half an hour. Carr (1979) showed that to sustain high discharges for hours or days, unrealistically high permeabilities were needed. However, if the pressure were high enough and the discharge violent enough, then the aquifer itself would be disrupted and carried along in the flow so that the permeability of the aquifer would no longer be constraining. The rubble-filled hollows we observe may indicate that this indeed did happen. As the aquifer drained, the hydrostatic pressure would fall, and the flow would ebb until the water could no longer reach the surface, at which time the cryosphere would refreeze. After the eruption was over, water could flow into the area from more distant parts of the aquifer system to rebuild pressure within the system and perhaps enable another eruption event.

As indicated above, not all outflow channels start in rubble-filled depressions. Some emerge from the east end of the canyons. The presence of layered deposits in the canyons, and the pattern of erosion of these deposits in Candor Chasma, suggested to McCauley (1978) that lakes were formerly present in the canyons and had catastrophically drained to the east. As discussed in Chapter 5, the widespread presence of layered deposits within the canyons has subsequently been confirmed (Nedell *et al.*, 1987; Lucchitta *et al.*, 1992; Malin and Edgett, 2000b), although the lacustrine nature of these deposits has been questioned. The start of several large outflow channels around the periphery of the canyons supports the supposition that the canyons formerly contained lakes that drained away through these peripheral channels (Coleman, 2002). The former presence of lakes is also supported by the detection of sulfates at several places within the canyons (Gendrin *et al.*, 2005).

The elevations of the canyon rims decrease to the west. The south rim of Coprates Chasma drops

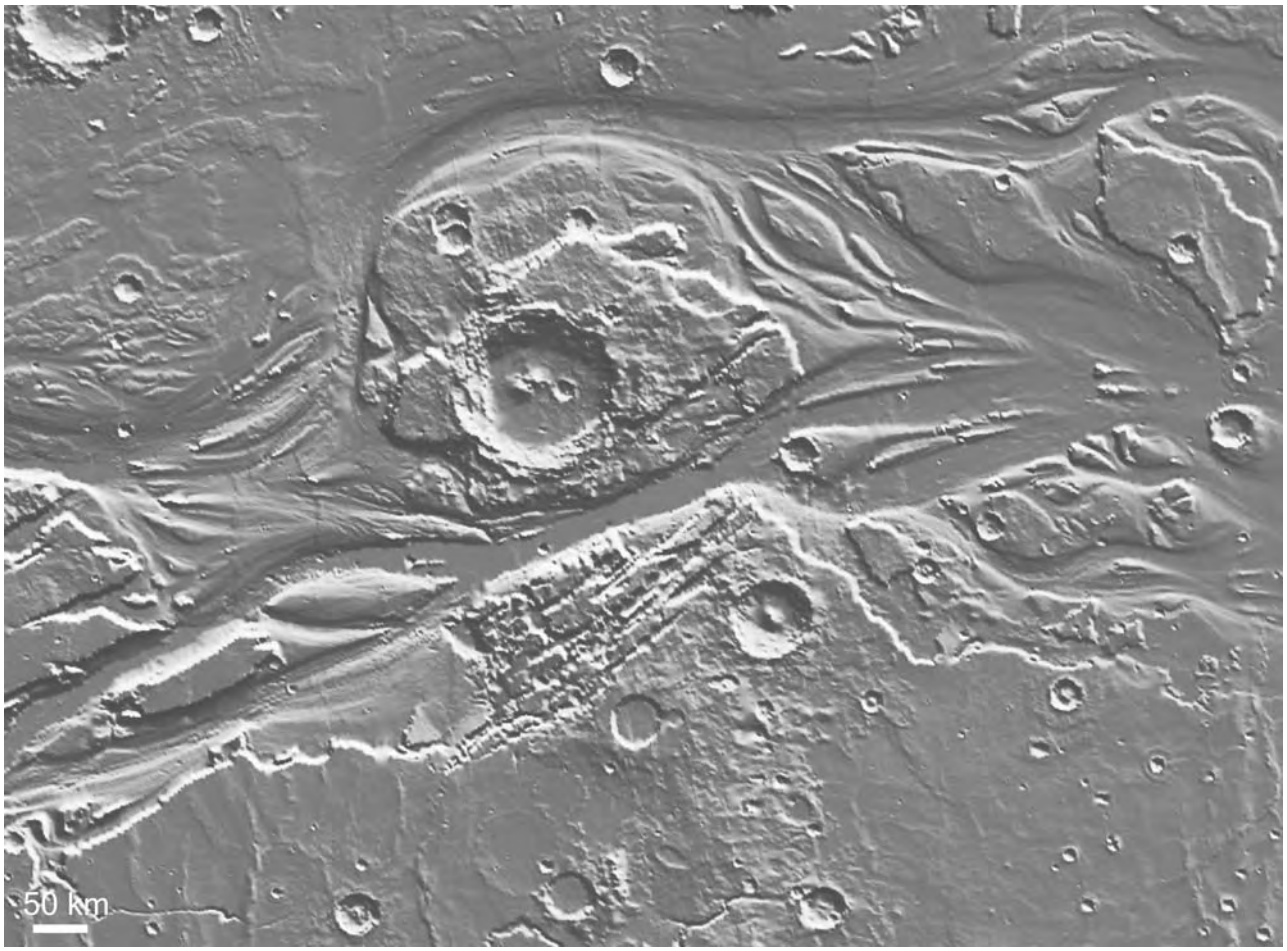

Figure 6.6. Streamlined islands and convergent and divergent striae in Kasei Vallis. The image is centered at 26°N, 302°E (MOLA).

below 3 km at 302°E and below 2 km at 303°E, so that if Coprates were closed around these longitudes the canyons could contain a lake with a surface at a 2–3 km elevation. Layered deposits within the Ius–Melas–Coprates system are all below 2 km. Those in Ophir and Candor Chasmata, however, reach elevations in excess of 3 km. Under temperate climatic conditions such a high-standing lake would tend to drain away by seepage to the surrounding low areas to the north and east. If the climate were similar to the present, the lake would have been ice-covered and losses by seepage to the surrounding areas would have been suppressed by a thick cryosphere. Such a high-standing lake, and accompanying water table, would have provided the high hydrostatic pressures needed to account for the high discharges estimated for the channels that start in the chaos-filled depressions to the east and north of the canyons, which are 3–5 km below the postulated lake level.

At present the canyons are open to the east. For lakes to have been present in the canyons there must have been barriers to eastward drainage. Possible locations are the divide between Melas Chasma and Candor Chasma, and where Coprates Chasma narrows at 300°E (Figure 5.9). Failure of the postulated eastern barrier would have resulted in rapid draining of the lake through the Hydraotes Chaos and Simud Vallis, and a rapid lowering of the regional water table. The process by which the postulated eastern barrier might have failed is illustrated by the Shalbatana–Ravi Valles north of Ganges Chasma (Figure 6.4). Both Shalbatana Vallis and Ravi Vallis start in rubble-filled depressions. Extending southward from the Shalbatana Vallis source is an ill-defined depression into which the surface appears to have collapsed. The depression almost reaches the rim of Ganges Chasma. The simplest explanation is that water within a lake in Ganges Chasma drained

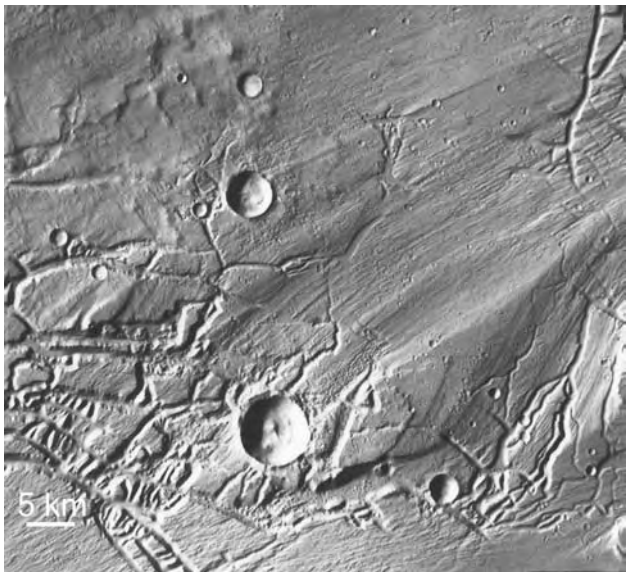

Figure 6.7. Detail from the west end of Kasei Vallis at 27°N, 289°E. The channel flow is characterized by streamlined islands, longitudinal scour, plucked zones, and inner channels, all features of terrestrial flood channels (Viking mosaic).

northward, underground, to the source of Shalbatana Vallis. Creation of a subsurface pathway by erosion or solution led to collapse of the surface. Further development of the pathway would have led to breaching of the barrier between Shalbatana and Ganges, and catastrophic drainage of Ganges Chasma. The barrier at the east end of Coprates Chasma may have been similarly undermined, but here the undermining likely continued to completion causing the barrier to collapse. The emptying of the canyons and lowering of the regional water table possibly ended the era of major outflow channel formation in the Chryse region. Such a sequence of events is consistent with the conclusion of Ivanov and Head (2001) that the Simud and Tiu Valles postdated all the other major channels that extended into the Chryse basin. The story is clearly speculative, and dependent on how credible the evidence is that the canyon formerly contained large lakes.

The origin of Kasei Vallis is even more uncertain than the other circum-Chryse channels. It starts within Echus Chasma, but the floor of the chasma is mostly hidden from view by young lava flows, so we cannot see the Kasei source. Where the scoured ground emerges from under the flows it is at an elevation of −0.5 km. Parts of the canyon floor along the eastern margin resemble chaotic terrain, but islands in the middle of the canyon do not. There are several possibilities. One is that Kasei Vallis formed as a result of one or several groundwater eruptions similar to those postulated for Ares Vallis, and that the rubble-filled source depressions have been buried by lava. A second possibility is that a lake formerly occupied Echus Chasma and that it drained catastrophically to the north. The maximum elevation that a lake in Echus Chasma could be is about 0 km. A higher elevation would have resulted in spillover across Lunae Planum to the east. The highest elevation at which scoured ground is observed is −0.5 km, so if a lake was formerly present, its surface elevation was likely between these two limits. The volume of such a lake ($\sim 4 \times 10^5\,km^3$) is, however, smaller than the volume of material eroded to form Kasei Vallis ($\sim 6 \times 10^5\,km^3$), so Kasei Vallis is unlikely to have formed simply by the draining of a lake comparable in size to the present Echus Chasma. A third possibility is that the Kasei Vallis formed from a lake significantly larger than the present Echus Chasma. At 20°N in Echus Chasma, prominent NE–SW trending scour marks emerge from under lava flows, as though there had been a water source under the flows to the southwest. An Echus Chasma lake could, therefore, have extended farther west than the present geometry suggests. A fourth possibility is that Kasei Vallis is not the result of large floods, but of some other process such as erosion by ice (Lucchitta, 1982) or disaggregation of the surface materials to form debris flows (Nummedal and Prior, 1981; Tanaka, 1999).

Estimates of the total volume of water involved in formation of the Chryse channels are very uncertain. The volume of the main interconnected canyons is $\sim 3 \times 10^6\,km^3$; the total negative volume of canyons, valleys, and chaos around Chryse is $\sim 6 \times 10^6\,km^3$. Part of this volume is the result of erosion and part the result of faulting. A lake within the canyon, with a surface level at 2 km above the datum, would have had a volume of $\sim 2 \times 10^6\,km^3$. From numbers similar to these, and assuming that all the water carried its maximum sediment load, Carr *et al.* (1987) estimated that at least $6 \times 10^6\,km^3$ of water, and probably considerably more, had flowed into the Chryse basin. The amount is equivalent to 40 m spread evenly over the whole planet.

Tharsis

Discriminating between lava channels and fluvial channels is particularly difficult in the volcanic plains of Tharsis, but several valleys there resemble outflow channels. Sections of the Olympica Fossae (25°N, 245°E), for example, combine fluvial and

tectonic characteristics (Figure 6.8). Valleys adjacent to the southeast margin of Olympus Mons also appear to start at graben (Figure 6.9). Both these sets of valleys suggest eruptions of groundwater from graben, as proposed for Mangala Vallis and the Cerberus valleys discussed below. Another valley in western Tharsis, along the 267°E meridian between 35 and 45°N, also resembles an outflow channel, but has no obvious source. The central section of the Olympica Fossae is at an elevation of over 2 km above the datum, possibly the highest outflow channel on the planet.

Amazonis and Elysium Planitiae

Description Several large valleys extend from the southern uplands into Amazonis and Elysium Planitiae between longitudes 165 and 215°E. Other seemingly water-worn features start at graben within the plains. These large valleys appear to have formed in ways different from those around the Chryse basin. The largest outflow channel in this region is Mangala Vallis. It has no tributaries and starts, almost full size, at a notch in a graben wall at 18°S, 210°E (Figure 6.10). From the graben it extends northward for 200 km where it branches. One branch goes northwest and ultimately is lost from view under a thick younger deposit, the Medusae Fossae Formation, which overlies the plains–upland boundary. The other branch continues northward across the plains–uplands boundary into Amazonis Planitia, to about 5°N, where traces of it are lost among the lava plains. The channel is roughly 1400 km in length and is in places 100 km wide. Like the Chryse outflow channels, it has a rich array of teardrop-shaped islands, convergent and divergent striations, and other streamlined forms. Other large upland valleys such as Al-Qahira and Ma'adim Valles are wide, deeply incised, and flat-floored like outflow channels but, unlike outflow channels, they have tributaries, albeit very few for their size. One possibility is that these valleys formed by a combination of floods and slow erosion. Irwin *et al.* (2002) showed, for example, that Ma'adim Vallis starts in a large depression within the uplands, and suggested that it could have formed in part by catastrophic release of water from a lake within the depression.

Some of the youngest outflow channels on the planet start at graben (Cerberus Fossae) among and to the west of the hills (Tartarus Colles) that separate Amazonis Planitia from Elysium. Athabasca Vallis starts at one of the Cerberus Fossae at 10°N, 157°E and extends to the southwest (Figures 6.11, 6.12). Teardrop-shaped islands, striae, and other sculpted

Figure 6.8. Olympica Fossae at 25°N, 245°E. The valley combines fluvial and tectonic characteristics, being sinuous in places and rectilinear elsewhere. The main valley appears to have been the source of fluids that have cut shallow, sinuous valleys with teardrop-shaped islands adjacent to the main valley. Whether the sinuous valleys were cut by lava or water or both is unclear.

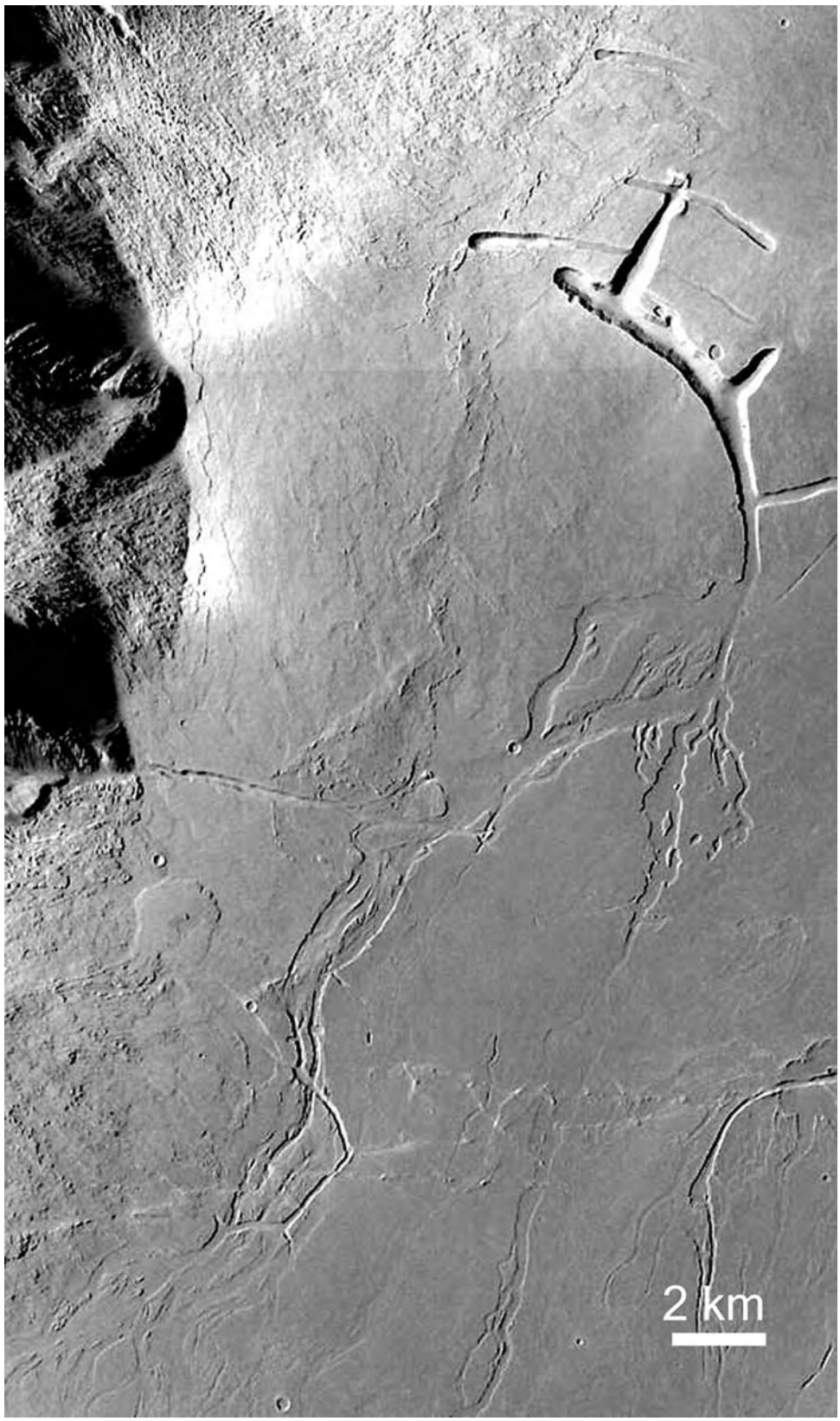

Figure 6.9. Channels at 14°N, 229°E emerging from graben just to the east of Olympus Mons, whose bounding cliff is visible along the left edge of the image. As in the previous figure, it is not clear whether the sinuous channels in the lower part of the figure were cut by water or lava (HRSC).

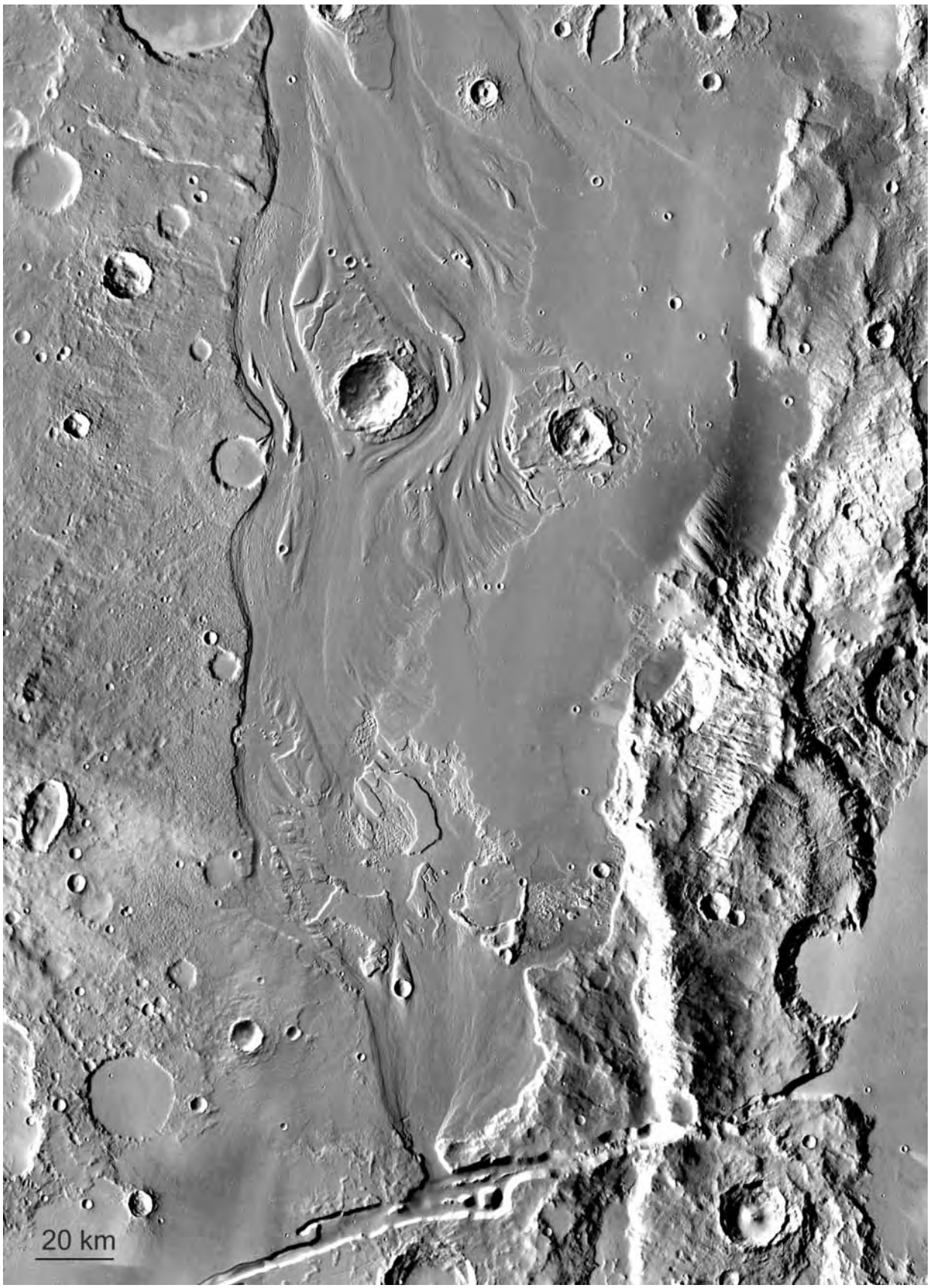

Figure 6.10. The source of Mangala Vallis at 18°S, 210°E. The channel starts at a 7 km wide gap in a graben wall and widens northward to display a rich array of streamlined forms (THEMIS).

Figure 6.11. Athabasca Vallis. The channel starts at one of the Cerberus Fossae at 10°N, 157°E, near the letter A, extends southwestward adjacent to a ridge, then spills southward through gaps in the ridge, as at C. The letters show the location of the frames in the next figure (THEMIS).

forms indicate that flow was channeled through gaps in a ridge and continued southward to about 5°N where traces of the channel are lost in the lava plains. Another channel, Grjota Vallis, which similarly starts at a graben at 16°N, 163°E, can be traced roughly 400 km eastward before it is lost among the Tartarus Colles. All these features have characteristics of outflow channels. They start full size, have no tributaries, and scour broad swaths of ground, leaving behind numerous streamlined islands.

Further east, a 100 km wide, shallow valley, Marte Vallis, starts near 10°N, 180°E in the low-lying

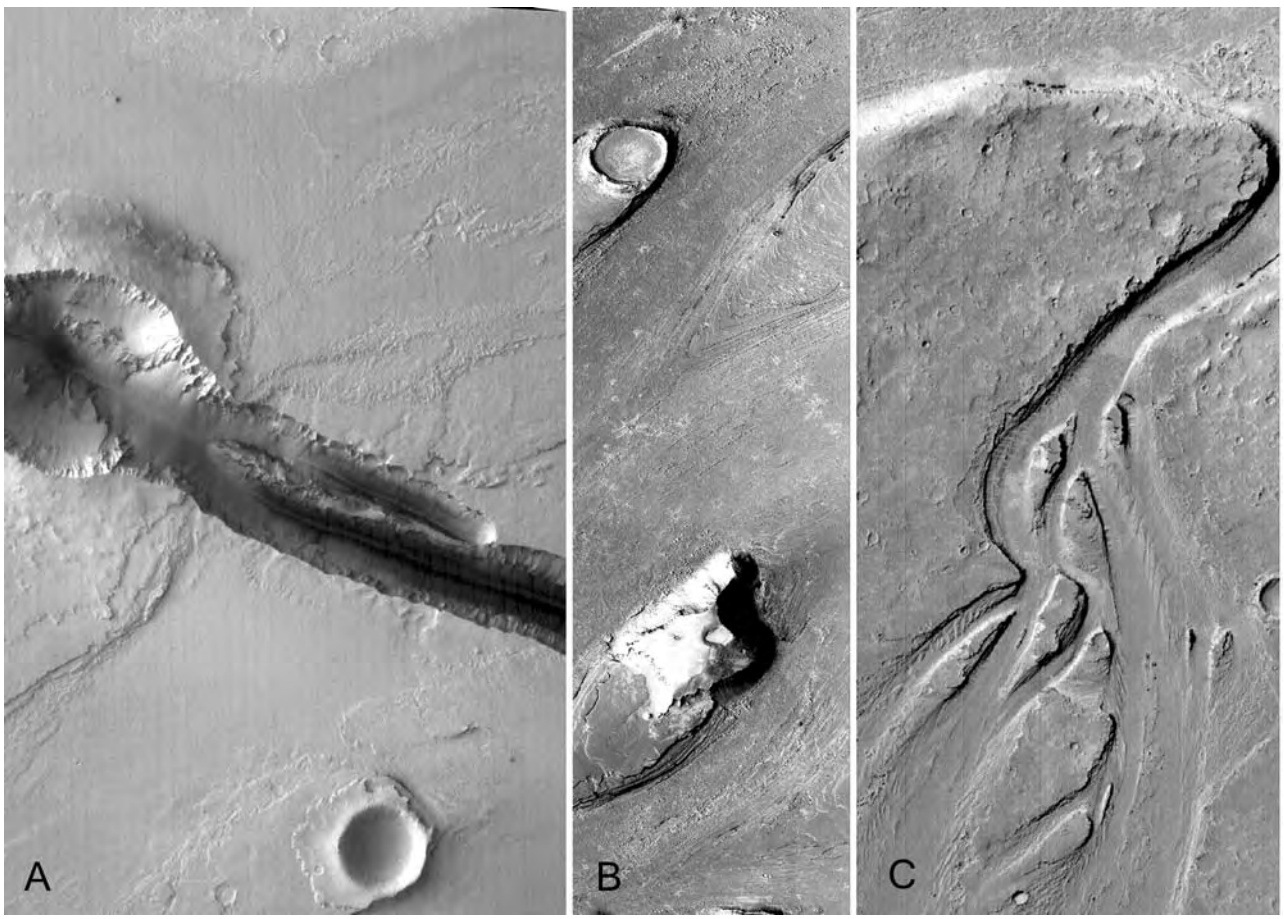

Figure 6.12. Detail of Athabasca Vallis. (A) The ground is eroded on both sides of the fissure at the channel source, suggesting fountaining of the water as it erupted from the channel. The image is 7.2 km across (MOC SP2−53103). (B) Streamlined islands within the main channel. The image is 2.8 km across (MOC E05−03124). (C) Streamlined forms where flow cut through the ridge to the southeast of the main channel. The image is 2.9 km across (MOC M21−01914).

Cerberus plains to the south of the Tartarus Colles (Figure 3.23). It extends north to roughly 20°N where it is lost among the ridged plains and hills along the western boundary of Amazonis Planitia. Although shallow, the valley is readily recognizable by teardrop-shaped islands. As discussed in Chaper 3, both lava and water appear to have flowed through it.

All the valleys on the Cerberus plains are young. The Cerberus plains lavas themselves have a crater age of roughly 10 Myr according to Berman and Hartmann (2002). Burr *et al*. (2002b) estimated the ages of Athabasca Vallis, Grjota Vallis, and Marte Vallis to be 2−8 Myr, 10−40 Myr, and 35−140 Myr respectively. If only approximately correct, these ages are so young as to suggest that outflow channels such as these could form today.

Mode of formation Mangala Vallis and the Cerberus channels all start at graben. Two models have been suggested to explain floods that start at graben. The first is that faulting caused rapid release of water from an aquifer confined below the crysophere by dislocating the cryosphere seal (Carr, 1979; Burr *et al*., 2002a; Manga, 2004; Hanna and Phillips, 2005). The second is that dike emplacement accompanied formation of the graben and caused the failure of the cryosphere (Head *et al*., 2003b). In the first case cryosphere failure was purely tectonic. In the second case there was accompanying volcanism. In both cases, large discharges were enabled by the large hydrostatic pressures within the aquifers. For the Cerberus channels, a hydrostatic head could have been provided by continuity of the aquifer to the Elysium rise to the west. For Mangala Vallis, the head may have been provided by Tharsis. In either case, the hydrostatic head could alternatively, or in addition, be the result of tectonic forces or explosive activity resulting from dike injection. The close association between the young

Cerberus channels and some of the youngest lavas on the planet supports the suggestion that the floods from the Cerberus Fossae were triggered by volcanism. Because of the lack of collapse around the channel sources, Burr *et al*. (2002a) suggested that the aquifer was buried to depths of several kilometers, which is consistent with the young ages of the channels and the likely low heat flows on present-day Mars (Solomon *et al*., 2005). Burr *et al*. (2002) estimated that the peak discharge for Athabasca Vallis was $10^6\,m^3\,s^{-1}$. This creates the same problem for these channels as for the Chryse channels. To sustain such large discharges for more than a few tens of minutes requires permeabilities that exceed almost all terrestrial rocks. For the Chryse channels it was suggested that the aquifer disintegrated and was withdrawn with the floodwaters, thereby leading to collapse. For the water that erupted from the Mangala and Cerberus Fossae, recharge could have been through the large-scale, horizontally connected, fracture systems (Head *et al*., 2003a).

The origin of Marte Vallis is obscure. It is at the outlet of an almost level plain on which water may have pooled. (For further discussion of the Cerberus plains and the possibility that water and lava may have pooled there, see Chapter 3.) In addition, several branching valleys converge on the start of Marte Vallis at 10°N, 179°E (Figure 3.23). The most prominent of the branching valleys, the Rahway Vallis, can be traced almost to Grjota Vallis to the northwest and to the Cerberus Fossae to the west. They may be downstream manifestations of floods from these sources. Other channels emerge from the uplands to join Marte Vallis from the south and southeast. None of these valleys is comparable in size to Marte Vallis and capable of feeding the required discharge into Marte Vallis. This led Burr *et al*. (2003a) to suggest that the floods that cut Marte Vallis originated from extensions of the Cerberus Fossae now buried by later lavas under the Cerberus plains.

Utopia Planitia

Several large channels start to the west of the Elysium volcanic complex between 125 and 140°E and 15 and 35°N (Figure 6.13). They extend northwestward for several hundred kilometers down into the Utopia basin. The larger ones extend almost to the center of the basin where traces of them are lost in the highly textured terrain there. Most of the valleys start at a break in slope along the western margin of the Elysium dome. Three large valleys, the Granicus, Tinjar, and Hrad Valles, and other minor valleys start within graben roughly radial to the Elysium dome. The graben are linear troughs, with flat floors or V-shaped cross-sections, depending on their width. They are typical of graben elsewhere on the planet. Here, however, they transition downslope into curvilinear depressions, or channels that are clearly erosional in origin rather than tectonic. Some of the broader channels have flat floors with teardrop-shaped islands; some of the narrower channels branch and join to make complex patterns.

The Utopia channels may form in a way similar to that proposed in the previous section for the Cerberus channels. Faulting and/or dike emplacement disrupted the cryosphere seal over a confined aquifer, thereby resulting in eruption of groundwater, the hydrostatic head being provided by Elysium dome to the east. Russell and Head (2003) point out that, at elevations above −3400 m, the graben are sources of only lava flows. Below this elevation, the graben are sources of fluvial-like channels. They suggest that the graben formed over dikes, as indicated by the lava flows, and that the −3400 m elevation represents that maximum elevation of the regional water table at the time that the channels formed.

The Elysium channels have significantly different morphologies from the Cerberus channels. Many of the Elysium channels have broad-textured rims, with lobate outer margins, as though the channels had overflowed and left a deposit on the rim. In addition, some channels terminate in lobate, flow-like deposits, some with a finely channeled surface. These observations suggested to Christiansen (1989) that the channels were cut by, or were at least utilized by, lahars or mudflows. Lahars result from mobilization of ice- or water-laden granular materials on the flanks of volcanoes, as a result of volcanic activity. They contain only a few to a few tens of percent water. Overflow of the channels through which they moved would leave behind the lobate rim deposits that are observed. Dewatering of the debris flows could explain the finely channeled surfaces of some of the flows.

Perhaps the most puzzling features in this general area are the Hephaestus Fossae and Hebrus Valles (Figures 6.14, 6.15). At the upper end of the Hephaestus Fossae a curvilinear, channel-like feature starts at an irregular depression, but most of the fossae are made of linear angular segments that join and branch at high angles to form a pattern similar to cracked pavement. Discontinuous lines of linear hollows make up the more distal segments of the network (Figure 6.15). The nearby Hebrus Valles also starts at an irregular depression, but here the upper reaches are more clearly fluvial, being curvilinear depressions containing teardrop-shaped islands. However, they transition northward into an angular

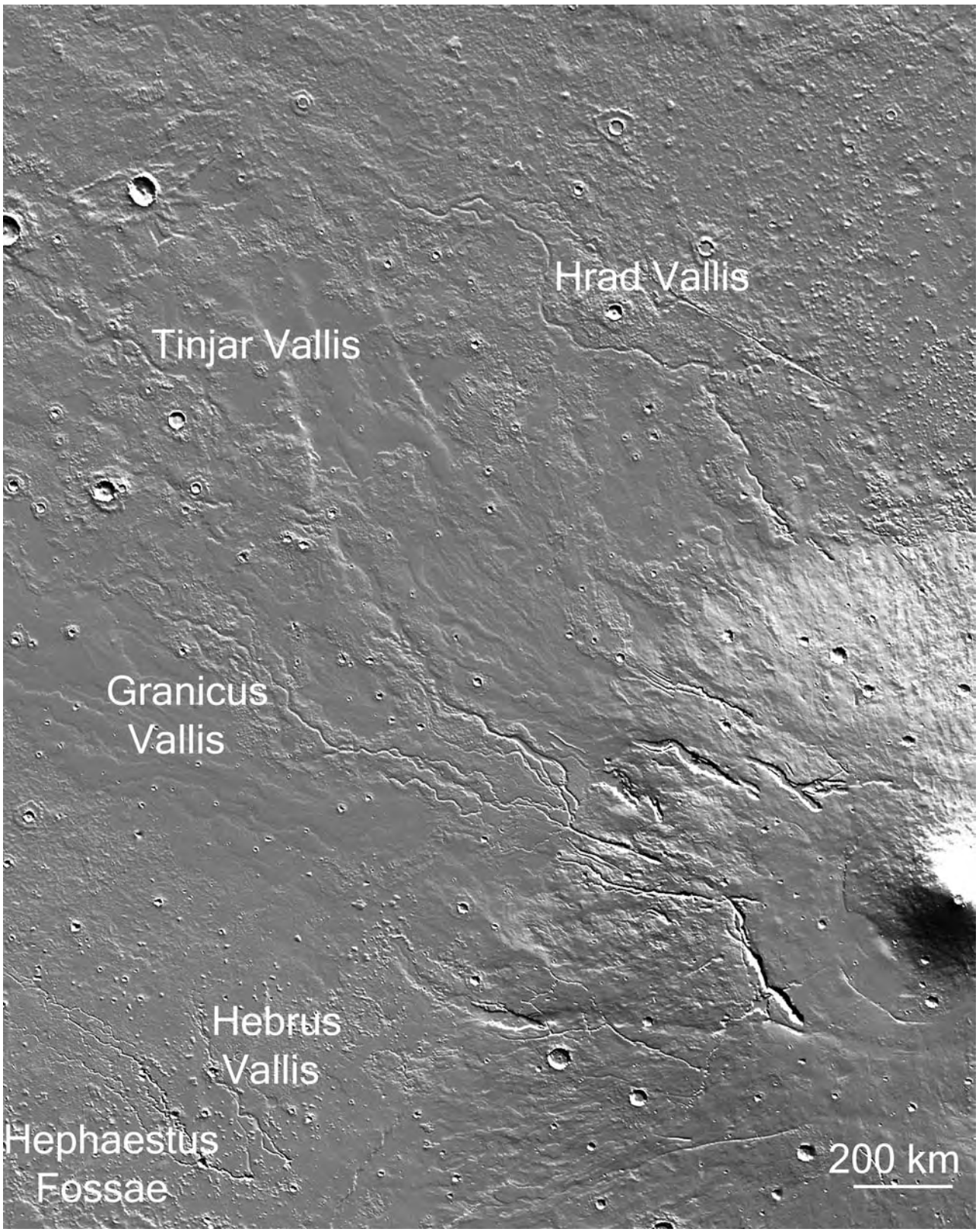

Figure 6.13. Channels extending from Elysium Mons (lower right) into the Utopia basin (upper left). The various branches of Granicus Vallis and Tinjar Vallis emerge from a graben at 27°N, 136°E at an elevation of −2700 m and extend down the regional slope to the northwest. At the western margin of the image Tinjar Vallis is at an elevation of −4800 m. The summit of Elysium Mons is at 14,028 m (MOLA).

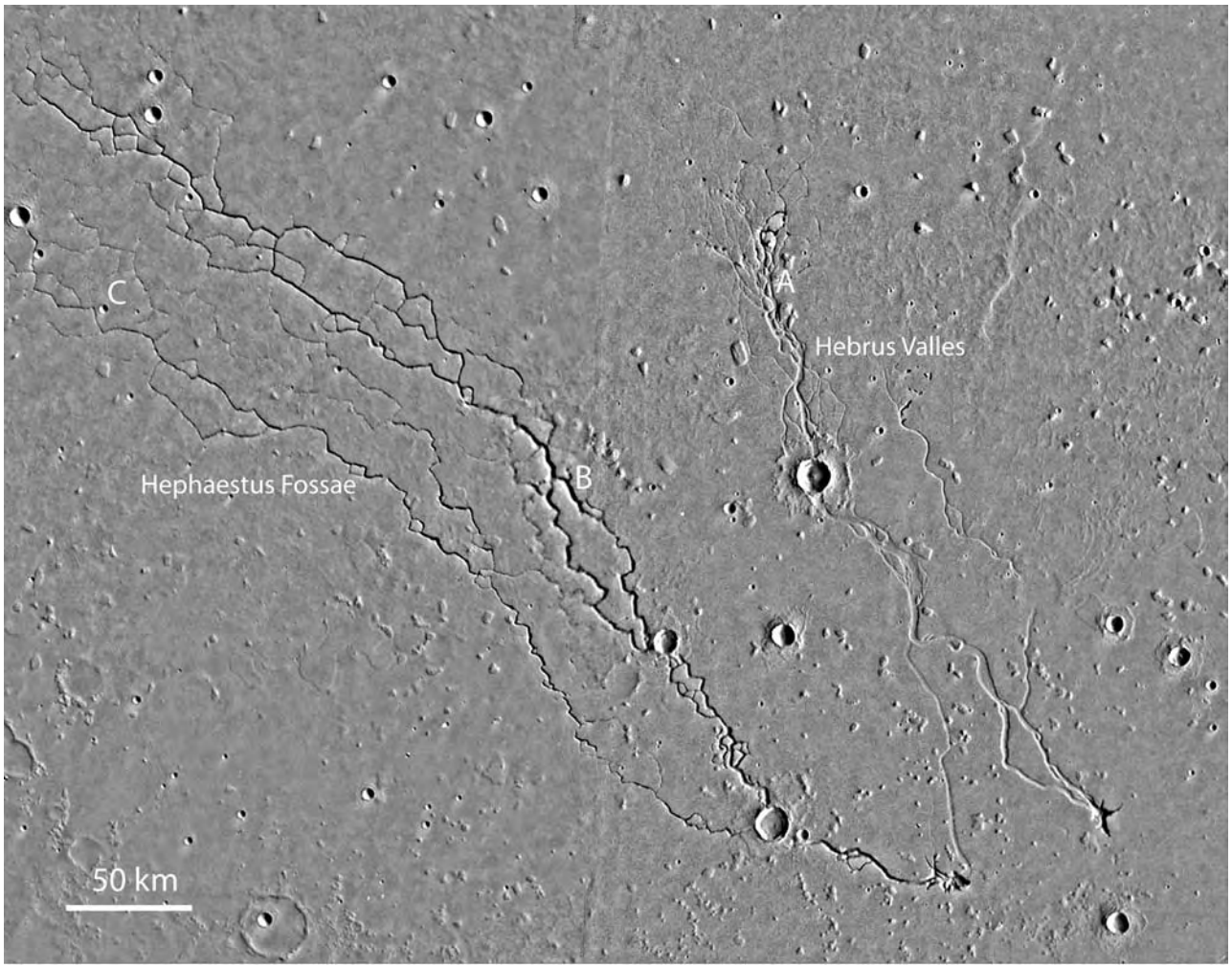

Figure 6.14. The Hephaestus Fossae and Hebrus Valles combine tectonic and fluvial attributes. Both start at an irregular depression. The Hebrus Valles have predominantly curvilinear forms but degenerate into linear discontinuous depressions north of A. Although the Hephaestus Fossae start with a curvilinear channel, most of the system consists of linear segments that become more discontinuous to the northwest. The image is centered at 20°N, 124°E (MOC).

network of discontinuous, linear depressions, similar to the Hephaestus Fossae. Thus, these two valley systems combine both tectonic and fluvial characteristics. Discontinuous lines of depressions commonly form in basaltic terrains over lava tubes. However, lava tubes follow sinuous traces and do not form grid-like patterns such as we observe in Hephaestus Fossae. Another possibility is that the upstream section of the Hephaestus Fossae was cut by water flow at the surface but that water infiltrated into the ground. Flow continued to the northwest below the surface, utilizing pre-existing fractures, and possibly enlarging them by solution or erosion, as occurs in terrestrial karst. This explanation is, however, also unsatisfactory in that no downstream outlet has been identified to carry away the solution or erosion products. The origins of the Hephaestus Fossae and Hebrus Valles remain a mystery.

Hellas

Three large valleys, Dao Vallis, Niger Vallis, and Harmakhis Vallis (Figure 6.16), start on the east rim of the Hellas basin and extend for over 1000 km down into the floor of the basin (Crown *et al.*, 1992). The plains that separate the valleys are in several places scoured into patterns that resemble those in Chryse Planitia. Dao Vallis starts in a well-delineated, 40 km wide, box canyon adjacent to the volcano Hadriaca Patera. The source of the nearby, similarly sized Niger Vallis is more obscure. Its main channel is

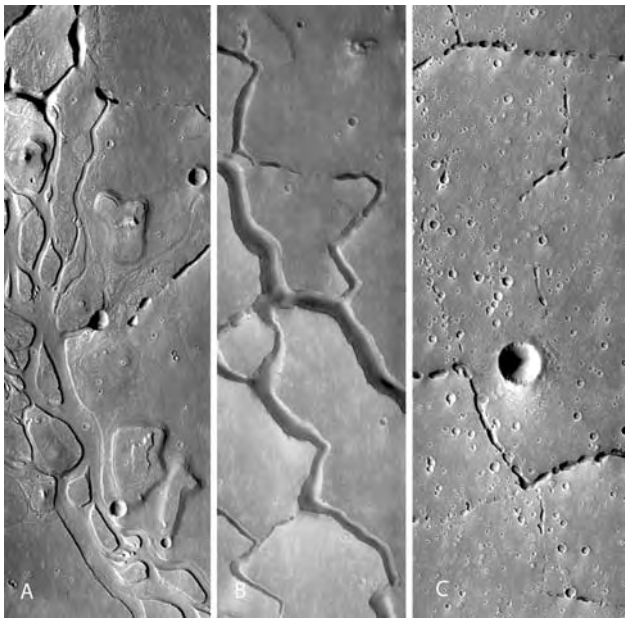

Figure 6.15. Detail of Hebrus Valles and Hephaestus Fossae. Letters on the previous image indicate location of images. (A) Hebrus Valles showing transition from streamline forms to discontinuous linear depressions. Image is 18 km across (THEMIS V01868003). (B) The middle section of the Hephaestus Fossae showing a grid of quasi-linear segments. The image is 17 km across (THEMIS V08921010). (C) A distal section of the Hephaestus Fossae with discontinuous segments. The image is 17 km across (THEMIS V01993007).

sharply defined but discontinuous. Upslope of it, a series of subdued depressions wrap around the periphery of Hadriaca Patera. Numerous narrow channels immediately adjacent to both valleys suggest overflow of the main channels. The abrupt start of the valleys, their location adjacent to Hadriaca Patera, the presence of numerous collapse depressions, and evidence of overflow suggest that the valleys formed by catastrophic release of groundwater or melting of ground ice triggered by volcanic activity at Hadriaca Patera.

Hamarkhis Vallis, 150 km to the east of Niger Vallis, resembles Niger Vallis but instead of starting next to a volcano it starts close to the end of another prominent valley, Reull Vallis, which extends 1500 km to the ENE. The source of Reull Vallis is unclear; it has few tributaries and the main channel simply fades away among the ridged plains of Tyrrhena Patera. Reull Vallis also ends abruptly, raising the question of where the material went that was eroded away to form the channel. One possibility is that Reull Vallis formerly connected with Harmakhis Vallis and that the material was carried down into the floor of Hellas. All these large valleys may have contributed to a lake that is postulated to have formerly occupied the floor of Hellas (Moore and Wilhelms, 2001).

Argyre

What may be the largest drainage system on the planet starts on the northern rim of the Argyre basin at 35°S, 325°E (Parker *et al.*, 2000). Although the drainage path is discontinuous, being interrupted by several large craters (Hale, Bond, Holden), it can be traced northward through the Uzboi, Ladon, and Margaritifer Valles until it merges with Ares Vallis and continues into Chryse Planitia. The southern section of the path with its numerous superimposed large craters is clearly older than Ares Vallis and its Chryse extension, which suggests that the younger Ares Vallis followed an older drainage path. Several large valleys (Surius, Dzigai, Palacopus), which originate peripheral to the south polar cap, feed into the Argyre basin. Parker *et al.* suggested that the large valley system formed by overflow of the Argyre basin as a result of melting of ice around the south pole. This concept has, however, been challenged by Heisinger and Head (2002) as discussed in Chapter 7. The entire drainage pathway from the south pole into the northern plains is over 8000 km long. If real, it is the longest such path in the Solar System.

The poles

Outflow channels may also have formed at the poles. A large valley is incised into the water ice cap at each pole, Chasma Boreale in the north and Chasma Australe in the south. Although these valleys lack the teardrop-shaped islands and other sculpted forms that typify outflow channels, one possibility is that they formed by catastrophic release of meltwater from beneath the caps (Clifford, 1987; Fishbaugh and Head, 2002), much like the formation of Icelandic jökulhlaups (Thorarinsson, 1957; Roberts, 2005). Another possibility is that they are eolian in origin, having formed as a result of katabatic winds blowing off the poles (Chapter 10; Howard, 2000).

Thus, large flood features have formed in several regions of the planet in several different ways. Most appear to be late Hesperian in age, but they have continued to form into the recent geological past. Most appear to have formed by eruptions of groundwater triggered by impact, volcanic or tectonic events, or by catastrophic drainage of lakes. Basal melting of surface ice may have been an additional cause at the poles. Their widespread occurrence must surely indicate the

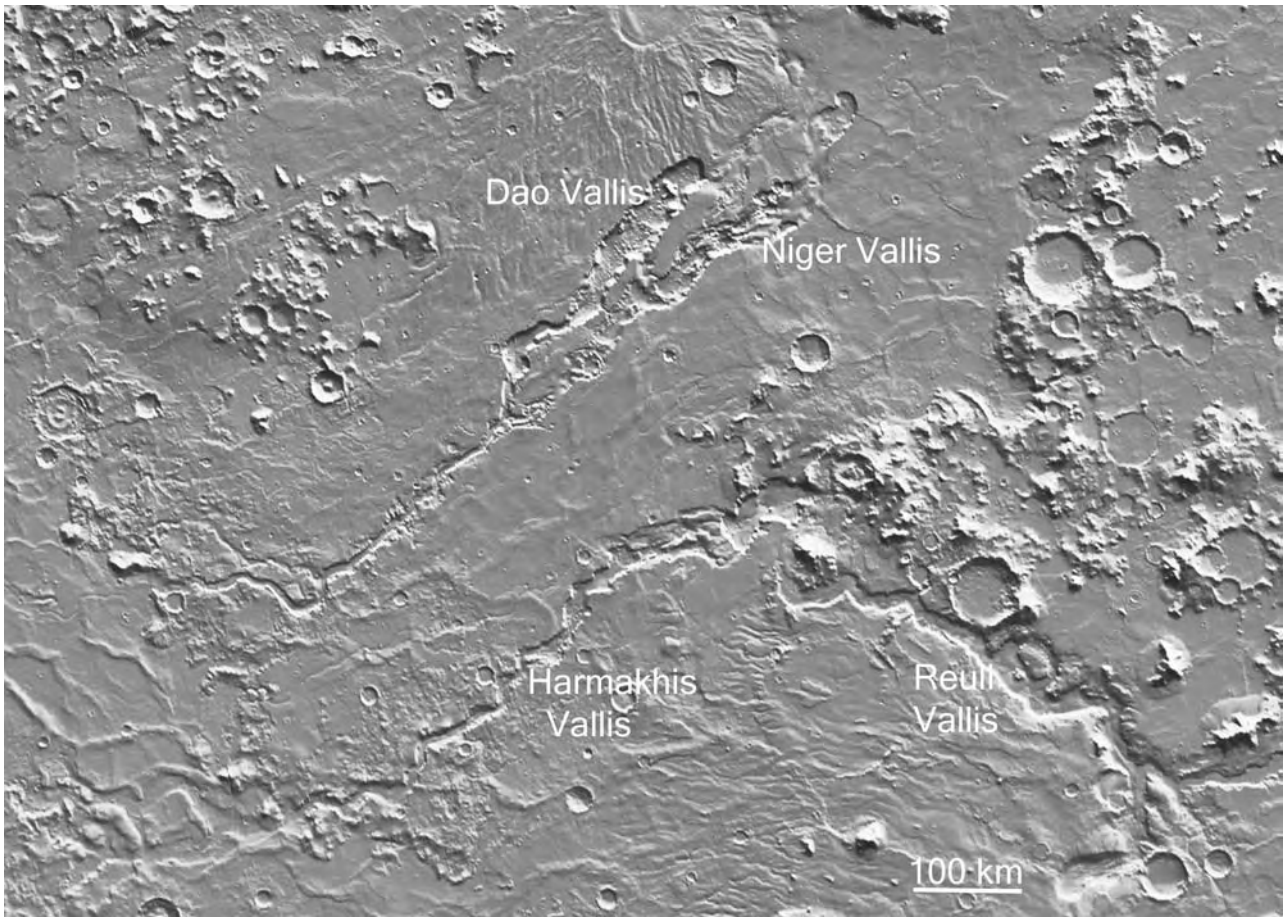

Figure 6.16. Channels in eastern Hellas. Dao and Niger Valles start adjacent to an ancient volcano, Hadriaca Patera (see Figure 3.30), at an elevation close to −2 km and extend down into the floor of Hellas where they terminate at an elevation of roughly −6 km. Harmakhis Vallis starts near the termination of another prominent valley, Reull Vallis, which extends many hundreds of kilometers to the east (MOLA).

abundant presence of water and water ice in the martian crust.

Valley networks

Most of the cratered uplands of Mars are dissected by networks of branching valleys, no more than a few kilometers wide but up to hundreds and even thousands of kilometers long (Figure 6.17). Most are readily distinguishable from the outflow channels discussed in the previous section. They were first observed in 1972 during the Mariner 9 mission (Masursky, 1973) and have been a focus of considerable interest and controversy ever since. One of the main issues is what the valleys imply for past climates on Mars. While most, although not all, researchers conclude that they were eroded by running water, conclusions about the climatic conditions required for their formation differ considerably. Some researchers argue that the valleys are close analogs to terrestrial fluvial valleys, and that they were cut primarily by surface runoff following rainfall under terrestrial-like conditions (e.g. Craddock and Howard, 2002). Others argue that the valleys are cold-climate features cut by groundwater emerging from below a thick cryosphere, and that they are telling us little about past climates (e.g. Squyres and Kasting, 1994; Gaidos and Marion, 2003). Another major issue is age. While most of the valleys are in the oldest terrains, more and more exceptions are found as we acquire more data. It is now clear that valley formation was not restricted to the Noachian, but continued at least through the Hesperian and possibly later, although at a much lower rate than in the Noachian. If all valleys required warm climates for their formation, then not only must early Mars have been warm but there must have been warm episodes in the more recent geological past.

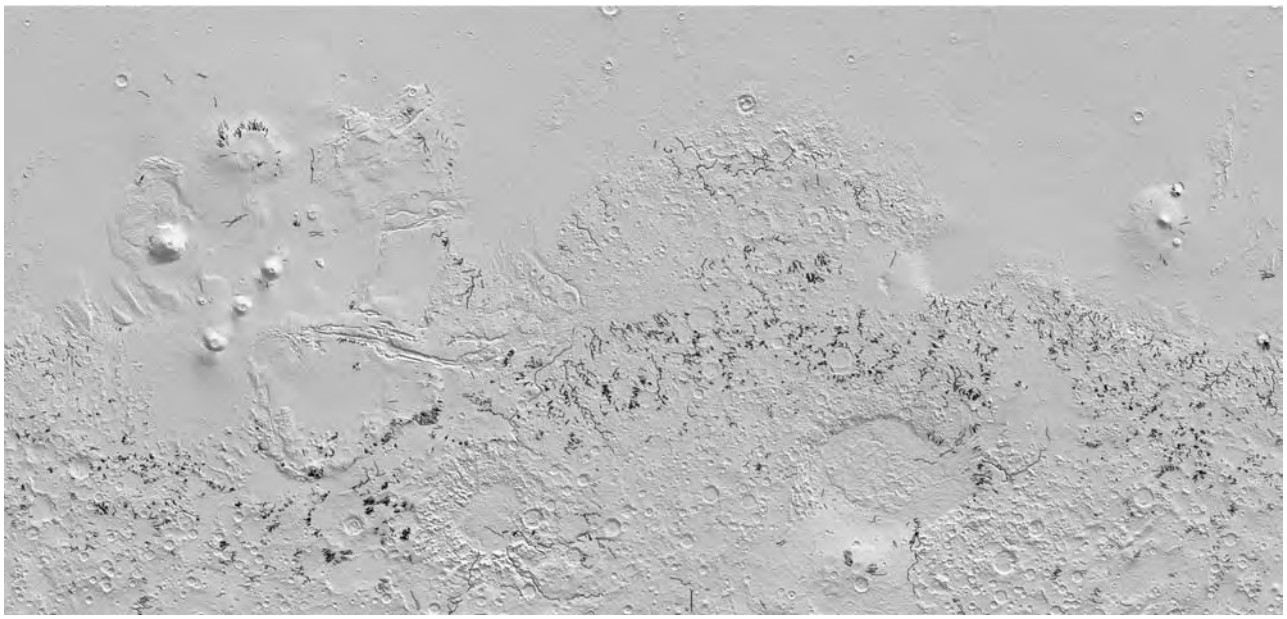

Figure 6.17. Global distribution of major valley networks. The figure shows only the large valleys; numerous additional smaller valleys are present locally. Most valleys are in the cratered uplands, but not all the cratered uplands are dissected. Extensive areas to the east and west of Hellas are poorly dissected, as is western Arabia.

Until recently, discussion of valley networks was largely restricted to what could be inferred from the appearance of the valleys in images. However, acquisition of MOLA data now allows analysis of the three-dimensional properties of valleys and drainage basins, which is providing additional clues as to the origin of the drainage system. In this chapter we describe the characteristics of the valley networks and what they might imply for past climates. Mechanisms for climate change, and other supporting and contrary evidence for climate change, are discussed more fully in Chapter 12.

General description

Valley networks are found mainly in the cratered uplands (Figure 6.17). They are distributed very unevenly. Northwest Arabia and large areas to the southwest and southeast of Hellas, for example, are sparsely dissected, whereas Terra Cimmeria and a broad swath of terrain just south of the equator from 20°E eastward to 180°E are highly dissected. Most of the valleys are short (< 200 km) and drain into local lows. However, several valleys, mostly those extending down the regional slope through Terra Meridiani toward the Chryse basin, are well over 1000 km long (Figure 6.18). In the dissected areas the valleys tend to cluster, particularly on steep slopes, such as crater walls, and on local highs (Figure 6.19). The flat areas between the craters tend to be less dissected. But these statements are rough generalizations. There are many exceptions. Valleys that wind between craters, for example, are not uncommon. Volcanoes vary widely in their dissection. Hecates Tholus, Ceraunius Tholus, and Alba Patera are well dissected (Figures 3.15, 3.20); other volcanoes are undissected.

Most martian valleys are narrow (1–4 km) with respect to their lengths, which can range to over 2000 km. They typically have steep walls and cross-sectional shapes that range from V-shaped in the upper reaches to U-shaped or rectangular in the lower reaches (Figure 6.20). Most have stubby tributaries and maintain their 1–4 km width over large distances. They therefore more resemble channels than most terrestrial valleys, which tend to become broader and shallower downstream. The most prominent martian valleys are incised into the martian surface to depths typically in the 50–200 m range (Williams and Phillips, 2001). Narrower, less incised valleys are much less common. Indeed, it is somewhat surprising that MOC images, with resolutions of a few meters, do not reveal more incised valleys with widths in the tens to a few hundreds of meters range. This may be in part an observational artifact, since vague, sinuous depressions are visible in some images of otherwise undissected terrains. Nevertheless, it appears true in general that most deeply incised, channel-like valleys do not divide into ever smaller, similar-shaped valleys with widths less than a few hundred meters. Commonly the valleys end with stubby, alcove-like terminations

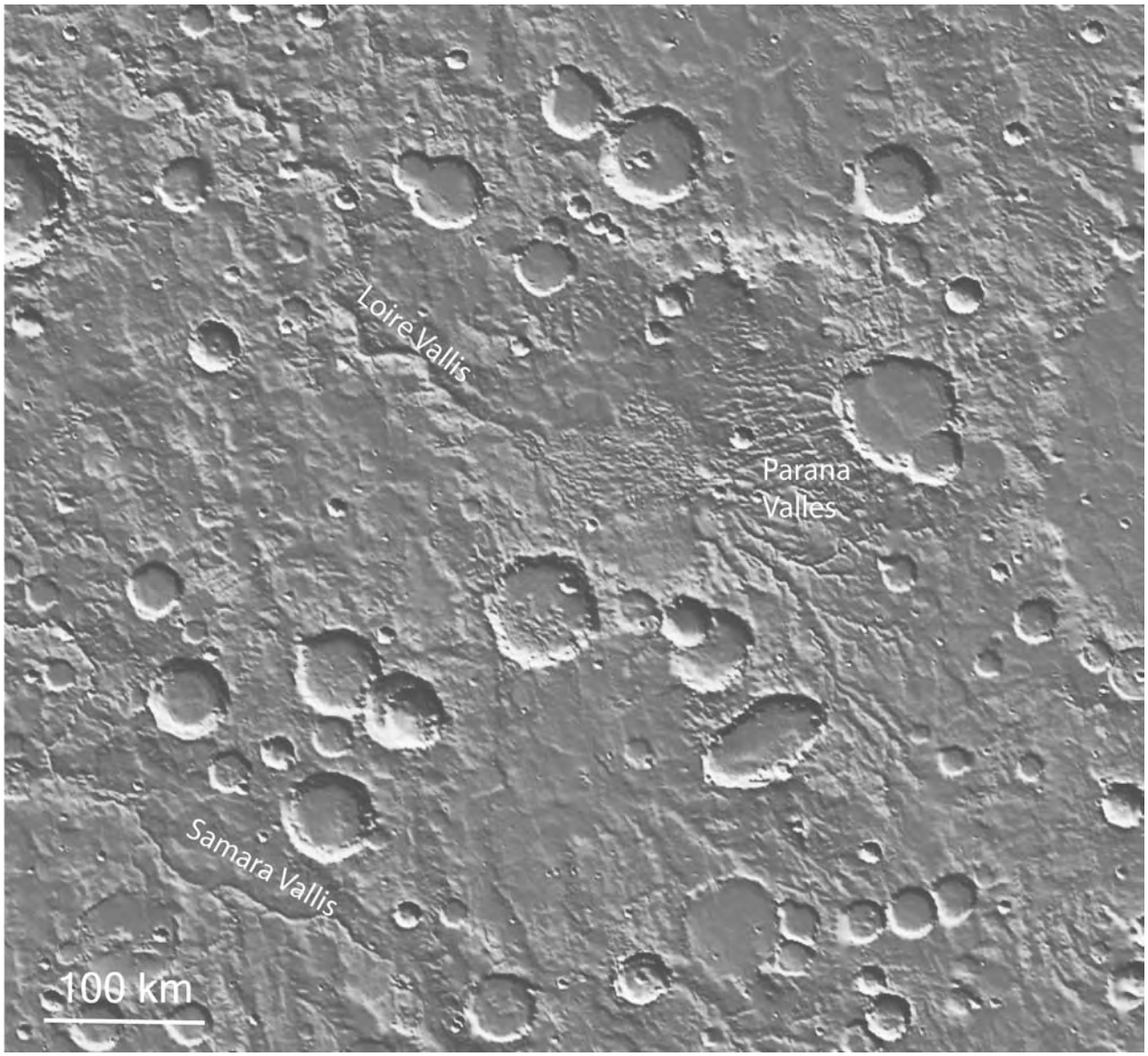

Figure 6.18. Terra Meridiani at 20°S, 345°E. The long regional slope toward the Chryse basin in this area has led to development of some of the longest valleys on the planet. Here the Parana Valles converge on a local, rubble-filled low out of which emerges the Loire Vallis, which extends for over 1000 km to the northwest (MOLA). Samara Vallis in the lower left may be the longest valley network on the planet (MOLA).

(Figures 6.21, 6.22) These characteristics (abrupt termination of tributaries and maintenance of valley width downstream) are more characteristic of streams that form mainly by release of groundwater from springs rather than those formed directly by surface runoff (Pieri, 1980; Laity and Malin, 1985; Baker, 1990).

The depths of the valleys likely control their width, the walls being eroded back as the valleys deepened. The original valleys were also likely V-shaped and became more U-shaped or rectangular as material from the walls and eolian or other debris accumulated in the valley floors. While most valleys may have originally contained a stream channel, as seen in Nanedi Vallis (Malin and Edgett, 2001), such channels are not commonly observed, although as more data is acquired, more are discovered (e.g. Jaumann *et al.*, 2005). The scarcity of such inner valleys is most likely due to their small size, which renders them vulnerable to burial by later deposits, although it is possible that many valleys do

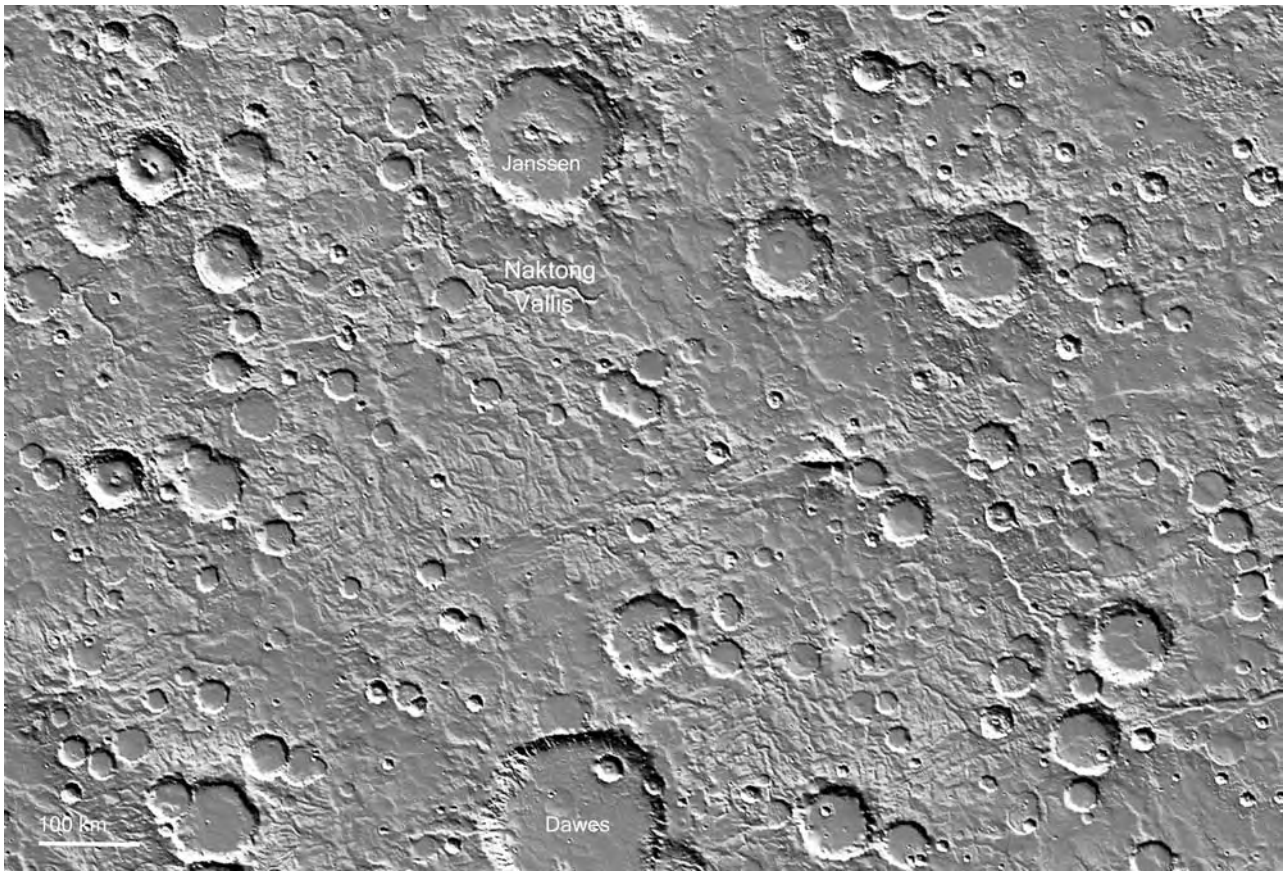

Figure 6.19. Typical dissected cratered upland centered at 5°S, 40°E. Local, heavily dissected areas are separated by ridged plains that are almost completely undissected. The high drainage densities in the dissected areas and extension of valleys up to crater rim crests suggests surface runoff. The smooth undissected areas are probably younger than the dissected areas (MOLA).

not form like most terrestrial valleys by downcutting of a stream much narrower than the valley itself.

In planimetric form most valley networks resemble terrestrial river systems. Terrestrial streams can be classified according to order. In the Strahler (1958, 1964) scheme, the smallest, most peripheral tributaries are designated order 1. Merging of two streams of equal order u results in a stream of order $u + 1$; merger of streams of unequal order results in a stream that retains the highest order of the two merging streams. The order of the network is the same as the highest-order stream in the network. Most martian valley networks can be similarly ordered and show the same relations between order and number of streams and stream lengths as do streams on Earth (Carr, 1996). These relations may, however, have little genetic significance. They probably simply reflect the random development of the tributary systems (Shreve, 1966a). Not all martian networks follow a simple hierarchical, ordered system. In some networks, the valleys not only branch upstream but also branch downstream to form complex patterns (e.g. Carr, 1996, Figure 3.4). Such valleys are topologically distinct from terrestrial river systems and cannot be ordered by the schemes used to portray terrestrial stream networks.

The statements in the two previous paragraphs are generalizations that apply mostly to intercrater areas of the uplands. In other locations the generalizations are less applicable. Crater walls, volcanoes, and other steep slopes are, for example, commonly dissected by parallel V-shaped valleys that do not form well-integrated networks. Some valleys have anastomoses (Carr and Malin, 2000), indicating that the valley had overflowed and that it did not form simply by downcutting of a small central stream. Other possible indications of overflooding are levee-like structures bounding a valley. Yet other valleys, notably Ma'adim Vallis, have median ridges on their floors that have yet to be satisfactorily explained. Finally, some valleys degenerate upstream into lines

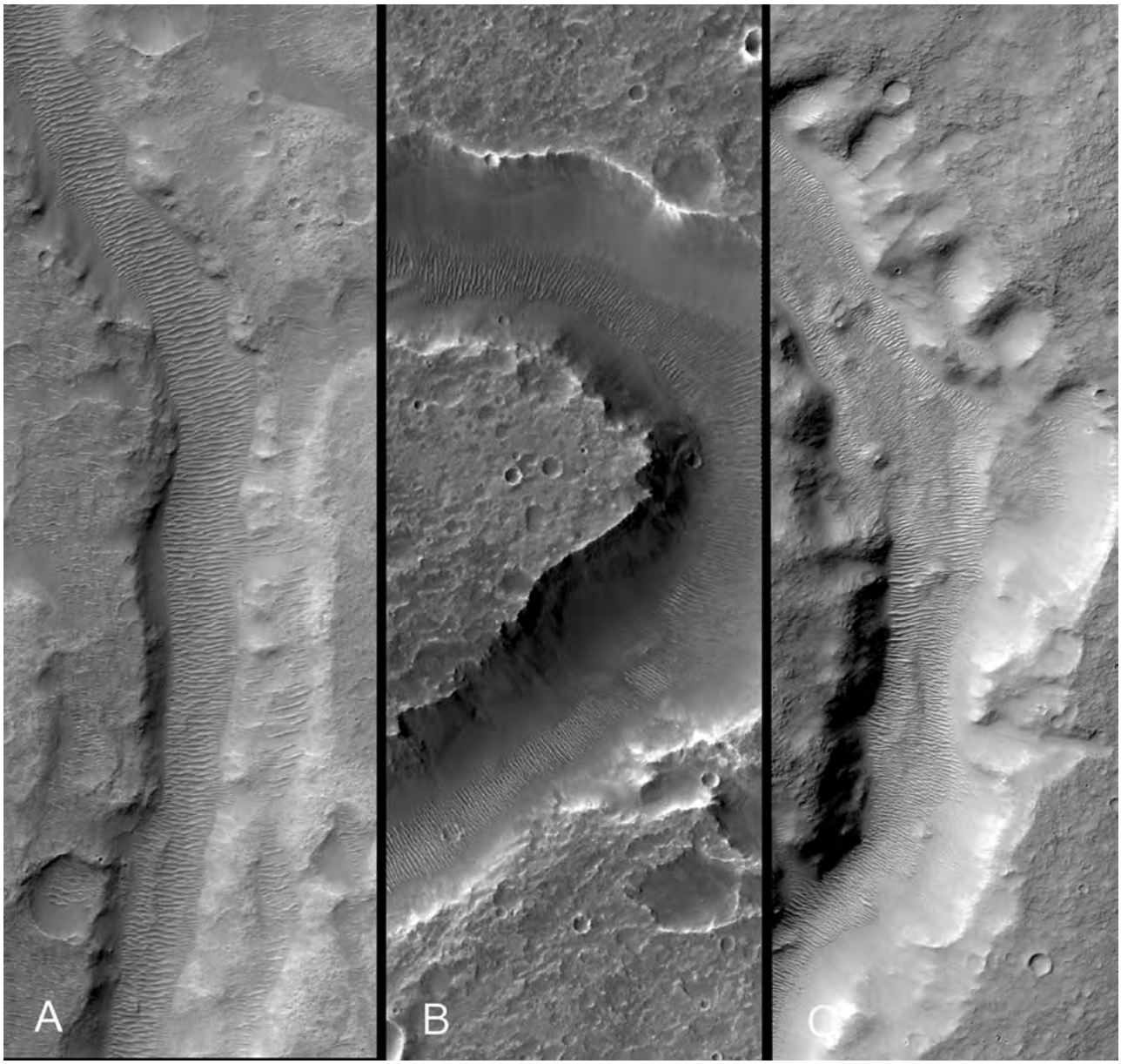

Figure 6.20. Detail from three different valleys showing the typically deep incision, rectangular to U-shaped cross-sections, absence of a central channel and dunes on the floor. (A) 22.1°S, 339.8°E, 3.5 km across (MOC E2300216). (B) 28.9°N, 349.4°E, 3.1 km across (MOC E0200972). (C) 31.8°N, 346.4°E, 2.9 km across (MOC E0301275).

of depressions, as though fed by subsurface streams (Carr and Malin, 2000). None of these variants is inconsistent with a fluvial origin of the valleys. Many of the valleys are old and have likely undergone modification by erosion, burial, faulting, and so forth, so that only remnants of the original drainage pattern survive. Other features can be attributed to occasional flood episodes, as already indicated.

Drainage density (stream length per unit area) varies greatly on both regional and local scales. Recently acquired high-resolution data shows that early estimates of drainage densities (Carr and Chuang, 1997) based on Viking data were much too low. The newer MOC and THEMIS data show that in some areas, drainage densities are very high (Figure 6.23). Hynek and Phillips (2001) estimated that in some areas of Meridiani Terra drainage densities are in the 10^{-2} to $10^{-1}\,km^{-1}$ range, close to the bottom end of the terrestrial range. In almost all areas drainage density varies greatly at the local scale,

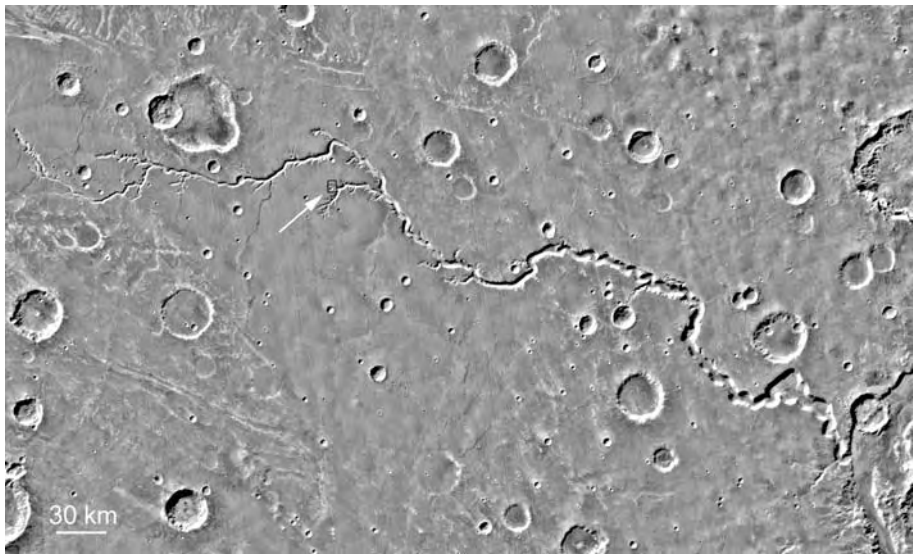

Figure 6.21. Nirgal Vallis at 28°S, 320°E. The valley has typical groundwater sapping characteristics. It is deeply incised into an otherwise undissected plain and has few tributaries. The valley cuts Hesperian plains, in contrast to the valleys in the previous three figures which are mostly incised into Noachian terrain. The arrow shows the location of the next image (Viking MDIM).

with densely dissected areas commonly being immediately adjacent to undissected or sparsely dissected areas (Figure 6.19). Many factors could cause the local variations. Slope is important. In dissected regions slopes tend to have more valleys than level areas. But this cannot be the only factor since much of the steeply sloping ground around Hellas and Argyre is undissected. Age may also be significant. At the local scale, hills tend to be dissected whereas the intervening plains, which may be younger, are less dissected. Burial and exhumation, which appears to have been common in the cratered uplands (Chapter 1), likely affected drainage densities, and variations in erodibility and infiltration probably also contributed.

Some of the most densely dissected surfaces on Mars are on the flanks of volcanoes (Gulick and Baker, 1990). The flanks of Hecates, Tholus, and Ceraunius are, for example, almost completely covered with numerous closely spaced, subparallel valleys, mostly under 100 m across (see Figures 3.15, 3.20). The northwestern flank of Alba Patera is also well dissected. Lava channels may be present on volcanoes, but as pointed out by Gulick and Baker (1990), the valleys on the volcanoes just mentioned branch upstream like fluvial valleys, and unlike lava channels which normally originate at a single source. The Alba valleys appear to be incised into an Amazonian surface. If truly fluvial they are among the youngest such valleys on the planet.

The ages of valleys are difficult to determine, in part because most individual valleys cover only a small area, so there are rarely statistically significant numbers of superimposed craters to determine a crater age. Moreover, most of the superimposed craters are small and so vulnerable to erosion and burial. The vast majority of the valleys are in the Noachian terrain as mapped at a scale of 1:15,000,000 (Scott and Tanaka, 1986; Greeley and Guest, 1987). In contrast, younger surfaces, such as the Hesperian plains of Syria, Solis, Hesperia, and Lunae Plana and Chryse Planitia, are mostly undissected. However, there are many exceptions to the general rule that valleys are restricted to Noachian terrains. Volcanoes have already been mentioned. In addition, some of the freshest-appearing valleys, such as Nanedi Vallis and Nirgal Vallis (Figures 6.21, 6.22), are incised into Hesperian terrains, and well-developed, dense networks cut Hesperian plains at the southern end of Echus Chasma (Mangold *et al*., 2004) (Figure 6.24). Hesperian plains in eastern Hellas are cut by valleys, and debris from valleys in the Isidis rim have deposited materials on the adjacent Hesperian plains. These are all unambiguous examples of post-Noachian valleys. In addition, there may be many valleys within the areas mapped as Noachian that are younger than Noachian. As already indicated, within dissected upland areas the valleys tend to be on locally higher, sloping ground and tend to converge on and terminate against lower,

Figure 6.22. Detail from the previous image. The deep, wide, stubby tributaries and lack of dissection of the adjacent plains indicate an origin by groundwater sapping. Dunes cover the valley floors (MOC E0202651).

smoother areas. This smoother fill in low areas is likely younger than the nearby hills, but the boundaries between the two units are transitional and age relations commonly ambiguous. While most valleys terminate against the smoother, and presumably younger, units, Scott and Dohm (1992) estimated that as many as 30 percent of the valleys are younger than Noachian. Although the details are uncertain, the widespread dissection of Noachian terrains and the lack of widespread dissection of post-Noachian terrains suggest that the rate of valley formation declined dramatically at the end of heavy bombardment, as did erosion rates (Golombek and Bridges, 2000). But the numerous exceptions to the generally undissected nature of post-Noachian terrains indicate that valleys continued to form through the Hesperian and into the Amazonian, albeit at much lower rates.

Drainage basins

Analysis of digital elevation models (DEMs) of martian valleys and drainage basins is providing new insights into the origin of the drainage system. Drainage pathways and basins can be derived directly from the DEMs. The first step is to compare the elevation of every pixel in the DEM with the elevations of the eight immediately adjacent pixels to determine a drainage direction for each pixel. Drainage paths can then be followed, pixel to pixel, through the DEM. In terrestrial studies, paths are followed until they reach the sea or a local low. If a local low is reached, the pixels within the low may be assigned a value, typically the elevation of the depression's outlet, to create a "flat," and tracing of the drainage path is continued beyond the depression. In the natural world a flat is commonly the site of a lake. A similar process can be followed for Mars, although in this case there is no sea level, so that some other arbitrary low level must be used as a baseline. When the process just described is applied to Mars the results differ significantly from those of most terrestrial landscapes. Typically flats constitute only a small fraction of terrestrial terrains. Major exceptions are recently glaciated areas such as the Canadian Shield. In contrast, closed depressions form a significant part of the dissected uplands of Mars. In Terra Cimmerium and Terra Sirenum, the areas with most depressions, the fraction reaches almost 50 percent. Most of the depressions are craters, but many are not. Fluvial processes tend to eliminate closed depressions created by other processes such as glaciation, volcanism, tectonism, and mass wasting One interpretation of the abundance of closed depressions on Mars, which is consistent with other indicators as discussed below, is that the martian drainage system is less well developed than the Earth's. Elimination of depressions by fluvial erosion has been less effective. Various adjectives such as immature and juvenile have been used to describe the arrested development.

Several global-scale basins can be extracted from the MOLA data as just described. These are not true drainage basins in the sense that drainage paths are continuous from the divides to the basin lows, as would normally be the case for large basins on Earth. They do, however, show how global drainage would converge and divide if all local lows were filled.

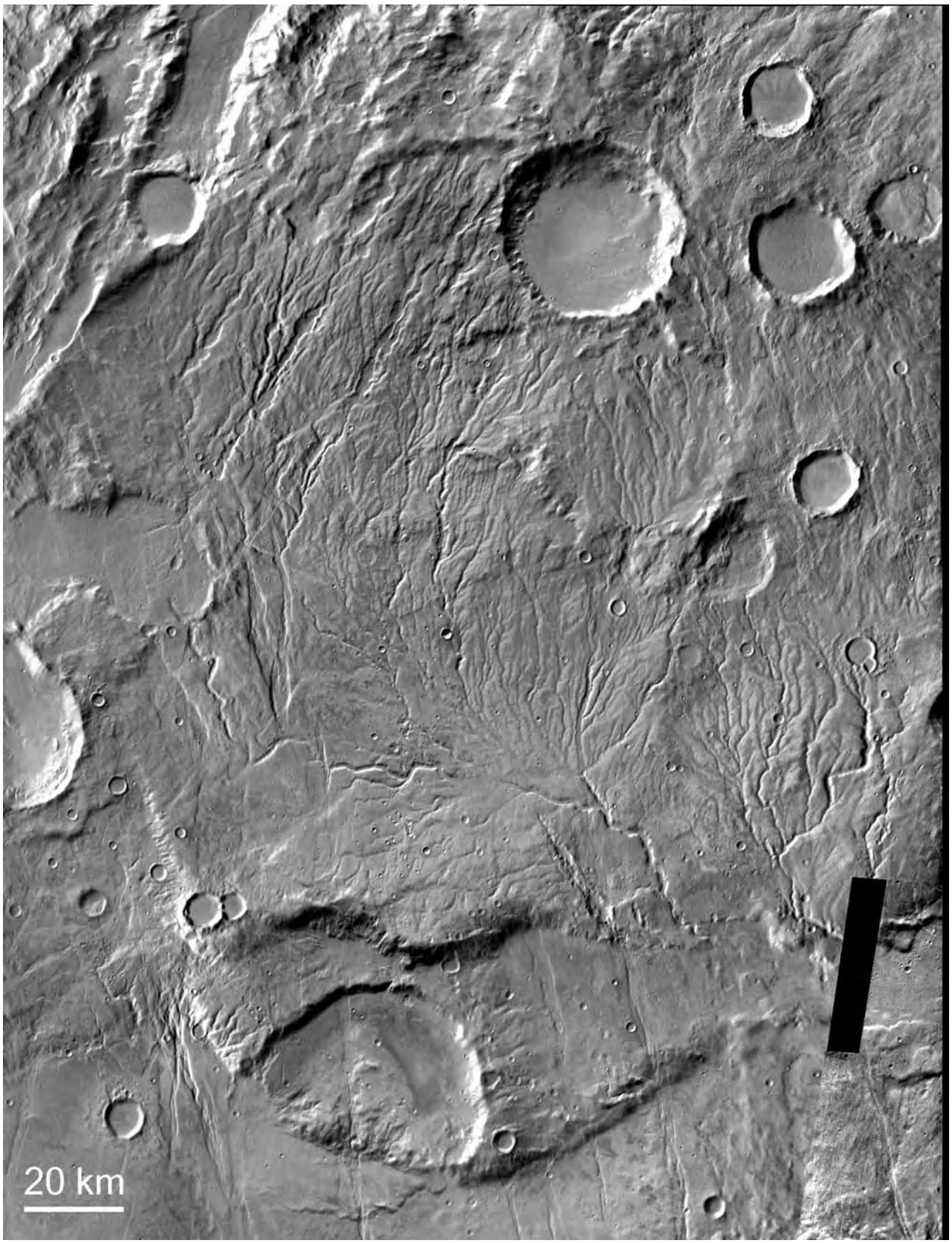

Figure 6.23. Warrego Vallis at 42°S, 267°E on the escarpment at the southern tip of the Syria–Thaumasia block (Figure 4.16). This is one of the most densely dissected areas of the planet. The drainage density strongly supports origin by surface runoff (THEMIS mosaic).

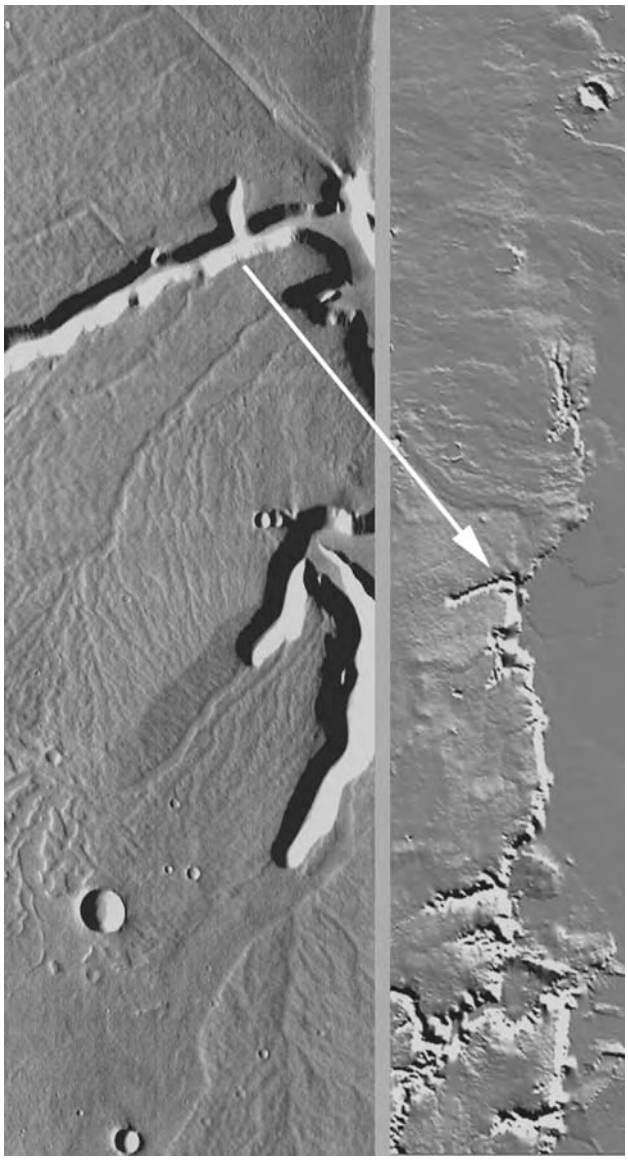

Figure 6.24. Well-developed drainage systems on Hesperian plains adjacent to Echus Chasma at 2.1°S, 277.7°E. The left image is 31 km across. The valleys are puzzling in that the high drainage density suggests precipitation and surface runoff, yet the valleys are largely restricted to the edge of the canyon. Dense drainage networks, while common on Noachian terrains, are rare on Hesperian surfaces. (Left: THEMIS I0195002; right: MOLA).

In the southern hemisphere, most of the regional drainage is either toward the Argyre basin or toward the Hellas basin. In the northern hemisphere, drainage is either into the Isidis or Utopia basins, or into the north polar basin through Chryse and Amazonis.

Quantitative measures of stream profiles and basin shapes support the supposition that most martian valley networks are less well developed than their terrestrial counterparts (Aharonson *et al.*, 2002; Stepinski and O'Hara, 2003). In most terrestrial basins, the local slope $S \sim A^{-\theta}$, where A is the area upstream of the given point, and θ is called the concavity exponent. The larger the upstream area that drains through a point in a basin, the lower the slope at that point. The exponent is a measure of how concave the basin is. Terrestrial basins typically have values that range from 0.3 to 0.7. The higher the value of the exponent, the more concave it is. Those basins with the smallest concavity exponents are those formed in areas of sporadic runoff and/or where groundwater sapping dominates. Concavity exponents of most martian basins are in the 0.2–0.3 range, indicating poor concavity. Another indicator of basin shape is how the circularity of the basin shape varies with elevation. The higher the elevation slice through a typical terrestrial basin, the more circular the basin outline. This tendency to higher circularities at higher elevations is significantly less pronounced with martian basins (Stepinski and O'Hara, 2003).

The low concavity of martian basins is reflected in the longitudinal profiles of streams. Figure 6.25 shows the longitudinal profile of Samara Vallis. The profile is almost linear; it shows little evidence of any concavity. In Terra Meridiani, where Samara Vallis is located, the regional slope is to the northwest, probably as a consequence of the lithospheric flexure under the Tharsis load. Samara Vallis, one of the largest of the martian valleys, is simply incised into this slope to an almost uniform depth. Gradation of the profile and development of a basin have been minimal. Linear stream profiles and poor basin development appear typical of martian valleys (Aharonson *et al.*, 2002; Stepinski and O'Hara, 2003). The poor development of basins is also reflected in the basin divides. Because terrestrial basins tend to have significant concavity, the steepest slopes tend to be around the periphery of a basin. Divides are commonly marked by steep opposing slopes. In contrast, because of the low concavities, martian basin divides are difficult to discern in images and most can only be determined from the MOLA data (Grant and Parker, 2002).

Origin

Glaciation, mass wasting, faulting, and erosion by CO_2, wind, and lava have at times been invoked to explain valley networks, but erosion by liquid water is now almost universally viewed as their primary cause. There can be little doubt about the availability of water. At the north pole is a thick and extensive water ice cap. Outside the north polar cap at latitudes higher

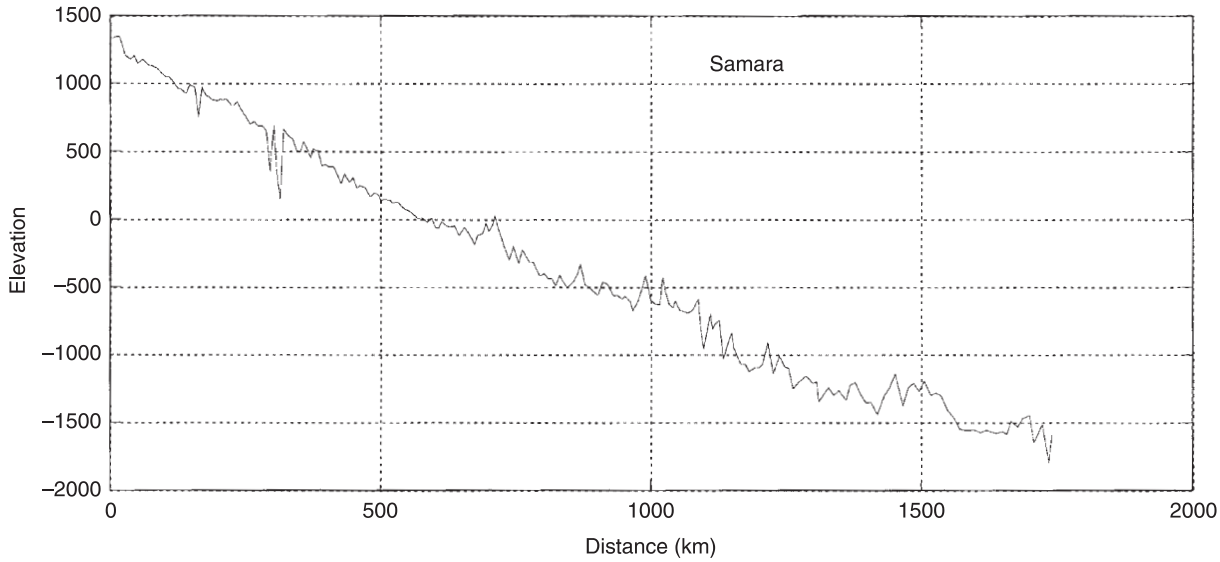

Figure 6.25. Longitudinal profile of Samara Vallis showing its almost linear profile. Terrestrial rivers tend to have a concave up profile, with higher slopes in the distal portions. We see little indication here of such concavity. The valley simply follows the regional slope.

than 60°, and everywhere in the southern hemisphere at latitudes higher than 60°, the ground a few centimeters below the surface contains 70–85 percent by volume of ice (Feldman *et al.*, 2004; Prettyman *et al.*, 2004). Evaporite deposits were found by the Spirit rover at Meridiani (Squyres *et al.*, 2004a), and extensive aqueous alteration was detected by the Opportunity rover in the Columbia hills of Gusev crater (Squyres *et al.*, 2006). Moreover, no other readily available fluid has the viscous properties and stability relations that enable it to form streams that run downhill, flow for thousands of kilometers, and erode into the surface materials. Strong confirmation of the role of water in cutting valleys is provided by fan-shaped deposits in Holden NE crater at 24°S, 326°E (Malin and Edgett, 2003) (Figure 6.26). The deposits are at the eastern end of a valley that has all the characteristics typical of martian valleys (steep walls, flat floor, uniform width over its length, abrupt distal terminations, and few tributaries). The fan deposits formed where the stream that cut the valley debouched onto the floor of the crater. The delta is highly eroded. The former watercourses are left as flat-topped ridges presumably because coarser debris on their floors left them more resistant to erosion than the intervening areas. Positive curvilinear features on the deposits mark the former watercourses, which show compelling evidence of superposition of successive streams, meander migration, and meander cutoffs.

While the role of water in cutting most of the valley networks is compelling, other processes have operated. Incision likely led to slope failure and mass wasting. We have clear evidence for flow of surface materials from the walls and down some valleys, particularly at high latitudes, as demonstrated in Figure 6.27. In addition, some valleys have been cut by lava. Lava channels are common in the volcanic provinces of Tharsis and Elysium, but lava channels may also be present in the Noachian uplands. Leverington and Maxwell (2004) point to several possible examples associated with what could be lava lakes. Nevertheless, the bulk of the valleys in the Noachian uplands branch upstream in a manner rarely seen with lava channels.

Noachian valleys Although most of the Noachian valleys were almost certainly cut by water, the source of the water and the conditions under which formation took place remain controversial. If the valleys were observed in isolation with no other knowledge of the planet, we would assume that some had been cut by surface runoff following rainfall, and that others had formed by sapping as a result of infiltration and emergence of some of the precipitation at springs to form sapping features, as happens on Earth. There has, however, been resistance to interpreting all the valleys as due to rainfall. For rain to fall, warm conditions are required (Haberle, 1998). The arguments against rainfall are not geomorphic, as discussed more fully in Chapter 12. They are based on (1) modeling studies that indicate that it is very difficult to warm Mars, particularly early in its history when the energy output

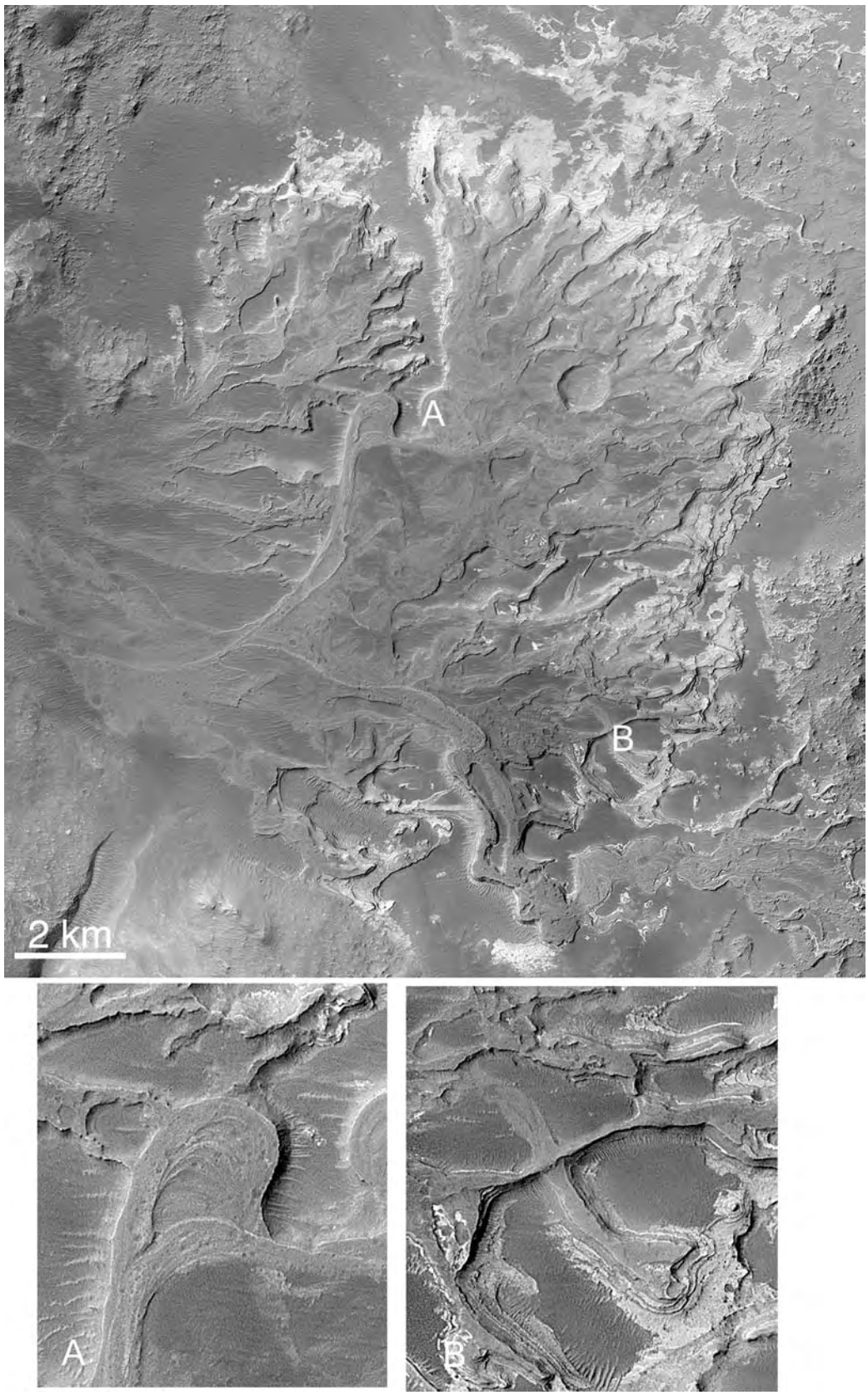

Figure 6.26. Distributary fan in a 64 km diameter crater at 24.3°S, 326.5°E. The fan, or delta, formed at the mouth of a valley, off the picture to the west, at a time when a lake was present in the crater. Subsequent erosion has left the former watercourses as highs, probably because of coarser, more resistant deposits on their floors. Cutoff meanders can be seen at A and superposed watercourses at B. The fan is compelling evidence of sustained water erosion and deposition. (Courtesy of Malin Space Sciences.)

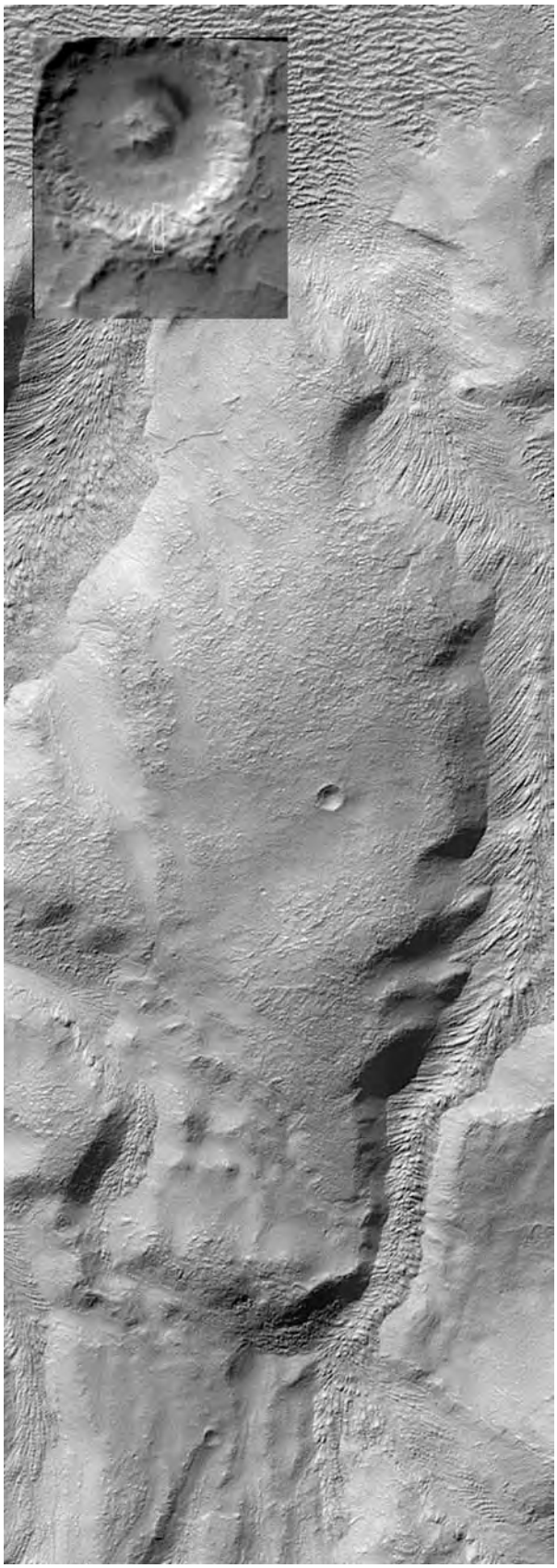

of the Sun was less than it is today (Kasting, 1991); (2) the difficulty of sustaining a thick CO_2–H_2O atmosphere on Mars against losses by weathering; (3) the vulnerability of Mars' early atmosphere to blow-off by large impacts; (4) the sparse indications in orbital spectral data of weathering products that would be expected if Mars had been warm (Bandfield *et al.*, 2000); and (5) the abundant detection of easily weathered minerals such as olivine (Hoefen *et al.*, 2003).

Partly because of difficulties in creating and sustaining warm conditions on Mars (see Chapter 12), several authors have suggested that the valley networks could have formed exclusively by groundwater seepage under cold conditions much like those that prevail today (e.g. Squyres and Kasting, 1994; Gaidos and Marion, 2003). Modeling suggests that groundwater-fed springs may be possible under present cold conditions (Goldspiel and Squyres, 2000) and that streams may be able to travel long distances under an ice cover in cold conditions (Wallace and Sagan, 1979; Carr, 1983). That groundwater seepage has played a prominent role in the formation of valley networks was recognized early (e.g. Sharp and Malin, 1975; Pieri, 1980). The open networks, amphitheater-like termination of tributaries, constant width downstream, steep valley walls, and U-shaped or rectangular cross-sections are all diagnostic. Sapping characteristics are particularly striking for some of the larger, younger valleys such as Nirgal Vallis and Nanedi Vallis, which both cut Hesperian plains (Figure 6.22). Nevertheless, formation of valley networks by groundwater seepage alone seems unlikely. Dense, area-filling drainage networks are common in the cratered uplands (Figures 6.19, 6.23) and many valleys start at local highs such as crater rims and central peaks where groundwater seepage is unlikely. Moreover, seepage results in drawdown of the water table. If seepage is to be sustained, some mechanism must exist to replenish the large amounts of lost water.

One possibility is that the valleys all formed by groundwater seepage under cold conditions and that the groundwater was replenished on a global scale by

Figure 6.27. Mass wasting in valleys on the wall of the 60 km diameter Prometheus crater at 39.5°S, 112.8°E. The image is 2.8 km across. Striae on the surface of material within the valleys indicates flow away from the walls and down the valleys to the crater floor at the top of the image. The original valley was likely cut by water, but was later covered by ice-rich surficial materials (see Chapter 8), which subsequently flowed down the valley (MOC M0001617).

polar recharge rather than by local precipitation. Water lost by groundwater seepage would sublimate into the atmosphere and be frozen out at the poles. As the polar ice thickened it could ultimately melt at its base as a result of the internal heat flow, thereby enabling water to re-enter the groundwater system (Clifford, 1993). Observational evidence that this actually occurs are channels that emerge from below what are likely ice-rich deposits at the south pole (Milkovich *et al.*, 2002). Thus a slow global groundwater circulation might have developed, driven by melting at the south pole. (Melting may also have occurred at the north pole, but it could not have driven a global circulation because of its low elevation.) While this mechanism may have operated, it is unlikely to have been the sole source of the water that cut the valleys, since a large fraction of them are at elevations that are higher than the base of south polar layered terrain (Carr, 2002). Another suggestion is that groundwater may be circulated locally, driven either by volcanic heat (Gulick, 1998) or impact heating (Newsome, 1980), but in both these cases, if subfreezing conditions prevailed at the surface, then water could have percolated back into the ground only very close to the heat sources where the surface was unfrozen. Water that traveled kilometers away from the hot spots would have been lost from the groundwater system because it could not have penetrated the frozen ground. Thus, both observational evidence and recharge considerations make it unlikely that formation of valley networks was solely by groundwater sapping under cold conditions. Craddock and Howard (2002) argue that the geomorphic evidence for surface runoff, and hence precipitation, is so compelling that some assumptions in the modeling studies must be wrong and that observational artifacts must be hindering our ability to detect weathering products from orbit. Precipitation and warm conditions appear to be required to explain the valley networks.

Warm conditions in the Noachian are supported by other observations. On Hesperian and Amazonian terrains, most impact craters are almost perfectly preserved, including the most subtle textures on their ejecta blankets. In contrast, in Noachian terrains almost all the larger, older craters are highly eroded, many being detectable only by subtle topographic signatures (Schultz and Frey, 1990). Golombek and Bridges (2000) estimate that erosion rates decreased by 3–6 orders of magnitude at the end of the Noachian. The most straightforward explanation is a climate change from dominantly warm to dominantly cold conditions. This change is also supported by detection of phyllosilicate weathering products in Noachian terrains but not in younger terrains (Bibring *et al.*, 2006).

As discussed in Chapter 12, the causes of the postulated warm conditions in the Noachian remains unresolved. Permanent warming by a CO_2–H_2O greenhouse appears unlikely because of the low solar flux for this early era. Also, no evidence has been found of the carbonates that would be expected if the late Noachian had a thick CO_2 atmosphere. Episodic warmings as a result of massive volcanic eruptions or large impacts are other possibilities.

Despite the likely warm conditions and an active hydrological cycle in the Noachian, large integrated drainage basins comparable to those of the Mississippi, Amazon, and Nile did not develop. Most of the valleys in the Noachian terrain drain into local lows. They typically do not merge with other networks to form large basins thousands of kilometers across, as has happened in many areas on Earth. The immaturity of the drainage system is also reflected in the poor concavity and relations between circularity and elevation within the basins as described above. These indications of immaturity may simply reflect the balance between the rate of terrain creation, which in the Noachian was largely by impacts and volcanism, and the rate of terrain degradation by fluvial erosion. On Noachian Mars the balance appears to have been more in favor of terrain creation than on present-day Earth. Whether this was the result of a higher rate of terrain formation or a lower rate of terrain degradation is unclear.

If the Noachian did have an active hydrological cycle with high erosion rates and high rates of valley formation, as appears likely, then other implications follow. High rates of erosion imply high rates of sedimentation, which is supported by abundant evidence for sedimentary rocks within the Noachian terrains (Malin and Edgett, 2000b). Widespread precipitation implies open bodies of water both as sources and sinks. Most of the discussion of oceans on Mars has focused on Hesperian oceans (Parker *et al.*, 1989, 1993; Baker *et al.*, 1991; Clifford and Parker, 2001) because of the possibility they could have resulted from the large Hesperian-aged floods, but a strong case can also be made for Noachian oceans as a source of the precipitation that cut the valleys and as a base level that controlled sedimentation (Howard and Moore, 2006). Indeed, if warm conditions prevailed at the end of the Noachian, as is implied by the widespread dissection, and the planet had a significant inventory of water ($\gg$100 m global equivalent), as is implied by the subsequent erosion

needed to form the large outflow channels, then Noachian Mars must have had large bodies of water in low areas such as Hellas and the northern plains (see Chapter 7).

Post-Noachian valleys As already indicated, the rate of valley formation appears to have declined rapidly at the end of the Noachian, along with erosion rates and weathering rates. The rate of valley formation did not, however, decline to zero. Dense networks are incised into the Hesperian plains adjacent to Echus Chasma (Figure 6.24), and into post-Noachian surfaces on several volcanoes. Isolated young valleys occur elsewhere. Indeed, some of the most prominent valley networks such as Nanedi Vallis and Nirgal Vallis cut Hesperian terrains. Nevertheless, the characteristic fluvial feature of the Hesperian and Amazonian is not the valley network but the outflow channel. Extremely low erosion rates (Golombek and Bridges, 2000), extremely low weathering rates (Haskins *et al.*, 2005), the scarcity of valley networks on post-Noachian plains, and the presence of outflow channels all suggest predominantly cold conditions and a thick cryosphere for most of the post-Noachian era. How then do we explain the young valleys?

Baker *et al.* (1991) and Baker (2001) suggested that the large post-Noachian floods created temporary oceans and released massive amounts of CO_2 and possibly SO_2 into the atmosphere, thereby causing a temporary global warming during which the young valleys formed. Segura *et al.* (2002) also suggested that the planet could have had short warm episodes, but suggested that large impacts were the cause. Gulick *et al.* (1997) noted that sublimation from temporary oceans could result in precipitation of snow on local highs such as volcanoes. Melting of the snow by volcanic heat could then result in erosion of valleys, particularly if the volcano flanks are formed of easily erodible ash. Another possibility is that during periods of high obliquity snow is precipitated in favored locations such as volcanoes (Head and Marchant, 2003). The young valleys could then have formed from meltwater released by melting of the snow either by solar heat or internal heat. All these ideas are discussed more fully in Chapter 12.

Thus, while most valley networks appear to be cut by running water, the conditions required for their formation and how those conditions were effected both remain unclear. One thing is clear, however, and that is that the hydrological regimes in the Noachian and post-Noachian eras were very different. Most surfaces that survive from the Noachian are dissected by valleys and have experienced considerable erosion; most post-Noachian surfaces are poorly dissected by valleys and have experienced almost no erosion, other than locally by outflow channels. A major change in surface conditions occurred around the end of the Noachian, but what caused the change is unknown.

Gullies

Gully is the term applied to small, linear, seemingly young erosional features incised into steep slopes. They typically consist of an upper, theater-shaped alcove that tapers downward to converge on one or more channels that extend further downslope, commonly terminating in triangular debris aprons (Malin and Edgett, 2000a) (Figure 6.28). The channels are mostly meters to tens of meters wide and hundreds of meters in length, so are much smaller than the valley networks just discussed. A young age is indicated by the absence of craters on the terminal deposits, and the fact that they cut across all other features in their path, including sand dunes. Their importance stems from the possibility that they may be indicators of recent erosion by liquid water.

They vary considerably in appearance, particularly in the extent to which they widen and branch upstream and form alcoves. Most occur in the southern hemisphere at latitudes higher than 30°, all on steep slopes such as crater walls, crater central peaks,

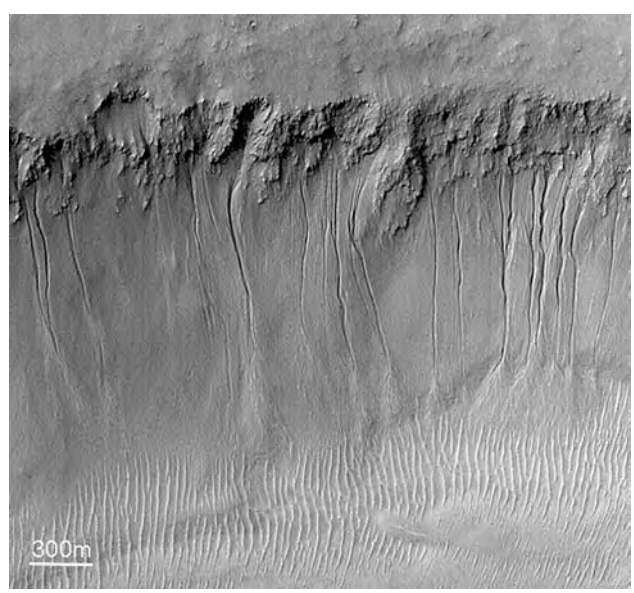

Figure 6.28. Gullies on the south, pole-facing slope of Nirgal Vallis at 29.7°S, 321.1°E (see Figure 6.21). The gullies, around 10 m across, typically start in an upper alcove and terminate in a triangular-shaped fan at the base of the steep valley wall (MOC M0322990).

the walls of valleys, and pits. They have a preference for the colder, pole-facing slopes. Their scarcity in the northern hemisphere may simply reflect the fewer steep slopes at high northern latitudes as compared with southern latitudes. Malin and Edgett (2000a) noted that at many locations, arrays of gullies started at the same horizon on a slope, commonly where there appeared to be a ledge or outcrop. They concluded that the gullies formed as a result of recent seepage of groundwater from the outcropping unit.

Origin by groundwater seepage has been questioned on two grounds. First, seepage of groundwater is difficult to reconcile with conditions on present-day Mars. With mean annual temperatures of 215 K or less the ground must, on average, be frozen to kilometer depths for all likely heat flows and thermal conductivities (Chapter 1). For liquid water to be stable at depths as shallow as 200 m, for example, the overlying materials must have very low conductivities, those equivalent to poorly consolidated, low-density soils (Mellon and Phillips, 2001), which is contrary to the observation of rock outcrops above the supposed sources. Thermal anomalies could facilitate movement of liquid water to the surface, but the distribution of the gullies shows no relation to volcanic areas where higher heat flows might be expected. In addition, many of the gullies are in locations were groundwater seepage is unlikely even under temperate conditions. They are observed, for example, at the crest of the central peaks, on isolated mesas, and extending up to, the rim crests of many craters (Figure 6.29). None of these is a plausible source of groundwater.

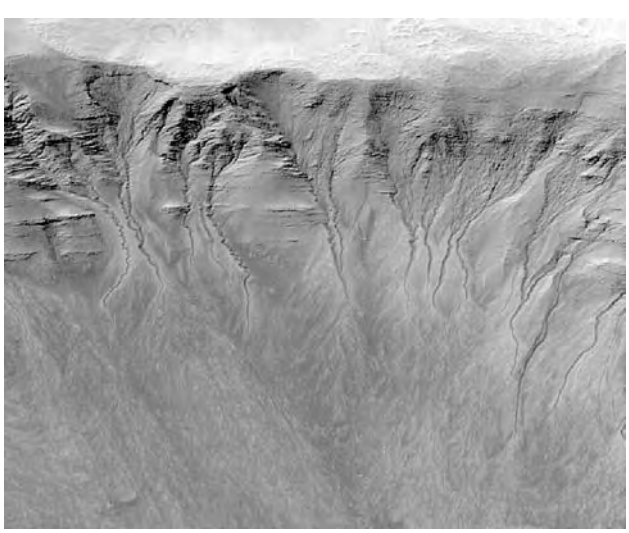

Figure 6.29. Gullies in the layered, south-facing wall of Newton crater at 41.8°S, 192°E (MOC E16-00043).

Three possible alternatives to groundwater sapping have been suggested: dry mass wasting (Treiman and Louge, 2004), erosion mediated in some way by CO_2, and erosion by water derived from the melting of ice. Although gullies can form by dry mass wasting in poorly coherent materials, close to the angle of repose, such as a sand, the mechanism is improbable for the ledge-forming materials into which many of the gullies are incised, especially in their upper reaches. The possibility that CO_2 might somehow be involved was considered by several authors immediately after their discovery (e.g. Musselwhite *et al.*, 2001; Hoffman, 2002b). Liquid CO_2 and CO_2 clathrate are stable at martian temperatures under pressures of several bars or more, equivalent to lithostatic pressures at depths of 100 m or more. It was argued that if liquid CO_2 is present, it could leak out to cut the gullies directly or provide gas to lubricate debris flows. Similarly, disassociation of clathrate could provide gas to lubricate flows. However, there are problems with these hypotheses (Stewart and Nimmo, 2002). A major issue concerns the stability of liquid CO_2 and clathrate in the pores of near-surface rocks. While lithostatic pressures at depths deeper than 100 m are several bars or more, pore pressures are likely to be close to atmospheric pressure. For liquid CO_2 or clathrate to exist close to the surface, they must be completely sealed off from the surface, otherwise they would dissipate and the CO_2 would diffuse into the atmosphere Not only is it difficult to prevent leakage and maintain the high CO_2 pore pressures, it is difficult to inject the CO_2 into the rock under pressure in the first place. Even if liquid CO_2 were present and erosion on a slope broke the seal, the liquid CO_2 would evaporate explosively, forming a jet, and would unlikely form a gully. These considerations led Stewart and Nimmo (2002) to reject the CO_2 hypothesis.

The possibility that the gullies formed by melting of ice has been suggested on the basis of terrestrial analogs, theoretical considerations, and observations of the emergence of gullies from under what could be ice deposits. Lee *et al.* (2001) and Costard *et al.* (2002) point out the close resemblance between the martian gullies and gullies that form in arctic regions of the Earth by the melting of snow and ice. However, conditions on Earth are far more favorable for accumulation and melting of snow than on Mars. As we saw in the previous section, accumulation and melting of snow on Mars is sensitive to the obliquity cycle. At the present obliquity of 25° most of the water on the surface is in the polar caps, precipitation outside the polar caps is negligible, and even though surface temperatures may rise above 273 K around midday,

above-freezing temperatures are restricted to the upper few millimeters of the surface. The daily, near-surface temperature fluctuations dampen out rapidly with depth to converge on the mean daily temperatures, which are well below freezing. Under these conditions, generation of enough liquid water to cut even the small gullies by melting of snow is unlikely (Clow, 1987). The situation is very different at high obliquities. At obliquities higher than 30–40°, water is driven off the polar caps and accumulates as snow in low to mid latitudes (Mischna *et al.*, 2003). During summer, poleward-facing slopes face the Sun and are illuminated for most of the long summer day. As a consequence, average daily temperatures on these slopes may rise well above freezing. The process is helped if the slope is also exposed to reflections from and radiation emitted by nearby slopes (Hecht, 2002). Under these conditions, enough meltwater may be produced to destabilize the slope underneath the snowpack and form a gully (Costard *et al.*, 2002). Emergence of gullies from beneath what may be ice deposits on pole-facing slopes provides observational support for origin of the gullies by this mechanism (Christensen, 2003) (Figure 6.30).

Finally, a different type of gully is occasionally seen on sand dunes (Figure 6.31). They are roughly 10 m across but may extend for 3 km down the slope of

Figure 6.30. Possible ice deposits in hollows on the wall of Dao Vallis at 33.1°S, 93.2°E. It has been suggested that gullies form by melting of snow and ice preferentially retained on cold, pole-facing slopes (see text). Here we see examples of the postulated ice deposits. The scene is 2.8 km across (MOC M11-01601).

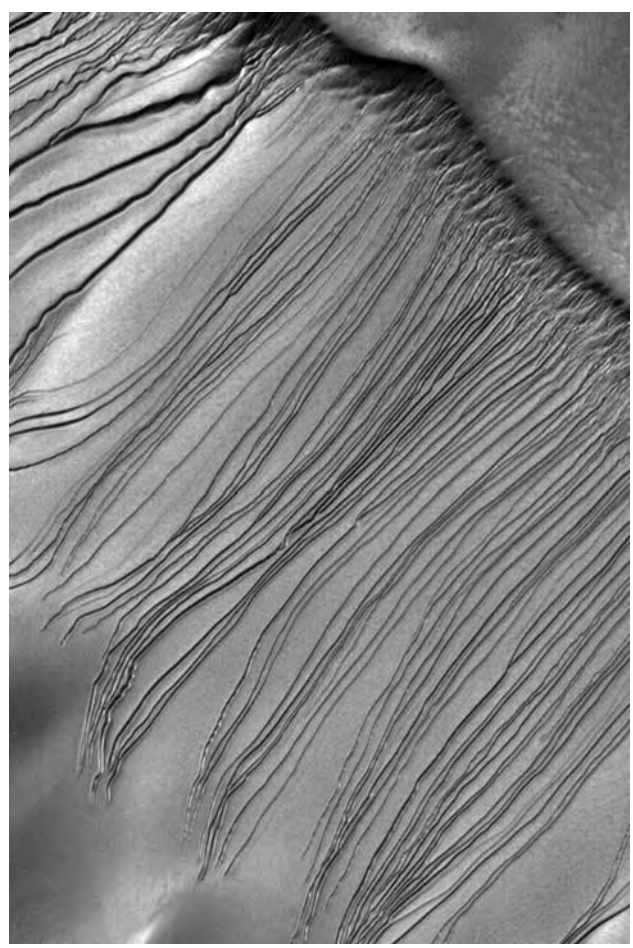

Figure 6.31. Gullies in a sand dune at 54.5°S, 12.7°E. Avalanching of the sand may have been triggered when the sand, containing small amounts of water or carbon dioxide ice, was warmed by the Sun. The image is 3 km across (MOC M19-01170).

the dune. Their precise origin is unknown. They likely formed as a result of avalanching of the dune materials, but the role of water, ice, or other volatiles is unclear.

Summary

Three types of water-worn features are recognized: outflow channels, valley networks, and gullies. Outflow channels are mostly tens to hundreds of kilometers wide, have complexly scoured floors, and contain teardrop-shaped islands. Most start full size in local rubble-filled hollows or at graben, but some of the largest emerge from the east end of the Valles Marineris. They are mostly Hesperian in age, and so younger than most of the valley networks. Outflow channels are thought to have formed by large floods with peak discharges orders of magnitude larger than any terrestrial river. Two likely causes of the floods are violent eruptions of groundwater and catastrophic draining of large lakes. Eruptions of groundwater could have resulted from the trapping of groundwater under high pressure beneath a thick cryosphere followed by disruption of the cryosphere seal by faulting, dike injection, or impacts. Catastrophic release of water stored in lakes within the canyons may have followed undermining of an eastern barrier by subsurface flow of groundwater into the low areas to the canyon's east.

Valley networks are mostly 1–5 km across, but may be hundreds to even thousands of kilometers long. They form branching, hierarchical systems of valleys like terrestrial rivers. Most are deeply incised into the surface, and have rectangular or U-shaped cross-sections. Most valleys are in the cratered uplands, where drainage densities vary greatly at local and regional scales from zero to the low end of terrestrial values. Some volcanoes are densely cratered, others are undissected. The rate of valley formation was high during the Noachian and declined rapidly at the end of the Noachian, but valleys continued to form through the Hesperian into the Amazonian. Some prominent valleys appear to have formed largely by groundwater sapping, but surface runoff appears to have been widespread. Warmer climates are almost certainly required to provide runoff irrespective of whether precipitation was rain or snow. If so, the ages of the valleys imply sustained warmer conditions in the Noachian and occasional warm conditions subsequently.

Gullies are typically about 10 m wide and hundreds of meters long and form on steep slopes, preferentially those that face the poles. They appear to be forming in the present epoch. Although they are likely water-worn, the source of the water is controversial. One possibility is groundwater seepage, but this is inconsistent with current climatic conditions on Mars and some of the geometric relations. Another possibility is that they form during periods of high obliquity by melting of snow deposited on steep, pole-facing slopes during winter. Melting occurs in summer when pole-facing slopes experience long, sustained illumination by the Sun.

7 Lakes and oceans

Numerous standing bodies of water of widely different sizes must have accompanied formation of the valley networks and outflow channels. The cratered uplands, in which most of the valley networks occur, are poorly graded. Closed depressions are common. Most are clearly impact craters, ranging in size up to the Hellas basin, but irregularly shaped basins of indeterminate origin are also common. The uplands somewhat resemble fluvially immature terrestrial landscapes, such as the Canadian Shield, where fluvial erosion has not yet eliminated many of the local hollows left by recent glaciation. Most of the hollows in the martian uplands were present at the time that the valley networks formed, as indicated by drainage directions that generally follow the present topography and converge on the hollows. Much of the precipitation that resulted in formation of valleys likely accumulated, therefore, in lakes, at least temporarily.

The possible presence of former seas or oceans on Mars presents us with some of the planet's most intriguing issues. A distinction must be made between possible Noachian oceans and possible post-Noachian oceans. The highly dissected and highly eroded nature of the Noachian uplands strongly suggests that conditions were warm and wet for extended periods of time during the Noachian. If so, then large bodies of water would have been present in low areas such as Hellas and the northern plains, also for extended periods of time. As on Earth, their size would have been controlled by the total near-surface water inventory. The situation for post-Noachian times was probably very different. The large outflow channels are the main reason for concluding that large bodies of water accumulated on the martian surface in post-Noachian times. As discussed in Chapter 6, formation of large floods may have required cold conditions and a thick cryosphere. If true, then the size of resulting bodies of water would have been controlled by the size of the floods, not the global inventory of water, and the resulting seas or oceans would have frozen within geologically short periods of time.

Since most outflow channels end in the northern plains, large bodies of water were likely left there after each flood. While the size of such northern seas may be controversial, their former presence is not. The upper estimates of the amounts of water that formed these seas are comparable to the volume of water per unit area on Earth today, the equivalent of a global layer roughly 3 km deep. The lower estimates are of a global equivalent of a few hundred meters. All but the lowest estimated volumes of water are difficult to hide and difficult to eliminate, such as by losses to space. Before we can speculate on how the water of former oceans might have been lost, and what effect these oceans might have had on global conditions, we have to know when and where oceans were present and how big they were. These are the main concerns of this chapter. The climatic implications of the oceans are discussed in Chapter 13.

Part of the geological evidence for lakes and oceans is the rock record. Depressions commonly contain stacks of horizontally layered rocks. While this is not proof of lacustrine or marine deposition, it is consistent with it. More compelling evidence has come from the rover landing site in Meridiani, where finely bedded evaporites provide evidence for former lakes, and from spectral data from orbit that indicates that sulfate-rich deposits in depressions are common. Other evidence is geomorphic. Seas and lakes could have left their mark on the landscape in various ways. Shorelines may outline former oceans. Smaller bodies may be identified by terraces, deltas, convergent valleys, outlet channels, and so forth.

In addition to examining the observational evidence, we also briefly discuss what the fate of a lake or ocean might be under different circumstances. The post-Noachian lakes and seas that formed as a result of outflow channels may have accumulated under sub-freezing conditions. We examine how long it would take such bodies to freeze and how long the resulting ice deposit might have survived.

Paleolakes in the cratered uplands

Several authors have attempted to identify paleolakes in the cratered uplands from orbital data. The criteria used include valleys entering and leaving a depression, and the presence of terraces, deltas, layered deposits, and light-toned materials suggestive of

evaporites (e.g. Goldspiel and Squyres, 2000; DeHon, 1992; Forsythe and Zimbelman, 1995; Newsome *et al*., 2003; Forsythe and Blackwelder, 1998; Cabrol and Grin, 1999). An example is provided by the Parana Valles, which converge on a depression partly filled with knobby or chaos-like deposits. Out of the depression emerges the Loire Vallis, which then continues for 1000 km to the northeast (Figure 6.18). If the Parana Valles and Loire Vallis were cut by water, as is highly likely, then water must have pooled in the depression between the Parana Valles and Loire Vallis. Goldspiel and Squyres (2000) interpret the knobby deposits in the depression as eroded remnants of sediments deposited there. At a larger scale, several depressions in the Terra Sirenum region (Figure 7.1), ranging in size up to 200 km across and over 1 km deep, contain knobby deposits similar to those downstream of the Parana Valles (Figure 7.2). Although convergent drainage is less obvious in these depressions, terraces around the periphery support the supposition that they formerly contained lakes. However, areas of convergent drainage containing knobby deposits are rare. More commonly depressions within the uplands contain ridged plains similar to extensive volcanic plains elsewhere, as in Tyrrhena Planum. In these depressions the sediments may be buried by younger volcanics.

The most common relationship interpreted as indicative of former lakes within a crater is the breaching of the crater rim by a valley, cut by a stream either entering or leaving the crater (Forsythe and Blackwelder, 1998). The best-known example is the crater Gusev whose southern rim is cut by Ma'adim Vallis. It was chosen as a landing site for the Spirit rover on the supposition that it formerly contained a lake. Valleys entering and leaving craters are common throughout the uplands. Figure 7.3 shows an area near the crater Palos where several craters have rims breached by valleys. Most such craters show little evidence to confirm that water did indeed pool in them. As viewed at moderate resolution (100 m/pixel), most

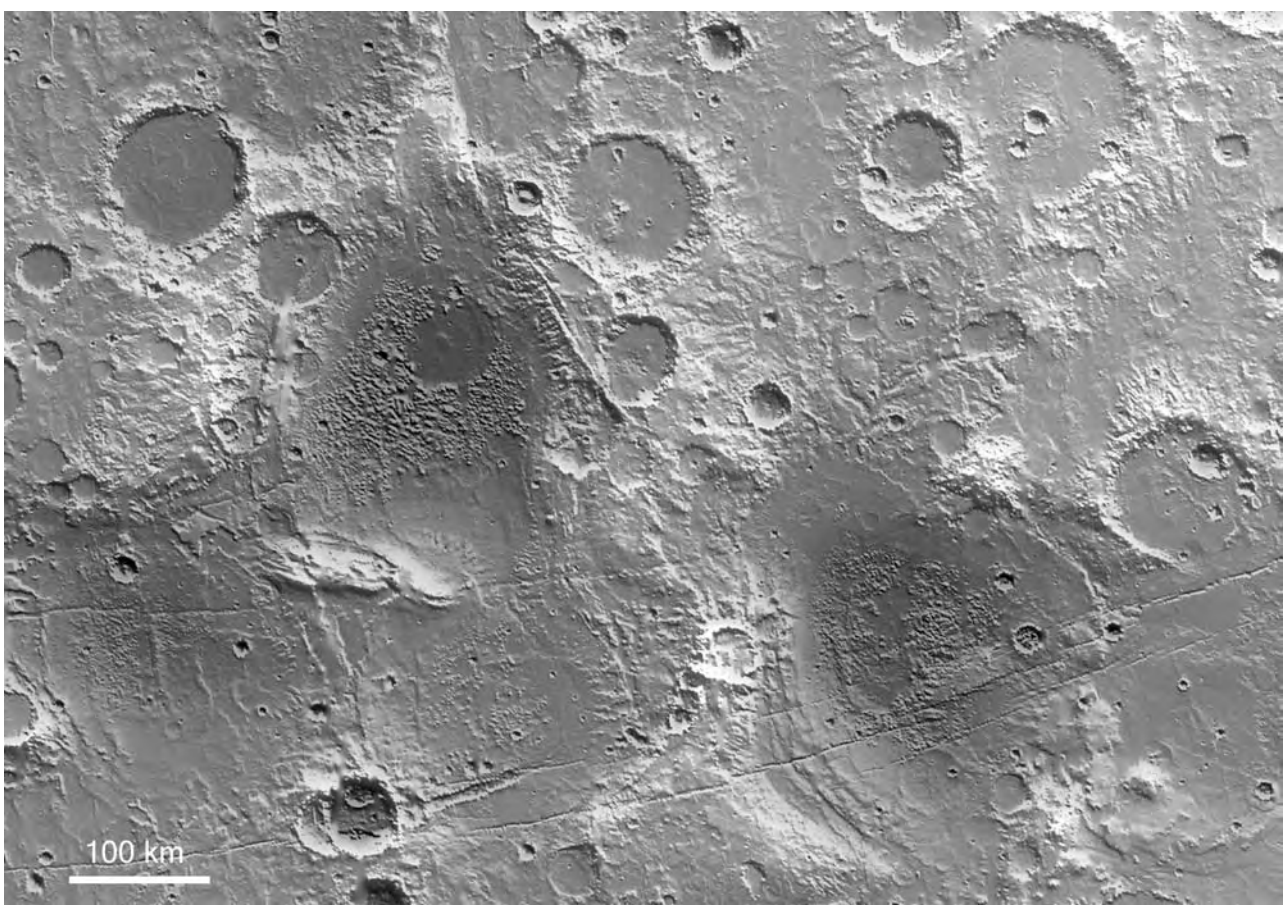

Figure 7.1. Closed depressions around 35°S, 185°E in Terra Sirenum that are partly filled with material eroded into closely spaced hills. These depressions may be part of an extensive former lake that ultimately drained through Ma'adim Vallis, which starts 1000 km to the north (Irwin *et al*., 2002).

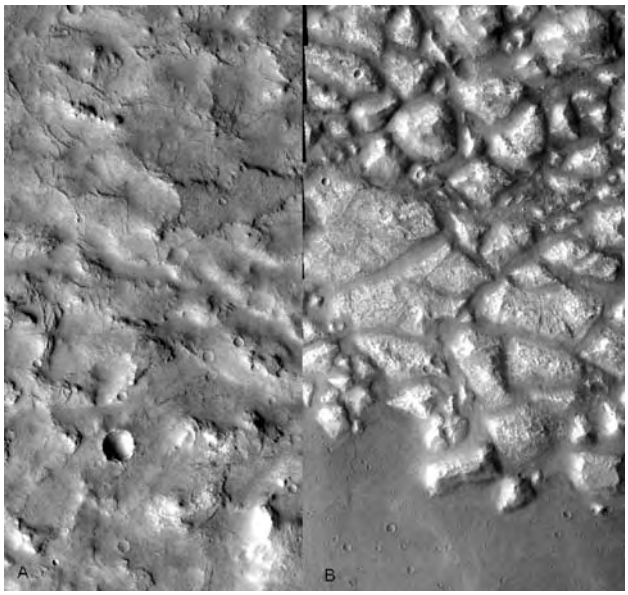

Figure 7.2. Detail of the eroded remnants of deposits in closed depressions. (A) Parana Chaos at 21.9°S, 347.3°E (THEMIS V08265003). The regional context is shown in Figure 6.18. (B) Detail of Atlantis Chaos at 35.1°S, 183°E shown in the previous figure (THEMIS V01330003). Both images are 17 km across.

have flat, cratered floors that are featureless, except for wrinkle ridges, as do most nearby unbreached craters. Leverington and Maxwell (2004) argue that many such crater floors and their associated valleys are volcanic. They point to similarities between these breached craters and features of unquestioned volcanic origin such as the summit caldera of Elysium Mons (Figure 3.19). Nevertheless, if most of the valleys in the Noachian uplands were cut by water, then water must have commonly pooled in closed depressions, despite our inability to unambiguously discriminate between lava pools and water pools in the imaging.

Some craters have additional features that support the former presence of a lake. Rarely, a terrace may be present at a constant elevation around the periphery of the crater (Figure 7.4). Such terraces could form in several ways. They may be remnants of a former level floor that is now almost completely eroded away as a result of a lowering of the basin outlet. They may have formed of material eroded from the crater walls, by fluvial and mass-wasting processes, and deposited close to the shore within the crater lake. They may be erosional terraces, but terraces cut into crater walls are rare, possibly because the small dimensions of the craters limit the fetch needed to generate wave action. Leverington and Maxwell (2004) argue here also for a volcanic origin. They point out the similarity between the terrace in Figure 7.4 and terraces left behind in terrestrial pit craters following withdrawal of magma. Occasionally, concentric rings are seen, possibly indicating successive shorelines or successive stages of removal of crater fill (Figure 7.5).

Deltas are more common than terraces. A particularly compelling example of a delta occurring where a valley enters a crater, in this case Holden NE crater, was discussed in Chapter 6, and shown in Figure 6.26. Other examples of deltas are seen in Figures 7.6 and 7.7. One issue with respect to these deposits where valleys enter craters is whether deposition was subaereal or subaqueous. Fassett and Head (2004) argue for a subaqueous origin, particularly where the surface of the deposit is at a lower elevation than a channel exiting the crater. Like Malin and Edgett (2003), they interpret the superposed ridges (Figure 7.6) as sites of former channels, whose bed deposits were more resistant to erosion than their surroundings. Hauber *et al.* (2005a) showed that the delta in Figure 7.7 had elevation profiles very similar to terrestrial deltas and that layering can be seen in the delta deposits around their periphery. A group of flat-topped hills where Ma'adim Vallis enters Gusev crater (Chapter 11) has also been interpreted as the remains of a delta that formed at the mouth of Ma'adim Vallis at a time when a lake formerly occupied the crater (Kuzmin *et al.*, 2000).

The vast majority of the Noachian impact craters have flat floors. The original bowl-shaped cavities have been largely filled, and the original central peaks are either absent or only small remnants poke up above the level of the flat floor. To what extent lacustrine processes contributed to the filling of the original craters is not known. As indicated above, if precipitation accompanied formation of the valley networks, as is likely, then many Noachian craters are likely to have at times contained lakes. When present, the lakes could have acted as traps for material entrained in the atmosphere as a result of impacts, volcanic eruptions, and wind erosion. Some lacustrine episodes may have ended with the deposition of evaporites. When lakes were not present, materials would still have been deposited in the craters but directly out of the atmosphere. Volcanic eruptions within the craters could also have contributed to the crater fill. The present crater floors give little insight into the relative importance of these different processes, although the common presence of ghost craters on the floors indicates that the filling of the host craters took place over extended periods of time. Pits eroded into some crater floors expose layered

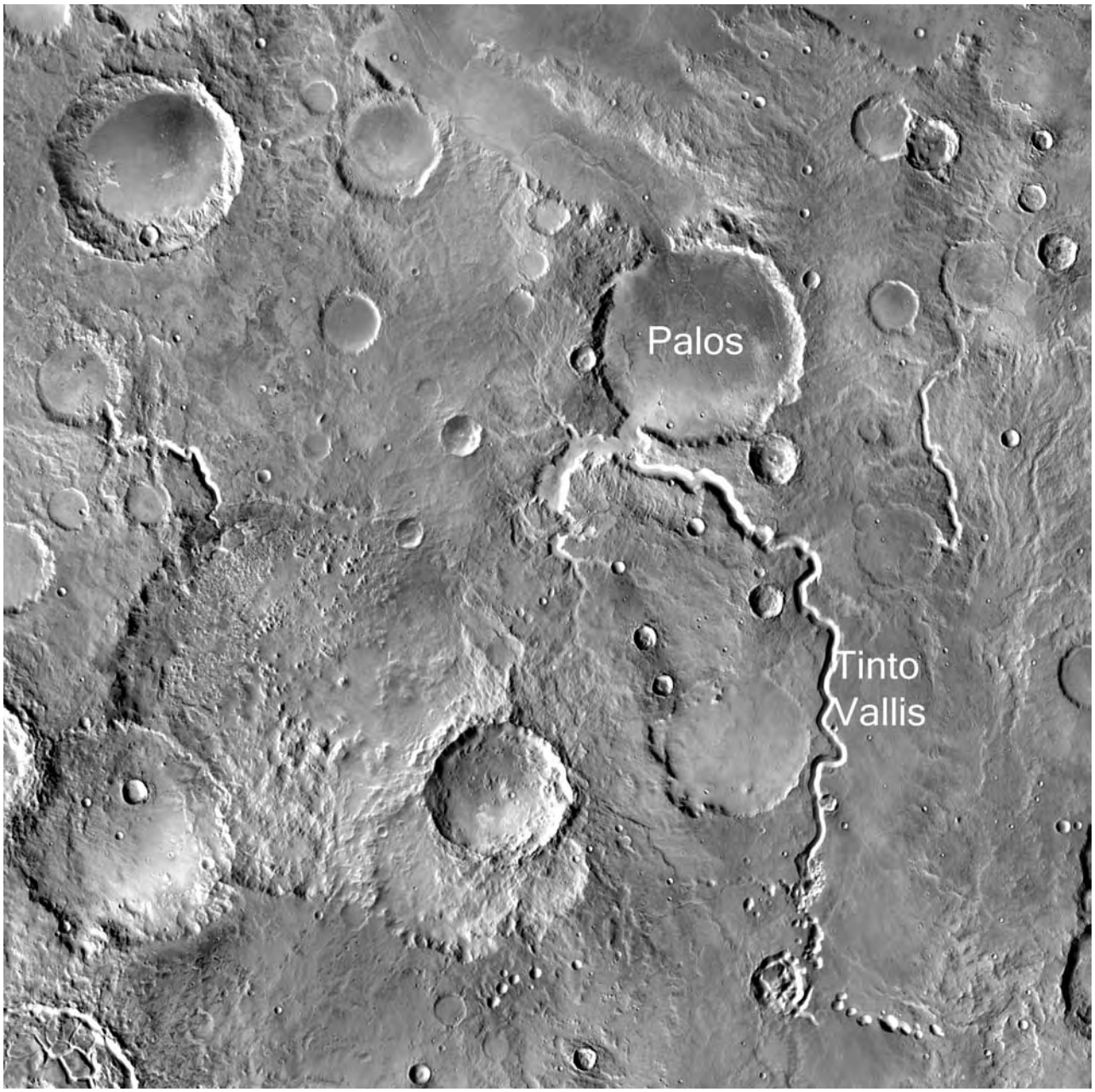

Figure 7.3. Possible paleocrater lakes near 4°S, 111°E. Near the center of the image, Tinto Vallis breaches the wall of the 60 km diameter crater Palos. Water likely pooled within Palos before exiting the crater through its north rim. Other breached craters occur elsewhere in the image. Tinto Vallis degenerates upstream into a line of pits, which suggests a subsurface source (THEMIS mosaic).

sequences, as might be expected (Figure 7.8), but again the images give little indication of what role lacustrine processes played in creating the layering.

In some upland areas, the larger craters may have mounds of layered sediments superimposed on their flat floors. Such mounds are particularly common in Terra Meridiani near the crater Schiaparelli (Figure 7.9). Cabrol and Grin (1999) used the presence of such mounds as one criterion for recognition of crater lakes. As viewed at the MOC scale (1.5 m/pixel), the layered deposits appear identical to sediment mounds in the canyons discussed in Chapter 5. Both are generally lighter toned than the surrounding materials and can be divided into different units,

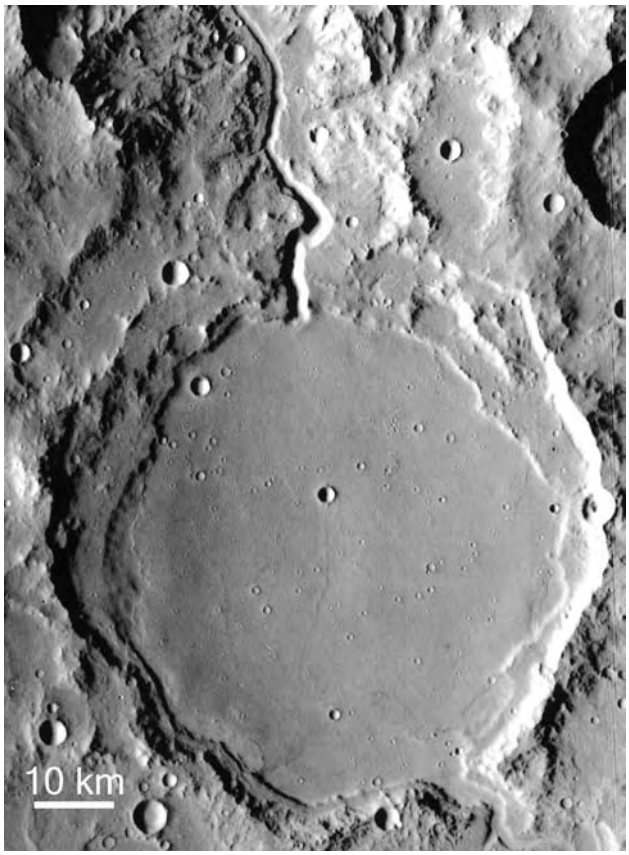

Figure 7.4. Terraced, 50 km diameter crater with breached rims at 14.2°S, 185.9°E. Water may have flowed into the crater from the south and out of the crater to the north. The terrace could represent the level of former fill that has since largely been removed. Alternatively, the crater floor is volcanic and a lava lake left the terrace behind (Viking 438S12).

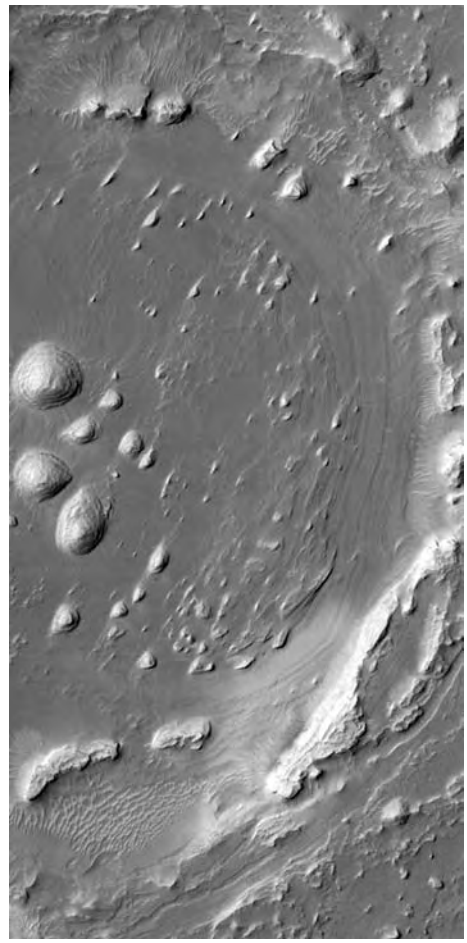

Figure 7.5. Possible paleocrater lake at 7.9°N, 354.1°E. Eroded remnants of the former crater fill form terraced hills on the crater floor. Rings around the periphery of the crater may mark former lake levels in the crater, or be simply remnants of the former layered fill, which has now been almost completely removed. The image is 3.1 km across (MOC E2200081).

possibly separated by unconformities (Malin and Edgett, 2000b). The most distinctive units are finely layered and erode to form arrays of closely spaced mesas with stair-stepped slopes (Figure 7.10). The more massive units erode to form an etched surface on which layering is barely visible. One of the largest deposits is in Gale crater (4.9°S, 138.2°E), where the sedimentary stack is over 2 km thick. The stack is so high that it overtops the crater rim. A small but well-studied example, nicknamed White Rock (8°S, 25°E), has been interpreted as an evaporite deposit (Forsythe and Zimbleman, 1995), although this has not been confirmed from spectral observations. Commonly, in the vicinity of craters with sediment mounds, what appear to be etched remnants of layered deposits occur in the intercrater areas. Malin and Edgett (2000), accordingly suggested that the crater mounds were eroded remnants of regional layered deposits, not simply local deposits within craters. This interpretation is also consistent with the overtopping of crater rims by the mounds.

Some of the issues associated with the former presence of lakes in the upland are well illustrated by Gusev crater and Ma'adim Vallis. Irwin *et al.* (2002) suggested that Ma'adim Vallis formed as a result of partial drainage of a 1,100,000 km^2 lake in the uplands to the south of Ma'adim (Figure 7.11). The lake is identified as a closed depression in the MOLA data. Its outlet is at the 950 m level, and the maximum possible elevation of the lake surface, as indicated by alternate overflow pathways, is at 1100 m. Around the proposed lake, valleys terminate at the 950 m level, as expected if a lake were formerly present, even though the slopes

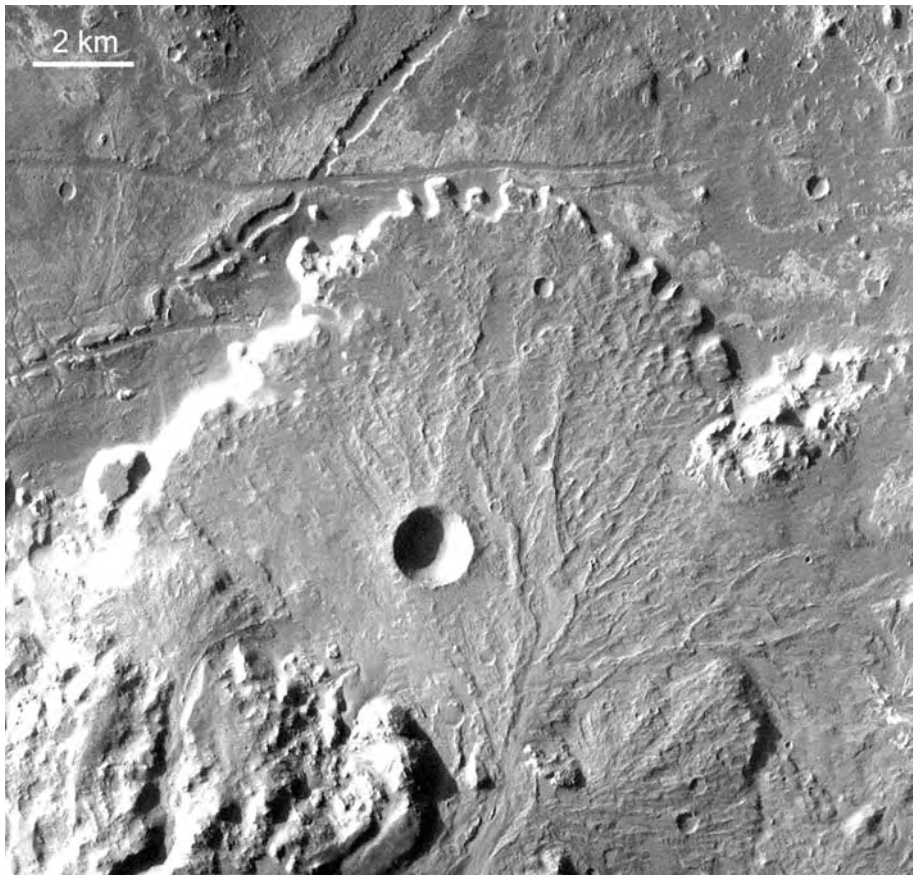

Figure 7.6. Delta in Holden crater at 26.6°S, 325.6°E. A valley has cut through the south rim of the crater, just visible at the bottom of the picture, and deposited its sediment load to form a fan within the crater. Coarse sediments within the former channels are resistant to erosion so have left the channels as branching ridges on the fan (THEMIS V03210003).

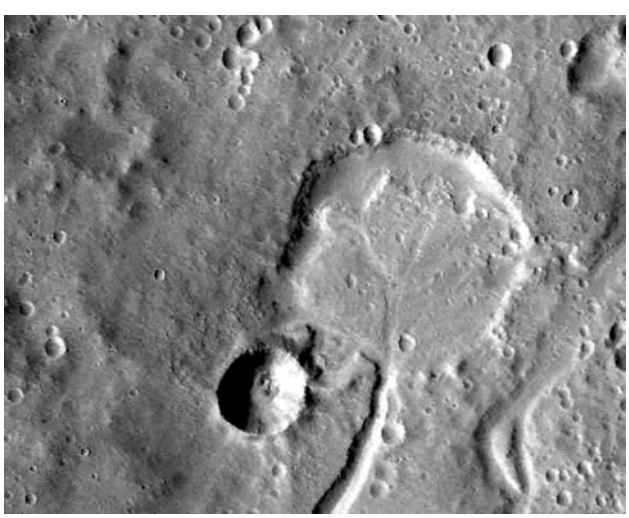

Figure 7.7. Delta in a 6.4 km diameter crater at 8°N, 312°E. Water appears to have entered the crater through the southern rim and exited through the eastern rim (THEMIS V01849011).

continue well below this level. Irwin *et al.* propose that this lake drained northward into a smaller, shorter-lived lake that occupied the remnants of an old impact basin. Ma'adim Vallis, the outlet to this secondary lake, was rapidly incised and extended headward as a result of the low base level near the plains–upland boundary. Ultimately, according to Irwin *et al.*, Ma'adim breached the barrier between the upper lake and lower lakes, resulting in drainage of the larger, upper lake. At some time during these events, the Ma'adim river breached the rim of Gusev crater forming a lake within the crater, and a delta where the river entered the lake. A group of hills at the mouth of Ma'adim Vallis is probably the remains of the delta. The top of the hills, at an elevation of −1600 m, 200–300 m above the level of the present floor, may indicate the former lake level.

Unfortunately, the Spirit rover found little to support the hypothesis that there had previously been a lake in Gusev crater (Chapter 11). The rover landed

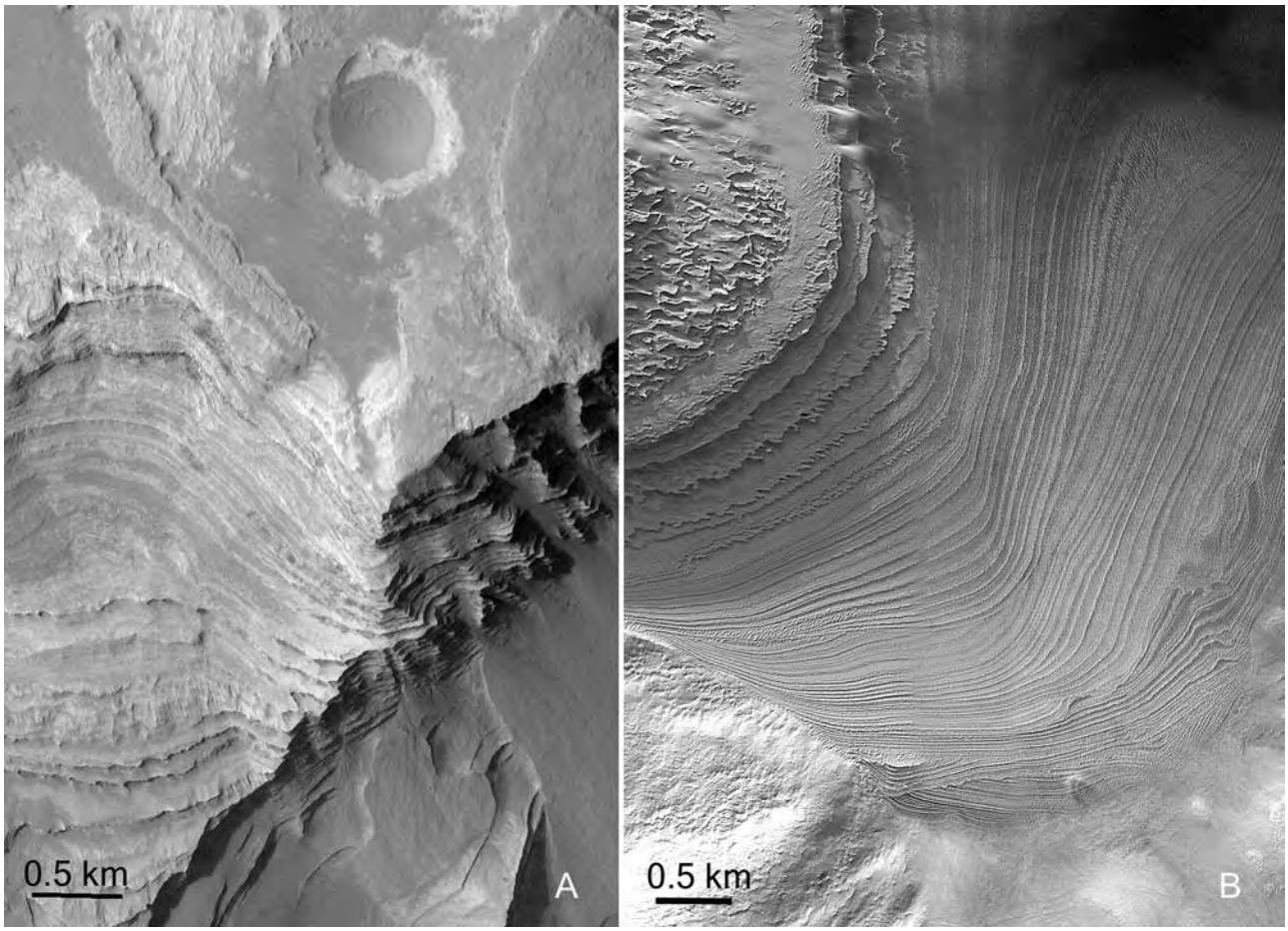

Figure 7.8. (A) Layers in the floor of the 185 km diameter crater Terby at 27.7°S, 161.9°E. Like most upland craters, Terby has a flat floor. The layers seen here are exposed in the wall of pits eroded into the floor. Such pits are rare, but this image gives an indication of what may typically be present under the flat floors of upland craters (MOC R0501482). (B) Layered sediments in Galle crater at 52.3°S, 329.9°E showing numerous unconformities (MOC mosaic, Malin Space Sciences).

on a plain strewn with angular basaltic rocks that were almost unaltered except for a millimeters-thick weathering rind (Squyres *et al.*, 2004b). No sediments were found on the plains. The rocks in the Columbia Hills southeast of the landing site are more altered, and some appear layered, but they still do not provide compelling evidence of lacustrine deposition. There are at least three explanations. The first, that Gusev never contained a lake, is unlikely. Ma'adim Vallis was surely cut by water, and if so water must have flowed into Gusev and some of the materials eroded away to form Ma'adim Vallis must have been deposited there. The second possibility is that the Ma'adim-derived materials are buried by younger volcanic deposits. The floor of Gusev crater likely has a complex origin (Kuzmin *et al.*, 2000). Materials from the volcano Amphitrites Patera, just to the north of the crater, could have been deposited in the crater. The thick, probably eolian deposits of the Medusae Fossae Formation just to the northeast may extend into the crater. Ejecta from nearby impact craters must have been deposited in the crater and there may have been volcanic eruptions within the crater itself. All these materials could have contributed to burial of the lacustrine deposits. A third possibility is that the plains on which the rovers landed were formerly covered by sediments that have since been removed. The etched deposits to the east of the landing site may be analogous to the hummocky deposits downstream from the Parana Valles, discussed above. They are at an elevation 100–200 m higher than the landing site. If they were formerly more extensive than at present, as appears likely from their etched appearance, they may have once covered the landing site. There are thus several plausible reasons why Spirit found no lacustrine deposits in Gusev despite the likely former

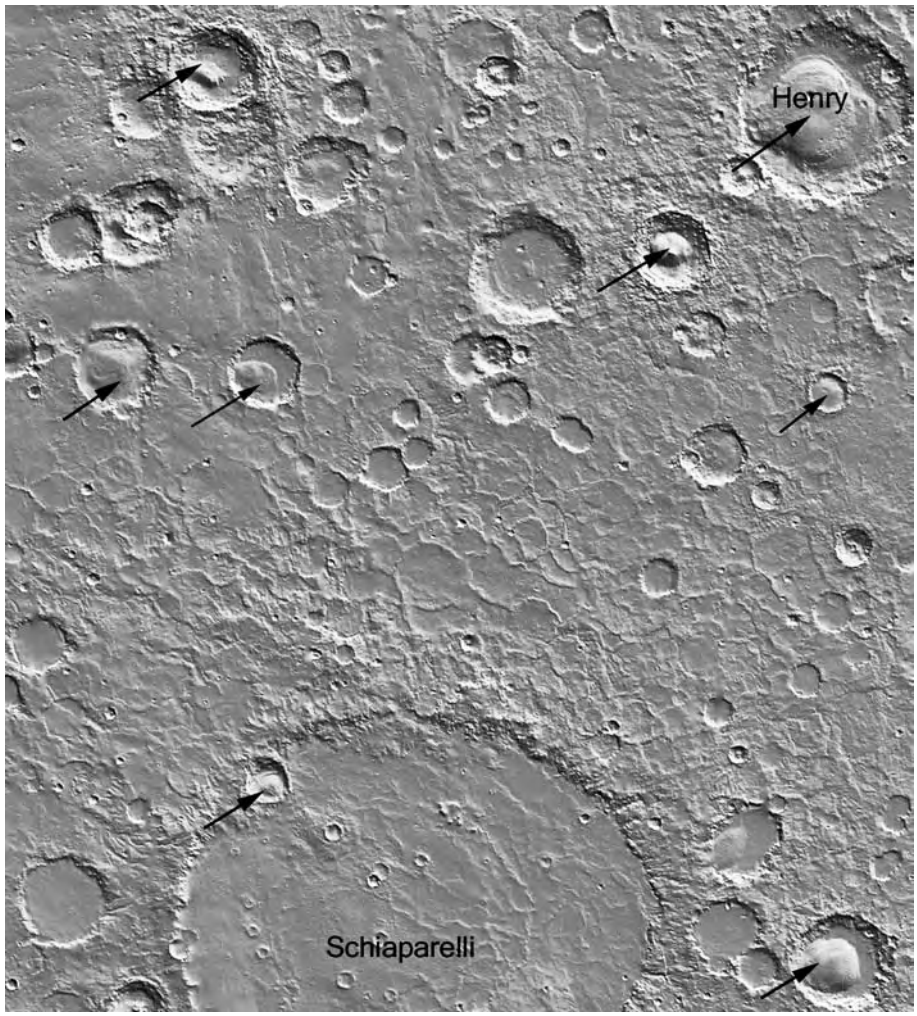

Figure 7.9. Sediment mounds in craters near the 460 km diameter crater Schiaparelli, centered at 2°S, 17°E. Most of the mounds, indicated by arrows, are finely layered (see next figure) and rest on the flat floors of the craters, as distinct from the layers beneath the flat floors seen in Figure 7.8A. Some of the mounds have been interpreted as remains of former lake sediments, although in places the mounds are higher than the crater rims. The mounds may alternatively be the remains of a layered deposit that formerly covered the entire region shown and that has since been almost entirely removed (MOLA).

presence of a lake. The experience indicates the hazards of geological interpretation from remote sensing data alone.

In summary, lakes must have been common in the cratered uplands during the Noachian when most of the valley networks formed. The uplands are, however, complex in origin. In addition to being an era with high rates of fluvial activity, the Noachian was an era with high rates of volcanism, impact, and probably other processes such as eolian erosion and deposition. Layered deposits, common in local lows such as craters throughout the Noachian terrain, may include lacustrine sections, but layering is no guarantee of a lacustrine origin.

Argyre and Hellas

Parker *et al*. (2000) suggested that, during the Noachian, the impact basin Argyre contained a large lake that overflowed to the north. The evidence is a string of short channel segments that extend from the north rim of Argyre to chaotic terrain in Margaritifer Terra, 1000 km to the north (Figure 7.12). The original channel may have extended further north into the Chryse basin, but it can no longer be confidently identified because of the presence of younger, Hesperian outflow channels that may have utilized the former Noachian watercourse. The channel segments, particularly Ladon Vallis, strongly resemble the younger outflow channels, which suggests that they formed

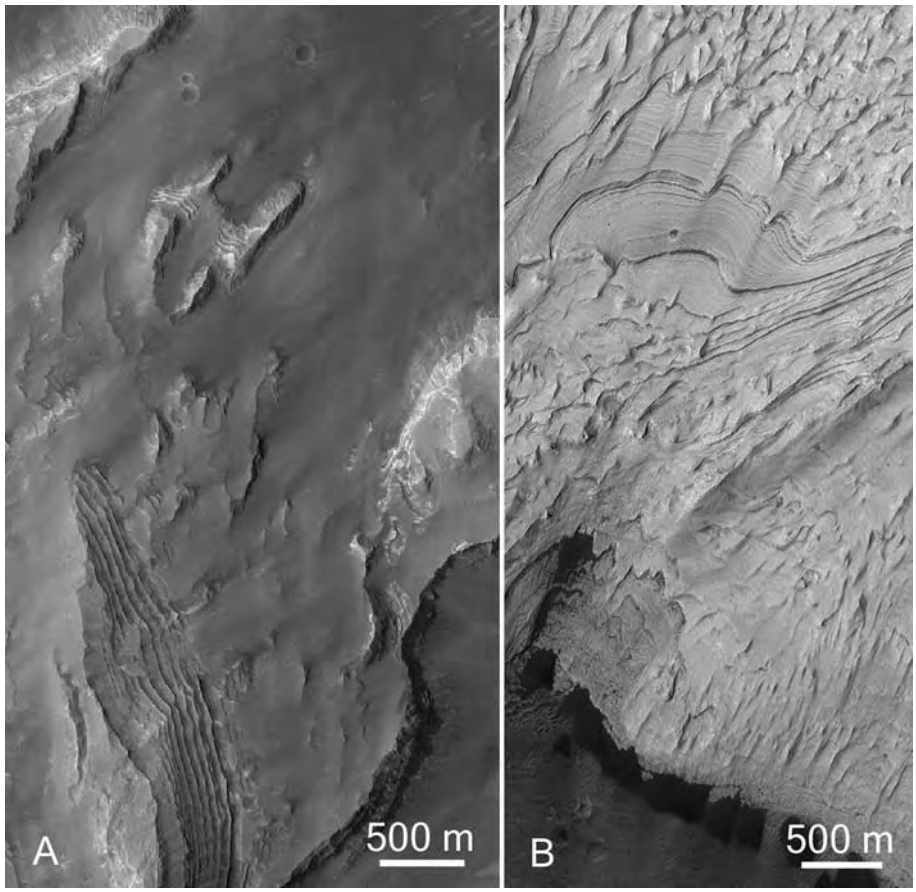

Figure 7.10. Layered deposits that form sediment mounds within upland craters. (A) Deposits in Gale crater at 4.9°S, 138.2°E (MOC S0300700). (B) Sediments in the 170 km diameter crater Becquerel at 21.3°N, 351.6°E. The rhythmic layering seen in the mounds resembles the rhythmic layering seen in the much more extensive sediment mounds in Valles Marineris. Compare with Figure 5.17 (MOC S0100156).

by floods rather than slow erosion. The pathway is discontinuous, partly because of the superposition of younger craters and partly because of the presence of local lows, such as the Ladon basin, in which water probably ponded. If this truly was an integrated watercourse, extending from the rim of Argyre into the Chryse basin, then it is the largest known river system in the Solar System. Several valleys feed into Argyre from the south and east. The three largest, shown in Figure 7.12, start near some flat-lying, possibly ice-rich sediments near the south pole, called the Dorsa Argentea Formation (Tanaka and Scott, 1987; Head and Pratt, 2001). Parker *et al*. speculated that, during the Noachian, meltwater from ice-rich deposits near the south pole fed into Argyre, filling the basin and periodically causing massive overflows. The outlet, Uzboi Vallis, is now partly blocked by the younger crater Hale. If the Noachian outlet was roughly the same elevation as the present-day outlet (+140 m), the lake within Argyre would have contained 2.1×10^6 km^3 of water (Heisinger and Head, 2002).

Heisinger and Head (2002) reviewed various models that have been proposed for the evolution of Argyre, and argued against the former presence of a lake at the elevation of the present outlet, as proposed by Parker *et al*. They note that the three main incoming valleys (Figure 7.13) are Hesperian in age, and significantly younger than Uzboi Vallis, which Parker *et al*. interpreted as Argyre's overflow. If the ages are correct, Uzboi cannot have formed as a result of meltwater from near the south pole entering the basin through these three valleys. Furthermore, the incoming valleys extend down into the basin to levels 2000 m below the outlet, which indicates that there was no lake present when the valleys were cut. They also point out that there are no terraces at the outlet level, despite the fact that if the lake did overflow through Uzboi, a substantial lake would have been left with a surface

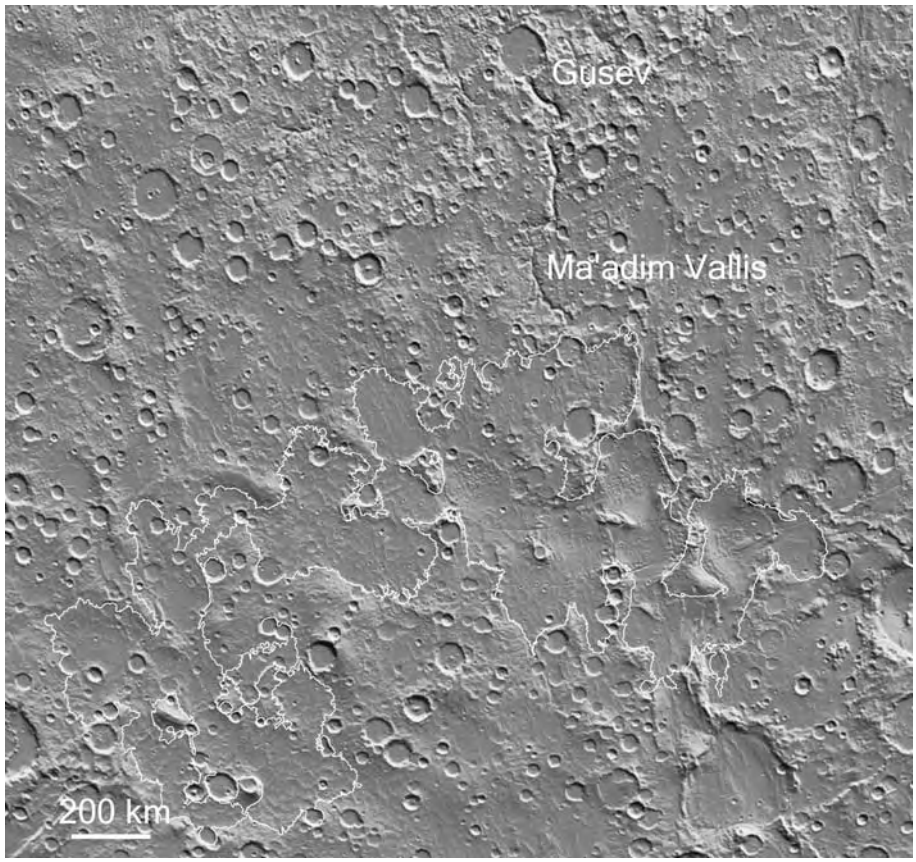

Figure 7.11. The outline of a possible former lake that was the source of water that cut Ma'adim Vallis and flowed through Gusev crater. The lake is outlined by the 1100 m contour. For a closer look at the Gusev–Ma'adim region see Figure 11.2 (MOLA).

at the outlet level. They argue further that, under temperate climatic conditions, such as are postulated for the Noachian, a lake could not be maintained in Argyre at the outlet level, since the water would be lost by infiltration and groundwater movement to the low areas to the north of the basin. Finally, they judge that the volume of water required for overflow is too large compared with what might reasonably be derived from melting the Dorsa Argentea Formation. Heisinger and Head prefer a model in which, during the Hesperian, meltwater from the south pole produced a much shallower lake in Argyre. This lake, estimated to be roughly 2000 m deep, would have slowly frozen then sublimated away if the climate were similar to today's. The presence of what appear to be eskers on the floor of Argyre (Figure 7.14) supports the supposition that ice deposits were formerly present on the floor of Argyre (Kargel and Strom, 1992). Thus, Parker *et al.* and Heisinger and Head all agree that a lake was formerly present in Argyre. Where they differ is in the timing and the volume of the lake, and whether it overflowed catastrophically to the north.

The ancient impact basin Hellas contains the lowest point on the planet at −8200 m, significantly lower than the lowest point in Argyre, which is at −4590 m. If Mars was ever warm and wet, runoff must surely have created a lake in Hellas, and if ever there was a globally interconnected aquifer system (Clifford, 1993), groundwater would tend to infiltrate into Hellas to create a lake. In contrast, a lake in Argyre would have been at a higher elevation than the northern plains, so might be expected to lose water by infiltration into the ground and then to the lower-lying Hellas basin and northern plains. Moore and Wilhelms (2001) examined the morphology of the Hellas basin for evidence of former lakes. They found two possible strandlines around the basin, one at −5800 m and one at −3100 m (Figure 7.14). The lower strand can be traced most of the way around the basin. It is missing only in the south, where it is buried by younger

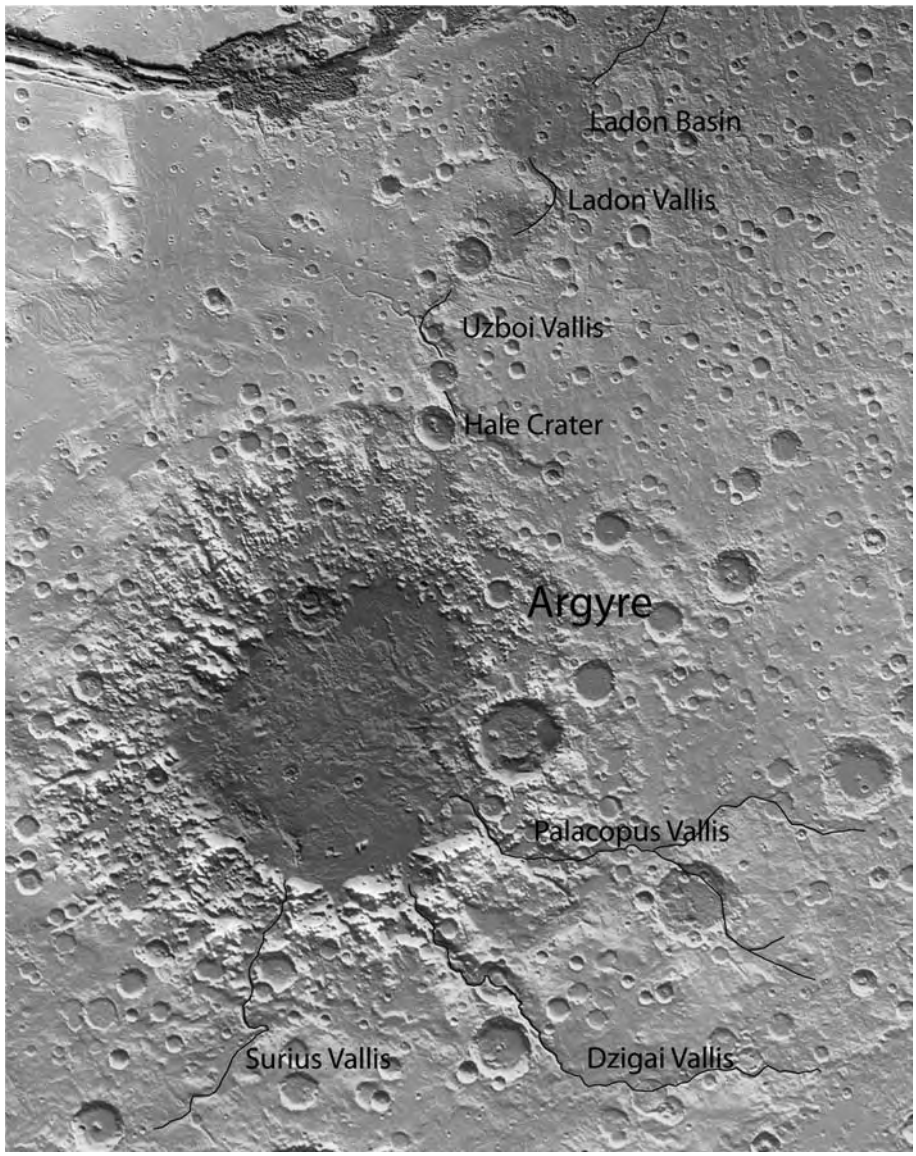

Figure 7.12. The Argyre basin. Three major valleys feed into the basin from the south. The proposed pathway of the overflow at Hale crater is shown to the north. The inner, level floor of Argyre is 750 km across (MOLA).

volcanics. Along most of its length, the contour is at a change in slope between the steeper basin wall and the more shallowly sloping basin floor. It also follows the contact between a ridged plains unit on the floor and an outer mantled unit on the basin rim in which large craters appear subdued. In addition, large outflow channels entering the basin from the east change their form where they cross the contour. Above the contour they are sharply defined; below the contour they are difficult to trace. The upper −3100 m line is marked by an escarpment that in places separates the mantled unit from unmantled terrain further from the basin. Although less well defined than the −5800 m line, it can be traced for over 2000 km around the north and west rim of the basin. There is also a shorter section in the southeast sector of the basin. The upper strandline encloses a volume of $1.4 \times 10^7\,km^3$; the lower one encloses $9 \times 10^6\,km^3$. The lower strandline appears to be the younger, since it was present when the outflow channels formed that enter Hellas from the east. In contrast, the upper strandline is buried by the materials into which the channels are cut. In addition to the two strandlines, Moore and Wilhelms point to layered sediments, common in the northern and eastern parts of the basin (Malin and Edgett, 2000b), as consistent with lacustrine deposition.

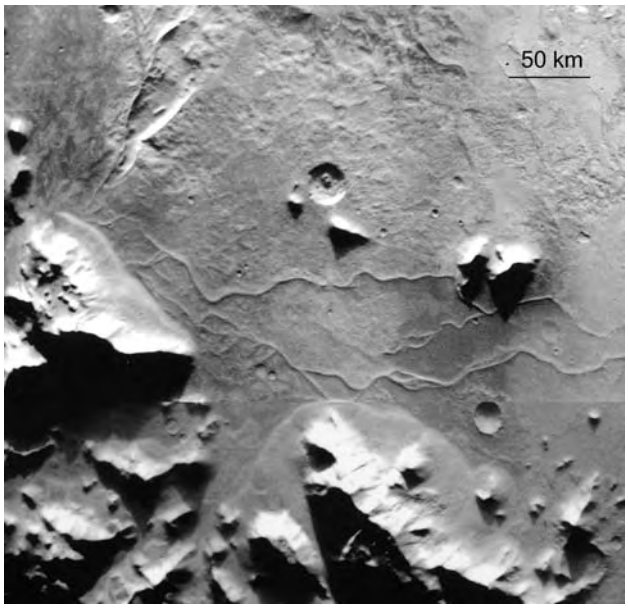

Figure 7.13. Sinuous ridges on the floor of Argyre. The ridges are just visible in the previous figure where Surius Vallis enters the Argyre basin through the southern rim. The ridges are interpreted as eskers, ridges that form along the path of former subglacial streams (Viking 352S36/34).

Kargel and Strom (1992) interpreted many of the features of the Hellas basin as the result of glaciation. They suggested that glaciers entered the basin from the south, covered much of the center of the basin, and created a proglacial lake between the ice in the center of the basin and the basin wall. They interpret the highly textured deposits in the Alpheus Colles Plateau in the center of the basin (Figure 7.14), not well explained in the Moore and Wilhelms model, as moraines. As support for their hypothesis, Kargel and Strom point to several features that resemble terrestrial glacial landforms, including terminal moraines, transverse moraines, drumlins (ice-sculpted hills), eskers (sinuous ridges), and strongly lineated terrain. Moore and Wilhelms also interpret some of the features of the floor of Hellas when viewed at high resolution (Figures 7.15, 7.16) as the result of ice-related processes. They suggest that the lake within the basin developed a kilometers-thick ice cover that ultimately grounded, thereby leading interaction between the ice and the basin floor to create a variety of peculiar landforms.

Thus, Hellas has two potential shorelines around its perimeter, which persist over large distances at constant elevations. In contrast, Argyre seemingly does not, despite having what might be an outlet that would control the lake level, given sufficient water. The strandlines in Hellas are well established, indicating that the lake levels that they may record persisted for a considerable time. But since there is no outlet from Hellas that would maintain the level of a lake, it is puzzling what mechanism sustained the lake at these two levels.

Northern oceans

The global dichotomy between the mainly high-standing cratered terrain in the south and the low-standing sparsely cratered plains in the north has long been recognized (Chapter 4). The low-lying plains have low slopes and are at elevations 5 km lower than the cratered southern uplands (Smith *et al.*, 1998, 1999b). Gravity data indicates that the crust is thinner in the north than in the south, being typically 30–40 km thick under the northern plains and 40–80 km thick under the southern uplands (Zuber *et al.*, 2000). Thus the dichotomy is expressed in three ways, elevation, crater density, and crustal thickness, although the three boundaries do not everywhere coincide. The boundary can be traced all the way around the planet except through Tharsis, where it is buried beneath a thick volcanic pile. The northern plains outside Tharsis thus form a vast depression into which drainage converges from much of the southern uplands.

The conclusion by most researchers that the large outflow channels discovered by Mariner 9 were formed by large floods (McCauley *et al.*, 1972; Masursky, 1973; Milton, 1973; Baker and Milton, 1974; Baker, 1982; Baker and Kochel, 1979) implies that the floods left behind substantial bodies of water in the northern plains. Yet until the late 1980s little was done to determine where such bodies of water might have been present, how big they might have been, and whether they had left behind any evidence of their former presence. It was recognized that the northern plains constitute an ancient depression, possibly formed by one or more giant impacts (Wilhelms and Squyres, 1984; McGill and Squyres, 1991), and that the depression is partly filled with deposits that, at the surface, are mostly Hesperian in age (Scott and Tanaka, 1986; Greeley and Guest, 1987; Tanaka and Scott, 1987). Many of the unique features of the northern plains were variously interpreted as due to repeated deposition and removal of debris blankets (Soderblom *et al.*, 1973), presence of pervasive ground ice (Carr and Schaber, 1977; Rossbacher and Judson, 1981), volcano–ice interactions (Chapman, 1994; Hodges and Moore, 1994), widespread volcanism (Tanaka and Scott, 1987), and large-scale mass wasting (Jons, 1985, 1986; Tanaka *et al.*, 2001).

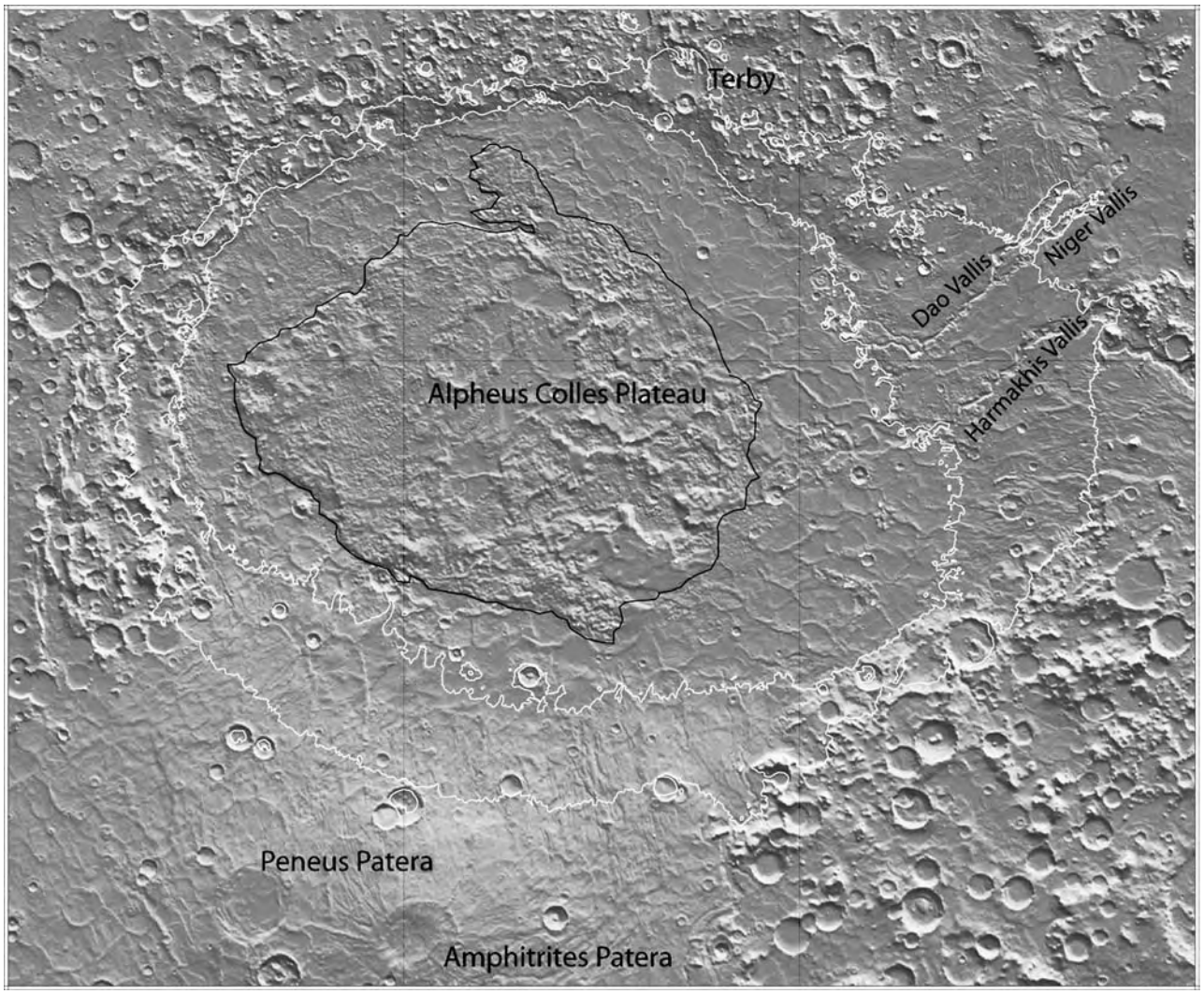

Figure 7.14. The Hellas basin. Shown in white are two levels that have been suggested as former shorelines: a lower −5.8 km level and an upper −3.1 km level. The lower level separates the basin wall from the basin floor. The upper level, visible mostly in the northern and western parts of the basin, is marked by a discontinuous escarpment. Large channels entering the basin from the east (see Figure 6.16) abruptly change their form at the −5.8 km level. The textured, and commonly layered, deposits in the center of the basin have been interpreted as remnants of glacial and lacustrine deposits (MOLA).

Among the first to discuss the possibility of former oceans in the northern plains were Lucchitta *et al.* (1986), who suggested that the polygonally fractured ground found in the plains downstream of outflow channels could be the result of compaction and warping of sediments deposited in standing bodies of water.

Within the northern plains are two subsidiary depressions: a circular Utopia basin centered at 45°N, 110°E, and a more elongate North Polar basin centered at roughly 70°N, 330°E (Figure 7.17). The Utopia basin reaches depths of −5000 m; the North Polar basin reaches depths of −5200 m. The barrier between the two basins has a minimum elevation of −4300 m. Floods that carved the large valleys around Chryse Planitia would have flowed into the North Polar basin, those that cut the valleys northwest of Elysium would have flowed into the Utopia basin. Water from southern Elysium Planitia would have flowed through Marte Vallis into Amazonis Planitia. Similarly, water that cut the channels along the highland front south of Amazonis Planitia would have flowed into Amazonis Planitia. Amazonis Planitia is extremely flat, having a slope of only 1:10,000

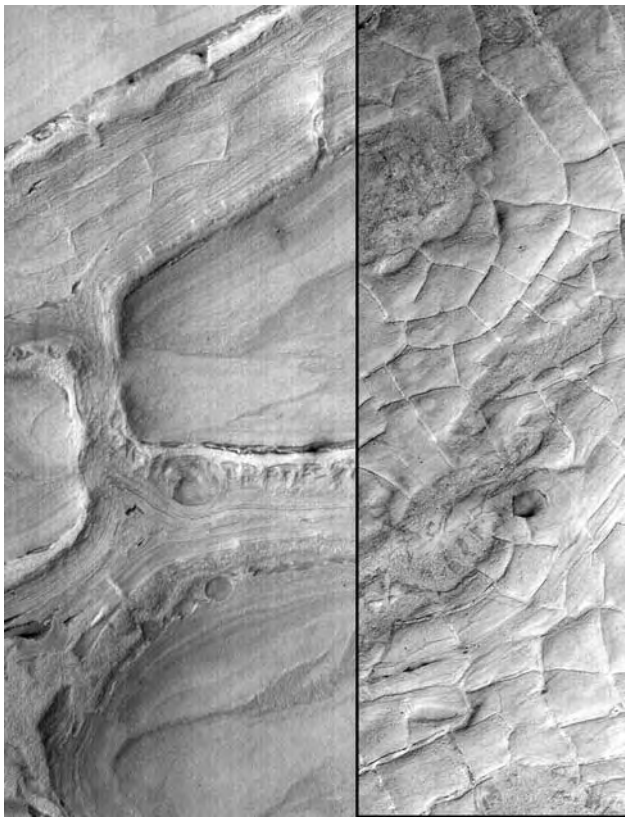

Figure 7.15. Honeycomb structures on the floor of Hellas at (left) 37.4°S, 54.8°E (MOC M0705324), and (right) 37.5°S, 54.1°E (MOC M1300892). Both images are 2.8 km across. Moore and Wilhelms (2001) speculate that the scene on the left is the result of ice blocks settling into a muddy substrate, and that the intersecting ridges seen in the right image are casts of ice cracks.

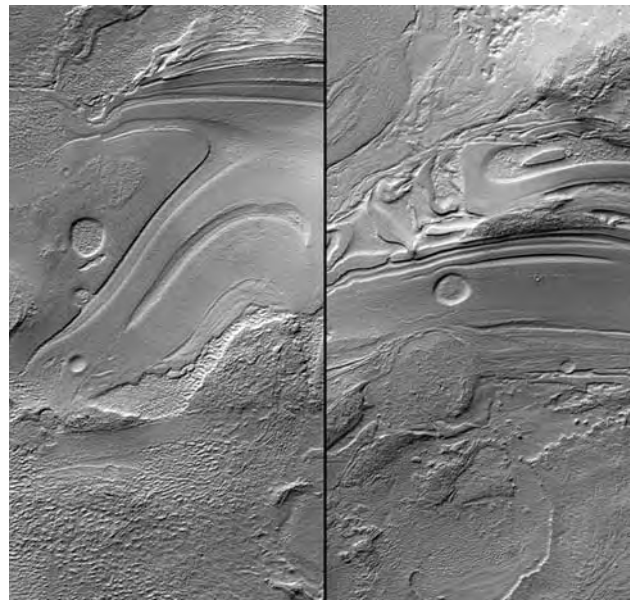

Figure 7.16. Enigmatic terrain at 40.2°S, 55.1°E. The deposits in the center of the Hellas basin display a wide variety of bizarre textures that defy interpretation. Here we see textures that suggest plastic deformation and exhumation. Possibilities are interaction between ice and soft, still waterlogged sediments or differential erosion of ice-rich sediments such as we see at the south pole. The images are 2.9 km across (MOC E2000933).

over a distance of 800 km, possibly as a result of lava flow that forms a dam between Amazonis Planitia and the northern plains (Fuller and Head, 2002b). Because of the low slopes it is not clear whether water flowing into Amazonis Planitia from the south during most of the Hesperian would ultimately reach the North Polar basin before flow was arrested by processes such as freezing and infiltration. Finally the Isidis basin, which reaches depths of −3900 m, and whose floor is tilted toward the south, is presently separated from the main northern depression by a ridge with a minimum elevation of −3500 m. Although most of the northern plains are Hesperian in age, low hills that outline remnants of large craters, MOC images showing subdued craters in numbers comparable to the southern highlands (Malin and Edgett, 2001) and faint circular depressions, detectable only in the MOLA data (Frey, 2002; Frey *et al*., 2002a), indicate that the Noachian surface is at depths of 0−5 km below the present plains.

Ridged plains dominate the topography of the northern plains at a regional scale (Withers and Neumann, 2001; Head *et al*., 2002). The materials that form the ridged plains likely constitute most of the post-Noachian fill within the northern basin. The extensive ridged plains further south, as in Lunae Planum, Solis Planum, and Hesperia Planum, are thought to be volcanic because of their resemblance to lunar maria, their wide range in elevation, and the occasional presence of flow lobes, cinder cones, and other likely volcanic features (e.g. Mouginis-Mark *et al*., 2002). The ridged plains in the northern basin are continuous with, and closely resemble, those further south. The most straightforward interpretation is that they are also volcanic (Head *et al*., 2002). The ridges in the northern plains of the western hemisphere form a coherent, parallel set that extends northward from Chryse, around the northern edge of Tharsis, then south through Amazonis Planitia and the Phlegra Montes. They are part of the ridge system that extends all around Tharsis (Banerdt *et al*., 1992). The ridges in the eastern hemisphere form a more random or

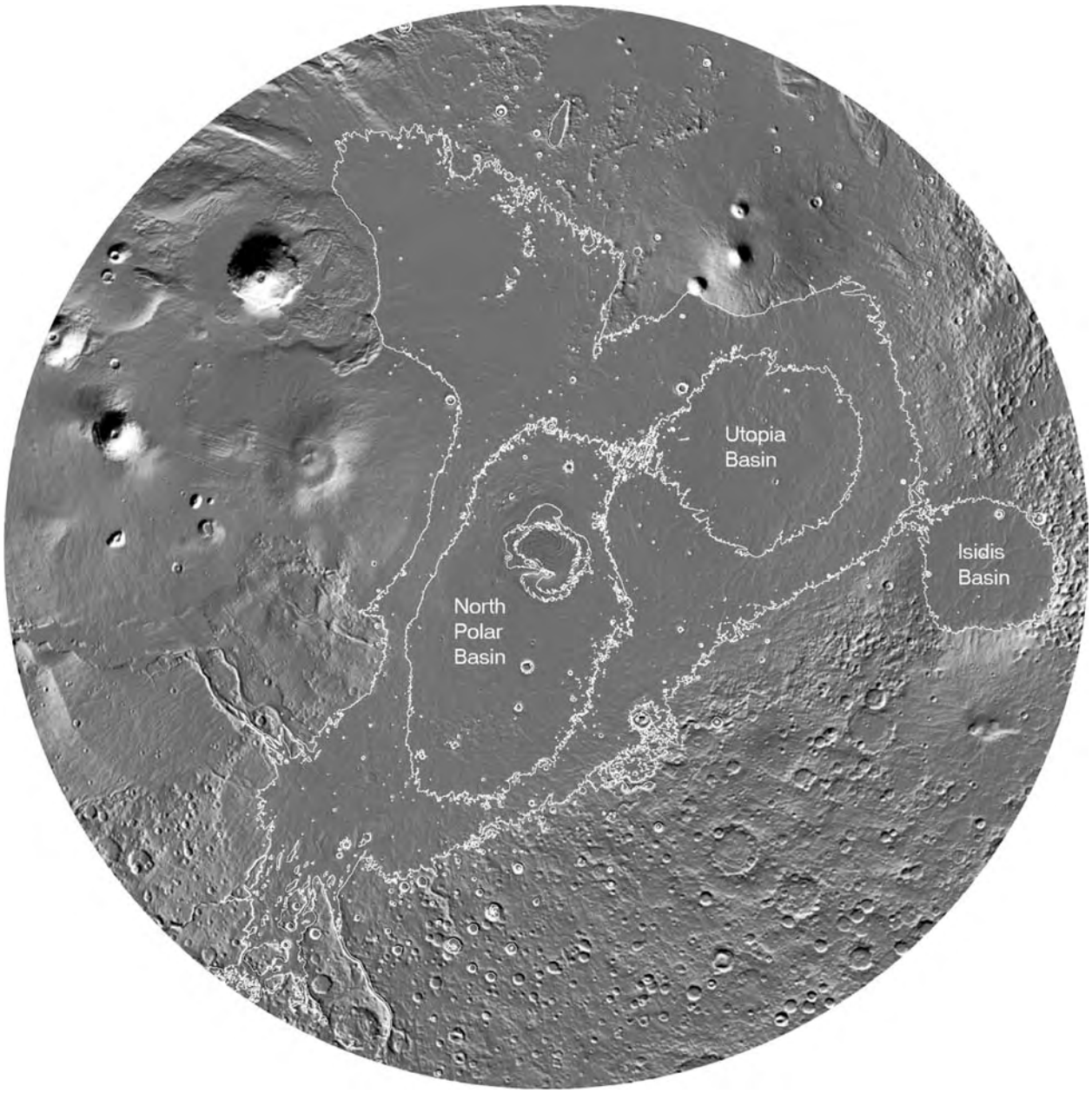

Figure 7.17. Polar stereographic projection of the northern hemisphere. Two contours are shown: an outer one at −3500 m, the height of the barrier between the Isidis basin and the northern plains, and an inner one at −4350 m, the height of the barrier between the Utopia basin and the North Polar basin. Channels through the Chryse basin (lower left) would have drained into the North Polar basin; the outflow channels west of Elysium (upper right) drain into the Utopia basin.

polygonal pattern related to local features such as the Isidis and Utopia basins (Head *et al*., 2002).

The low regional slopes within the northern plains have been compared with the Earth's oceanic abyssal plains (Aharonson *et al*., 1998; Smith *et al*., 1998), but the regional slopes are dominated by the ridged plains surface so, like the ridged plains themselves, the generally low regional slopes are probably the result of volcanic processes (Head *et al*., 2002). Even where ridges are absent, the regional-scale topography appears to be the result of volcanism. The flattest region of the planet is Amazonis Planitia (Aharonson *et al*., 1998). Although parts of its surface are almost featureless in the MOLA reconstructions of the topography and in all but the highest resolution Viking images, lava flows are visible in almost all the

MOC images of the region (Keszthelyi *et al*., 2000; Malin and Edgett, 2001). Thus even the extremely low slopes of Amazonis Planitia appear to be covered mainly by volcanic deposits, although several large fluvial channels feed into Amazonis Planitia (notably Marte Vallis and Mangala Vallis) and the volcanics there may be interbedded with fluvial deposits (Fuller and Head, 2002a,b). It should be noted in passing that Murray *et al*. (2005) interpreted as lacustrine some features in southern Elysium Planitia (Figures 3.25, 3.26), similar to those of Amazonis Planitia that have been interpreted as volcanic.

Shorelines

The idea that oceans were formerly present in the northern plains was elaborated upon in some detail in pioneering work by Parker *et al*. (1989, 1993). They noted a variety of features around and within the plains that they interpreted as indicative of former shorelines (Figures 7.18, 7.19). The features are particularly common in the so-called fretted terrain, where the plains–upland boundary is poleward of 30°N. They include (1) cliffs separating the plains from the uplands; (2) contacts between geomorphic units with different characteristics; (3) plains with subdued parallel, sinuous ridges or ''thumbprint'' textures; (4) terraces on valley walls; (5) abrupt termination of outflow channels as they debouch onto the plains; (6) massifs and ''islands'' within the plains with terraced slopes; and (7) evidence for local upstream flow within some outflow channels. Some features (cliffs, benches, stepped massifs) were interpreted to be the result of wave erosion, some (spits, curvilinear ridges) the result of wave transport. Other features were thought to result from the former presence of water (indications of upslope flow, abrupt termination of channels and valleys). Boundaries separating different textured units could be the result of differential deposition or erosion at the ocean's edge. Parker and co-workers initially identified two major contacts around the northern plains that were tentatively interpreted as shorelines (Figure 7.20). Contact 1 for most of its length follows the abrupt geomorphic boundary between the heavily cratered uplands and the sparsely cratered plains. The boundary, subsequently labeled the Arabia shoreline by Clifford and Parker (2001), can be traced all the way around the planet except through Tharsis where it is buried by younger deposits. Contact 2, subsequently labeled the Deuteronilus shoreline by Clifford and Parker, is more subtle. It lies wholly within the northern plains and is identifiable by textural differences within the plains. The two boundaries differ significantly in age. Contact 1, the boundary between the uplands and the plains, is clearly very ancient, having formed deep within the period of heavy bombardment. Contact 2 is post-Noachian. Of course, if post-Noachian oceans were of sufficient volume, they could lap up to Contact 1 despite its old age.

One possible test as to whether these contacts are truly shorelines is whether they are everywhere at the same elevation. Head *et al*. (1999) pointed out that Contact 1 has a wide range of elevations, almost 11 km, and suggested that it is unlikely to be a shoreline. However, if Tharsis is excluded, the range is much less. Figure 7.20 shows the −2000 m contour superimposed on the shaded relief. This contour is a good proxy for the boundary between the cratered uplands and the plains in much of the eastern hemisphere and southwest of Chryse Planitia. Major deviations of the boundary from the contour occur

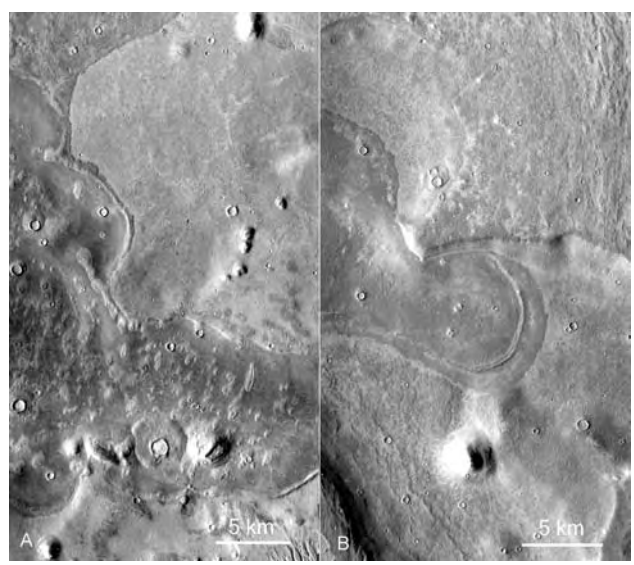

Figure 7.18. Possible shorelines in the fretted terrain of Deuteronilus, along the margin of the North Polar basin. The relations show the difficulty of identifying shorelines. (A) The low cliff or ridge that separates the smooth higher unit from the mottled lower unit may be a former shoreline. The mottling is a common characteristic of parts of the northern plains where other features such as partly buried craters suggest sedimentation from a former water body. The image is 19 km across and located at 45.05°N, 10.67°E (THEMIS V04581003). (B) A dark unit laps onto a lighter unit in the center of the frame. Such relations are common throughout the fretted terrain, where plains materials complexly interfinger with upland materials. Onlaps such as seen here have a variety of possible causes, but some have been interpreted as the result of encroachment of a northern ocean onto the adjacent uplands. The image is 19 km across and located at 46.43°N, 14.65°E (THEMIS V04481003).

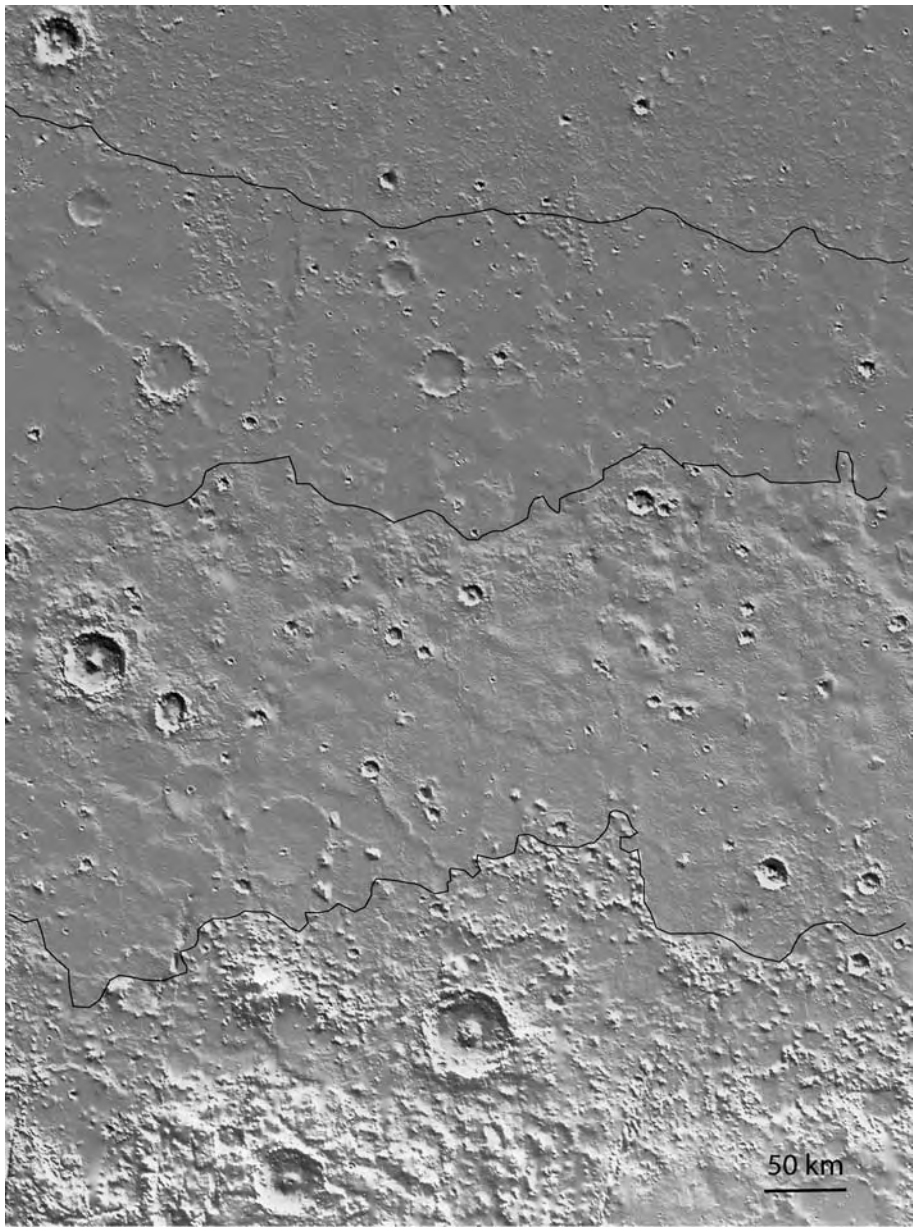

Figure 7.19. Possible shorelines south of Elysium. At latitudes higher than about 30°N the plains–upland boundary has been extensively modified by mass-wasting processes (see Chapter 8), which hinders identification of shorelines. Here we see a section of the boundary at 15°N, between 100 and 110°E. Three contacts are readily identified. The upper contact separates the Vastitas Borealis Formation, with its numerous closely spaced low hills, from ridged plains to the south. The middle contact separates the ridged plains from a smooth bench which follows the plains–upland boundary through this region. The lower contact separates the bench from the main body of the cratered uplands to the south. The upper contact is the Deuteronilus shoreline of Clifford and Parker (2001), the lower contact is close to the Arabia shoreline. The middle contact they call ''Mamers level 2'' (MOLA).

mainly in western Arabia, where the boundary between the uplands and plains is 1–2 km lower than elsewhere. To accommodate the shoreline hypothesis, the lower elevations in western Arabia could be attributed to tectonic deformation or extensive erosion (Hynek and Phillips, 2001) after the contact formed. Howard and Moore (2006) alternatively suggested that part of western Arabia was under water during the late Noachian and early Hesperian. From dissection patterns and the degradation and frequency of craters,

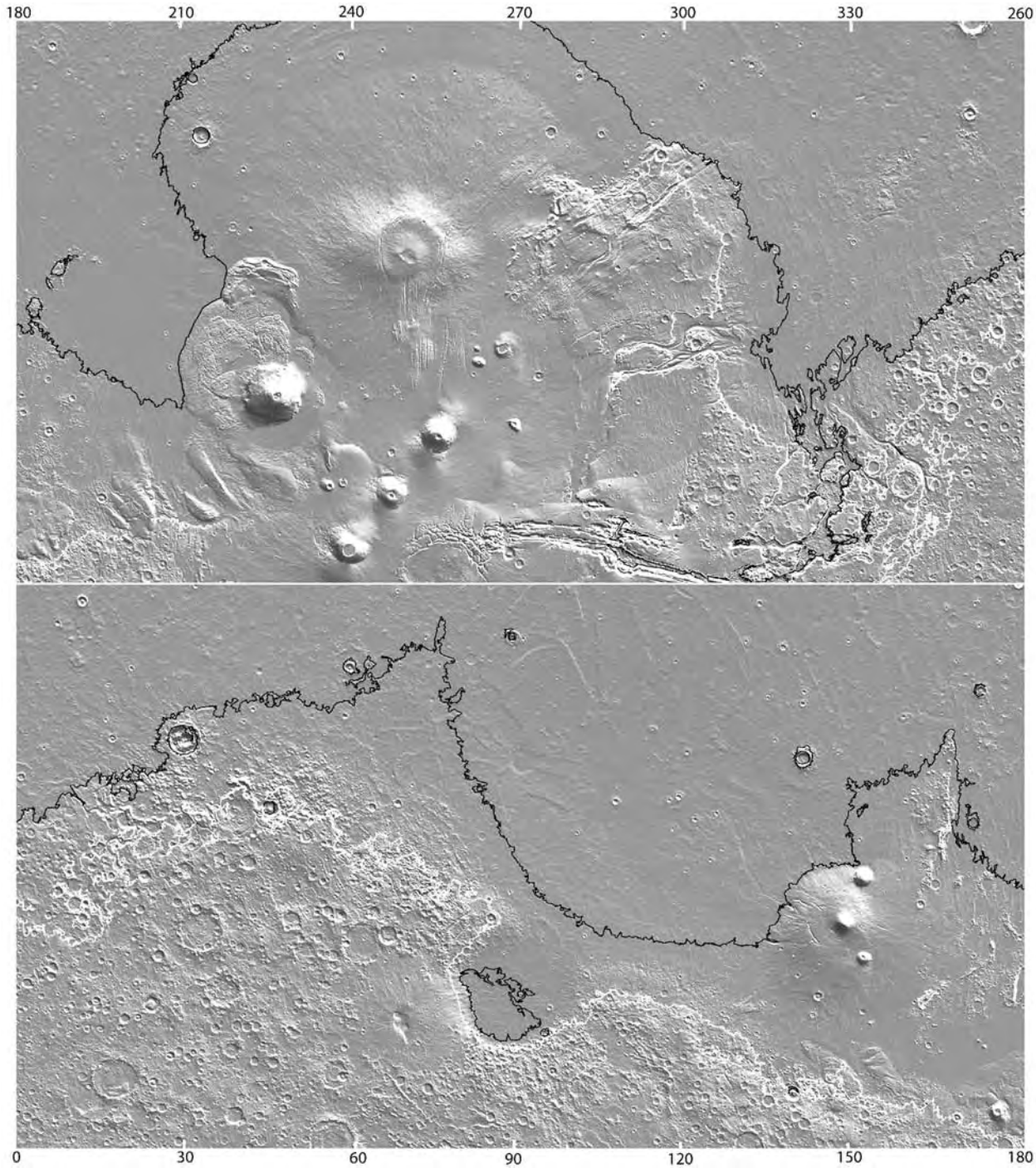

Figure 7.20. Possible strandlines around the northern basin. The black line is the −3760 m contour, which closely follows the Deuteronilus shoreline of Clifford and Parker (2001). The main deviation of the shoreline from the contour is between 40 and 80°E. The white line is the −2000 m contour. It closely follows the Arabia shoreline between 80 and 180°E and in southeast Chryse around 310°E. Elsewhere the shoreline is below the −2000 m level.

they estimated that the shoreline of a northern ocean was at an elevation of roughly −1500 m at this time.

Contact 2, the Deuteronilus shoreline, is much closer to an equipotential surface. Except to the north of Tharsis, where it is difficult to identify, the contact is at an elevation close to −3760 m (Head *et al.*, 1999), consistent with it being a shoreline. Since the original work that identified the two contacts just discussed, Parker and his co-workers have proposed several other possible shorelines. Eight are listed in Clifford and Parker (2001). The Deuteronilus shoreline, the lowest, would have enclosed an ocean with a volume of 1.9×10^7 km^3, or the equivalent of 130 m spread over the whole planet. The Meridiani shoreline, the highest, at an elevation of 0 m, would have enclosed a volume of over 2.2×10^8 km^3 or 1.5 km spread evenly over the whole planet (Figure 7.21).

The plausibility of the various proposed shorelines is difficult to assess. The large floods must have left behind large seas that had long shorelines. The features mapped by Parker and co-workers are real. There are terraces, benches, escarpments, parallel ridges, and textural changes along the postulated shorelines, and they are arrayed around the lows where water would have accumulated. But how do we know that they are truly shorelines? The difficulties are illustrated by two examples in Tharsis. Volcanic flows are visible all along the contact between the plains and the Acheron Fossae at 40°N, 215–230°E, and along the edge of the Olympus Mons aureole at 210°E between 15 and 30°N (Carr and Head, 2002).

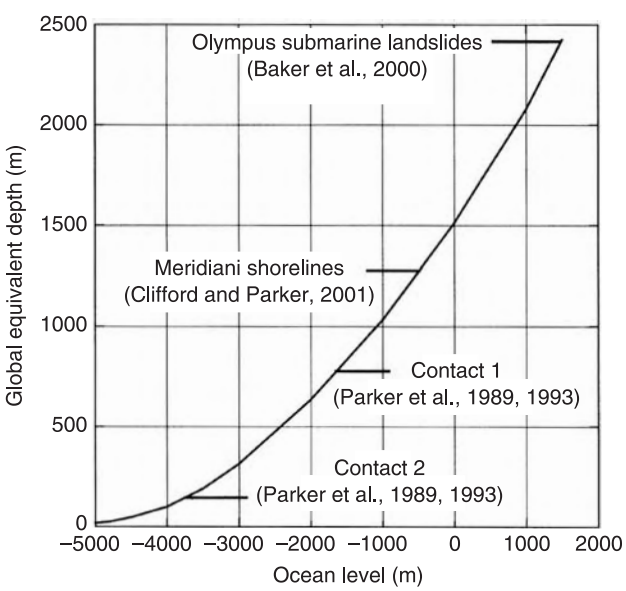

Figure 7.21. The volumes of water, expressed as global depth equivalents, for different elevations of an ocean surface.

The former was identified as part of the Arabia shoreline, the latter as part of the Deuteronilus shoreline. The present relief along these two shoreline segments was unambiguously created by non-marine processes. Yet given seas of the appropriate size, both could have been shorelines. Other difficulties arise in other areas. In the fretted terrain, the focus of much of the original work by Parker *et al.* (1989, 1993), sharp breaks in slope have been created by mass wasting (Squyres, 1979; Chapter 10) and horizontally bedded rocks crop out on valley walls (Carr, 2001). Discriminating these breaks in slope from those that might be produced by marine processes is challenging. The problem becomes more difficult the further back in time we go, particularly into the Noachian when erosion rates were likely high. It should not be surprising, therefore, that many of the proposed shorelines remain controversial.

Evidence for marine sediments

Alternative approaches to assessing the extent of any former oceans are to look within the northern plains for deposits that might have been left after the large floods, and to look for evidence of a former ice cover on the assumption that any post-Noachian ocean would have frozen. This approach can be followed only for post-Noachian oceans. The surface of most of the northern plains is Hesperian in age, so any deposits associated with Noachian oceans are buried beneath younger deposits. Head *et al.* (2002) noted that the height and spacing of the ridges in the northern plains are different from those of the ridges further south, with which they are continuous. The ridges in the north are systematically lower and more widely spaced. In addition, there are two populations of craters in the northern plains: a fresh-appearing population and a more subdued, "ghost" population (Figure 7.22). Both observations can be explained by burial of the volcanic, ridged plains in the north by a deposit roughly 100 m thick. They called the deposit the Vastitas Borealis Formation (VBF), a term used previously in a more general sense for all the deposits of the northern plains (Tanaka and Scott, 1987). We will continue to use the term VBF here to refer only to the roughly 100 m thick deposit that is thought to overlie the ridged plains. The number of fresh craters superimposed on the VBF indicates that it is Upper Hesperian in age, as are most of the outflow channels. Head *et al.* conclude that the inferred deposit is the result of flooding by the outflow channels. The area within which ghost craters and muted ridges occur may therefore provide another indicator of the extent of an Upper Hesperian ocean. Kreslavsky and Head (2002)

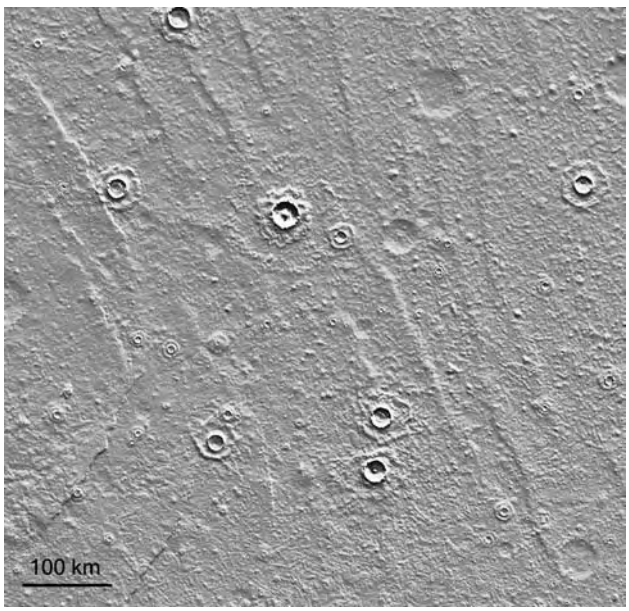

Figure 7.22. Typical Vastitas Borealis Formation at 60°N, 135°E. This unit covers much of the northern plains inside the Deuteronilus shoreline. The characteristic knobby texture is caused by closely spaced low hills, which in places line up to form parallel, discontinuous ridges. Two populations of craters are seen: fresh ones superimposed on the present surface and subdued "ghosts" superimposed on the underlying ridged plains (MOLA).

estimated that the volume of the VBF is $3 \times 10^6\,km^3$, a volume very similar to the amount of erosion estimated to have been effected by the large circum-Chryse floods (Carr *et al.*, 1987).

The Vastitas Borealis Formation can be readily recognized independently of burial of ridges and craters. The unit is richly textured when viewed at resolutions of a few tens of meters. Textural features include polygonal fractures, parallel ridges and grooves, labyrinths of curvilinear valleys, ridges with summit pits and grooves, thumbprint patterns of regularly spaced curvilinear ridges and aligned hills, arrays of low, pitted domes, and mottled patterns (Figures 7.23, 7.24). At MOC resolutions (a few meters) the plains are mostly bland, in part because of a thin pervasive cover with a characteristic "basketball" texture (Carr, 2001; Mustard *et al.*, 2001). However, in places there are arrays of cratered cones, irregular hollows, polygonal and parallel cracks, shadowy craters outlined by boulders, and boulder-strewn knobs (Malin and Edgett (2001)). These textures provide a sharp contrast to the uncovered ridged plains which, at resolutions of a few tens of meters, are mostly featureless, except for craters and ridges. The contact around the VBF is thus easily recognized, and for most of its length was identified as Contact 2 by Parker *et al.* (1989, 1993). An ocean with a surface at around −3760 m, the average elevation of Contact 2 (Figure 7.20), would have encompassed most of the VBF. Thus the validity of Contact 2 of Parker *et al.* as a shoreline is supported both by its nearly constant elevation and by its enclosure of terrain with characteristics suggestive of deposition of sediment.

Evidence for ice

If the outflow channels formed under climatic conditions similar to those that prevail today, water that ponded in the northern plains would have rapidly frozen. We should therefore expect to see evidence of ice in the areas formerly covered by water. Several types of features within the area mapped as the Vastitas Borealis Formation have been interpreted as the result of the former presence of ice (for a comprehensive summary see Kargel *et al.*, 1995). The most striking are the "thumbprint" terrain and labyrinthine valleys (Figures 7.23, 7.24). "Thumbprint" terrain is common around the edge of the area mapped as the Vastitas Borealis Formation. It consists of whorled patterns of subparallel, curvilinear ridges 0.5–2.5 km wide. Many of the ridges have summit pits or depressions. They have been variously interpreted as glacial moraines, lines of kames (sand and gravel hills that form where subglacial streams emerge from a glacier), ice-pushed ridges, ice-cored ridges, or other indicators of successive positions of retreating ice or ice-rich materials (e.g. Carr and Schaber, 1977; Lucchitta, 1981; Rossbacher and Judson, 1981; Kargel *et al.*, 1995). In several areas, also toward the edge of the Vastitas Borealis Formation, are labyrinths of intersecting curvilinear troughs, some with central ridges. Kargel *et al.* (1995) point out their strong resemblance to terrestrial tunnel channels and eskers that form by meltwater under an ice sheet. They also point out the absence of drumlins (ice-sculpted hills in glacial till) within the northern plains, and suggest that this may be due to lack of till within the ice or lack of movement of the ice, suggestions that are consistent with a stationary ice sheet as might be expected from the freezing in place of a lake formed by floods.

Possible fate of a northern ocean

Several authors have examined what would happen to a frozen body of water on Mars under present climatic conditions (Carr, 1983; Kargel *et al.*, 1995; Moore *et al.*, 1995; Kreslavsky and Head, 2002). Kreslavksy and Head (2002) identified three stages in the emplacement of a large body of water: a warm

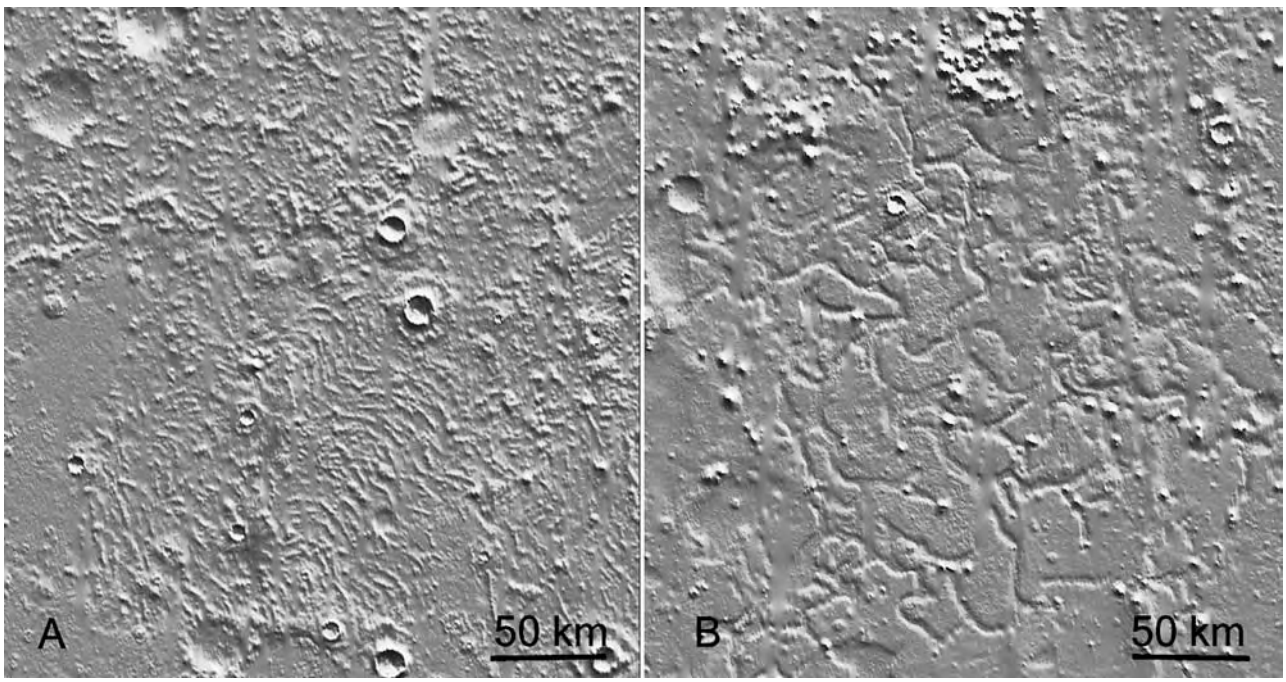

Figure 7.23. Thumbprint and labyrinth textures in the Vastitas Borealis Formation. (A) Closely spaced, curvilinear ridges create a thumbprint texture at 57°N, 186°E. When observed at high resolution, many of the ridges are seen to have summit depressions. (B) Labyrinth at 45°N, 176°E. Both these textures are preferentially found around the periphery of the area covered by the Vastitas Borealis Formation. They are thought to be analogs of features found at the margin of terrestrial glaciers (Kargel *et al.*, 1995) (MOLA).

convecting stage, a freezing stage, and a sublimation stage. If the floodwaters were initially above freezing, as would be the case if they were derived from groundwater well below the cryosphere, then rapid heat losses by evaporation and radiation from the surface would initially cause convective overturn (Lane and Christensen, 2000), thereby keeping the surface warm, preventing an ice cover from forming, and causing the ocean to be stirred and its sediment suspended. Rapid evaporation (3–9 mm per day) would result, and the water would condense over and downwind of the ocean. Heat would also be lost into the ocean floor. Convection would cease when the temperature fell to 277 K, the temperature at which water reaches its maximum density. Kreslavsky and Head (2002) estimate that a 100 m deep ocean would cool at 7–20 K per year so that the convecting stage would last only a few years, depending on the ocean depth and its initial temperature. If the temperature of the water were initially close to 273 K, as would be expected if the water erupted from just below the cryosphere, then this stage would be very short or non-existent.

In the second stage, when convection ceased, an ice cover would form and heat losses from the surface would be rapidly reduced. Moore *et al.* (1995) and Kargel *et al.* (1995) estimate that, as a result of heat losses through the surface alone, a 1 km deep lake would take roughly 10^5 years to freeze solid, the precise time depending on factors such as the ice albedo and wind speed. Kreslavsky and Head (2002), taking into account heat losses both through the ice cover and into the lake floor, derive a significantly shorter time of $1-2 \times 10^4$ years. During this time any sediment load kept suspended during the first stage by convection would be deposited on the floor.

In the final sublimation stage, the ice deposit slowly sublimates and the water condenses elsewhere on the planet. The rate at which this occurs is extremely sensitive to whether or not the ice was covered with debris, such as eolian deposits or a lag. Clean polar ice under the present obliquity may sublimate at rates as high as 0.8 mm per year (Jakosky and Haberle, 1992). For a high obliquity with strong winds, Toon *et al.* (1980) estimated that polar sublimation rates for bare ice could be as high as 50 cm per year. In contrast, at high latitudes under the present obliquity, ice buried below a few tens of centimeters of rock or soil is permanently stable because temperatures never get above the frost point (Farmer and Doms, 1979).

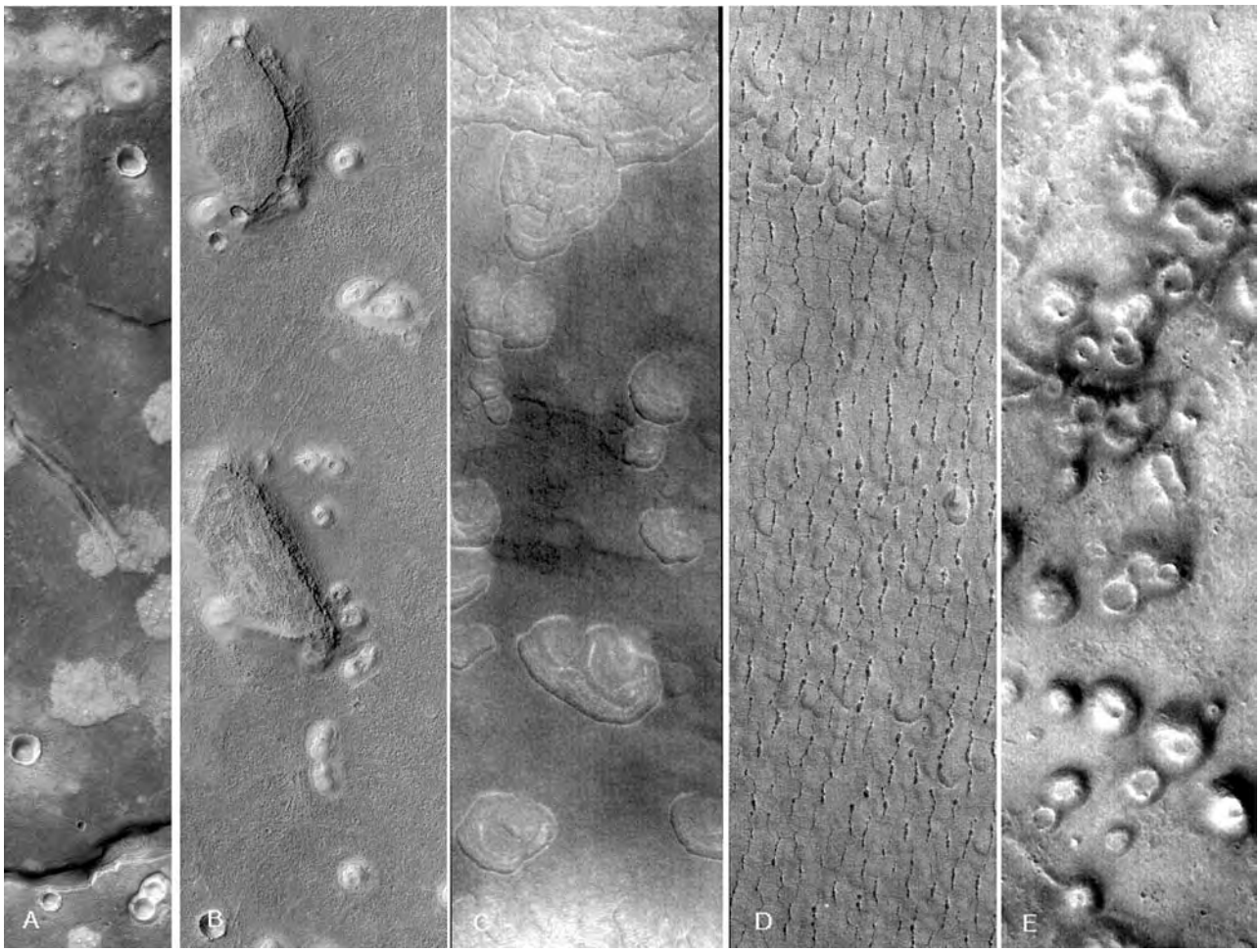

Figure 7.24. MOC-scale textures on the northern plains. (A) Mottled terrain within an "island" surrounded by the Vastitas Borealis Formation (VBF) in Acidalia Planitia at 47.7°N, 333.2°E. The mottling is caused by bright haloes around impact craters, bright low, cratered cones, and bright irregular patches with little relief. The strip is 3.2 km across (M21-01816). (B) Thumbprint terrain close to the outer boundary of the VBF at 32.9°N, 87.7°E. The thumbprint texture is caused by low cratered hills and domes that have a higher albedo than their surroundings. The areas between the hills and domes have the fine-scale pitted texture typical of most surfaces at these latitudes. The strip is 3.1 km across (M23-02053). (C) Possible deflation hollows within the VBF at 47.5°N, 91.2°E. The hollows may be exposing layering within the VBF. This strip and the next two are 1.6 km wide (M07-04451). (D) Lines of pits within the VBF at 45.1°N, 84.2°E (M08-07602). (E) Pitted cones near the outer boundary of the VBF at 39.2°N, 320.8°E. Such cones are common throughout the VBF (M11-02050).

Sublimation occurs only at high obliquities and then probably at rates of only 10^{-6} to 10^{-4} cm per year (Carr, 1990). Thus, if the ice remains clean, a 1 km thick ice sheet could sublimate in a few hundred thousand years. If covered with a few tens of centimeters of debris, the ice could remain for the lifetime of the planet. Neither extreme is likely.

Kargel *et al.* (1995) note that during the sublimation phase, net sublimation at the more southerly parts of the former ocean and net accumulation at the pole would have resulted in a transition from a frozen ocean to a polar cap. The amount of water in today's north polar cap (1.6×10^6 km^3) is, however, much smaller than the volume enclosed even by the Deuteronilus shoreline (1.9×10^7 km^3).

The most puzzling issue with respect to the former presence of oceans is where the water went. The amount of water enclosed by Contact 1 and Contact 2 of Parker *et al.* (1989, 1993) is roughly equivalent to 700 m and 130 m respectively spread over the whole planet. Even larger numbers are implied by other interpretations of other authors. No more than 50 m is estimated to have been lost to space since the end of the Noachian (Kass 2001; Hodges, 2002), so most of

the water postulated for the oceans probably remains on the planet. What little water is at the surface today is in the polar caps, which contain the global equivalent of 10 m. Large fractions of ice exist just below the surface at high latitudes (Prettyman *et al.*, 2004), but how deep the ice-rich zone extends is unknown. If large amounts of water are present on Mars today they are probably in the cryosphere or the underlying hydrosphere. Their combined holding capacity is probably adequate to accommodate the ocean volumes (Clifford, 1993; Clifford and Parker, 2001). Presence of subsurface water is supported by geologically recent eruptions of groundwater (Chapter 6), but how the water was transferred from the surface to the subsurface remains puzzling despite suggestions of infiltration under warm climate conditions (Baker, 2001) and infiltration by polar basal melting (Clifford, 1993).

Summary

Local closed depressions, mostly craters, are common throughout the cratered uplands. Paleolakes probably occupied many of these depressions during the Noachian, when most of the valley networks formed. A particularly large lake in Terra Sirenum–Terra Cimmeria may have drained catastrophically to form Ma'adim Vallis. The evidence for lakes in craters includes valleys entering and leaving craters and, less commonly, deltas and terraces within craters. Most Noachian craters are partly filled and have flat floors. Horizontally layered sediments, observed to underlie some of the flat floors, may be in part lacustrine. Mounds of sediments within large craters in some areas have also been suggested as lacustrine, but many mounds are higher than the rims of the crater that they are in. Even though lacustrine processes may have contributed to the accumulation of fill within large upland craters, the MER experience at Gusev demonstrates that other processes also likely contributed.

If the Noachian had warm, wet periods, as is suggested by extensive erosion and dissection by valleys, then large bodies of water would have occupied low areas such as Hellas, Argyre, and the northern plains. Strandlines of possible Noachian age have been identified around Hellas, and a possible Noachian Arabian shoreline at roughly the −2000 m level has been tentatively identified around the northern plains. A large lake may also have formerly occupied Argyre and overflowed in the Noachian to form a large channel complex extending from the Argyre rim into the Chryse basin over 2000 km to the north.

Formation of the large late Hesperian floods must have created large lakes in the northern plains. Arrays of linear features around the northern plains have been proposed as shorelines. The lowest and youngest of the proposed shorelines is supported by several observations. It can be traced almost continuously around the northern basin; it maintains a roughly constant altitude close to −3760 m over large distances; it encloses an area within which ridges and craters are partly buried; and it encloses an area within which features suggestive of a former ice cover are present. Counts of craters superimposed on materials within the contact indicate late Hesperian age, an age similar to that of most of the large floods. The higher and older shorelines are less convincing. Their identification is almost solely dependent on our ability to discriminate between shorelines and other linear topographic features. Our ability to do this is questionable, even with the relatively young late Hesperian contacts, so prospects are not good for authenticating proposed Noachian shorelines, which have been exposed to more erosion and for which other possible evidence of the presence of oceans has been largely buried.

8 Ice

Ice has likely played many different roles in the evolution of the surface, depending on where and when the ice was located. One can think of ice as being in two reservoirs: one on the surface exchanging with the atmosphere and with the upper meter or so of the surface, and one deep below the surface. The amount at the surface is rather modest, probably no more than 50 m spread over the whole planet, and most is at the poles (Chapter 10). We have known that the northern remnant cap is composed of water ice since the time of Viking (Farmer *et al.*, 1976; Kieffer *et al.*, 1976). Suspicion from that time that a water-ice cap also underlies the remnant CO_2 cap in the south has recently been confirmed (Byrne and Ingersoll, 2003b; Bibring *et al.*, 2004). The amount buried deep in the ground is probably substantially larger than the amount on the surface. While we have no direct measure of how much is there, radar sounding suggests that significant amounts may be present (Picardi *et al.*, 2005). In the present epoch, ice is continually being redistributed across the surface and exchanged with the near-surface materials as a result of seasonal changes in insolation and astronomically induced changes (Mellon and Jakosky, 1995). During periods of high obliquity, much of the water now locked up in the poles may move to lower latitudes, and there may be a redistribution of ice that resides within a few meters of the surface. Possible geomorphic evidence for such a redistribution are thin mantling units at high latitudes, possible ice deposits on poleward-facing slopes, and indications of glacial activity.

The large flood channels and evidence for ancient seas and lakes suggest that larger amounts of water were on the surface at times in the past. What happened to the water is one of Mars' major mysteries. It could have been mostly lost to space or it could have been frozen into the planet's kilometers-thick cryosphere (Clifford, 1993). Irrespective of its fate, there must have been times in the past when much more water was on the surface than at present, and this water would have been subject to similar redistribution as a result of seasonal and astronomical changes as is present-day ice. At low obliquities, large polar ice caps probably developed; at high obliquities, large amounts of ice probably moved equatorward. Evidence for ancient glaciers, and for frozen seas and lakes, all supports the presence of abundant near-surface ice in the past.

Some surface features, such as terrain softening, suggest that there are massive amounts of ground ice to kilometer depths at high latitudes. It is difficult, if not impossible, to introduce water from the surface to these depths under present conditions, even with the astronomically induced variations. However, during warmer climatic episodes, such as must surely have occurred at least during the Noachian to cause the pervasive dissection of the cratered highlands, the cryosphere may have been thin or non-existent, and groundwater could have percolated through the upper few kilometers of the crust. A change to a colder climate, much like today's, would then have caused ice to be frozen into the deep subsurface. Extensive ground ice may thus have been inherited from early in the planet's history or from later warm climatic episodes. Climate change has another implication for ice-related phenomena. Most terrestrial permafrost features result from processes in the active zone that undergoes thawing every spring, and for which there is no present-day martian equivalent. Yet if Mars experienced climate changes, it may have gone through periods when there was an active zone much as in terrestrial permafrost regions, and martian equivalents of terrestrial permafrost features may have developed.

In this chapter, the stability of ice under present conditions, and how it might be affected by perturbations in orbital and rotational parameters, are first discussed. This is followed by an examination of the observational evidence for the redistribution of ice during the present epoch. We then move back in time and look at the geological evidence for both surface and ground ice. The fretted terrain in northern Arabia, where massive, probably ice-abetted, mobilization of the surface materials has taken place, is examined in some detail. One issue in the fretted terrain is the extent to which ground ice or surface ice is responsible for what we observe. The evidence for frozen lakes and seas was discussed in Chapter 7 and will be only briefly revisited, but we will also look at the evidence for other

forms of surface ice such as mountain glaciers. Ice at the poles is discussed in Chapter 10.

The stability of ice

The stability of ice at the surface depends on the frost point. At temperatures above the frost point, ice on the surface in contact with the atmosphere is unstable, and will tend to sublimate; at temperatures below the frost point, ice will freeze out of the atmosphere. From Viking measurements that indicate that the atmosphere is well mixed and contains 12 pr μm of water, that is, if all the water precipitated out of the atmosphere it would form a layer one micrometer deep, Farmer and Doms (1979) estimated that the frost point is 198 K on average. The frost point will, however, vary according to season and location. Column abundances of water in the atmosphere, measured by Viking, ranged from almost zero around the edge of the CO_2 ice cap to over 100 pr μm over the north polar cap in summer, so frost point temperatures could be a few degrees higher or lower depending on the local water vapor abundances. Temperatures everywhere exceed the frost point at some time during the year, so that a block of ice on the surface will tend to sublimate away, with the water ultimately condensing onto the winter pole. The ice caps at the poles survive because sublimation losses in the summer are replenished by condensation in winter. The losses and gains at the poles may not be in balance. Jakosky and Haberle (1990) suggest, for example, that the northern cap is slowly losing water to the south.

The stability of ice in the ground depends on ground temperatures, which in turn depend on the properties of the surface. At latitudes higher than 40° the temperature at depths of several centimeters below the surface are mostly below the frost point, so water will tend to diffuse from the atmosphere into the soil and condense. For present average conditions at these latitudes, ground temperatures at depths greater than a few tens of centimeters, but less than several kilometers, never reach the frost point, so ice is permanently stable. At latitudes less than about 40°, ground temperatures are always above the frost point, so ground ice is unstable at all depths (Farmer and Doms, 1979). If ground ice were ever present at these latitudes it would be lost to the atmosphere at rates dependent upon the rate of diffusion of water vapor through the soil. If the soils were fine-grained, however, diffusion rates could be so low that ice could survive for geologically significant time scales. Thermodynamic instability does not necessarily mean absence.

The above is for average conditions today. But the surface materials have a considerable range of albedo and thermal inertia, which affect the surface temperatures and hence ground temperatures. Paige (1992) pointed out that lower thermal inertia areas have a wider daily range of surface temperatures than high thermal inertia areas, so lose more heat by radiation because of dependence of radiation losses on T^4. As a result, mean annual temperatures are lower. In low thermal inertia areas such as Tharsis, Elysium, and Arabia, therefore, ground ice should be found at lower latitudes than elsewhere. Stability of ice is also favored by a high thermal inertia material, such as ice, just below the surface. According to Paige's models, in low thermal inertia areas at latitudes higher than about 40°, ice should be found at all depths more than a few centimeters below the surface. Without the effect of the high thermal inertia ice, the depth would be tens of centimeters.

The stability of ice is also affected by the planet's obliquity. Increasing the obliquity has two main effects. First, a smaller fraction of the Sun's insolation falls in the equatorial regions, so equatorial surface and ground temperatures fall. Second, water is driven off the polar caps, thereby increasing the amount of water in the atmosphere and increasing the frost point temperatures. Lowering the obliquity has the reverse effect. As we saw in Chapter 1, the present obliquity is 25.19°, but it undergoes large changes. During the current epoch it is thought to oscillate between 15° and 35°, about a mean of 24° with periods of 1.2×10^5 years and 2 Myr (Laskar *et al.*, 2002) (Figure 1.3). However, the obliquity variations are chaotic on time scales larger then 10 Myr. Over geological time, values for the obliquity may have occasionally reached as low as 0° and as high as 70°, the average being around 40° (Laskar *et al.*, 2004).

Mellon and Jakosky (1995) modeled how variations in obliquity might affect the stability of ground ice. In their model they varied the column abundance of water with obliquity, assuming that the amount of water in the atmosphere scales directly with the sublimation rate at the poles. This results in high water abundances and frost point temperatures at high obliquities, and the reverse at low obliquities. For example, they estimate that at an obliquity of 40° the atmosphere contains 1000 pr μm of water and the frost point temperature is 236 K. At an obliquity of 10° the atmosphere contains 0.02 pr μm of water and the frost point temperature is 164 K. The combination of the lower equatorial temperatures and higher frost point temperatures results in ground ice being stable at low latitudes during periods of high obliquity, in contrast to the present situation where it is unstable. At the present obliquity of 25.19° and lower, ground ice

is unstable for all latitudes less than 40–50°. At obliquities of 32.3° and higher, ground ice is stable everywhere, with the top of the ice being mostly 5–10 cm below the surface. However, how deeply water can diffuse into the ground during the periods of high obliquity and build a significant ice layer is unclear. Creation of an ice table a few centimeters below the surface will tend to block pathways to deeper levels and so hinder growth of the ice layer (Schorghofer and Aharonson, 2004).

Spectral evidence for ice

Until recently we had only models of the distribution of ice in the near-surface materials, but now we have measurements from which the ice contents can be estimated, and the models have proved quite reliable. The measurements were made by the gamma ray and neutron spectrometers on the Mars Odyssey spacecraft (Boynton *et al.*, 2001; Feldman *et al.*, 2002, 2004; Mitrofanov *et al.*, 2002; Prettyman *et al.*, 2004). Cosmic rays, which are mostly protons and alpha particles, interact with the atmosphere and the surface materials, and initiate a series of nuclear reactions that lead to production of neutrons and to excitation of the constituent nuclei in the near-surface materials. The hydrogen content, and thus the water content, of the near-surface materials is estimated in two ways. The first is from the flux of hydrogen gamma rays emitted from excited hydrogen nuclei as they revert to a lower energy state. The effective source depth of the gamma rays is about 10 cm. The second method is from the flux of different energy neutrons. Neutrons produced in the soil by cosmic-ray-induced reactions are slowed down by collisions with surrounding atoms. Hydrogen atoms are particularly effective in slowing down neutrons because their mass is close to that of a neutron, so the flux of the lower-energy thermal and epithermal neutrons from the surface provides a measure of the hydrogen content of the soil. The effective depth of the neutrons is about 20–30 cm. The hydrogen detected is assumed to be all in the form of water.

Derivation of the absolute amounts of hydrogen is complicated since the neutron and gamma ray fluxes depend on the composition of the host rock and the distribution of hydrogen with depth, which are both unknown. Prettyman *et al.* (2004) and Feldman *et al.* (2004) examined two models: one in which the composition is uniform with depth, and a two-layer model in which an ice-rich layer is overlain by a more desiccated layer containing only 2 percent ice. The latter model is favored from the ratio of the thermal and epithermal neutrons. According to this model, poleward of 50° latitude the ground below the upper desiccated layer a few centimeters thick contains at least 20 percent ice and possibly as much as 100 percent. The equatorial deposits ($< 50°$ latitude) below the desiccated layer contain at least 2 percent water and possibly as much as 11 percent.

While the high concentration of ice below a near-surface desiccated layer at high latitudes is expected from the models of ice stability, abundances of 10 percent H_2O below the desiccated layer at the equator are not. According to the models, ice is unstable at all depths at the equator. One possible explanation is that the water is in hydrated minerals. But a few percent water would imply that the materials are dominantly hydrated minerals, which is contrary to what is seen on the ground and in the orbital spectral data (Bandfield *et al.*, 2000; Bibring *et al.*, 2005). There are at least two other possibilities (Jakosky *et al.*, 2005). One is that the water detected is largely ice, and that the ice was inherited from an earlier era of high obliquity when ground ice was stable at low latitudes. This interpretation is consistent with the observation of possibly ice-cemented surficial deposits at high latitudes as discussed below. For this to occur, however, the ice would have had to survive for over 10^5 years, which would imply that the ice was diffusively isolated from the atmosphere, such as by a cemented layer or duricrust. Jakosky *et al.* considered this unlikely. They suggest, alternatively, that the water is indeed ice, but is present as a result of more recent changes. They suggest that slight changes in surface conditions could result in elimination of the southern residual CO_2 cap and more fully expose the underlying H_2O cap. Evidence of instability of the CO_2 cap is the "Swiss cheese" texture on the residual cap (Malin *et al.*, 2001). Sublimation from the southern water cap would then enhance the average water content of the atmosphere, possibly up to as much as 100 pr μm, and thereby increase the frost point temperature and stabilize ice at low latitudes.

In summary, both models and measurements suggest that ground ice should be widespread at depths greater than a few centimeters below the surface at latitudes higher than about 40–50°, and that it should be much less common at lower latitudes. As we shall see below, this is somewhat at odds with the surface morphology, which suggests that 30° is the critical latitude. Above 30° there is abundant morphological evidence of ground ice; below 30° there is little.

Permafrost

As discussed in Chapter 1, the surface of Mars is permanently frozen to depths of several kilometers.

The permafrost zone of the Earth is defined as that part of the ground where temperatures do not get above 273 K for two successive years. In Siberia the permafrost can reach depths of 1400 m; the maximum recorded thickness for North America is 610 m (Washburn, 1980). The term permafrost is defined strictly on temperature. Ground ice may or may not be present depending on local conditions. Overlying terrestrial permafrost is an active zone that undergoes an annual freeze–thaw cycle. Every spring a melting front penetrates from the surface down to the top of the permafrost. Every fall the active zone is refrozen. During spring and summer, water from precipitation or the thawing of ground ice cannot penetrate the permafrost so it tends to saturate the surface materials. Most ice in terrestrial permafrost is within 50 m of the surface, and commonly segregated into sheets, lenses, and wedges. These ice deposits may have been incorporated directly into the permafrost, such as by injection and burial; they also may grow in places as water vapor migrates through host rock to the freezing front. Most terrestrial permafrost is warmer than −5°C. Consequently, there is usually a significant quantity of water co-existing with the ice (Williams and Smith, 1989). Because of its warm temperature, ground ice tends to be unstable and vulnerable to dissipation due to slight changes in climate, surface albedo, vegetation cover, and so forth. In fact, permafrost stability is one of the most sensitive indicators of global climate change on Earth.

Terrestrial permafrost regions commonly have a rich array of unique landforms (French, 1976; Washburn, 1980; Williams and Smith, 1989). These result from a variety of causes: the annual freeze–thaw cycle, the saturated ground in spring and summer, and the growth and thawing of ground ice. Polygonally cracked ground may result from contraction of the permafrost during winter, in a process somewhat analogous to the formation of desiccation cracks in lake sediments. The cracks may partly fill with water or sediment in early spring, thereby leading to compressive stresses within the polygons when temperatures in the permafrost fall later in the year. The polygons may range in size up to about 100 m across. A similar process can lead to striped ground if the surface is sloping. Other forms of patterned ground are circles, polygons, and stripes formed of rocks, which may be sorted or non-sorted. They form by frost heaving, a process whereby coarser rocks are preferentially brought to the surface. It is thought to result from a combination of upward pulling, caused by expansion of the wet, finer-grained, enclosing materials during freezing, and upward pushing as a result of freezing of water that collects in gaps below the rocks.

Mass wasting is particularly common in permafrost regions. Frost creep is the "ratchet-like downslope movement of particles as the result of frost heaving of the ground and subsequent settling upon thawing, the heaving being predominantly normal to the slope and the settling more nearly vertical" (Washburn, 1980). Gelifluction is the slow downslope movement of water-saturated sheets of rock over permanently frozen ground and occurs only in the active layer due to seasonal thawing. Gelifluction is particularly common in permafrost regions because the permafrost table prevents seepage of rainwater and meltwater into the ground. Movements of centimeters per year have been measured on slopes of a few degrees. Rock glaciers are glacier-like tongues of rock debris that also move at rates measured in centimeters per year, although the precise mechanism whereby rock glaciers move is uncertain (Wahrhaftig and Cox, 1959; Whalley and Aszizi, 2003). They may be ice-cemented or ice-cored, and grade into true glaciers as the proportion of ice increases.

Thermokarst is a general term applied to areas where ground ice has been removed as a result of climate change or disturbances in the local thermal regime. The stability of ground ice is sensitive to the annual cycle of ground temperatures. Changes in the albedo of the surface can result, for example, from erosion, fires, or changes in vegetation. The consequent dissolution of the ground ice results from a combination of downwearing and backwearing at slopes. Local hollows, called alases, may form in which lakes can accumulate. The depressions may merge to form continuous valleys. The general result is a poorly integrated drainage system with numerous lakes and closed depressions. Within some lakes pingos form. These are ice-cored mounds that form in the final stages of the freezing of a lake, when water and sediments on the lake floor are forced upward, through the overlying ice, by the high artesian pressures that build as the lake progressively freezes.

Many features on the martian surface have been compared to those in terrestrial permafrost regions, but care should be taken in making such comparisons. Many of the landforms in terrestrial permafrost result from freeze–thaw and water saturation of the active zone. On Earth the active zone is typically a few to several meters thick. On Mars today the near-surface zone where temperatures get above 273 K is normally no more than a centimeter thick, although there are exceptions such as at high latitudes in summer, particularly at high obliquities on pole-facing slopes

(Costard *et al.*, 2002; Hecht, 2002). Even where temperatures do get above freezing, there is unlikely to be enough liquid water to cause gelifluction, frost heaving, and other permafrost phenomena. This may not have always been the case, however. If Mars ever underwent significant climate change in the past, as seems likely (see Chapters 6 and 12), then Mars may have had permafrost zones with active near-surface layers, much like the Earth's.

Ice-rich surficial deposits at high latitudes

Much of the surface at latitudes between 30° and 60° in both hemispheres has a distinctive, stippled appearance when viewed at the MOC scale of a few meters per pixel (Carr, 2001; Mustard *et al.*, 2001). The stippled texture is rarely observed equatorward of 30° and only occasionally at latitudes higher than 60°, yet almost all the terrain in 30–60° bands shows it. The stippled texture is caused largely by closely spaced pits 10–30 m across (Figure 8.1). The pitted unit is draped over pre-existing topography but appears itself to be only sparsely cratered. Mustard *et al.* estimate that the thickness is in the 1–10 m range. In places, the pitted unit is in contact with a smooth-surfaced unit, and small patches of smooth terrain may occur amidst the pitted (Figure 8.2). The smooth unit is also draped over the pre-existing topography. It seems clear from the relations that much of the terrain in the two latitude bands was formerly covered by a thin, smooth-surfaced veneer that has been partly removed by a process that has left the surface pervasively pitted. In some places the unit has been almost entirely removed to leave low mounds and linear ridges of possibly more resistant material.

The veneer is probably ice-cemented dust or soil. Head *et al.* (2003a) suggest that it is material that was deposited during the recent epoch of high obliquity that extended from 0.4 to 2.1 Myr ago (Figure 1.3; Laskar *et al.*, 2002). During this time, water was driven off the poles and accumulated as surface ice at latitudes as low as 30°, trapping dust with it. Subsequently, with the onset of lower obliquities, the ice started to sublimate away at the lower latitudes, leaving uncemented dust susceptible to being carried away by the wind to form the pits that we observe. They note that the pits are mostly equidimensional, not oriented in some specific direction such as would occur if wind were the controlling process. They suggest, therefore, that wind can remove the dust only where the ice cement has been removed. The texture is rarely observed at latitudes higher than 60°, possibly because the ice there is still stable, and the veneer remains intact.

Figure 8.1. Thin, possibly ice-rich veneer at 40.1°S, 188.2°E. Most of the terrain at latitudes higher than 30° in both hemispheres is draped with a veneer that has a characteristic pitted texture. The veneer may have been deposited during a recent period of high obliquity and has now been partly removed, as evidenced by the pitting (MOC M0003091).

Another type of veneer is commonly seen in the 30–60° latitude belt (Carr, 2001). At these latitudes, many slopes, such as those around mesas and on valley walls, are covered with faintly lineated deposits with a well-defined outer margin (Figure 8.3). The lineations are normally at right angles to the slopes. The almost smooth surface of the deposits commonly contrasts markedly with the rougher underlying base on which they are deposited. The deposits are particularly common in alcoves. They also appear to prefer poleward-facing slopes, although this is not well documented. We have little information upon which to judge what the deposits are, but since they occur

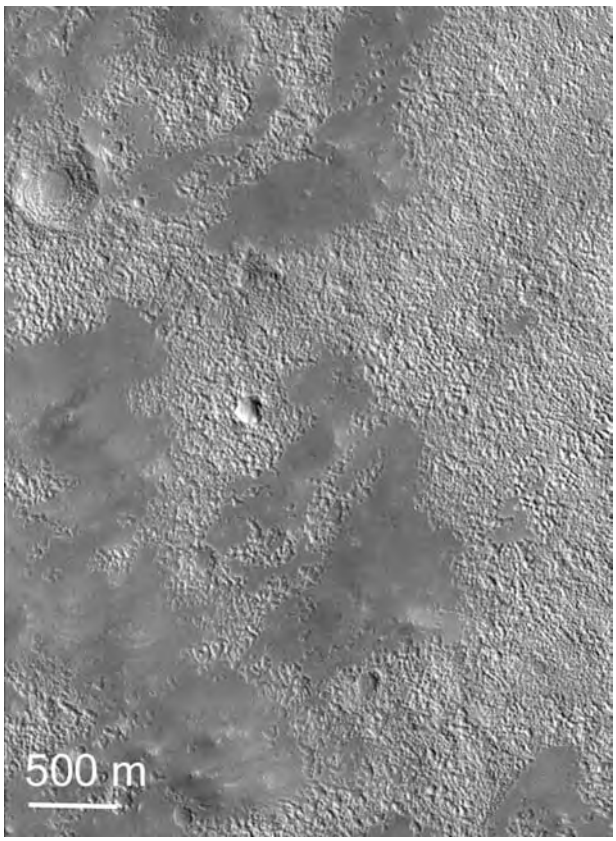

Figure 8.2. A formerly smooth surface at 31.9°N, 20.3°E in transition to a pitted surface like that in the previous figure, possibly as a result of sublimation of the ice cement of the veneer (MOC M0401878).

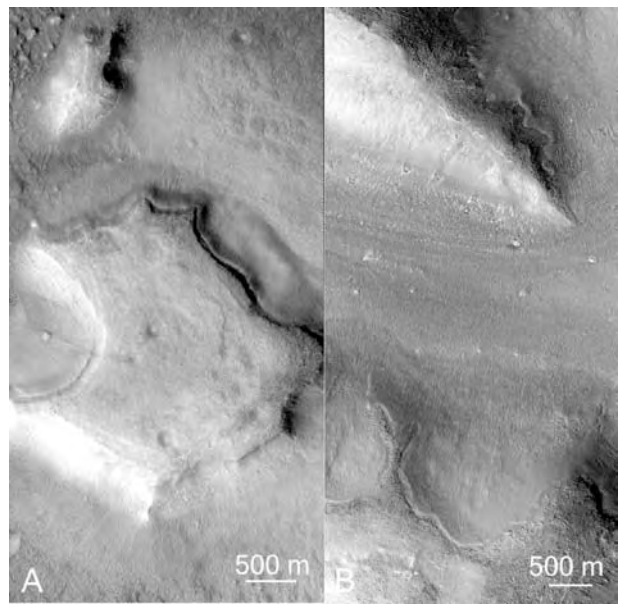

Figure 8.3. Possible ice deposits on poleward-facing slopes. (A) A mesa in the fretted terrain at 41.4°N, 12.1°E. Faintly lineated, clearly outlined deposits are on north-facing slopes (MOC M0800546). (B) North-facing alcoves at 40.1°N, 350.3°E in the lower half of the image containing similar deposits (MOC M0304566).

at latitudes where ice is stable, possibly preferentially on colder poleward-facing slopes, and in alcoves, a reasonable assumption is that they, like the much thinner and more widespread veneer discussed above, are ice-rich deposits. They may have been inherited from an earlier era, when there was a pervasive ice cover at these latitudes, and they have been retained preferentially in alcoves where the ice was thicker, and on colder, poleward-facing slopes. Consistent with this interpretation, Christensen (2003) suggests that many gullies found on steep slopes may be the result of melting of these deposits (see Chapter 6). In places these alcove-occupying deposits may be so thick as to flow and become true glaciers, as discussed later.

Fretted terrain

The term "fretted terrain" was coined by Sharp (1973b) to refer to the area that straddles the plains–upland boundary between 30–50°N and 0–60°E. In this area, numerous steep-walled, flat-topped upland remnants are separated by low-lying, almost level plains (Figure 8.4). The uplands decrease in elevation northward through the area. Mesas close to the continuous upland are 1–2 km high, but the heights diminish northward until ultimately the mesas disappear beneath the northern plains. The region is of interest in the context of this chapter because several types of surface features, thought to be in some way related to the presence of surface or ground ice, are well developed there. These include terrain softening, lobate debris flows, and lineated valley fill. All these features occur elsewhere at similar latitudes, but their best development is in the fretted terrain.

One characteristic of the fretted terrain is that wide, flat-floored, steep-walled valleys extend from the plains into the uplands. The most prominent is the 1200 km long Mamers Vallis. Like valleys elsewhere, the fretted valleys have a meandering course and few tributaries. They differ from most other valleys, however, in having strongly lineated, highly textured deposits on their floors. This is true both of the valleys in the type area of the fretted terrain and of those in other areas at similar latitudes, such as Reull Vallis, east of Hellas. Some of the valleys in the fretted terrain are discontinuous or simply isolated linear depressions (Figure 8.5). They clearly cannot have formed in the same way as typical fluvial valleys by erosion of the surface materials and transport of the eroded materials

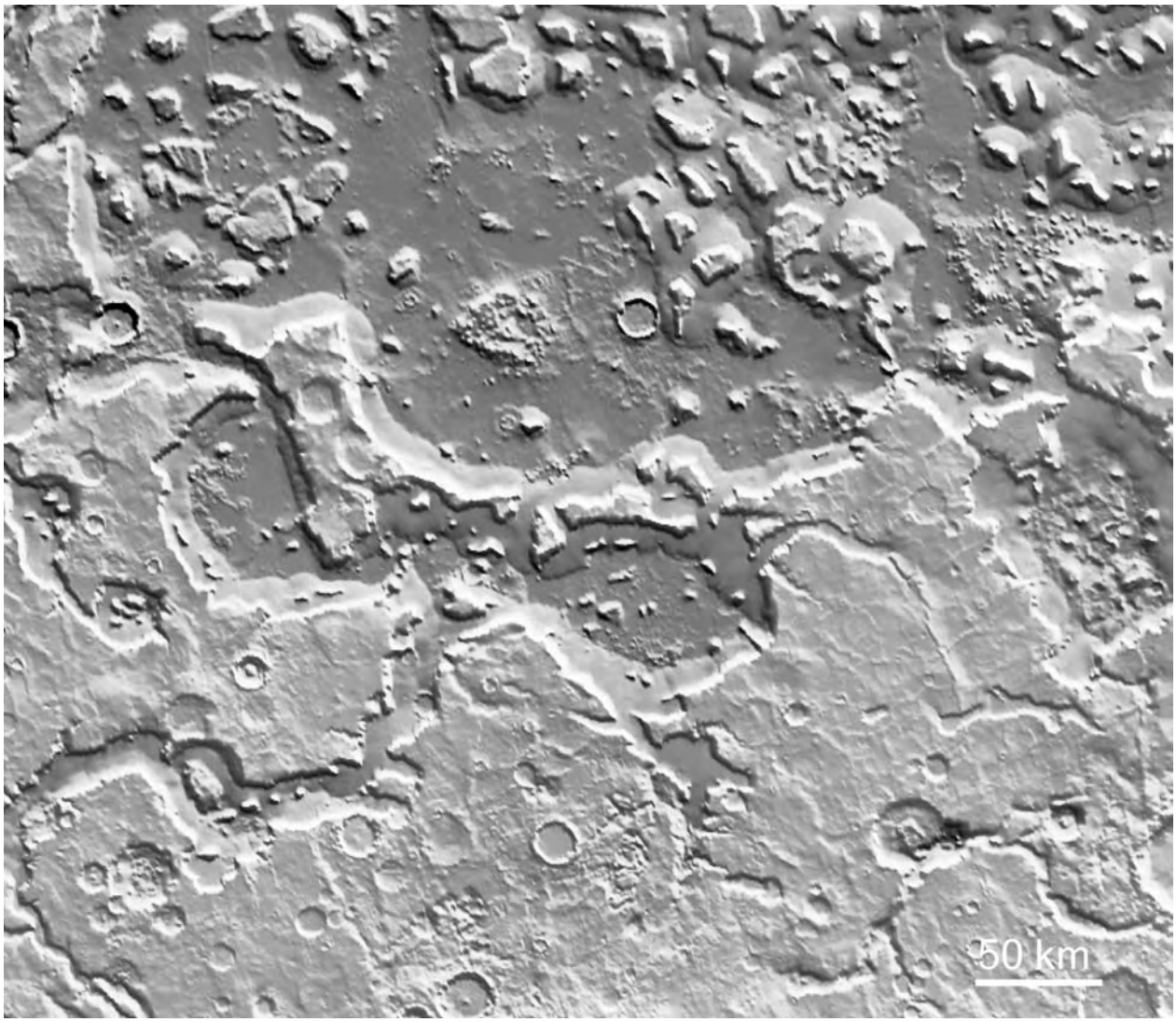

Figure 8.4. Fretted terrain centered at 40°N, 25°E. Cratered upland in the bottom half of the image transitions northward into isolated 1–2 km high mesas separated by plains. The mesas decline in elevation north of the image and ultimately the upland remnants disappear beneath the northern plains. Debris flows that extend roughly 20 km away from the base of all steep slopes are thought to be lubricated by ice shed from the slopes (MOLA).

downstream, unless they have been blocked by later materials, for which there is no evidence. To form the depression at B in Figure 8.5, for example, approximately 1000 km^3 of material had to be removed and there is no outlet. In some places a discontinuous channel appears to have formed partly by collapse as though there had been subsurface erosion or solution. Faulting is unlikely to be the cause of these sinuous discontinuous valleys. They surely are ice- or water-worn. One possibility is that water cut the original valleys, but it flowed partly on the surface and partly underground as in karst regions on Earth. The surface then collapsed and the depression so formed was partly filled with material that flowed away from the depression walls.

Terrain softening

Terrain softening is a term coined by Squyres and Carr (1986) to describe the difference in the appearance of cratered terrain at high and low latitudes, when viewed at resolutions of 50 m/pixel or better. At latitudes lower than 30° (Figure 8.6) craters of all sizes are crisply defined. Most large (>20 km diameter) craters have well-defined rims, steep walls, and a flat floor on which there is normally a population of small, fresh-appearing, bowl-shaped craters.

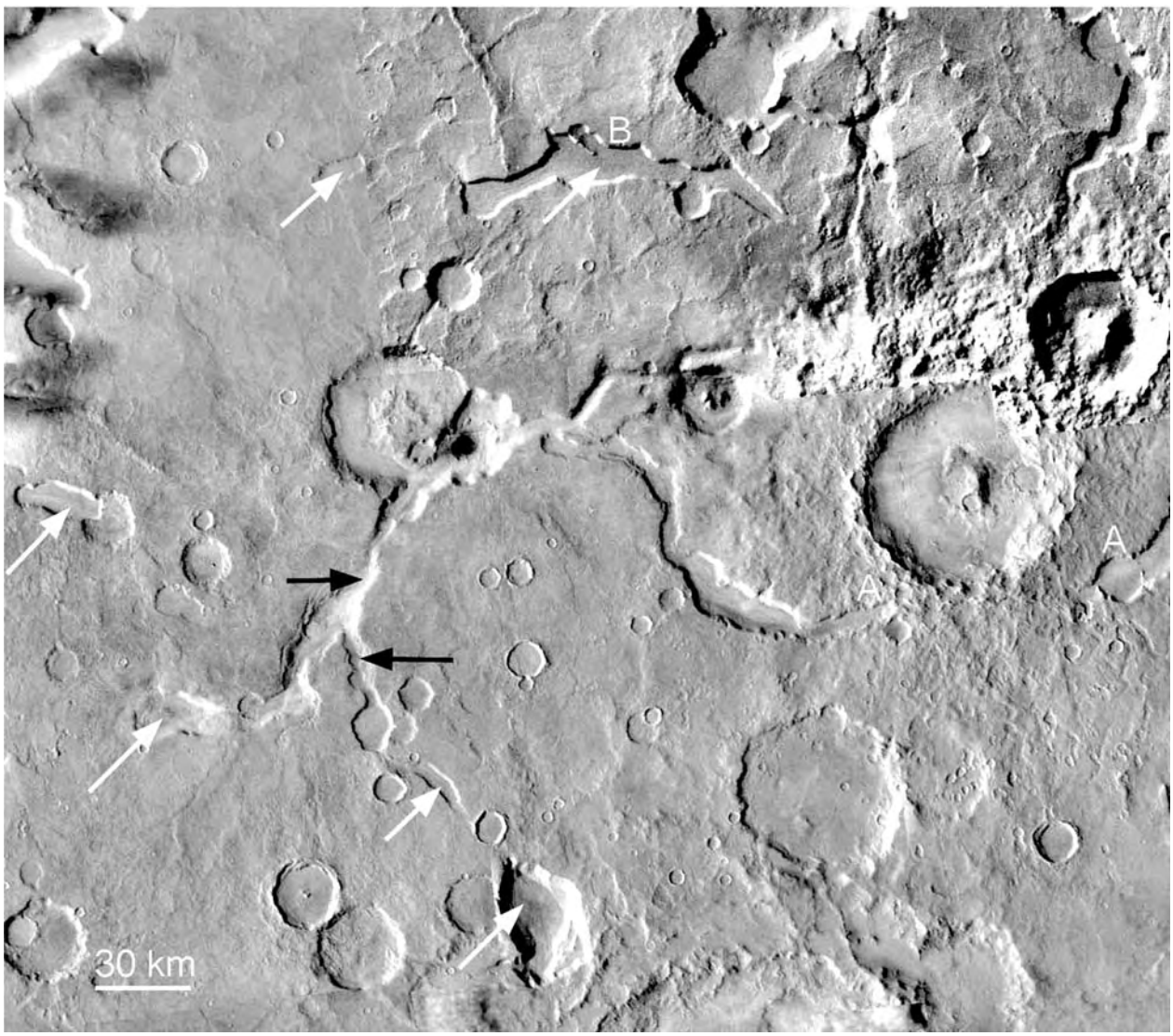

Figure 8.5. Fretted terrain between 34–39°N, 24–32°E. The white arrows indicate closed depressions partly filled with lineated valley fill, indicating that the lineations in the fill are not caused by down-valley flow. Black arrows indicate where the surface has collapsed to form a linear depression. At the two locations marked A, B a valley is incised into ejecta from a large crater, yet between the two locations ejecta fills the valley. The implications are discussed in the text (Viking MDIM).

Ridges on the intercrater plains are sharply defined. At latitudes higher than 30°, the scene is usually very different (Figure 8.7). Rim crests and intercrater ridges are commonly rounded, and smaller craters are much more sparsely distributed. Fill within the larger craters commonly has a concentric pattern as though material had flowed from the walls to the center of the crater. In addition, the ridges and escarpments outlining the ejecta around craters are commonly rounded. In general the terrain has a softer appearance. Squyres and Carr attributed the softening to viscous creep of the near-surface materials caused by the presence of ground ice. While other suggestions have been made to account for the latitudinal differences (e.g. Clifford and Zimbelman, 1988), ice-abetted creep still appears to be the most plausible cause, particularly with the detection of large fractions of ice very close to the surface at these latitudes, as discussed above.

Lobate debris aprons

Lobate debris aprons occur almost universally at the base of steep cliffs in the 30–50° latitude belts in both hemispheres (Figure 8.4) (Squyres, 1979). The aprons extend 10–30 km from the cliff, are convex

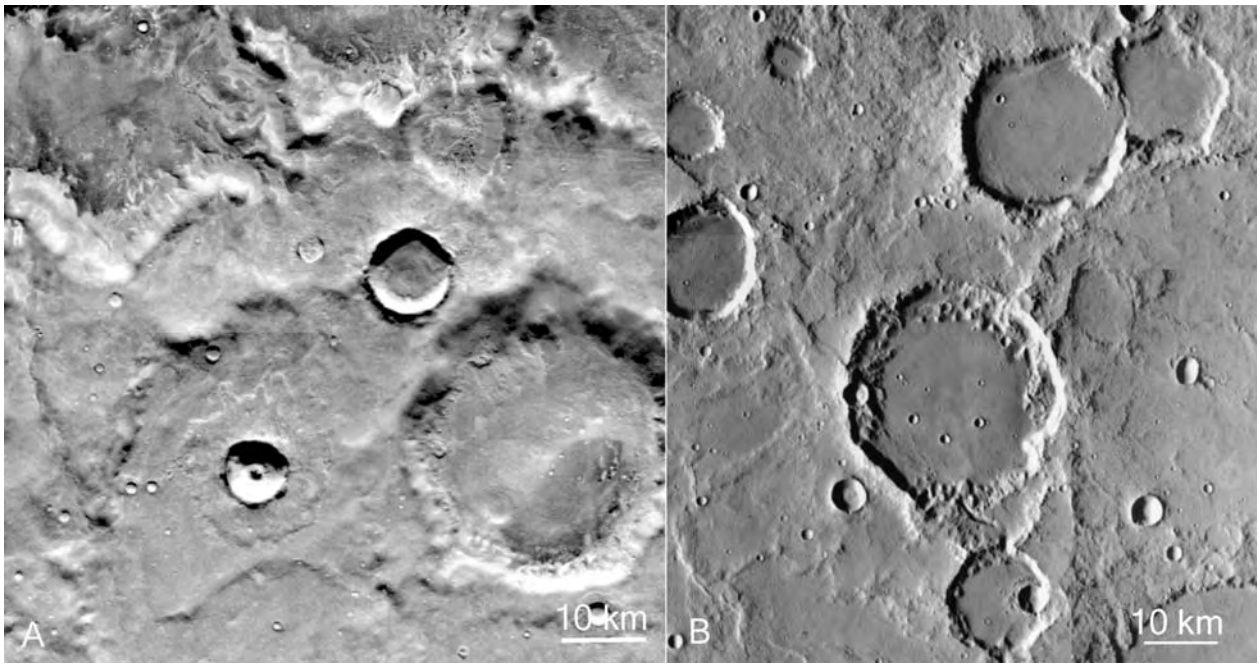

Figure 8.6. Comparison of softened terrain at high latitudes with unsoftened terrain at low latitudes. (A) Softened terrain at 48.8°S, 20.0°E. Rims of old craters and ridges are rounded. Fresh-appearing small craters are rare (Viking 57B). (B) Unsoftened terrain at 12°S, 197°E. Rim crests of old craters and ridges are sharply defined. Numerous small, fresh-appearing craters are present (Viking 443S). The differences are thought to be due to creep of near-surface materials caused by presence of ground ice at high latitudes.

upward, and most have striations at right angles to the cliff. The striations may be deflected downstream of alcoves in the cliff. Where obstacles are in the path of the flow, the striations diverge around them (Figure 8.8). If there is a gap in the obstacle, the flow lines converge on the gap (Figure 8.9). It seems clear that the aprons formed by flow of material away from the cliffs. (However, for an alternative view, see Malin and Edgett, 2000c.) The apron surfaces typically have 1–3° slopes but they steepen to several degrees at the outer margin (Malin and Edgett, 2000c; Carr, 2001). While debris aprons are best developed in the fretted terrain between 0–60°E and 30–50°N, they occur wherever there are cliffs to feed the flows in the 30–50°N latitude bands. In the southern hemisphere, debris aprons are less common, probably because of the fewer cliffs at the appropriate latitudes, but they are found next to steep slopes around Hellas and Argyre. Steep slopes at low latitudes do not have debris aprons. Debris shed from low-latitude slopes simply accumulates as talus, close to the angle of repose. Debris aprons are also rare at latitudes higher than 50°. This may simply be the result of the scarcity of steep slopes at these latitudes. Alternatively, the colder temperatures may inhibit flow.

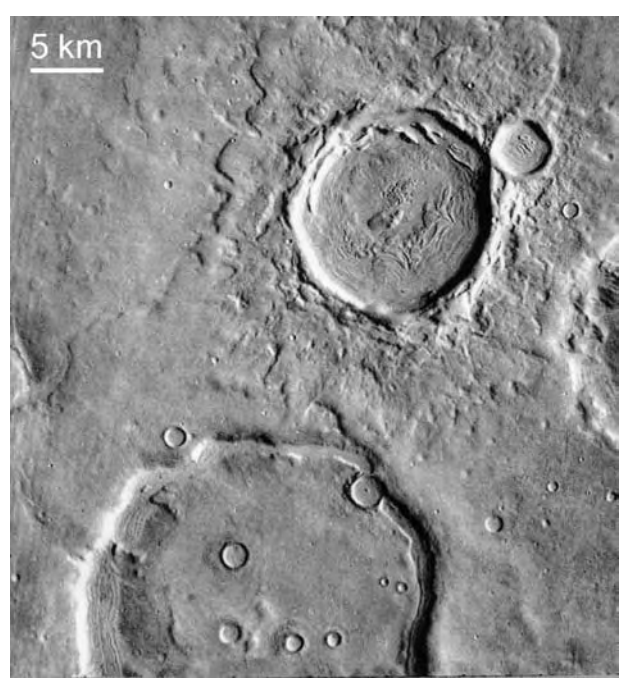

Figure 8.7. Concentric valley fill and muted ejecta patterns in softened terrain at 33°N, 48°E. The concentric fill is thought to form as a result of ice-abetted flow from the crater walls toward the center of the crater (Viking 196S11).

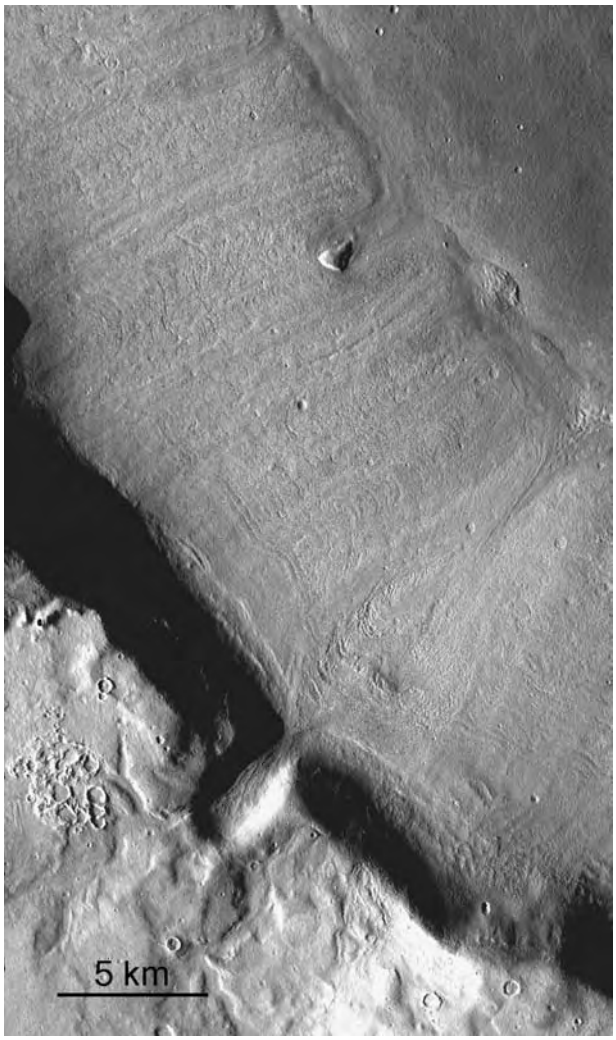

Figure 8.8. Detail of a typical debris flow at 41.2°N, 20.1°E. The flow has lineations both at right angles to the cliff and parallel to the cliff. The flow is deflected around a small obstacle. The surface is pitted with small impact craters, and irregular pits may indicate ice sublimation (THEMIS V05442018).

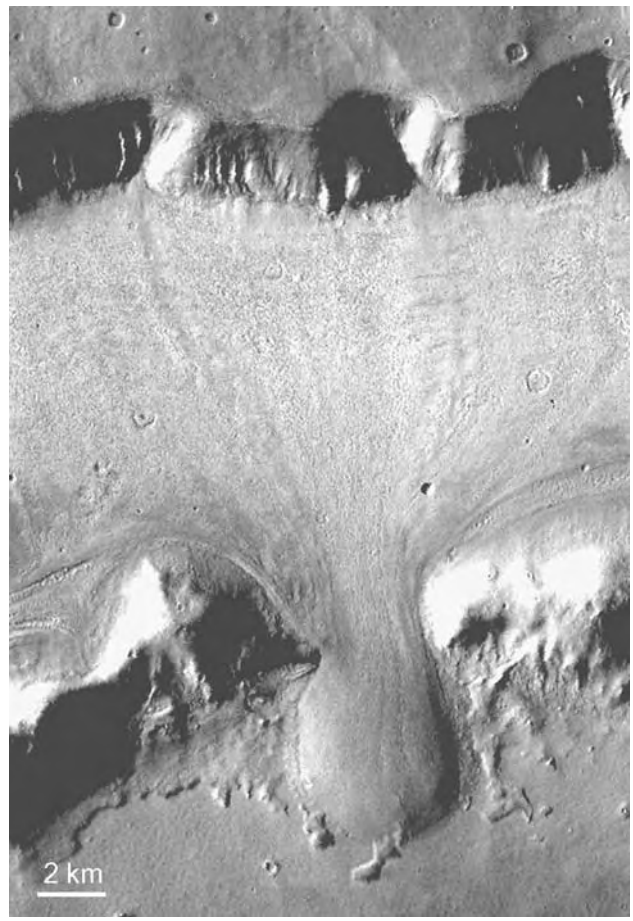

Figure 8.9. Debris flow deflected through a gap in an obstructing ridge at 40.0°N, 25.0°E. On the surface of the flow are both fresh-appearing craters and circular remnants of older impact craters. Relations such as this suggest that the debris aprons may contain large fractions of ice, and be akin to terrestrial rock glaciers (THEMIS V12057009).

At resolutions of a few tens of meters per pixel or poorer, all that can be seen on the surface of the aprons are the striations and the remnants of craters 100 m across or larger. At MOC resolution, however, the surfaces are richly textured (Figure 8.10). Most of the surfaces are covered with closely spaced hillocks and pits, 10–30 m across. These may be arrayed in parallel lines that give the surface its striated appearance. In places the lineations form complex sinuous patterns, particularly downstream of alcoves or where different aprons meet. Elsewhere, especially toward the outside edge of the aprons, gaps in the hillocky unit commonly form complex patterns.

The ages of the aprons are difficult to determine. Fresh-appearing small (< 0.5 km) craters are common on the surface of the flows, as well as remnants of larger, probably older craters (Figure 8.10). Mangold (2003) compared counts of all craters with counts of fresh-appearing craters on debris aprons in the fretted terrain and found that the all-crater counts gave ages of several hundred million years, while the fresh-appearing craters gave ages of a few million years. He suggested that the debris aprons are ice-cemented but that ice is continuously sublimating and so facilitating erosion of the surface. The smaller craters are more easily eroded and so give younger ages. Crater counts by Head *et al.* (2005b) yield similar results. The crater counts cut across isochrons, indicating preferential destruction of the smaller craters. They give a minimum age of 40 Myr for a debris flow

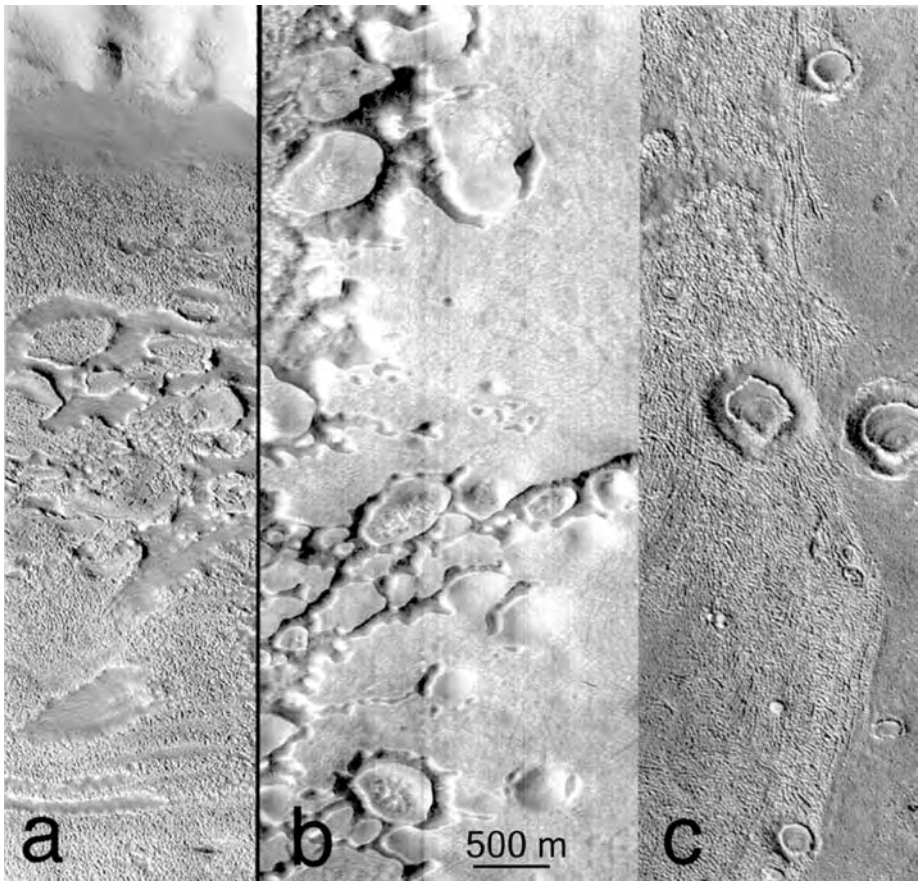

Figure 8.10. Detail of textures on the surface of debris flows between 41–44°N and 25–36°E. The most pervasive texture is a fine-scale, sandpaper-like texture composed of closely packed pits and hillocks. Interrupting this texture may be irregular hollows or long linear gaps as in (a). Not all the flows have a sandpaper texture. Some have a smooth surface broken only by cracks, which in places form circles as in (b). Circular remnants of impact craters in (c) suggest that the flows have not been active for geologically significant lengths of time. Fill within the craters indicates a complex history of deposition and removal of material. (a, M0700734; b, M0300046; c, SP200506).

east of Hellas, but emphasized that the true age could be significantly older. Counts of the larger, circular remnants suggest that most of the debris flows are at least 1 Gyr old and that they have moved little since that time.

Restriction of the flows to latitudes above 30°, the distance that the materials have flowed, the convex upward profiles, and pitting of the flow surfaces, suggestive of sublimation, all indicate that ice played a prominent role in formation of the flows. Different suggestions have been made for the source of the ice. Squyres (1979) suggested that annual precipitation of frost, under conditions similar to those that prevail today, could have resulted in incorporation of ice into the flows. This seems unlikely, however, since the amount of frost deposited on the ground today is minute, and large amounts of ice need to be mixed into the aprons to enable them to flow. Mangold *et al.* (2002), for example, estimated, on the basis of experimental work, that at least 28 percent ice is needed to produce the viscous deformation observed in the fretted terrain. Lucchitta (1984) alternatively suggested that ground ice is pervasive in the fretted regions, and that it would be incorporated in any talus that accumulated on slopes and so mobilize the talus to form a debris flow. The suggestion is consistent with the experimental findings of Mangold *et al.* and with terrain softening discussed above. Another possibility is that the ice is derived from water discharging from a regional aquifer (Hamlin *et al.*, 2000).

Head *et al.* (2005) proposed that some of the debris flows, particularly those that emerge from alcoves, are glaciers that formed during periods of enhanced precipitation of snow, such as during periods of high obliquity. One example from the Hellas region is shown in Figure 8.11. Two craters are at the mouth of

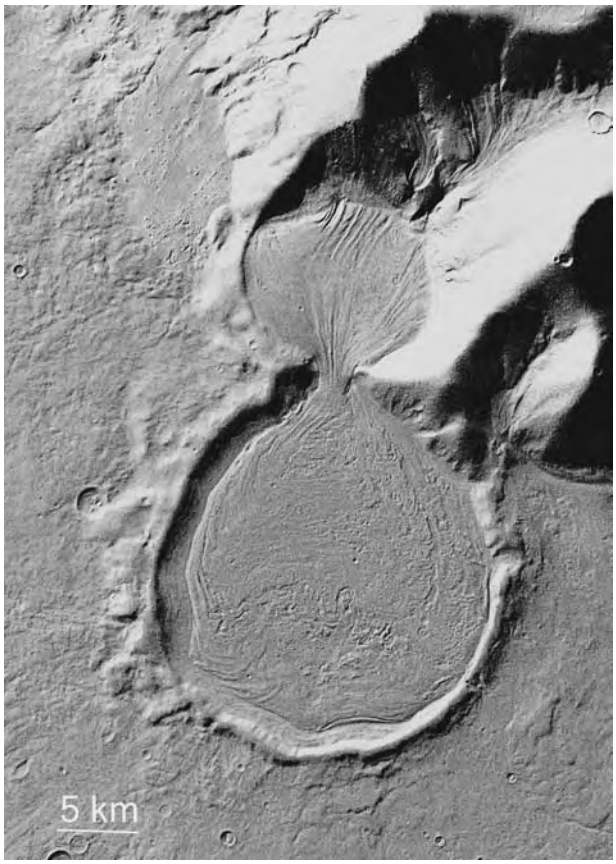

Figure 8.11. Possible glacier east of Hellas at 38°S, 104°E. Material has flowed from an alcove in a massif at the upper right into a nearby crater and from there through a gap in the crater to another larger crater, 500 m lower in elevation (HRSC).

a valley in a massif. Flow lines extend away from the valley walls and down the valley to converge on the upper crater, which in turn appears to have filled and overflowed through a notch into the lower crater. The lineations suggest viscous flow and an ice-like rheology, and the complex pattern of pits on the flow suggests sublimation. Head *et al.* interpret the Hellas features as the result of accumulation of snow and ice precipitated from the atmosphere, rather than incorporation of ground ice. While this may be true of this particular flow, it is unlikely to be the cause of most of the debris flows in the 30–60° latitude belts since they form at the base of almost all cliffs at these latitudes, irrespective of their shape or orientation. Whatever process caused the flows, it must be ineffective at low latitudes because the cutoff at the 30° latitude is quite sharp.

Lineated valley fill

Most valleys in the fretted terrain have flat floors with a pronounced linear texture when viewed at

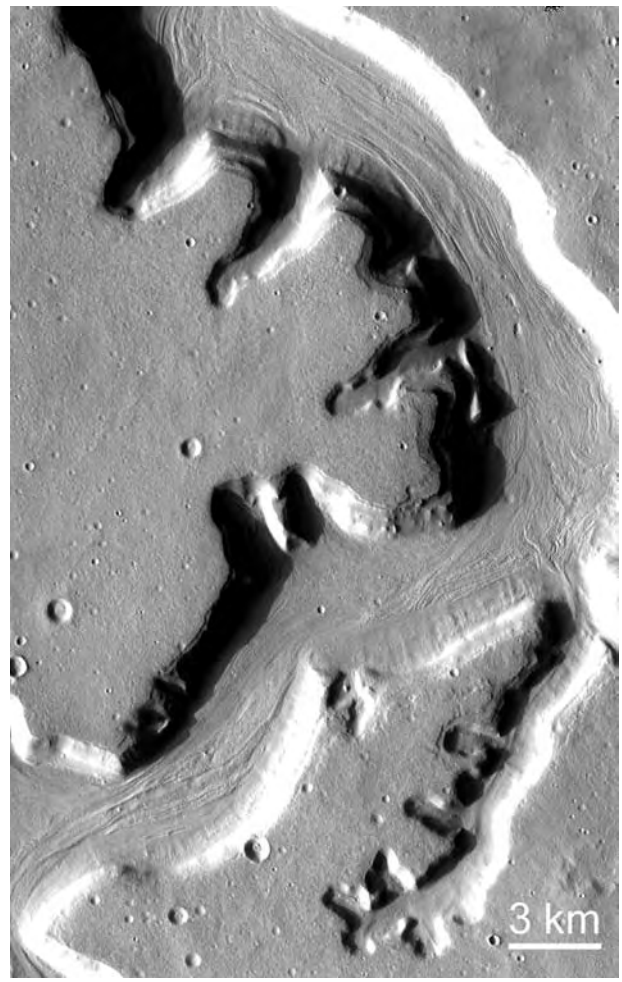

Figure 8.12. Lineated valley fill in Mamers Vallis at 31.3°N, 19.1°E. One issue with respect to the fill is whether the linear texture is due to down-valley flow, cross-valley flow, or some other cause. Fretted valleys such as these may have formed by widening and filling of typical V-shaped valleys by flow of material away from the valley walls, as seen in Figures 8.8 and 8.9 (THEMIS V05055010).

a few tens of meters per pixel (Figure 8.12). When viewed at the MOC scale of a few meters per pixel, the texture is resolved into lines of closely packed pits and mounds a few tens of meters across (Figure 8.13). It has been likened to the surface of a corncob. The linear patterns are caused by alignment of the pits and mounds in long strings and by smooth, linear pathways through the dominant bumpy texture. The lineations mostly run along the length of the valleys, but minor crenulations commonly reflect indentations and protuberances on the valley walls. In places the textured materials seem to ride part way up the valley walls. In other places the lineated fill is separated from the valley wall by smoother material with a faint

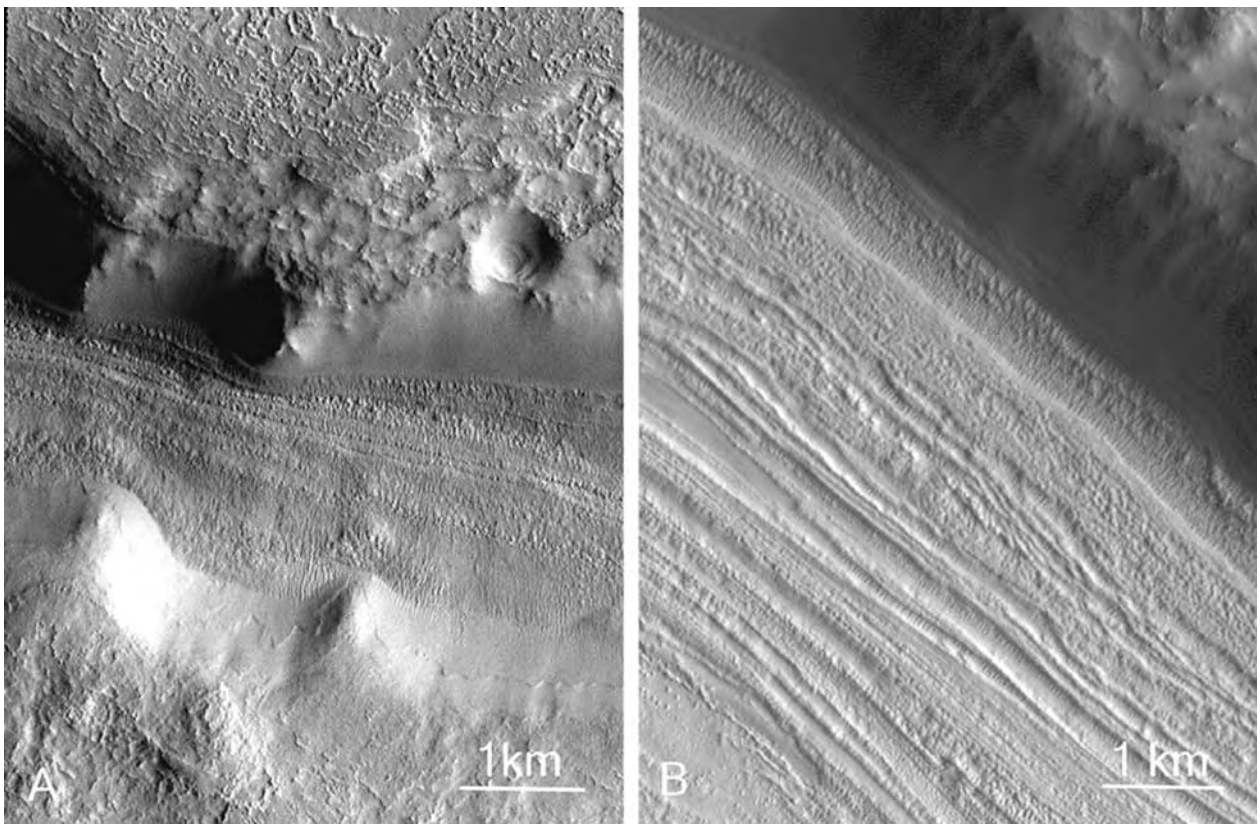

Figure 8.13. Lineated valley fill. (A) A thin deposit that appears to be draped on the valley walls and on the surface outside the valley may be the same veneer shown in Figures 8.1 and 8.2 (MOC SP243014). In (B) the valley fill consists of linear ridges with a beaded texture separated by linear troughs that are either smooth or filled with small transverse ridges (MOC SP241204). These areas appear to have had complicated histories with down-valley flow, cross-valley flow, and deposition and removal of veneers.

lineation at right angles to the wall. While most valleys in the fretted terrain have lineated fill, some have a smooth fill, commonly with crevasse-like depressions adjacent to the valley walls (Figure 8.14).

When first observed, the lineations were thought to be analogous to median moraines in glaciers, and to indicate down-valley flow. This is almost certainly not the case in most instances. Completely enclosed linear depressions such as those shown in Figure 8.5, for which there can be no down-valley flow, have identical textures to open-ended valleys. More likely, the lineations are caused mostly by convergence of debris aprons from opposing valley walls. There are, however, some indications of down-valley flow. In some places, faint lineations on the smoother material close to the wall curl downstream, and at some valley junctions material appears to have pushed a short distance out of a tributary valley into the main valley. But there is little reason to conclude that the material in the valleys has flowed any further than the 20–30 km that is typical of debris flows elsewhere in the fretted terrain that are not confined in valleys. As with debris aprons, flow of material away from the valley walls was likely enabled by incorporation of ground ice.

Origin of the fretted valleys

Valleys in the 30–60° latitude belts tend to be much wider than valleys at lower latitudes, and those close to the plains–upland boundary, instead of maintaining their width downstream as low-latitude valleys mostly do, tend to widen considerably downstream. We have just concluded that downstream flow is unlikely to be the main cause of lineations on the valley fill. One possibility for the formation of the valleys (Carr, 2001) is that the fretted terrain underwent dissection during the Noachian to form valley networks like terrain elsewhere, except that the valleys subsequently were modified by the process that formed the debris flows. Because of the drop in elevation across the plains–upland boundary, the original valleys were deeper closer to the boundary. When the

Figure 8.14. Fretted valley tributaries. (A) Smooth valley fill at 39.7°N, 25.4°E. Crevasse-like cracks around the edge of the fill suggest that the fill pulled away from the valley walls like a glacier (MOC M0202164). (B) Concentric crater fill at 36.5°N, 24.5°E has breached the crater wall and flowed into an adjacent valley (THEMIS V12319006).

main era of valley formation was over, the valleys started to slowly widen and fill as a result of ice-abetted flow of material away from the valley walls. The valleys widen downstream because the original valleys were deeper downstream and so could accommodate more fill. Support for this suggestion is seen at A in Figure 8.5. As pointed out by McGill (2000), conflicting age relations are observed between the large crater and the channel. Ejecta fills the part of the valley close to the crater rim, indicating that the crater is younger than the valley, but the ejecta is dissected by the valley elsewhere, indicating that the valley is younger. These relations are simply explained by the origin suggested above. When the crater formed, the original fluvial channel was filled with ejecta close to the rim and partly filled further from the rim. Where the valley was only partly filled with ejecta, the valley walls continued to provide material to debris flows, so the valley continued to widen and all traces of ejecta on the floor were erased. The result is that the valley is buried close to the crater rim but cuts the peripheral parts of the ejecta and has typical lineated valley fill on its floor.

Thus, in the fretted terrain and other areas at the same latitude, the near-surface materials appear to have flowed viscously, leading to a softening of the terrain and to formation of a variety of landforms such as broad aprons at the base of slopes, concentric crater fill, and lineated valley fill. Terrain softening suggests pervasive ground ice. Flow of the near-surface materials was probably enabled by presence of large fractions of ice. Large amounts of ground ice may also have become incorporated into talus on steep slopes, thereby enabling talus to flow and form the aprons and the various kinds of fill. Flow of material away from slopes resulted in backwasting of scarps and widening of pre-existing valleys. The timing of these events is unclear, but counts of the larger craters on the aprons suggest that the aprons formed in the order of Gyrs ago. Younger ages derived by counting smaller craters

suggest a continual slow resurfacing. These tentative conclusions apply not just to the fretted terrain in northern Arabia but to all upland regions in the 30–60° latitude belts in both hemispheres.

Glaciers

Bodies of surface ice, as opposed to ground ice, have been invoked to explain many surface features. They may occur in two different topographic situations: in confined basins, where flow is restricted, and in unconfined locations where the ice is free to flow. In Chapter 7 we discussed the likelihood that large bodies of water pooled and froze in basins such as the northern plains, Hellas and Argyre. Several authors have proposed morphological evidence for such ice sheets (e.g. Allen, 1979; Hodges and Moore, 1979; Rossbacher and Judson, 1981; Kargel and Strom, 1992; Lucchitta, 1993; Chapman, 1994; Costard and Kargel, 1995; Head and Pratt, 2001). The evidence is summarized briefly in Chapter 7 and more comprehensively and compellingly in Kargel *et al.* (1995). It will not be discussed further here.

The role of moving glaciers is more controversial. Lucchitta (1982, 2001) suggested that the outflow channels around Chryse and Amazonis were carved by glaciers. She made detailed comparisons between the outflow channels and landforms sculpted by terrestrial glaciers and showed that there is a strong resemblance both in form and scale. She favored two possible origins for the glaciers. In the first, eruptions of groundwater built thick bodies of ice within pre-existing valleys that ultimately became thick enough to move. A second possibility she suggested is that a flood or debris flow moving down a valley could have stalled and frozen as a result of ice dams and so formed a glacier which continued to move and modify the valley. This would explain why some channels have characteristics of both large floods and sculpture by ice. Lucchitta (1984) also suggested that many features of the fretted terrain may be glacial in origin. Kargel and Strom (1992) interpret many features of Argyre and Hellas as glacial. They suggested that striations on the south wall of Hellas are glacial scour, that various ridges within the basin are moraines, and that a low area around the periphery of the basin's interior is the former site of a proglacial lake. However, while ice may have once occupied the floors of Hellas and Argyre as a result of the freezing of water that formerly pooled there (Chapter 7), the role of alpine glaciation and the presence of terminal moraines and glacial scour is more controversial.

A stronger case can be made for glaciers on the flanks of the large Tharsis volcanoes (Lucchitta, 1981; Head and Marchant, 2003; Shean *et al.*, 2005). Fan-shaped deposits occur adjacent to the western flanks of each of the Tharsis Montes and Olympus Mons (Figures 8.15). They occur at low latitudes, where ice is unstable, so are unlikely to be the result of presence of ground ice, as many of the features in the fretted terrain may be. The deposits normally contain three facies: (1) an outermost ridged facies consisting of a broad thin sheet, with numerous subparallel ridges, tens of kilometers long and spaced hundreds of meters apart, which pass undeflected across topographic barriers such as craters (Figure 8.16); (2) a knobby facies consisting of closely spaced hills a few kilometers across; and (3) a smooth facies with elongate, lobate margins and arcuate lineations. The most puzzling characteristic of these deposits is the way that the ridged unit drapes over pre-existing topography, such as impact craters and lava flows. If the ridged material were deposited from a landslide, a debris flow, or a temperate glacier, the ridges would be deflected by the obstacles, but they are not. By analogy with glaciers in Antarctica, Head and Marchant (2003) proposed, alternatively, that the ridges are drop moraines, deposited from cold-based glaciers. The basal temperature of cold-based glaciers is below the pressure melting point and so all movement occurs within the ice, in contrast to temperate glaciers where significant slip and erosion occur at the base. Deposits from temperate glaciers would be deflected by obstacles, which is contrary to what is observed. In contrast, drop moraines deposited by advance and retreat of cold-based glaciers in the Dry Valley of Antarctica are superposed with almost no modification on the underlying rock surface, as we observe at Arsia Mons. Consistent with this interpretation, Head and Marchant interpret the knobby facies as a sublimation till, in which a debris-laden glacier dissipates by sublimation rather than melting. The smooth facies with its elongate tongue-like forms, they interpret as rock glaciers (Figure 8.17). Similar glacier-like features are see on the western flanks of other volcanoes, for example, Olympus Mons (Figure 8.18)

Some support for the glacier interpretation is provided by general circulation models. Preliminary results show that the western flanks of the Tharsis volcanoes are preferred sites of ice deposition when water is transferred from the poles to lower latitudes during periods of high obliquity (Haberle *et al.*, 2004). However, whether this preference can lead to thick permanent ice deposits is unclear from the simulations. The lobate features adjacent to the Tharsis volcanoes appear to be young since they override Amazonian lava flows. The simulations of Haberle *et al.* were at an obliquity of 45°. According to calculations by

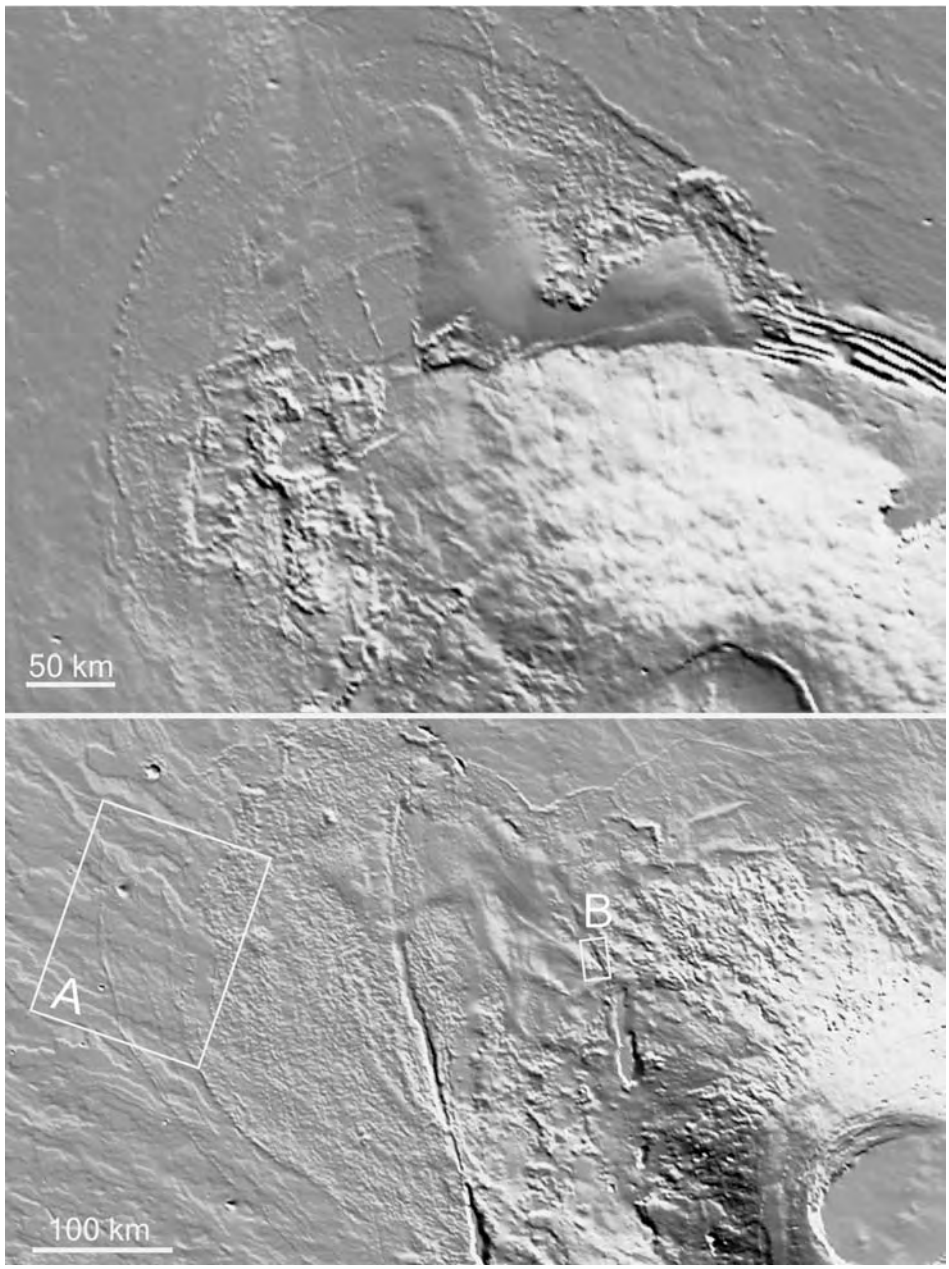

Figure 8.15. Possible glacial deposits off the northwest flanks of Pavonis Mons (top) and Arsia Mons (bottom). The fan-shaped deposits are draped over the surrounding terrain. Three facies are recognized: an outer ridged facies, a knobby facies, and an inner smooth facies. The boxes indicate the location of Figures 8.16 and 8.17.

Laskar *et al*. (2002), the last time obliquities were as high as 45° is 5.5 Myr ago. Lobate, flow-like forms are also observed at the base of a cliff on the western periphery of Hecates Tholus in Elysium. Hauber *et al*. (2005a) interpret the flows as glacial in origin, and derive crater retention ages of 11 and 95 Myr. They suggest that these flows are also glaciers formed by accumulation of ice during periods of high obliquity.

Other possible indicators of ground ice

Crater ejecta patterns

As discussed in Chapter 2, the unique patterns of ejecta around martian impact craters, variously described as rampart, pancake, petal-like, and fluidized, have been ascribed to incorporation into the ejecta of ice or water that was originally present in the surface materials. The patterns have also been

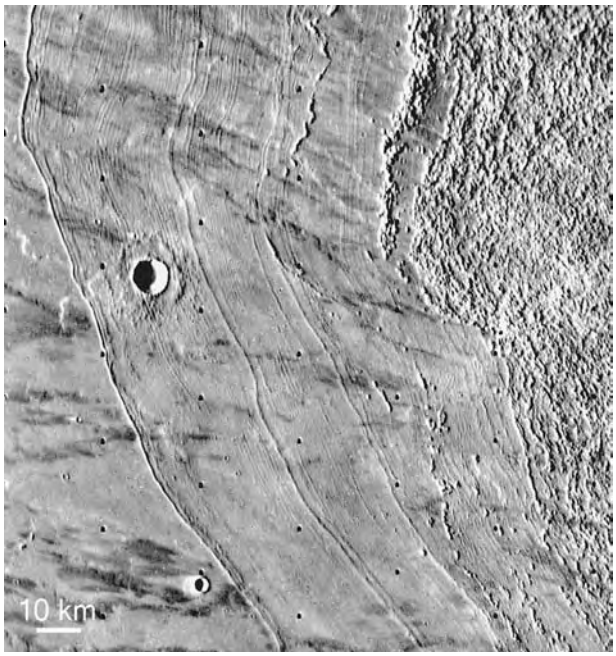

Figure 8.16. The outer ridged facies in area A of Figure 8.15. The ridges, which pass undeflected across the crater in the upper left, have been interpreted as drop moraines from a cold-based glacier (Viking 42B35).

Figure 8.17. Possible rock glacier in area B of Figure 8.15.

attributed to atmospheric effects. As discussed in Chapter 2, however, incorporation of liquid water into the ejecta appears an unlikely cause of the patterns because it would imply that liquid water had been at depths of a few hundred meters below the surface everywhere on the planet for much of Mars' history, which is geophysically implausible. Incorporation and volatilization of ground ice possibly caused the patterns, but again there are problems. We should expect the patterns to change across the 30° latitude, as do other possible indicators of ground ice such as terrain softening, concentric crater fill, and debris aprons. But changes in ejecta across this boundary, if any, are subtle. The patterns appear equally common at low latitudes where ice is unstable at all depths, as at 40° latitudes, where it is stable up to within a few centimeters of the surface. Fluidization of the ejecta by incorporation of ice has also been questioned on theoretical grounds. The usefulness of the patterns as an index of the presence of ice or water in the surface is thus questionable.

Polygonal fractures

Polygonally fractured ground occurs at a wide range of scales, with polygons ranging in size from a few meters to 20 km across. Most, but not all, the polygonal ground is at high latitudes where ice is stable. The terrain has been likened to a commonly occurring terrain in the terrestrial arctic characterized by ice-wedge polygons (Lachenbruch, 1962). The terrestrial polygons are typically 3–30 m across. They are formed by shallow cracks that are generally underlain by wedge-shaped masses of clear ice up to 10 m deep and 2 m across at the top. The polygonal pattern superficially resembles desiccation cracks in mud, although at a larger scale. Most of the terrestrial polygons are thought to form by repeated fracturing of the permafrost in winter as a result of thermal contraction, and filling of the cracks with water during the spring thaw. When the much coarser martian polygons (Figure 8.19) were first observed they were likened to terrestrial ice-wedge polygons, but Pechman (1980) demonstrated convincingly that the polygons are too large to have formed by shrinkage, even that caused by thermal effects of long-term cycles such as obliquity. Most of the large-scale polygonal ground is found near the floor of the Utopia basin where water is thought to have at one time pooled. The fracturing may have been caused by regional warping

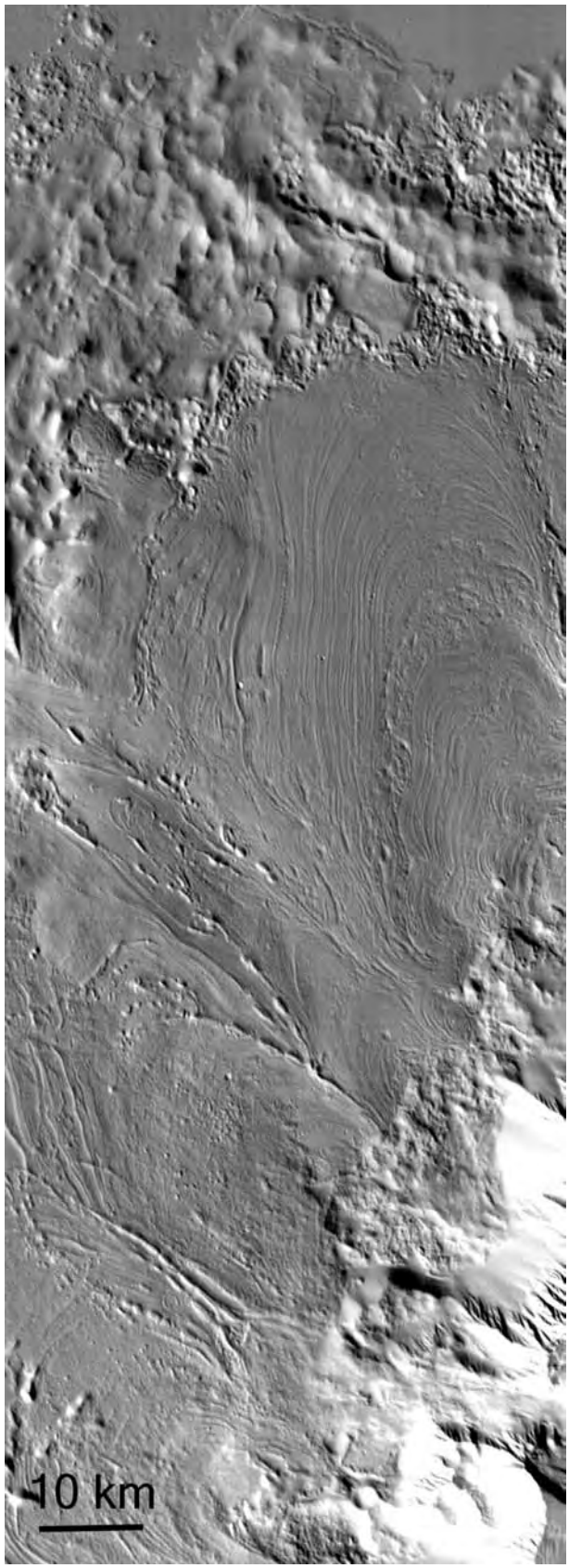

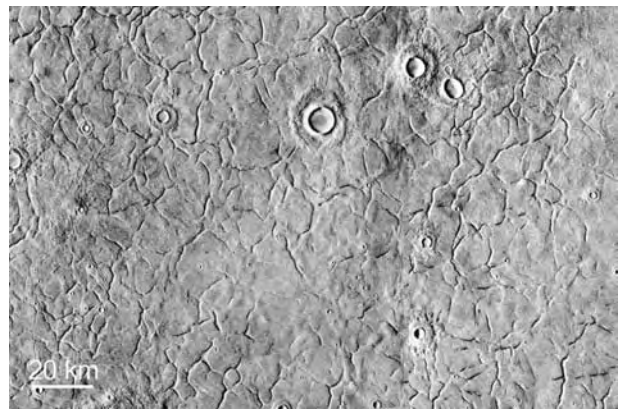

Figure 8.19. Coarse, polygonally fractured ground in the Utopia basin at 38°N, 103°E. The fractures are spaced too far apart to have formed by thermal contraction. They occur at the end of large channels where water may once have pooled. One possibility is that they formed as a result of extension caused by rebound after the water dissipated (Viking 573A10/12).

after removal of the water-ice load (Pechman, 1980; Heisinger and Head, 2001) or convection in water-saturated sediments (Wenrich and Christensen, 1996). So even though the fractures did not form in the same way as terrestrial ice-wedge polygons, they may still be indicative of ice.

Acquisition of higher resolution images has revealed that polygonally patterned ground with polygons similar in size to their terrestrial counterparts is common at high latitudes (Figure 8.20). The terrestrial-scale polygons appear not to be associated with the large-scale polygons and most appear to be in closed basins such as craters (Seibert and Kargel, 2001). Seibert and Kargel interpret these smaller polygons as either desiccation cracks or ice-wedge polygons and inferred, therefore, that they formed at times when the climate was such that liquid water could exist, at least temporarily, at the surface. It is not certain, however, that liquid water is needed to form polygonal ground. If the cracks are filled each winter with other materials, such as wind-blown sand, the same polygonal pattern might still result. Nevertheless, the fact the polygons are almost all found at high latitudes suggests that ice may be a requirement for their formation.

Figure 8.18. Lobate flows off the northwest flank of Olympus Mons at 22°N, 222°E. The outer scarp of Olympus Mons is at the lower right. The lobate flows appear to have originated near the scarp and spread over the adjacent plains, leaving a finely ridged deposit with local pits and elongate hollows (THEMIS mosaic).

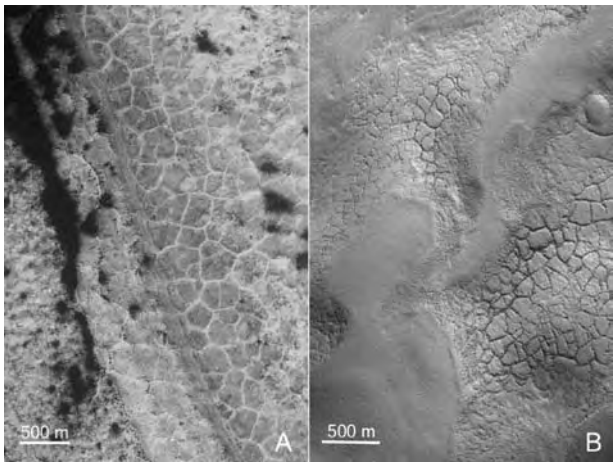

Figure 8.20. Polygons similar in size to polygons that form by freeze–thaw of terrestrial permafrost. (A) 81.8°S, 269.4°E (MOC R1001796). (B) 54.6°N, 33.2°E (MOC R1001555).

Thermokarst

In terrestrial permafrost regions, removal of ground ice can lead to collapse of the surface and formation of irregular depressions, commonly occupied by lakes. Further enlargement and merging of the depressions may lead to formation of irregular, flat-floored, steep-walled valleys. For collapse to occur, ice must be present in amounts in excess of the pore volume of the host materials. Terrain with irregular, shallow, steep-walled pits and valleys in southern Chryse Planitia has been interpreted as thermokarst (Carr and Schaber, 1977; Costard and Kargel, 1995). Irregular pits are also common in bedded sediments in the Utopia basin (Figure 8.21). Almost all the pitted areas in Utopia Planitia are, in addition, polygonally fractured. The basin location, the layering, the polygonal fracturing, and the pits all combine to suggest that waterlogged sediments once accumulated in the basin and later froze, setting the stage for subsequent development of polygonal ground and thermokarst features.

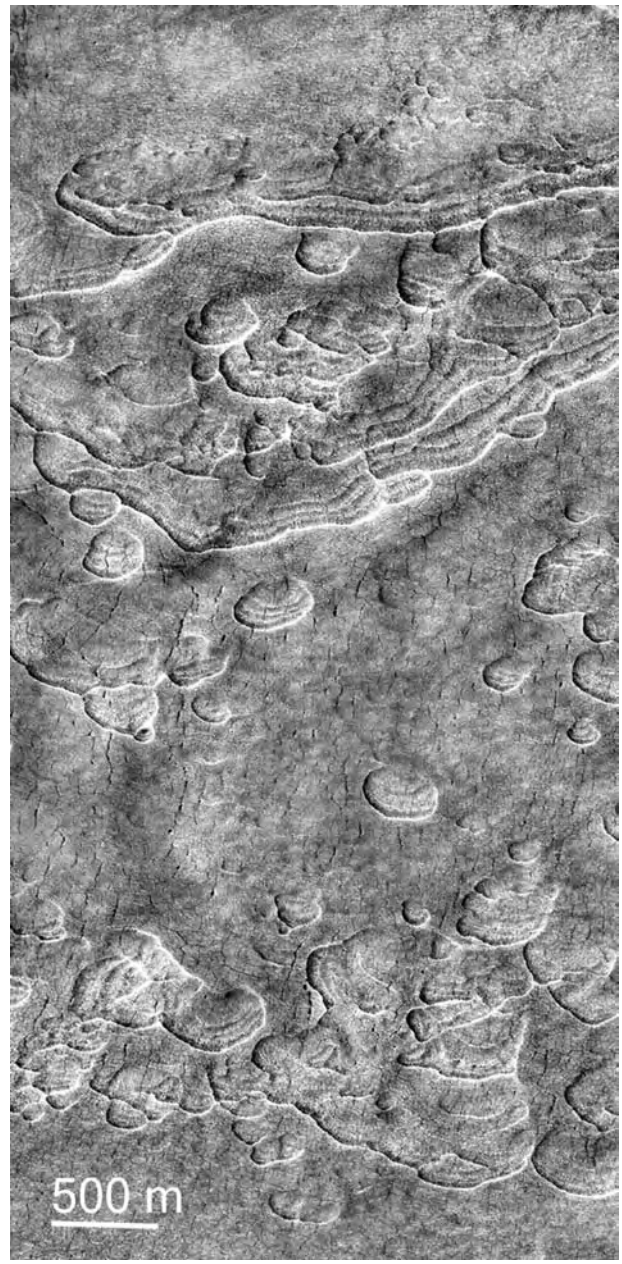

Figure 8.21. Hollows possibly created by sublimation of ice from ice-rich sediments in the Utopia basin at 46.2°N, 94.6°E (MOC M0203335).

Summary

Ice occurs in two reservoirs: (1) on the surface, exchanging with the atmosphere and the near-surface materials; and (2) deep within the surface as semi-permanent ground ice. Under present conditions, at latitudes lower than 40° ground ice is unstable at all depths below the surface; at latitudes higher than 40° it is permanently stable at depths below a few centimeters. We therefore expect ground ice to be present at high latitudes, and this has been confirmed by direct measurement. Small amounts of near-surface water or ice detected at low latitudes may be inherited from an earlier era when stability relations were different. During periods of high obliquity ice becomes stable at low latitudes, and water now frozen at the poles may be redistributed to lower latitudes. A thin deposit with a characteristic stippled texture, at the surface almost everywhere in the 30–60° latitude belt in both hemispheres, is thought to be the partly eroded remnant

of a surficial ice-rich layer deposited during a recent period of high obliquity.

Large fractions of ground ice in the fretted terrain of northern Arabia and other upland terrains at similar 30–60° latitudes have led to enhanced mobility of the near-surface materials and development of landforms not found at lower latitudes. These include a general smoothing of the terrain, formation of debris aprons at the base of all steep slopes, and accumulation of lineated fill in valleys. While ground ice appears to have played a major role in the formation of these features, surface ice may also have contributed. Polygonally patterned ground and local hollows at high latitudes may be additional indications of ground ice. Glaciers appear to have modified the western flanks of volcanoes in Tharsis and Elysium, and may have been active elsewhere. The glaciers may be another indication of the redistribution of surface ice during periods of high obliquity.

9 Wind

Wind is one of the few geological agents for change that has been seen in action at the martian surface. Local and global dust storms have been observed to wax and wane. Dust devils have been observed both on the ground and from orbit. Changes in the configuration of wind-created albedo patterns have been followed from year to year, and disturbances of loose debris at the surface have been noted both from orbit and on the ground. In addition, almost all high-resolution images taken from orbit show ripple-like features and dunes, clear evidence of pervasive wind activity. Yet it appears that the efficacy of wind in modifying the landscape is limited. The wind mostly redistributes loose or poorly cohesive material across the surface. Wind erosion of primary volcanic and impact terrains is mostly minor. The only parts of the surface that are significantly eroded by the wind are where poorly coherent, layered sedimentary rocks are present.

The cycling of fragmental debris that can be moved by the wind is very different on Earth and Mars. On Earth most of the rock debris of a size most easily moved by the wind is quartz sand, most of it originally derived by the mechanical and chemical breakdown of granitic rocks. The sand spends only a geologically short time on the land surface participating in eolian processes before it is transported to the oceans where it is buried and ultimately lithified and incorporated into the sedimentary rock record. Tectonic forces may then return the sand to the surface in sandstones and other rocks, so that the sand is reintroduced into the eolian regime. There is thus an inventory of materials that can be easily moved by the wind that is recycled on geological time scales. Finer-grained particles such as dust and clay also become rapidly incorporated into sediments, but are permanently removed from the eolian regime.

For Mars the situation is very different. First, quartz rich granitic rocks, if present at all, are minor components of the surface, so that any sand present is unlikely to be quartz. Second, although burial of fragmental debris in oceans may have occurred, it has been limited, at least since the end of the Noachian, and recycling of marine rocks to the surface by tectonic forces has not occurred. This implies that once fragmental material is produced at the surface it largely remains available to be moved around by the wind. As a consequence, much of the loose debris at the surface may be very ancient, having been inherited from the Noachian era when rates of volcanism, impact, and erosion, all of which could produce fragmental material, were much higher than they were subsequently. Later additions of loose debris to the surface inventory were probably modest, except locally in the vicinity of new impact craters. Thus, on Earth fragmental material is rapidly removed from the surface and incorporated into the rock record, whereas on Mars it remains at the surface for billions of years to be moved around by the wind. While thick sedimentary rock deposits did form on Mars, for example, the Medusae Fossae Formation and those at Meridiani Planum (Malin and Edgett, 2000b), they remain at the surface where they can still be affected by the wind. Some of the most spectacular examples of eolian erosion on Mars are from these deposits.

This chapter mostly concerns the effects of wind in the post-Noachian era. Eolian activity may have been very different during the Noachian when the atmosphere was probably thicker and liquid water was probably more common. But the Noachian eolian record is largely lost, or difficult to separate from later eolian effects.

Entrainment of particles by the wind

Material is transported by the wind either as a load suspended within the atmosphere, or by saltation, the bouncing of particles across the surface, or by creep, the slow, almost imperceptible movement of particles across the surface as they are impinged upon by other particles (Figure 9.1). For terrestrial conditions, and probably for Mars also, movement of particles larger than approximately 1000 μm is mostly by creep (Table 9.1). For particles in the 100–1000 μm size range, movement is mostly by saltation. Particles finer than 100 μm move mostly in suspension. The exact numbers depend on wind speed, surface roughness, and other factors such as vegetation. The three types of movement can result in efficient separation of

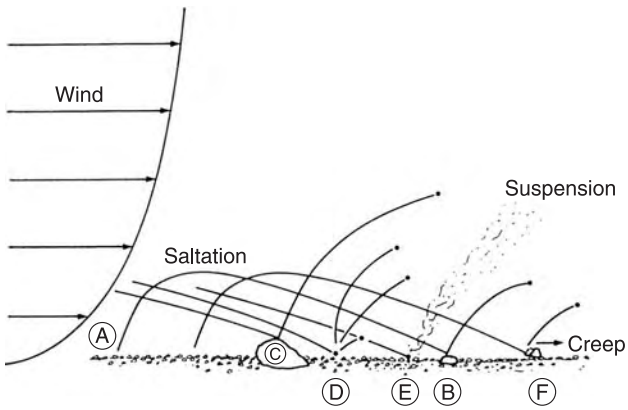

Figure 9.1. Different modes of grain transport. In saltation, wind shear causes grain A to lift off the surface and to be carried downwind to B where it bounces off the surface back into the air stream. At C a grain hits a rock, possibly causing some erosion, and lifting the grain high into the air stream on a long saltation trajectory. At E a particle dislodges material too fine-grained to saltate and lifts it into suspension in the atmosphere. At F a particle hits a small rock fragment and causes it to shift slightly downwind (from Greeley and Iverson, 1985, copyright Cambridge University Press).

particles of different sizes. Most terrestrial desert sand is in the 100−500 μm size range (Bagnold, 1941). Finer particles are carried away in suspension, coarser debris is left behind as a lag.

The ability of wind to dislodge and move particles around the surface depends on the particle size, the atmospheric pressure, the wind speed, and the roughness of the surface (Greeley and Iverson, 1985; Greeley *et al.*, 1992). When wind blows across the surface, a turbulent boundary layer develops in which the wind decreases from its free-stream value at high altitude to a much lower value right at the surface. If the surface is aerodynamically smooth, there may be a thin laminar boundary layer, a few millimeters thick, at the surface. Particles immersed in the laminar layer are difficult to entrain in the wind unless dislodged by more easily moved grains. With increasing surface roughness the laminar layer breaks down and ultimately ceases to exist. The entire boundary layer becomes turbulent and the velocity profile becomes

$$U/u^* = 2.5\ln(z/z_0)$$

where U is the wind velocity at height z, u^* is the surface friction speed, and z_0 is the equivalent roughness height (Greeley *et al.*, 1992). The roughness height is determined by measuring the wind speed at two elevations or more. Greeley and co-workers, using

Table 9.1. *Terminology and mode of transportation of particulates*

Size mm	μm	Terminology[a]	Dominant mode of eolian transport[b]
		Cobbles	
>64			
		Very coarse pebbles	
32			
		Coarse pebbles	
16			
		Medium pebbles	Stable?
8			
		Fine pebbles	Creep?
4			
		Granules	Creep
2	2000		
		Very coarse sand	Creep/ saltation
1	1000		
		Coarse sand	Saltation/ creep
0.5	500		
		Medium sand	Saltation
0.25	250		
		Fine sand	Saltation/ suspension
0.125	125		
		Very fine sand	Suspension/ saltation
0.063	63		
		Very coarse silt	Suspension
0.031	31		
		Coarse silt	Suspension
0.016	16		
		Medium silt	Suspension
0.008	8		
		Fine silt	Suspension
0.004	4		
		Very fine silt	Suspension
<0.002	<2		
		Clay/dust	Supension

[a]Adapted from Wentworth (1922) and Friedman and Sanders (1978).
[b]Adapted from Greeley *et al.* (1992).

wind tunnels that simulate martian conditions, have determined the winds needed to dislodge different-sized particles on Mars under different conditions. The results are summarized in Figure 9.2. The optimum size for dislodgement is 100 μm. Dislodgement typically requires a surface friction speed of $1-2\,\mathrm{ms}^{-1}$ and free-stream wind velocities (those above the boundary layer) of a few tens to hundreds of meters per second, depending on the surface roughness. The increase in wind speeds needed to dislodge particles smaller than 100 μm may be due in part to immersion of smaller particles in the laminar layer, and in part to the increased cohesion of smaller particles because of moisture and electrostatic effects.

The wind speeds required to raise dust particles $< 10\,\mu\mathrm{m}$ in diameter simply by wind shear, as described above, are so large that they are probably only rarely achieved. Yet dust is commonly raised into the atmosphere, so other effects must be involved. Among the suggestions are (a) dust fountaining by desorbed CO_2 and H_2O, (b) clumping of dust grains to form larger, more easily moved particles, (c) raising of dust by impacts of larger particles, and (d) dust devils (Greeley *et al.*, 1992). Dust devils appear to be an efficient dust-raising mechanism. They were first observed in Viking images (Thomas and Gierasch, 1985) and subsequently were filmed by the Spirit rover in Gusev crater (Greeley *et al.*, 2006). In addition, large areas of the martian surface are crossed by dust devil tracks (Figure 9.3) whose pattern changes from year to year (Malin and Edgett, 2001). Dust devils are common in several regions including Amazonis Planitia, Cimmerium, Sinai, and Solis (Fisher *et al.*, 2005). Experimental data shows that the raising of dust by dust devils is fundamentally different from the dislodgement of larger particles by wind shear, since dust can be raised when the unidirectional winds are very gentle (Greeley *et al.*, 1981). A primary factor in raising dust particles by dust devils may be the transient difference in atmospheric pressure experienced by the top and bottom of the particles as the dust devil passes over the surface. This results in lifting of the particle into the winds of the dust devil's vortex.

Dust storms

Dust storms on Mars have been observed for centuries (Kahn *et al.*, 1992). They tend to recur in southern spring and summer. Most are regional in

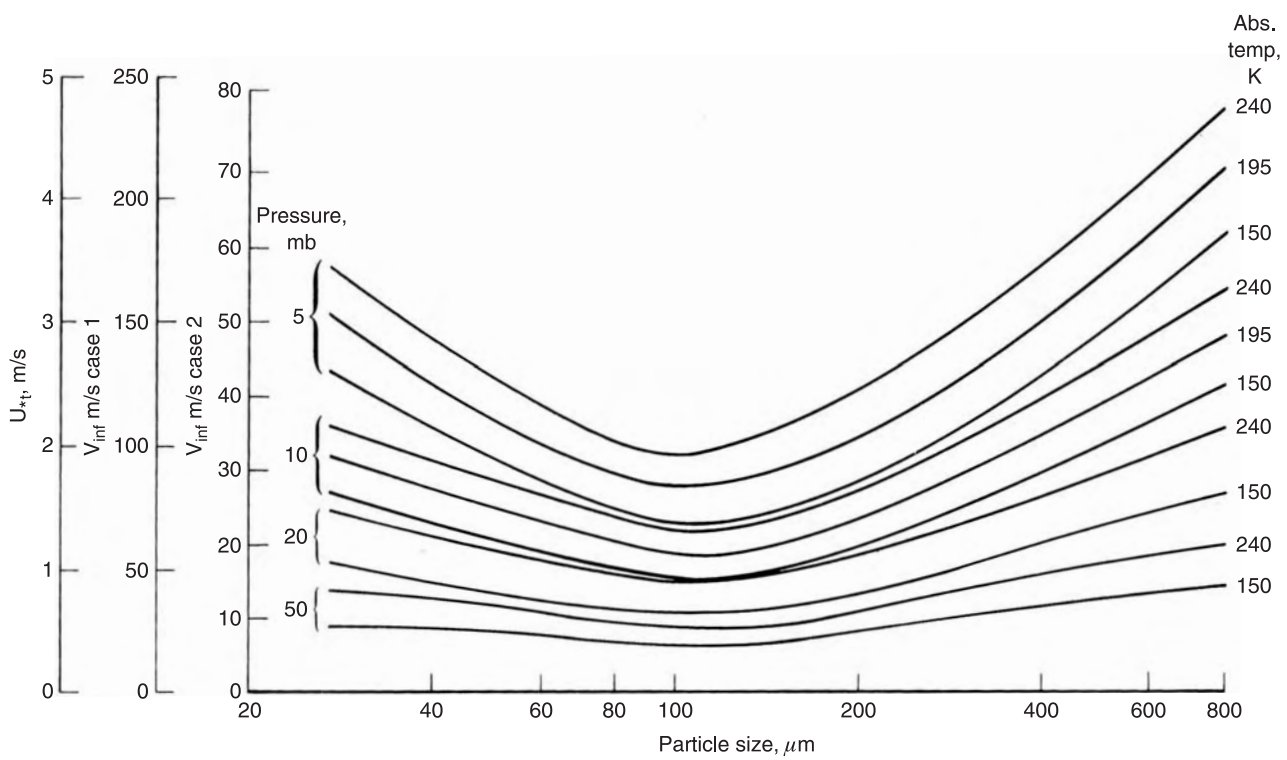

Figure 9.2. Threshold wind speeds for dislodgement of particles of different sizes as a function of atmospheric pressure and temperature. Wind is given as a surface friction speed and as the free-stream value above the boundary layer for two cases. Case 1 is for a flat surface of erodible grains, case 2 is for a surface with cobbles and boulders (from Greeley *et al.*, 1980).

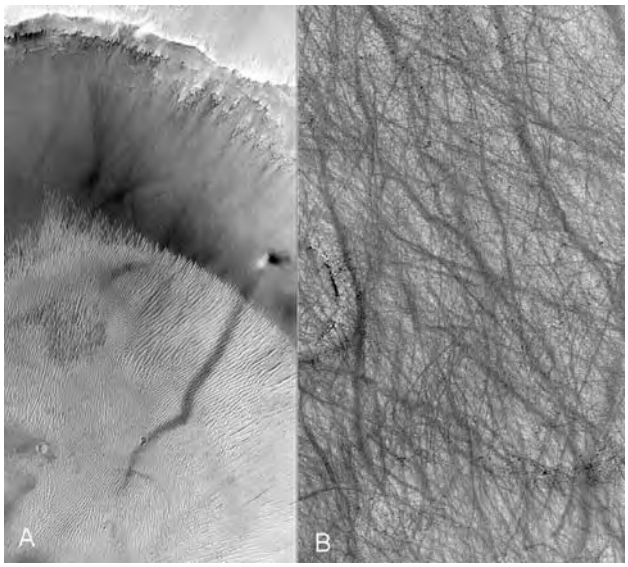

Figure 9.3. Dust devils. (A) A dust devil climbing up the wall of a crater at 4.1°S, 350.5°E. Megaripples cover the floor of the crater (MOC E1601487). (B) Dust devil tracks at 59.6°S, 31.2°E (MOC 2-541). Both images are 3 km across.

extent, but in some years, as in 1971, they become truly global. Favored places for recurrence of dust storms are the edge of each polar cap and the 10–30°S latitude band. Other favored regions are Hellas, the Noachis uplands to the west of Hellas, Argyre, and the Solis–Syria–Sinai Planum region in the southern hemisphere and Chryse–Acidalia, Isidis–Syrtis, and Cerberus in the northern hemisphere.

The geological significance of the dust storms is unclear. The observational effects, such as obscuration of the surface by dust in the atmosphere and changing the surface albedo patterns, are substantial (Figures 9.4, 9.5). Geissler (2005) shows that more than one-third of the planet's surface has brightened or darkened by at least 10 percent during the era of spacecraft observations. All of the changes are consistent with burial of rocky surfaces by thin dust layers deposited during dust storms and subsequent exposure by removal of the dust. Nevertheless, the amount of dust involved in the dust storm is small, equivalent to a surface layer of only a few micrometers thick even for the largest storms (Kahn *et al.*, 1992). Most of this material is probably recycled with each new storm.

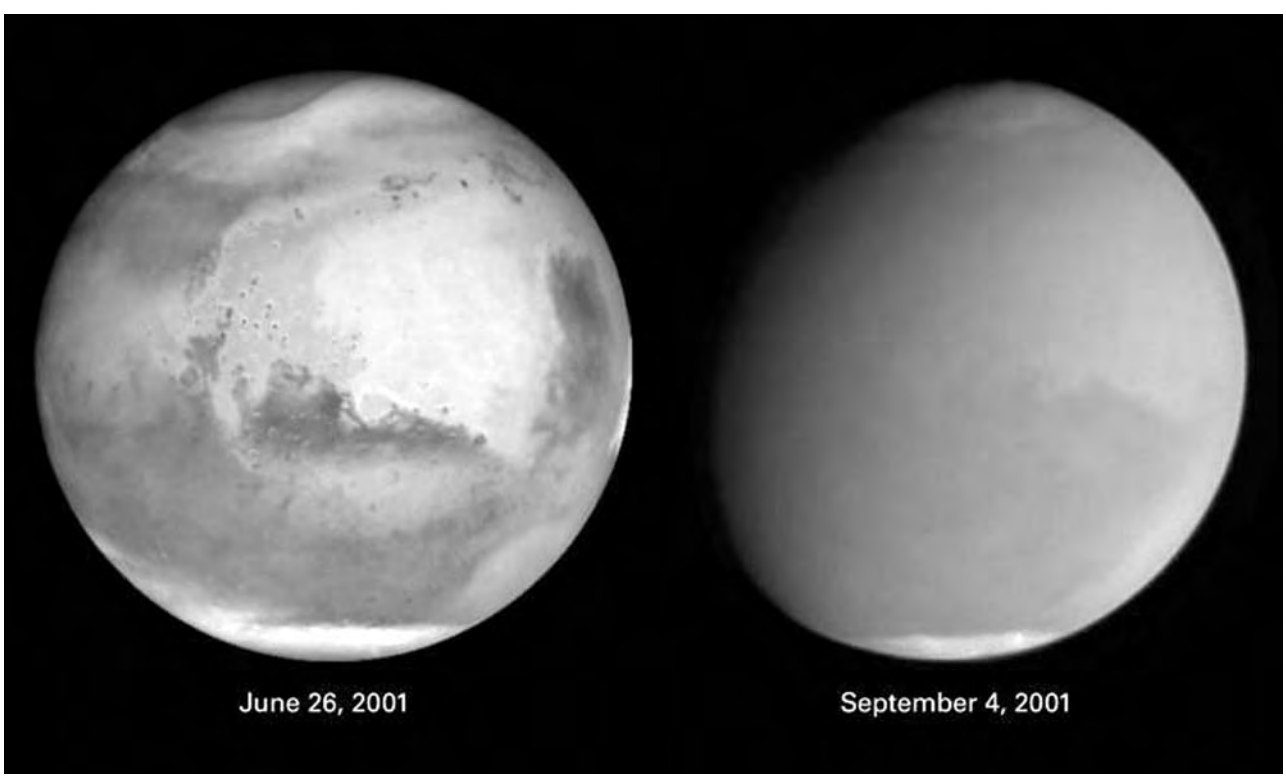

Figure 9.4. Hubble Space Telescope image of Mars before and during the 2001 global dust storm. The image is centered at 10°E longitude. The storm started in southern spring in Hellas, just visible in the lower right, and spread over the rest of the planet (see next image).

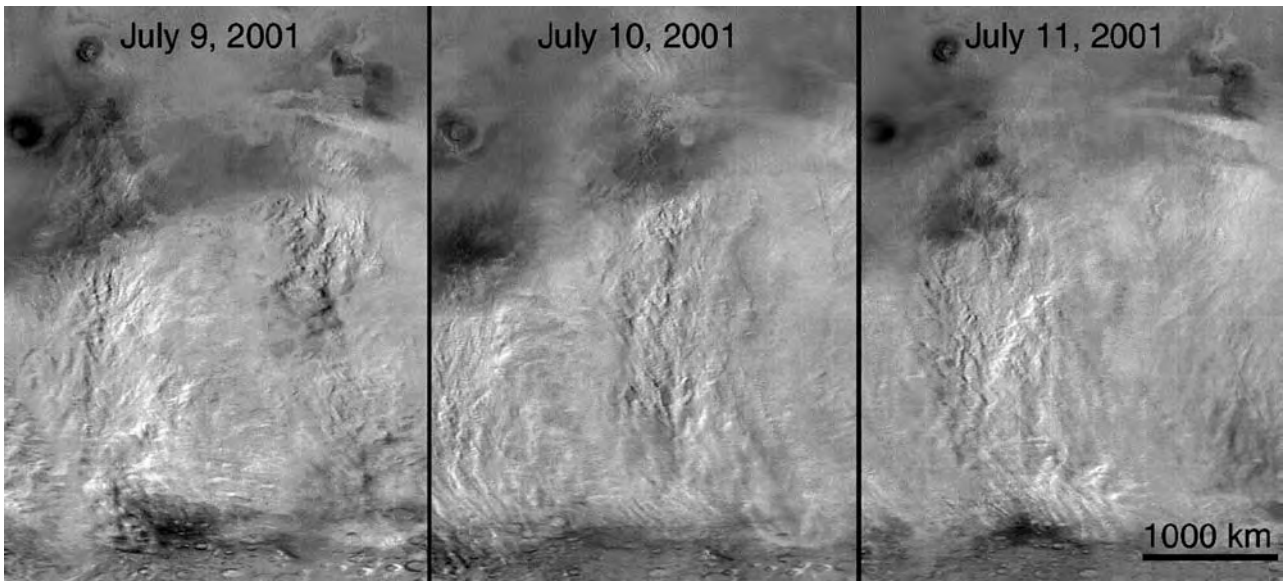

Figure 9.5. 2001 dust storm spreading northward across Sinai Planum. Arsia Mons and Pavonis Mons are visible as dark circles in the upper left of each image. The western sections of the canyons appear bright to the north of the main storm front (MOC 2-291).

Of more geological interest is whether the storms result in net transport from region to region. Despite changes observed during the last few decades, the face of Mars has not changed dramatically over centuries of telescopic observations. Two dust sinks have, however, been proposed. One possibility is that, in the present era, dust is incorporated into the northern CO_2 cap, which is typically growing during the dust storm season (Pollack *et al.*, 1979). Subsequent sublimation of the cap may then leave behind dust that is incorporated into the residual cap and ultimately the polar layered terrain. Although there is little observational evidence for a dusty residual cap, the layered deposits at the poles indicate that the poles must be a long-term sink for dust. The volumes are unclear because of a poor understanding of the relationship of polar layered terrain brightness variations and actual dust contents. The bright, low thermal inertia regions of Tharsis, Arabia, and Elysium are a second possible sink. Their low thermal inertia indicates that they may have a meter or two of dust at the surface, but the radar characteristics indicate that the surface is still rough. Christensen (1986) suggested that wind removes dust from dark regions such as Syrtis Major and the dust then becomes trapped in the rough lighter regions.

Wind streaks and tails

Wind streaks are elongate albedo markings downstream of topographic obstacles, particularly craters (Figure 9.6). Wind tails is the term given to accumulations of debris downwind of rocks observed from landers on the surface. Four types of wind streaks have been recognized: bright depositional streaks, dark erosional streaks, dark depositional streaks, and frost streaks (Greeley *et al.*, 1992, 1999, 2004).

Bright depositional streaks are the most common. They form downwind of craters and positive relief features, mostly at low southern latitudes and in the northern plains. Most are stable, but those in Tharsis and Elysium show seasonal changes. Their directions correlate well with wind directions predicted by general circulation models for the dust storm season (southern spring and southern summer). They probably form mostly by deposition of dust in the waning stages of dust storms. If so, they may be just a thin veneer, no more than a few tens of micrometers thick. Other bright streaks, however, must be thicker accumulations since they affect the thermal inertia of the surface (Zimbelman and Greeley, 1982). These may be more akin to the wind tails observed at landing sites, which are centimeter to meters thick and typically brighter than their surroundings.

Dark erosional streaks also form downwind of obstacles, but are more restricted in location than the bright streaks. Most form in late southern summer and fall and are obliterated in the following dust storm season. Both dark and light streaks can form from the same obstacles. The dark streaks probably

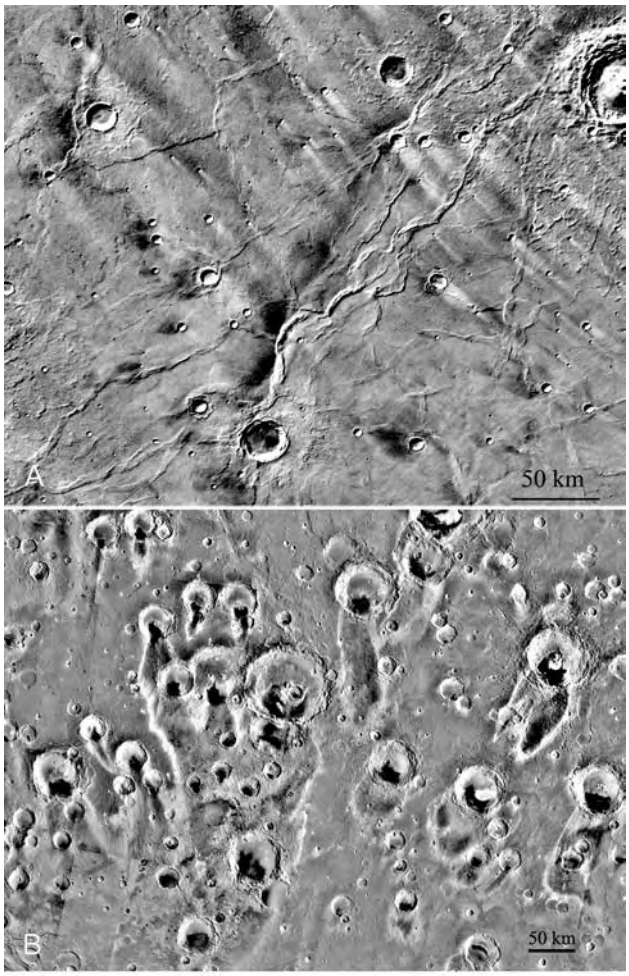

Figure 9.6. Wind streaks. (A) Bright and dark streaks at 25°S, 110°E in Hesperia Planum. The bright streaks are elongate; the dark streaks are irregularly shaped and occur downwind of mare ridges as well as craters. (B) Dark depositional streaks in Oxia Palus at 10°N, 350°E. Almost all the streaks start at dark accumulations within craters (MDIM2).

form when turbulence downstream of topographic obstacles scours away dust that was deposited during the waning phases of the previous dust storm.

Dark depositional streaks form downwind of sedimentary deposits, usually sand dunes inside craters. Thermal inertias indicate that they are composed of sand-sized particles. Some lengthening of such streaks in the Oxia Palus region in the late 1970s indicates that saltation of sand-size particles had occurred (Thomas and Veverka, 1979). They are commonly more irregularly shaped that the other streaks. Frost streaks are accumulations of CO_2 frost downwind of obstacles.

Many slopes, particularly in dust-mantled regions at low latitudes, have dark streaks that extend downslope (Aharonson *et al.*, 2003). They appear to be forming today (Malin and Edgett, 2001). Fresh streaks are dark and they become lighter with age until they merge with the background (Figure 9.7). They clearly result from slope failure, which temporarily removes the light near-surface dust on the affected part of the slope. Wind may not be involved. They are referred to here merely for comparison.

Dunes, ripples, and drifts

The terminology that has been used for eolian depositional landforms is somewhat confusing. Accumulations of wind-blown debris can occur in a wide range of sizes from centimeters across to kilometers across. The term "ripple" refers to accumulations that have wavelengths in the centimeter to a few meters size range, and is used for both free-standing accumulations and for features on the surface of other eolian landforms such as dunes. Greeley and Iverson (1985) use the term "megaripples" for linear, parallel ridges of fragmental material that are in the few meters to 25 m wavelength range. They restrict the term "dune" to accumulations that are greater than 25 m across. Although size is used to define the features, ripples, megaripples, and dunes may differ in origin and not be simply different-size features that grade into one another.

According to Bagnold (1941), ripples form as saltating particles exploit chance irregularities of a surface composed of granular materials. Wind-facing slopes are eroded by the saltating particles, and lee slopes are protected. As a result the ripple moves downwind with a wavelength controlled by the saltation path length. In an alternative model, Sharp (1963) suggested that ripple height may be a more important factor in controlling ripple wavelength than saltation path length since it controls the effectiveness of the ripple as a barrier to saltating particles. Ripple height also affects the wind speed at the ripple crest and hence erosion of sand from the crests. Ripples form mostly on dunes where there is a monomodal supply of sand-size particles.

In contrast, the larger megaripples form where there is a bimodal distribution of particles and the winds are strong enough to move the fine particles but not strong enough to move the coarse particles (Greeley and Iverson, 1985). The result is a lag concentration of coarse grains on the surface with the coarsest grains at the megaripple crest. The wavelength of megaripples is probably controlled more by aerodynamic effects than by saltation path length.

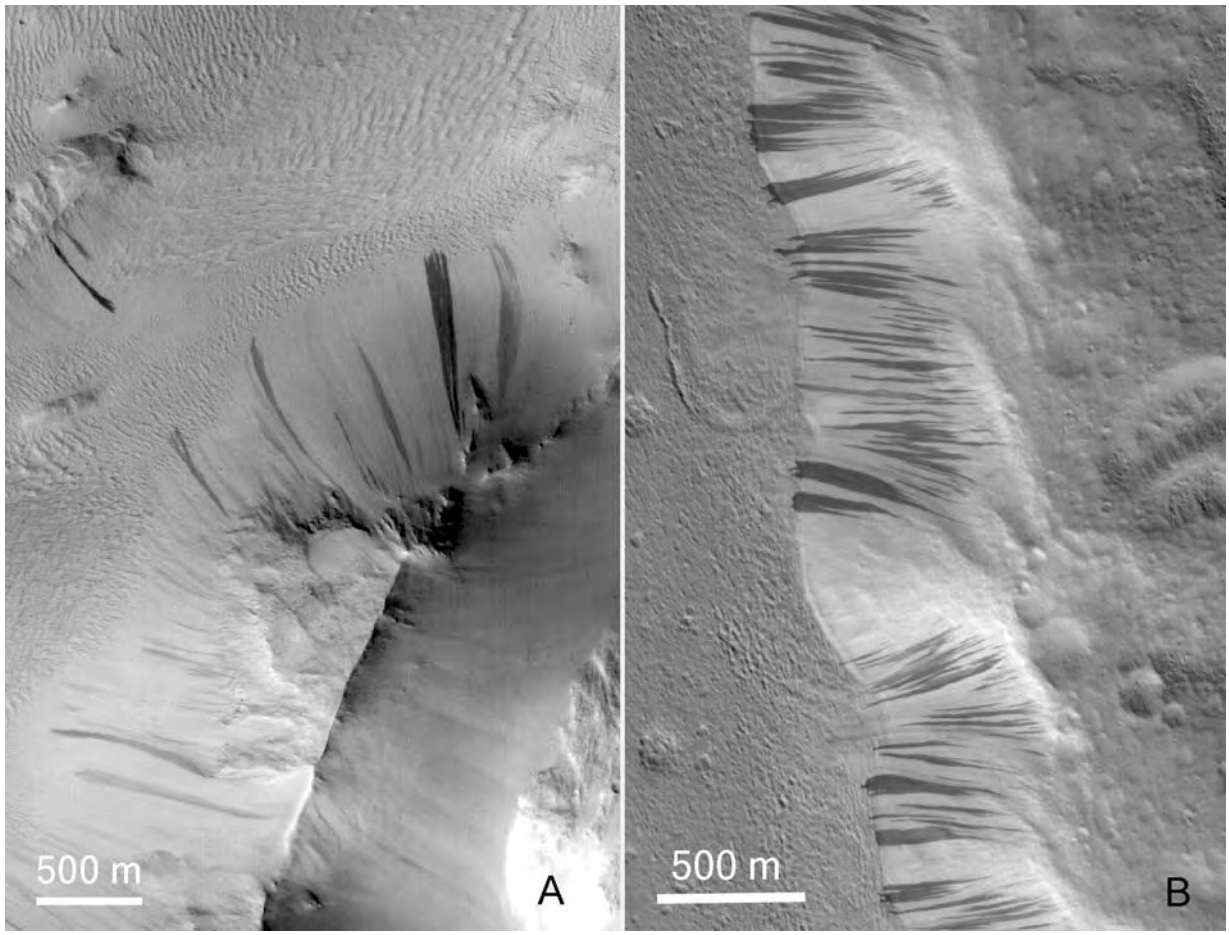

Figure 9.7. Slope streaks. Steep slopes in terrain with low thermal inertia at low latitudes commonly have darks streaks that indicate recent slope failures. They are distinctively different from wind streaks. (A) Slope streaks in the Olympus Mons aureole at 27°N, 227°E (MOC M-16-00596). (B) Slope streaks at 37.5°N, 229°E. Illumination is from the lower left (MOC 513-01131).

On Mars, megaripples are more widespread than true dunes. They are visible in almost all images with resolutions of a few meters per pixel or better (Figures 9.8, 9.9). They are particularly common in low areas such as inside craters and on valley floors. In contrast to dunes, megaripples are mostly lighter than their surroundings.

Terrestrial dunes typically form where accumulations of sand exceed 4–6 m across and 30 cm in height (Bagnold, 1941). The sand particles saltate up the windward slopes and cascade in avalanches down the lee slopes. The sand is usually unimodal in size. Dunes are common in orbital images of Mars. They have a wide variety of forms that are similar on both Earth (McKee *et al*., 1979) and Mars (Greeley and Iverson, 1985; Malin and Edgett, 2001). The morphology is controlled largely by the wind patterns, the availability of sand, and on Earth, stabilizing factors such as vegetation and moisture (McKee *et al*., 1979). The most common and best-known dune type is the crescent-shaped barchan dune (Figures 9.10, 9.11). It has a shallow (5–15°) windward slope up which the wind-driven particles saltate, and a steep (30–32°) lee face down which the particles avalanche. Two lateral horns point downwind. If sand is abundant the barchans may merge to form ridges transverse to the wind. If the ridge crest is wavy, it is referred to as a barchanoid ridge. If it is linear it is usually referred to as a transverse dune (Figure 9.12). These three dune types – barchans, barchanoid ridges, and transverse dunes – are sometimes called simple dunes because they have only one slip face, a consequence of a constant wind direction. A variety of different shaped dunes may develop from the basic barchan

Figure 9.8. Megaripples. Dune-like forms less than 25 m across are referred to as megaripples. Those here are light-toned and less than 20 m across (MOC 1002671). (A) Isidis Planitia at 18.2°N, 87.4°E. (B) Megaripples on a valley floor at 29°N, 60°E (MOC 1200991).

type (Figure 9.13). The horns on one side may lengthen so that an array of barchans may transition into linear longitudinal dunes. The two horns may wrap around the main body of the barchan to form a single, downwind-pointing extension. Such variants typically develop because of variable wind directions.

Other dune forms may result if the wind comes from several directions. Long linear dunes or seif dunes have slip faces on both sides, and are thought to result from wind from two directions at angles $< 90°$ to each other. The dune bisects the angle between the two directions. Star-shaped dunes, with several arms and slip faces with different orientations, may form if the wind comes from several directions, and reversing dunes may form with opposing winds. All these different kinds of dunes may merge to form complex patterns.

On Mars dunes are most common around the northern polar cap where there are vast arrays of barchans and transverse dunes, mostly spaced 300–800 m apart. Dunes are also common in mid-southern latitudes (40–50°S), where they form clusters, mostly within craters. Lancaster and Greeley (1990) recognized two types of clusters. The first type consists of transverse dunes 100–1200 m apart, some surrounded by a dune wall or rampart. In the second type of cluster the dunes are also mostly transverse ridges but are spaced further apart (1600–4000 m) and tend to intersect to form rectilinear patterns. Barchan dunes are common around the periphery of the clusters. The dunes of both types usually have a low albedo.

Drift is a term that is normally used for accumulations of material in the lee of obstacles. It was, however, used in reference to the large dune-like hills

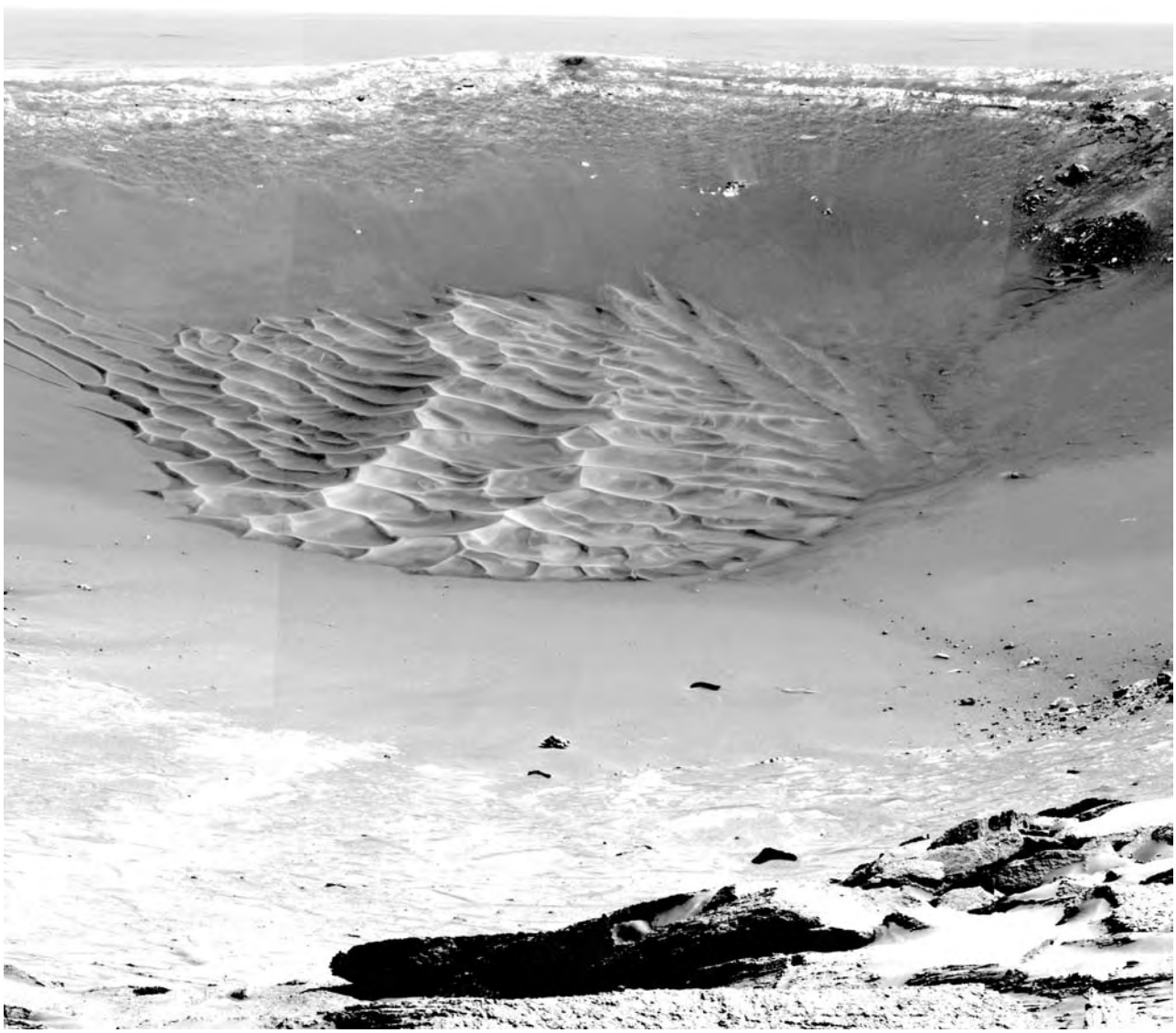

Figure 9.9. Megaripples in Endurance crater at the Opportunity landing site. The field is 30 m across and the individual ripples have a wavelength of 2–3 m. The rover is on the south rim, which is just visible in the foreground. The north rim is in the background beyond the dune field.

seen at the Viking 1 site, which are not in the lee of any obvious obstacles (Figure 9.14). One reason for a reluctance to call these hills dunes was the unknown size of the constituent particles. The term "dune" is normally restricted to accumulations of sand-sized particles, and by implication accumulations that form mainly by saltation. The drifts at the Viking 1 site were initially thought to be composed of very fine-grained material in the 1–10 μm size range rather than the 100–500 μm size range typical of saltating particles, so the more neutral term "drift" was used. The large drifts at the Viking landing sites are not moving but rather undergoing erosion, since bedding is visible in several places.

Although there are still uncertainties, basaltic fragments appear to constitute the bulk of the megaripples, dunes, and drifts. The source of the loose debris that formed the drifts at the Viking landing sites was an issue after the Viking mission. On Earth, most dunes are of quartz sand. The quartz is derived mostly

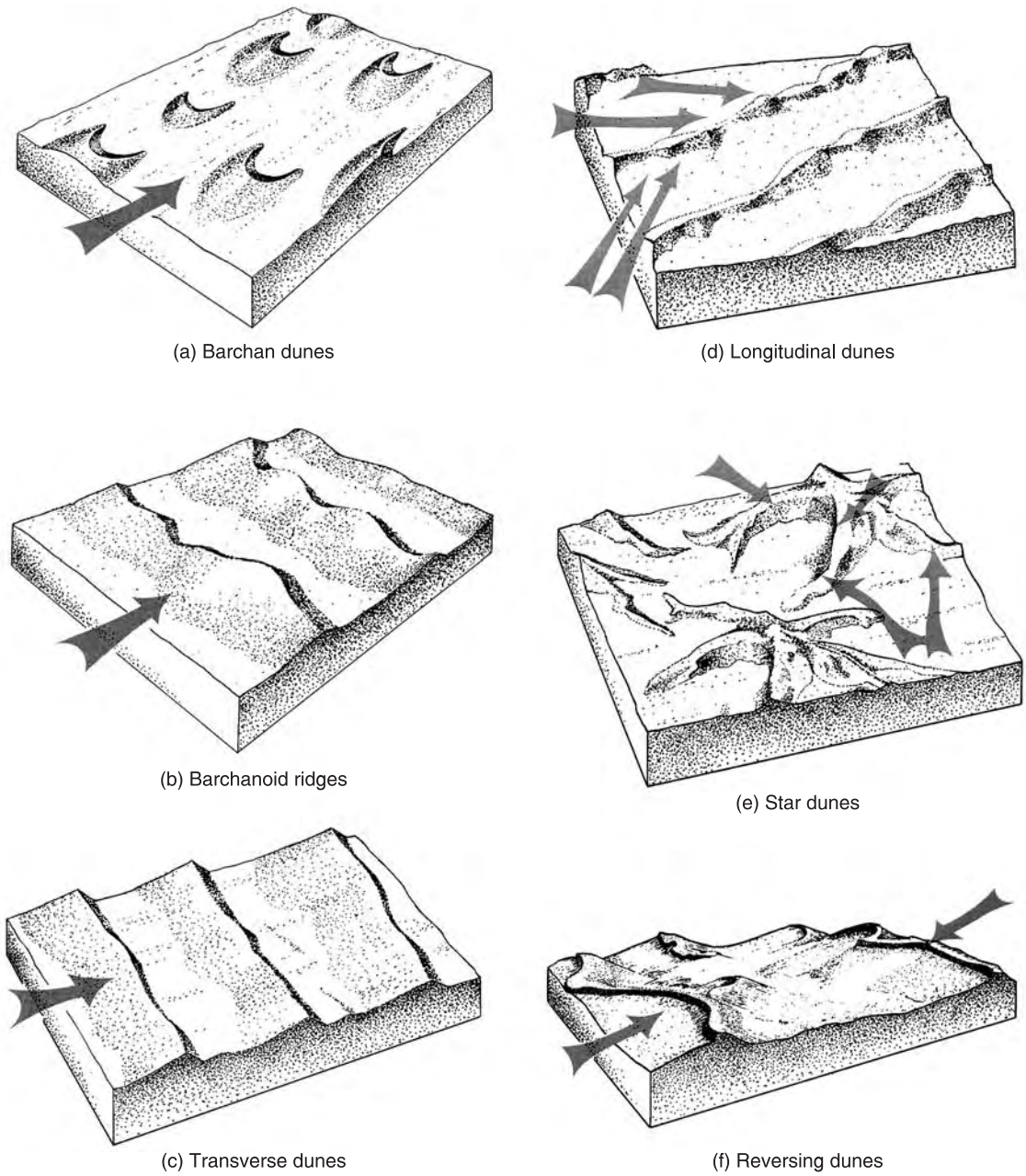

Figure 9.10. Different types of dunes. Simple dunes on the left have a single slip face and form where winds are from one direction. Complex dunes on the right have multiple slip faces and form where winds are from different directions (from McKee *et al*., 1979).

from continental granitic rocks, of which there are none on Mars that we know of. The loose debris in the vicinity of the Viking sites was interpreted to be fine-grained (1−10 μm) alteration products such as nontronite, an iron-rich clay, or palagonite, a poorly crystalline hydrated basaltic alteration product. The nontronite and palagonite appeared to be too fine-grained to saltate and too soft to survive as coherent sand grains even if they could. Various other possibilities were suggested, such as that the drifts were composed of aggregates of fine particles, cemented by salts or frost, or that they were not true dunes that formed by saltation. This is now less of an issue. We now know that the dark, loose materials beneath the surface veneer of dust at both MER landing sites are composed mostly of primary basaltic minerals.

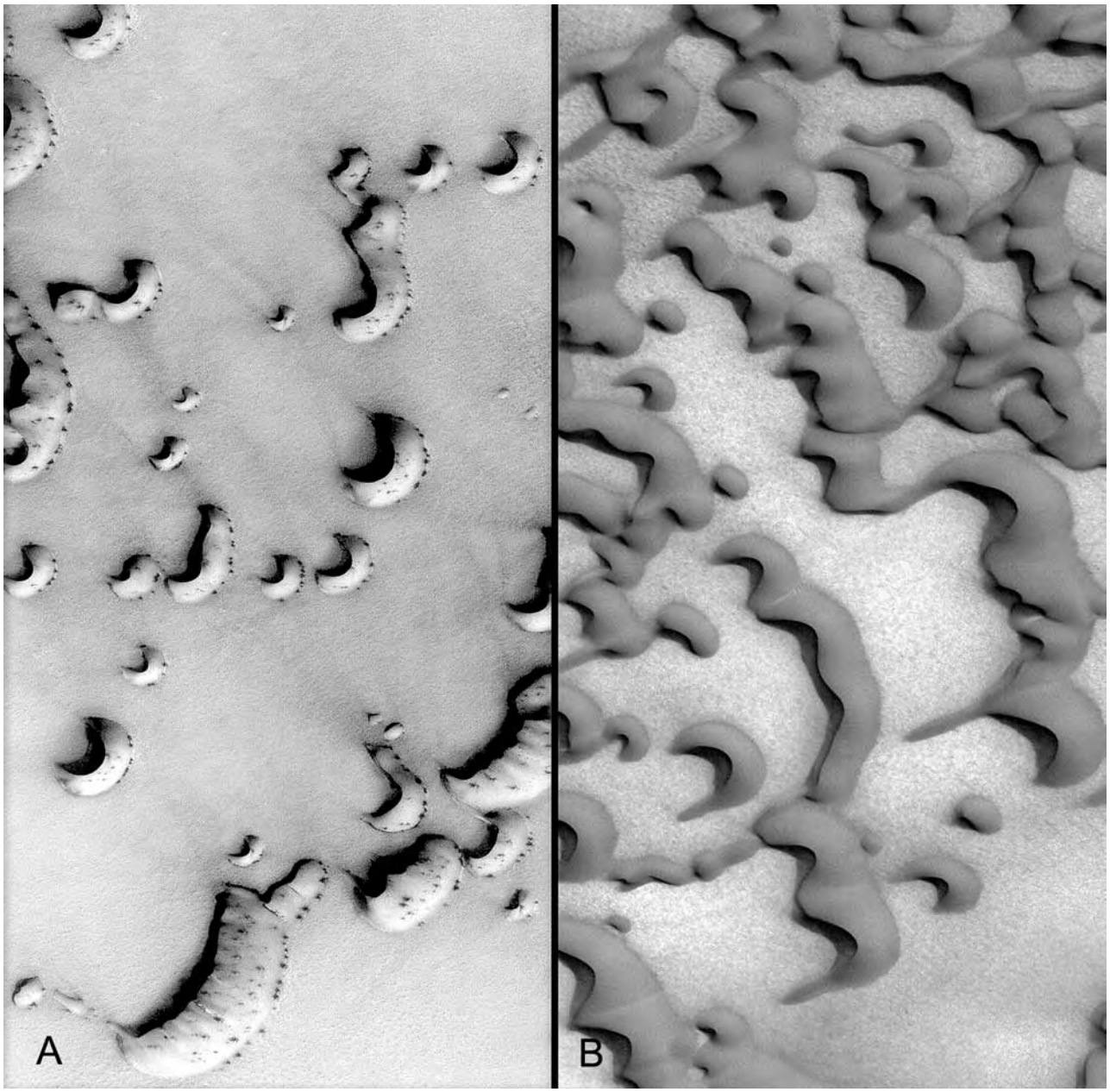

Figure 9.11. Barchanoid dunes in the north polar erg. (A) Frost-covered dunes at 76.0°N, 93.8°E. The dunes appear spotted as they are just beginning to lose their winter frost cover. Illumination from the lower right (MOC R1600306). (B) Defrosted dunes and ridges at 76.6°N, 10.1°E. Illumination from the upper right (MOC M0001460). Both images are 3 km across.

The dunes and other eolian landforms that form elsewhere on Mars are probably also formed largely of these minerals or fragments of basaltic rock. Sulfate-rich particles may also be present as they are in the fossil dunes at Meridiani, which are interpreted to be sulfate-cemented muds from playa deposits (Grotzinger *et al*., 2005; McLennan *et al*., 2005).

Thus, dunes and dune-like landforms are common on the surface of Mars, more common than on the Earth and a natural result of surface winds and the abundant availability of clastic debris, particularly sand-sized particles.

Regional eolian deposits

While dunes and megaripples are common features almost everywhere on the martian surface, they probably represent only a small fraction of the total inventory of fragmental material at the surface.

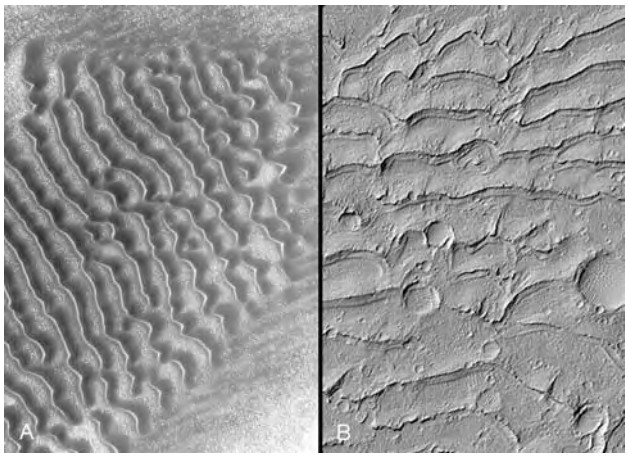

Figure 9.12. (A) Transverse dunes at 47°S, 40.2°E. Wind is from the upper right (MOC R0902524). (B) Fossil transverse dunes at 12.5°S, 359°E. Impact craters preserved on the dunes indicate that these dunes have not moved for millions of years (MOC 2-204). Both images are 3 km across.

There are two other major reservoirs. The first is the polar layered deposits, discussed in Chapter 10; the second is the Medusae Fossae Formation, and other similar deposits (Figures 9.15, 9.16). The Medusae Fossae Formation is by far the thickest and most extensive deposit of possible eolian origin outside the polar regions. The term refers to thick layered deposits that straddle the plains–upland boundary at several locations along the equator between 130 and 240°E (Scott and Tanaka, 1986; Greeley and Guest, 1987). In places the deposit is several kilometers thick. Their total volume is estimated to be $2 \times 10^6\,km^3$, enough to cover the entire planet to a depth of 7 m (Hynek *et al.*, 2003). The deposits have in places been eroded to expose layers and exhume craters. Mesas of layered rocks, mounds of sediments in craters, pedestal craters, and other features around the periphery of the deposits indicate that the deposits have shifted in location in post-Noachian times. The deposits appear to be massive accumulations of loosely cemented, fragmental debris that have, over geological time, been successively reworked by the wind, so that in some areas the deposits appear freshly deposited, in other areas the deposits are deeply eroded, and in yet other areas only scattered remnants of the deposits remain.

The origin of the unit is uncertain. Scott and Tanaka (1986) and Hynek *et al.* (2003) suggested that the Medusae Fossae Formation is a sequence of volcanic ash deposits, or ignimbrites. The suggestion was made mainly because of the proximity of most of the deposits to the volcanic provinces of Tharsis and Elysium. Because of their resemblance to polar layered deposits, Schultz and Lutz (1988) alternatively suggested that these and similar layered deposits elsewhere are former polar deposits. They suggested that, over time, the positions of the martian poles had changed, and that these deposits traced the former path of the poles. Another possibility is that they are accumulations of friable, fine-grained materials from a wide variety of origins such as impacts, volcanism, and erosion. As suggested in the introduction to this chapter, any such materials, irrespective of their origin, may simply accumulate at the surface and become redistributed by the wind as wind regimes change. High rates of impact, volcanism, and erosion during the Noachian may have left large volumes of fragmental debris at the surface, which over time has accumulated into these thick piles of friable, easily erodible sediments. A similar deposit at Meridiani Planum, like the Medusae Fossae Formation, unconformably overlies the dissected cratered uplands, and appears to be composed largely of wind-deposited materials derived from playa deposits (Chapter 11).

Elsewhere, both within the uplands (Figure 9.17) and the plains (Figure 9.18), etched terrain and pedestal craters indicate that surface layers have been partly removed by the wind. The source of the material that makes up these deposits is unknown, but some form of airfall appears likely. Particularly large areas of etched terrain occur northwest of Isidis Planitia and around the Meridiani deposits on which Opportunity landed. Pedestal craters also suggest that large areas of the northern plains were at one time covered with a layer of friable material that has since been removed except around the craters to form the pedestals. Thus, while dunes and megaripples are observed in almost every region of the planet, they may represent only a small fraction of the inventory of movable fragmental debris at the surface. The bulk of the fragmental debris is in the form of thick deposits such as the Medusae Fossae Formation and the Meridiani Planum deposits, and widespread, partly eroded, sheet-like deposits both in the uplands and the northern plains.

Wind erosion

Wind erosion has left little recognizable imprint on primary volcanic and impact surfaces. Fine features of volcanic flows and impact crater ejecta are commonly preserved despite exposure to billions of years of wind erosion. The main imprint of the wind has been on sedimentary deposits, such as those just discussed. Wind erosion is recognizable by a general sculpting of the surface into curvilinear forms or by distinctive patterns left by removal of layers. Some of the best examples of wind erosion are from the

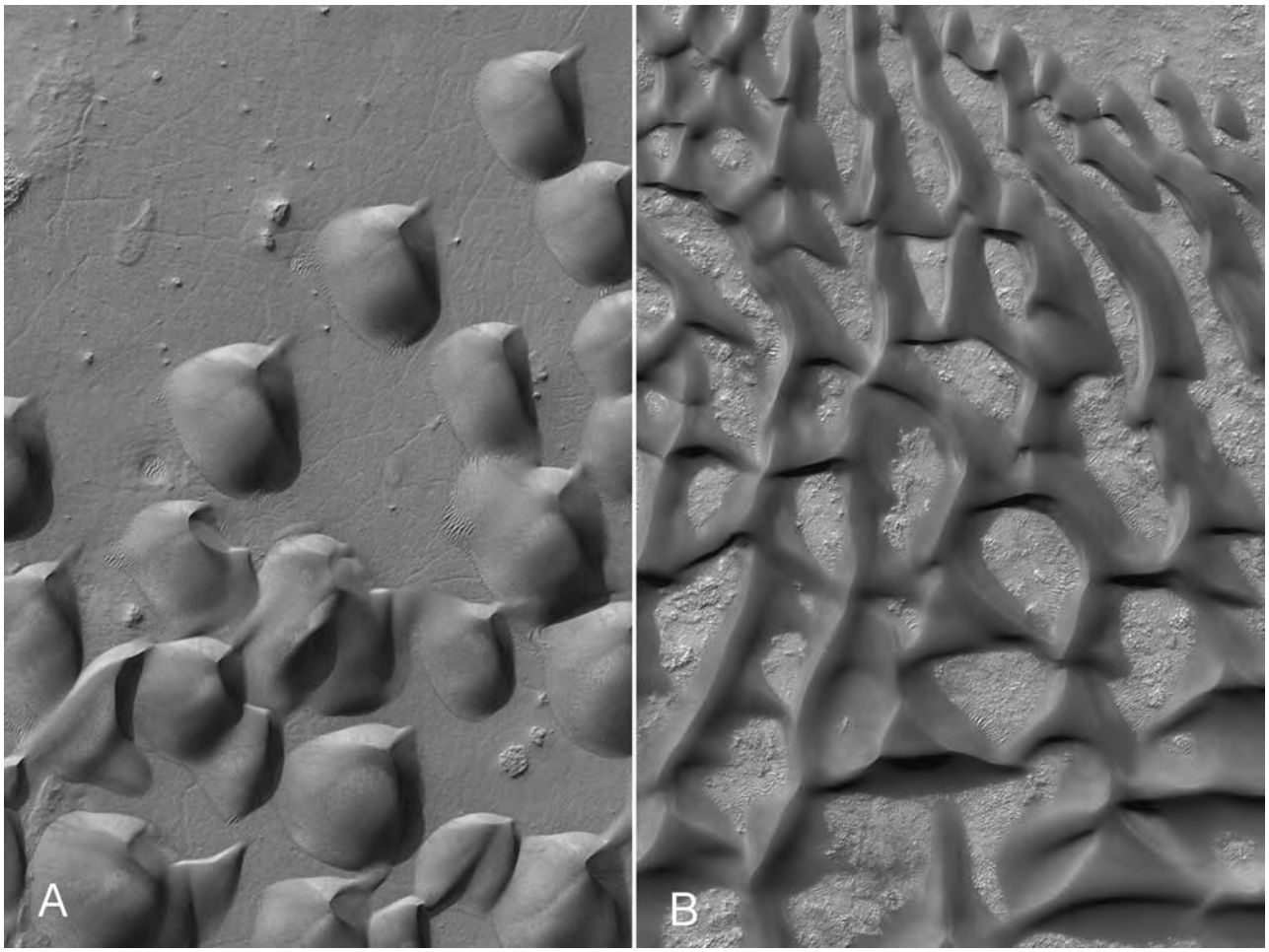

Figure 9.13. Odd dunes. Not all dunes fit the categories illustrated in Figure 9.10. In (A), sand mounds at 48.6°S, 334.5°E have a downwind ridge that may have formed by fusion of the two horns of a barchan-like dune. Illumination is from the top (MOC E2100192). (B) Overlapping star-shaped dunes at 33.8°S, 311.1°E with steep lee slopes facing in different directions. Illumination is from the left (MOC M2200197). Both images are 3 km across.

Medusae Fossae Formation. Whatever the original origin of the materials that form the formation, they have been extensively reworked by the wind. Wind has carved intricate patterns into the surface (Figure 9.19) and exposed formerly buried craters. Similar patterns are observed on sedimentary deposits in the canyons and in some large craters, a prominent example being ''White Rock'' in Pollack crater (Figure 9.20). As mentioned in the previous section, wind has also deflated large areas of both the uplands and the northern plains, where easily erodible sediments were or are present at the surface. The process has exhumed craters buried by the sediments and left behind rampart craters and etched remnants of the surface layers. Less common in the northern plains are local hollows that have probably been excavated by a combination of sublimation of ice and removal of material by the wind (Figure 8.21).

Despite the low erosion rates on coherent rock surfaces, the effects of wind erosion are commonly seen on individual rocks (Figure 9.21). Bridges (1999) pointed out that about half the rocks at the Pathfinder landing site show evidence of wind abrasion to form ventifacts, with a variety of forms including faceted edges, flutes, grooves, and finger-like projections. Evidence of abrasion is also common on the cohesive basaltic rocks of the Gusev plains (Greeley *et al.*, 2004).

Summary

Wind mostly redistributes loose or poorly cohesive material across the surface. The optimum

Figure 9.14. Drifts at the Viking 1 landing site in Chryse Planitia. Many of the small rocks in the foreground have tails that suggest winds from upper left to lower right. Bedding is visible in some of the larger drifts, suggesting that the drifts are not presently moving but are instead undergoing erosion. The large rock on the left is 2 m across.

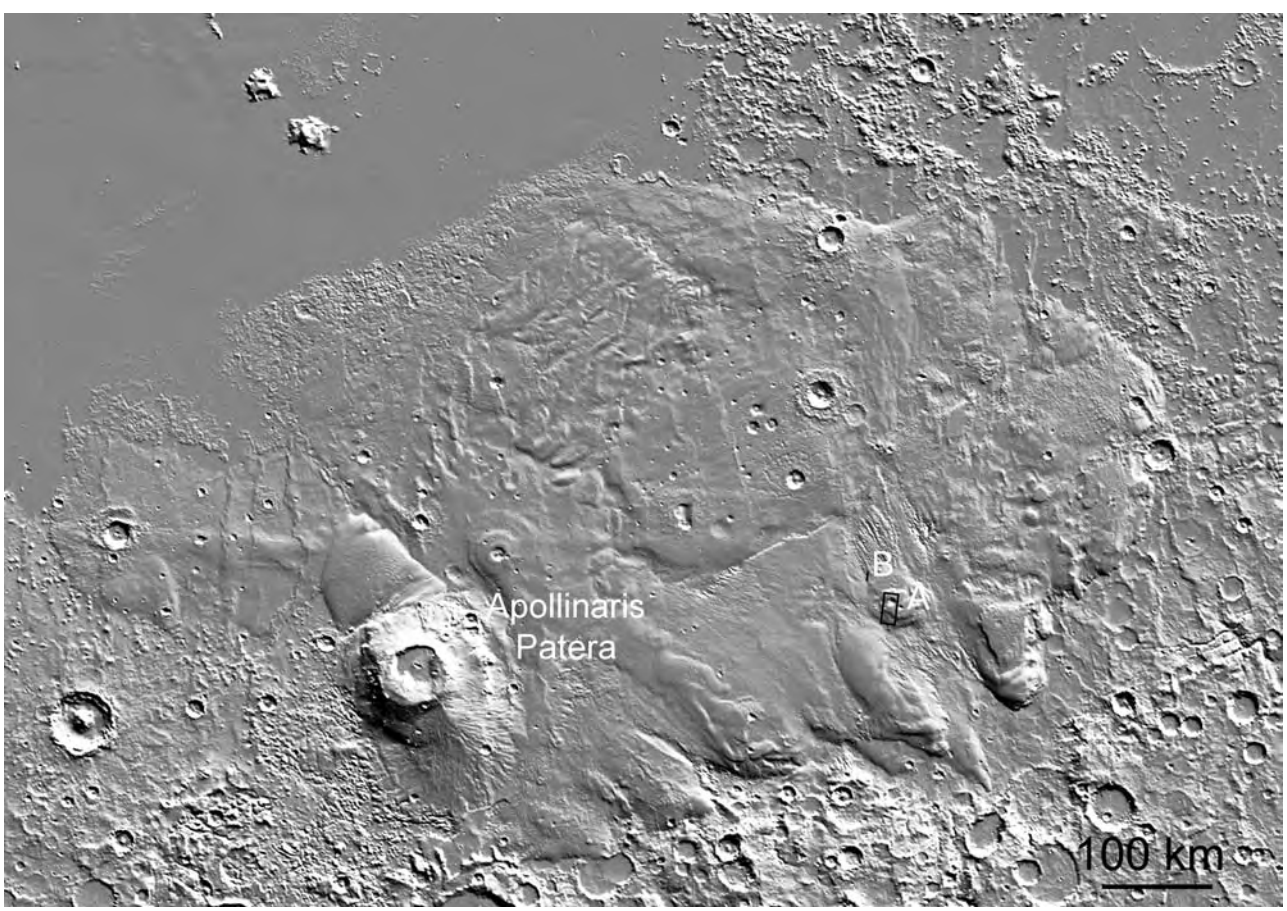

Figure 9.15. The Medusae Fossae Formation forms several kilometers-thick outcrops along the plains–upland boundary between 130 and 240°E. Here we see one such outcrop centered at 4°S, 180°E. The outcrop is easily recognized by its smooth to wavy surface. A and B show the locations of the frames in the next image (MOLA).

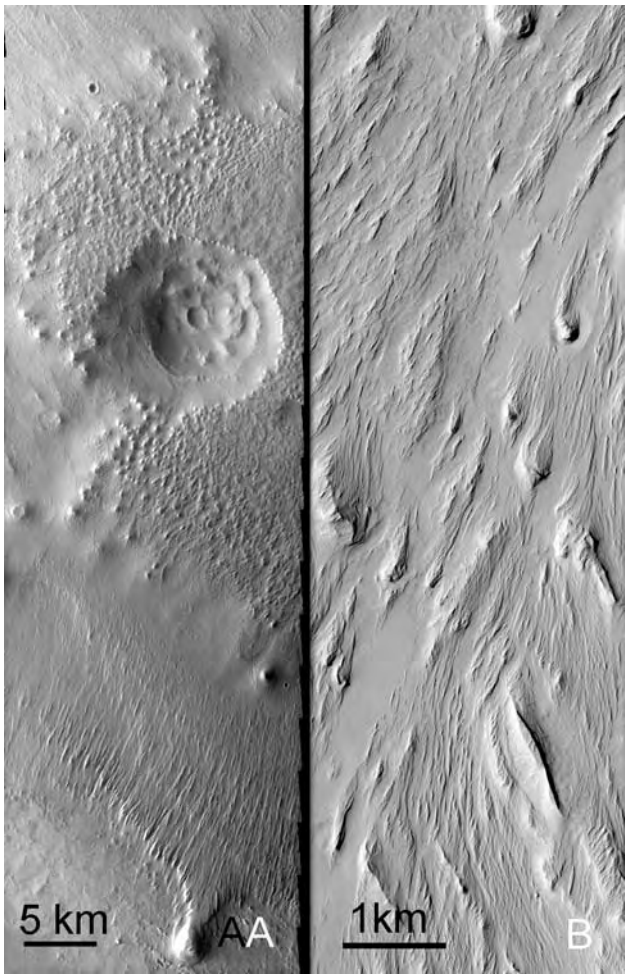

Figure 9.16. Details of the surface of the Medusae Fossae Formation. (A) A partial removal of near-surface layers by the wind has partly exhumed an impact crater at 7.1°S, 184.5°E. Ejecta has been preferentially retained around the impact crater (THEMIS V13867001). (B) Sculpting of the surface of the wind to form closely spaced curvilinear ridges, as seen here at 5.1°S, 183.4°E, is typical of much of the Medusae Fossae Formation (MOC M0303174).

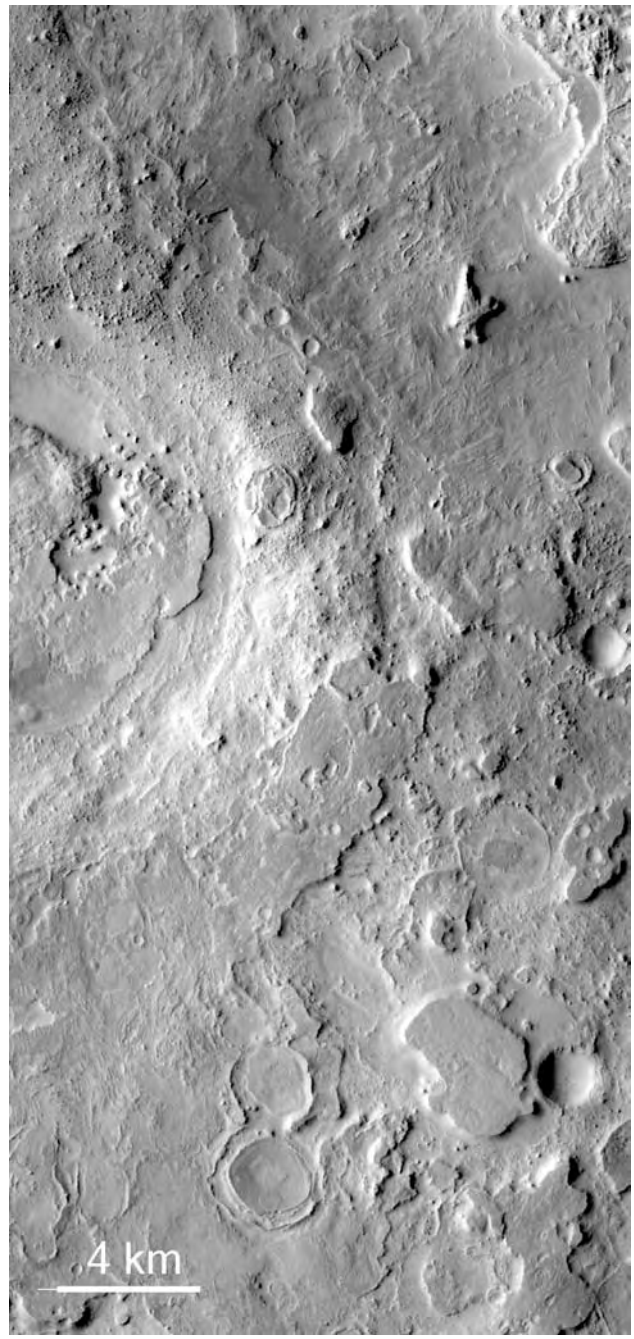

Figure 9.17. Etched upland terrain north of Syrtis Major at 27.7°N, 61.7°E. Large areas of the uplands in this region appear to have been formerly covered with layered materials that have been partly removed, leaving behind irregularly shaped mesas and exhumed craters (THEMIS V04679003).

size of dislodgement of particles by the wind is 100 μm. Dust storms indicate that much smaller particles (1−10 μm) are commonly dislodged, probably as a result of dust devils, which have been directly observed from orbit and from the surface and which have left tracks over large areas of the planet. Light-toned materials may accumulate downwind of obstacles to form bright streaks. Dark streaks can form both by scouring the area downwind of an obstacle and by accumulations of coarser debris. Megaripples and dunes are common in all regions of the planet. They form from particles mostly in the 50−500 μm size range that can saltate. The term megaripple refers to arrays of ridges transverse to the wind, a few to 25 m across. They are light-toned and common in low areas in all parts of the planet. Terrestrial megaripples have a bimodal distribution of particles, with the coarser

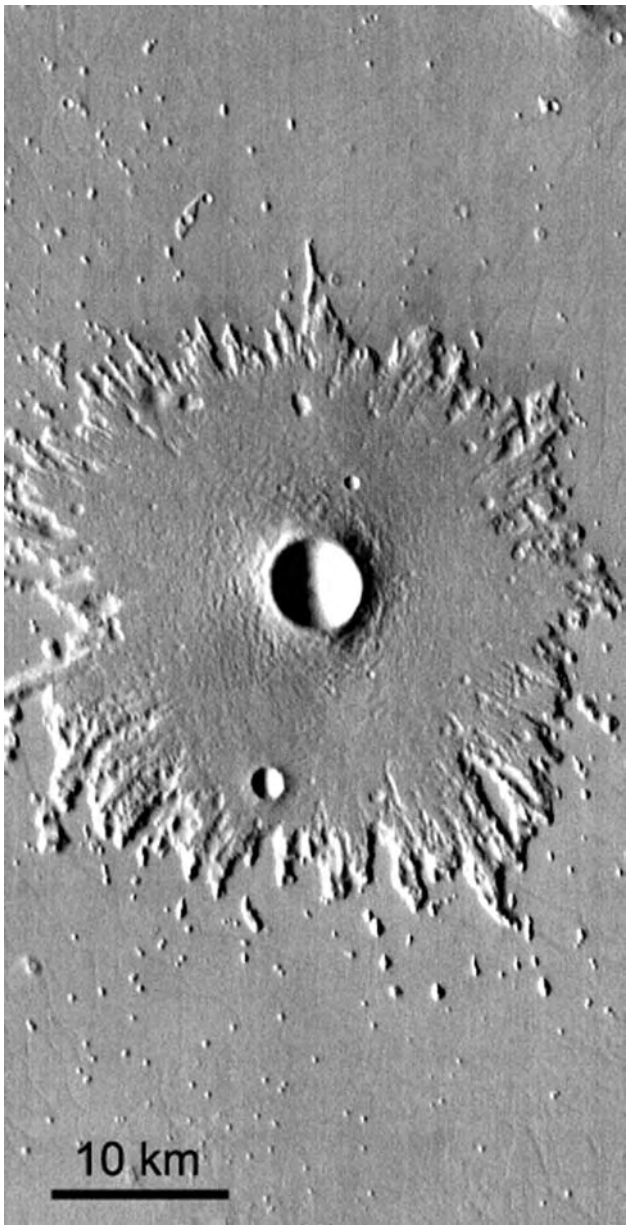

Figure 9.18. Pedestal crater adjacent to the Medusae Fossae Formation at 14.7°N, 197.5°E. The presence of a crater such as this indicates that the nearby Medusae Fossae Formation once covered this area and has since been largely removed by the wind except where protected by crater ejecta. Pedestal craters are common in many parts of the northern plains, and are a clear indication that these plains were once partly covered with layers of fragmental debris that has since been removed (THEMIS V02215005).

particles forming a lag on the surface. Dunes are 25 m to kilometers across and mostly dark-toned. They are most common around the northern polar cap and in mid-southern latitudes. Dunes assume a wide variety of

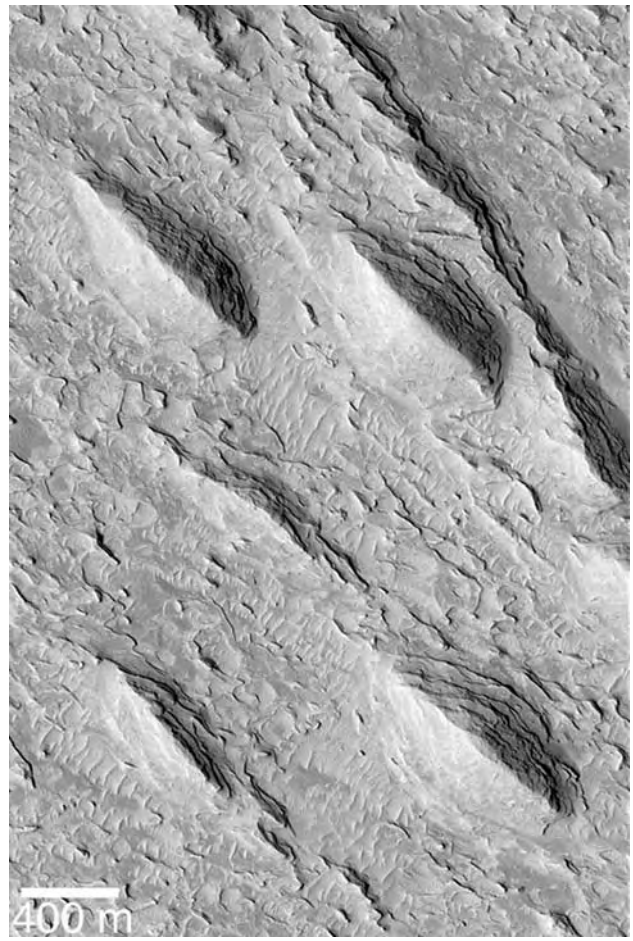

Figure 9.19. Yardangs eroded from the Medusae Fossae Formation at 1.5°N, 145.6°E. The term yardang refers to aerodynamical hills aligned parallel to the wind in terrestrial deserts. They are typically in layered, soft rocks, and commonly have the shapes of inverted hulls, as seen here (MOC M0702180).

forms according to the availability of sand and the directions and magnitude of the winds.

Thick accumulations of layered, easily erodible deposits occur along the equator between latitudes 130 and 240°E and in Meridiani Planum close to 0°N, 0°E. The particulate materials that make up the deposits may be from diverse sources such as volcanic eruptions, impacts, and erosion, and may be of ancient origin, even though some of the present landforms are young. Other easily erodible, layered deposits occur locally within craters and other depressions. Many of the deposits have been intricately carved by the wind. Pedestal craters and local etched patterns indicate that the materials have been eroded by the wind from some areas, such as the northern plains, and deposited in others. Although wind has been effective in eroding

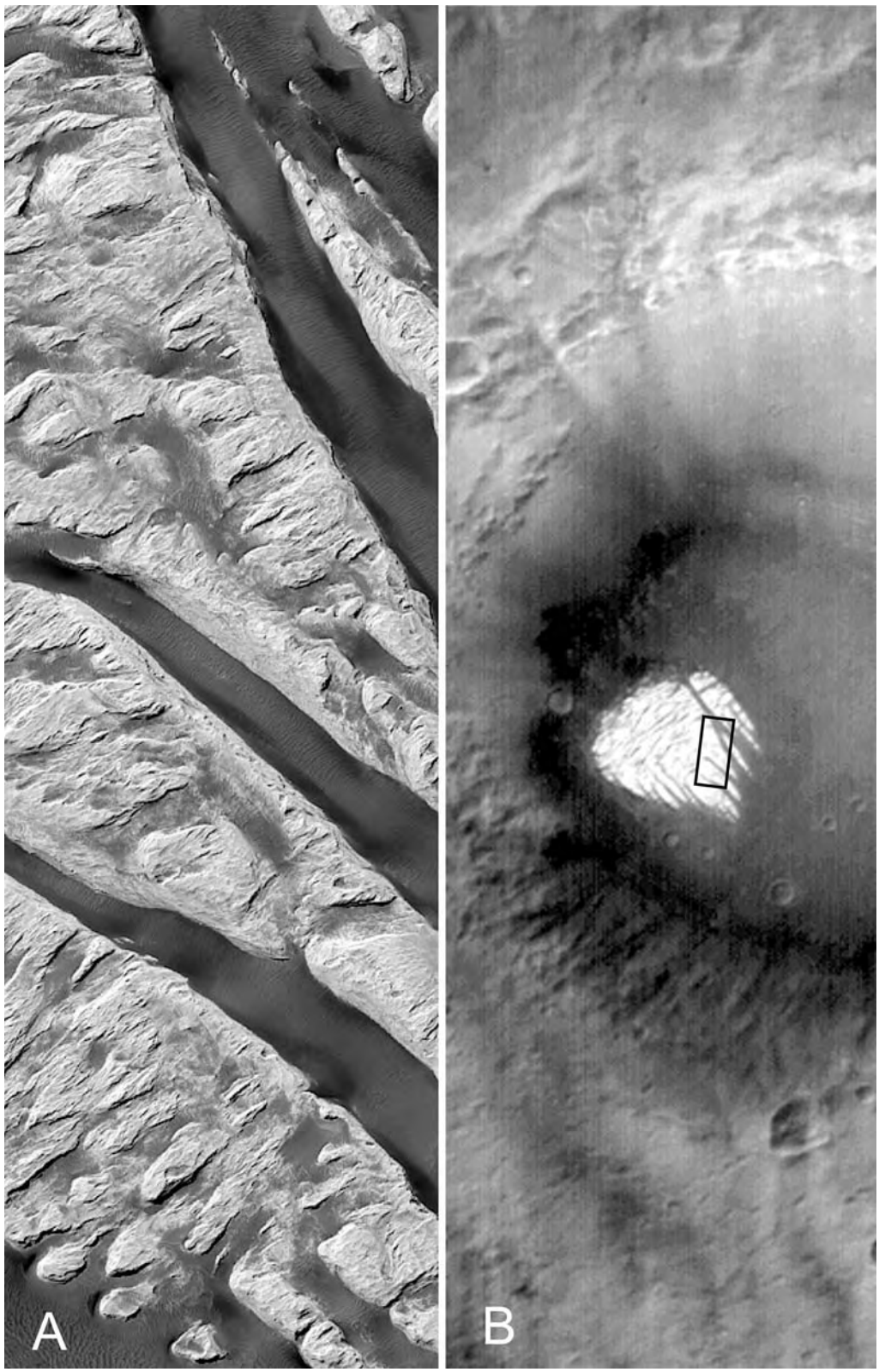

Figure 9.20. White Rock inside Pollack crater at 7.9°S, 25.3°E. Many craters in this region of Mars have stacks of layered sediments on their floors. They are probably remnants of a much more extensive cover that has been largely removed by the wind. They may have been formerly continuous with sediments on which the Opportunity landed several hundred kilometers to the east (Chapter 11). (A) The sediments have been carved into NW–SE trending ridges, most likely by the wind. The image is 3 km across. Note the megaripples in the low areas between the ridges (MOC M100309). (B) Context image showing the location of White Rock within the crater (MOC M0100824).

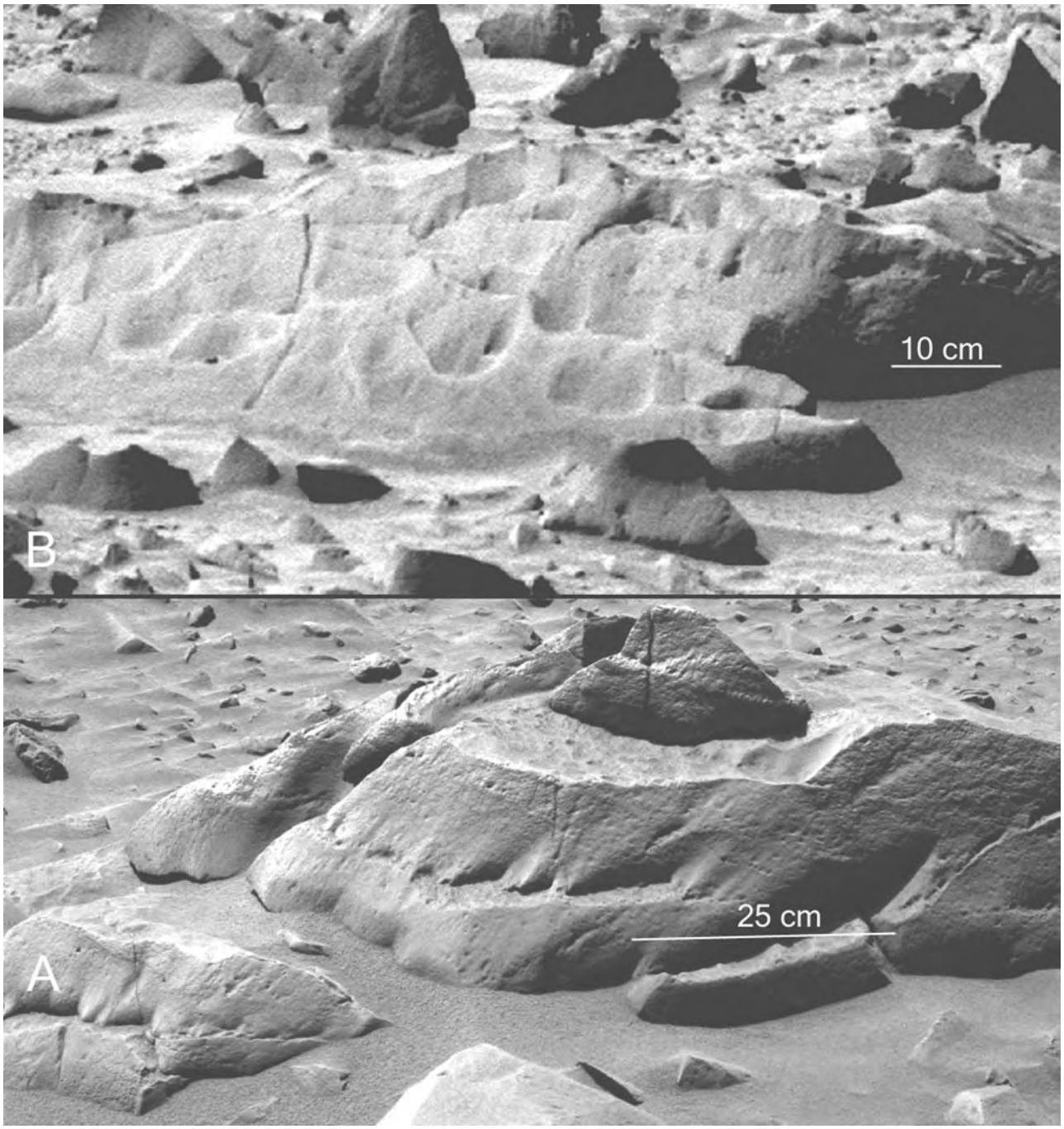

Figure 9.21. Wind-abraded rocks on the Gusev plains. (A) Terrace rock. Flutes starting at a common horizon in the large rock in the center and the one in the lower left suggest that the rocks were at one time partly buried. (B) Mazatzal.

and redistributing poorly cohesive accumulations of fragmental debris across the surface, erosion of primary volcanic and tectonic features by the wind has been small despite exposures over billions of years. The wind has primarily redistributed fragmental materials produced by other agents.

10 Poles

The advance and retreat of the martian polar caps have been observed for almost two hundred years. The seasonal caps are solid CO_2, a possibility that was recognized as early as the end of the nineteenth century. The prevailing view until the 1960s was, however, that the seasonal caps are water ice. This view changed when in 1965 Mariner 4 determined the surface pressure and it was realized that Mars had a thin atmosphere composed predominantly of CO_2. In 1966 Leighton and Murray published a remarkably prescient paper in which they demonstrated not only that the seasonal caps are composed of CO_2, but also that the atmospheric pressure must vary seasonally because of growth and dissipation of the caps. From temperature measurements and spectra, Mariners 6 and 7 soon confirmed that the seasonal caps are indeed CO_2. Subsequently, the Viking orbiter instruments showed that during northern summer, the northern CO_2 cap dissipates almost completely and uncovers a residual water-ice cap (Farmer *et al.*, 1976; Kieffer *et al.*, 1976). No water ice was detected at the south pole. More recently, however, water ice has been detected there beneath a meters-thick veneer of CO_2 ice (Byrne and Ingersoll, 2003b). The CO_2 ice appears to be dissipating on decadal time scales, creating strange patterns at the surface.

The unique geological characteristic of the poles is the presence of 3 km thick mounds of finely layered deposits. Because of the hemispheric dichotomy, those in the south are at an elevation 6 km higher than those in the north. The layering is exposed around the edge of the deposits and in the walls of valleys that form quasi-spiral patterns around both poles. The layered deposits are among the youngest sediments exposed on the planet's surface. They have been the object of considerable speculation since they were first observed in that they might record, in some way, recent climate changes that result from astronomical perturbations in the planet's orbital and rotational motions. In the north the finely layered deposits rest on a more coarsely layered unit that may be the source of the sand that forms a vast dune field around the central mound of layered deposits. Surprisingly, gypsum appears to be a significant component of parts of the dune field (Langevin *et al.*, 2005). The area covered by layered deposits in the south is less certain but the southern deposits may be more extensive, and parts of them may be older than those in the north.

The bulk of the chapter concerns the layered terrains. After a brief discussion of conditions at the poles, the layered deposits are described and various proposals as to how they and their incised valleys may have formed are examined. The deposits are thought to be composed mostly of water ice. But what caused the layering and the spiral troughs is controversial. The chapter concludes with a discussion of evidence for long-term changes in the inventory of CO_2 in the southern residual cap.

The present polar environments

Seasonal CO_2 caps form and dissipate at both poles. Because of the longer southern winters, the southern seasonal cap is significantly larger than that in the north, extending to roughly 40° latitude as compared with 55° latitude in the north. Formation and dissipation of the seasonal caps causes a 25 percent variation in atmospheric pressure. From the pressure variations, Kieffer *et al.* (1992) estimate that 3.5×10^{15} kg of CO_2 condense to form the northern cap, and 8.1×10^{15} kg condense to form the southern cap. The maximum thickness of the CO_2, as determined by MOLA, is 1.5 m in the north and 0.9 m in the south (Smith *et al.*, 2001). Temperatures at the surface of the ice are close to 150 K, substantially colder than the unfrosted terrain, where surface temperatures can range from 180 K to over 280 K depending on season, time of day, albedo, and so forth. The domal topography and the low temperatures of the poles may result in strong off-pole winds analogous to katabatic winds off the terrestrial Antarctic plateau (Magalhaes and Gierasch, 1982; Howard, 2000).

Dissipation of the north polar cap in spring exposes a remnant water-ice cap roughly 1000 km across. Surface temperatures rise from 150 K, the frost point temperature of CO_2, to around 200 K, the frost point temperature of H_2O. (The exact temperature depends on factors such as the local humidity and presence of dust in the ice.) Under present conditions,

sublimation of as much as 1 mm of ice may occur during the summer (Haberle and Jakosky, 1990). The sublimation results in a substantial increase in atmospheric water vapor over the northern pole in summer. Since the southern residual cap is mostly CO_2, no comparable increase in water vapor is observed there in summer. However, spectral measurements and local variations in the temperature on the southern residual cap, together with the morphology of the surface, suggest that water ice is present beneath a thin veneer of CO_2 ice (Byrne and Ingersoll, 2003b).

General description of polar terrains

At both poles is a stack of layered deposits 2–3 km thick. Those in the north extend from the pole to just beyond the 80° latitude circle (Figure 10.1). They have a total volume of $\sim 1.2-1.7 \times 10^6\,km^3$ (Zuber *et al.*, 1998). The deposits at the south pole are less symmetrically arrayed around the pole and they do not form a neatly defined mound like those in the north (Figure 10.2). From longitude 30°E to longitude 130°E the outer boundary of the southern deposits is well defined just inside the 80° latitude circle, but elsewhere the boundary is uncertain and the deposits may extend as far north as the 70°S latitude. They are estimated to have a volume of roughly $2-3 \times 10^6\,km^3$ (Smith *et al.*, 1999). The northern deposits rest on the surface of the northern plains, which are at an elevation of roughly 5 km below the reference level. The southern deposits lie on the heavily cratered southern uplands at an elevation of roughly 1.5 km. Thus the deposits at the south pole reach elevations over 6 km higher than those in the north (Figure 10.3). Both deposits have a maximum thickness of just over 3 km.

In the north, valleys spiral out from the pole in a counter-clockwise (anti-coriolis) direction. The valleys deepen from tens of meters near the center of the deposits to kilometers around their periphery. Toward the edge of the deposit the valleys are 20–70 km apart, but between the valleys are shallow undulations that follow the trend of the adjacent valleys. A large, kilometers-deep valley, Chasma Boreale (Figure 10.4), cuts across the general trend of the other valleys to divide the northern polar deposits into two unequal parts. Equatorward of this valley, smaller valleys spiral around a secondary center, also in a counter-clockwise direction. In the 180° direction a crescentic-shaped rise, the Olympia Planitia, abuts against the main body of layered deposits, and stands roughly 1 km above the surrounding Vastitas Borealis and 2 km below the maximum height of the central mound. Olympia Planitia lacks the spiral valleys that characterize the main body of the layered terrain, so appears smooth in MOLA reconstructions. Surrounding much of the layered terrain and covering Olympia Planitia is a vast sea of dunes, whose low albedo contrasts sharply with the lighter-toned, layered deposits (Figure 10.5).

In the south, the layered deposits have a wider range of characteristics (Figure 10.6). Close to the pole they are 2–3 km thick and, like those in the north when viewed at the regional scale, have a smooth surface except for superimposed curved valleys. These have a crudely clockwise spiral pattern, but the pattern is less distinct than in the north. In the 90°E direction the deposits lie unconformably on an impact basin, Prometheus, outlined by a prominent escarpment. Within the basin, the edge of the layered deposits is clearly marked by an outward-facing escarpment. Also in this sector, a major valley, Chasma Australe, is incised into the deposits. Elsewhere, the edge of the layered deposits is less clear. In the 180° direction the main body of the layered deposits is separated from more peripheral deposits by an escarpment or by deep valleys. Equatorward of these features, the layered deposits are only 1 km thick, and lack the spiral valleys. The surface is smooth except for low, scalloped, equator-facing escarpments. These 1 km thick deposits can be traced almost to the 70° latitude circle. On the opposing side of the pole, particularly in the sector from 270°E eastward to 40°E, the layered deposits are thin and discontinuous. Lows within the cratered uplands appear to be partly filled with a unit whose surface is in places heavily pitted. Tanaka and Scott (1987) interpreted the pitted unit as a deposit that is older than the layered deposits at the pole and called it the Dorsa Argentea Formation, after some branching ridges at 83°S, 320°E that resemble terrestrial eskers.

Northern polar deposits

Upper unit

The north polar layered deposits can be divided into two distinct units: an upper, finely layered, mostly lighter-toned unit and a dark, basal, platey unit (Kolb and Tanaka, 2001; Byrne and Murray, 2002; Edgett *et al.*, 2003; Fishbaugh and Head, 2005). The upper unit constitutes the bulk of the deposits. The layered unit was first recognized in Mariner 9 images. Detailed descriptions of the unit are given in Howard *et al.* (1982), Thomas *et al.* (1992), Malin and Edgett (2001), and Milkovich and Head (2005). The layering is best seen in northern spring and summer when the sunward-facing slopes of the spiral troughs become defrosted to expose the fine layering of the underlying

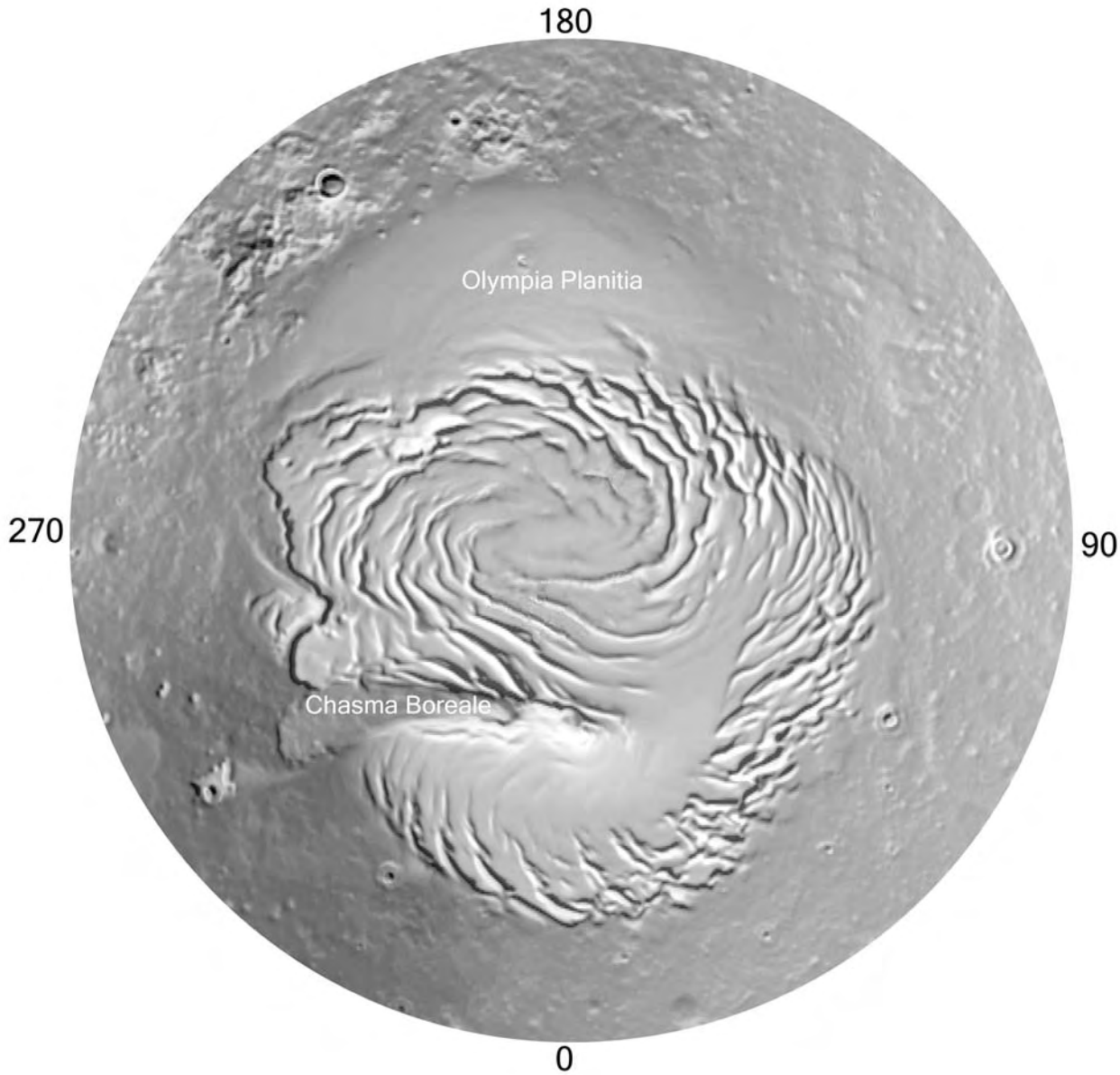

Figure 10.1. MOLA reconstruction of the relief at the north pole out to the 75° latitude circle. Valleys (troughs) that spiral out from the poles increase in depth toward the edge of the central mound, which is composed of young, finely layered deposits. Olympia Planitia is at an elevation 2 km lower than the central mound. It may consist of older deposits that extend under the main layered unit.

unit (Figure 10.7). The layers are also visible on the equatorward-facing slopes around the outer margin of layered terrain. The layering is expressed both as bright and dark bands, and as breaks in slope. Some of the layers form simple or beaded escarpments on the valley walls, as though they were more resistant to erosion than the adjacent layers. Although unconformities are present (Howard *et al.*, 1982), most of the layers persist without interruption over long distances. Individual layers can be traced across Viking images for tens of kilometers (Thomas *et al.*, 1992), and MOC images taken 100 km apart (Figure 10.8) have sequences in which tens of layers are repeated with barely any perceptible change in thickness or appearance of the individual layers (Malin and Edgett, 2001). Milkovich and Head (2005) used techniques that have been used to correlate layers in terrestrial sea cores, in order to assess the continuity and characteristics of the layering in the upper part of the deposits. They were able to identify the same marker beds and make

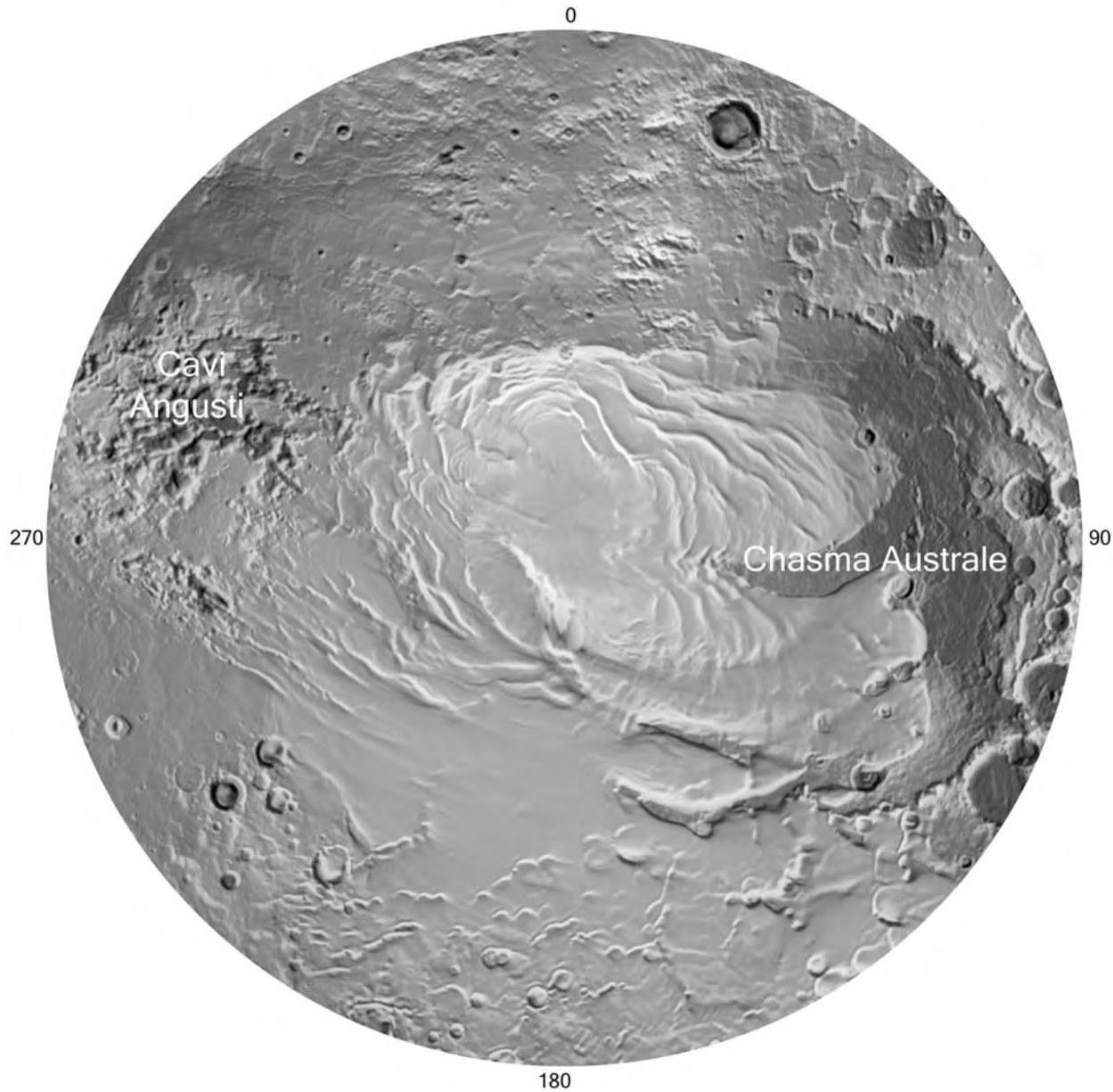

Figure 10.2. MOLA reconstruction of the area around the south pole out to the 75° latitude circle. The various polar features are less symmetrically arrayed around the pole than in the north, and the polar deposits are superimposed on heavily cratered upland rather than sparsely cratered plains. At the pole is a mound of layered terrain with spiral valleys as in the north, but the surrounding terrain is very different as described in the text.

correlations between sequences seen in MOC images spaced hundreds of kilometers apart. They show that the dominant wavelength in most of the sequences is ~30 m; secondary wavelengths range from 17 to 37 m. The sequences show a high degree of correlation over the entire cap, although the thickness of individual layers may vary by a factor of ~2.5. They also show that the layers dip away from the center of the deposits at an angle of 0.5°, as does the cap surface. While 30 m may be the dominant wavelength, in the MOC images with 1.5 m/pixel resolution, layers are visible down to the limiting resolution, and likely continue below the limit.

Increases in water vapor over the northern cap in summer (Jakosky and Haberle, 1992) indicate that water ice accumulates and dissipates on the cap with

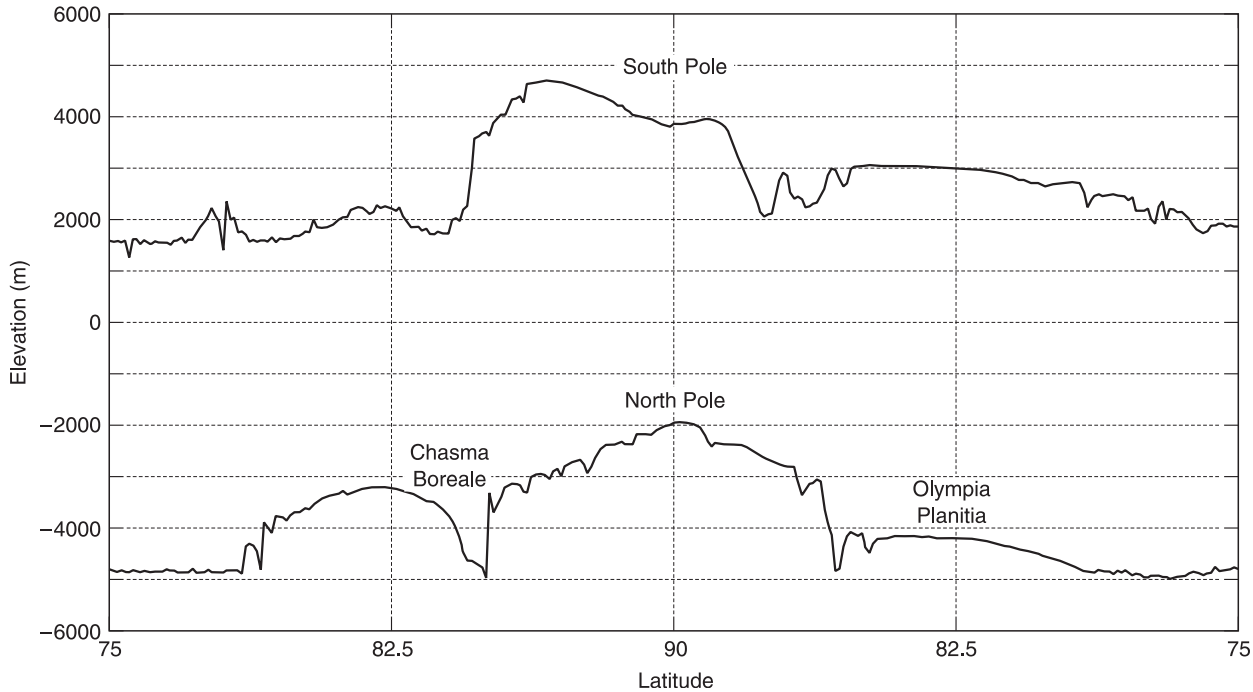

Figure 10.3. Profiles across the north and south poles in the 0° to 180° direction. The south pole is at an elevation over 6 km higher than that in the north. At both poles the layered deposits reach thicknesses of 3 km.

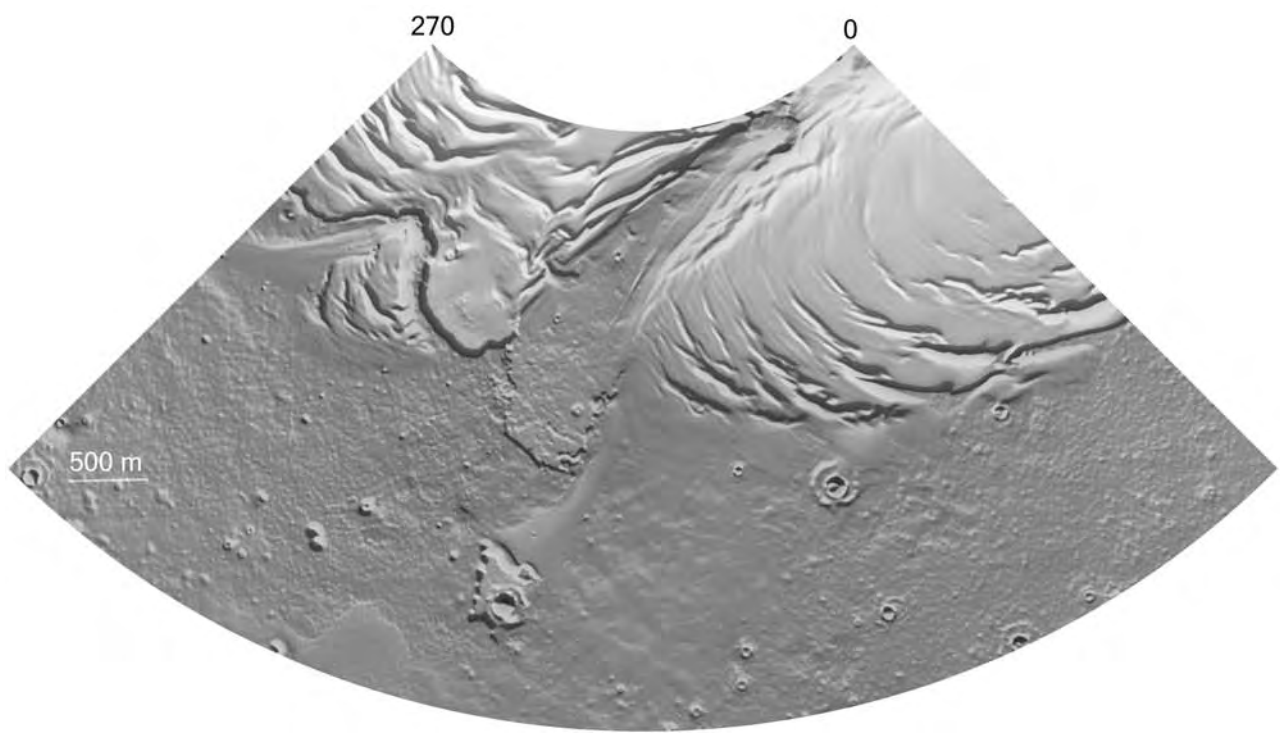

Figure 10.4. Chasma Boreale. The area shown is from 270−0°E and 75−85°N. Large valleys are cut into the main body of layered terrain at both poles. Their origin is controversial. Two suggestions are that they formed as a result of floods that followed melting of the ice-rich layered deposits, or that they were eroded by strong winds blowing off the pole. Also visible on this image are the undulations on the upper surface of the layered terrain between the deep valleys.

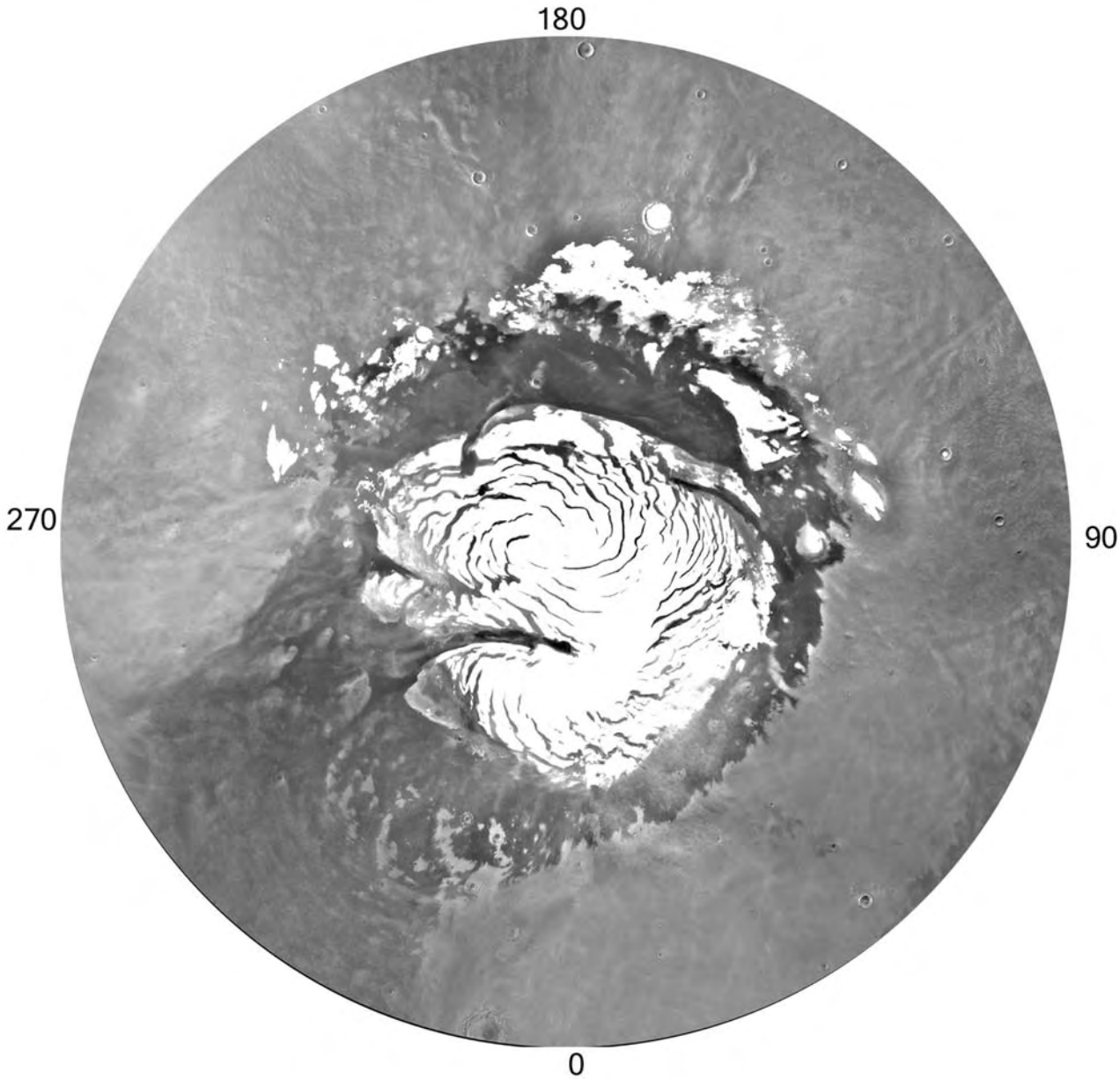

Figure 10.5. The appearance of the northern summer pole out to the 75° latitude during the Viking missions. The bright areas are mostly water ice left behind after recession of the seasonal CO_2 cap. The central body of layered terrain is surrounded by a dark collar that is mostly caused by dunes, although the dark area to the lower left of the cap is the intrinsically dark surface of Acidalia Planitia.

the seasons. Episodic dust storms must also deposit dust on the caps. The composition of the deposits is poorly constrained, but the albedo and color suggest that they are mixtures of dust and young, fine-grained, water ice (Thomas *et al*., 1992). Crater counts indicate that they are very young (< 120,000 years) (Herkenhoff and Plaut, 2000). Pathare and Paige (2005), however, question the validity of crater ages on these ice-rich deposits because of possible viscous relaxation of the craters. The deposits are probably dust and ice accumulations that result from processes that are occurring in the present epoch. Variations in the rates of accumulations of dust and ice to form the layers could result in a variety of ways. From their first discovery, the variations were thought to be related in some way to perturbations in the orbital and rotational

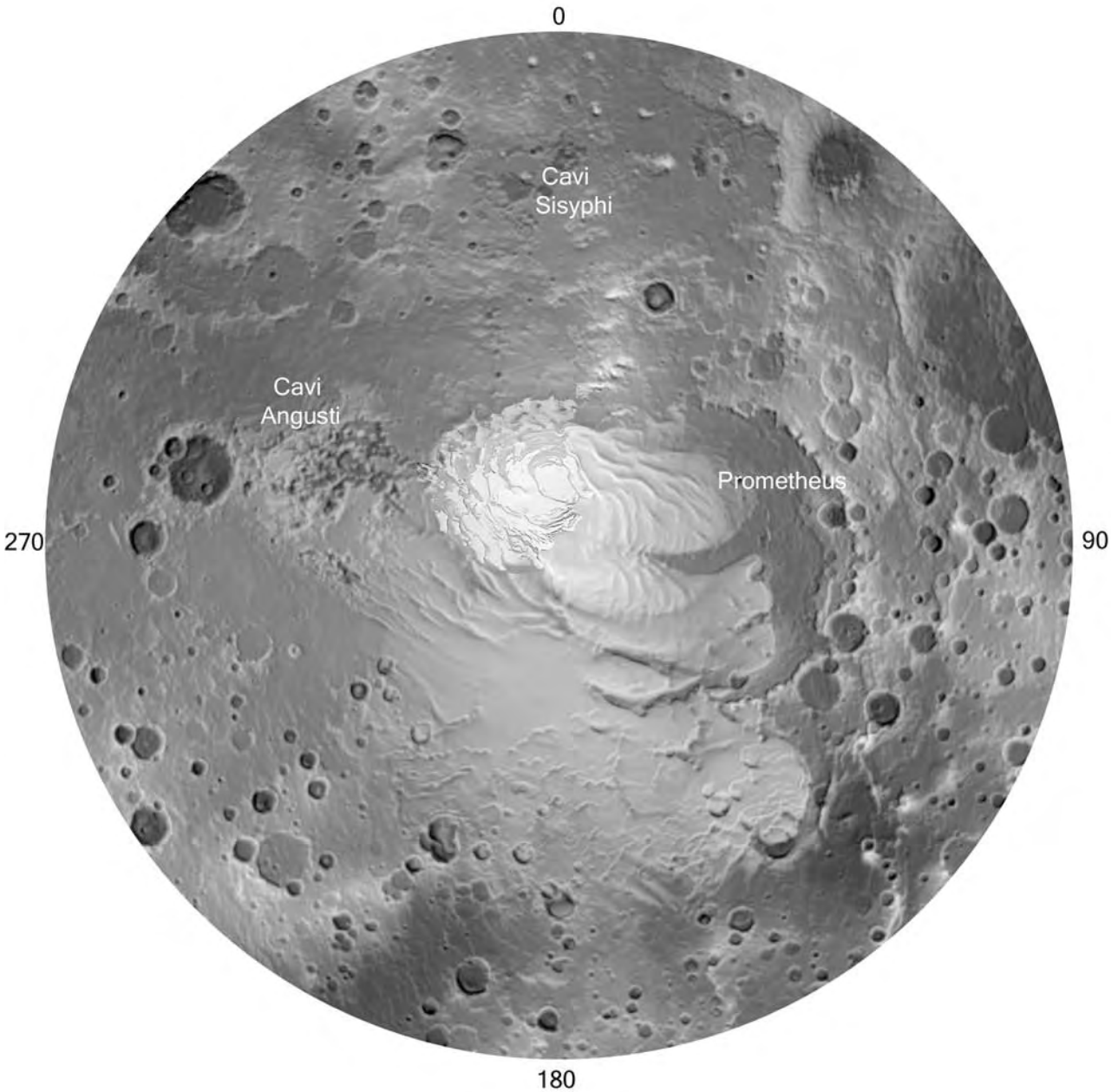

Figure 10.6. MOLA reconstruction of the south polar region out to the 65° latitude circle with the residual summer cap superimposed. The residual cap occupies the highest part of the mound of layered deposits at the pole. Young, 1 km thick layered deposits cover much of the area from the pole out to the 70° latitude in the 180° direction. Between 0°E and 270°E much older Hesperian deposits fill lows in the underlying cratered terrain. Prominent pits or cavi have formed in these deposits.

motions of the planet, which could affect both the stability of ice and the incidence of dust storms.

What controls the overall shape of the northern cap is poorly understood. Zuber *et al.* (1998) suggested that the cap is predominantly water ice and that its convex upward profile is caused by flow of ice from an accumulation zone at the center to the ablation zone around the cap's periphery, much like the profile of a terrestrial glacier. In contrast, Ivanov and Muhleman (2000) showed that the shape could be simulated by sublimation alone. They did not rule out flow, but implied that it may not be required.

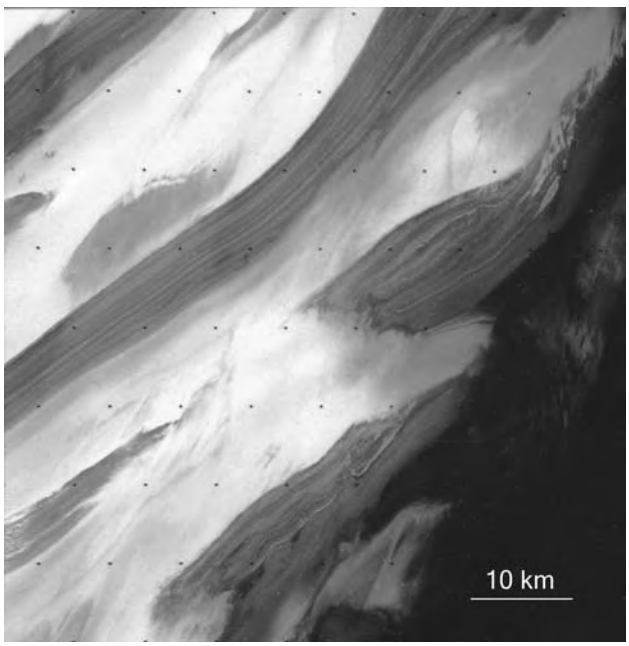

Figure 10.7. Polar layers on defrosted, sun-facing slopes within the residual north polar cap at 82°S, 100°E. Bright water ice is retained on the flats between the valley. Many of the layers are continuous for tens of kilometers across the image (Viking 65B68).

Models for accumulation of the layers can be divided into two classes. In the first class each layer is deposited across the entire cap such as might result from a global dust storm or a volcanic eruption. The second class of model envisages local factors affecting accumulation. The continuity of the layers and correlation of sequences over large distances favor the first class of models. Observation of unconformities favors the second class. Howard *et al.* (1982) proposed that accumulation of the layers was the result mainly of local factors and intimately related to formation of the spiral troughs. They proposed that undulations on the surface of the layered deposits would become amplified and form troughs as ice is preferentially ablated from equatorward-facing slopes and deposited on the intervening flats and poleward-facing slopes. As ablation continues, the troughs migrate toward the poles and unconformities develop in the wake of the troughs as new layers are deposited over the older, partly ablated and eroded sequence. They point to several unconformities in support of their model.

Milkovich and Head (2005) invoked the first class of model, suggesting that the layers are due to variations in deposition of dust and ice across the entire cap, as indicated by the wide-scale continuity of the stratigraphic sequences. They attempted to correlate the sequence of layers in the upper part of the layered terrain with the recent history of orbital and rotational motions calculated by Laskar *et al.* (2002, 2004). From their correlations of layers in MOC images they divide the uppermost sequence into four zones. Zone 1, roughly 300 m thick, has a periodic signal with a characteristic wavelength of 30 m. Zone 2 below it is 100 m thick but has no periodic signal, then below it the periodic signal is re-established. Superimposed on these variations is a general darkening with depth. Laskar *et al.* estimate that, as we go back in time, the obliquities were higher, particularly before about 0.4 million years ago. We seemingly have just emerged from a period of high obliquities. Milkovich and Head interpret the darkening with depth as a result of these changes in obliquity. They suggest that the darkening results from increased dust storm activity and decreased deposition of ice at the higher obliquities. An additional factor may be accumulation of a lag as ice is lost from the poles and deposited at low latitudes. Zone 1 may represent the present epoch of low obliquities and zone 2 the previous epoch of high obliquities. If true, then the roughly 30 m layers that characterize zone 1 must represent some shorter cycle, possibly the 51 kyr precessional cycle that affects the length and intensity of the seasons in the different hemispheres (Chapter 1). The scenario just outlined is only one of a wide range of possibilities. Until we can accurately date the layers, correlations between the layers and astronomical motions will remain speculative.

Basal unit

Throughout much of the cap, particularly the area between Chasma Boreale and Olympia Planitia, the finely layered deposits appear to rest upon a dark, coarsely layered unit (Figure 10.9). The elevation of the contact ranges from −4.9 km to −4.3 km. The unit is seen best in Chasma Boreale, where it comprises most of the floor, and in the deeper, outer troughs and scarps between the main body of the layered terrain and Olympia Planitia. Where the layers crop out at the base of scarps, they commonly form horizontal shelves with convoluted outer margins or isolated mesas in marked contrast to the finely banded, uniform slopes above. The elevation of the contact and the geometric relations suggest that the unit is the same as that which forms Olympia Planitia. The unit appears to extend from Olympia Planitia, beneath the main part of the cap, to wedges out south of Chasma Boreale.

Dunes cover much of Olympia Planitia. They are also associated with most of the outcrops of the

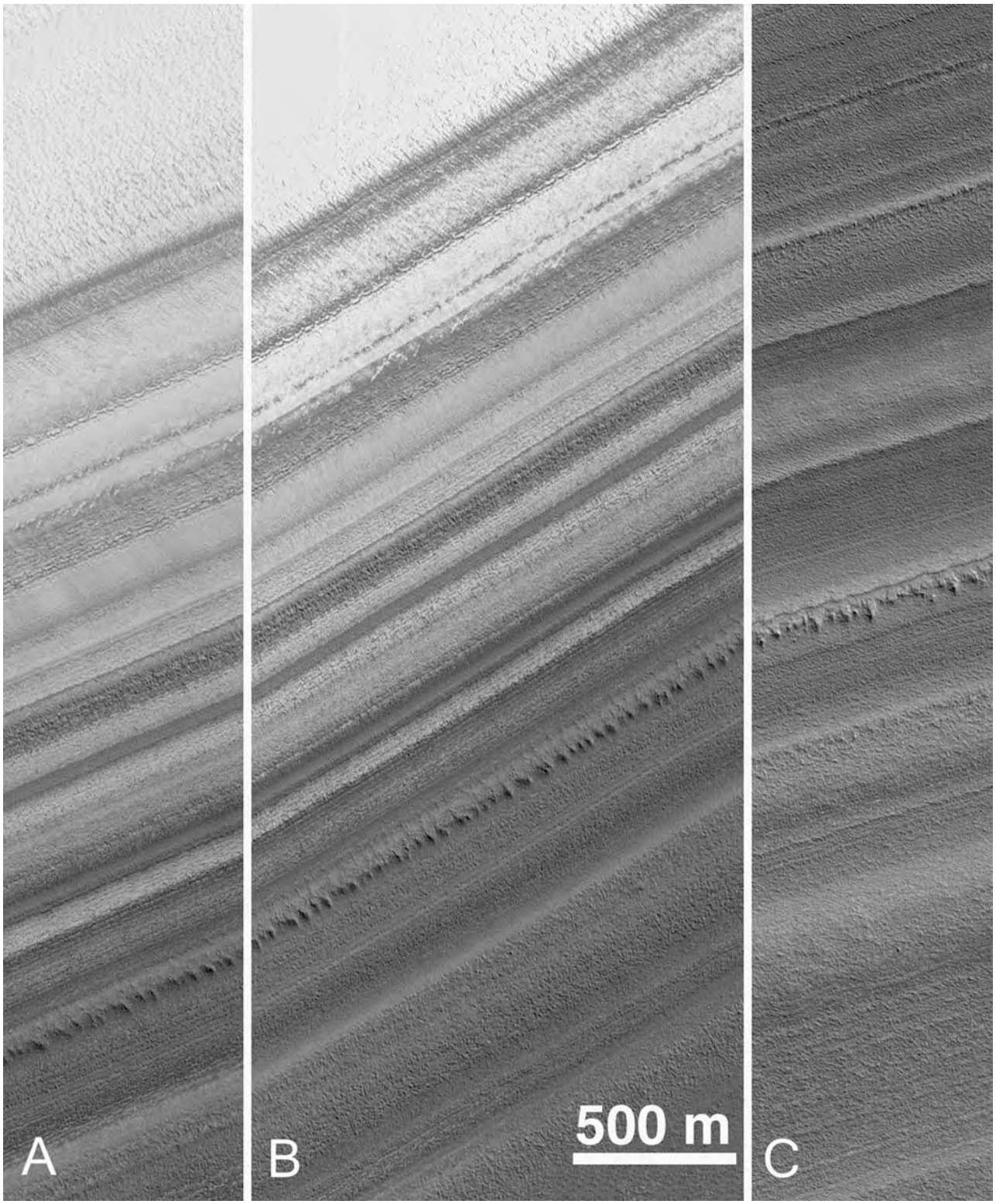

Figure 10.8. North polar stratigraphy. Here we see three images of the same trough. The right and middle images are separated by 13 km, the left and right images by 104 km. The same marker horizon can be seen in each image, and roughly the same stratigraphic sequence. The layering is visible down to the limiting resolution of the images (~3–5 m). Even the finest layers are continuous across all three images. (A) 86.5°N, 78.5°E. (B) 86.4°N, 81.3°E. (C) 85.9°N, 102.1°E (MOC 2-148).

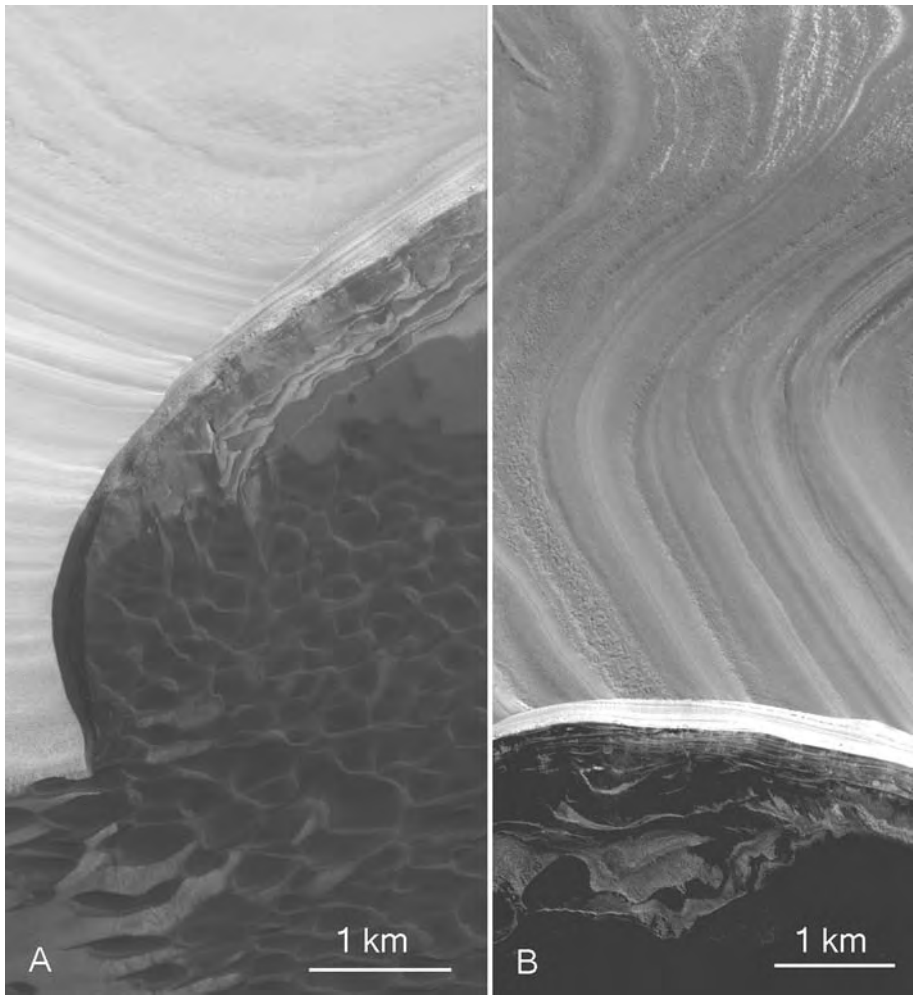

Figure 10.9. Boundary between the upper and basal units in the north pole layered terrain. (A) In the upper left of the image, layers of the upper unit crop out on a gently sloping surface at 83.6°N, 118°E. In the center of the image this surface is cut by an escarpment in which the bright, fine layering of the upper unit is exposed. This is underlain by the coarse layers of the basal unit. Dunes encroach on the escarpment from the lower part of the image (MOC E0101772). (B) The boundary between the two units at 83.8°N, 122.2°E is also marked by an escarpment that separates the upper unit exposed on a gentle slope in the upper part of the image, from the darker, more platey basal unit in the lower part of the image (MOC E0201209).

basal unit around the edge of the main cap and in Chasma Boreale. Byrne and Murray (2002) accordingly suggested that the basal unit was the source of much of the sand in the circumpolar erg. They proposed that the basal unit is a weakly cemented sandstone that formed before the present polar cap. Presence of gypsum at the surface of Olympia Planitia (Langevin *et al.*, 2005) indicates that the dunes, and probably the basal unit, are not simply accumulations of basaltic sand. Evaporites are the most likely source of gypsum. There is a wide range of possibilities for forming evaporites, ranging from evaporation of extensive bodies of water, such as postulated by Parker *et al.* (1989, 1993), to local interdune pools as suggested by Grotzinger *et al.* (2005) and McLennan *et al.* (2005) for the deposits at Meridiani. Clearly, the boundary between the basal unit and the finely layered upper unit represents a major change in environmental conditions at the pole.

Chasma Boreale cuts through the entire finely layered sequence to expose the basal unit on its floor. One possibility is that the chasma was cut by catastrophic draining of a subglacial lake at the base of the layered deposits (Clifford, 1987; Benito *et al.*, 1997; Fishbaugh and Head, 2002). The young age of the present surface of the deposits implies that the chasma is also young. Melting as a result of warm surface conditions or high heat flows is unlikely for

such recent deposits. One possibility is that the cap was melted by volcanic eruptions at its base. Another possibility, supported by the abundance of eolian features in the chasma, is that Chasma Borealis was not cut by water but instead was eroded by katabatic winds flowing off the cold pole (Howard, 2000; Edgett *et al.*, 2003).

Southern polar deposits

The relationships at the south pole are much less clear than those in the north. Both poles have a 3 km thick stack of finely layered deposits with spiral valleys close to the pole, but they differ in almost all other respects. The south polar deposits are older than those in the north, 10^7 years versus 10^5 years if the crater ages are valid (Herkenhoff and Plaut, 2000). The outer margin of much of the layered deposits in the south is less clearly defined than in the north, and the deposits are less symmetrically arrayed around the pole. No equivalent of Olympia Planitia is present in the south, nor has a basal unit analogous to that in the north been identified. Pitted deposits around the south pole have no northern equivalent. Around the south pole dunes are present only locally, mainly in craters, instead of forming an encircling erg. The reason for the differences between the poles is unknown. They could arise from a variety of causes such as the 6 km difference in elevation, differences in the nature of the underlying terrains, presence of a CO_2 residual cap, and differences in depositional rates, insolation, wind regimes, and lengths of seasons that result from variations in precession and eccentricity. The following discussion refers to three basic units in the south polar region: (1) a 3 km thick central mound of layered deposits offset from the pole in the 0° direction and roughly outlined by the 3 km contour; (2) similar but much thinner deposits, roughly outlined by the 2 km contour, which extend from the central mound almost to the 70° latitude in the 180° direction; and (3) a much older, lower-lying deposit called the Dorsa Argentea Formation.

Much of the discussion above on the characteristics and origin of the layers and spiral valleys of the upper unit at the north pole is applicable to the central mound at the south pole and will not be repeated. There are some differences. MOC images of the south polar layered deposits, for example, show much more obvious stair-stepped patterns (Figure 10.10) on slopes than the upper unit in the north, and mesa-like remnants of layered deposits are more common within valleys than in the north. A 1–2 km deep valley radial to the southern remnant cap with strong longitudinal striations and convoluted patterns of

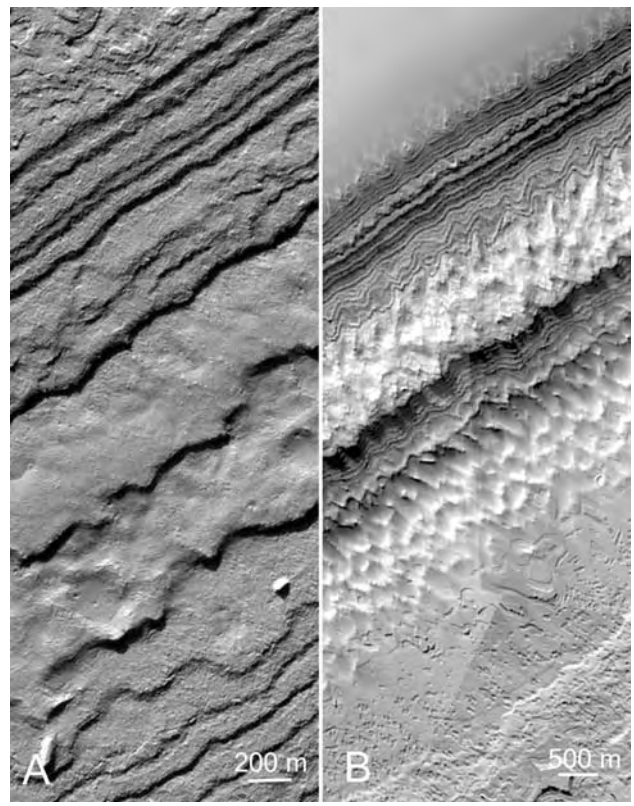

Figure 10.10. Southern layered deposits on opposites sides of the pole. (A) Layers at 87°S, 153.4°E step down from a nearby flat at the upper left of the image into a valley whose floor is to the lower right (MOC E1300797). (B) Layers at 87°S, 350°E. Flats in the upper left and lower right of the image are separated by a valley with a central ridge (MOC 2-223). Illumination of both images is from the upper left.

layers on its walls and floor (Figures 10.11, 10.12) has no obvious northern equivalent (Koutnik *et al.*, 2002). Nevertheless, the main differences between the deposits of the north and south are the presence in the south of extensive young deposits peripheral to the central 3 km thick mound, and the presence of the older Dorsa Argentea Formation.

For purposes of discussing the deposits around the central mound, the area around the pole is divided into three sectors. In the first sector, from 30°E to 150°E, lobes of layered deposits (Figure 10.13) roughly 1 km thick extend outward from the central 3 km thick mound into the Prometheus basin and over the adjacent cratered terrain to the east. The lobes are separated from each other by large re-entrants, the largest being Chasma Australe. The question of whether these lobes were emplaced by flow, or were eroded out of more continuous deposits, is difficult to answer. Radial striations in the upper reaches of Chasmal Boreale, the

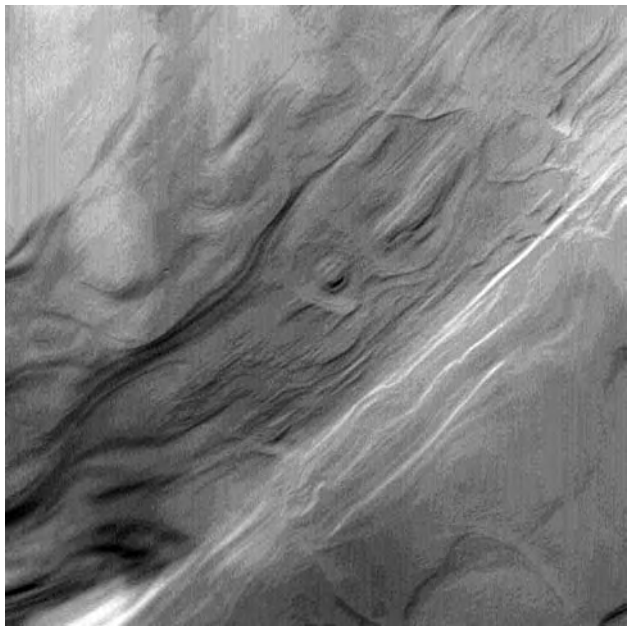

Figure 10.11. Wind-eroded valley in the layered deposits at 86.7°S, 154.5°E indicates the efficacy of wind in eroding the layered deposits.

other re-entrants, and the valley mentioned in the previous paragraph strongly support some erosion by winds off the poles, and Howard (2000) suggested that wind was the main cause of the re-entrants. Clifford (1987) had earlier suggested that the re-entrants resulted from basal melting of the ice-rich layered deposits. The lobes may have been formerly more extensive, as indicated by the pattern of secondary craters around craters at the lobes' margin (Carr, 1981; Head, 2001).

The next sector extends from 150°E to 240°E. In this sector the layered deposits extend to varying distances out from the central mound, in some places as far as the 70° latitude circle. The surface of the unit is mostly at an elevation between 2 and 3 km, well below the 3–5 km elevation of the central mound. Its extent is roughly outlined by the 2 km contour. The main characteristic of these deposits is that the surface is smooth, except for arrays of scalloped ridges. Howard (2000) suggested that the ridges might be related in some way to erosional and depositional processes associated with standing atmospheric waves. The smooth deposits appear to be similar to those at the poles except that they are only 1 km thick and lack the spiral valleys and re-entrants.

The third sector from 240°E eastward to 30°E is characterized by discontinuous smooth deposits that are commonly highly pitted. The deposits occur mostly in local lows at elevation below 2000 m, unlike the

Figure 10.12. Details of the center of the previous image. (A) In the lower left corner a crater that formed in the layered deposits is being exhumed as the wind erodes deeper into the layers (THEMIS V00979003). (B) The slope of the valley stepping down the same crater in the upper left of the image. Each layer forms a pitted surface outlined with a low escarpment with a serrated margin (THEMIS V084690004).

smooth unit in the previous sector. The unit appears to be older and distinctly different from the deposits at the pole. It was named the Dorsa Argentea Formation by Tanaka and Scott (1987), and assigned a Hesperian age based on crater counts.

The Dorsa Argentea Formation

The Dorsa Argentea Formation (DAF) partly covers the cratered uplands to form patches of level, pitted plains between the layered deposits at the pole and the 60° latitude circle. The plains-forming deposits were originally interpreted as volcanic or eolian in origin (Tanaka and Scott, 1987), but an alternative that we will explore further here is that they are

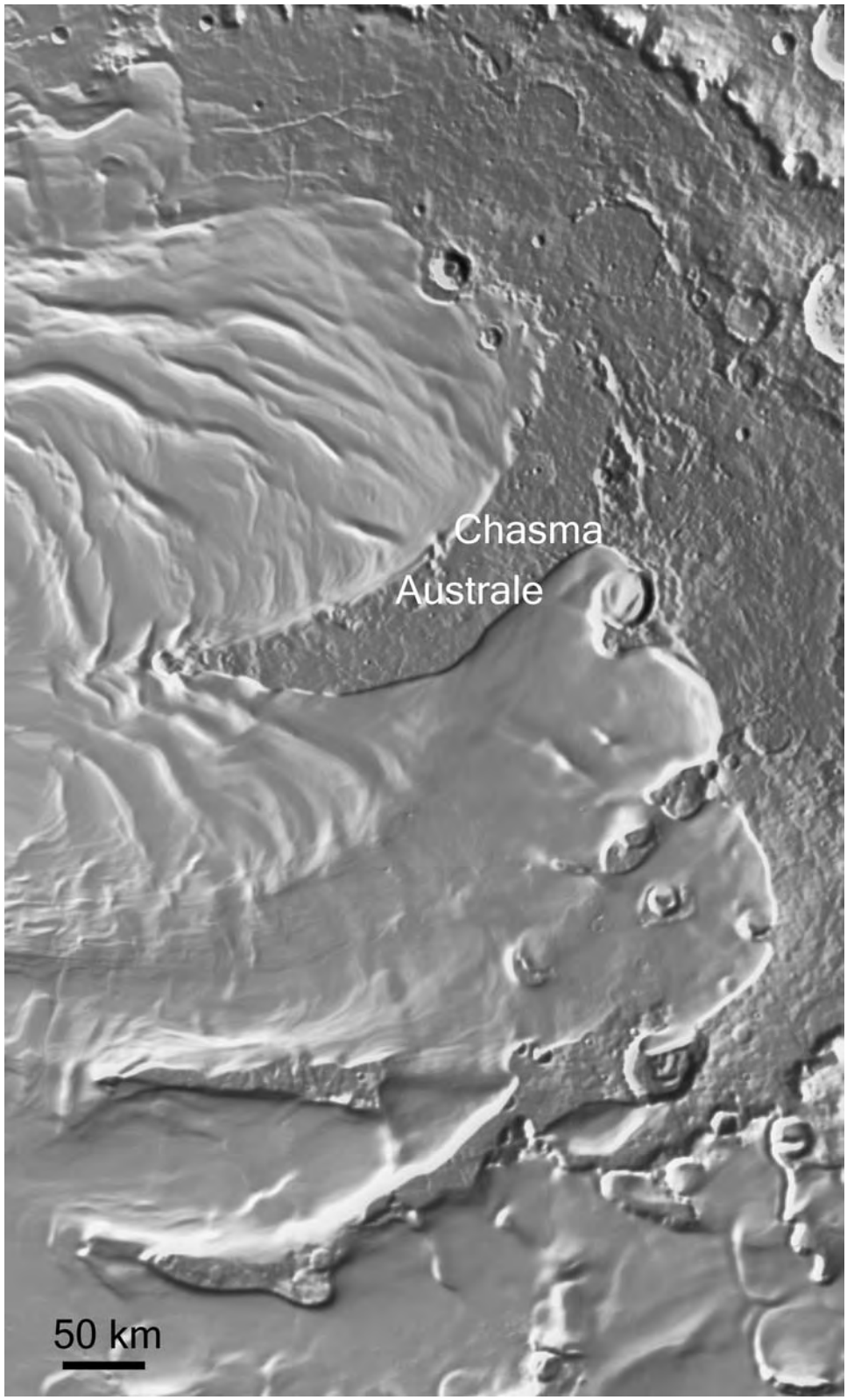

Figure 10.13. Lobes of southern layered deposits in the vicinity of Chasma Australe. For location see Figure 10.2. In this area the extent of the polar deposits is sharply defined. Around the periphery of the lobes the layered unit partly covers several craters, having possibly flowed into them. Valleys curl around the pole, which is just to the center left of the area. Several re-entrants and hollows extend all the way through the layered deposits to expose the underlying older surface.

ancient, ice-rich polar deposits, analogous to the deposits that are at the pole today. The formation is named after the Dorsa Argentea, a group of branching, sinuous ridges of Hesperian age at 78°S, 320°E (Figure 10.14). The ridges are typically 2–4 km wide and 50–100 m high. In plan, their pattern resembles that of anastomosing streams. Similar ridge systems are found elsewhere on the planet, such as in southern Amazonis and Argyre, commonly where other indicators, such as pedestal craters, suggest that a former cover has been removed. While numerous proposals have been made as to how such ridges might form, the most plausible is that they are analogous to terrestrial eskers (Kargel and Strom, 1991; Metzger, 1991; Kargel, 1993). Eskers are ridges of glacial drift deposited by subglacial or intraglacial streams. When the glacier retreats or dissipates, the stream deposits are left as ridges on the underlying terrain. The martian examples have all the characteristics of terrestrial examples including sinuosity, branching upstream and downstream, superposition of ridge on ridge, discontinuities, and so forth. The esker interpretation appears solid. Their presence suggests that, at some time in the past, the surface at their present location was covered by ice-rich deposits, possibly similar to those thought to be at the pole today. They further indicate that the deposits melted, a result either of climate change or volcanic heating from below, and ultimately disappeared. Superimposed impact craters (Figure 10.14) and stratigraphic relations (see below) suggest that the ridges are Hesperian in age.

The general area where the Dorsa Argentea Formation crops out is also characterized by numerous pits in its surface. Most, but possibly not all, are in the Dorsa Argentea Formation. They are particularly common at two locations to form the Cavi Angusti at 72°S, 355°E (Figure 10.15) and the Cavi Sisyphi at 83°S, 285°E (Figure 10.16). The Cavi Angusti cover a roughly 600 × 600 km region. They are inset into a broad high that stands 500–1000 m above the surrounding terrain. The pits are steep-sided and irregularly shaped, although with a north–south elongation. They range in size up to 50 km across and over 1 km deep. Most have flat floors. Terraces on the pit walls suggest that they are incised into a layered unit. The Cavi Sisyphi are also irregularly shaped, flat-floored pits, but they are inset into a plain, formed by the Dorsa Argentea Formation, rather than a high. The areal extent and dimensions of the Cavi Sisyphi are difficult to define because of the complex boundaries between the Dorsa Argentea Formation, into which the pits are incised, and the underlying Noachian cratered terrain. Nevertheless, the pits

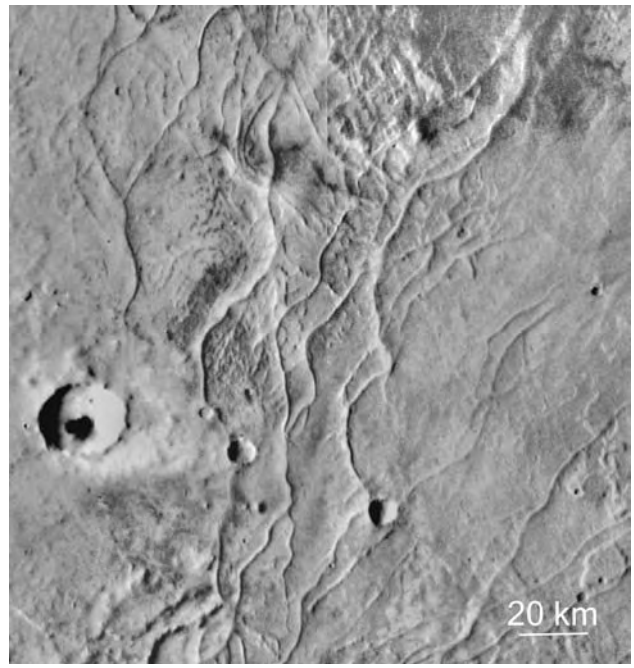

Figure 10.14. Branching ridges at 77.7°S, 319.6°E. The ridges are believed to be eskers, accumulations of sand and gravel deposited by subglacial streams, then left behind when the glacier retreats. They suggest that this area was formerly covered by ice-rich deposits. Illumination is from the left (Viking 421B53/55).

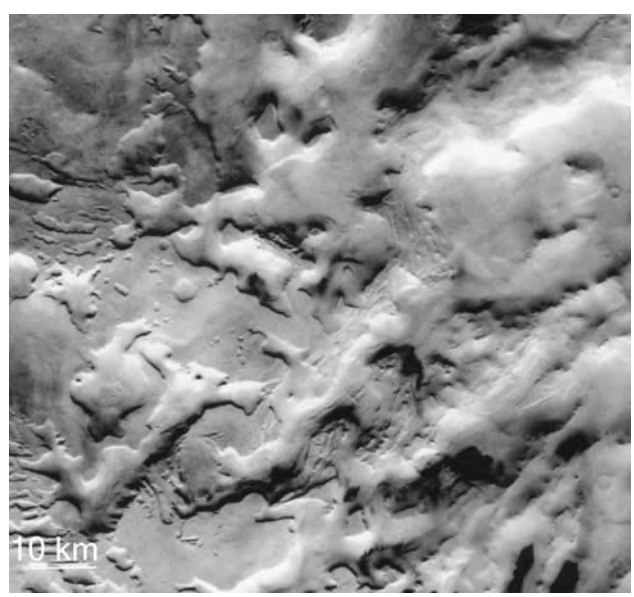

Figure 10.15. The Cavi Angusti at 78.4°S, 291.0°E. These pits are similar to those in the next image except that the pitted deposit is on a local high. The origin of the pits is uncertain. Possibilities include excavation by the wind or melting of an ice-rich deposit (Viking 390B88).

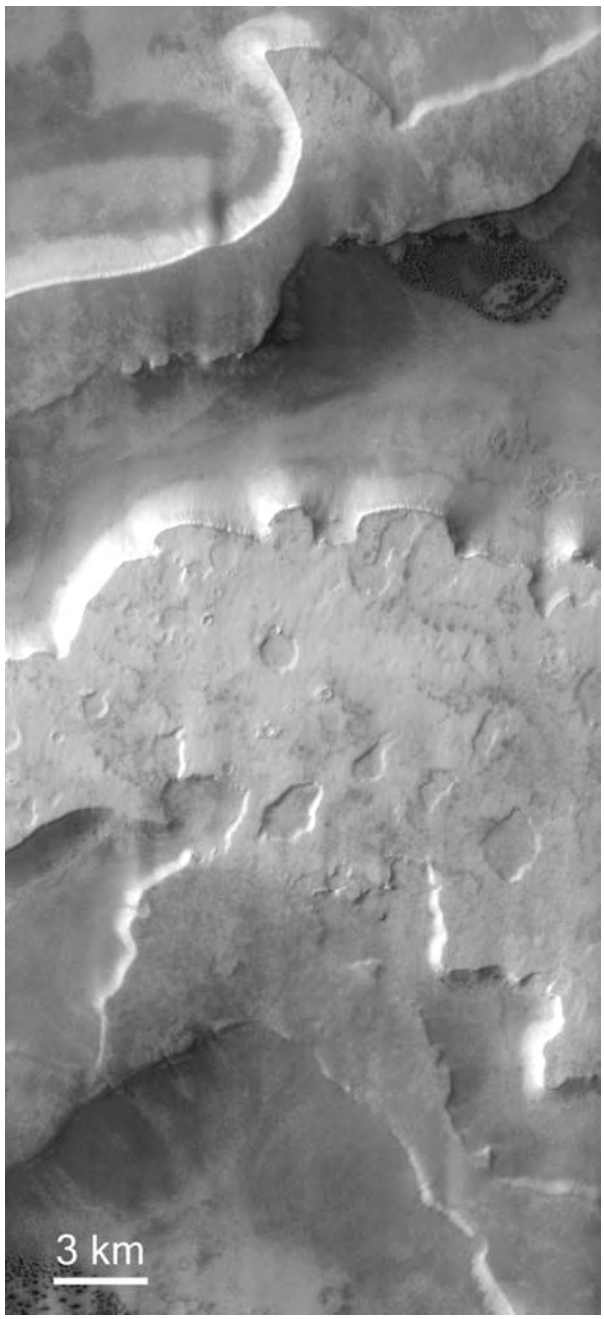

Figure 10.16. The Cavi Sisyphi at 73.5°S, 351.3°E. Much of the cratered terrain around the periphery of the southern polar layered terrain is partially buried by a deposit with a flat upper surface. In places, the deposit has been partly removed to form irregularly shaped pits, termed cavi, with flat-topped remnants between, as seen here (THEMIS PIA05479).

may be over several tens of kilometers across and over 1 km deep.

Most early workers supported the idea that the Dorsa Argentea Formation was a sedimentary blanket of eolian or volcanic origin that had been partly removed by the wind. Howard (1981) alternatively suggested, however, that the pits could be the result of basal melting of ground ice. In support of the proposal he noted that the braided ridges that he interpreted as eskers. Head and Pratt (2001), Ghatan *et al.* (2003), Ghatan and Head (2002, 2004), and Milkovich *et al.* (2002) elaborated on this proposal, and suggested that the cavi, the braided ridges, and several large channels that originate within the area are all the result of basal melting of the Dorsa Argentea Formation, which is interpreted to be an ice-rich deposit. In support of the proposal they note evidence for the emergence of the braided ridges (eskers) from beneath the Dorsa Argentea Formation, the presence of small volcanoes in the area, the start of four large channels at the outer margin of the formation, and the difficulty of eroding small 1 km deep pits by the wind. A small volcano at 73°S, 342°E with radially elongate pits on its flanks and irregular pits further out provides direct evidence of a connection between volcanism and the pits. The suggestion that ice-rich deposits may have been melted at the poles has broad implications for global hydrology. Clifford (1987, 1993) suggested that slow, global circulation of groundwater could result from recharge at the south pole as water derived from melting of the ice-rich deposits there seeps into the ground. The eskers and pits around the south pole support the supposition that melting did indeed occur, but whether it resulted in significant groundwater recharge is unclear.

Thus we have evidence for ice-rich deposits at the poles today, and plausible evidence for extensive ice-rich deposits around the poles during the Hesperian, but there is little, if any, evidence for polar deposits that formed during the intervening 3 Gyr. Did they not form, or were they continually reconfigured so that intermediate-aged units do not survive?

The CO_2 residual cap

The residual CO_2 south polar cap is roughly 300 × 200 km across, on the highest part of the layered terrain, centered at a point offset from the pole by 150 km in the 340°E direction. Its surface has characteristics that are unique to the residual cap (Thomas *et al.*, 2000, 2005; Malin *et al.*, 2001; Byrne and Ingersoll, 2003a,b). The most distinctive type of terrain, informally called Swiss-cheese terrain, has irregular to circular pits of uniform depth with flat floors and steep sides (Figure 10.17). The pit floors may be smooth or complexly patterned. Merging of the pits may isolate irregularly shaped mesas outlined

Figure 10.17. Swiss-cheese terrain at 85.6°S, 283.8°E. The surface of the remnant CO_2 cap is carved into strange patterns not seen elsewhere on the planet. A common pattern is seen here, where an upper layer has been eroded or sublimated away to form intersecting circular pits, roughly 10 m deep. Pits similar to these have been observed to enlarge from year to year. The upper layer may be CO_2 that is being removed to expose an underlying water-rich layer (MOC M0306646).

by walls with concave outward segments. Elsewhere, interconnected linear depressions form polygonal patterns or patterns that resemble fingerprints (Figure 10.18). Byrne and Ingersoll (2003a,b) suggest that the quasi-circular pits form as the result of sublimation of a thin (~10 m) layer of CO_2 ice that exposes underlying water ice, as indicated by the warmer surface temperatures detected by THEMIS. Thomas *et al*. (2005) suggest a more complicated stratigraphy in which an upper unit B, 8 m thick, with layers 1 m thick, overlies an older unit A with 2 m thick layers. Both units have undergone backwasting to form complicated geometric patterns, but the patterns on unit A were made before it was partly covered by unit B.

Malin *et al*. (2001), by comparing images taken one year apart, estimated that the depressions are expanding at a rate of 1–4 m/year. Given this rate, the size of the depressions indicates that unit A started eroding ~100 Mars years ago, and unit B started eroding ~45 Mars years ago (Thomas *et al*., 2005). Malin *et al*. estimate that during each decade formation of the pits results in augmenting the amount of CO_2 in the atmosphere by 1 percent. At the present time, therefore, the atmospheric pressure is increasing, unless additions to the atmosphere are offset by increased adsorption in the regolith or condensation elsewhere on the polar cap.

Summary

1. At each pole is a CO_2 cap roughly 1 m thick, and more extensive in the south than the north, which advances and recedes with the seasons causing global changes in atmospheric pressure.
2. In the north a water-ice residual cap is left in summer. In the south the residual cap appears to be a meters-thick veneer of CO_2 ice overlying water ice. The CO_2 is currently dissipating on decadal time scales to form terrain characterized by numerous shallow circular depressions with uniform depth.
3. At each pole are stacks of young, layered deposits up to 3 km thick that are incised by valleys that spiral around the poles. The deposits in the north form a mound roughly symmetrical about the poles. Those in the south are less uniformly distributed about the poles. The northern deposits are at an elevation roughly 6 km below those in the south. The deposits at both poles are thought to be mixtures of dust and ice,

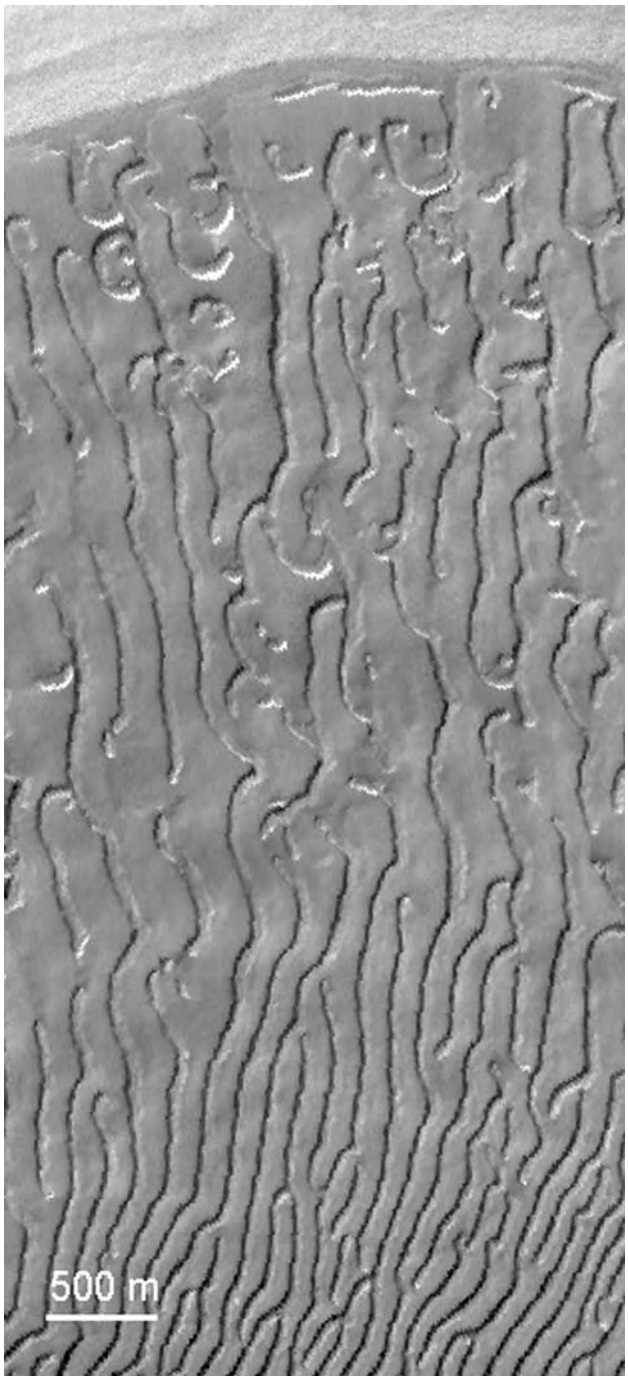

Figure 10.18. South polar cap fingerprint terrain at 85.9°S, 304.2°E. In several places on the residual cap, terrain like that in the previous image transitions into a surface with a fingerprint pattern such as is seen here. This pattern also shows progressive year-to-year changes (MOC M0306756).

and may record changes at the poles caused by recent variations in the orbital and rotational motions of the planet.

4. The mode of formation of the deposits and their incised valleys is controversial. The deposits may result from progressive accumulations of new material deposited over the entire cap, or they may have formed by reworking of the same materials by sublimation and wind. The valleys may form by a combination of preferential sublimation on sunlit slopes and katabatic winds flowing off the poles.
5. The northern layered deposits overlie a darker, gypsum-rich unit that appears to have been the source of sand that forms a vast erg around the north pole.
6. Peripheral to the layered terrains in the south, the cratered uplands are partly blanketed by the Dorsa Argentea Formation of Hesperian age. The presence of esker-like ridges and deep pits suggests that this may be an ice-rich unit that has undergone melting at its base, possibly as a result of volcanic activity.

11 The view from the surface

Our approach to elucidating the geology of Mars has of necessity been very different from the approach used for the Earth. Almost all our geological knowledge of the Earth is based on measurements made on the ground, on the chemistry, mineralogy, lithology, and orientation of rocks at the surface. In contrast, our perceptions about how Mars has evolved have been mostly derived from remote sensing data and a few martian meteorites of unknown provenance. However, geological processes and their sequence can rarely be uniquely identified solely by the configuration of the surface, and composition and lithology can only be coarsely inferred from spectra. This is particularly true on an alien planet where geological processes operate on different materials and under different conditions from our terrestrial experience. Generally, in situ measurements provide much more definitive clues about geological evolution. They also greatly enhance the value of any remote sensing data by providing ground truth against which the interpretation of the remote sensing data can be tested and extrapolated to other areas. At the time that this book was written we had made direct measurements on the martian surface at only five sites: the two Viking sites, the Pathfinder site, and the two Mars Exploration Rover sites. In this chapter we discuss what was found at these sites. The discussion mainly concerns the MER sites because of the diversity of materials that they were able to access and the quality of the data they returned.

Vikings 1 and 2

On July 10, 1976, Viking Lander 1 landed at 22.5°N, 312°E on the rock-strewn plains of Chryse Planitia to give us our first close-up views of the martian surface (Figure 11.1). This success was followed by a second landing in Utopia Planitia at 48.0°N, 134.4°E. While elaborately instrumented for biology, the only geology-oriented instruments on the landers were the cameras and an x-ray fluorescence spectrometer that could analyze loose soil for major elements heavier than Na. The Viking 1 site is downstream of several large channels that enter Chryse Planitia from the south. The site, however, shows little, if any, morphological evidence for fluvial activity. The site has a gentle, rolling topography partly covered by drifts of fine-grained materials, and a population of pitted rocks that cover roughly 6 percent of the surface. Analyses of the soil are consistent with a basaltic composition except for large fractions of sulfur, which is concentrated, probably as sulfate, in a crusty material just below the surface. The vehicle had no means of determining directly the composition of the local rocks. Viking 2 landed on a level plain within an ejecta lobe of the 90 km diameter crater Mie. It is considerably more rocky than the Viking 1 site, with rocks covering roughly 15 percent of the surface. The composition of the soils is similar to those at the Viking 1 site, which suggests that they are not true soils, derived from weathering of the local rocks, but rather material that has been redistributed over the planet's surface. For detailed descriptions of the two sites see Binder *et al.* (1977) and Mutch *et al.* (1977). For discussions of the implications of the chemistry of the soils see Banin *et al.* (1992).

The main goal of the Viking landers was to look for life. Toward this end they carried a complex payload that included a gas chromatograph mass spectrometer (GCMS) and a biology experiment designed to detect metabolism in three different ways. The results were disappointing. The GCMS failed to detect any organics in the soil, despite sensitivities of the order of a ppb and the expectation that detectable amounts would be present from meteorite infall (Biemann *et al.*, 1977). While the biology experiment yielded results not anticipated from a non-biological setting, almost all the experimenters concluded that there were plausible non-biological explanations for what was observed (see Klein, 1979; Horowitz, 1986, and for an alternative view, Levin, 1988). The absence of organics and some initially confusing results from the biology experiments, were attributed to small amounts of oxidants in the soil. When water was added to the soils during the biology experiments oxygen was evolved. The oxidants probably form as a result of photodissociation of water in the atmosphere to produce OH and HO_2, which condense on the surface and migrate through the pores of the soil (Hunten, 1979). The excess hydrogen

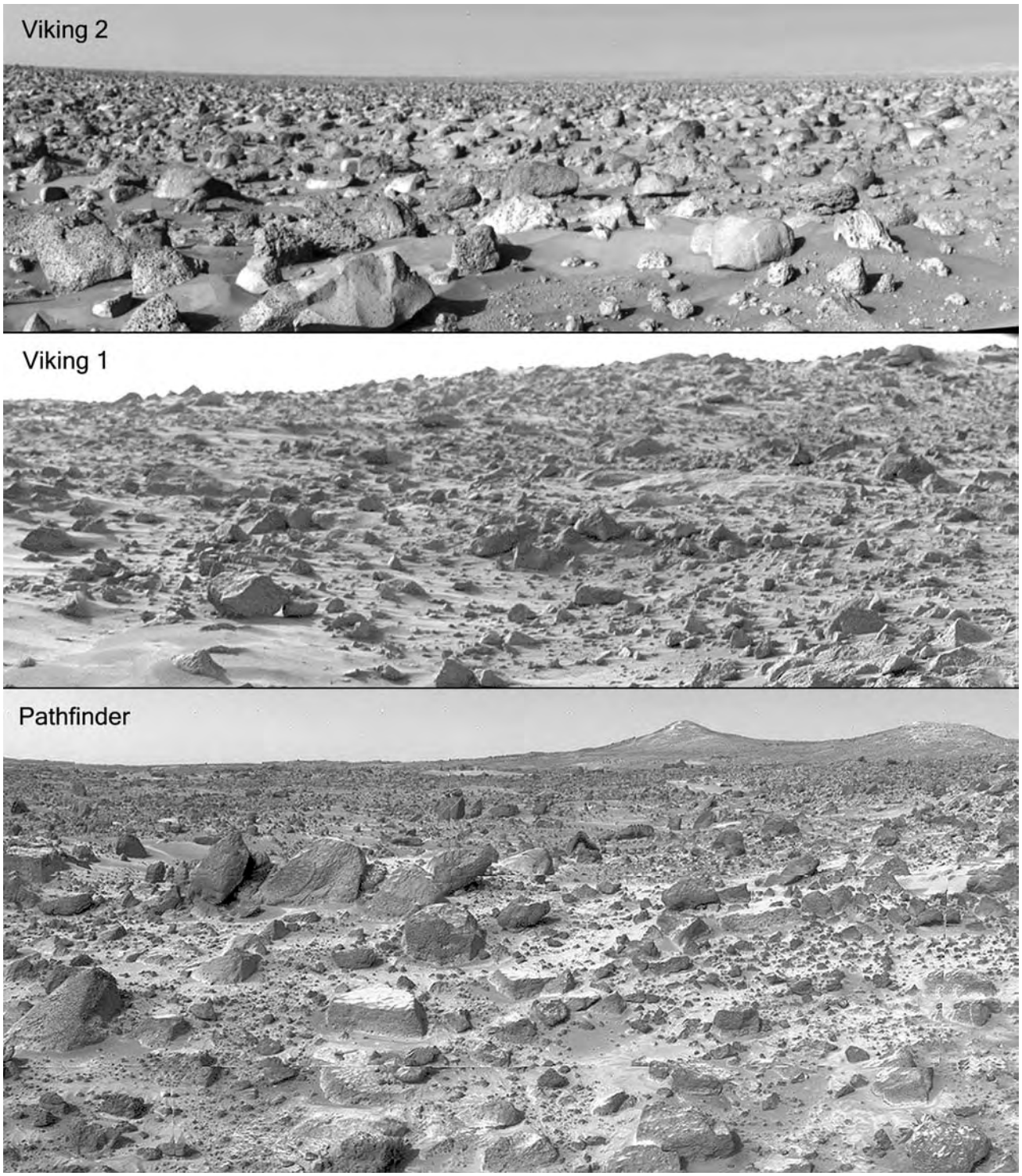

Figure 11.1. Scenes from three landing sites. Viking 2 (upper image) landed on the almost level plains of Utopia Planitia on what may be a lobe of ejecta from the 90 km diameter crater Mie, whose rim is 170 km to the east of the site. The largest rock in the foreground is 1 m across. Viking 1 (middle image) landed in Chryse Planitia on a gently rolling, rock-strewn plain downstream from several large channels that enter the plain from the west and from the south. The rocks are mostly in the centimeter to meter size range. Interspersed among the rocks are drifts of fine-grained material up to 10 m across. Pathfinder (lower image) also landed in Chryse Planitia on what is thought to be the depositional fan of Ares Vallis, a large flood channel that enters the plain from the south. The twin peaks in the background are 1 km away and have a streamlined outline in orbiter images. Many of the rocks in the foreground appear to be standing on end and leaning left to right in the direction of flow of the flood inferred from the regional setting.

ultimately escapes to space leaving the surface oxidized.

Mars Pathfinder

Mars Pathfinder, the first mission to Mars to deploy a rover, was initially conceived as an engineering experiment designed to explore ways of performing small, inexpensive missions to planets. The spacecraft landed on July 4, 1997, in Chryse Planitia, 800 km southeast of the Viking 1 site and at the mouths of Ares and Tiu Valles. The rover, which could travel roughly 10–15 m away from its parent lander, carried cameras and an alpha-proton x-ray spectrometer (APXS) to characterize the rocks and soils. The lander carried a camera with high spatial and spectral resolution, an atmosphere experiment, and a variety of other sensors. The following brief overview of the site geology is abstracted from Golombek *et al.* (1999). For more detail see the more than sixty papers in three special issues of the *Journal of Geophysical Research*, vols. 102(E2), 104(E4), and 105(E1).

In general, the landing area is consistent with its being a depositional plain from the Ares and Tiu floods. The surface, covered with subangular to subrounded pebbles, cobbles, and boulders, resembles depositional surfaces produced in terrestrial catastrophic floods such as the Ephrata Fan in the Channeled Scabland of Washington State. Some of the rocks are imbricated or inclined in the direction of flow as inferred from the orbiter data. Other large rocks are perched as though deposited by a flood. Troughs, visible throughout the scene and aligned in the direction of the flow, may result from late-stage drainage that preferentially carried away the fines leaving a blocky armored surface. Fine-grained windblown material is common throughout the site, as light-toned drifts and tails downwind of rocks. Barchanoid and other dune forms indicate, in addition, the presence of sand-size material. Some of the rocks appear to have been fluted and grooved by saltating particles, but in general wind erosion is minor. The rocks have a variety of textures. Many are pitted, resembling vesiculated volcanic rocks. Others are subtly layered. Some have textures suggestive of breccias. One rock with rounded hemispherical indentations was thought by some experimenters to be a conglomerate out of which had fallen some of its constituent pebbles.

Like the soils at the Viking sites, the Pathfinder soils contain a significant fraction of sulfur (6–8 percent SO_3). All the rocks are partly covered with soil so the APXS rock analyses had to be corrected for the soil contaminant to derive a rock analysis. The high sulfur content of the soils and the likely low sulfur content of unaltered rocks allowed sulfur to be used as a proxy to make the correction (Foley *et al.*, 2003). The soil-free rocks have andesitic compositions. They are distinctively different from martian meteorites, being more Si-rich and Mg- and Fe-poor. It is unclear, however, whether this composition represents a primary volcanic rock or a silicic weathering rind (McSween *et al.*, 2003). The presence of up to 4 percent water in the analyses (Foley *et al.*, 2003) supports the supposition that what was analyzed was a thin alteration rind. The soils appear to be a mixture of comminuted basaltic material and volatiles rich in sulfur and chlorine derived from volcanic exhalations.

Mars Exploration Rovers

In mid 2003 the United States launched two identical rovers to Mars named Spirit and Opportunity. They were to be sent to sites that were thought, from orbiter and other data, to have a high probability of containing physical and/or chemical evidence for the action of liquid water. They were then to reconnoiter these sites, and to characterize the rocks and soils there, looking for aqueous activity such as water-bearing minerals, and minerals deposited by precipitation, evaporation, aqueous sedimentation, and/or hydrothermal activity. In this task, they were extraordinarily successful. Although the two rovers went to two very different sites, they both found unequivocal evidence for the action of water.

The two rovers had an identical array of instruments (Squyres *et al.*, 2003). On a pointable mast were a high-resolution, stereo color imager (Pancam) and a miniature thermal emission spectrometer (Mini-TES). The two instruments could image the surrounding scene at a wide range of wavelengths, thereby providing information on the morphology, composition, and physical properties of the rocks and soils within view, information that was not only of scientific interest but was also required for operating the rover's arm and navigating the vehicles. There were several other cameras in addition to the Pancam, primarily to support rover operations. Hazard identification cameras (Hazcams), mounted low to the front and rear, provided fish-eye views of the immediate vicinity of the rovers. Navigation cameras (Navcams), mounted on the mast, provided stereo, wide-angle views. Although designed primarily for operations, these cameras also provided invaluable science support. In addition, each rover had a movable arm that could place instruments on nearby rocks and soils. On the arm were a microscopic imager (MI) that could take

images at a resolution of 30 μm/pixel, a Mössbauer spectrometer (MB) for determination of iron minerals, and an alpha-particle x-ray spectrometer (APXS) to provide chemical analyses. The arm also carried a rock abrasion tool (RAT) that allowed the experimenters to abrade away surface alteration rinds and expose rock interiors. Magnets of different strengths, designed to capture magnetic components of the airborne dust, were mounted on each rover deck. The landing sequence involved deceleration by a heat shield during atmospheric entry, followed by deployment of a parachute, then inflation of protective airbags for touchdown. After bouncing several times and coming to rest, the airbags were retracted and the landers were unfolded, freeing the rovers for science operations.

The landing sites were selected by a process that took over two years and involved broad participation of the science and engineering communities (Golombek *et al.*, 2003). The goal of landing site selection was to find safe sites that had a high probability of satisfying the science goal of yielding insights into the aqueous history of the planet. Safety and other operational considerations dictated a set of engineering constraints that included (1) latitudes 15°S to 10°N for maximum solar power; (2) elevation < 1.3 km for sufficient atmosphere to slow the parachute during descent; (3) low horizontal winds, wind shear, and turbulence to minimize horizontal velocities at landing; (4) low slopes to minimize bounce on landing; (5) modest rock abundances to reduce airbag abrasion; and (6) a coherent, load-bearing surface for trafficability. The engineering constraints for each potential site had to be inferred indirectly from remotely sensed properties of the surface, such as thermal inertia and radar reflectivity, and from modeling the atmosphere. Considerations of scientific desirability and engineering acceptability narrowed an initial set of ~150 sites down to the chosen two: Gusev crater and Meridiani Planum.

Spirit

The Spirit rover landed in Gusev crater on January 3, 2004. Gusev is a 160 km diameter, flat-floored, Noachian-aged crater near the plains–upland boundary at 14°S, 175°E (Figure 11.2). Its interest as an exploration site stems from the possibility that it may have once contained a lake (Cabrol *et al.*, 2003). The southern wall of the crater is breached by a large channel, Ma'adim Vallis. If the channel was cut by water, as is likely, then water must have pooled in Gusev. The hope was, therefore, that we would find lacustrine sediments on the floor of the crater, and that these sediments would provide insights into aqueous processes and climatic conditions that prevailed during the Noachian era. While lacustrine deposits were not found on Gusev's flat floor, low hills within the crater did provide abundant evidence for aqueous alteration.

Gusev crater regional context Ma'adim Vallis is one of the largest valleys on the planet. It combines characteristics of a valley network and an outflow channel. It starts abruptly at 28°S, 178°E and extends for 1000 km northward before it ends in Gusev crater. Over much of this length it is 8–10 km wide and up to 1 km deep. The abrupt start and large dimensions of the channel are more typical of an outflow channel than a valley network. On the other hand, the valley has numerous tributaries like a valley network. Irwin *et al.* (2002) suggested that the large dimensions and abrupt start of the channel resulted from rapid draining of a large Noachian lake in the uplands to the south of the present valley. MOLA data shows that the valley starts at the outlet of a closed basin ~3,000,000 km^2 in area (Figure 7.11). They argue that the basin's outlet was formerly at the 1100 m level and was downcut to its present 950 m level, and in so doing discharged roughly 100,000 km^3 of water down Ma'adim Vallis and through Gusev crater, hence its resemblance to an outflow channel. The numerous tributaries result simply from drainage unconnected with that of the main lake. Where Ma'adim enters Gusev crater are a group of flat-topped hills that have been interpreted as delta deposits (Figure 11.3). If this interpretation is correct, then the water level must have been at least at the −1500 m elevation of the hills, roughly 300 m above the present level of the crater floor. An outlet from the crater through the northwest rim at an elevation of −1800 m is mostly blocked by a younger crater.

Although the main justification for choosing Gusev crater as a landing site was the expectation of finding lake sediments there, the deposits in the floor of Gusev are probably of diverse origin. To the north of the crater is a large volcano, Apollinaris Patera, whose flanks extend to within 80 km of Gusev's northern rim. Pyroclastic deposits from this volcano may have been deposited within the crater. To the northeast of Gusev an extensive, thick, eroded deposit, called the Medusae Fosssae Formation, straddles the plains–upland boundary. It can be traced to within 40 km of the rim and may actually be present in the eastern half of the crater. The origin of the Medusae Fossae Formation is unclear. Suggestions include a pyroclastic origin or simply a thick accumulation of weakly cemented, wind-blown debris. There may also have been volcanic intrusions within the crater,

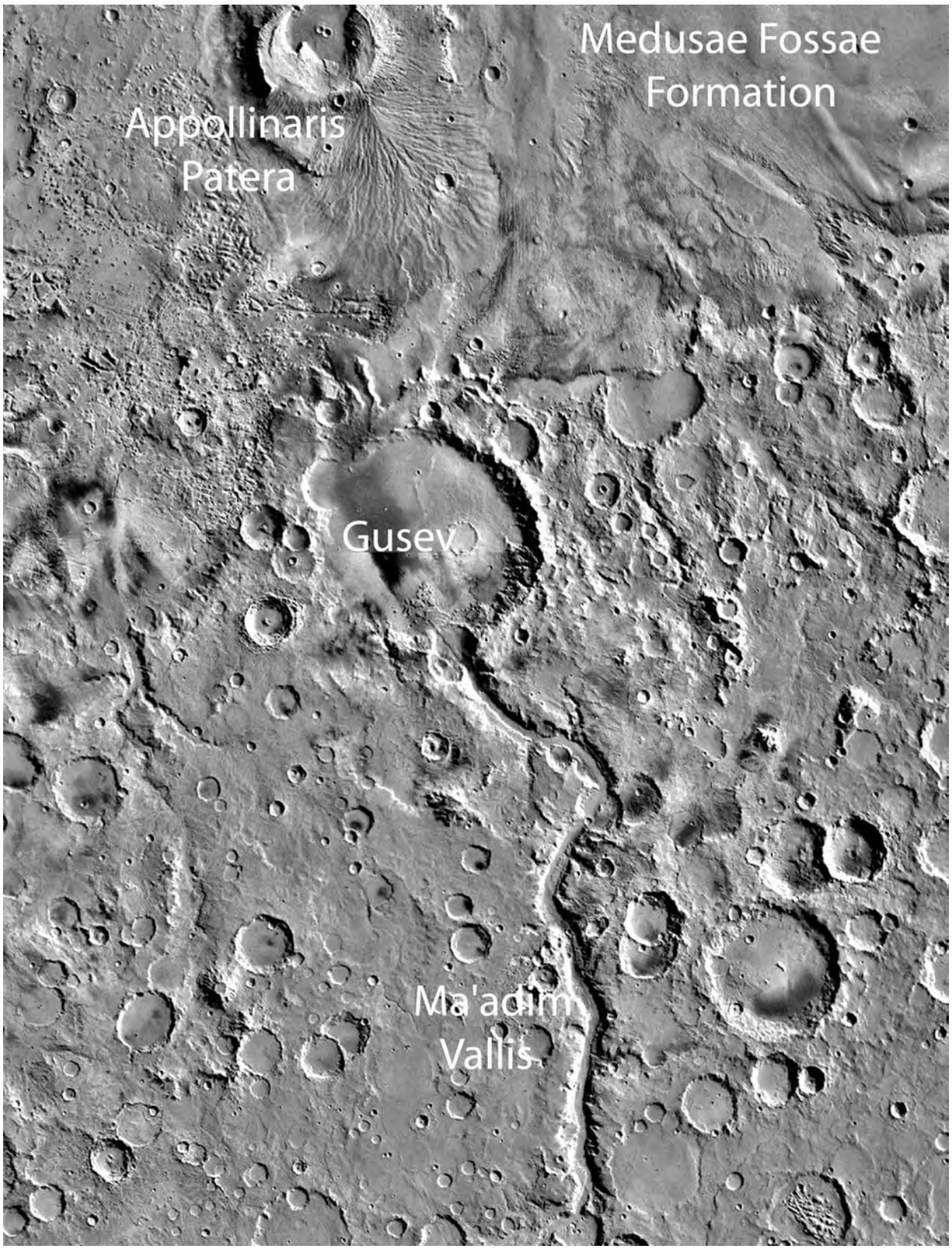

Figure 11.2. The regional setting of the 160 km diameter Gusev crater. A large valley, Ma'adim Vallis, breaches the southern rim of the crater. It is thought to have been fed by a large lake to the south of the image area (see Figure 7.11). Water from the valley probably pooled within the crater, then exited to the north through a gap now blocked by an impact crater. Ash from the volcano Apollinaris Patera to the north may have been deposited within the crater. The Medusae Fossae Formation, an extensive eolian deposit to the northeast, may also have contributed to the fill in Gusev (MOC WA).

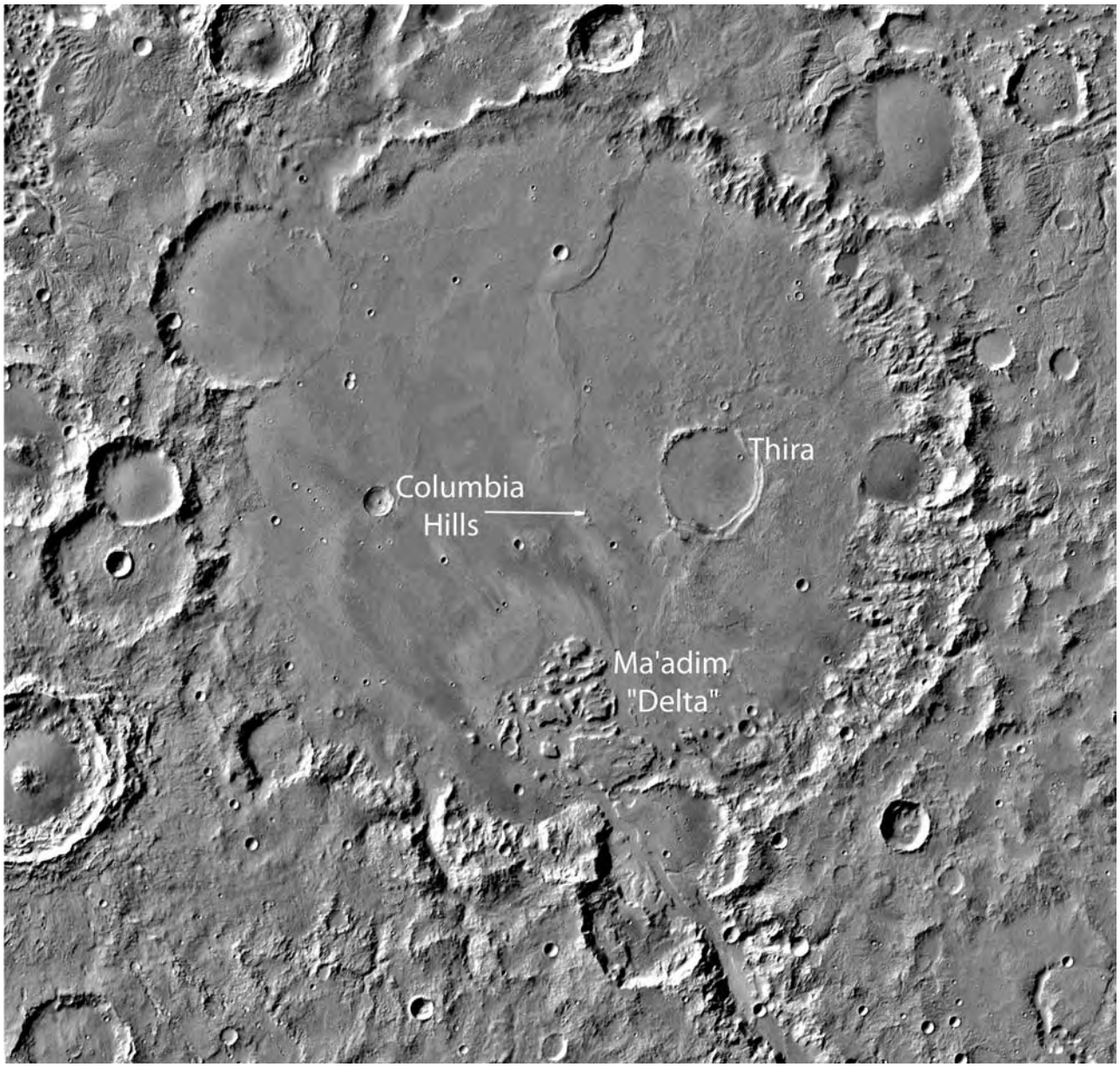

Figure 11.3. Gusev crater. A group of hills at the mouth of Ma'adim Vallis have been interpreted as a delta. The floor in the eastern third of the Gusev, around Thira, is covered with a hilly deposit of unknown origin that appears etched in high-resolution images. The rest of the crater floor is a level cratered plain with wrinkle ridges, except for some low hills such as the Columbia Hills, and some local areas where the regional plains unit has been stripped away to expose the underlying materials (Viking mosaic).

and impact debris and wind-blown material must also have contributed to the crater fill.

A complex history of Gusev is supported by features on the crater floor. Several large, partly filled or completely filled craters are present, identifiable by rims that stand above the almost level plains that constitute the floor, or detectable as shallow circular depressions in the MOLA data. The most prominent is the 20 km diameter crater Thira in the eastern half of the crater. These post-Gusev craters suggest that a significant time elapsed between formation of Gusev and accumulation of all its interior deposits, during which successive impacts disturbed and redistributed previous fill. Prior to the landing, several geological and thermophysical units were identified on the floor (Kuzmin *et al*., 2000; Milam *et al*., 2003). Ridged

plains, the most widespread unit, cover much of the western half of the crater, and is the unit on which Spirit landed. Much of the eastern half of Gusev's floor, particularly around the crater Thira, is covered with an etched unit, consisting of numerous closely spaced hills that appear to be remnants of a formerly more extensive cover. The unit stands at an elevation 50–150 m higher than the ridged plains. Locally, hollows in the ridged plains, surrounded by low, inward-facing escarpments, have a similar etched appearance. Also locally, low hills poke up above the plains. Finally, a flow-like feature with a rumpled surface and lobate margins extends 150 km across the floor from the mouth of Ma'adim (Rice *et al.*, 2003). The origin of all these units is very uncertain.

Gusev plains Spirit landed at 14.57°S, 175.47°E on a rock-strewn, cratered plain near the center of Gusev, and 20 km to the west of the rim of the crater Thira. A 210 m diameter crater, Bonneville, lies 300 m to the northeast of the landing point; 2.6 km to the southeast are a small group of roughly 100 m high hills called the Columbia Hills (Figure 11.4). Spirit first characterized the materials in the immediate vicinity of the landing point, then traveled the 300 m up to the rim of Bonneville crater. From there it made the 2.6 km journey across the plains to the Columbia Hills, then up into the hills. We first discuss the plains where the surface materials consist of minimally altered basaltic rocks, sitting on and embedded in a matrix of mostly comminuted basaltic debris. Then we discuss the hills, where the rocks are very different, being highly altered, and likely of a variety of origins.

The plains form a rock-strewn surface crossed by poorly defined ridges up to hundreds of meters long and a few meters high, and pitted with numerous shallow, circular hollows that are probably secondary impact craters formed in unconsolidated rubble (Golombek *et al.*, 2006). In the immediate vicinity of the landing site, rocks >1 cm across cover about 5 percent of the surface; on the rim of Bonneville crater they cover 29 percent of the surface. Between the rocks, the surface is covered with a light-toned, reddish soil. The rock sizes have an exponential distribution as do those at the Viking and Pathfinder sites. Rock frequencies are higher on the rims of hollows whereas hollow interiors are almost rock-free, so they appear lighter-toned in the images. Most of the rocks are angular to subangular; they show no sign of rounding that might indicate water transport (Figure 11.5). Almost all are massive and poorly foliated. They are fine-grained with irregular vesicles and vugs, suggesting a volcanic origin. No stratified rocks that might be interpreted as sedimentary were observed on the plains, nor were any impact breccias. The rocks are intrinsically dark gray in color but they are variably coated with the bright, reddish soil materials. Some rocks have a distinctive two-toned appearance, with upper portions that look fresh and dark, and lower portions that are brighter and coated. Many, having beveled sides, facets, and grooves, appear to have been shaped by the wind. A few rocks have flutes that start at a common level above the present plains surface, as though the flutes had developed when the lower portions of the rock were buried and protected. No unambiguous outcrops were observed on the plains, even within the walls of Bonneville crater, where outcrops would be present if the Bonneville impact had been into coherent rocks. The lack of outcrops in Bonneville implies that bedrock is at least 10 m below the present surface. The survival of a Hesperian crater population down to small sizes, the minimal abrasion of the rocks ejected from these craters, and estimates of total deflation from rock markings indicate that the average erosion rates over the last $\sim$3 billion years have been very low, between 0.01 and 0.1 nm/year, several orders of magnitude less than even the lowest terrestrial rates (Golombek *et al.*, 2006).

Mineralogical and chemical analyses show that the plains rocks are olivine basalts, similar in composition to a class of martian meteorites called shergottites (Gellert *et al.*, 2004; McSween *et al.*, 2004; Morris *et al.*, 2004). All the rocks analyzed had surface alteration rinds that differed in composition from the rock interiors. The normative mineralogy of the unaltered rocks, that is, the hypothetical mineral composition derived from the chemical analyses, suggests that the rocks are composed of olivine, plagioclase, and pyroxene with accessory magnetite, chromite, ilmenite, and phosphate. Olivine, pyroxene, magnetite, and a nanophase iron oxide were detected in unaltered rocks by the Mössbauer spectrometer (Morris *et al.*, 2004). The rocks also have vugs and veins partly filled with lighter-toned materials of unknown composition. Although similar in composition to the Pathfinder rocks, the Gusev rocks are higher in Mg and lower in K than those at Pathfinder. While the rocks are clearly volcanic, having formed either as intrusives or surface flows, their source is unclear. There are no obvious extrusive centers within Gusev and no flows from the volcano Apollinaris Patera can be traced into the crater. The lavas are likely the result of fissure eruption within the crater, and the original vents have been covered by lava or destroyed by impacts. Since no outcrops were observed, it is not clear how far below the present

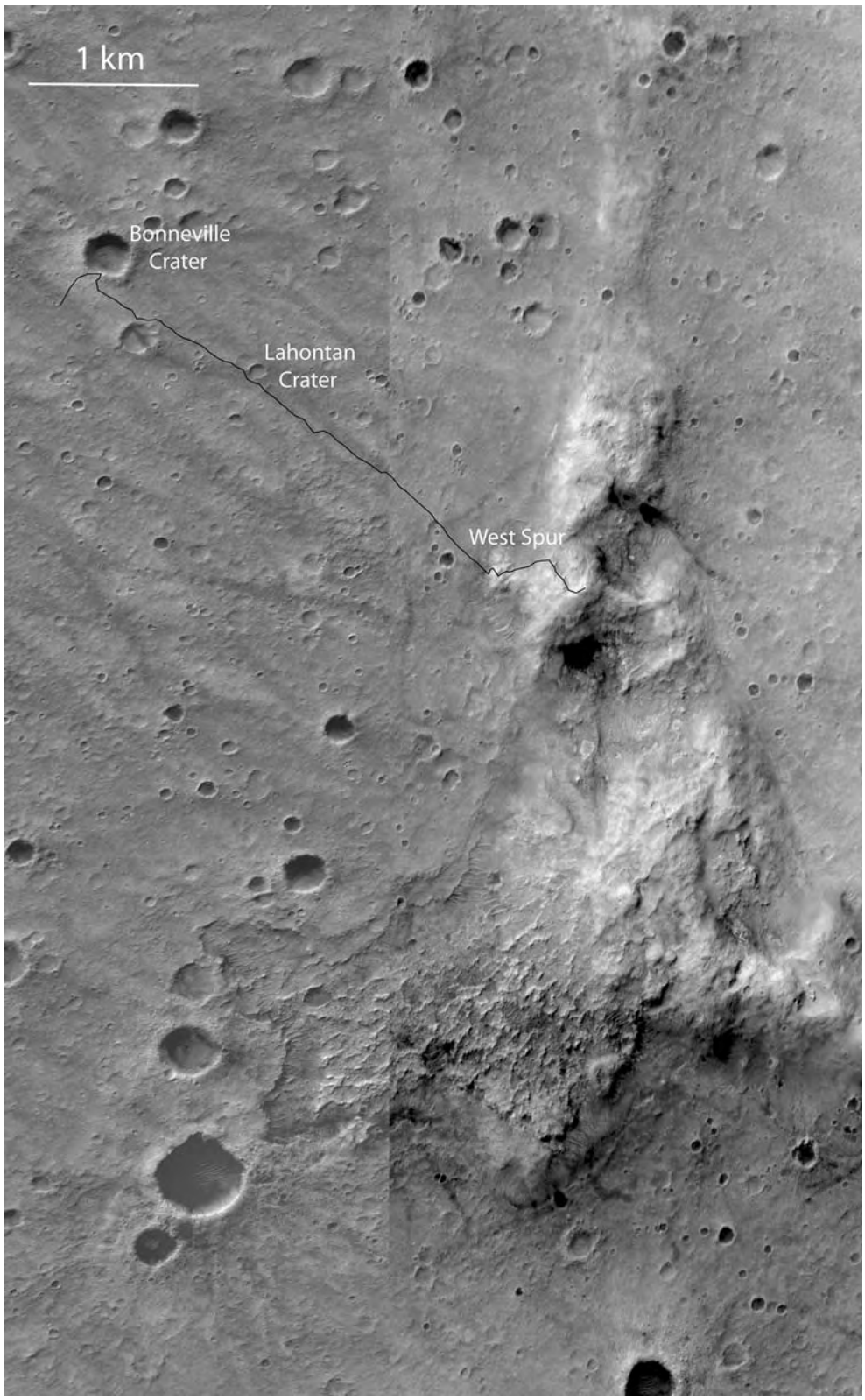

Figure 11.4. The traverse of Spirit from its landing site to the summit of the Columbia Hills. Numerous shallow craters, probably mostly secondary craters, are inset into the plains. Dark streaks on the plains are dust devil tracks. The plains lap onto the older Columbia Hills. Closed basins northeast and southeast of the summit to the east of West Spur may be ancient impact craters. The southern end of the hills has an etched appearance as though a former surface cover had been partly removed (MOC frames R1001924, E0300012).

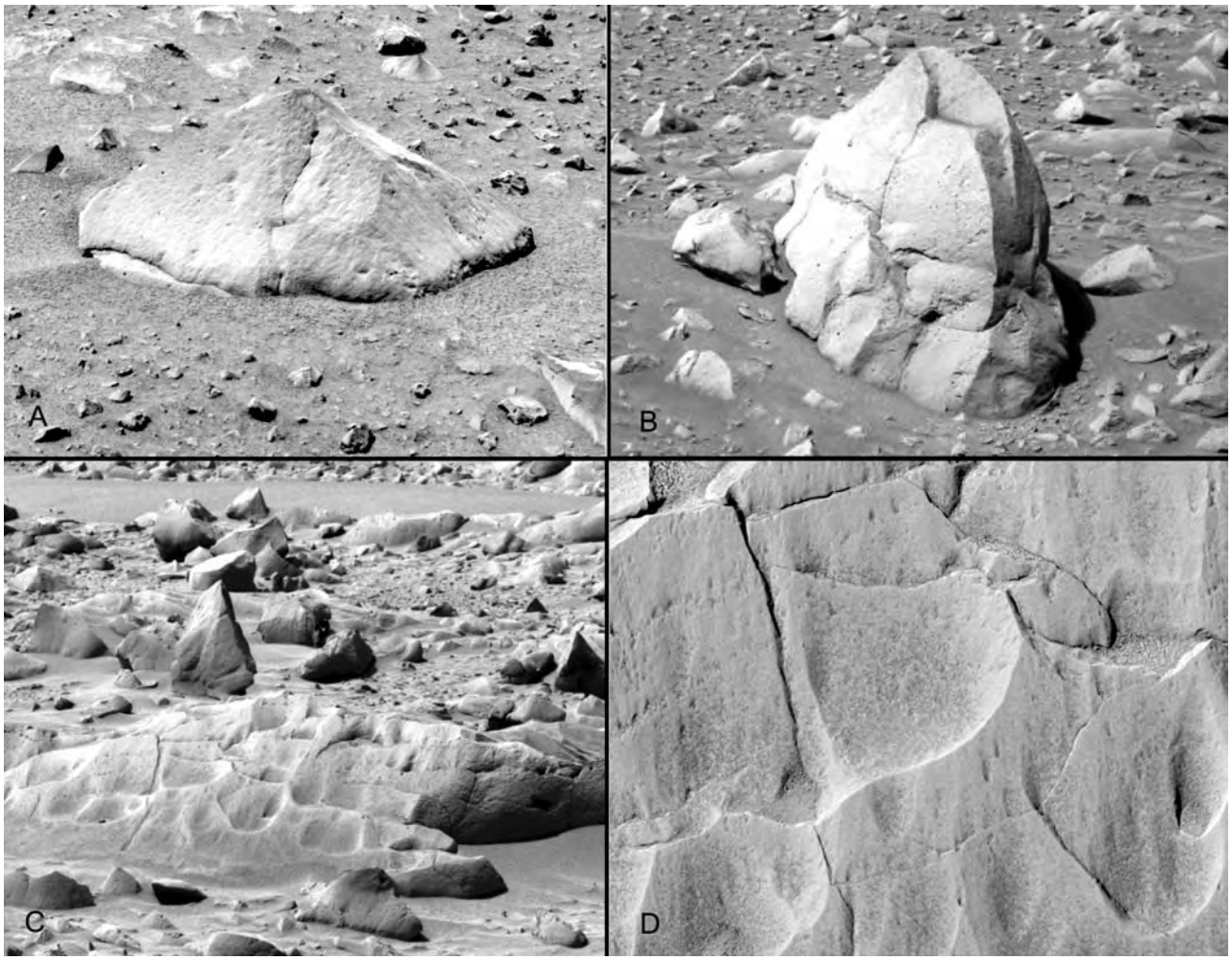

Figure 11.5. Rocks on Gusev plains. All are massive to slightly foliated basalts, almost unaltered except for a millimeters-thick weathering rind. Most are angular and show no evidence of transport by water. (A) Adirondack, 20 cm high. (B) Humphrey, 50 cm high. (C) Mazatzal, 20 cm high. In the background is a light-toned, rock-free hollow, thought to be the remains of a secondary impact crater. (D) Detail of the fluting on Mazatzal.

surface the rocks were originally emplaced. The absence of lake sediments on the plains likely results because the present plains surface is younger than Ma'adim. The plains are Hesperian in age, whereas Ma'adim Vallis and any sediments that might have been derived from it are probably Noachian in age.

All the rocks have a millimeters-thick rind formed of altered rock and adhering soil particles. On some rocks, analyses were made on the original surface, on the surface after a light brushing, and on the interior after the rind had been ground away. From interior to exterior, S, Cl, and the oxidation state of the Fe increase, whereas Br and Mg decrease. Various processes probably have contributed to alteration of the rocks' surfaces. Oxidants, formed by UV-mediated reactions in the atmosphere and then precipitated onto the surface, have likely contributed to oxidation of the original basaltic components (Hunten, 1979). Volcanogenic exhalations of HCl and SO_3 could, when combined with minor amounts of liquid water, possibly in acid fogs or in thin films, break down the primary minerals. Ice, deposited during periods of high obliquity, could have melted to also produce small amounts of water, which could have mediated alteration, particularly if combined with oxidants and volcanogenic acids. Whatever processes operated, they were extremely slow and probably involved only minute amounts of water, since the alteration rinds are only millimeters thick, despite exposures of billions of years to conditions at the surface. There is no chemical

evidence from the rocks to support the supposition that they have been exposed to warm climatic conditions or submerged beneath a lake's surface.

The soils at Gusev are similar in composition of those at the Viking and Pathfinder sites, which supports the hypothesis of global mixing of fine-grained materials by global dust storms. They are essentially basaltic in composition except for higher concentrations of S and Cl. The main difference between the Gusev soils and those at the Pathfinder site is that the Gusev soils have less K but so do the rocks, which suggests that, despite global mixing, the chemistry of soils is affected by local source materials. The iron mineralogy of the soils is still dominated by primary basaltic minerals such as olivine and pyroxene. These minerals are, however, present in smaller proportions than in the rock interiors, and the soils contain larger fractions of oxidative weathering products, such as nanophase ferric oxide particles (Morris *et al.*, 2004).

The soils have a sulfur-rich component in addition to basalt and its oxidation products. The highest sulfur contents among the soils on the Gusev plains were in the upper layers of trenches (Burroughs and Laguna) dug by the rover. If all the sulfur in soils from the trench Burroughs were in the form of Mg, Fe, and Ca sulfates, then the sulfate content in the trench would range from 7 to 22 wt percent. S, Br, Cl, and Mg are strongly correlated in the soils, suggesting that Mg is transported with the soluble elements, in contrast to the rock rinds where S is anticorrelated with Mg. Transport of soluble salts over scales of at least centimeters has clearly taken place in the soils, and water is clearly implicated. What remain unclear are how much water was involved, and what conditions led to breakdown of the silicates, production of magnesium salts, and their transport through the soil profile. While Haskins *et al.* (2005) invoke processes involving very low water to rock ratios to explain the weathering rinds on the rocks, they acknowledge that somewhat wetter conditions than at present may be needed to mobilize the S-rich components in the soil.

As expected, wind features are common on the Gusev plains. In addition to the fluting and faceting of rocks, already mentioned, there are depositional features such as drifts, ripples, tails downwind of rocks, and mantles on rocks. Dust devils, known to be common in the areas from their tracks seen from orbit, were observed and filmed directly by the rovers. The loose material available to be mobilized by the wind ranges widely in size from dust, which probably is in the micrometer size range (Smith *et al.*, 1997), through silt ($\sim$0.01–0.1 mm), sand (0.1–1 mm), to coarser granules ($\sim$1–3 mm). Away from ripples, most of the Gusev soils are composed of very fine grains ($<200\,\mu$m) or agglomerations of fine grains (Herkenhoff *et al.*, 2004a). Eolian bedforms consist primarily of meter-size ripples that have crests with a surface layer of coarse sand and troughs with poorly sorted, finer-grained sand. The size distribution of the particles on the ripples has a bimodal distribution with peaks at 0.3 mm and 1.4 mm. The coarse debris appears to be well-rounded lithic fragments (Figure 11.6); the fine debris appears to be agglomerations of finer particles. The presence of crusts on the bedforms and absence of dunes with steep slip faces suggest that the ripples and drifts are not currently active.

Columbia Hills The Columbia Hills are a chain of hills roughly 8 $\times$ 4 km across, elongate in a north-south direction, and standing 90 m above the adjacent plain (Figure 11.7). As viewed from orbit they have a rough, textured surface, particularly at their southern end, where the surface of the hills has an etched appearance (Figure 11.4). Some roughly circular depressions, several hundred meters across, within the hills may be remnants of old impact craters. In most places the plains lap onto the hills, indicating that the hills are older than the plains. At the southern end of the hills, however, the plains appear, in places, to have been stripped back to form areas that are lower than the adjacent plains, and surrounded by escarpments that face the hills. Opportunity crossed from the plains into the hills at an east–west promontory of the hills called West Spur, then it slowly moved upward and westward to a local summit called Husband Hill, analyzing rocks and soils, and assessing the local geology along its way.

The rocks of the hills are very different from those of the plains, and highly variable in texture and composition. Some have cavernous textures as though the wind had hollowed out the soft interiors and left only the harder exterior rinds or coatings (Figure 11.8). Others have a deeply eroded surface with stalk-like protrusions (Figure 11.9). Yet others are strongly foliated. Many of the rocks have a granular appearance in contrast to the massive, igneous textures typically encountered on the plains. Grinding of rocks with the rock abrasion tool indicates that the hills rocks are, in general, much softer than those on the plains.

Squyres *et al.* (2006) identify six distinct classes of rocks from Gusev crater on the basis of their elemental composition. All the rocks on the plains are

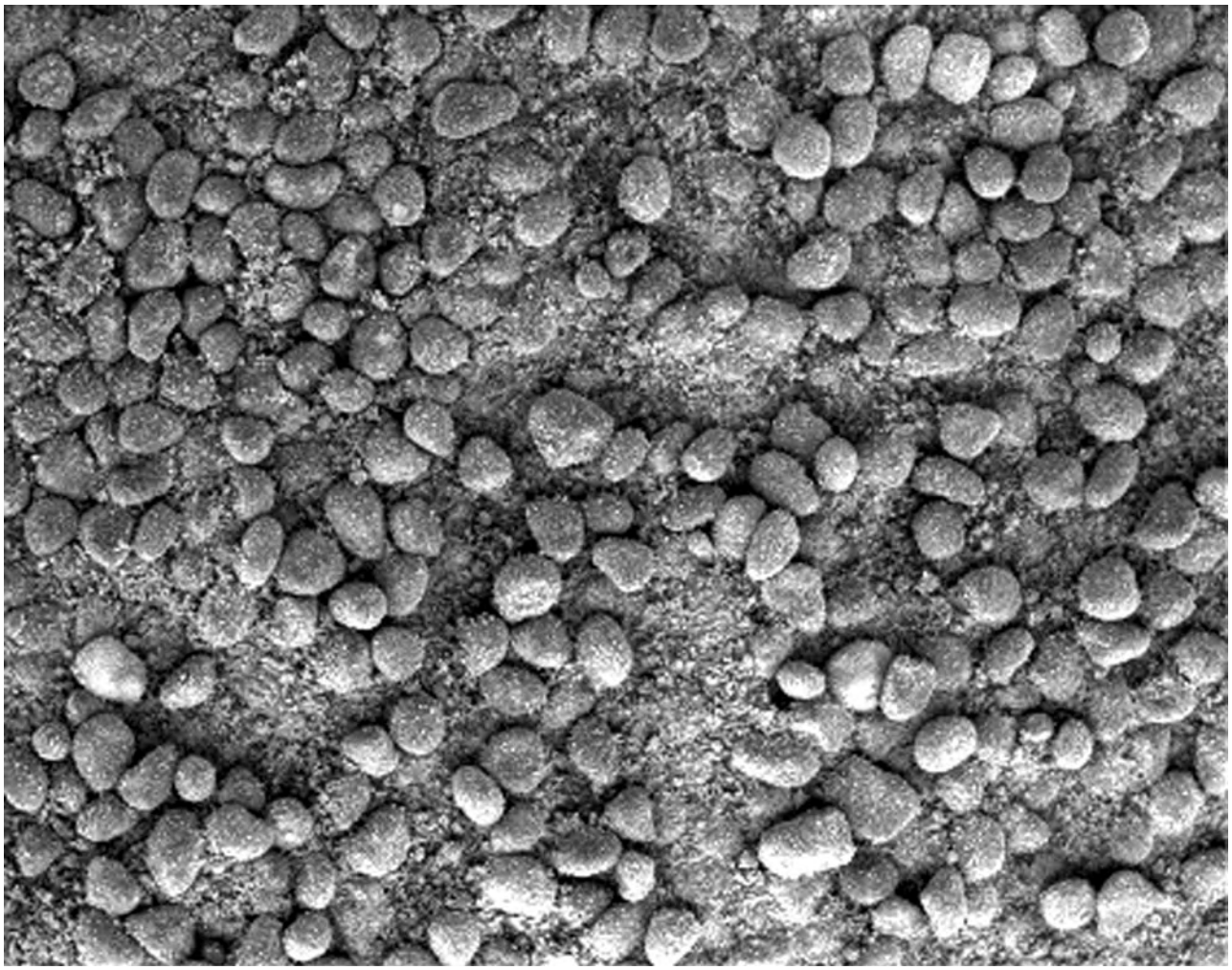

Figure 11.6. Well-sorted coarse (1.8 mm) sand grains on the windward side of an eolian ripple at Arena (2M130001885EFF0506P2943M2M1).

olivine basalts, which they call the Adirondack class, after the informal name of one of the plains rocks that was examined in detail. The five other classes, which occur only in the Columbia Hills, are lithologically and chemically diverse. Again the different classes are named after rocks that were examined in detail. The following descriptions are abstracted from Squyres *et al.* (2006).

CLOVIS CLASS. Clovis-type rocks dominate on West Spur, both in outcrops and in the float (Figure 11.10). At the time this was written, none had been found on Husband Hill. They have similar Si, Ti, Al, and Fe contents as the plains rocks, but have significant enrichments of S, Cl, and Br, even in their interiors. S correlates with Na, K, and Ca, suggesting that these elements are present mainly as sulfates; Mg correlates with Cl, suggesting that it is present as a chloride. The Clovis-type rocks are also enriched in Ni as compared with the plains basalts, indicating that there may be a meteoritic component. The Clovis rocks are also highly oxidized, with most of the Fe existing as Fe^{3+} in the minerals goethite, hematite, and magnetite. Primary minerals such as olivine and pyroxene are much reduced or absent.

The Clovis-class rocks show a wide variety of characteristics at the outcrop scale. Some are massive and have little structure. Others appear finely laminated (Figure 11.11). The hollowed-out textures have already been mentioned. The rocks are soft. The RAT required only 10–20 percent of the energy drill into

Figure 11.7. View of the Columbia Hills looking southeast from the rim of Bonneville crater. Failure to find lacustrine rocks in the ejecta and walls of Bonneville crater and elsewhere on the Gusev plains prompted a drive to the Columbia Hills where it was thought that there would be a greater chance of finding evidence of aqueous processes in the older rocks there.

Clovis-class rocks as was required to drill the same distance into the Adirondack-class olivine basalts. Finally, some of the rocks contain clasts that ranged in size up to several millimeters across. On the surface of some of the rocks, wind erosion has left the more resistant clasts on long stalks.

Thus, the Clovis-class rocks are poorly sorted, pervasively altered, clastic rocks of basaltic composition. Their characteristics are consistent with their being emplaced by explosive volcanism or impact. After deposition they were extensively altered by S-, Cl-, and Br-laden acid fluids.

WISHSTONE CLASS. The Wishstone-class rocks were first found on the northwest flank of Husband Hill. They are also common in the float on Cumberland Ridge. No outcrops of Wishstone class were observed. The Wishstone-class rocks have a distinctively different elemental composition from the Adirondack and Clovis-class rocks, being lower in Fe and Cr and higher in Al, Ti, and P. The dominant primary minerals are plagioclase, pyroxene, and olivine, possibly with minor ilmenite and a calcium phosphate. MI images show that the Wishstone rocks are composed of poorly sorted, shard-like, angular clasts in a fine-grained matrix. The textures resemble terrestrial ash-flow tuffs.

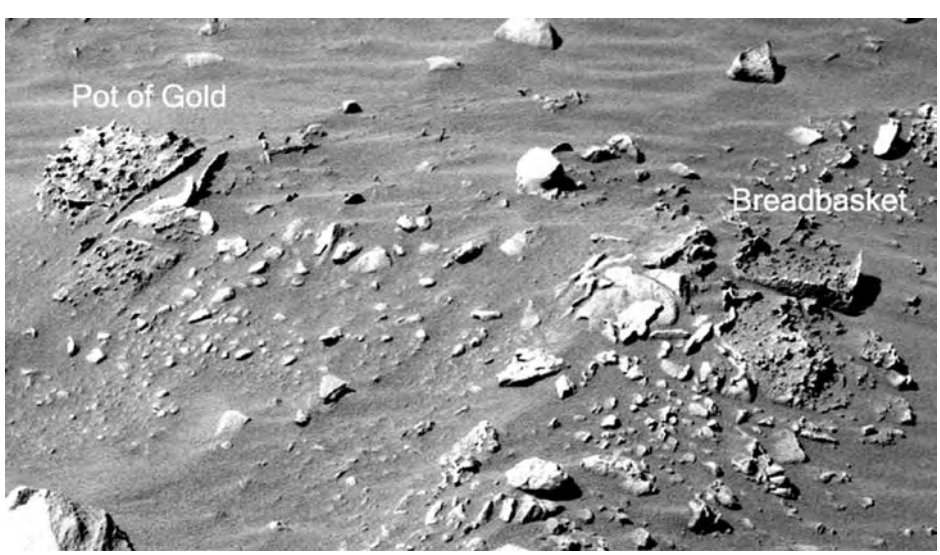

Figure 11.8. Highly altered rocks on West Spur. Immediately upon leaving the plains and crossing onto West Spur, Spirit encountered soft, highly altered rocks. On the surface of Pot of Gold are stalk-like protrusions, which may have resistant nodules at their tips (see the next figure). Breadbasket appears to be the weathered-out shell of a former rock, of which only the harder, outer rind remains. Both rocks are enriched in hematite and nanophase iron oxides and depleted in olivine relative to the plains rocks.

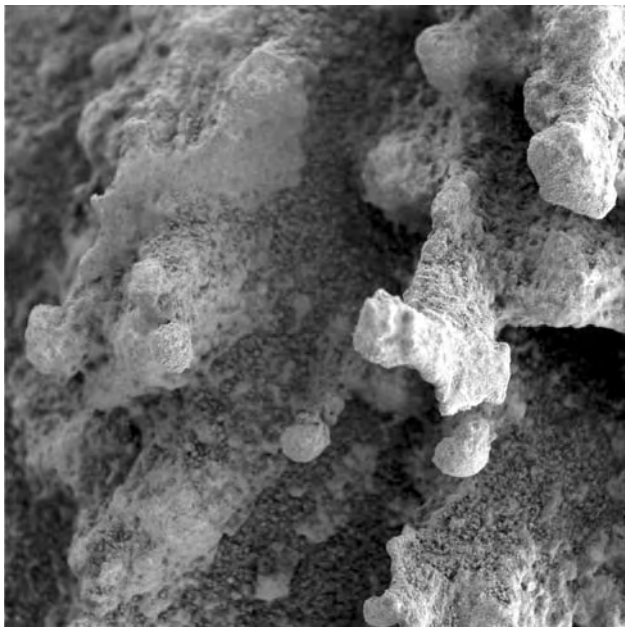

Figure 11.9. Microscopic image of the surface of Pot of Gold showing the stalks that constitute the rock's surface (Spirit sol 171).

The rocks have been only minimally altered since they were deposited. They are less oxidized than the Clovis rocks, having Fe^{3+}/Fe_{total} ratios of ~0.4–0.45 as compared with 0.58 to 0.85 for Clovis rocks, and they show no significant enrichment in S, Cl, or Br compared with the Adirondack-class rocks. Grinding energies required to RAT were several times larger than those required for Clovis rocks. All these characteristics suggest that the Wishstone-class rocks formed by an explosive event, either volcanism or impact, which created the clasts, and that the original rocks have been only slightly altered since deposition. The paucity of Ni in the rocks and the resemblance of the rock textures to ash-flow tuffs favors a volcanic origin.

PEACE CLASS. Only two exposures of Peace-class rocks had been found at the time of this writing, both outcrops (Figure 11.12). The Peace rocks are fine-grained, cemented, and clastic. Most of the grains are in the fine to medium sand range, but larger clasts up to a few millimeters across are present. They form mostly finely layered outcrops, but where the layering is not present, the rocks display a spongy texture. They are soft rocks. The energies needed for grinding by the RAT were less than any other rocks in Gusev and comparable to the sulfate-rich sedimentary rocks at Meridiani Planum. The rocks are very low in Al, Na, and K compared with other Gusev rocks, which indicates that they are low in plagioclase. The chemical composition of the silicate (clast) component is similar to a lherzolite (an ultramafic rock consisting of olivine, clinopyroxene, and orthopyroxene). The primary basaltic components of the rocks appear to be only slightly altered since the Fe^{3+}/Fe_{total} is only 0.35 and hematite, goethite, and Fe sulfates were not detected. However, the Peace rocks have significant fractions of salts, probably as a cement. They have high sulfur contents, and the sulfur correlates with Mg and Ca, suggesting that the sulfates are of Mg and Ca. If so, these two salts make up ~16–17 percent of the rocks. The only rocks examined by the rovers that contain more S are the evaporitic rocks at Meridiani Planum.

The Peace rocks therefore have two very different components: a minimally altered utramafic, clastic component and a Mg–Ca sulfate cement. Although the high quantities of sulfates suggest that they were deposited from water, the lack of significant alteration of the mafic minerals, particularly olivine, suggests that the exposure to an aqueous environment was limited.

WATCHTOWER CLASS. This class of rock has been found only on the Cumberland Ridge where it forms prominent, rugged, stratified outcrops (Figure 11.13). The rocks are very variable in composition and texture (Figure 11.14). Like the Wishstone rocks they have high Ti, high P, and low Cr. Like the Peace rocks they are enriched in S, Cl, and Br. The elemental variability can be mimicked well by the mixing of two components, one with the composition of the Wishstone-class rocks, the other with the composition of the Peace rocks. The group is also highly variable in its level of alteration. The Fe^{3+}/Fe_{total} ranges from 0.43 to 0.95, and alteration products such as hematite, goethite, and nanophase oxyhydroxides have a correspondingly wide range. The rocks are texturally diverse. Watchtower rock itself has a surface that is composed of closely spaced knobs and pits. Some rocks are finely layered, others finely pitted on a millimeter scale, yet others have bulbous textures.

Squyres *et al.* (2006) conclude that these rocks are fine-grained ejecta from an impact into a mixture of Wishstone and Peace-class rocks. They ascribe the different textures to different modes of deposition during the impact event. While the rocks do have a salt component, the levels are no higher than those predicted from the Wishstone–Peace mixing model. Alteration is isochemical, being mostly oxidation with

Figure 11.10. Clovis after RATing. This soft rock is high in sulfates, chlorides, and bromides. It is also rich in hematite and goethite, but has no jarosite. It may originally have been an impact breccia or volcanoclastic rock of basaltic composition but was altered by S-, Cl-, and Br-rich fluids (Spirit sol 226).

minor hydration. They accordingly suggest that the alteration was at low water/rock ratios, possibly shortly after the impact events by hydrothermal fluids in the hot ejecta blanket.

BACKSTAY CLASS. Only one rock of this class has been examined in detail. The rock was in the float. No outcrops were observed. The class was defined because the rock has a characteristic Mini-TES spectrum, and several other rocks with the same spectrum have been observed in Gusev. The rock is an olivine basalt that resembles the Adirondack-class rocks on the plains, except that it is higher in Ti, Al, and K and lower in Fe. It is less altered than any other rocks in the Columbia Hills. The source of the rocks is unknown. They may have been introduced into the hills by impacts. However, while several Backstay-class rocks have been identified from Mini-TES spectra on the upper slopes of Husband Hill, none has been observed on the lower slopes, which suggests a local source.

In summary, at least five distinctively different geological materials have been identified in the Columbia Hills: (1) the Ni-enriched basaltic source that was stirred by impacts and deposited to form the Clovis-class rocks; (2) the Wishstone-class rocks rich in Ti and P and low in Cr, interpreted to be a pyroclastic deposit; (3) the cemented, ultramafic sands of the Peace class, representing a time when basaltic debris was transported into the area and became permeated with sulfate-rich brines; (4) fine-grained impact ejecta of mixed Wishstone and Peace materials; and (5) the Backstay basalts. All classes except Backstay are significantly more altered than the plains basalts. Some of the Clovis and Watchtower rocks are so pervasively altered that they have a chalk-like

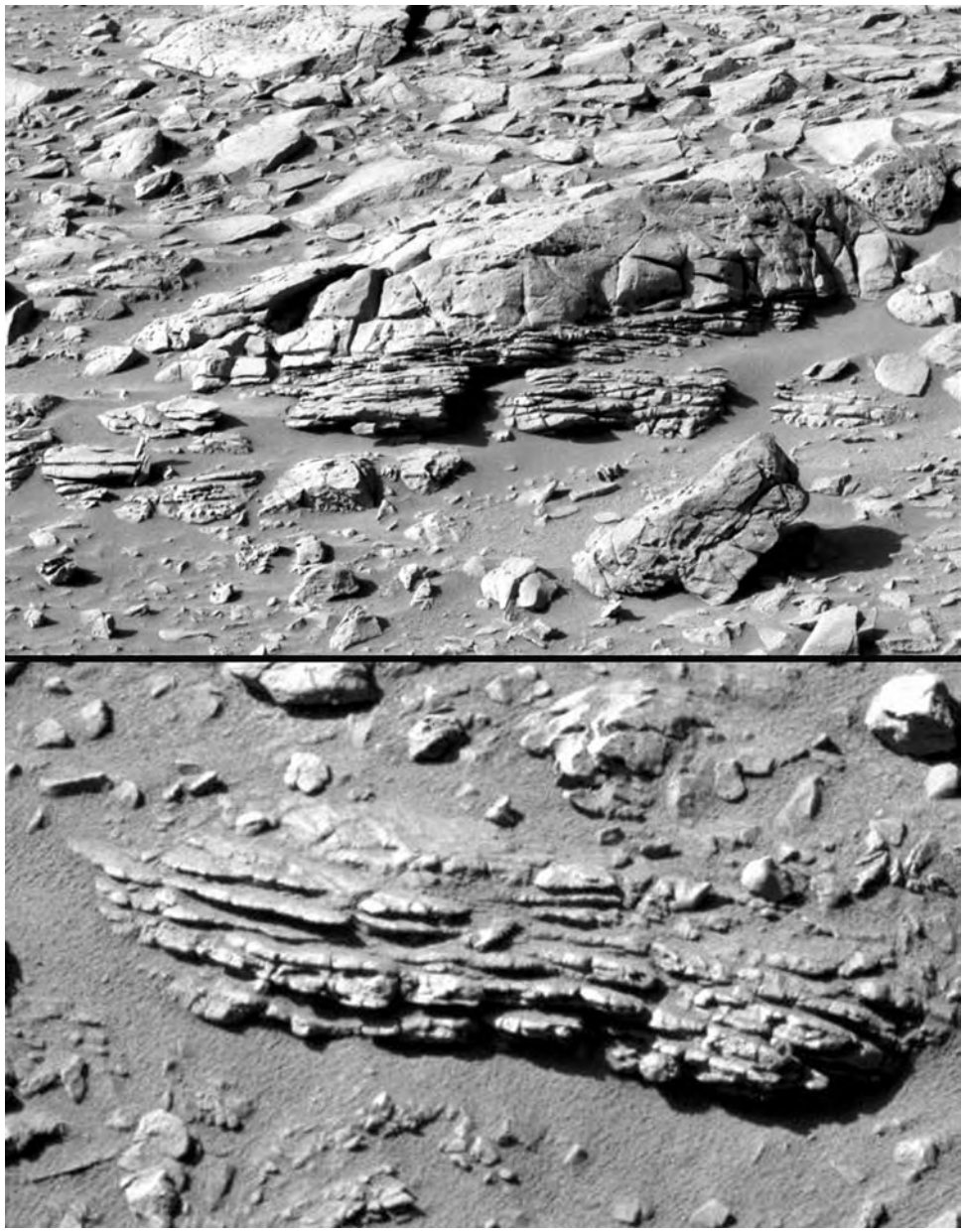

Figure 11.11. Foliated Clovis-class rocks on West Spur. The upper image is of Palenque, the lower of Tetl (Spirit sols 269, 264).

consistency and only traces of the original primary minerals remain.

The Columbia Hills rocks are almost certainly Noachian rocks that postdate the formation of Gusev crater but predate formation of the plains on which Spirit landed. Whether they postdate or predate the formation of Ma'adim Vallis is unclear. None of the Columbia Hills rocks, with the possible exception of the Peace class, appear to be lacustrine. As indicated above, several large impact craters identified from MOLA and imaging data on the floor of Gusev are partly or completely buried by crater fill, and the Columbia Hills were likely formed by uplift as a result of an impact, although they cannot be tied to a specific crater. If uplift occurred after formation of Ma'adim, then lacustrine rocks may occur somewhere within the Columbia Hills. If uplift occurred before formation of Ma'adim, then the hills would probably have been covered with water since they are at a lower elevation than the "delta" deposits at the mouth of Ma'adim.

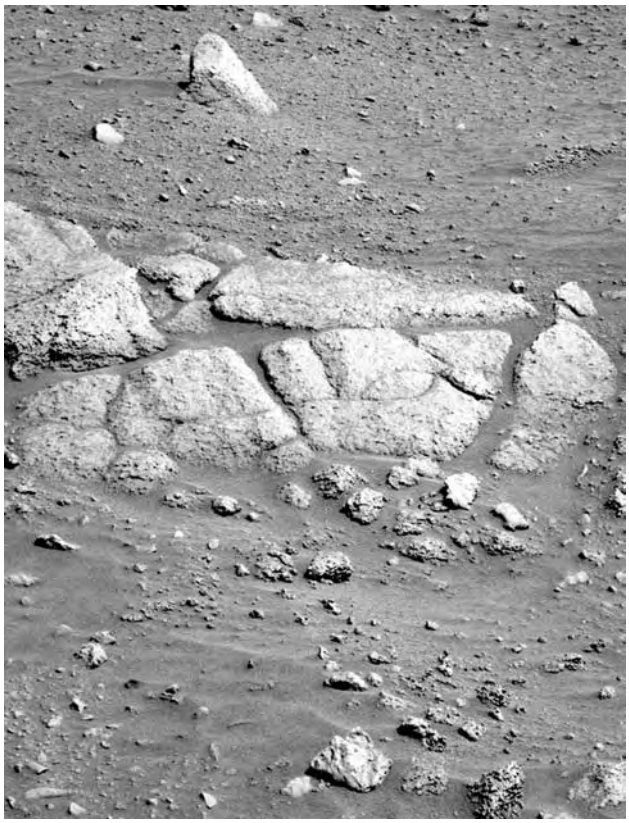

Figure 11.12. The Peace-class rock, Alligator. This class of rock has a high sulfate content and an only slightly altered ultramafic, silicate component (Spirit sol 382).

However, deposition could have been restricted to the lower parts of Gusev's floor and the lake may have been short-lived and left no trace in the hills. The Columbia Hills rocks have been substantially altered. Water is clearly implicated, but alteration by lake waters appears unlikely in view of the large local variations in the amount of alteration and of the dependence in the amount of alteration on class type. Much of the alteration may have occurred at the time of rock formation, particularly if deposited as warm ejecta or pyroclastic flows at a time when water was locally available. Only the Peace-class rocks can plausibly be interpreted as water-lain. Thus although there are many uncertainties, the rocks of the hills differ radically from those on the plains. They have a variety of origins and almost all have been exposed to aqueous alteration. In contrast, the rocks on the plains are all basaltic lavas that have barely been altered despite being exposed to conditions at the surface for probably more than 3 billion years.

Opportunity

Opportunity rover landed on Meridiani Planum, at 1.948°S, 354.474°E, on January 24, 2004, twenty-one days after Spirit landed in Gusev crater. Being a level, sparsely cratered plain, the site was attractive from an engineering standpoint. It was one of the safest sites under consideration. Its science interest stemmed from detection of abundant hematite at the surface by the thermal emission spectrometer on Mars Global Surveyor (Christensen *et al.*, 2000). Hematite can exist in different forms. The infrared spectra suggested that the that form of hematite in Meridiani is a gray, coarse-grained, crystalline variety. This type of hematite can form in several different ways such as by precipitation from oxygenated, iron-rich, surface waters, precipitation from iron-rich hydrothermal fluids, leaching of iron-rich soils, and oxidation of magnetite-rich lavas (Christensen *et al.*, 2000). Most of the possible origins involve liquid water, so the site had a high potential for providing insights into the aqueous processes, which was the main thrust of the MER project.

Regional context Opportunity landed on the upper surface of a widespread sequence of layered rocks, at least 600 m thick, that lie unconformably on an ancient cratered surface (Figure 11.15). Where the rover landed, the upper surface of the sequence forms an almost level plain. To the south the boundary between the layered sequence and the dissected Noachian terrain is sharp. The layered unit clearly cuts across pre-existing craters and valleys. Elsewhere the boundary with the cratered terrain is poorly defined. Complex patterns of ridges, mesas, and hills, mostly outlined by cliffs, give the peripheral areas of the unit an etched appearance as though parts of the sequence had been removed (Figure 11.16). As a result, the areal extent of the layered deposits cannot be precisely determined. However, they extend for at least 800 km in both the east–west and north–south directions. Pedestal craters, outward-facing cliffs, mounds of sediments within craters, and etched remnants of the sedimentary sequence beyond the periphery of the main exposure suggest that the formation was at one time considerably more extensive than it is at present (Edgett and Malin, 2002).

Hematite is not detected over the entire area of the layered sequence. It appears to be the uppermost unit of the sequence, and where the layered sequence has been partly eroded away to form the etched terrain, hematite is generally absent (Arvidson *et al.*, 2003). In its appearance in orbiter images, the layered sequence resembles units elsewhere on the planet that

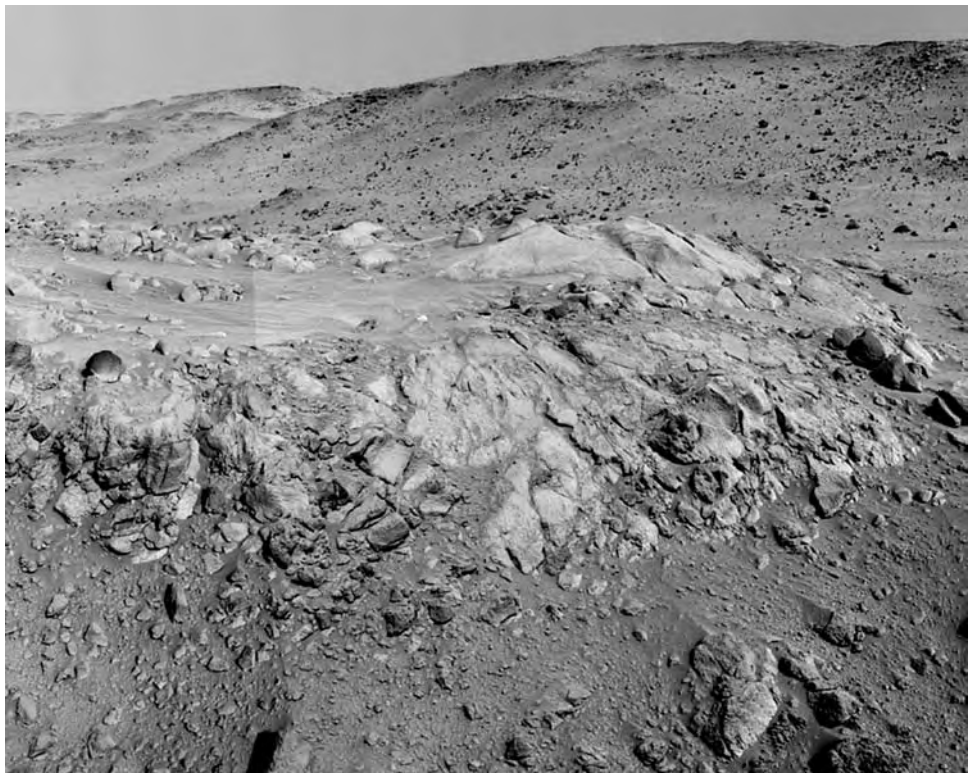

Figure 11.13. Watchtower-class rocks form rugged outcrops on Cumberland Ridge. The crest of Husband Hill is on the horizon to the upper right (Spirit sol 410-413).

have been deposited unconformably on the pre-existing terrain, a prominent example being the Medusae Fossae Formation. Prior to the landing, the Meridiani deposits (and the Medusae Fossae Formation) had been variously interpreted as a volcanic or eolian mantle (Scott and Tanaka, 1986; Greeley and Guest, 1987; Arvidson *et al*., 2003), former polar deposits (Schultz and Lutz, 1988), and subaqueous sedimentary deposits (Edgett and Parker, 1997). The deposits do not lie within any clearly defined basin, as might be expected if they were deposited from some extensive body of water, although there may have been local closed basins around the periphery of the deposit (Newsome *et al*., 2003).

The appearance of the layered sequence in orbiter images with resolutions better than 50 m/pixel varies considerably according to location. Near the landing site, where the unit is minimally eroded, the unit forms a level plain that is mostly smooth except for scattered craters that have a wide range of preservation, from almost fresh-appearing to barely discernible shallow depressions. Most of the surface has a two-toned appearance. Some areas have an irregular mottled pattern; other areas are mostly dark except for bright circles, formed where rims of craters in the brighter underlying material poke up through the darker surface unit (Figure 11.17). Most of the craters contain fields of dunes. Before the landing, the area was interpreted to have a dark, hematite-rich layer at the surface that partly covered an older, brighter, cratered unit. It was hoped that both units could be sampled at the landing site, a hope that was fully realized.

The age of the layered unit is poorly defined, mainly because of the effects of infilling and erosion. Crater counts by Lane *et al*. (2003) show that the size-distribution curve for craters on the unit does not follow a crater production function (see Chapter 2) but is instead flat. The number of small craters (< 500 m) falls far short of the number expected from the number of larger craters (> 500 m). This implies that the smaller craters have been preferentially destroyed by erosion and infilling. The small crater population cannot, therefore, be used to date the unit. Hynek *et al*. (2002) suggested that the plains on which Opportunity landed are probably Upper Noachian to Lower Hesperian in age, based on the number of large bright circles that are seen in the MOC images, but the younger bound of Lower Hesperian is very uncertain.

Figure 11.14. The Watchtower-class rocks are highly variable in texture. Some are massive, but the globular to spongy texture seen here on Jibsheet is common. Most are highly altered, but the degree of alteration varies on small length scales, which suggests that only small amounts of water were involved. Alteration may have occurred by hot aqueous fluids at the time of deposition as an ash flow or from a cloud of impact debris (Spirit sol 482).

Around the periphery of the area where the layered sequence is exposed, well away from the landing site, the appearance of the surface is dramatically different. In these peripheral regions, the layered rock sequence has been eroded into complex patterns in which bright hills and mesas are separated by dark, low, flatter areas (Figure 11.16). The hills commonly have stair-stepped slopes, presumably because of the layers' varying resistance to erosion. The bedding appears to be all horizontal, and individual beds can commonly be traced for several kilometers. Exhumed craters on the stair-stepped slopes suggest that accumulation of the layers took place over an extended period of time (Edgett and Malin, 2002). Even further out from the main outcrop area, only isolated remnants of sediments remain, commonly within craters as stacks that in places overtop the crater rims.

The Meridiani rocks and soils The Opportunity lander came to rest on dark, fine-grained soil inside a shallow, 20 m diameter crater, subsequently named Eagle (Figure 11.18), in a level plain that extends to the horizon in all directions (Squyres *et al.*, 2004a). Ten meters away from the lander, lighter-toned rocks, exposed in the wall of the crater, appeared to be bedrock. Subsequent examination of the rocks showed that they are sandstones composed of roughly equal amounts of silicic clastic debris and chemical constituents, dominated by evaporitic minerals. The ferric sulfate mineral jarosite was specifically identified, but calcium and magnesium sulfates are inferred from the chemical analyses. Scattered throughout the rocks, and weathering out at the surface, are spherules, 4–5 mm across, informally termed blueberries, that contain large fractions of hematite (Figure 11.19A). The rocks exposed in Eagle crater form a widespread pavement, which probably extends to the horizon at a shallow depth just below the loose soil and eolian debris at the surface. The soils are dominated by basaltic sands with a mean grain size of 50–150 μm, the size most easily moved by saltation on Mars (Figure 11.19B). In addition, there are minor amounts of dust derived locally from the sulfate-rich outcrops and globally from airfall. Hematite spherules are scattered across the soil surface. Trenches dug in the soil show that the spherules are a lag, concentrated right at the surface. It is estimated that a 1 m layer of rock needs to be eroded away to produce the density of spherules observed at the surface.

The rocks are of pivotal importance for understanding past environmental conditions at the surface, since they provide almost unequivocal evidence for aqueous activity at or near the surface. Water was almost certainly involved in the formation of the evaporitic minerals, in the deposition of some of the rocks, and in their subsequent alteration. Moreover the rocks appear to have been deposited at the surface where they are now located, unlike those of the Columbia Hills, which may have been formerly buried and structurally emplaced in their current location. The rock sequence exposed in Eagle crater is only 30–50 cm thick. Subsequently, Opportunity examined a 7 m thick section in a nearby crater called Endurance (Figure 11.20), then traveled for several kilometers across the Meridani plains, examining the rocks and soils encountered on the way.

THE BURNS FORMATION. The best-documented rock section at Meridiani is that of Burns cliff in Endurance crater (Figure 11.21). The cliff was named after Roger Burns, who predicted that ferric sulfate minerals, including jarosite, would be found on the surface of Mars. The rock sequence, called the Burns Formation, consists almost entirely of sandstones, whose component sand grains are composed of mixtures of silicic debris of basaltaic provenance and evaporitic minerals.

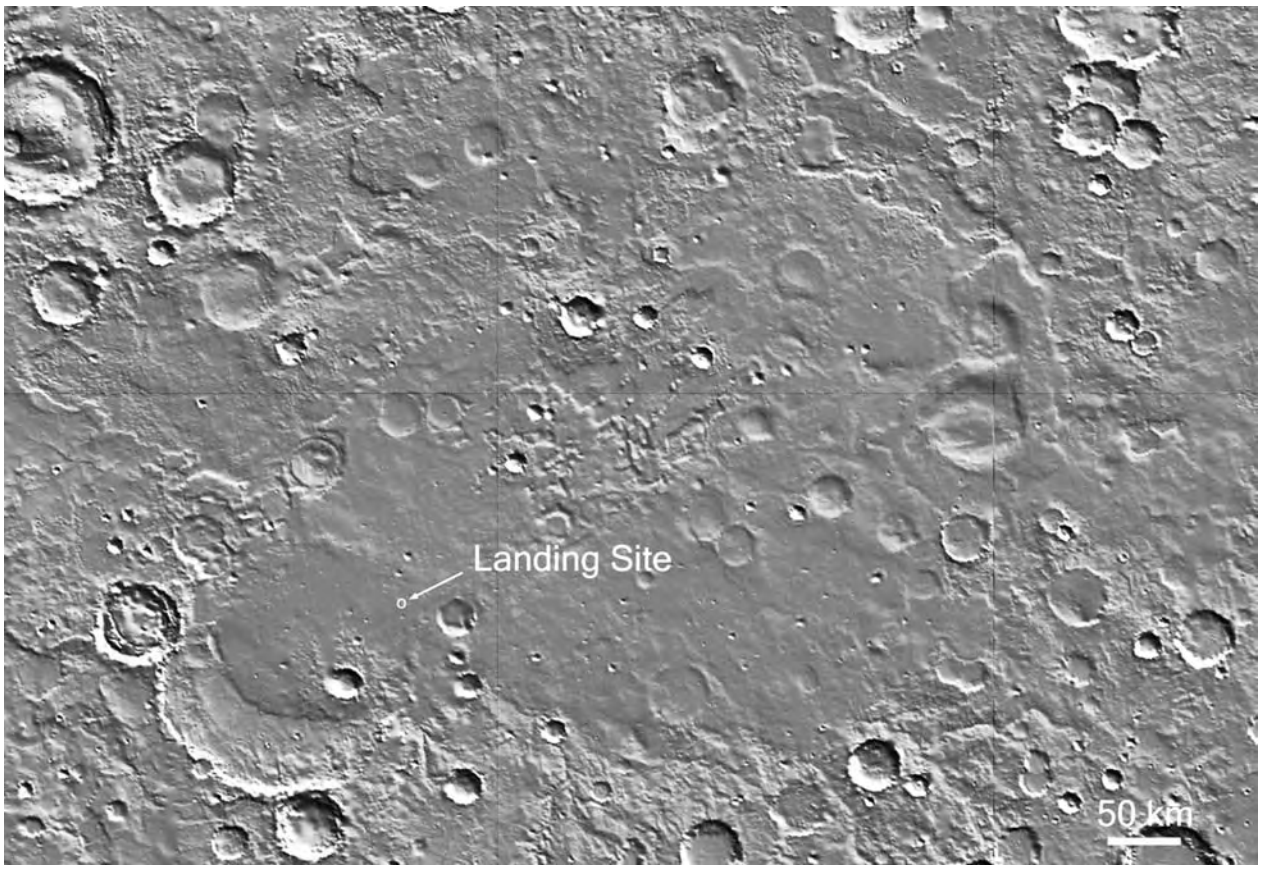

Figure 11.15. Opportunity landing site. Opportunity landed on layered sediments that extend for several hundred kilometers to the north and east of the landing site. They appear dark in this MOLA image. The upper surface of the sediments is mostly smooth, but in places, particularly around the periphery of the deposit, the sediments are partly eroded away to give the surface an etched appearance.

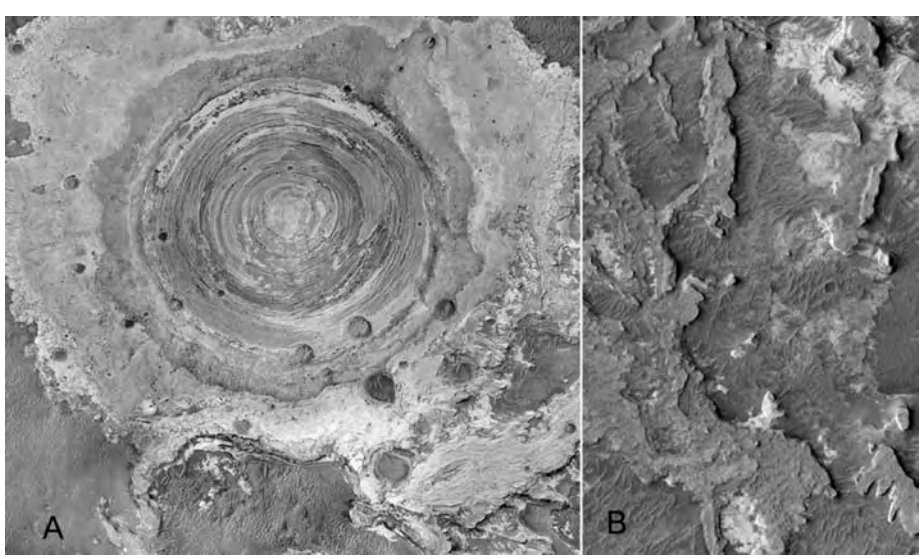

Figure 11.16. Etched remnants of the Meridiani sediments at 4.6°N, 357.2°E. Erosion of the sediments on which Opportunity landed can produce a variety of patterns. (A) Here a crater was filled with sediments and then the sediments were partly removed, leaving layers in the crater and a bright rim around the crater outlined by an irregular outward-facing escarpment. 2.3°N, 7.4°E (MOC 2-316). (B) Here parts of the sedimentary sequence have been eroded away. The remains of the upper layers of the sediments form bright ridges, outlined by steep escarpments. Between the ridges are darker plains partly covered by dunes (MOC M0301935).

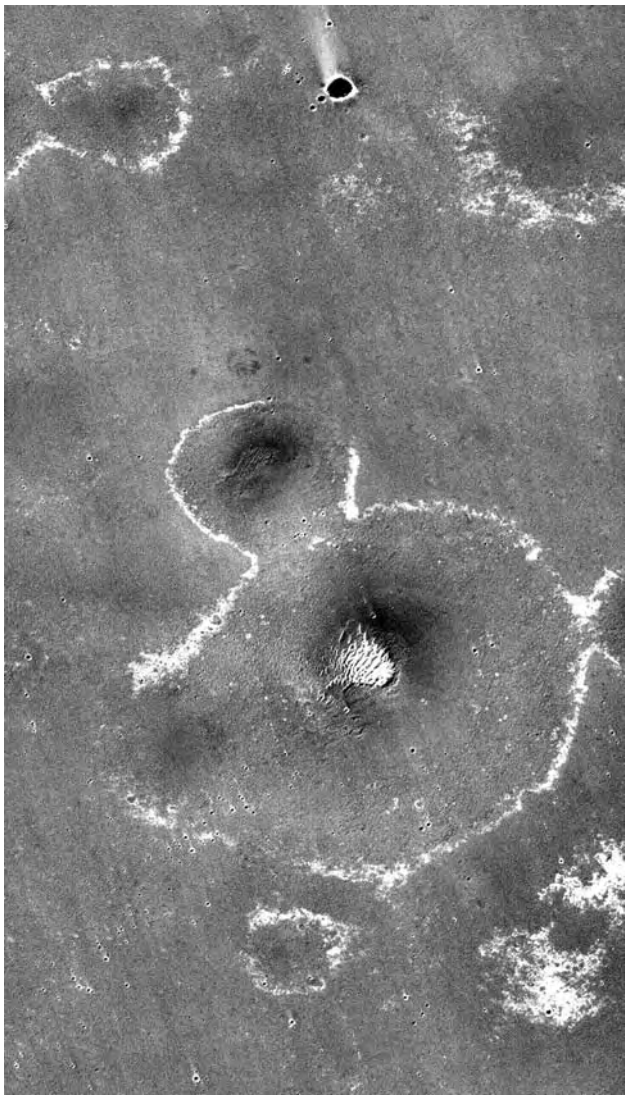

Figure 11.17. Meridiani plain north of the landing site at 6.2°N, 353.8°E. Most of the plains around the landing site have a two-toned appearance. Bright rings outline the rims of craters in light-toned sediments that poke up through darker surface materials. Mottled areas are bedrock pavements where the darker materials have been removed. The image is 3 km across (MOC E2201660).

Because the Mössbauer spectrometer on the rovers could determine only iron minerals, the other minerals in the rocks had to be inferred from the chemical analyses. While varying considerably in their sedimentary characteristics and origin, the rocks do not vary greatly in composition. Models of the mineralogical make-up of the rocks that are consistent with their chemical composition and with elemental correlations, suggest that the rocks are composed of roughly 20 percent basaltic rock debris, 10 percent oxides, 30 percent hydrated silicate alteration products, and 40 percent salts, which are mainly sulfates but include chlorides and phosphates (Clark *et al.*, 2005). McLennan *et al.* (2005) suggest that the sandstone grains are reworked, evaporite-cemented basaltic mud derived from contemporaneous playa deposits. They cite several lines of evidence to support the supposition that the chemical constituents were derived by alteration of olivine-bearing rocks under low pH conditions. The evaporites differ significantly from typical terrestrial evaporites, which are normally dominated by chlorides and carbonates, and have only minor amounts of sulfate. In contrast, the evaporites of the Burns Formation are dominantly sulfates.

The Burns Formation is the uppermost member of the layered sequence recognized from orbital observations. It extends over an area of at least 500,000 km^2. On the basis of primary sedimentary structures, secondary alteration features, and the color and the morphology of the weathered surface, the Burns Formation can be divided into three units (Figure 11.22). The following description of these units is summarized from Grotinger *et al.* (2005).

(1) The lowest unit is a large-scale, cross-bedded sandstone with hematitic concretions (Figure 11.23). (Cross-bedding refers to deposition of layers at an angle to the original depositional surface. It may form in both eolian and subaqueous environments, by the transport of silt and sand-sized particles (0.01−1 mm) as a moving bedload at velocities that suspend finer particles.) The multi-meter scale of the cross-bedding in this unit is interpreted to result from migration of eolian sand dunes. Fine lamination within the beds indicates accretion of the sand and silt particles from migrating ripples up the windward slopes of the dunes; the coarser lamination indicates accretion by avalanching grains on the lee slopes. Although the rock characteristics indicate transport of sand by the wind, the grains themselves came from an evaporitic source, so water was involved in their formation. The contact between the lower unit and the middle unit is erosional. By analogy with terrestrial dune deposits it is interpreted to be an interdune deflation surface that was created when a rise in ground water dampened and partially cemented the dune strata making it more resistant to erosion, thereby arresting the dune motion and enabling the beds to survive.

(2) The middle unit is dominated by finely laminated sandstones with low-angle cross-bedding and hematitic concretions (Figure 11.24). The fine laminations truncate the coarse cross-bedding of the lower unit. The unit is interpreted as an accumulation of an ancient sand sheet deposit, composed of sand

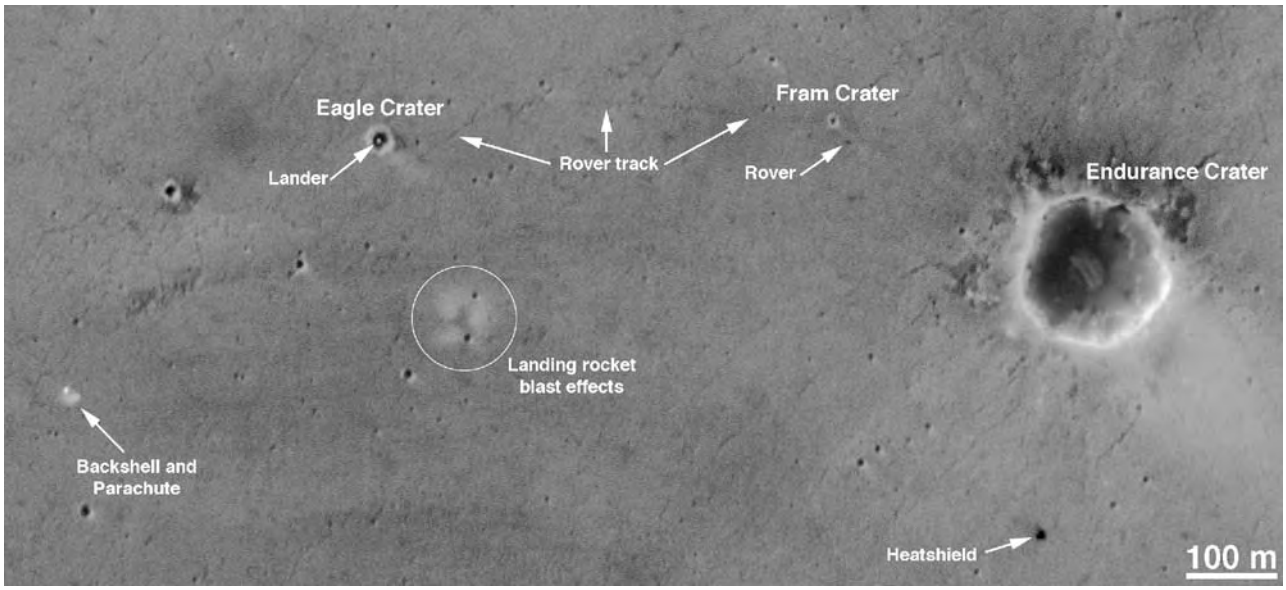

Figure 11.18. Detailed aerial view of the Opportunity landing site. The rover landed in Eagle crater, around whose rim bedrock is exposed. The rover then traveled to Endurance crater. After surveying the possibilities around the southern rim, the rover entered the crater from the southwest to characterize the section exposed in the walls (MOC 2-981).

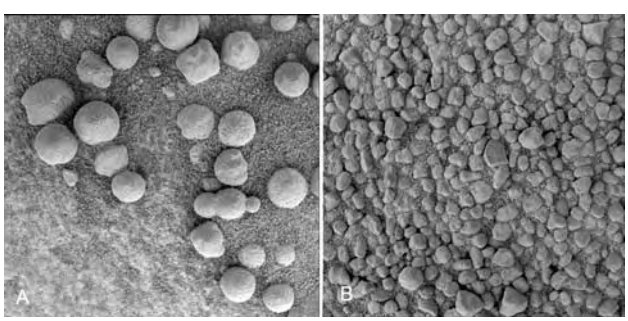

Figure 11.19. (A) Hematite-rich spherules with a mean grow diameter of 4.2 mm grow within the local rocks and weather out and form concentrations in local hollows as seen here (Opportunity sol 28). (B) Soils at Lanikai near the landing site consist of well-sorted, millimeter-sized, subangular particles, mostly of basaltic composition (MI, Opportunity sol 52).

from reworked evaporites, as with the lower unit. The fine laminations formed as ripples migrated across the accreting sand sheet. High-angle cross-beds are largely absent because of the absence of the steep lee slopes that occur on dunes. Low-angle discordances may occur as a result of migrating low mounds of sands without slip faces. The result is a sandstone with fine laminations and only low-angle discordances. The sand sheet deposits represent a transition between the high-angle dune deposits of the lower unit and the more varied interdune deposits of the upper unit. The middle unit also contains some cross-laminated sandstones that may record an occasional flood event, as described below in discussing the upper unit.

Almost the entire middle unit has been pervasively recrystallized to give it a nodular texture, and some dissolution of the evaporite minerals has occurred, causing an increase in rock porosity. The recrystallization postdates formation of the hematite concretions, since overgrowths have been deposited on them. Some of the finely laminated sandstones also appear to have undergone secondary deformation at the time that they were deposited to produce wavy or convoluted forms (Figure 11.25). By analogy with terrestrial deposits, these wavy forms are thought to result from evaporation of saline capillary water at the air–sand interface (Grotzinger *et al.*, 2005). The accumulated surface salts cause expansion, forcing lightly cemented layers to deform, and create folds or buckles according to their degree of cementation. The close association of planar to low-angle cross-stratified sandstones with wavy to irregularly bedded deposits is diagnostic of deposition in a dry to intermittently damp or wet, interdune setting. The convoluted forms are most common in the upper part of the middle unit. They are also found in the upper unit.

(3) The upper unit. The boundary between the middle and the upper unit is marked by an abrupt decrease in the nodular recrystallization.

Figure 11.20. Looking north across Endurance crater. Burns cliff is to the upper right (Pancam mosaic, sols 115, 116).

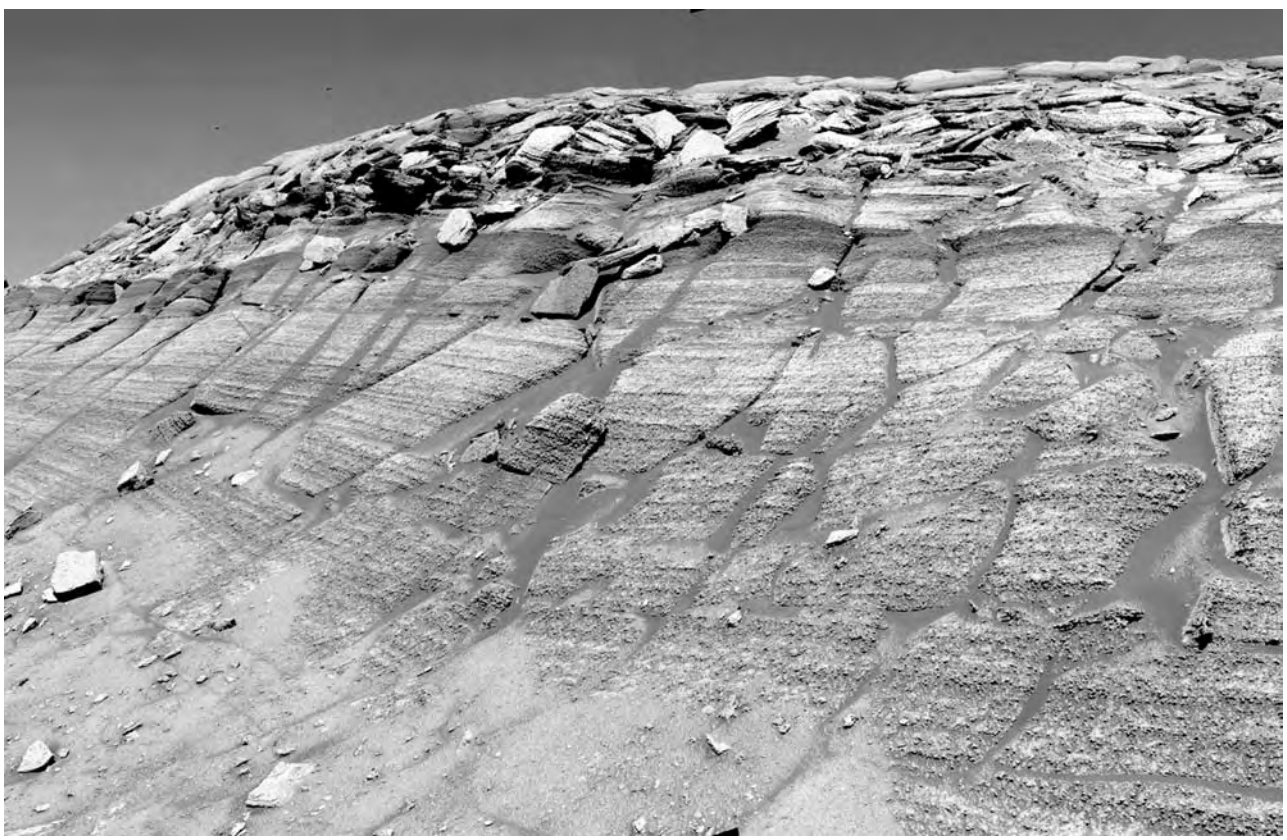

Figure 11.21. Burns cliff. Most of the section here is of the middle unit of the Burns Formation. The Whatanga contact between the middle and upper units is at the top of the dark layer in the upper part of the cliff. It is a zone of recrystallization interpreted to have formed just above the water table. Ripple cross-laminations indicative of subaqueous sedimentation are rare in the middle unit but more common in the upper unit.

The boundary is thus not a primary depositional boundary but one formed by subsequent alteration. Finely laminated sandstones are common in the upper unit as they are in the middle unit, but a characteristic of the upper unit is the more common occurrence of a coarsely cross-laminated sandstone, with laminae 0.3–1.8 cm in thickness, an order of magnitude thicker than the finely laminated sandstones common in the middle unit. The laminae may be planar or have a festoon geometry that consists of mutually intersecting, concave upward sets no more than a few centimeters across (Figure 11.26). The festoon cross-laminations are important, since on Earth festoons of this fine scale form only in subaqueous conditions. Laminations result as ripples migrate across the aggrading surface. Ripple bedforms of the type

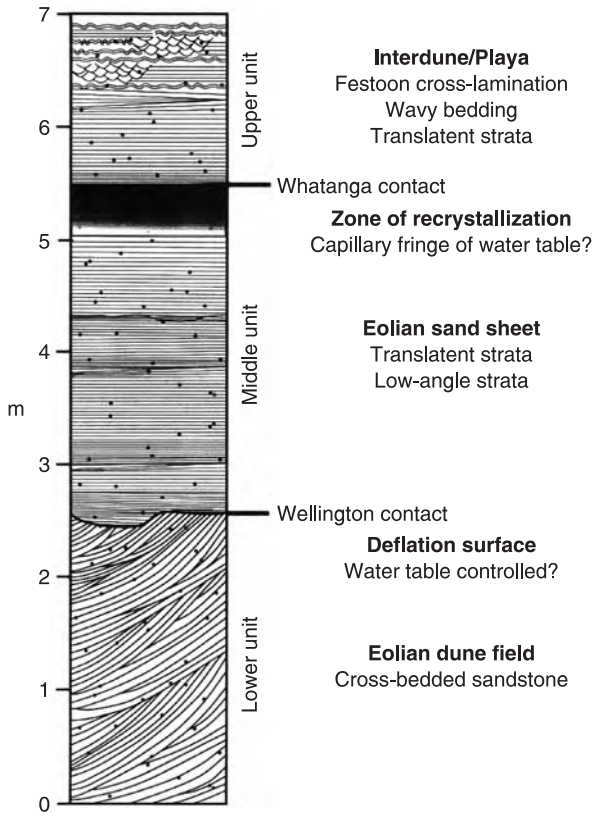

Figure 11.22. The stratigraphic section at Burns cliff. Three units are defined on the basis of primary sedimentary structures and alteration attributes. The Wellington contact (see next figure) between the lower and middle units is interpreted as a deflation surface. The contact between the middle and upper units is an alteration zone, in which the evaporitic minerals were recrystallized near the top of the water table (from Grotzinger *et al*., 2005, reproduced with permission from Elsevier).

observed in the Burns Formation have been well studied in laboratory and natural systems on Earth (see references in Grotinger *et al*., 2005). If the ripples have straight crestlines, tabular laminations form; if the crestlines are sinuous, festoon cross-laminations form. Highly sinuous, centimeter-scale crestlines are known to develop only in subaqueous ripples. Eolian ripples normally have straight crestlines and do not produce festoon cross-lamination. Small-scale eolian dunes can develop sinuous crestlines but the sinuosity is decimeter-scale rather then centimeter-scale, as is observed in the Burns Formation. Moreover, centimeter-scale sinuous ripples have not been observed by either Spirit or Opportunity despite travel of several kilometers over terrains with abundant eolian landforms. Thus the cross-laminated sandstones likely

Figure 11.23. The Wellington contact on Burns cliff separating the high-angle, thickly bedded eolian dune deposits on the left from the finely bedded, low-angle, dominantly sand sheet deposits on the right (Opportunity sol 288).

Figure 11.24. Planar to low-angle cross-stratification in a 30–40 cm section at the top of the finely layered middle unit. It is interpreted to have been deposited mainly from sand sheets (Opportunity sol 307).

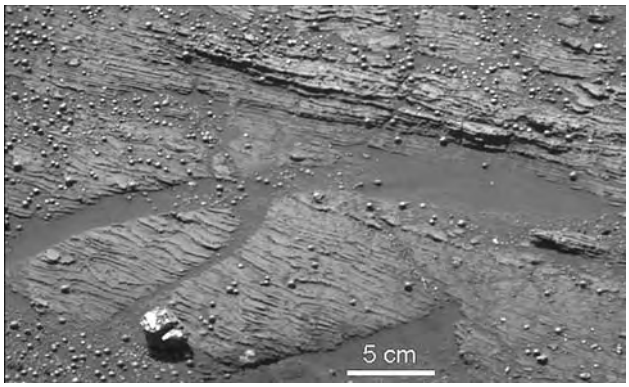

Figure 11.25. Wavy laminations thought to have formed in damp interdune environments where evaporation of saline water causes accumulation of salts that deform the layers (Opportunity sol 45).

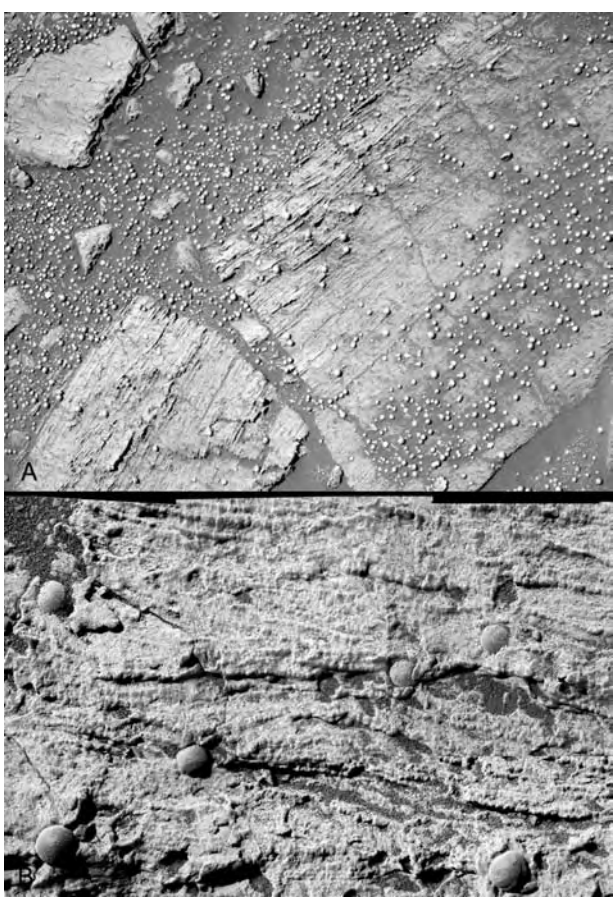

Figure 11.26. Festoon cross-bedding. (A) Slightly curved, mutually intersecting fine-scale laminae in the upper left side of the largest slab are interpreted to result from migration of subaqueous ripples (Pancam, Opportunity sol 41). (B) High-resolution view of the same type of ripples (MI, Opportunity sol 41). For scale on both images, the blueberries average 4 mm across.

record occasional flood events in an otherwise dry climatic regime.

In summary, the Burns Formation consists of sandstones with grains that are a mixture of silicate debris and evaporitic minerals. The lowest unit consists almost entirely of cross-bedded sandstones deposited in dunes. The middle unit consists mainly of finely laminated sand sheet deposits with rarer cross-laminated sandstones that record fluvial events. Festoon cross-bedding, indicative of interdune flooding, is most common in the upper unit. Convoluted bedding, caused by salt recrystallization of the saline components during periods of a high water table, is common in both the middle and upper units.

POST-DEPOSITIONAL ALTERATION. A variety of features indicate that the sedimentary rocks at Meridiani Planum underwent secondary alteration after deposition (Figure 11.27). These features include cements, nodules, convoluted bedding, concretions, vein filling, enlargement of fractures, and crystal molds (McLennan *et al.*, 2005). However, despite the reactive nature of the rock constituents, alteration is rarely so pervasive that the primary depositional features are destroyed. The presence of cement is inferred from MI images. They show that wherever individual grains can be resolved they are of uniform size, well sorted, and moderately well rounded, consistent with being transported by wind and water. The fine-grained intergranular material is thus interpreted as a cement rather than a population of finer grains. Cement also forms as 1–2 mm thick overgrowths on spherules and other grains. Such cements are common terrestrial eolian deposits that have become partly submerged below the water table.

Hematitic spherules (blueberries) present the most striking evidence of secondary alteration (McLennan *et al.*, 2005). They are dispersed throughout all the outcrops at the Meridiani site, constituting a few percent of the total rock volume. Almost all are perfectly spherical and have a uniform size with a mean diameter of 4.2 mm. They do not appear to disrupt the primary laminations. Their composition could not be directly measured because there were no concentrations of them that were sufficiently dense that the background rock or soil could be excluded from the APXS and Mössbauer analyses. However, mini-TES spectra, and mixing models of the APXS and Mössbauer data, suggest that they contain at least 50 percent hematite and possibly as much as 90 percent, and less than 10 percent sulfates. Their distribution is non-random. Growth of a concretion in one location

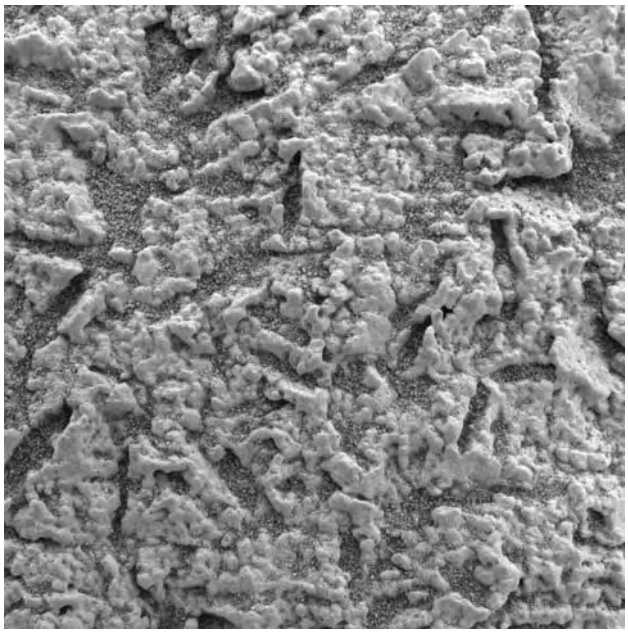

Figure 11.27. Rectangular crystal molds in the upper unit of the Burns Formation. The molds are elongate and have sharply defined margins and angular terminations. They are thought to mark the original locations of highly soluble, euhedral crystals that formed within the sediments around the time of their deposition, and then were subsequently dissolved. The image is 3 cm across (MI sol 28).

diminishes the chances of growth of another in close proximity. They are found in all rocks of the Burns Formation irrespective of whether they formed from dunes, sand sheets, or subaqueously. Thus, their formation is thought to have occurred some time after deposition of the entire Burns cliff sequence, since all the units were affected irrespective of their initial origin. The concretions probably formed quite rapidly (< 1000 years) under conditions of stagnant to slow movement of dilute groundwater (Tosca *et al*., 2005). The hematite probably formed by the breakdown of jarosite or oxidation of ferrous sulfates.

Void spaces of various sizes and shapes occur throughout the outcrops (Herkenhoff *et al*., 2004a). The voids are typically larger than the surrounding sand grains. Tabular-shaped pores, 0.5–1.5 mm wide and 1–8 mm long, with well-defined straight edges, are common. They are thought to be molds of crystals that were formerly present but that have now been dissolved away. Growth of the original crystal does not appear to have disrupted the primary laminations. In terrestrial sediments deposited in dune–interdune environments, growth of evaporitic minerals shortly after deposition by evaporation of pore-filling brines is common. Geometric relations between the pores, the rock laminations, and the hematitic spherules suggest that the crystals formed early, but were dissolved after formation of the spherules (McLennan *et al*., 2005). Whatever minerals formed the molds, they must have been highly soluble, since surrounding evaporitic minerals remain intact. Possible candidates are magnesium sulfate, melanterite (a hydrated ferrous sulfate), and iron and magnesium chlorides.

GROUNDWATER MOVEMENT. McLennan *et al*. (2005) suggest that the Burns Formation records a complex history of groundwater movement with at least four recharge episodes. The first was infiltration of groundwater to the surface to produce a playa lake in which basaltic mud was cemented with evaporitic mineral to produce the sand-size particles that formed the dunes. However, as discussed below, it is not clear that this took place locally. The precipitation of jarosite from these waters indicates they must have been sulfate-rich and highly acidic, with pH < 3. A second infiltration took place after deposition of dunes of the lower unit to form the deflation surface that marks the boundary between the lower and middle units. A third episode of groundwater recharge culminated in the wet, interdune conditions recorded in the cross-laminated rocks of the upper unit. The fourth recharge event resulted in formation of the hematitic concretions at the expense of jarosite and other minerals. Waters during the last episode probably had a higher pH than those in the earlier episodes, thereby leading to dissolution of jarosite to form hematite, but they must have still had high ionic strengths because there was no widespread dissolution of the evaporitic components. All these events took place before formation of Endurance crater. There is little or no evidence of any solution of the soluble salts that were exposed to the surface after formation of the crater, which suggests that the surface has not been exposed to liquid water since the crater formed.

Although the bulk composition of the rocks is similar at all the locations where rocks were analyzed in Meridiani, there are variations. The variations suggest that sulfates (mainly Mg and Ca) migrated up the section, whereas Na and Cl migrated down the section. Bromine is highly variable. Upward migration of sulfates is consistent with evaporation of water from the top of the sequence (Clark *et al*., 2005). Migration of Cl and Br appears to be decoupled from that of sulfates. One possibility is that this is a consequence of freezing point depression. Sulfates are poor freezing point depressors whereas chlorides and bromides are

strong depressors. When temperatures fall below a certain threshold, therefore, the chlorides and bromides may remain mobile whereas the sulfates are frozen. An additional contributor to the high variability of Br may be the hypersolubility of bromides, which enables them to remain labile under conditions when only minor amounts of water are available.

EVAPORITIC SOURCES. The deposits of Meridiani Planum provide almost unequivocal evidence for the widespread evaporation of brines at the surface at times in the past. The brines likely formed as a result of the interaction between sulfate-rich acidic groundwater and basaltic minerals, particularly olivine (Burns, 1987). Volcanic exhalations are the most likely source of the sulfur, which may have been scavenged out of the atmosphere as acid rain. The specific areas where evaporation occurred are not known, but they must have been extensive. The sedimentary sequence, of which the Burns Formation is a part, is several hundred meters thick. It now covers over 500,000 km^2, and appears to have formerly been significantly more extensive. Although Opportunity could analyze only those rocks immediately around the landing site, spectral data suggests that the entire exposure of layered rocks in Meridiani is sulfate-rich (Arvidson *et al.*, 2003; Gendrin *et al.*, 2005). McLennan *et al.* (2005) prefer local, interdune playas as sources of the sulfate minerals, but extensive, more distant sources cannot be ruled out. The sedimentary sequence itself does not lie within any well-defined basin, which is consistent with its deposition being dominantly eolian. The northern plains is an obvious large basin in which water could have evaporated to provide the copious source of evaporites needed. If there was an active hydrological cycle during the Noachian, which seems likely, then bodies of water would have at least episodically occupied the lower parts of the northern plains and left behind evaporites. In addition, drainage convergent on local lows is common throughout the Noachian terrain (Chapter 6), so there could have been many local sources throughout the uplands. Hesperian volcanics now cover much of the northern lowlands and fill many local hollows within the Noachian terrain, so many possible sources may now be buried.

The age of the sediments is poorly defined. As indicated above, Hynek *et al.* (2002), on the basis of transection relations and crater counts, suggest an age of Noachian to Lower Hesperian, but the young limit on the age is poorly defined.

Summary

At the time this was written, spacecraft had successfully landed at five locations on the surface of Mars. The two Viking landers carried an array of experiments designed to search for life. No evidence of life was found, nor were any organics detected in the soil, probably as a result of the presence of small amounts of oxidants. Pathfinder landed on a flood-scoured plain strewn with volcanic rocks of basaltic to andesitic composition. All the soils at the Viking and Pathfinder sites are similar in composition, being basaltic except for enhancements in sulfur.

The Spirit rover landed on a level plain within the 160 km diameter crater Gusev whose wall is breached by a large channel, Ma'adim Vallis. The hope was that products of fluvial erosion of the channel would be found within the crater. No evidence of aqueous activity was found where the spacecraft landed. The area was strewn with basaltic rocks, which are unaltered except for millimeters-thick, S- and Cl-rich rinds that probably formed by interaction of the rocks with acid fogs. Lack of outcrops implies that bedrock is at least 10 m below the surface. The soils are essentially basaltic in composition but with an additional S–Cl-rich component that is concentrated at the surface. The pristine nature of the rocks and the minimal evidence for erosion suggest that the plains have been resting undisturbed except for minor eolian and impact activity since the present surface materials were deposited in Hesperian times. The rover traveled 2.6 km across the plains to some low hills, called the Columbia Hills. Here the rocks are very different. The primary rocks are still of basaltic provenance, but in many of the rocks most of the primary minerals have been replaced by oxidized and hydrated species such as hematite, goethite, and nanophase oxyhydroxides, and by salts, mainly sulfates and chlorides. The alteration of some of the rocks may have occurred close to the time of their deposition as volcanic ash flows or impact breccias. Other alterations may have resulted subsequent to deposition as a result of hydrothermal activity or circulation of groundwater. Irrespective of the timing and type of alteration, all involved aqueous processes. Thus the rocks of the Columbia Hills appear to date from a time when aqueous processes were common, in contrast to the younger plains rocks which have barely been affected by aqueous processes.

At Meridiani Planum is a sequence of sediments partly covered with eolian deposits (Figure 11.28). The sediments are several hundred meters thick, cover an area in excess of 500,000 km^2, and consist mostly of sand and silt-sized grains. Individual grains are

Figure 11.28. Tracks across the dune field to the south of Endurance crater.

composed of a mixture of evaporitic minerals, mostly sulfates and chlorides, and silicic minerals, mostly basaltic alteration products, in roughly equal proportions. The sediments are mostly eolian, but include some of fluvial origin. They are thought to have been laid down in a desert with dunes and ephemeral, interdune acid ponds. The mineral-rich waters probably result from interaction of sulfate- and chloride-rich groundwater with basaltic constituents, primarily olivine. Several episodes of groundwater recharge resulted in alteration of the sediments during which some evaporitic minerals were recrystallized and others were dissolved away leaving vugs and molds. A late alteration event resulted in formation of hematitic concretions. The section was viewed mostly in the walls of a 150 m crater called Endurance. There is no evidence of an aqueous activity after the formation of Endurance.

12 Climate change

Throughout this book we have described features on the surface that almost certainly imply that climatic conditions in the past were different from those that prevail today. Among others, these include valley networks, lakes, oceans, deltas, hydrated minerals, water-lain sediments, evaporites, glacial deposits, ice-rich veneers, and ice at low latitudes. In this chapter we briefly re-examine what these features might imply about the climatic history of the planet and explore what might have caused the climatic variations.

The discussion is broken down into three pieces. The first piece of the story is the Noachian. This is the era for which we have the best evidence for dramatically warmer climatic conditions. The main evidence is the presence of valley networks, seemingly formed by slow erosion of running water. But warmer conditions are also implied by high erosion rates, indications of lakes, deltas, and water-lain sediments, and detection of hydrous minerals. The second part of the story concerns the post-Noachian era. The geological evidence here is more conflicting. While the mineralogical evidence and the bulk of the geomorphic evidence suggest persistent cold conditions, there may have been occasional climatic excursions. We will look at the evidence for such excursions and examine possible causes. The third part of the story concerns geologically recent changes that have been induced by obliquity variations. These were discussed in Chapters 8 and 10 and will be summarized only briefly here. Although the most obvious effects of obliquity variations are geologically recent, obliquity-induced changes must have occurred throughout the planet's history, and their effects may have been greater earlier when climates were different and when there may have been a thicker atmosphere and much more water at the surface.

For each era, mechanisms for changing the climate are examined. We will see that despite strong evidence for warmer climates on early Mars, we have no satisfactory explanation as to what caused the warmer conditions or how they could have been maintained. For the bulk of the post-Noachian era the situation is equally bleak. Do the occasional examples of young, densely dissected terrain indicate major, temporary climate changes, or do they result from other effects such as obliquity variations, groundwater seepage, or hydrothermal activity? If they result from climate changes, what caused the changes? What were the climatic effects of the large floods? These various questions are explored but no compelling answers are provided. We are on firmer ground when discussing changes in the geologically recent past, although even here the uncertainties are still large. We are reasonably certain that recent obliquity changes have affected the distribution of near-surface ice. They may also be responsible for layering at the poles, glaciers at low to mid latitudes, and other features.

Noachian climate

The evidence for warmer climate during the Noachian was discussed in Chapter 6. Much of the heavily cratered Noachian terrain is dissected by valley networks that in plan resemble terrestrial river systems. There is little reason to doubt that they were cut by running water. Since they were first observed, the relative roles that surface runoff and groundwater seepage played in their formation have been debated, and the controversy may have climatic implications. In most terrestrial fluvial systems, part of the precipitation collects into streams fed by surface runoff, part infiltrates into the ground and emerges at springs downslope. Where surface runoff dominates, dense, area-filling networks develop, valleys divide upstream into ever smaller branches, and the tributaries tend to have V-shaped cross-sections. Where groundwater sapping dominates, the networks are open and the distal tributaries tend to have abrupt terminations and U-shaped or rectangular cross-sections. These are generalizations. Most terrestrial networks form by a combination of surface runoff and sapping, and have attributes of both types. Much of the early work on Mars emphasized the role of groundwater sapping, partly because most of the networks appeared to be open, and many of the larger networks such as Nirgal Vallis have classic sapping attributes (Figure 6.22). Theoretical modeling suggested that springs could continue to flow despite

a thick cryosphere (Squyres and Kasting, 1994), and, once initiated, streams may be able to travel long distances below an ice cover, even with temperatures well below freezing (Wallace and Sagan, 1979; Carr, 1983). The supposition that the valley networks required warm conditions was therefore questioned. But how the groundwater system below the cryosphere could be recharged to sustain the flow remained a problem, despite the suggestion of a possible global recharge through the poles (Clifford, 1987).

With the acquisition of better data, it has become clear that the open nature of some of the valley networks was simply a resolution effect, and that dense, area-filling networks, with distal V-shaped tributaries indicative of surface runoff, are common (Figures 6.19, 6.23). In addition, many valleys start at places, such as crater rim crests, where groundwater seepage is unlikely. That precipitation and surface runoff played a role in formation of the valley networks, in addition to groundwater sapping, now appears compelling. (For a comprehensive summary of the fluvial arguments for warm conditions, see Craddock and Howard, 2002.) Warm surface conditions and an active Noachian hydrological cycle is also supported by high erosion rates during the Noachian (Carr, 1996; Golombek and Bridges, 2000), water-lain sediments at Meridiani (Grotzinger *et al*., 2005), dissolution and deposition of soluble minerals in the sediments at Meridiani (McLennan *et al*., 2005), detection of hydrous silicates in Noachian terrains (Bibring *et al*., 2006), and by details of delta deposits in Eberswalde and other craters (Malin and Edgett, 2003).

Greenhouse warming

Haberle (1998) summarized the attributes of various climate models that had been proposed at that time. Much of the discussion here on modeling of the early Mars climate is abstracted from that summary. To warm early Mars requires a very effective greenhouse. According to stellar evolution models, 3.8 Gyr ago the Sun's luminosity was 75 percent of its present value (Newman and Rood, 1977; Gough, 1981). With this luminosity, the mean surface temperature would be 196 K if there were no greenhouse, so to raise the global mean temperature to 273 K requires 77 K of greenhouse warming. To achieve this, the martian atmosphere must intercept 85 percent of the radiation coming from the surface, substantially more than the 56 percent intercepted by the Earth's atmosphere (Haberle, 1998).

Until the 1970s it was thought that the early atmospheres of Earth and Mars were reducing. If so, then several greenhouse gases (CH_4, NH_3, H_2S, H_2O) could have provided an effective greenhouse. However, geochemists now believe that early core formation (Chapter 4) and massive hydrogen loss from the interior (Pepin, 1994) both left the mantle oxidized and stripped away any reducing atmosphere that might have been acquired during accretion. The evidence for massive early loss of volatiles is mainly from the noble gases. Martian atmospheric Xe is mass fractionated against Xe in C1 carbonaceous chondrites, with the heavier isotopes being preferentially retained. Xe is too heavy to be lost by thermal escape or by any of the processes currently occurring in the upper atmosphere. The fractionation is thought to have resulted from massive loss of hydrogen during the first few hundred million years of the planet's history, driven by an intense, rapidly decaying solar EUV flux (Pepin, 1991). The lighter Xe isotopes and essentially all the other lighter gases were lost to space as they were carried along in a hydrogen wind. After hydrodynamic escape was over, the planet is thought to have acquired a second atmosphere by outgassing of the interior and meteorite and cometery infall.

The atmosphere that subsequently outgassed from the interior is thought to have been oxidizing because of removal of iron from the mantle to form the core. Another problem with invoking reduced gases to explain an early greenhouse is that they are destroyed by ultraviolet photolysis on time scales of tens to hundred of years (Kuhn and Atreya, 1979). If they are responsible for climate change, there must have been a persistent source for the gases or some protection from the ultraviolet, such as an organic haze (Sagan and Chyba, 1997). Most of the modeling studies from the 1970s onward have assumed that reduced species played either no role or only a minor role and that any warming of early Mars would have been mainly by a CO_2-H_2O greenhouse. This assumption is, however, becoming increasingly hard to justify in view of the difficulty of demonstrating how early Mars could have been warmed by such an atmosphere, and in view of the failure to detect carbonates on the surface despite increasingly sophisticated methods of detection.

Greenhouse models (Table 12.1) can be grouped into three types: globally averaged energy balance models, one-dimensional radiative-convection models, and latitudinally resolved energy-balanced models (Haberle, 1998). The globally averaged models are very simple. The model of Sagan (1977) merely balanced the incoming solar radiation against two sources of outgoing radiation, the surface and a single isothermal layer of atmosphere. This type of model will not be discussed further. The 1-D models divide

Table 12.1. *Estimates of atmosphere properties required to raise mean global surface temperature to 273 K (adapted from Haberle, 1998)*

Model	Comment
Sagan (1977)	1 bar H_2 1 bar foreign gas + minor NH_3
Pollack *et al.*(1979)	10 bar CO_2–H_2O) 0.6 bar CO_2 + minor NH_3, CH_4, H_2
Postawko and Kuhn (1986)	10 bar CO_2–H_2O + minor SO_2
Pollack *et al.* (1987)	5 bar CO_2–H_2O
Kasting (1991)	No amount of CO_2–H_2O can raise temp. to 273 K
Forget and Pierrehumbert (1997)	0.5–2 bar depending on water content and CO_2 cloud properties
Yung *et al.* (1997)	2 bars CO_2 plus 0.1 ppmv SO_2
Colaprete and Toon (2003)	>5 bars even with CO_2 clouds

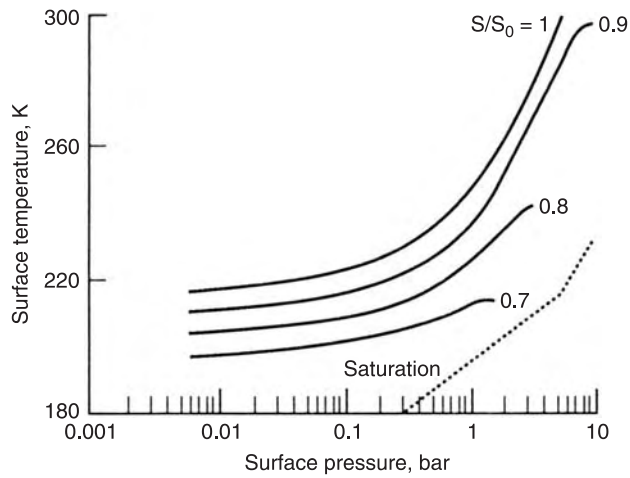

Figure 12.1. Surface temperatures as a function of surface pressure for four values of solar luminosity according to the model of Kasting (1991). The solar luminosity at the end of the Noachian is thought to be close to 0.7. For this luminosity, formation of CO_2 clouds and condensation of CO_2 on the surface limits surface pressures to under 2 bars, and surface temperatures remain well under 220 K, no matter how much exchangeable CO_2 is at the surface. (Copyright Elsevier, 1991. Reproduced by permission from Elsevier.)

the atmosphere into a number of layers. Estimates of the temperature of each layer are made by balancing the solar and infrared fluxes so that no heating occurs. Finally, lapse rates are adjusted to take into account the stabilizing effects of atmospheric motions. Pollack *et al.* (1979), using a 1-D model for a CO_2–H_2O atmosphere, estimated that 10 bars of CO_2 were required to raise the global temperature on early Mars to 273 K. For an atmosphere containing 10 ppm of NH_3, CH_4 and H_2, the figure is only 0.6 bars of CO_2, which demonstrates the effectiveness of the reduced gases (mainly NH_3) in producing a greenhouse. Pollack *et al.* (1987) subsequently refined their model and estimated that the 273 K mean global temperature could be achieved with only 5 bars of CO_2 with a purely CO_2–H_2O atmosphere. Around the same time, Postawko and Kuhn (1986) ran some latitudinally resolved models that took into account latitudinal variations in heating and global circulation. These models result in lower equatorial temperatures than the 1-D models because, if transport is vigorous, energy is consumed by atmospheric circulation. If the transport is less vigorous, then cold polar temperatures cause condensation of CO_2 at the poles and limit the amount of CO_2 that can remain in the atmosphere. The results suggest that Mars could not sustain more than a 3 bar atmosphere, so could not achieve equatorial temperatures of 273 K or higher. All these results may, however, have been too optimistic. Kasting (1991) pointed out a problem with all the Pollack *et al.* models. They did not take into account formation of CO_2 clouds. According to Kasting, cloud formation limits a CO_2–H_2O atmosphere on early Mars to 2.5 bars (Figure 12.1), which would result in a mean surface temperature of only 220 K, well short of that required to stabilize liquid water at the surface.

Different ways out of this dilemma have been proposed. Yung *et al.* (1997) suggested that very small amounts (0.1 ppm) of SO_2 in the atmosphere, while having a negligible direct effect on surface temperatures, could raise temperatures in the mid-atmosphere and suppress formation of CO_2 clouds. It is not clear, however, whether this would raise or lower surface temperatures because of another effect suggested by Forget and Pierrehumbert (1997). They point out that the CO_2 clouds scatter infrared radiation and so could provide a greenhouse. They modified Kasting's code to take into account this effect, which requires persistent clouds with large (>5 μm) particles. According to their model, clouds with an optical depth of 10 and particles in the 10–50 μm size range could raise the mean global temperatures to 273 K with atmospheric pressures in the 0.5–2 bar range, so this could be significant. However, more detailed modeling of the scattering effects of such clouds suggests that their effectiveness in warming the planet may have been overemphasized (Colaprete and Toon, 2003). Cloud formation may be

self-limiting, since heating the atmosphere causes the clouds to dissipate within several days. Colaprete and Toon estimated that surface temperatures would not rise above freezing on early Mars even with a 5 bar atmosphere, despite the scattering effects of CO_2 clouds.

A very different way of warming early Mars and forming the valley networks was proposed by Segura *et al.* (2002). They suggested that massive amounts of rock vapor and water vapor would be injected into the atmosphere by large impacts. The hot (~1600 K) rock would rain out of the atmosphere shortly after the impact, blanketing the planet, thereby heating the ground and causing evaporation of near-surface groundwater and ground ice, so adding to the water vapor in the atmosphere that had been injected directly during the impact. The impact would be followed by years to decades of rainfall, with an active hydrological cycle, during which the valleys were cut. They suggested that the rate of valley formation declined rapidly at the end of the Noachian because the impact rate declined. The original proposal considered only very large impacts. For example, according to their model a 100 km diameter asteroid, which makes a 600 km diameter crater, deposits a 10 m layer of hot rock over the entire planet, and precipitates out 5 m of water over a period of 10 years. The plausibility of the process depends on how effective it is for smaller impacts. There are fewer than ten 600 km diameter craters preserved well enough to have formed roughly contemporaneously with the valleys, but the cumulative effect of the more numerous smaller craters may be significant.

Retention of a dense CO_2 atmosphere

Even if a thick atmosphere were to cause surface temperatures to rise above freezing, such an atmosphere may be difficult to maintain against losses by impact erosion and weathering. Melosh and Vickery (1989) developed a simple model to estimate the effectiveness of large impacts in removing parts of the atmosphere. The impacts must be large enough that the vapor plume created expands to escape velocity and the mass of the plume must exceed the mass of the atmosphere above the planet tangent to the point of impact. When this happens the atmosphere above the tangent point is removed. Using this model, they suggested that if an atmosphere 100 times the present atmosphere was present shortly after accretion, then it would have eroded to the atmosphere's present size by roughly 4 Gyr ago. Clearly this scenario cannot explain the valleys at the end of the Noachian since, by this time, the atmospheric pressure was close to its present value. This does not, however, negate the importance of impact erosion. A characteristic of the process is that its effectiveness depends on atmospheric pressure. The thicker the atmosphere, the more energetic the impact needed to cause erosion. This means that as the atmosphere thins, the efficiency of erosion increases. Thus a thick atmosphere could be maintained for some time and then rapidly decline, even though the population of impactors had not changed. Carr (1999), using their model, estimated that if Mars had a 4 bar atmosphere 4.4 Gyr ago, it would have been reduced to 700 mbar by 4 Gyr ago. Brain and Jakosky (1998) estimated that 50–90 percent of the atmosphere could have been lost by this mechanism as a result of formation of the observed population of impact craters in Noachian terrains.

Weathering would also remove CO_2 from the atmosphere if conditions were such that liquid water was at the surface. Pollack *et al.* (1987) estimated weathering rates on early Mars by scaling terrestrial rates to hypothetical martian conditions. According to their model, removal of CO_2 by weathering is remarkably efficient. A 5 bar atmosphere with surface temperatures of 273 K would, for example, be removed in 50 Myr. However, using a very different model of geochemical cycles involving weathering and precipitation in a Noachian ocean, Schaeffer (1993) concluded that Pollack *et al.* had greatly overestimated weathering rates, and that a thick atmosphere could survive for a significant length of time. Impact erosion and weathering rates may be interdependent. If impact erosion is effective, the atmosphere thins, temperatures fall, and weathering rates decline. Most of the atmosphere is lost to space; carbonate formation is minor. If impact erosion is low, an originally thick atmosphere would be retained, resulting in higher temperatures and hence higher weathering rates. As a result, most of the CO_2 forms carbonates instead of being lost to space, unless the Schaeffer model is more correct. In both cases it is difficult to maintain an atmosphere until the end of heavy bombardment when most of the valleys formed, unless there is some way of replenishing the CO_2. No matter how thick the starting atmosphere, without replenishment it is mostly lost by the end of the Noachian, either by weathering or by impact erosion.

Pollack *et al.* (1987) suggested that the CO_2 atmosphere was maintained by recycling back into the atmosphere the CO_2 that had been scavenged out of the atmosphere during weathering to form carbonates. They suggested that, as a consequence of the likely high heat flows on early Mars, rates of volcanism (both extrusions and intrusions) would have been high so

that weathering products would have been rapidly buried and heated and the CO_2 returned to the atmosphere. Another possible way that CO_2 buried as carbonates could be returned to the atmosphere through the effects of heating is by large impacts, but simple modeling suggests that this is probably not as effective as volcanism (Carr, 1989). Extensive carbonate deposits have not been detected at the surface (Bandfield *et al.*, 2000; Bibring *et al.*, 2005). This does not mean that carbonates were not scavenged out of the atmosphere. Acid, sulfate-rich waters are implied by the evaporites at Meridiani (Klingelhöfer *et al.*, 2004; Squyres *et al.*, 2004a), the alteration of the rocks in the Columbia Hills (Squyres *et al.*, 2006), and sulfate-dominated evaporites elsewhere (Gendrin *et al.*, 2005; Langevin *et al.*, 2005). Carbonates would dissolve in the acid waters. However, if acid, sulfate-, and carbonate-rich rain infiltrated into the ground and remained in contact with basalt, the pH of the water would increase as the sulfate was consumed by weathering of the basalt. Ultimately carbonates would form if HCO_3^{-1} ions were originally present in the water (Tosca *et al.*, 2005). Thus, even though carbonates have not been detected at the surface, they could be present below the surface. Nevertheless, it is troubling that carbonates have not been detected in such places as the walls of canyons and craters.

Another unresolved issue is the fate of the CO_2 present in the atmosphere at the time valley formation rapidly declined at the end of the Noachian. From the above discussion and ignoring the CO_2 condensation problem, it appears that 0.5–5 bars of CO_2 must have been present when equatorial temperatures fell below freezing, thereby causing the rate of valley network formation to rapidly decline. The absence of carbonates from the era when temperatures were above freezing can be explained away by infiltration and equilibration with basalt as described above. But after temperatures fell below freezing, infiltration would be much more difficult. Presence of small amounts of carbonate in martian meteorites (Gooding *et al.*, 1988; Bridges *et al.*, 2001) suggest that some of the CO_2 could have infiltrated into the ground despite the likely low temperatures for much of Mars' history, a small amount may be present in atmospheric dust (Pollack *et al.*, 1990; Bandfield *et al.*, 2000), and a small amount may be adsorbed in the regolith. But none of these sinks appears large enough to account for the CO_2 needed to keep Mars warm so that valleys could form at the end of the Noachian.

The most significant losses of CO_2 since the main era of valley formation may have been to space by sputtering. This is a process whereby atoms, ionized in the upper atmosphere, are accelerated by the solar magnetic field, then collide with other atoms at high velocities and eject them into space (Luhmann and Kozyra, 1991). Because of diffusive separation of species with different masses in the upper atmosphere, the process favors loss of the lighter isotopes. From the isotopic composition of the present atmosphere, Jakosky and Jones (1997) estimated that since the end of the Noachian, roughly 90 percent of the exchangeable surface reservoir of CO_2 has been lost by this process. The total amount of exchangeable CO_2 at the surface today is unknown, but is unlikely to be large. Brain and Jakosky (1998) estimate that there are no more than a few tens of millibars in the polar caps and adsorbed on the regolith. If so, then a few hundred millibars may have been lost by sputtering since the end of the Noachian. Brain and Jakosky also estimated that 50–90 percent of the atmosphere would have been lost by erosion as a result of formation of the observed population of craters in Noachian terrains. They concluded, therefore, that 95–99 percent of the atmosphere had been lost since the start of formation of the observed craters by a combination of impact erosion and sputtering. Although sputtering could have started earlier, most of the isotopic enrichment due to sputtering would have taken place after the size of the exchangeable reservoir had been reduced by impact erosion. If 95–99 percent of the near-surface CO_2 was lost by these two processes, then we should not expect to find extensive carbonate deposits. It would also mean that any warm episodes subsequent to the end of the Noachian cannot be attributed to a CO_2–H_2O greenhouse since most of the CO_2 had, by that time, been lost to space either by impact erosion or sputtering.

To conclude this section on Noachian climate, geological evidence strongly supports warmer climates in the Noachian. Unless CO_2 clouds prove to be effective infrared scatterers, or the early Sun was not as faint as standard models, then CO_2–H_2O alone would not have been able to provide the necessary warming. Even if early Mars was warmed with a CO_2–H_2O greenhouse, the atmosphere would have needed to be maintained against losses by weathering and impact erosion, such as by burial and heating of carbonates as a result of high rates of volcanism. An additional major problem with the CO_2–H_2O model is failure to detect significant carbonate reservoirs. Possible solutions to these problems are that (1) trace greenhouse gases played a more prominent role than has been generally assumed; (2) the early Sun was brighter than standard models predict; (3) CO_2 clouds are more efficient infrared scatterers than has been assumed;

(4) warm conditions were sporadic, as a result of large impacts or volcanic events; or (5) the valley networks and other features that seemingly result from liquid water could form under cold conditions.

Post-Noachian climate history

The global fluvial regime changed at the end of the Noachian. The rate of formation of valley networks seems to have declined significantly, despite the presence of prominent Hesperian valleys such as the Nirgal and Nanedi Valles. The decline is indicated by the vast expanses of Hesperian plains (Chryse, Solis, Syria, Sinai, Lunae, Hesperia, Syrtis, Malea Plana) that are almost completely undissected by valley networks. The rapid decline is also supported by relations in the cratered uplands where valleys on locally higher ground are commonly transected by younger ridged plains in the local lows. It could be argued that these volcanic plains are poorly dissected because they are resistant to erosion, or because they have high infiltration rates. However, the simplest explanation is that surface conditions changed at the end of the Noachian. Along with the decline in valley formation, there was an increase in the rate of formation of outflow channels. There may have been large floods in the Noachian, for example in Ma'adim Vallis (Irwin *et al*., 2002). Nevertheless, the overwhelming majority of outflow channels are post-Noachian. After the Noachian, occasional massive eruptions of groundwater appear to have become the dominant fluvial process rather than the slow, persistent erosion that likely formed the valley networks.

The differences between the Noachian and post-Noachian regimes can be explained in part by a change from warm and wet surface conditions to cold and dry surface conditions. Such a change is consistent with (1) the scarcity of highly dissected post-Noachian terrains; (2) the massive post-Noachian eruptions of groundwater, which may require a thick cryosphere; (3) the dominance of sapping features on large pristine Hesperian valleys (Baker and Partridge, 1986; Gulick, 2001) such as Nirgal and Nanedi; (4) the 4–5 orders of magnitude decline in erosion rates at the end of the Noachian (Golombek and Bridges, 2000); (5) the failure to detect hydrated minerals in post-Noachian terrains despite their detection in Noachian terrains (Bibring *et al*., 2006); and (6) the low weathering rates implied by the almost pristine nature of basalts on the Gusev plains (Haskins *et al*., 2005) and by the detection of easily weathered olivine elsewhere (Mustard *et al*., 2005).

Haberle *et al*. (1994) attempted to model how conditions on Mars would change after the Noachian on the assumption that Mars started out with a thick atmosphere at the end of the Noachian, then conditions changed as the CO_2 was lost to space and to carbonates and the luminosity of the Sun increased. They tracked how the amount of CO_2 in different reservoirs (atmosphere, regolith, polar cap, and carbonates) changed with time, and what the atmospheric reservoir implied for surface temperatures. They conclude that any CO_2–H_2O atmosphere thick enough to create an effective early greenhouse could not evolve to present conditions with its very limited total inventory (caps–regolith–atmosphere) of CO_2 that is exchangeable with the atmosphere. The large amount of CO_2 that would be retained today in the polar caps is too large to be consistent with what is currently observed. A 0.5–1 bar atmosphere at the end of the Noachian, for example, is compatible with present inventories but would not have provided the necessary greenhouse. A characteristic of the model is that for large initial inventories of CO_2 (>1–2 bars), the atmosphere at some point collapses as a result of formation of permanent CO_2 caps (Figure 12.2). Despite the increase in solar luminosity with time, for almost all starting conditions, global mean temperatures remain below 240 K for the entire post-Noachian era.

Despite the strong case for a change in surface conditions from warm and wet to cold and dry at the end of the Noachian, this cannot be the whole story. Some post-Noachian surfaces are dissected by valley networks. The surfaces of several volcanoes (Ceraunius, Hecates, Alba) are, for example, densely dissected and some of the Hesperian plains adjacent to Valles Marineris are so densely dissected that surface runoff is implied (Mangold *et al*., 2004). In addition, some of the Hesperian features of the northern plains and the floor of Hellas have been interpreted as the result of meltwater from glaciers (Kargel and Strom, 1992; Kargel *et al*., 1995), which may require warm conditions, although the ice deposits could have been so thick that they could have been melted from below as has been suggested for the Dorsa Argentea Formation near the south pole (Head and Pratt, 2001). Thus, while low erosion and weathering rates, and formation of large floods, are consistent with cold conditions and a thick cryosphere for most of the post-Noachian era (Carr, 1996; Clifford and Parker, 2001), there may have been short, warmer episodes and/or local deviations from the global conditions. Possible causes of the young valleys and possible glacial features include temporary global warming as a result of formation of oceans by large floods (Baker *et al*., 1991; Baker, 2001), melting of snow deposited

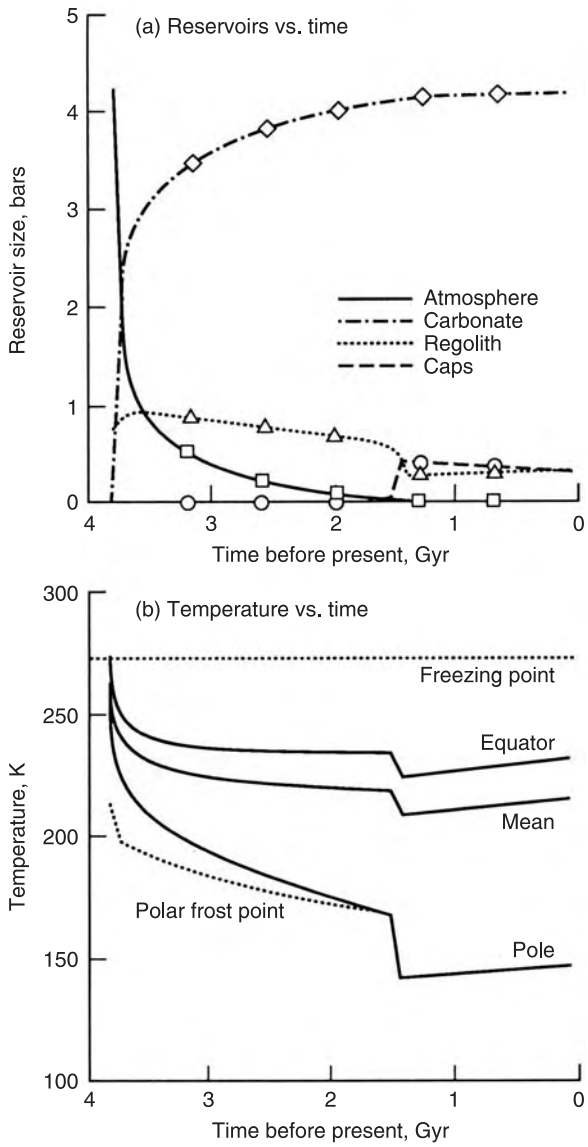

Figure 12.2. Model of the post-Noachian evolution of CO_2 on the assumption of a 5 bar atmosphere at the end of the Noachian (Haberle *et al.*, 1994). The strong greenhouse model of Pollack *et al.* (1987) is assumed. Formation of carbonates rapidly consumes the atmosphere. The step function at 1.2 Gyr results when polar temperatures fall to the frost point temperature and a CO_2 cap forms. Despite increasing solar luminosity through the entire period, equatorial temperatures remain well below freezing and a thick cryosphere develops (from Haberle, 1998, Copyright 1998, American Geophysical Union, reproduced by permission of the American Geophysical Union).

downwind of oceans (Moore *et al.*, 1995), possibly coupled with hydrothermal circulation of the meltwater (Gulick *et al.*, 1997), melting of snow deposited during periods of high obliquity (Jakosky and Carr, 1985), temporary changes in the global climate as a result of large impacts (Segura *et al.*, 2002), or large volcanic eruptions.

Baker *et al.* (1991) and Baker (2001) proposed that the large, post-Noachian floods episodically created temporary oceans and released massive amounts of CO_2 and possibly SO_2 into the atmosphere, thereby causing temporary greenhouse warming. They suggested that Mars was cold and dry for most of its post-Noachian history, except for short (10^3–10^4 years), warm, marine episodes. The CO_2 released to the atmosphere was derived from that dissolved in the groundwater brought to the surface during the floods, from breakdown of clathrates (CO_2–H_2O compounds) in the cryosphere, from release of CO_2 adsorbed or frozen at the surface, and from volcanic emanations. The warm wet conditions caused by the CO_2–H_2O–(SO_2) greenhouse resulted in an active hydrological cycle accompanied by cutting of the young valleys and formation of glaciers, such as those proposed for Hellas (Kargel and Strom, 1992). The warm conditions are unstable. The oceans evaporate. Where the evaporated water precipitated on land, it infiltrates into the ground carrying CO_2 scavenged out of the atmosphere to form carbonates or clathrates, and within 10^3–10^4 years the planet reverts to its stable cold dry state. Gulick *et al.* (1997) used the model of Haberle *et al.* (1994) to estimate the amount of CO_2 that was needed to be injected into the atmosphere during the oceanic episodes to warm the planet. They also calculated the length of time that the warm conditions would last (Figure 12.3). They suggested that to explain the observed fluvial and glacial features, global temperatures must be raised to 240–250 K for over 10^6 years. This would require at least 2 bars and possibly several bars of CO_2 at 3 Gyr ago and no more than 1 bar at 1 Gyr ago. (Most of the large floods are Upper Hesperian in age, or 3–3.5 Gyr old.)

The episodic ocean hypothesis suffers from some of the same problems encountered with the Noachian greenhouse models, particularly in accounting for where all the CO_2 went. According to the models, when equatorial temperatures drop below freezing and CO_2-charged water can no longer infiltrate into the ground, the atmosphere typically still contains bars of CO_2. Any carbonates formed subsequently would have remained at the surface, yet no carbonates have been detected, despite the fact that they have to be younger than most other features on the surface. This problem may be alleviated if, during the post-flood period, there was significant volcanic activity that maintained high levels of SO_2, for then the

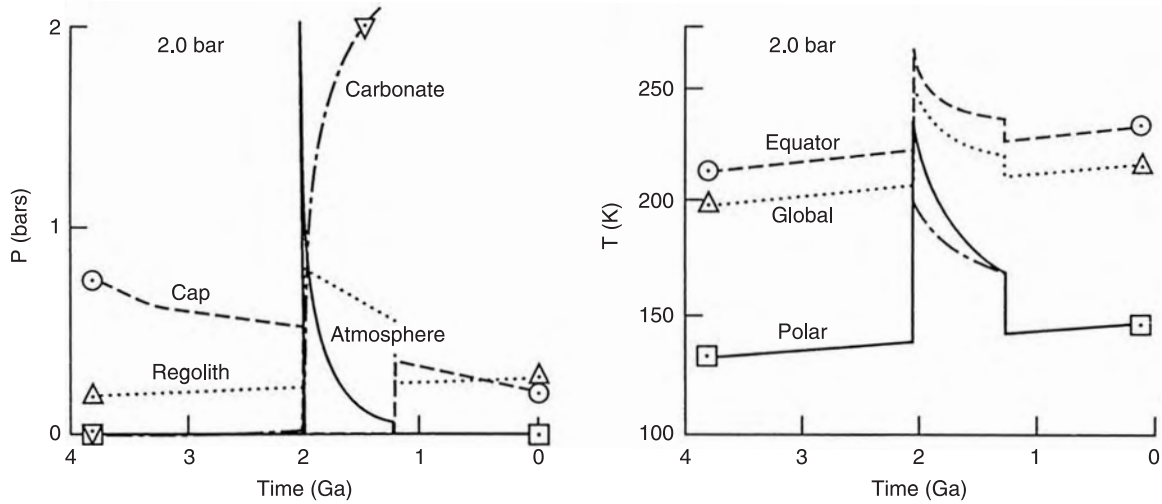

Figure 12.3. Model similar to the previous figure except that a total inventory of 1 bar of CO_2 is assumed for the end of the Noachian, at which time most of the CO_2 is in the cap or regolith. An additional 2 bars of CO_2 are injected into the atmosphere at 2 Gyr ago, as might occur during a large flood. After the flood, equatorial temperature rise to over 250 K, then decline as carbonates form, and ultimately a polar cap forms as in the previous figure (from Gulick *et al.*, 1997, reproduced by permission from Elsevier).

atmosphere could have been much thinner when equatorial temperatures fell below freezing. Another possible problem is that the proposed mechanism results in global warming, yet the post-Noachian valleys are very unevenly distributed, being mostly on a few volcanoes. Gulick *et al.* (1997) recognized this problem and suggested that infiltration could have been at active hydrothermal zones, or other areas where volcanic heat has thawed the ground (Figure 12.4). Alternatively, the preferential distribution of young valley networks on mid-latitude volcanoes could be explained by deposition of snow and ice on the volcanoes during periods of high obliquity followed by melting when the volcanoes were active (Fassett and Head, 2006).

The large floods may not have injected significant amounts of CO_2 into the atmosphere and changed the global climate. Large bodies of water that were left after the floods may simply have frozen in place to form large bodies of ice (Kargel *et al.*, 1995; Moore *et al.*, 1995; Kreslavsky and Head, 2002), which wholly or partly sublimated away, under cold conditions without an enhanced CO_2 greenhouse. Winds blowing over the frozen oceans could have carried away the sublimated water and precipitated it elsewhere as snow. Some young valley networks could have formed by the melting of ice and snow by volcanic heating, or by some combination of internal and solar heating, but clearly, the process would be aided if there were also some greenhouse warming. Some minor greenhouse warming is expected for the Hesperian if the Jakosky and Jones (1997) and Brain and Jakosky (1998) model is correct and that at the beginning of the Hesperian the planet had an atmosphere a few hundred millibars thick, which was mostly lost subsequently by sputtering. But the warming expected from such an atmosphere falls far short of that required to raise equatorial temperatures above freezing.

Episodic warming could have resulted from the occasional large meteorite impact or volcanic event. However, there are no post-Noachian craters that even approach the smallest crater (600 km diameter) that Segura *et al.* (2002) considered. Furthermore, the largest post-Noachian crater, Lyot (220 km diameter), shows no sign of water erosion. Large volcanic events could have injected large amounts of SO_2 into the atmosphere, as suggested by the sulfur-rich nature of the surface. A CO_2 atmosphere a few hundred millibars thick with abundant SO_2 may have provided an effective greenhouse, but it would have been very short-lived, particularly if water was present.

Finally, variations of orbital and rotational motions must have affected climate. Studies of the effects of varying obliquity and eccentricity have focused on recent changes (see below), but changes have been occurring throughout martian history, including times when there may have been substantially more exchangeable CO_2 and water at the surface. Obliquity changes could have affected the stability of the polar caps; the magnitude of the eccentricity

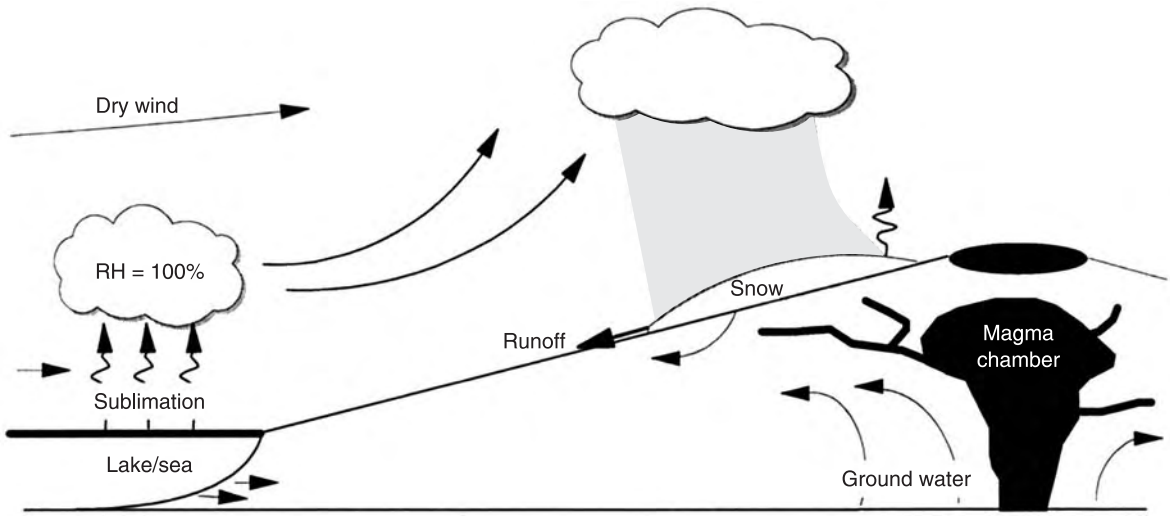

Figure 12.4. Possible mode of formation of young valleys on volcanoes. Large floods result in saturation of the atmosphere and precipitation of snow on volcanoes. Volcanic heating of the snow pack results in cutting of valleys on the volcano flanks (from Gulick *et al.*, 1997, reproduced by permission from Elsevier).

and the timing of periapsis could have affected surface temperatures. Whether some combination of orbital and rotational parameters could have significantly affected global climates, or facilitated other processes, such as melting of snow, remains to be demonstrated.

Recent climate changes

Possible effects of changes in orbital and rotational motions on various surface processes have been discussed elsewhere (Chapters 6, 8, and 10) and are here only briefly summarized. Mars appears to be emerging from a period of high obliquity (Laskar *et al.*, 2002) during which there may have been a martian "ice age" (Head *et al.*, 2003c). For the last 0.3 Myr, the obliquity has ranged from 23–27° about its present value of 25.19°, whereas from 0.3 to 1 Myr ago obliquities were mostly higher, ranging from 15–35°. Obliquity variations affect the stability of ground ice. Ice is stable just below the surface everywhere when obliquities are greater than 30°, but it is unstable at latitudes less than 60° when obliquities are less than 20° (Mellon and Jakosky, 1995). Possible results of the recent higher obliquities are deposition of an ice-rich veneer over much of the terrain between latitudes 30° and 60° in both hemispheres (Mustard *et al.*, 2001) and possible survival of ground ice at low latitudes where it is currently unstable (Jakosky *et al.*, 2005). Obliquity variations may also have modulated deposition of ice and dust at the poles (Milkovich and Head, 2005).

High obliquities result in enhanced sublimation of water ice at the poles, and possibly deposition of snow at low latitudes (Jakosky and Carr, 1985). Evidence of recent glaciation has been found to the northeast of Hellas and on the northwest flanks of volcanoes in Tharsis, where ice is now unstable (Head and Marchant, 2003a; Head *et al.*, 2005c). Recent global circulation models suggests that these are preferred sites for deposition of ice during periods of high obliquity (Mischna *et al.*, 2003), which lends support to the supposition that the glaciers are the result of changes in the stability of ice induced by obliquity changes.

Summary

High erosion rates, high rates of valley formation, details of fluvial features such as deltas, presence of aqueous sediments at Meridiani, dissolution of minerals by groundwater at Meridiani, and detection of hydrated Noachian weathering products from orbit, together are compelling evidence that early Mars was warm and wet and had an active hydrological cycle. Yet how Mars could have been warmed and how the warm conditions could have been maintained remain elusive. Warming by a CO_2–H_2O greenhouse appears inadequate if the energy output of the early Sun was low as standard models predict. Moreover, it is difficult to maintain an early thick CO_2 atmosphere against impact erosion and weathering, and significant carbonate deposits have not been found at the surface. Possible solutions are that (1) the energy output of the

early Sun was not as low as models predict; (2) other greenhouse gases contributed to global warming; and (3) the warmings were not sustained but rather episodic and the result of large impacts or large volcanic eruptions.

The post-Noachian era was mostly cold and dry as indicated by low erosion rates, low weathering rates, and large floods, which probably required a thick cryosphere. The large floods may have temporarily changed the global climate, enabling occasional young valley networks and glacial feature to form. Alternatively, these young features are the result of some combination of astronomical motions, sublimation from oceans, and volcanic heating that resulted in deposition and melting of ice at low latitudes.

Mars may at present be emerging from an ''ice age'' extending from 0.3 to 2 million years ago during which obliquities ranged up to 35°, as compared with the more recent limit of 27°. The higher obliquities may have resulted in accumulation of the ice-rich surficial deposits observed at the surface down to latitudes as low as 30^0 and which are now undergoing removal. The higher obliquities may also have resulted in accumulation of ice just below the surface at lower latitudes where it is now unstable.

13 Implications for life

From the beginnings of telescopic observations of Mars, people have speculated about whether life could have started on the planet and what that life might be like. While the concerns of early observers were mostly with intelligent beings with whom we might communicate, the focus now is on life's origins, microbial communities, and the limits to their survival. Views on the prospects for life on Mars have varied greatly in recent decades. During the 1960s it was thought plausible that vegetation could be present on the martian surface. Some observers noted a seasonal wave of darkening that moved from the poles to the equator in spring and attributed it to vegetation. The Mariner-Mars program originally planned to launch two spacecraft to the planet in 1971. One was to systematically map the planet, the other was to be put into a Mars-synchronous orbit to carefully monitor surface changes that might have a biological cause. One of the spacecraft was lost at launch and the two objectives were ultimately combined in Mariner 9. The search for life continued with the Viking landers. Each carried a sensitive instrument for detecting organic molecules and an elaborate array of biology experiments devoted to detecting metabolism. The negative results from both these experiments in the late 1970s, and a better understanding of the harsh conditions that prevail at the surface today, resulted in considerable pessimism about the prospects for life on Mars, which persisted through the 1980s. Several factors subsequently contributed to a change in how the prospects for life were viewed. The first was the discovery that life could survive in a far wider range of environments than was formerly thought possible, as in deep-sea smokers at temperatures above 100°C, and in basaltic rocks deep below the Earth's surface. The second factor was recognition of the wide diversity of microbial life and the variety of its energy sources. A third factor was the suggestion that life started very early on Earth, possibly during the period of heavy bombardment. A fourth factor was a better understanding of the geological history of Mars, particularly the role of water. Announcement of the finding of possible evidence for life in the martian meteorite ALH84001 further focused attention on the issue.

In this chapter we examine the prospects for life on Mars in light of past conditions on Mars outlined in the previous chapters. Conditions at the surface today are very hostile to life, but we have seen that Noachian Mars was probably very different from present-day Mars. In addition, there may have been episodes in the post-Noachian era when conditions were more clement than at present. When life started on Earth, conditions on the two planets may have been similar. Did some form of life start very early on Mars also? If it did start, did it survive to the present day in niches protected from the current hostile surface conditions? We also know that Mars and Earth exchange surface materials as a result of ejection by large impacts and subsequent capture of the ejected materials. Our finding of over 30 martian meteorites testifies to the efficacy of the process. On early Mars, with impact rates hundreds to thousands of times the present rate, exchange of material must have been common. While it is more difficult for Earth rocks to reach Mars, the high rates of impact almost guarantee that Earth rocks were transported to Mars (Gladman *et al.*, 1996). A few percent of material ejected from Earth would have reached Mars within several years. Since microbes can survive exposure to space conditions for years if protected from radiation, it is not unreasonable to conclude that if life started on Earth during heavy bombardment, viable microbial life could have been delivered to Mars in the interstices of Earth meteorites, and similarly, if life ever started on Mars, viable forms could have been delivered to the Earth.

These two possibilities for early life on Earth and Mars, independent origin and mutual colonization, have different implications for the origin of life outside our Solar System. If life arose independently on the two planets, it would imply that the origin of life is not a low-probability chance event but instead will follow naturally given the right conditions. If so, then life could be common throughout the universe.

Of course, none of the questions just raised can yet be answered. This chapter merely gives an overview of some of the issues. The chapter is different from the previous chapters in that the topic is outside the area of expertise of the author. It was felt important,

however, to include the chapter because the search for life and its origins is the main thrust of the Mars exploration program and because the search has such broad philosophical implications.

The origin of life

We will not explore here the "how" of life's origins but rather the "when" and the "under what conditions." For a summary of the major questions regarding the " how," see National Research Council (1990) and Lazcano and Miller (1996). In the following discussion we will assume that life started on Earth and had not been introduced from outside the Solar System or from Mars (Davies, 1995). We do not know how life started on Earth, but it appears to have arisen remarkably quickly. Isotopic evidence suggests that life may have started 3.85 Gyr ago (Mojzsis *et al.*, 1996) and organic remains in microbial fossils may have been found in rocks as old as 3.46 Gyr (Brasier *et al.*, 2002; Schopf *et al.*, 2002). These findings remain very controversial in part because the geological record from this early era, when the Earth was just emerging from the period of heavy bombardment, is poorly preserved. The period from the origin of the planet 4.5 Gyr ago until 4 Gyr ago is called the Hadean era and roughly corresponds to the pre-Noachian and Noachian on Mars. The following Archean era refers to the period of the Earth's history that extended from 4 Gyr ago to 2.5 Gyr ago. Archean rocks are exposed within all the continental shields, but the largest exposures are in southern Africa, western Australia, and around Hudson Bay in Canada. Two kinds of Archean rock associations are generally distinguished: a high-grade metamorphic association consisting mostly of gneisses of tonalitic–granodioritic composition, and low-grade greenstone belts. The high-grade gneisses commonly enclose volcanic–sedimentary sequences, including banded iron formations (BIFs), bright-red banded rocks rich in chert and hematite. The presence of water-lain rocks, including BIFs and pillow lavas enclosed by 3.7–3.8 Gyr gneisses of Isua in west Greenland, attests to the presence of a hydrosphere with an already mature cycling of sediments by this time (Ernst, 1983).

Part of the evidence for early life is the fractionation of carbon isotopes in Archean rocks (Schidlowski, 1983). Biologic fixation of carbon typically results in depletion of ^{13}C. Organic carbon from extant plants and organisms mostly have $\delta^{13}C$ value of -10 to -30 per mil, as compared with 0 per mil for marine carbonates Figure 13.1. Fossil carbon, including that from many Archean rocks has a range similar to modern organic carbon, which suggests

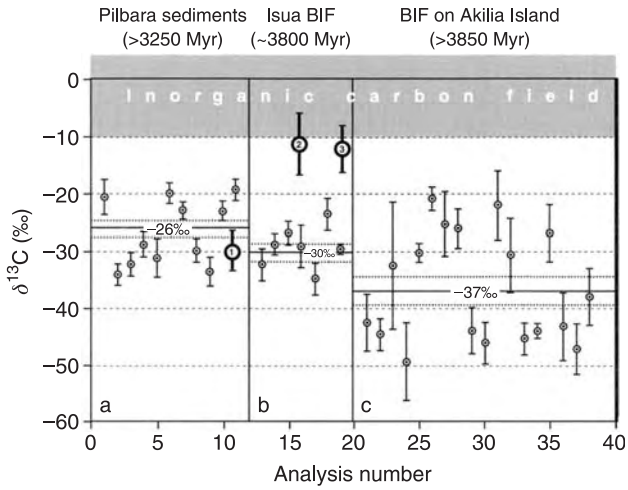

Figure 13.1. Isotope compositions of carbonaceous inclusions in individual apatite grains from early Archean sediments. The lower the δ^{13} number, the lighter the carbon. Transformation of inorganic carbon to organic carbon results in lowering the δ^{13} value. The terrestrial biomass as a whole has a δ^{13} value of -25 per mil as compared with 0 per mil for oceanic carbonate, which represents the bulk of the inorganic carbon. The carbon from the different Archean rocks shown all have the organic carbon values. The numbers in circles represent whole rock analyses (from Mojzsis *et al.*, 1996, copyright © 1996, Nature Publishing Group).

that Archean carbon is organic. The age of the oldest organic carbon is, however, controversial. Mojzis *et al.* (1996) and Mojzis and Mark (2000) claim to have found low δ^{13} values in carbon extracted from 3.85 Gyr old apatites in gneisses from Akilia, Greenland. Modern microorganisms actively nucleate apatite, a chemically resistant calcium phosphate mineral. As a result, apatites in both modern and ancient sediments are commonly intertwined with organic remains. Enclosure of the carbon in the apatite protects it from isotopic exchange with groundwater and so preserves the initial isotopic compositions. Because of the light carbon extracted from the 3.85 Gyr rocks Mojzsis *et al.* concluded that life had started on Earth by this time, the tail end of heavy bombardment. However, the age of the gneisses, the presence of carbon in theapatites, and the sedimentary nature of the deposits have all been questioned (Lepland *et al.*, 2005).

Claims for very ancient fossils may be more questionable. Schopf (1999) has pioneered the search for Earth's earliest fossils. Because fossils from the Archean are all microbial, they are small and difficult to identify. The difficulty is compounded by the fact that most Archean rocks have undergone at least

some metamorphism. Schopf's approach has been conservative. To be authenticated, a fossil must satisfy the following criteria: (1) be relatively abundant, (2) be carbonaceous, or be the product of mineral replacement, (3) resemble other modern and/or fossil microorganisms, (4) occur in a geologically plausible context, (5) exhibit a level of organization consistent with known fossils of similar age, and (6) be dissimilar from coexisting abiological organic bodies (Schopf and Walter, 1983). Using these criteria, Schopf has identified possible fossils in various Precambrian sediments ranging in age up to 3.5 Gyr (Figure 13.2). Until recently the carbonaceous nature of the oldest fossils could not be confirmed. However, Raman imagery of some of the putative fossils has now established that some as old as 3.465 Gyr are indeed carbonaceous. The fossils resemble filamentous prokaryotes and have been taken as evidence that oxygen-producing photosynthesis had started by this time. This conclusion has, however, been vigorously challenged by Brasier *et al.* (2002), who claim that the carbon is abiotic.

Another controversial issue is the age of the oldest stromatolites. These are banded formations visible to the naked eye. They form from microbial mats in shallow water. Sediment becomes trapped in the mats, thereby obscuring the sunlight, and the photosynthesizing organisms then move upward to survive leaving organic detritus behind. Upon lithification a banded structure is preserved. Stromatolite-like formations have been identified in the 3.5-Gyr-old Warrawoona Group in Australia (Walter, 1983) in association with filamentous, cyanobacteria-like features (Schopf and Walter, 1983). However, as with the postulated fossils, the claims of an organic origin for the structures has been questioned because abiotic processes can also produce banded formations that resemble stromatolites (Lowe, 1994). Nevertheless, despite all the uncertainties, the combination of isotopic evidence, possible stromatolites, and suggestive fossil morphologies all combine to support the supposition that life started very early, possibly during the period of heavy bombardment.

Molecular phylogeny indicates that all life on Earth had a common ancestor. Woese and co-workers (Woese, 1987, 1990; Pace, 1991) used the sequence of bases on ribosomal RNA to determine the relatedness of different forms of terrestrial life. Ribosomes are small structures within cells that translate genetic information into the production of proteins. They are therefore fundamental to the basic metabolism of the cell. Ribosomal RNA was chosen as a measure of the relatedness of organisms because it appears to have retained its function over large evolutionary

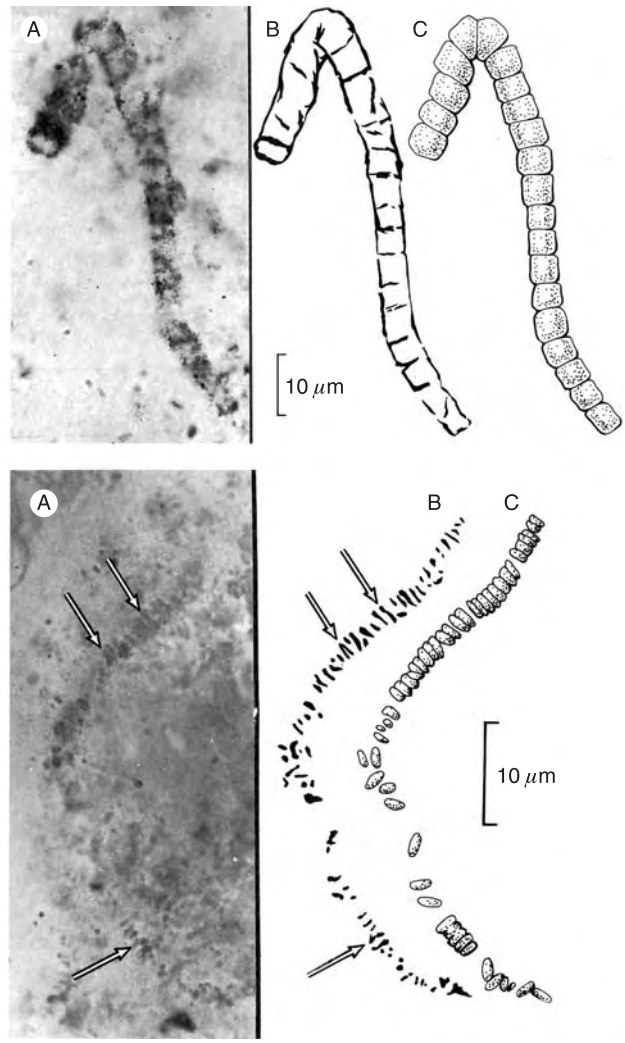

Figure 13.2. Possible Archean fossils. Photographs are on the left, reconstructions on the right. The upper example is a filamentous prokaryote from the 3.5-Gyr-old Warrawoona Group from western Australia. The lower example is a filamentous prokaryote from a stromatolite of the 2.8-Gyr-old Fortescue Group of western Australia (from Schopf and Walter, 1983, copyright © Princeton University Press).

distances and has been modified only slowly so that deep ancestral sequences have been retained. The ribosomal phylogeny indicates that the last common ancestor of all terrestrial life was thermophilic, as were several branches close to the origin of the RNA tree (Figure 13.3). The most primitive life forms that survive on Earth today appear to be anaerobic hyperthermophiles that grow at temperatures in excess of 90°C, utilizing geochemical energy sources such as sulfur and hydrogen, and deriving their carbon from CO_2 (Achenback-Richter *et al.*, 1987; Pace, 1991).

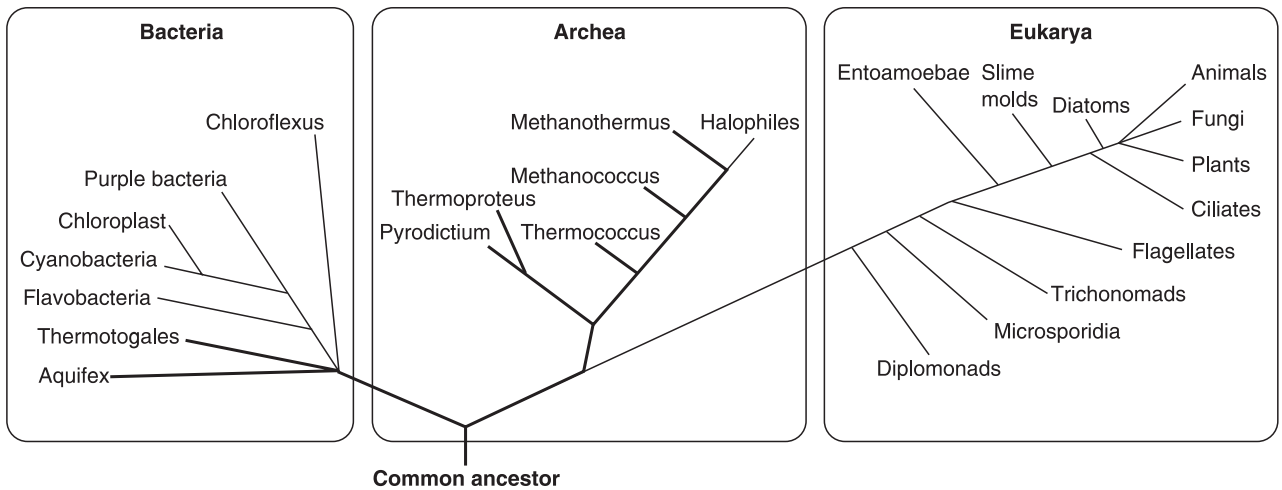

Figure 13.3. The "tree of life" based on ribosomal RNA showing the genealogical relations between all living organisms. Three main branches of life are recognized as shown. The heavy lines show hyperthermophiles, groups of organisms that live at high temperatures (adapted from Woese *et al*., 1990; Stetter, 1996).

We saw above that life may have already started by the end of heavy bombardment. Sleep and Zahnle (1998) examined what conditions might have been like during the era of heavy bombardment and what the implications might be for any life that had taken hold. The main concern is with very large impacts that had the potential for sterilizing the planet, impacts that released ten to hundreds of times more energy than the impact at the K/T boundary. The impact rate can be estimated from the age of the basins on the Moon, where there were roughly ten such events between 3.8 and 4.1 Gyr ago. Sleep and Zahnle estimate that there would have been hundreds of such events on the Earth. Ryder (2002) suggested, however, that there would have been far fewer events than Sleep and Zahnle assumed. He claims that the large number of basins on the Moon is the result of a spike late in the heavy bombardment and that preceding the spike was a more benign era of cratering. But even with the Sleep and Zahnle assumptions, the spacing between the mega-events would have been millions of years, time enough for colonizing much of the Earth if life ever arose. The threat to life from these events is mainly thermal. The oceans would have boiled away and the planet been enveloped in hot rock vapor, which would have condensed and rained hot rock back onto the surface. All life would probably have been extinguished. The effects of smaller events intermediate in size between the largest basin-forming events and that at the K/T boundary may have been less lethal. Only the upper few hundreds of meters of the oceans may have been boiled away, and all life at the surface dependent on energy from the Sun would have been eliminated. However, ocean-bottom communities in hydrothermal vents living off chemical energy may have survived. Thus the fact that the common ancestor and many of the life forms at the root of the phylogenetic tree are thermophiles does not necessarily imply that life started in hot environments such as hydrothermal systems. Life could have started in some low-temperature environment, such as a tidal pool or Darwin's warm little pond, then multiplied and adapted to different environments, only to be annihilated except for the thermophilic ancestor. The thermophilic common ancestors are not primitive. They contain most of the enzymes of modern organisms, the same elaborate protein biosynthesis, and the same replication and translation machinery (Lazcano and Miller, 1996). Impacts probably created a bottleneck allowing only thermophillic autotrophs to survive that ultimately give rise to all of subsequent life. For a more complete summary of habitats on early Earth and the nature of early life, see Nisbet and Sleep (2001).

Sleep and Zahnle (1998) also explored how life might have survived large impacts on Mars, if life ever started there or was colonized from Earth. They concluded that survival of life in the deep subsurface was more likely on Mars than on Earth because a lower gravity and lower heat flow would have allowed life to penetrate deeper and because the thermal pulse from large impacts would have been shorter, since much of the hot ejecta would have left the planet rather than falling back as on Earth.

Conditions on Earth and Mars may have been similar during the Hadean–Noachian. Both appear to have had abundant liquid water at the surface,

a supply of organic materials from comets and asteroids, a similar surface composition, and, at least episodically, a thick enough atmosphere to permit precipitation and flow of water across the surface. Both had widespread volcanism with accompanying hydrothermal environments and volcanogenic gases. Both were protected from the solar wind by a magnetic field, and both were subject to repeated large impacts. Large potential but unknown differences are the composition and thickness of the atmosphere, the size of the oceans, and the presence of plate tectonics. The biggest differences were size and distance from the Sun. Since we do not know how life originated (or even on which planet it originated), it is difficult to assess how these various similarities and differences affected life's start.

The nature of Mars' early atmosphere is a big unknown. Because of the planet's smaller size, Mars' atmosphere would have been more vulnerable to blow-off by large impacts than was the Earth's. While CO_2 lost from the martian atmosphere by weathering may have been recycled back into the atmosphere by high rates of volcanism, CO_2 losses to space as a result of impact would have been permanent. Such losses would have been more efficient on early Mars than on early Earth because of Mars' smaller size. The result may have been a progressive depletion of recyclable CO_2 through the Noachian, which would explain the failure to detect significant amounts of carbonate at the surface. Nitrogen, so essential to life, may have been severely depleted since it is much less readily fixed in minerals. Another big unknown is how long-lasting surface conditions were such that liquid water was stable at the martian surface during the Noachian. We saw in Chapter 12 that one possible explanation for the extensive fluvial dissection of Noachian terrains is that the fluvial activity resulted from temporary conditions caused by large impacts rather than sustained conditions imposed by a semi-permanent, thick atmosphere. If so, then this would probably render the origin of life less likely on early Mars than on the Earth. Nevertheless, since we do not know what conditions were necessary for life's start and what condition were incidental, we cannot come to a definite conclusion as to what the probability is that life started on Mars.

Habitability

The habitability of post-Noachian Mars was likely very different from the Noachian Mars just described. The cold temperatures, the scarcity of organic materials, the high UV flux, and the lack of liquid water combine to make the present surface of Mars hostile to all forms of terrestrial life. Present-day conditions are probably representative of conditions for much of the last 3.5 Gyr, so even if life started on early Mars, it would have been challenged to survive for any length of time after the end of the Noachian. The first challenge is temperature. The mean equatorial temperature of 215 K is close to the mean annual temperature of the Earth's south pole (223 K) and the mean polar temperature of 160 K is well below the lowest temperature ever recorded on Earth (185 K). The second challenge is the scarcity of organic compounds. The Viking GCMS experiment failed to detect any organic compounds in the surface materials at the ppb level despite infall of meteorites that typically contain 1–10 percent of reduced carbon compounds (Biemann *et al.*, 1997). The absence has been attributed to oxidation of organics by oxidants that were synthesized either by photolytic reactions in the upper atmosphere or by UV radiation of minerals at the surface. The third challenge is the high UV flux. On Earth a deep ozone absorption band at 2550 Å prevents most of the UV from reaching the surface, whereas on Mars, at least at low latitudes and in summer at high latitudes, the full solar flux at wavelengths greater than 1900 Å falls unattenuated onto the surface. While some organisms can adapt to high UV fluxes, the flux at the martian surface is sterilizing for most terrestrial organisms. Because Mars has no magnetic field, the surface is also unprotected from the flux of solar particles.

Scarcity of liquid water at the surface may be the most difficult environmental factor with which life must cope. As discussed in Chapter 1, ice is present everywhere just below the surface at latitudes higher than 60° and small fractions may be present at low latitudes. Liquid water is stable at temperatures between 273 and 283 K if the partial pressure of water vapor exceeds 6.1 mbar. This temperature condition is achieved at midday during summer in the upper centimeter of low thermal inertia soils. The partial pressure condition is unlikely ever to be met at the surface under present conditions, it being typically 2–3 orders of magnitude lower than the requirement. However, at the lowest parts of the surface where the total surface pressure is in excess of 6.1 mb liquid water brought to the surface would not boil; it would remain until eliminated by freezing and sublimation.

Pockets of liquid water could also exist transiently just below the surface in an ice-rich soil if it were heated and if the water vapor was prevented from diffusing to the surface, such as by a cement. Such pockets are, however, unlikely under present conditions, at least at low to mid latitudes. At these latitudes, the required temperatures are met only in

the upper centimeter or so of low thermal inertia soils. If cement were present, the thermal inertia would be increased and the temperatures required for liquid would not be reached. Transient pockets of liquid water may be more likely at certain times at high latitudes where there is more water ice and where long summer days allow deeper penetration of the diurnal wave, for example on poleward-facing slopes. The conditions are much more likely to be met during periods of high obliquity (Costard *et al.*, 2002).

Young, seemingly water-worn features of different kinds were described in Chapter 6. Gullies are common on poleward-facing slopes at high latitudes. Their appearance strongly suggests that water was involved in their formation, either as a result of groundwater seepage, or the melting of ice retained in hollows on poleward-facing slopes at high obliquity. If the latter, they may have formed as recently as 0.5 Myr ago when obliquities were higher than in the present epoch. Young, seemingly water-worn channels that originate at fissures in several locations, as in southern Elysium and southeast of Olympus Mons (Chapter 6), have been roughly dated at a few tens of millions of years. They suggest that water has episodically erupted on to the surface from a deep hydrosphere until geologically recent times.

Young martian meteorites and young crater ages on various volcanic features indicate that Mars has been volcanically active throughout its history, up to the present. Active volcanism combined with a water-rich cryosphere and hydrosphere must inevitably have led to hydrothermal activity, which on Earth results in a variety of warm, wet, chemically rich environments with prolific and varied biologies. Although no active hydrothermal sites have been identified from orbit, some of the mineral anomalies being identified in spectral data (Bibring *et al.*, 2005) may turn out to be hydrothermal. Finally, extensive dissection of some volcanoes (Figures 4.15, 4.20) suggests that liquid water was available at least episodically on their flanks. One possibility among many is that the water derived from the melting of ice is deposited on the volcano flanks during periods of high obliquity.

The examples of possible episodic availability of liquid water just described probably apply to most of the time since the end of the Noachian, when surface conditions were predominantly cold. But we saw in Chapters 7 and 12 that Mars may also have experienced short ($10-10^3$ years) warm episodes as a result of large floods (Baker, 2001). During these short episodes, liquid water may have been widely available at the surface and large bodies of water may have been present in low areas, particularly the northern plains.

Survival

If life started on Mars, or was colonized from the Earth, to survive it would have had to either adapt to the hostile surface conditions, find more hospitable niches below the surface, or be able to survive in a dormant mode waiting for the next moist episode. Microbial life is remarkably adaptive, so it is not outrageous to suppose that life may have survived to the present had some form of life taken hold in the Noachian. In recent decades, life has been found almost everywhere on Earth where liquid water is available no matter what the physical and chemical conditions.

The following summary of the range of conditions under which life is found on Earth is from Rothschild and Mancinelli (2001). The most hyperthermophilic organisms are Archea. *Pyrolobus fumarii*, a chemolithoautotroph, thrives at deep-sea smokers and is capable of growing at 113°C. At the other end of the scale, many microbes can be preserved at liquid nitrogen temperatures (−196°C) and active microbial communities have been observed at −18°C. Some species (e.g. *Deinococcus radiodurans*) can withstand high levels of UV and gamma radiation. Microorganisms have, for example, been found in the core of the Three Mile Island reactor (National Research Council, 1992). High pressures are not a problem. Obligate piezophiles, found in the Mariana trench, can grow at pressures of 70−80 MPa but not at pressures below 50 MPa. Organisms can also adapt to extremes of pH ranging from 0.5 for the red alga *Cyanidium caldarium* to alkophiles living at a pH of 10.5. They can also adapt to extremes of salinity such as are found within salt crystals. While most of these extremes may not be applicable to Mars, they are indicative of life's adaptability.

Perhaps more important for Mars are dormancy and the ability to live at low metabolic rates. As we saw above, normal conditions at the martian surface are very hostile to life because of the UV radiation and the lack of liquid water. But we also saw that liquid water may be episodically available as a result of melting of ice or leakage of groundwater. Could spore-like or seed-like forms survive at the surface during the extended cold dry periods and episodically revive when water becomes available? Endospores from gram-positive bacteria are among the most resistant and survivable life forms on Earth. They are thought to be capable of surviving for thousands of years and are resistant to freezing, desiccation, and vacuum

conditions (National Research Council, 1992). Experiments with NASA's Long Duration Exposure Facility showed that, when shielded from radiation, bacterial spores had good survival rates even after 6 years' exposure in space. Survival was, however, considerably reduced if the spores were exposed to UV radiation. If spores at the martian surface are to resist being deactivated by radiation they must be below the surface, sheltered from the UV. They do not need to be deeply buried, just a few millimeters would suffice.

In Antarctica, organisms have adapted to living within rocks to avoid the harsh conditions at the surface (Friedman, 1980). These diverse cryptoendolithic communities live within the interstices of porous sandstones where adequate water for growth and light penetration for photosynthesis is present no more than 2–5 days a year. Inorganic nutrients come from the host rock and photosynthesis occurs at temperatures as low as −8°C. Metabolism is so slow that the time for carbon turnover is of the order of 10,000 years (Johnston and Vestal, 1989). Another low metabolic-rate community lives several hundred meters below the surface in the Columbia River basalts of Washington State. The community is supported by lithoautotrophs that consume hydrogen generated by slow interaction between water and basalt. They appear to be independent of any photosynthetic support from the surface. Doubling time for the organisms is estimated to be between 10,000 and 20,000 years. They clearly have the capacity to live in a dormant state for long periods of time. We saw above that the deep subsurface may be a favored place for survival of life from the large impacts on Noachian Mars, had any life been present at that time. But could such hypothetical communities have survived the billions of years of Mars' subsequent history? And if life did survive and adapt to living below the ground, could it have temporarily colonized parts of the surface, such as lakes and seas, after being introduced onto the surface by eruptions of groundwater? Despite the extraordinary feats of survival by life on Earth, they appear minor compared with the feats that martian life must perform.

ALH84001

In August 1996, McKay *et al.* (1996) shocked the scientific world by announcing that they had found evidence for life in the martian meteorite ALH84001. The meteorite is a very ancient, coarse, grained orthopyroxenite that crystallized 4.5 billion years ago, roughly 40 million years after global differentiation to form the core (Chapter 4). In support of their claim for biogenic activity in the meteorite they listed the presence of (1) objects shaped like bacteria in scanning electron microscope imagery, (2) polycyclic aromatic hydrocarbons (PAHs), (3) disequilibrium mineral assemblages, and (4) magnetic particles similar to magnetofossils produced by terrestrial bacteria. They noted that "Although there are alternative explanations for each of these phenomena taken individually, when they are considered collectively . . . we conclude that they are evidence of primitive life on Mars." The announcement triggered a massive public and scientific debate into the validity of the claims. The scientific consensus now is that there are plausible abiological explanations of all the observations, and that the claims of biological causes are likely invalid. For a highly informative account of the ensuing debate about the validity of the claims, see the site http://www.lpi.usra.edu/lpi/meteorites/alhnpap.html formerly maintained by Alan Treiman of the Lunar and Planetary Institute.

The episode, coupled with the claims and counterclaims for discovery of the earliest life on Earth, is illustrative of the difficulties that we will continue to encounter as we pursue our quest to determine if life ever arose on Mars. We will quickly review here why the claim of finding evidence for life in ALH84001 is now viewed with skepticism. The claim that some of the objects viewed in the meteorite at high resolution could be bacteria was immediately doubted because of the small size of the objects. The bacteria-like forms are 100 nm long and as little as 20–30 nm wide, much smaller than the generally accepted size of the smallest bacteria. A special panel convened by the National Research Council (1999) to assess how big an organism must be to enclose all the metabolic and genetic machinery that modern terrestrial life requires concluded that independent free-living bacteria must be at least 200–300 nm in diameter. If the objects that McKay *et al.* describe are organisms, they must have had a much simpler chemistry than modern terrestrial organism. Bradley *et al.* (1997) alternatively suggested that the objects might be artifacts caused by the Au–Pd conductive coatings used by McKay *et al.* in the SEM work. Similar objects have not been found when other coatings are used. It should be noted here that there are claims of terrestrial nanobacteria of comparable size to those in the martian meteorite (e.g. Folk, 1993), but these claims are not widely accepted. Shortly after publication of McKay *et al.* (1996), Anders (1996) pointed out that production of PAHs does not require biology. Abiotic causes have been proposed for PAHs found in carbonaceous chondrites, Moreover, some phases (magnetite, clay minerals) associated with the carbonates in ALH84001 are

known to catalyze Fischer–Tropsch reactions, which convert simple carbon compounds such as CO into more complex ones, including PAHs. Anders also pointed out that the disequilibrium mineral assemblages described by McKay *et al.* could be produced abiotically. Finally, while the size, purity, and mineral structure of the magnetite grains in ALH84001 do resemble those produced by bacteria, similar magnetites have been produced experimentally without the intervention of biology (Golden *et al.*, 2004).

Looking for life

Even if some form of life, indigenous or terrestrial, established itself on early Mars, finding evidence for it will be extremely difficult, whether or not some form of it survived to the present day. Two broad approaches can be followed in the search. We can focus on the past and look for fossil evidence, or we can focus on the present and look for evidence of extant life, as was done with Viking.

It could be argued that the best approach is to look for fossil life. Life on Noachian Mars was more likely than on post-Noachian Mars. We saw above that conditions on Noachian Mars may have been similar to the contemporary Earth, where life may have already taken hold. In addition, seeding from Earth was more likely at this time. Life subsequent to the Noachian would have had the additional burden of coping with the hostile surface conditions that prevailed for most of the planet's subsequent history. So perhaps the best strategy is to focus on early Mars. However, the experience with ALH84001 and the controversies over when life first started on Earth illustrate the difficulty of finding unambiguous evidence of microbial fossil life in ancient rocks. It is possible that the cold, dry conditions that prevailed for most of Mars' history would have led to better preservation of organic molecules and organic structures than on Earth. A compelling case is likely to be made only with information on morphology, organic chemistry, possible chemical disequilibria, isotopics, and the contemporary environment. Such comprehensive information will only be obtainable from samples returned to Earth. A focus on fossil life implies returning to Earth samples from favorable fossil environments, such as former hydrothermal systems, lakes, or seas, then using the full array of analytical techniques available in terrestrial laboratories for their analysis.

Alternatively, it could be argued that the best strategy is to look for present-day life. Should living organisms be present, molecular analysis and detection of growth are much more likely to give definitive, unambiguous results than is evidence from fossils. There are also drawbacks to this approach. The main one is that even if life started on early Mars it may not have survived to the present. A second is that the present surface is so hostile that if life is present it probably is in protected niches, and we do not where those niches are. Drilling into the surface to access materials shielded from the UV and oxidizing surface conditions has, for example, been suggested. Another problem is that detecting growth may require culturing, and we do not know how to culture possible Mars organisms. Even on Earth, most microbes elude culturing in the laboratory. On alien Mars the problem will be much more severe. Organic chemistry may offer the best hope for life detection. Clearly detection of a diagnostic molecule such as RNA would be definitive, but it is also very unlikely. More likely is the detection of anomalous distributions of isomers or anomalous isotopic compositions. Isomers are molecules of the same compound but with different properties. They may for example be mirror images of each other or have some other geometric difference. Biological processes tend to prefer one isomer to another. Similarly, biological process that produce arrays of macromolecules, such as lipids, do so with preferred numbers of carbon atoms, in contrast to a more random distribution by abiotic processes (Brooks *et al.*, 1999). Any strategy directed at detecting present-day life would have to include both *in situ* analysis to detect growth and samples returned to Earth for more comprehensive analysis.

Finally, life may be detected indirectly. Formisano *et al.* (2004) and Krasnapolsky *et al.* (2004) report detecting methane in the martian atmosphere. Methane cannot survive long in the martian atmosphere (Kuhn and Atreya, 1979), so if the reported detection proves true, there must be a source. Possibilities include meteoritic infall, magmatic exhalations, and methanogenic bacteria.

Summary

Life on Earth started or was seeded from Mars very early, possibly during the period of heavy bombardment that ended 3.8 Gyr ago. Conditions on Earth and Mars may have been similar at that time. Both appear to have had abundant liquid water at the surface, a supply of organic materials from comets and asteroids, a similar surface composition, and, at least episodically, a thick enough atmosphere to permit precipitation and flow of water across the surface. Both had widespread volcanism with accompanying hydrothermal environments and volcanogenic gases. Both were protected from the solar wind by a magnetic field, and both were subject to repeated large impacts.

Close to the end of heavy bombardment all life on Earth may have been destroyed by large impacts except for hyperthermophiles living deep within hydrothermal systems protected from the sterilizing effects of impacts. The hyperthermophiles ultimately gave rise to all subsequent life on Earth.

Early Mars could have been seeded by the Earth, or given rise to life independently, possibly including seeding the Earth. Survival beyond the end of heavy bombardment would have been much more difficult on Mars than on Earth because of the hostile surface conditions. Terrestrial life is very adaptive. Life could have adapted to changing conditions at the end of the Noachian by retreating to refugia underground or becoming dormant, and reviving episodically when the necessary conditions arose.

Detecting life on Mars will be challenging. Fossil life is more likely than extant life, but unambiguous detection of fossil life on Mars will be extremely difficult, as exemplified by ALH84001 and controversies surrounding detection of early life on Earth. Detection of extant life will also be difficult, requiring culturing of unknown life forms and sophisticated organic chemistry. Detection of both extinct and extant life will require return of samples to Earth from carefully chosen sites.

14 Summary

From the discussion in the previous chapters we can reconstruct the broad outlines of the geological history of the planet. The history that is potentially decipherable from the surface morphology has been divided into three eras: the Noachian, which extends from roughly 4.1 Gyr ago to 3.7 Gyr ago, the Hesperian from roughly 3.7 to 3 Gyr ago, and the Amazonian from 3 Gyr ago to the present. The era prior to the Noachian has not been formally named because the geological record for that era has been largely erased. Arguably the most important era of the planet's history was the first 800 million years. When Mars emerged from the Noachian around 3.7 Gyr ago it was on an evolutionary path very different from that of the Earth and the other terrestrial planets. Its geology had a distinctively martian style that was sustained for the rest of the planet's history.

Mars accreted and differentiated to form a core remarkably quickly. The core formed within 20 Myr of the age of the formation of the Ca–Al-rich inclusions in carbonaceous chondrites, which, with an age of 4.567 Gyr, are the oldest objects in the Solar System (Chapter 4). It had formed before creation of the Earth's Moon, which is regarded as the terminal event in the formation of the Earth and dated at 30–50 Myr after the formation of the Solar System. Core formation probably released enough energy to leave the core liquid and convecting, thereby creating a magnetic field around 4.5 Gyr ago. A 4.5 Gyr age for the martian meteorite ALH84001 indicates that Mars also had a stable crust by that time. The crust appears to range in thickness roughly from 5 km to 100 km with an average thickness of 45 km. It is unequally distributed, with thicknesses that are typically 30 km in the northern hemisphere and 50 km in the southern hemisphere. Although spectral data suggests that there may be an andesitic component, most of the crust appears to be basaltic in composition. The spectral differences may be due to alteration. Differences in crustal thickness are the basic cause of the global dichotomy expressed by predominantly high-standing, heavily cratered terrain in the south and low-lying, sparsely cratered plains in the north. The cause of the dichotomy is unclear. Contending suggestions are that it results from one or a few very large impacts, or that it is the result of internal convection. Whatever the cause, it occurred very early in the planet's history.

The main characteristic that distinguishes the Noachian and pre-Noachian from the subsequent eras is the high impact rate. It is not clear whether the high impact rates at the end of the Noachian are typical of the entire period from the time of accretion to the end of the Noachian around 3.7 Gyr ago, or whether they result from a late spike as has been suggested for the Moon. Formation of large impact basins over 1000 km across, such as Hellas, Argyre, Isidis, Utopia, and Chryse, would have had devastating effects. It has been estimated that formation of the 2300 km diameter Hellas would have heated the surface hundreds of degrees, deposited 70 m of molten ejecta planetwide, and produced a 10 bar rock atmosphere that would have condensed out in a few days dropping an additional 10 m of molten rock onto the surface. While Hellas-sized impacts must have been rare (there may have been only one), the more frequent, smaller basin-forming events would also have had significant environmental effects, including precipitation of rain for months to years depending on the size of the impact, and deposition of layers of ejecta over the entire planet. Impacts would have resulted in deep gardening and brecciation of the near-surface materials leading to a high-porosity crust, probably with a low density compared with undisturbed volcanic rocks and meteorites.

The Noachian was also an era with high rates of volcanism. The pile of volcanic rocks that straddles the dichotomy boundary in the Tharsis region appears to have largely accumulated by the end of the Noachian (Chapter 4), but the region continued to be a focus of volcanic activity for the rest of the planet's history. Formation of Tharsis resulted in deformation of the lithosphere to create a shallow topographic and gravity low around the rise that affected the orientation of late Noachian and younger water-worn features. In addition, stresses caused by the presence of Tharsis resulted in extensive fracturing of the Noachian lithosphere around Tharsis. The fracturing also continued for the rest of the planet's history. Formation of Tharsis was

probably also accompanied by massive outgassing of volatiles such as water from the interior. What caused so much of the planet's volcanism to be focused in this region is unknown. Possibilities include convective patterns in the mantle, and a feedback mechanism whereby once the volcanic province had been established, it maintained a thin lithosphere which enabled further volcanism.

Two characteristics of Noachian surfaces, in addition to high crater densities, that distinguish them from younger surfaces are that they are mostly highly eroded and mostly highly dissected by valley networks. Estimates of erosion rates from preservation of craters suggest that erosion rates declined by at least 3–4 orders of magnitude at the end of the Noachian. Thus, large Noachian basins such as Hellas and Isidis thousands of kilometers across have undergone significant degradation, whereas intricate details of the ejecta around small (10 km diameter) Hesperian craters, only a few hundred million years younger, are perfectly preserved. Similarly, the rate of dissection by valley networks appears to have dropped dramatically at the end of the Noachian. Elaborate area-filling, branching valley networks up to thousands of kilometers long are common throughout the Noachian terrains. In contrast, most (but not all) Hesperian plains are barely dissected, if at all. The Noachian valley networks are commonly accompanied by arrays of other fluvial features such as central channels, alluvial fans, and deltas. Convergence of drainage on local lows suggests that lakes were common. Layered deposits appear to underlie much of the Noachian terrain. The layers are commonly exposed in craters, both in their walls and in their floors. In addition, over extensive areas of the Noachian terrains, the upper layers have been partly stripped away to exhume craters and form terrain with an etched-like appearance. The layers are probably of diverse origins, including fluvial, lacustrine, and eolian sediments, impact ejecta, and volcanic materials. The array of rocks encountered by the Spirit rover in the Columbia Hills in Gusev crater may be representative of Noachian rocks in general. They include primary basaltic rocks and clastic rocks, such as impact ejecta and tuffs derived from basalts, and have highly variable degrees of alteration, and highly variable contents of volatiles such as S, Cl, and Br.

Formation of the dense valley networks, common throughout the Noachian terrains, appears to require surface runoff, which would have had to be supplied either by rainfall or melting snow (Chapter 6). This in turn almost certainly implies conditions significantly warmer and wetter than those that prevail today. Warm conditions are also supported by the finding of evaporites at Meridiani, by indications of a shallow water table at Meridiani, and by detection of clay minerals from orbit in Noachian terrains. The valley networks suggest an Earth-like, active hydrological cycle in the late Noachian with large lakes or oceans that acted as evaporative sources, base levels for erosion, and sinks. Under warm, Earth-like conditions, the size of the oceans would have been controlled by the total surface inventory of water for which geological estimates range from 0.4 to >2 km global equivalent. The persistence and cause of the warm conditions at the end of the Noachian are both unknown. While there may have been a pulse of fluvial activity at that time, high erosion rates clearly prevailed for much of the Noachian period, as indicated by the extensive erosion of Noachian impact basins and large craters. Warm conditions may have been created episodically by large impacts, or by large volcanic eruptions. Alternatively, the warm conditions may have resulted from a semi-permanent atmospheric greenhouse, although failure to demonstrate how a CO_2–H_2O greenhouse could raise surface temperatures sufficiently and failure to detect significant carbonate reservoirs are troubling. As already indicated, warm conditions imply that large bodies of water were present in low areas such as Hellas and the northern plains. Possible shorelines have been tentatively identified around both these basins, but their identification is very uncertain. If there were cold periods during the Noachian, the large surface inventory of water coupled with variations of obliquity could have periodically caused massive transfer of water ice between the poles and lower latitudes.

At the end of the Noachian, impact rates declined dramatically and remained low for the rest of the planet's 3.7 Gyr history. As a result, Noachian surfaces are all heavily cratered, while younger surfaces are only sparsely cratered. Average erosion rates also fell dramatically by 4–5 orders of magnitude from the Noachian rates, which were at the low end of terrestrial rates. As a result, post-Noachian craters are almost all perfectly preserved. The main exceptions are where the craters are in loose materials that could be moved by the wind. The most distinctive feature of martian craters is the pattern of their ejecta. Around most fresh craters the ejecta is arrayed in lobes each surrounded by a low ridge or an outward-facing escarpment. The distinctive martian patterns have been attributed to presence of ice or water in the martian surface, or interaction between the ejecta and the thin atmosphere.

Most Noachian volcanic features have been destroyed by subsequent impacts or subsequent volcanic activity, except for a few volcanoes near Hellas and elsewhere. In contrast, younger volcanic features are almost perfectly preserved. While the Tharsis bulge had largely formed by the end of the Noachian, volcanic activity continued in the province, probably up to the present day, judging from young crater ages on parts of the volcanoes. The volcanism was mostly basaltic but because of conditions on Mars, basaltic volcanism was more likely to produce ash clouds and pyroclastic flows than on Earth, and lava flows tend to be thicker and longer. Some of the largest volcanoes in the Solar System accumulated in Tharsis. The large volcanoes likely accumulated over billions of years from large eruptions, widely spaced in time, and fed by semi-permanent magma sources deep within the mantle. Olympus Mons, 100 times larger than any volcano on Earth, may have been even larger at one time, but its outer flanks appear to have collapsed to form huge lobes that extend hundreds of kilometers away from the present volcano's periphery. The most striking characteristic of the planet's second largest volcanic province, Elysium, is the presence of large, seemingly fluvial channels that emerge from graben to the northwest of the province center. The channels are thought to have formed by release of groundwater or melting of ground ice as a result of faulting and injection of dikes. Extensive lava plains formed in and around Tharsis and Elysium, locally within the southern uplands, and possibly throughout the northern plains. Most of the lava plains are Hesperian in age.

After the end of the Noachian, the lithosphere continued to deform mostly as a result of the presence of the Tharsis bulge, although the deformation center of the province shifted with time. The result is an array of Tharsis-radial faults that cover roughly a third of the planet's surface and an array of circumferential ridges that surround the province. Deformation was not, however, restricted simply to radial faults and circumferential ridges. A well-delineated, rectangular block of terrain 3000 km across, on the southeast flank of Tharsis, is a major structural feature of the planet, whose origin remains obscure.

The equatorial canyons present some of the most puzzling issues of martian geology. They may have started to form within the Noachian, but they continued to form through much of the rest of the planet's history. Their orientation radial to Tharsis was clearly controlled by the stress field created by Tharsis, but the precise mechanism that caused the canyons is unclear. Some, such as Coprates Chasma, appear to be downfaulted rifts bound by fault scarps. Others, such as the Tithonium and Ius Chasmata, appear to have formed by the merging of lines of pits, as though the surface had collapsed into fault-created voids at depth. Other canyons, such as Hebes Chasma, are highly irregular in shape and show little indication of faulting. Nevertheless, tectonic activity likely caused much of the vertical relief, which then allowed other processes such as landsliding and fluvial erosion to cause further enlargement. Another puzzle is the origin of the layered deposits within the canyons, many of which are rich in sulfates. A minority view is that most are simply remnants of the layered deposits into which the canyons incised. The prevailing view, based on stratigraphic relations, is that the internal deposits accumulated after the canyons formed. One possibility is that the sediments were deposited in lakes formerly present within the canyons, but this still leaves the source of the sediments unresolved, a problem that is particularly puzzling for the thick stack of sediments in the completely enclosed Hebes Chasma. The lake hypothesis is supported by the merging of Ganges and Coprates Chasmata eastward with fluvial features and with finding of sulfates within the layered deposits, but the hypothesis appears at odds with the seemingly non-horizontal nature of some of the layering. Another puzzling feature of the internal layered deposits is that they are mostly separated by a moat from the canyon walls. Yet another puzzle is the source of the water, if indeed the canyon once contained lakes.

Three types of fluvial features are generally recognized: valley networks, outflow channels, and gullies. The Noachian valley networks have already been discussed. The rate of valley network formation declined after the end of the Noachian, but did not decline to zero. Some of the most prominent valley networks, such as Nirgal and Nanedi Valles, are Hesperian in age. The Hesperian valleys commonly have characteristics more indicative of origin by groundwater sapping than the runoff patterns typical of the Noachian valleys. However, Hesperian runoff patterns occur, for example, adjacent to Echus Chasma. The most densely dissected post-Noachian surfaces are on volcanoes, such as Ceraunius Tholus, Hecates Tholus, and Alba Patera. The rapid fall off in dissection at the end of the Noachian suggests that the planet cooled and a thick cryosphere started to develop, a conclusion consistent with extremely low rates of weathering and erosion after the Noachian. But this leaves unexplained the origin of the dense Hesperian networks just discussed.

Outflow channels result from large floods. They are characterized by scoured ground and teardrop-shaped islands, and start full size at local sources.

The dimensions of the largest, Kasei Vallis, suggest that it had a peak discharge of 10^8 to $10^9\,m^3\,s^{-1}$, significantly larger than any known terrestrial flood. Most outflow channels occur around the Chryse basin, commonly merging with, or starting adjacent to, the canyons. They almost all start at rubble-filled depressions or faults. While the largest are Hesperian in age, in southern Elysium and Tharsis, several young (<100 Myr) outflow channels start at faults. Massive release of groundwater from below a thick cryosphere as a result of faulting, impacts, dike injection, or some other process appears to be the outflow channels' most common cause. The larger floods must have left large bodies of water at their ends. Flood-deposited sediments at the end of the large Chryse channels is suggested by partial burial of craters and ridges in the northern plains. The sizes of the bodies of water left by the floods are unclear, because the total volume involved in each flood is unknown, and identification of Hesperian shorelines is ambiguous. If the channels formed under cold conditions, as is likely, then the lakes or seas would have frozen and sublimated away in a geologically short period of time (10^2–10^4 years). Esker-like ridges and other features that resemble terrestrial glacial features, suggest the former presence of ice sheets in several places including the northern plains, Argyre, and Hellas, where former large bodies of water may have been present. Formation of the oceans may have temporarily affected global climates.

Gullies are recent features. They are a few to a few tens of meters across and hundreds of meters long and occur mostly on steep, poleward-facing slopes at high to mid latitudes. While their origin is controversial, they most likely form by melting of snow or ice during periods of high obliquity when melting temperatures can be reached on poleward-facing slopes at high latitudes in midsummer.

At latitudes higher than 60° large fractions of ice have been detected just below the surface, where temperatures never exceed the frost point under current climatic conditions. Small fractions of hydrogen detected just below the surface at lower latitudes, where ice is unstable, may result in part from chemically bound water, ice in local cold spots, or ice inherited from an earlier era of higher obliquity when stability conditions were more favorable. Most of the 30–60° latitude belt in both hemispheres is covered with an ice-rich deposit, a few meters thick, now undergoing removal. It is thought to have been deposited prior to 0.3 Myr ago when obliquities were higher and ground ice was stable at lower latitudes than it is today. In the same 30–60° latitude belt, debris flows that extend 20–30 km away from all steep slopes are probably ice-rich, having incorporated ground ice shed from the slopes. The flow of the ice-rich material away from valley walls has widened pre-existing valleys to form broad, flat-floored valleys, particularly along the plains–upland boundary, thereby creating the so-called fretted terrain. Lobate glacier-like features are also found around the periphery of several large Tharsis volcanoes, particularly on their western sides. They have been attributed to glaciers that formed on the volcanoes during some former period of high obliquity when ice was stable closer to the equator than it is today.

At each pole is a stack of young, layered deposits up to 3 km thick into which are incised valleys that spiral out from the poles. At the north pole a basal, platey, gypsum-rich unit appears to have been the source of sand that has formed a vast dune field around the pole. Deposition of finely layered sediments that overlie the basal unit may have been modulated by recent changes in obliquity. Alternatively, or in addition, layering may been as a consequence of formation of the spiral valleys as ice sublimated from equator-facing slopes and re-froze on opposing slopes or adjacent flats. The layered deposits in the south appear to be older than those in the north and their stratigraphy is less clear. The water-ice-rich layered deposits are overlain in winter by the seasonal CO_2 cap. In summer the CO_2 cap completely evaporates in the north, but in the south a remnant cap remains with small windows that expose the underlying water-rich deposits. In the present epoch, the windows are growing larger, indicating that the residual southern CO_2 cap is dissipating.

Much of the martian surface, including the poles, has been scoured by the wind, but eolian erosion of primary igneous rocks appears to have been minor. Wind erosion is most evident where there are layered, presumably granular, materials at the surface. The result is a surface with an etched-like appearance in which successive layers are outlined by steep escarpments. Eolian deposits, mainly dunes, are visible in almost every image of the surface, and kilometers-thick eolian deposits straddle the plains–upland boundary in many places. The source of the eolian debris is uncertain, but it may be a long-term accumulation of debris from various sources such as impacts, volcanic eruptions, and fluvial erosion, which has been redeposited and re-eroded throughout the history of the planet.

The climate history of the planet is very uncertain. As already indicated, the high erosion rates and high rates of fluvial dissection strongly suggest warm conditions in the Noachian, but how sustained

those conditions were and how they were achieved both remain unknown. Low erosion rates, low weathering rates, and lack of hydrous minerals in post-Noachian terrains suggest that if post-Noachian Mars was ever warm and wet, the episodes were very short. The cumulative amount of erosion on most post-Noachian primary rock surfaces since the end of the Noachian 3.7 Gyr ago has been minuscule. Dissection of some Hesperian surfaces suggests that fluvial dissection tailed off at the end of the Noachian more slowly than did the impact rates. Suggestions of causes of post-Noachian valley networks include groundwater sapping, short-lived climate changes caused by large floods or impacts, hydrothermal circulation of groundwater induced by volcanic activity, and melting of ice deposits during periods of high obliquity.

Life may have been present on Earth when the period of heavy bombardment ended around 3.7 Gyr ago. Conditions on Earth and Mars may have been similar prior to that time. Both experienced high rates of volcanism and impacts, both probably had warm climates and oceans, both were protected from the solar wind by a magnetic field, and both had a copious supply of organics from comets and asteroids. The two planets were also exchanging materials as a result of the high impact rates, and some small fraction of the material would have been transported to the other planet in only a few years, insufficient time to sterilize microbes in the rock pores. Thus if life arose on either planet, it could have seeded the other. The most primitive life forms on Earth are hyperthermophiles. The large impacts late in the heavy bombardment period may have sterilized almost all of the Earth. The only survivors may have been organisms living in hydrothermal systems, which then gave rise to all subsequent life on Earth. Conditions on Mars changed dramatically at the end of the Noachian. If life ever started on Mars or was seeded from Earth during heavy bombardment, in order to survive it would have had to adapt to cold conditions on the surface under a high UV flux where liquid water is only intermittently available, or adapt to living in moist, protected regions below the surface.

Despite the summary just outlined, there are major gaps in our understanding of how the surface of the planet has evolved. While there are many uncertainties with respect to impacts, tectonism, volcanism, and eolian processes, arguably the most intriguing problems concern water, climate, and life. What is the present global inventory of water and how did it change with time? If there were oceans in the Noachian and episodically at later times, as was argued from the surface morphology, how big were they and where is all the water now? Did the canyons once contain large lakes? We may be even more in the dark with respect to climate. The geological evidence for warmer climates in the Noachian is compelling. Yet greenhouse models demonstrate that with a faint young Sun, Mars cannot be warmed sufficiently with a CO_2-H_2O greenhouse to enable widespread precipitation. Moreover, major carbonate deposits have not been detected despite the geological evidence that the uppermost Noachian is extensively dissected, which according to the models would require bars of CO_2. Other greenhouse gases must be involved or the warming mechanism was not a stable greenhouse but some transitory state such as might be induced by large impacts or volcanic eruptions. While low, cumulative amounts of erosion and weathering indicate that the post-Noachian era was mostly cold and dry, did the era experience short, warm climatic episodes, as has been suggested? What effects did high obliquities have on global climates, both during the Noachian and in subsequent times?

While the geological questions are all intriguing, the most important unanswered questions concern biology. Did life ever take hold on the planet and, if so, did it survive in some form to the present? Only a vigorous Mars exploration program combining *in situ* life-detection experiments and returned samples will tell.

References

Achenback-Richter, L., Gupta, R., Stetter, K. and Woese, C., (1987). Were the original eubacteria thermophiles? *Syst. Appl. Microbiol.*, **9**, 34–9.

Acuna, M. H., Connerny, J. E., Wasilewski, P., *et al.*, (1999). Global distribution of crustal magnetism discovered by the Mars Global Surveyor MAG/ER experiment. *Science*, **279**, 1676–80.

Aharonson, O., Zuber, M. T., Neumann, G. A. and Head, J. W. (1998). Mars: northern hemisphere slopes and slope distributions. *Geophys. Res. Lett.*, **25**, 4413–16.

Aharonson, O., Zuber, M. T. and Rothman, D. H. (2001). Statistics of Mars' topography from the Mars Orbiter Laser Altimeter: slopes, correlations and physical models. *J. Geophys. Res.*, **106**(E10), 23,723–35.

Aharonson, O., Zuber, M. T., Rothman, D. H., Schorghofer, N. and Whipple, K. X. (2002). Drainage basins and channel incision on Mars. *Proc. Natl. Acad. Sci. U.S.A.*, **99**, 1780–3.

Aharonson, O., Schorghofer, N. and Gerstell, M. F. (2003). Slope streak formation and dust deposition rates on Mars. *J. Geophys. Res.*, **108**(E12), doi:10.1029/2003JE002123.

Allen, C. C. (1979). Volcano-ice interactions on Mars. *J. Geophys. Res.*, **84**, 8048–59.

Amelin, Y., Krot, A. N., Hutcheon, I. D. and Ulyanov, A. (2002). Lead isotope ages of chondrules and calcium-aluminum rich inclusions. *Science*, **297**, 213.

Anders, E. (1996). Evaluating the evidence for past life on Mars. *Science*, **274**, 2119–20.

Anderson, F. S. and Grimm, R. E. (1998). Rift processes at the Valles Marineris, Mars: constraints from gravity on necking and rate-dependent strength evolution. *J. Geophys. Res.*, **103**, 11,113–24.

Anderson, R. C., Dohm, J. M., Golombek, M. P., *et al.* (8 authors) (2001). Primary centers and secondary concentrations of tectonic activity through time in the western hemisphere of Mars. *J. Geophys. Res.*, **106**(E9), 20,563–85.

Armstrong, J. C. and Leovy, C. B. (2005). Long term wind erosion on Mars. *Icarus*, **176**, 57–74.

Arvidson, R. E., Carusi, A., Coradini, A., *et al.* (8 authors) (1976). Latitudinal variation of wind erosion of crater ejecta deposits on Mars. *Icarus*, **27**, 503–16.

Arvidson, R. E., Seelos, F.P., Deal, K. S., *et al.* (2003). Mantled and exhumed terrains in Terra Meridiani, Mars. *J. Geophys. Res.*, **108**(E12), doi:10.1029/2002JE001982.

Bagnold, R. A. (1941). *The Physics of Wind-Blown Sand and Desert Dunes*. London: Methuen.

Baker, V. R. (1979). Erosional processes in channelized water flows on Mars. *J. Geophys. Res.*, **84**, 7985–93.

Baker, V. R. (1982). *The Channels of Mars*. Austin: Texas University Press.

Baker, V. R. (1990). Spring sapping and valley network development. *Geol. Soc. Am. Sp. Paper,* **252**, 235–65.

Baker, V. R. (2001). Water and the martian landscape. *Nature*, **412**, 228–36.

Baker, V. R. and Kochel, R. C. (1979). Martian channel morphology: Maja and Kasei Vallis. *J. Geophys. Res.*, **84**, 7961–83.

Baker, V. R. and Milton, D. J. (1974). Erosion by catastrophic floods on Mars and Earth. *Icarus*, **23**, 27–41.

Baker, V. R. and Nummedal, D. (1978). *The Channeled Scabland.* Field Guide. Washington DC: NASA.

Baker, V. R. and Partridge, J. (1986). Small martian valleys: pristine and degraded morphology. *J. Geophys. Res.*, **91**, 3561–72.

Baker, V. R., Strom, R. G., Gulick, V. C., *et al.* (6 authors) (1991). Ancient oceans, ice sheets and the hydrologic cycle on Mars. *Nature*, **352**, 589–94.

Baker, V. R., Strom, R. G., Dohm, J. M., *et al.* (2000). Oceanus Borealis, ancient glaciers, and the MEGAOUTFLO hypothesis. LPSC XXXI, Abstract 1863.

Bandfield, J. L. (2002). Global mineral distributions on Mars. *J. Geophys. Res.*, **107**(E6), doi:10.1029/2001JE001510.

Bandfield, J. L., Hamilton, V. E. and Christensen, P. R. (2000). A global view of martian surface compositions from MGS-TES. *Science*, **287**, 1626–30.

Banerdt, W. B. and Golombek, M. P. (2000). Tectonics of the Tharsis region of Mars: insights from MGS topography and gravity. LPSC XXXI, Abstract 2038.

Banerdt, W. B., Golombek, M. P. and Tanaka, K. L. (1992). Stress and tectonics on Mars. In *Mars*, ed. H. H. Kieffer, B. M. Jakosky, C. W. Snyder and M. S. Matthews. Tucson: University of Arizona Press, pp. 249–97.

Banin, A., Clark, B. C. and Wänke, H. (1992). Surface chemistry and mineralogy. In *Mars,* ed. H. H. Kieffer, B. M. Jakosky, C. W. Snyder and M. S. Matthews. Tucson: University of Arizona Press, pp. 594–625.

Barlow, N. G. and Perez, C. B. (2003). Martian impact crater ejecta morphologies as indicators of the distribution of subsurface volatiles. *J. Geophys. Res.*, **108**(E8), doi:10,1029/2002JE002036.

Barlow, N. G., Boyce, J. M., Costard, F. M., *et al.* (9 authors) (2000). Standardizing the nomenclature of martian impact crater ejecta morphologies. *J. Geophys. Res.*, **105**(E11), 26,733–8.

Becker, R. H. and Pepin, R. O. (1984). The case for a martian origin of the shergottites: nitrogen and noble gases in EETA79001. *Earth Planet. Sci. Lett.*, **69**, 225–42.

Benito, G., Mediavilla, F., Fernandez, M., Marquez, A., Martinez, J., and Aguita, F. (1997). Chasma Boreale, Mars. A sapping and outflow channel with a tectonic-thermal origin. *Icarus*, **129**, 528–38.

Berman, D. C. and Hartmann, W. K. (2002). Recent fluvial, volcanic and tectonic activity on the Cerberus plains of Mars. *Icarus*, **159**, 1–17.

Bibring, J. P., Langevin, Y., Poulet, F., *et al.* (2004). Perennial water ice identified in the south polar cap of Mars. *Nature*, **428**, 627–30.

Bibring, J., Langevin, Y., Gendrin, A., *et al.* (10 authors) (2005). Mars surface diversity as revealed by the OMEGA/Mars Express observations. *Science*, **307**, 1576–81.

Bibring, J., Langevin, Y., Mustard, J. F., *et al.* (2006). Global mineralogical and aqueous history derived from OMEGA/Mars Express data. *Science*, **312**, 400–4.

Biemann, K., Oro, J., Toulmin, P., *et al.* (12 authors) (1977). The search for organic substances and inorganic volatile compounds on the martian surface. *J. Geophys. Res.*, **82**, 4641–58.

Binder, A. B., Arvidson, R. E., Guinness, E. A., *et al.* (8 authors) (1977). The geology of the Viking 1 landing site. *J. Geophys. Res.*, **82**, 4439–51.

Blasius, K. R., Cutts, J. A., Guest, J. E. and Masursky, H. (1977). Geology of Valles Marineris: first analysis of imaging from the Viking 1 orbiter. *J. Geophys. Res.*, **82**, 4067–91.

Bogard, D. D. and Johnson, P. (1983). Martian gases in an Antarctic meteorite. *Science*, **221**, 651–4.

Bogard, D. D., Nyquist, L. E. and Johnson, P. (1984). Noble gas content of shergottite and implications for the martian origin of SNC meteorites. *Geochim. Cosmochim. Acta.*, **48**, 1723–39.

Boice, D. and Huebner, W. (1999). Physics and chemistry of comets. In *Encyclopedia of the Solar System,* ed. P. R. Weissman, *et al.* San Diego: Academic Press, pp. 519–56.

Borg, L. E., Nyquist, L. E., Taylor, L. A., Wiesmann, H. and Shih, C.-Y. (2003). Constraints on martian differentiation processes from Rb-Sr and Sm-Nd isotopic analysis of the basaltic shergottite QUE94201. *Geochim. Cosmochim. Acta.*, **61**, 4915.

Boynton, W., Feldman, W. C., Squyres, S. W., *et al.* (2001). Distribution of hydrogen in the near surface of Mars: evidence for subsurface ice deposits. *Science*, **297**, 81–5.

Bradley, J. P., Harvey, R. P. and McSween, H. Y. (1997). No nanofossils in martian meteorite. *Nature*, **390**, 454.

Brain, D. A. and Jakosky, B. M. (1998). Atmospheric loss since the onset of the martian geologic record: combined role of impact erosion and sputtering. *J. Geophys. Res.*, **103**(E10), 22,689–94.

Brasier, M. D., Green, O. R., Jephcoat, A. P., *et al.* (2002). Questioning the evidence for Earth's oldest fossils. *Nature*, **416**, 76–81.

Brass, G. W. (1980). Stability of brines on Mars. *Icarus*, **42**, 20–80.

Braun, M. G. and Zuber, M. T. (2000). Formation and evolution of large chasms in the Elysium region of Mars: influence of tectonic loading and water flow. *Eos Trans. AGU*, **81**, 48.

Bridges, J. C., Catling, D. C., Saxton, J. M., Swindle, T. D., Lyon, I. C., and Grady, M. M. (2001). Alteration assemblages in martian meteorites: implications for near-surface processes. *Space Sci. Rev.*, **96**, 365–92.

Bridges, N. T. (1999). Ventifacts at the Pathfinder landing site. *J. Geophys. Res.*, **104**(E4), 8595–615.

Brooks, J. J., Logan, G. A., Buick, P. and Summons, R. E. (1999). Archean molecular fossils and the early rise of eukaryotes. *Science*, **285**, 1033–6.

Burns, R. G. (1987). Ferric sulfates on Mars. *J. Geophys. Res.*, **92**, e570–4.

Burr, D. M., Grier, J. A., McEwen, A. S. and Keszthelyi, L. P. (2002a). Repeated aqueous flooding from the Cerberus Fossae: evidence for very recently extant, deep groundwater on Mars. *Icarus*, **159**, 53–73.

Burr, D. M., McEwen, A. S. and Sakimoto, S. E. (2002b). Recent aqueous floods from the Cerberus Fossae, Mars. *Geophys. Res. Lett.*, **29**(1), 10.1029/2001Gl013345.

Byrne, S. and Ingersoll, P. (2003a). A sublimation model for martian south polar ice features. *Geophys. Res. Lett.*, **299**, 1051–3.

Byrne, S. and Ingersoll, P. (2003b). Martian climatic events on timescales of centuries: evidence from feature morphology in the residual polar ice cap. *Geophys. Res. Lett.*, **30**(13), doi:.10.1029/2003GL017597.

Byrne, S. and Murray, B. C. (2002). North polar stratigraphy and the polar erg of Mars., *J. Geophys. Res.*, **107**(E6), doi:10.1029/2001JE001615.

Cabrol, N. A. and Grin, E. A. (1999). Distribution, classification and ages of martian impact crater lakes. *Icarus*, **142**, 160–72.

Cabrol, N. A., Grin, E. A., Carr, M. H., *et al.* (20 authors) (2003). Exploring Gusev crater with Spirit: review of science objectives and testable hypotheses. *J. Geophys. Res.*, **108**(E12), doi:10.1029/2002JE002026.

Cailleau, B., Walter, T. R., Janle, P. and Hauber, E. (2003). Modeling volcanic deformation in a regional stress field: implications for formation of the graben structures on Alba Patera, Mars. *J. Geophys. Res.*, **108**(E12), doi:10.1029/2003JE002135.

Carr, M. H. (1979). Formation of martian flood features by release of water from confined aquifers. *J. Geophys. Res.*, **84**, 2995–3007.

Carr, M. H. (1981). *The Surface of Mars*. New Haven, Conn.: Yale University Press.

Carr, M. H. (1983). The stability of streams and lakes on Mars. *Icarus*, **56**, 476–95.

Carr, M. H. (1989). Recharge of an early atmosphere of Mars by impact-induced release of CO_2. *Icarus*, **79**, 311–27.

Carr, M. H. (1990). D/H on Mars: effects of floods, volcanism, impacts and polar processes. *Icarus*, **87**, 210–27.

Carr, M. H. (1992). Post-Noachian erosion rates: implications for Mars climate change. LPSC XXIII, 205–6.

Carr, M. H. (1996). *Water on Mars*. Oxford: Oxford University Press.

Carr, M. H. (1999). Retention of an atmosphere on early Mars. *J. Geophys. Res.*, **104**, 21,897–909.

Carr, M. H. (2001). Mars Global Surveyor observations of martian fretted terrain. *J. Geophys. Res.*, **106**, 23,571–94.

Carr, M. H. (2002). Elevation of water-worn features on Mars: implications for circulation of groundwater. *J. Geophys. Res.*, **107**(E12), 5131, doi:10.1029/2002JE001845.

Carr, M. H. and Chuang, F. C. (1997). Martian drainage densities. *J. Geophys. Res.*, **102**(E4), 9145–52.

Carr, M. H. and Malin, M. C. (2000). Meter-scale characteristics of martian channels and valleys. *Icarus*, **146**, 366–86.

Carr, M. H. and Head, J. W. (2002). Oceans on Mars: an assessment of the observational evidence and possible fate. *J. Geophys. Res.*, **108**(E5), doi10.1029/2002JE001963.

Carr, M. H. and Head, J. W. (2003). Basal melting of snow on early Mars: a possible origin of some valley networks. *Geophys. Res. Lett.*, **30**(24), doi10.1029/2003GL018575.

Carr, M. H., Crumpler, L. S., Cutts, J. A., Greeley, R., Guest, J. E. and Masursky, H. (1977). Martian impact craters and emplacement of ejecta by surface flow. *J. Geophys. Res.*, **82**, 4055–65.

Carr, M. H. and Schaber G. G. (1977). Martian permafrost features. *J. Geophys. Res.*, **82**, 4039–55.

Carr, M. H., Wu, S. C., Jordan, R. and Schafer, F. J. (1987). Volumes of channels, canyons and chaos in the circum-Chryse region of Mars. LPSC XVIII, pp. 156–7.

CATWG (1979). Standard techniques for presentation and analysis of crater size-frequency data. *Icarus*, **37**, 467–74.

Chapman, M. G. (1994). Evidence, age and thickness of a frozen paleolake in Utopia Planitia, Mars. *Icarus*, **109**, 393–406.

Chapman, M. G. (2002). Layered, massive and thin sediments on Mars: possible Late Noachian to Late Amazonian tephra? In *Valcano-Ice Interactions on Earth and Mars*, ed. J. L. Smellie and M. G. Chapman. *Geol. Soc., London, Sp. Publ.*, **202** pp. 273–93.

Chapman, M. G. and Tanaka, K. L. (2001). Interior trough deposits on Mars: subice volcanoes? *J. Geophys. Res.*, **106**, 10,087–100.

Chen, J. H. and Wasserburg, G. J. (1986). Formation ages and evolution of Shergotty and its parent planet from U-Th-Pb systematics. *Geochim. Cosmochim. Acta.*, **50**, 955–68.

Christensen, P. R. (1986). Regional dust deposits on Mars: physical properties, age, and history. *J. Geophys. Res.*, **91**, 3533–45.

Christensen, P. R. (2003). Formation of recent martian gullies through melting of extensive water-rich snow deposits. *Nature*, **422**, 45–8.

Christensen, P. R. (2004). Mineralogy at Meridiani Planum from the Mini-TES experiment on the Opportunity rover. *Science*, **306**, 1733–9.

Christensen, P. R., Bandfield, J. L., Clark, R. N., *et al.* (2000). Detection of crystalline hematite mineralization on Mars by the Thermal Emission Spectrometer. Evidence for near surface water. *J. Geophys. Res.*, **105**, 9623–42.

Christiansen, E. H. (1989). Lahars in the Elysium region of Mars. *Geology*, **17**, 203–6.

Chyba, C. F. (1990). Impact delivery and erosion of planetary oceans in the early inner solar system, *Nature*, **343**, 129–33.

Chyba, C. F. (1991). Terrestrial mantle siderophiles and the lunar impact record. *Icarus*, **92**, 217–33.

Clague, D. A. and Dalrymple, G. B. (1987). The Hawaiian-Emperor volcanic chain. In *Volcanism in Hawaii*, ed. R. W. Decker *et al.* U.S. Geol. Survey Prof. Paper 1350, 5–73.

Clark, B. C., Morris, R. V., McLennan, S. M., *et al.* (2005). Chemistry and mineralogy of outcrops at Meridiani Planum. *Earth Planet. Sci. Lett.*, **240**, 73–94.
Clayton, R. N. and Mayeda, T. K. (1983). Oxygen isotopes in euchrites, shergottites, nakhlites and chassignites. *Earth Planet. Sci. Lett.*, **62**, 1–6.
Clifford, S. M. (1987). Polar basal melting on Mars. *J. Geophys. Res.*, **92**, 9135–52.
Clifford, S. M. (1993). A model for the hydrologic and climatic behavior of water on Mars. *J. Geophys. Res.*, **98**, 10973–1016.
Clifford, S. M. and Parker, T. J. (2001). The evolution of the martian hydrosphere: implications for the fate of a primordial ocean and the current state of the northern plains. *Icarus*, **154**, 40–79.
Clifford, S. M. and Zimbelman, J. R. (1988). Softened terrain on Mars. LPSC XIX, pp. 199–200.
Clow, G. D. (1987). Generation of liquid water on Mars through the melting of a dusty snowpack. *Icarus*, **72**, 95–127.
Colaprete, A. and Toon, O. B. (2003). Carbon dioxide clouds in an early dense martian atmosphere. *J. Geophys. Res.*, **108**(E4), doi:10.1029/2002/JE001967.
Coleman, N. M. (2002). Aqueous flows formed the outflow channels on Mars. LPSC XXXIII, Abstract 1059.
Comer, R. P., Solomon, S. C. and Head, J. W. (1985). Mars: thickness of the lithosphere from the tectonic response to volcanic loads. *Rev. Geophys.*, **23**, 61–92.
Connerny, J. E., Acuna, M. H., Wasukewski, P. J., *et al.* (1999). Magnetic lineations in the ancient crust of Mars. *Science*, **284**, 794–8.
Costard, F. M. and Kargel, J. S. (1995). Outwash plains and thermokarst on Mars. *Icarus*, **114**, 93–112.
Costard, F., Forget, F., Mangold, N. and Peulvast, J. P. (2002). Formation of recent Martian debris flows by melting of near-surface ground ice at high obliquity. *Science*, **295**, 110–13.
Craddock, R. A. and Howard, A. D. (2002). The case for rainfall on a warm, wet early Mars. *J. Geophys. Res.*, **107**(E11), doi:10.1029/2001JE001505.
Craddock, R. A. and Maxwell, T. A. (1993). Geomorphic evolution of the martian highlands through ancient fluvial processes. *J. Geophys. Res.*, **98**, 3453–68.
Crown, D. A. and Greeley, R. (1993). Volcanic geology of Hadriaca Patera and the eastern Hellas region of Mars. *J. Geophys. Res.*, **98**(E2), 3431–51.
Crown, D. A., Price, K. H. and Greeley, R. (1992). Geologic evolution of the east rim of the Hellas basin, Mars. *Icarus*, **100**, 1–25.
Crown, D. A., McElfresch, S. B., Pierce, T. L. and Mest, S. C. (2003) Geomophology of debris aprons in the eastern Hellas region of Mars. LPSC XXXIV, Abstract 1126.
Davies, P. (1995). *Are We Alone* ? London: Penguin.
Davis, P. A. and Golombek, M. P. (1990). Discontinuities in the shallow martian crust at Lunae, Susria and Sinai Plana. *J. Geophys. Res.*, **95**, 14,231–48.
DeHon, R. A. (1992). Martian lake basins and lacustrine plains. *Earth, Moon, and Planets*, **56**, 95–122.
Dohnanyi, J. S. (1972). Interplanetary objects in review: statistics of their masses and dynamics. *Icarus*, **17**, 1–48.
Edgett, K. S. and Malin, M. C. (2002). Martian sedimentary rock stratigraphy: outcrops and interbedded craters of northwest Sinus Meridiani and southwest Arabia Terra. *Geophys. Res. Lett.*, **29**(24), 2179 doi:10.1029/2002GL016515.
Edgett, K. S. and Parker, T. J. (1997). Water on early Mars: possible subaqueous sedimentary deposits covering ancient cratered terrain of Western Arabia and Sinus Meridiani. *Geophys. Res. Lett.*, **24**, 2897–900.
Edgett, K. S., Williams, R. M., Malin, M. C., Cantor, B. A. and Thomas, P. C. (2003). Mars landscape evolution: influence of stratigraphy on geomorphology of the north polar region. *Geomorphology*, **52**, 289–98.
Ernst, W. G. (1983). The early earth and the Archean rock record. In *TheEarth's earliest biosphere*, ed. J. W. Schopf. Princeton, pp. 41–52.
Eugster, O., Weigel, A. and Palnau, E. (1997). Ejection times of martian meteorites. *Geochim. Cosmochim. Acta.*, **61**, 2749–58.
Fahrig, W. F. (1987). *Geol. Assoc. Canada Sp. Paper 34*, ed. H. C. Halls and W. F. Fahrig., pp. 331–48.
Farmer, C. B. and Doms, P. E. (1979). Global and seasonal water vapor on Mars and implications for permafrost. *J. Geophys. Res.*, **84**, 2881–8.
Farmer, C. B., Davies, D. W. and LaPorte, D. D. (1976). Northern summer ice cap – water vapor observations from Viking 2. *Science*, **194**, 1399–41.
Farmer, C. B., *et al.* (1977). Mars: water vapor observations from the Viking orbiters. *J. Geophys. Res.*, **82**, 4225–8.
Fasset, C. I. and Head, J. W., (2004). Snowmelt and the formation of valley networks on martian volcanoes, LPSC XXXV, Abstract 1113.
Fassett, C. I. and Head, J. W. (2005). Fluvial sedimentary deposits on Mars: ancient deltas in a crater lake in the Nili Fossae region. *Geophys. Res. Lett.*, **32**(14), doi:10.1029/2005GL023456.
Feldman, W. C., Boynton, W. V., Tokar, R. L., *et al.* (2002). Global distribution of neutrons from Mars: results from Mars Odyssey. *Science*, **297**, 75–8.
Feldman, W. C., Prettyman, T. H., Maurice, S., *et al.* (2004). The global distribution of near surface hydrogen on Mars. *J. Geophys. Res.*, **109**(E9), doi:10.1029/2003JE02160.
Fernandez, J. A. (1999). Cometary dynamics. In *Encyclopedia of the Solar System*, ed. P. R. Weissman *et al.* San Diego: Academic Press, pp. 537–56.
Ferril, D. A. and Morris, A. P. (2003). Dilational normal faults. *J. Struct. Geol.*, **25**, 183–96.
Ferrill, D. A., Wyrick, D. Y., Morris, A. P., Sims, D. W. and Franklin, N. M. (2004). Dilational fault slip and pit chain formation on Mars. *GSA Today*, **14**(19), 4–12.
Fishbaugh, K. E. and Head, J. W. (2000). North polar region of Mars: topography of circumpolar deposits form Mars Orbiter Laser Altimeter (MOLA) data and evidence for asymmetric retreat of the polar cap. *J. Geophys. Res.*, **105**(E9), doi:10.1029/1999JE001230.
Fishbaugh, K. E. and Head, J. W. (2002). Chasma Boreale, Mars: topographic characterization from Mars Orbiter Laser Altimeter data and implications for mechanisms of formation. *J. Geophys. Res.*, **107**(E3), doi:10.1029/2001JE001351.
Fishbaugh, K. E. and Head, J. W. (2005). Origin and characteristics of the Mars north polar basal unit and implications for polar geologic history. *Icarus*, **174**, 444–74.
Fisher, J. A., Richardson, M. I., Newman, C. E., *et al.* (2005). A survey of martian dust devil activity using Mars Global Surveyor Mars Orbiter Camera images. *J. Geophys. Res.*, **110**(E3), doi:10.1029/2003JE002165.
Fiske, R. S. and Jackson, E. D. (1972). Orientation and growth of Hawaiian volcanic rifts – the effect of regional structure and gravitational stresses. *Proc. Roy. Soc., London, Ser. A.*, **329**, 299–326.
Foley, E. N., Economou, T. and Clayton, R. M. (2003). Final chemical results from the Mars Pathfinder alpha proton X-ray spectrometer. *J. Geophys. Res.*, **108**(E12), doi:10.1029/2002JE002019.
Folk, R. L. (1993). SEM imaging of bacteria and nanobacteria in carbonate sediments and rocks. *J. Sed. Pet.*, **63**, 990–9.
Folkner, W. N., Yoder, C. F., Yuan, D. N., Standish, E. M. and Preston, R. A. (1997). Internal structure and seasonal mass redistribution on Mars from radio tracking of Mars Pathfinder. *Science*, **278**, 1749–52.
Forget, F. and Pierrehumbert, R. T. (1997). Warming early Mars with carbon dioxide clouds that scatter infrared radiation. *Science*, **278**, 1273–6.

Formisano, V., Atreya, S., Encranaz, T., Ignatiev, N., and Guiranna, M. *et al.* (2004). Detection of methane in the atmosphere of Mars. *Science*, **306**, 1758–61.

Forsythe, R. D. and Blackwelder, C. R. (1998). Closed drainage basins of the martian highlands: constraints on the early martian hydrologic cycle. *J. Geophys. Res.*, **103**(E13), 31,421–32.

Forsythe, R. D. and Zimbelman, J. R. (1995). A case for ancient evaporite basins on Mars. *J. Geophys. Res.,* **100**, 5553–63.

Francis, P. W. and Wadge, G. (1983). The Olympus Mons aureole: formation by gravitational spreading. *J. Geophys. Res.*, **88**, 8333–44.

French, H. M. (1976). *The periglacial environment*. New York: Longman.

Frey, H. V. (1979). Pseudocraters on Mars. *J. Geophys. Res.*, **84**, 8075–86.

Frey, H. V. (2002). Age and origin of the crustal dichotomy in eastern Mars. LPSC XXXIII, Abstract 1727.

Frey, H. V., Roark, J. H., Shockey, K. M., Frey, E. L. and Sakimoto, S. E. (2002a). Ancient lowlands on Mars. *Geophys. Res. Lett.*, **29**, 1384, doi.10.1029/2001GL013832.

Frey, H. V., Roark, J. H., Hohner, G. J., Wernecke, A. and Sakimoto, S. E. (2002b). Buried impact basins as constraints on the thickness of ridged plains and northern lowland plains on Mars. LPSC XXXIII, Abstract 1804.

Frey, H. V. and Schultz, R. A. (1988). Large impact basins and the mega-impact origin for the crustal dichotomy on Mars. *Geophys. Res. Lett.*, **15**, 229–32.

Friedman, E. I. (1980). Endolithic microbial life in hot and cold deserts. *Origins of Life*, **10**, 223–35.

Friedman, G. M. and Sanders, J. E. (1978). *Principles of Sedimentology*. New York: Wiley

Fuller, E. R. and Head, J. W. (2002a). Geologic history of the smoothest plains on Mars (Amazonis Planitia) and astrobiological implications. LPSC XXXIII, Abstract 1539.

Fuller, E. R. and Head, J. W. (2002b). Amazonis Planitia: the role of geologically recent volcanism and sedimentation in the formation of the smoothest plains on Mars. *J. Geophys. Res.*, **107**(E10), doi:10.1029/2002JE001842.

Gaidos, E. and Marion, G. (2003). Geologic and geochemical legacy of a cold early Mars. *J. Geophys. Res.*, **108**(E6), doi:10.1029/2002JE002000.

Gault, D. E. and Greeley, R. (1978). Exploratory experiments of impact craters formed in viscous-liquid targets: analogs for martian impact craters? *Icarus*, **34**, 486–95.

Gault, D. E., Quaide, W. L. and Oberbeck, V. R. (1968). Impact cratering mechanics and structures. In *Shock Metamorphism of Natural Materials*, ed. B. M. French and N. M. Short. Baltimore: Mono Book Corp., pp. 87–99.

Geissler, P. E. (2005). Three decades of martian surface changes. *J. Geophys. Res.*, **110**(E2), doi:10.1029/2004JE002345.

Gellert, R., Rieder, R., Anderson, R. C., *et al.* (16 authors) (2004). Chemistry of rocks and soils in Gusev crater from the alpha particle X-ray spectrometer. *Science*, **305**, 829–32.

Gendrin, A., Mangold, N., Bibring, J., *et al.* (11 authors) (2005). Sulfates in martian layered terrains: the OMEGA/Mars Express view. *Science*, **302**, 1587–91.

Ghatan, G. J. and Head, J. W. (2002). Candidate subglacial volcanoes in the south polar region of Mars: morphology, morphometry, and eruption conditions. *J. Geophys. Res.*, **107**(E7), doi:10.1029/2001JE001519.

Ghatan, G. J. and Head, J. W. (2004). Regional drainage of meltwater beneath a Hesperian-age south circumpolar ice sheet on Mars. *J. Geophys. Res.*, **109**(E7), doi:10.1029/2003JE002196.

Ghatan, G. J., Head, J. W. and Pratt, S. (2003). Cavi Angusti, Mars: characterization and assessment of possible formation mechanisms. *J. Geophys. Res.*, **108**(E5), doi:10.1029/2002JE001972.

Gierasch, P. J. (1974). Martian dust storms. *Rev. Geophys. Space Phys.*, **12**, 730–4.

Gladman, B., Burns, J. A., Duncan, M., Lee, P. and Levinson, H. G. (1996). The exchange of impact ejecta between terrestrial planets. *Science*, **271**, 1387–90.

Golden, D. C., Ming, D. W., Lauer, H. V., *et al.* (2002). Inorganic formation of ''truncated hexa-octahedral'' magnetite: implications for inorganic processes in martian meteorite ALH84001. LPSC XXXIII, Abstract 1839.

Golden, D. C., Ming, D. W., and Morris, R. V., *et al.* (2004). Evidence for exclusively inorganic formation of magnetite in martian meteorite ALH84001. *Am. Mineral.*, **89**, 681–95.

Goldspiel, J. M. and Squyres, S. W. (1991). Ancient aqueous sedimentation on Mars. *Icarus*, **89**, 393–410.

Goldspiel, J. M. and Squyres, S. W. (2000). Groundwater sapping and valley formation on Mars. *Icarus*, **148**, 176–92.

Golombek, M. P. and Bridges, N. T. (2000). Erosion rates on Mars and implications for climate change: constraints from the Pathfinder landing site. *J. Geophys. Res.*, **105**(E1), 1841–53.

Golombek, M. P., Tanaka, K. L. and Franklin, B. J. (1996). Extension across Tempe Terra, Mars from measurements of faults scarp widths and deformed craters. *J. Geophys. Res.*, **101**, 26,119–30.

Golombek, M. P., Cook, R. A., Economou, T. E., *et al.* (14 authors) (1997). Overview of the Mars Pathfinder mission and assessment of landing site predictions. *Science*, **278**, 1743–52.

Golombek, M. P., Anderson, R. C., Barnes, J. R., *et al.* (53 authors) (1999). Overview of the Mars Pathfinder mission: launch through landing. Surface operations, data sets and science results. *J. Geophys. Res.*, **104**, 8523–53.

Golombek, M. P., Anderson, F. S. and Zuber, M. T. (2001). Martian wrinkle ridge topography: evidence for subsurface faults from MOLA. *J. Geophys. Res.*, **106**(E10), 23,811–21.

Golombek, M. P., Anderson, R. C., Barnes, J. R, *et al.* (22 authors) (2003). Selection of the Mars Exploration Rover land sites. *J. Geophys. Res.*, **108**(E12), doi:10.1029/2003JE002074.

Golombek, M. P., Crumpler, L. S., Grant, J. A., *et al.* (18 authors) (2006). Geology of the Gusev cratered plains from the Spirit rover traverse. *J. Geophys. Res.*, **111**(E2), doi:10.1029/2005JE002503.

Gooding, J. G., Wentworth, S. J. and Zolensky, M. E. (1988). Calcium carbonate and sulfate of possible extraterrestrial origin in EETA79001 meteorite. *Geochim. Cosmochim. Acta.*, **52**, 909–15.

Gough, D. O. (1981). Solar interior structure and luminosity variations. *Solar Phys.*, **74**, 21–34.

Grant, J. A. and Parker, T. J.(2002). Drainage evolution in the Margaritifer Sinus region of Mars. *J. Geophys. Res.*, **107**(E9), doi:10.1029/2001JE001678.

Greeley, R. and Crown, D. A. (1990). Volcanic geology of Tyrrhena Patera, Mars. *J. Geophys. Res.*, **95**(B5), 7133–49.

Greeley, R. and Fagents, S. A. (2001). Icelandic pseudocraters as analogs to some volcanic cones on Mars. *J. Geophys. Res.*, **106**, 20,527–46.

Greeley, R. and Guest, J. E. (1987). Geologic map of the eastern equatorial region of Mars. U. S. Geological Survey, Misc. Inv. Map I-1802-B.

Greeley, R. and Iverson, J. D. (1985). *Wind as a Geological Process on Earth, Mars, Venus and Titan*. Cambridge: Cambridge University Press.

Greeley, R. and Schneid, B. D. (1991). Magma generation on Mars: amounts, rates and comparisons with Earth, Moon and Venus. *Science*, **254**, 996–8.

Greeley, R., Leach, R., White, B., Iverson, J. and Pollack, J. (1980). Threshold windspeeds for sands on Mars: wind tunnel simulations. *Geophys. Res. Lett.*, **7**, 121–4.

Greeley, R., White, B. R., Pollack, J. B., Iverson, J. D. and Leach, R. N. (1981). Dust storms on Mars: considerations and simulations. *Geol. Soc. Am. Sp. Paper*, **186**, 101–21.

Greeley, R., Lancaster, N., Lee, S. and Thomas, P. (1992). Martian eolian processes, sediments and features. In *Mars,* ed. H. H. Kieffer, B. M. Jakosky, C. W. Snyder and M. S. Matthews. Tucson: University of Arizona Press, pp. 730–66.

Greeley, R., Draft, M., Sullivan, R., Wilson, G., *et al.* (1999). Aeolian features and processes at the Mars Pathfinder landing site. *J. Geophys. Res.*, **104**, 8573–84.

Greeley, R., Squyres, S. W., Arvidson, R. E., *et al.* (2004). Wind-related processes detected by the Spirit Rover at Gusev Crater, Mars. *Science*, **305**, 810–21.

Greeley, R., Arvidson, R. E., Barlett, P. W., *et al.* (2006). Wind-related features and processes observed by the Mars Exploration Rover, Spirit. *J. Geophys. Res.*, **111**(E2), doi10.1029/2005JE002491.

Grieve, R. A. (2001). The terrestrial cratering record. In *Accretion of Extraterrestrial Matter Through Earth's History*, ed. B. Peuker-Ehrenbrink *et al.* Dordrecht: Kluwer, pp. 379–402.

Grieve, R. A. and Shoemaker, E. M. (1994). The record of past impacts on Earth. In *Hazards due to Comets and Asteroids*, ed. T. Gehrels. Tucson: University of Arizona press, pp. 417–62.

Grotzinger, J. P., Arvidson, R. E., Bell, J. F., *et al.* (2005). Stratigraphy, sedimentology and depositional environment of the Burns Formation, Meridiani Planum, Mars. *Earth Planet. Sci. Lett.*, **240**, 11–72.

Grun, E. (1999). Interplanetary dust and the zodiacal cloud. In *Encyclopedia of the Solar System*, ed. P. R. Weissman, *et al.* San Diego: Academic Press, pp. 673–96.

Gulick, V. C. (1998). Magmatic intrusions and a hydrothermal origin for fluvial valleys on Mars. *J. Geophys. Res.*, **103**, 19,365–87.

Gulick, V. C. (2001). Origin of the valley networks on Mars: a hydrologic perspective. *Geomorphology*, **37**, 241–68.

Gulick, V. C. and Baker, V. R. (1990). Origin and evolution of valleys on martian volcanoes. *J. Geophys. Res.*, **95**, 14,325–44.

Gulick, V. C., Tyler, D., McKay, C. P. and Haberle, R. M. (1997). Episodic ocean-induced CO_2 greenhouse on Mars: implications for fluvial valley formation. *Icarus*, **130**, 68–86.

Haberle, R. M. (1998). Early climate models. *J. Geophys. Res.*, **103**(E12), 28,467–79.

Haberle, R. M. and Jakosky, B. M. (1990). Sublimation and transport of water from the north residual polar cap on Mars. *Icarus*, **90**, 187–204.

Haberle, R. M., Tyler, D., McKay, C. P., Davis, W. L., *et al.* (1994). A model for the evolution of CO_2 on Mars. *Icarus*, **109**, 102–20.

Haberle, R. M., Monmessin, F., Forget, F., Levrard, B., Head, J. W. and Laskar, J. (2004). GCM simulations of tropical ice accumulations: implications for cold-based glaciers. LPSC XXXV, Abstract 1711.

Halliday, A. N., Wänke, H., Birck, J.-L. and Clayton, R. N. (2001). The accretion, composition and early differentiation of Mars. In *Chronology and Evolution of Mars,* ed. R. Kallenbach *et al.* Dordrecht: Kluwer, pp. 197–230.

Hamlin, S. E., Kargel, J. S., Tanaka, K. L., Lewis, K. J. and MacAyeal, D. R. (2000). Preminiary studies of icy debris flows in the martian fretted terrain. LPSC XXXI, Abstract 1785.

Hanna, J. C. and Phillips, R. J. (2005). Tectonic pressurization of aquifers in the formation of Mangala and Athabasca Valles on Mars. LPSC XXXVI, Abstract 2261.

Harder, H. and Christensen, U. R. (1996). A one plume model of martian mantle convection. *Nature*, **380**, 507.

Harris, S. A. (1977). The aureole of Olympus Mons, Mars. *J. Geophys. Res.*, **82**, 3099–107.

Harrison, K. P. and Grimm, R. E. (2003). Rheological constraints on martian landslides. *Icarus*, **163**, 347–62.

Hartmann, W. K. (1977). Relative crater production rates on planets. *Icarus*, **31**, 260–76.

Hartmann, W. K. (1999). Martian cratering. IV: Crater count isochrons and evidence for recent volcanism from Mars Global Surveyor. *Meteoritics Planet. Sci.*, **34**, 167–77.

Hartmann, W. K. and Neukum, G. (2001). Cratering chronology and the evolution of Mars. In *Chronology and Evolution of Mars*, ed. R. Kallenbach *et al.* Dordrecht: Kluwer, pp. 165–94.

Haskins, L. A., Wang, A., Jolliff, B., *et al.* (34 authors) (2005). Water alteration of rocks and soils on Mars and the Spirit rover site in Gusev crater. *Nature*, **436**, 66–9.

Hauber, E., Gwinner, K., Reiss, D., *et al.* (2005a). Delta-like deposits in Xanthe Terra, Mars as seen with the high resolution stereo camera (HRSC). LPSC XXXVI, Abstract 1661.

Hauber, E., van Gasselt, S., Ivanov, B., *et al.* (2005b). Discovery of a flank caldera and very young glacial activity at Hecates Tholus, Mars. *Nature*, **434**, 356–61.

Hauber, G., Gwinner, K., Gendrin, A., *et al.* (2006). An integrated study of interior layered deposits in Hebes Chasma, Valles Marineris, Mars, using MGS, MO and MEX data. LPSC XXXVII, Abstract 2022.

Head, J. W. (1974). Orientale multi-ring basin interior and implications for the petrogenesis of lunar highland samples. *The Moon*, **11**, 327–56.

Head, J. W. (2001). Evidence for geologically recent advance of the south polar cap. *J. Geophys. Res.*, **106**(E5), 10,075–85.

Head, J. W. and Marchant, D. R. (2003). Cold based mountain glaciers on Mars: western Arsia Mons. *Geology*, **31**, 641–4.

Head, J. W. and Pratt, S. (2001) Extensive Hesperian-aged south polar ice sheet on Mars: evidence for massive melting and retreat, and lateral flow and ponding of meltwater. *J. Geophys. Res.*, **106**, 12,275–99.

Head, J. W. and Wilson, L. (2002). Mars: a review and synthesis of general environments and geologic settings of magma-H_2O interactions. In *Volcano-Ice Interactions on Earth and Mars*, ed. J. L. Smellie and M. G. Chapman. *Geol. Soc., London, Sp. Publ.,* **202**, pp. 27–57.

Head, J. W., Heisinger, H., Ivanov, M. A., Kreslavsky, M. A., Pratt, S. and Thomson, B. J. (1999). Possible ancient oceans on Mars: evidence from Mars Orbiter Laser Altimeter data. *Science*, **286**, 2134–7.

Head, J. W., Kreslavsky, M. A. and Pratt, S. (2002). Northern lowlands of Mars: evidence for widespread volcanic flooding and tectonic deformation in the Hesperian Period. *J. Geophys. Res.*, **107**(E1), doi:10.1029/2000JE001445.

Head, J. W., Wilson, L. and Mitchel, K. L. (2003b). Generation of recent water floods at Cerberus Fossae, Mars by dike emplacement, cryosphere cracking and confined aquifer groundwater release. *Geophys. Res. Lett.*, **30**(11), 1577, doi:10.1029/2003GL017135.

Head, J. W., Mustard, J. F., Kreslavsky, M. A., Milliken, R. E. and Marchant, D. R. (2003a). Recent ice ages on Mars. *Nature*, **426**, 797–802.

Head, J. W., Neukum, G., Jaumann, R., *et al.* (2005a). Tropical to mid-latitude snow and ice accumulation, flow and glaciation on Mars. *Nature*, **434**, 346–51.

Head, J. W., Marchant, D. R., Agnew, M. C., Fassett, C. I. and Kreslavsky, M. A. (2005b). Extensive valley glacier deposits in the northern mid-latitudes of Mars: evidence for late Amazonian obliquity-driven climate change. *Earth Planet. Sci. Lett.*, **241**, 663–71.

Hecht, M. H. (2002). Metastability of liquid water on Mars. *Icarus*, **156**, 373–86.

Heisinger, H. and Head, J. W. (2001). Characteristics and origin of polygonal terrain in southern Utopia Planitia, Mars: results from Mars Orbiter Laser Altimeter and Mars Orbiter Camera data. *J. Geophys. Res.*, **105**, 11,999–2,022.

Heisinger, H. and Head, J. W. (2002). Topography and morphology of the Argyre basin, Mars: implications for its geologic and hydrologic history. *Planet. Space Sci.*, **50**, 939–81.

Herkenhoff, K. E. and Plaut, J. J. (2000). Surface ages and the resurface rates of the polar deposits on Mars. *Icarus*, **144**, 243–53.

Herkenhoff, K. E., *et al.* (23 authors) (2004a). Textures of the soils and rocks at Gusev crater from Spirit's microscopic imager. *Science*, **305**, 824–6.

Herkenhoff, K. E., Squyres, S. W., Arvidson, R. E., *et al.* (2004b). Evidence from Opportunity's microscopic imager for water on Meridiani Planum. *Science*, **306**, 1727–30.

Hess, S. L., Ryan, J. W., Tillman, J. E., Henry, R. M. and Leovy, C. N. (1980). The annual cycle of pressure on Mars measured by Viking 1 and 2. *Geophys. Res. Lett.*, **7**, 197–200.

Hodges, C. A. and Moore, H. J. (1979). The sub-glacial birth of Olympus Mons and its aureoles. *J. Geophys. Res.*, **84**, 8061–74.

Hodges, C. A. and Moore, H. J. (1994). Atlas of volcanic landforms on Mars, U.S. Geol. Survey Prof. Paper 1534.

Hodges, R. R. (2002). The rate of loss of water from Mars. *Geophys. Res. Lett.*, **29**, 1038, doi:10.1029/2001GL013853.

Hoefen, R. M., Clark, R. N., Bandfield, J. L., Smith, M. D., Pearl, J. C. and Christensen, P. R. (2003). Discovery of olivine in the Nili Fossae region of Mars. *Science*, **302**, 627–30.

Hoffman, N. (2000). White Mars. *Icarus*, **146**, 326–42.

Hoffman, N. (2002). Active polar gullies on Mars and the role of carbon dioxide. *Astrobiology*, **2**, 313–23.

Horowitz, N. H. (1986). *To Utopia and Back: The Search for Life in the Solar System*. New York: W. H. Freeman.

Howard, A. D. (1978). Origin of the stepped topography of the martian poles. *Icarus*, **34**, 581–9.

Howard, A. D. (1981). Etched plains and braided ridges of the south polar region of Mars: features produced by basal melting and ground ice. NASA Tech. Memo 84211, pp. 286–8.

Howard, A. D. (2000). The role of eolian processes in forming surface features of the martian polar layered deposits. *Icarus*, **144**, 267–88.

Howard, A. D. and Moore, J. M. (2006). A geomorphic transect across the martian highlands-lowlands boundary near the prime meridian: evidence for a sedimentary platform graded to a deep ocean. *J. Geophys. Res.*

Howard, A. D., Cutts, J. A. and Blasius, K. R. (1982). Stratigraphic relationships within the martian polar cap deposits. *Icarus*, **50**, 161–215.

Howard, A. D., Moore, J. M. and Irwin, R. P. (2005). An intense terminal epoch of widespread fluvial activity on early Mars. I. Valley network incision and associated deposits. *J. Geophys. Res.*, **110**(E12), S14, doi:10.1029/2005JE002459.

Hungr, O. (1995). A model for runout analysis of rapid flow slides, debris flows and avalanches. *Can. Geotech.*, **32**, 610–23.

Hunten, D. M. (1979). Possible oxidant sources in the atmosphere and surface of Mars. *J. Mol. Evol.*, **14**, 71–8.

Hynek, B. M. and Phillips, R. J. (2001). Evidence of extensive denudation of the martian highlands. *Geology*, **29**, 407–10.

Hynek, B. M., Arvidson, R. E. and Phillips, R. J. (2002). Geologic setting and origin of Terra Meridiani hematite deposits. *J. Geophys. Res.*, **107**(E10), doi:10.1029/2002JE001891.

Hynek, B. M., Philips, R. J. and Arvidson, R. E. (2003). Explosive volcanism in the Tharsis region: global evidence in the martian geologic record. *J. Geophys. Res.*, **108**(E9), doi:10.1029/2003JE002062.

Ingersoll, A. P. (1970). Mars: occurrence of liquid water. *Icarus*, **79**, 3404–10.

Irwin, R. P., Maxwell, T. A., Craddock, R. A. and Leverington, D. W. (2002). A large paleolake basin at the head of Ma'adim Vallis, Mars. *Science*, **296**, 2209–12.

Irwin, R. P., Howard, A. D. and Maxwell, T. A. (2002). Geomorphology of Ma'adim Vallis, Mars and associated paleolake basins. *J. Geophys. Res.*, **109**(E12), doi:10.1029/2004JE002287.

Ivanov, A. B. (2001). Mars/Moon cratering rate ratio estimates. In *Chronology and Evolution of Mars*, ed. R. Kallenbach. Dordrecht: Kluwer, pp. 97–104.

Ivanov, M. A. and Head, J. W. (2001). Chryse Planitia, Mars: topographic configuration, outflow channel continuity and sequence and tests for hypothesized ancient bodies of water using Mars Orbiter Laser Altimeter (MOLA) data. *J. Geophys. Res.*, **106**(E2), doi:10.1029/20000JE001257.

Ivanov, M. A. and Head, J. W. (2003). Syrtis Major and Isidis basin contact: morphological and topographic characteristics of Syrtis Major lava flows and material of the Vastitas Borealis Formation. *J. Geophys. Res.*, **108**(E6), doi:10.1029/2002JE001944.

Ivanov, A. B. and Muhleman, D. O. (2000). The role of sublimation for the formation of the northern ice cap: results from the Mars Orbiter Laser Altimeter. *Icarus*, **144**, 436–48.

Ivanov, M. A. and Head, J. W. (2006). Alba Patera, Mars: Topography, structure and evolution of a unique late Hesperian-Early Amazonian shield volcano. *J. Geophys. Res.*, in press.

Jakosky, B. M. and Carr, M. H. (1985). Possible precipitation of ice at low latitudes of Mars during periods of high obliquity. *Nature*, **315**, 559–61.

Jakosky, B. M. and Haberle, R. M. (1990). Year-to-year instability of the south polar cap. *J. Geophys. Res.*, **95**, 359–365.

Jakosky, B. M. and Haberle R. M. (1992). The seasonal behavior of water on Mars. In *Mars.*, ed. H. H. Kieffer, B. M. Jakosky, C. W. Snyder and M. S. Matthews. Tucson: University Arizona Press, pp. 969–1019.

Jakosky, B. M. and Jones, J. (1997). The history of martian volatiles. *Rev. Geophys.*, **35**, 1–16.

Jakosky, B. M., Mellon, M. T., Varnes, E. S., Feldman, W. C., Boynton, W. V. and Haberle, R. M. (2005). Mars low-latitude neutron distribution: possible remnant near-surface water ice and a mechanism for its recent emplacement. *Icarus*, **175**, 58–67.

Jaumann, R. (2005). Martian valley networks and associated fluvial features as seen by the Mars Express High Resolution Camera (HRSC). LPSC XXXVI, Abstract 1815.

Johnston, C. G. and Vestal, J. R. (1989). Distribution of inorganic species in two cryptoendolithic communities. *Geomicrobiol. J.*, **7**, 137–53.

Jons, H.-P. (1985). Late sedimentation and late sediments in the northern lowlands on Mars. LPSC XVI, pp. 414–15.

Jons, H.-P. (1986). Arcuate ground undulations, gelifluxion-like features and "front tori" in the northern lowlands of Mars – what do they indicate? LPSC XVII, pp. 404–5.

Kahn, R. A., Martin, T. Z., Zurek, R. W. and Lee, S. W. (1992). The martian dust cycle. In *Mars*, ed. H. H. Kieffer, B. M. Jakosky, C. W. Snyder and M. S. Matthews. Tucson: University of Arizona Press, pp. 1017–53.

Kargel, J. S. (1993) Geomorphic processes in the Argyre-Dorsa Argentea region of Mars. LPSC XXIV, pp. 753–4.

Kargel, J. S. (2004). *Mars – A Warmer, Wetter Planet*. New York: Springer Praxis.

Kargel, J. S. and Strom, R. G. (1991). Terrestrial glacial eskers: analogs for martian sinuous ridges., LPSC XXII, 683–4.

Kargel, J. S. and Strom, R. G. (1992). Ancient glaciation on Mars. *Geology*, **20**, 3–7.

Kargel, J. S., Baker, V. R., Beget, J. E., *et al.* (7 authors) (1995). Evidence for ancient continental glaciation in the martian northern plains. *J. Geophys. Res.*, **100**, 5351–68.

Kass, D. M. (2001). Loss of water to space from Mars: processes and implications. Eos Trans. AGU, 82, (Fall Meeting Suppl.), Abstract P12E-02.

Kasting, J. F. (1991). CO_2 condensation and the climate of early Mars. *Icarus*, **94**, 1–13.

Keszthelyi, L., McEwen, A. S. and Thordarson, Th. (2000). Terrestrial analogs and thermal models for martian flood lavas. *J. Geophys. Res.*, **105**, 15,027–49.

Kieffer, H. H., Chase, S. C., Martin, T. Z., Miner, E. D. and Palluconi, F. D. (1976). Martian north pole summer temperatures: dirty water ice. *Science*, **194**, 1341–4.

Kieffer, H. H., Martin, T. Z., Peterfreund, A. R. and Jakosky, B. M. *et al.* (1977). Thermal and albedo mapping of Mars during the Viking primary mission. *J. Geophys. Res.*, **82**, 4249–91.

Kieffer, H. H., Jakosky, B. M., Snyder, C. W. and Matthews, M. S. (1992). *Mars*, Tucson: University of Arizona Press.

Klein, H. P. (1979). The Viking mission and the search for life on Mars. *Rev. Geophy.*, **17**, 1655–1662.

Kleine, T., Munker, C., Metzger, K. and Palme, H. (2002). Rapid accretion and early core formation in asteroids and the terrestrial planets from Hf-W chronometry. *Nature*, **418**, 952–5.

Kleine, T., Palme, H., Mezger, K. and Halliday, A. N. (2005). Hf-W chronometry of lunar metals and the age and early differentiation of the Moon. *Science*, **310**, 1671–4.
Klingelhöfer, G., Morris, R. V., Bernhardt, B., *et al.* (2004). Jarosite and hematite at Meridiani Planum from Opportunity's Mössbauer spectrometer. *Science*, **306**, 1741–5.
Kochel, R. C., Howard, A. D. and McLane, C. (1985). Channel networks developed by groundwater sapping in fine-grained sediments: analogs to some martian valleys. In *Models in Geomorphology*, ed. M. J. Woldenberg. Boston: Allen and Unwin, pp. 313–41.
Kolb, E. J. and Tanaka, K. L. (2001). Geologic history of the polar regions of Mars based on Mars Global Surveyor data. II. Amazonian period. *Icarus*, **154**, 22–39.
Komar, P. D. (1979). Comparisons of the hydraulics of water flows in martian outflow channels with flows of similar scale on Earth. *Icarus*, **42**, 317–29.
Komatsu, G., Geissler, P. E., Strom, R. G. and Singer, R. B. (1993). Stratigraphy and erosional landforms of layered deposits in Valles Marineris. *J. Geophys. Res.*, **98**, 11,105–21.
Koutnik, M., Byrne, S. and Murray, B. (2002). South polar layered deposits of Mars: the cratering record. *J. Geophys. Res.*, **107**(E11), doi:10.1029/2001JE001805.
Krasnapolsky, V. A., Mailliard, J. P. and Owen, T. (2004). Detection of methane in the martian atmosphere: evidence for life? *Icarus*, **172**, 537–47.
Kreslavsky, M. A. and Head, J. W. (2002). Fate of outflow channel effluents in the northern lowlands of Mars: the Vastitas Borealis Formation as a sublimation residue from frozen, ponded bodies of water. *J. Geophys. Res.*, **107**(E12), doi:10.1029/2001JE001831.
Kuhn, W. R. and Atreya, S. W. (1979). Ammonia photolysis and the greenhouse effect in the primordial atmosphere of the Earth. *Icarus*, **37**, 207–13.
Kuzmin, R. O., Greeley, R., Landheim, R., Cabrol, N. A. and Farmer, J. D. (2000). Geologic map of the MTM-15,182 and MTM-15,187 quadrangles, Gusev Crater-Ma'adim Vallis region, Mars. U.S. Geol. Survey, Misc. Inv. Map I-2666.
Lachenbruch, A. H. (1962). Mechanics of thermal contraction cracks and ice wedge polygons in permafrost. *Geol. Soc. Am. Sp. Paper* 70.
Laity, J. E. and Malin, M. C. (1985). Sapping processes and the development of theater-headed valley networks in the Colorado Plateau. *Geol. Soc. Am. Bull.*, **96**, 203–17.
Lancaster, N. and Greeley, R. (1990). Sediment volume in the north polar sand seas of Mars. *J. Geophys. Res.*, **95**, 10,921–7.
Lane, M. D. and Christensen, P. R. (2000). Convection in a catastrophic flood deposit as the mechanism for the giant polygons on Mars. *J. Geophys. Res.*, **105**, 17,617–27.
Lane, M. D., Christensen, P. R. and Hartmann, W. K. (2003). Utilization of the THEMIS visible and infrared imaging for crater population studies of the Meridiani Planum landing site and southwest Arabi Terra. *Geophys. Res. Lett.*, **29**, doi10.1029/2002GLO16515.
Langevin, Y., Poulet, F., Bibring, J. and Gondet, B. (2005). Sulfates in the north polar region of Mars detected by OMEGA/Mars Express. *Science*, **307**, 1584–6.
Laskar, J. and Robutel, P. (1993). The chaotic obliquity of the planets. *Nature*, **362**, 608–12.
Laskar, J., Levrard, B. and Mustard, J. F. (2002). Orbital forcing of the martian polar layered deposits. *Nature*, **419**, 375–7.
Laskar, J., Correia, A., Gastineau, F., Joutel, F., Levrard, B. and Robutel, P., *et al.* (2004). Long term evolution and chaotic diffusion of the insolation quantities of Mars. *Icarus*, **170**, 343–64.
Laul, J. C., Smith, M. R., Wänke, H., *et al.* (1986). Chemical systematics of the Shergotty meteorite and the composition of its parent body (Mars). *Geochim. Cosmochim. Acta*, **28**, 3035–8.
Lazcano, A. and Miller, S. L. (1996). The origin and early evolution of life: prebiotic chemistry, the pre-RNA world and time. *Cell*, **85**, 793–8.
Lee, P., Cockell, C. S., Marinova, M. M., McKay, C. P. and Rice, J. W. (2001). Snow and ice melt flow features on Devon Island, Nunavut, arctic Canada as possible analogs for recent slope flow features on Mars. LPSC XXXII, Abstract 1809.
Leighton, R. B. and Murray, B. C. (1966). Behavior of carbon dioxide and other volatiles on Mars. *Science*, **153**, 136–44.
Lemoine, F. G., Smith, D. E., Rowlands, D. D., *et al.* (2001). An improved solution of the gravity field of Mars (GMM-2B, from Mars Global Surveyor. *J. Geophys. Res.*, **106**(E10), 23,359–76.
Lepland, A., van Zuilen, M. A., Arrhenius, G., Whitehouse, M. J. and Fedo, C. M. (2005). Questioning the evidence for Earth's earliest life – Akilia revisited. *Geology*, **33**, 77–9.
Leverington, D. W. (2004). Volcanic rilles, streamlined islands, and the origin of outflow channels on Mars. *J. Geophys. Res.*, **109**(E11), doi:10.1020/2004JE002311.
Leverington, D. W. and Maxwell, T. A. (2004). An igneous origin for features of a candidate crater-lake system in western Memnonia, Mars. *J. Geophys. Res.*, **109**(E6), doi:10.1029/2004JE002237.
Levin, G. V. (1988). A reappraisal of life on Mars. *Adv. In Aeronautice*, **71**, 187–297.
Lipschutz, M. E. and Schultz, L. (1990). Meteorites. In *Encyclopedia of the Solar System*, ed. P. R. Weissman *et al.* San Diego: Academic Press, pp. 629–71.
Lopes, R., Guest, J. E. and Wilson, L. (1980). Origin of the Olympus Mons aureole and the perimeter scarp. *Moon and Planets*, **22**, 221–34.
Lopes, R., Guest, J. E., Hiller, K. and Neukum, G. (1982). Further evidence for a mass movement origin of the Olympus Mons aureole. *J. Geophys. Res.*, **87**, 9917–28.
Lowe, D. R. (1994). Abiological origin of described stromatolites older than 3.2 Ga. *Geology*, **22**, 387–90.
Lucchitta, B. K. (1979). Landslides in Valles Marineris, Mars. *J. Geophys. Res.*, **84**, 8097–113.
Lucchitta, B. K. (1981). Mars and Earth: comparison of cold climate features. *Icarus*, **45**, 264–303.
Lucchitta, B. K. (1982). Ice sculpture in the martian outflow channels. *J. Geophys. Res.*, **87**, 9951–73.
Lucchitta, B. K. (1984). Ice and debris in the fretted terrain, Mars. *J. Geophys. Res.*, **89**, B409–B418.
Lucchitta, B. K. (1987). Valles Marineris, Mars: wet debris flows and ground ice. *Icarus*, **72**, 411–29.
Lucchitta, B. K. (1989). Young volcanic deposits in the Valles Marineris, Mars. *Icarus*, **86**, 476–509.
Lucchitta, B. K. (1993). Ice in the northern plains: relic of a frozen ocean? LPI Tech. Rept. 93–04, 9–10.
Lucchitta, B. K. (2001). Antarctic ice streams and outflow channels on Mars. *Geophys. Res. Lett.*, **28**, 403–6.
Lucchitta, B. K., Ferguson, H. M. and Summers, C. (1986). Sedimentary deposits in the northern lowland plains, Mars Proc. 17th Lunar Planet. Sci. Conf. *J. Geophys. Res.*, **91**, E166–174.
Lucchitta, B. K., McEwen, A. S., Clow, G. D., *et al.* (7 authors) (1992). The canyon system on Mars. In *Mars*, ed. H. H. Kieffer, B. M. Jakosky, C. W. Snyder and M. I. Matthews. TUCSON: University of Arizona Press, pp. 453–92.
Lucchitta, B. K., Isbell, N. K. and Howington-Kraus, A. (1994). Topography of Valles Marineris: implications for erosional and structural history. *J. Geophys. Res.*, **99**, 3783–98.
Luhmann, J. G. and Kozyra, I. U. (1991). Dayside pick-up oxygen ion precipitation at Venus and Mars: spatial distributions, energy deposition and consequences. *J. Geophys. Res.*, **96**, 5457–67.
Magalhaes, J. A. and Gierasch, P. (1982). A model of martian slope winds: implications for eolian transport. *J. Geophys. Res.*, **87**, 9975–84.
Malin, M. C. and Edgett, K. S. (2000a). Evidence for recent groundwater seepage and surface runoff on Mars. *Science*, **288**, 2330–5.
Malin, M. C. and Edgett, K. S. (2000b). Sedimentary rocks of early Mars. *Science*, **290**, 1927–37.

Malin, M. C. and Edgett, K. S. (2000c). Observations of aprons in martian frettted terrain. LPSC XXXI, Abstract 1053.
Malin, M. C. and Edgett, K. S. (2001). Mars Global Surveyor Mars Orbiter Camera: interplanetary cruise through primary mission. *J. Geophys. Res.*, **106**, 23,429–570.
Malin, M. C. and Edgett, K. S. (2002). Martian sedimentary rock stratigraphy: outcrops and interbedded craters of northwest Sinus Meridiani and southwest Arabia Terra.. *Geophys. Res. Lett.*, **29**(24), 2179 doi:10.1029/2002GL016515.
Malin, M. C. and Edgett, K. S. (2003). Evidence for persistent flow and aqueous sedimentation on early Mars. *Science*, **302**, 1931–4.
Malin, M. C., Caplinger, M. A. and Davis, S. D. (2001). Observational evidence for an active surface reservoir of solid carbon dioxide on Mars. *Science*, **294**, 2146–8.
Manga, N. (2004). Martian floods at Cerberus Fossae can be produced by groundwater discharge. *Geophys. Res. Lett.*, **31**, L02702 doi:10.1029/2003GL018958.
Mandl, G. (1988). *Mechanics of Tectonic Faulting*. New York: Elsevier.
Mangold, N. (2003). Geomorphic analysis of lobate debris aprons on Mars at Mars Orbiter Camera scale. Evidence of ice sublimation initiated by fractures. *J. Geophys. Res.*, **108**(E4), doi:10.1029/2002JE001885.
Mangold, N., Allemand, P., Thomas, P., Duval, P. and Geraud, Y. (2002). Experimental and theoretical deformation of ice-rock mixtures: implications on rheology and ice content of Martian permafrost. *Planet. Space Sci.*, **50**, 385–401.
Mangold, N., Costard, F. and Forget, F. (2003). Debris flows over sand dunes on Mars: evidence for liquid water. *J. Geophys. Res.*, **108**(E4), doi:10.1029/2003JE001958.
Mangold, N., Quantin, C., Anson, V., Delacourt, C. and Allemand, P. (2004). Evidence for precipitation on Mars from dendritic valleys in the Valles Marineris area. *Science*, **305**, 78–81.
Martin, L. J., James, P. B., Dollifus, A., Iwasaki, K. & Beish, J. D. (1992). Telescopic observations. In *Mars*, ed. H. H. Kieffer, B. M. Jakosky, C. W. Snyder and M. S. Matthews. Tucson: University of Arizona Press, pp. 34–70.
Masson, P. (1985). Origin and evolution of the Valles Marineris region of Mars. *Adv. Space Sci.*, **5**, 83–92.
Mastin, L. G. and Pollard, D. D. (1988). Surface deformation and shallow dike intrusion processes at Inyo Crater, Long Valley, California. *J. Geophys. Res.*, **93**, 13,221–35.
Masursky, H. (1973). An overview of geological results from Mariner 9. *J. Geophys. Res.*, **78**, 4009–30.
McCauley, J. F. (1978). Geologic map of the Coprates quadrangle of Mars. U.S. Geol. Surv. Misc. Inv. Map I-897.
McCauley, J. F., Carr, M. H., Cutts, J. A., *et al.* (8 authors) (1972). Preliminary Mariner 9 report on the geology of Mars. *Icarus*, **17**, 289–327.
McEwen, A. S. (1989). Mobility of large rock avalanches: evidence from Valles Marineris, Mars. *Geology*, **17**, 1111–14.
McEwen, A. S., Malin, M. C., Carr, M. H. and Hartmann, W. K. (1999). Voluminous volcanism on early Mars revealed in Valles Marineris. *Nature*, **397**, 584–6.
McEwen, A. S., Preblich, B. S., Turtle, E. P., *et al.* (9 authors) (2005). The rayed crater Zunil and interpretations of small impact craters on Mars. *Icarus*, **176**, 331–50.
McGill, G. E. (1986). The giant polygons of Utopia, northern martian plains. *Geophys. Res. Lett.*, **13**, 705–8.
McGill, G. E. (1989). Buried topography of Utopia, Mars: persistence of a giant impact depression. *J. Geophys. Res.*, **94**, 2853–759.
McGill, G. E. (2000). Crustal history of north Arabia Terra, Mars. *J. Geophys. Res.*, **105**, 6945–59.
McGill, G. E. (2001). The Utopia Basin revisited: regional slope and shorelines from MOLA profiles. *Geophys. Res. Lett.*, **28**, 411–14.
McGill, G. E. and Squyres, S. W. (1991). Origin of martian crustal dichotomy: evaluating hypotheses. *Icarus*, **93**, 386–93.
McGovern, P. J., Solomon, S. C., Head, J. W., Smith, D. E., Zuber, M. T. and Neumann, G. A. (2001). Extension and uplift at Alba Patera, Mars: insights from MOLA observations and loading models. *J. Geophys. Res.*, **106**(E4), 23,769–809.
McGovern, P. J., Solomon, S. C., Smith, D. E., *et al.* (10 authors) (2002). Localized gravity/topography admittance and correlation spectra on Mars: implications for regional and global evolution. *J. Geophys. Res.*, **107**(E12), doi:10.1029/2002JE001854.
McKay, D. S., Gibson, E. K., Thomas-Keprta, K. L., Vali, H., Romanek, C. S. and Clemett, X. D., *et al.* (1996). Search for past life on Mars. Possible relic biogenic activity in martian meteorite ALH84001. *Science*, **273**, 924–30.
McKee, E. D. (1979). A study of global sand seas. U.S. Geol. Surv. Prof. Paper 1052.
McKenzie, D. and Nimmo, F. (1999). The generation of martian floods by the melting of ground ice above dikes. *Nature*, **397**, 231–3.
McLennan, S. M., Bell, J. F., Calvin, W. M., *et al.* (2005). Evidence for groundwater involvement in the provenence and diagenesis of the evaporite-bearing Burns formation, Meridiani Planum. *Earth Planet. Sci. Lett.*, **240**, 95–121.
McSween, H. Y. (1994). What have we learned about Mars from SNC meteorites. *Meteoritics*, **29**, 757–79.
McSween, H. Y. (1999). SNC meteorites: clues to martian petrologic evolution. *Rev. Geophys.*, **23**, 391–416.
McSween, H. Y. (2001). The rocks of Mars, from far and near. *Metoritics and Planet. Sci.*, **37**, 7–25.
McSween, H. Y. and Treiman, A. H. (1998). Martian meteorites. In *Planetary Materials*, ed. J. J. Papike. America Washington, D. C.: Mineralogical Society.
McSween, H. Y., Murchie, S. L., Crisp, J. A., *et al.* (20 authors) (1999). Chemical, multispectral and textural constraints on the composition and origin of rocks at the Mars Pathfinder landing site. *J. Geophys. Res.*, **104**(E4), 8679–715.
McSween, H. Y., *et al.* (2001). Geochemical evidence for magmatic water within Mars from pyroxenes in the Shergotty meteorite. *Nature*, **409**, 487–90.
McSween, H. Y., Grove, T. L. and Wyatt, M. B. (2003). Constraints on the composition and petrogenesis of the martian crust. *J. Geophys. Res.*, **108**(E12), doi:10.1029/2003JE002175.
McSween, H. Y., Arvidson, R. E., Bell, J. F., *et al.* (34 authors) (2004). Basaltic rocks analyzed by the Spirit rover in Gusev crater. *Science*, **305**, 842–5.
Mège, D. and Masson, P. (1996). Amounts of crustal stretching in Valles Marineris, Mars. *Planet. Space Sci.*, **44**, 749–82.
Mellon, M. T. and Jakosky, B. M. (1995). The distribution and behavior of martian ground ice during past and present epochs. *J. Geophys. Res.*, **100**, 11,781–99.
Mellon, M. T. and Phillips, R. J. (2001). Recent gullies on Mars and the source of liquid water. *J. Geophys. Res.*, **106**(E10), 23,165–79.
Melosh, H. J. (1983). Acoustic fluidization. *Am. Sci.*, **71**, 158–65.
Melosh, H. J. (1984). Impact ejection, spallation and the origin of meteorites. *Icarus*, **59**, 234–60.
Melosh, H. J. (1989). *Impact Cratering*. Oxford: OUP.
Melosh, H. J. and Vickery, A. M. (1989). Impact erosion of the primordial martian atmosphere. *Nature*, **338**, 487–9.
Metzger, S. M. (1991). A survey of esker morphometries, the connection to New York state glaciation and criteria for sub-glacial melt-water channels. LPSC XXII, pp. 891–2.
Michaux, C. M. and Newburn, R. L. (1972). Mars Scientific Model. Jet Propulsion Lab., Doc. 606–1.
Milam, K. A., Stockstill, K. R., Moersch, J. E., *et al.* (9 authors) (2003). THEMIS characterization of the MER Gusev crater landing site. *J. Geophys. Res.*, **108**(E12), doi:10.1029/2002JE002023.
Milkovich, S. M. and Head, J. W. (2005). North polar cap of Mars: polar layered deposit characterization and identification of a fundamental climate signal. *J. Geophys. Res.*, **110**(E5), doi:10.1029?2004JE002349.

Milkovich, S. M., Head, J. W. and Pratt, S. (2002). Meltback of Hesperian-aged ice-rich deposits near the south pole. Evidence for drainage channels and lakes. *J. Geophys. Res.*, **107**(E6), doi:10.1029/2001JE0018−02.

Milton, D. J. (1973). Water and processes of degradation in the Martian landscape. *J. Geophys. Res.*, **78**, 4037−48.

Milton, D. J., Barlow, B. C., Breett, R., *et al.* (10 authors) (1972). Gosses Bluff impact structure, Australia. *Science*, **175**, 1119−207.

Mischna, M. A., Richardson, M. I., Wilson, R. J. and McCleese, D. J. (2003). On the orbital forcing of martian water and CO_2 cycles: a general circulation model study with simplified volatile schemes. *J. Geophys. Res.*, **108**(E6), doi:10.1029/2003JE002051.

Mitrofanov, L., Anfimov, D., Kozyrev, M., *et al.* (2002). Maps of subsurface hydrogen from the High Energy Neutron Detector, Mars Odyssey. *Science*, **297**, 78−81.

Mojzsis, S. J., Arrhenius, G., McKeegan, K. D., Harrison, T. M., Nutman, A. P. and Friend, C. R. (1996). Evidence of life on Earth before 3,800 million years ago. *Nature*, **384**, 55−9.

Mojzsis, S. J. and Mark, T. (2000). Vestiges of a beginning: clues to the emergent biosphere recorded in the oldest known sedimentary rocks. *GSA Today*, **10**(4), 1−6.

Montesi, L. and Zuber, M. T. (2003). Clues to the lithospheric structure of Mars from wrinkle ridge set and localization instability. *J. Geophys. Res.*, **108**(E6), doi: 10.1029/2002 JE001974.

Moore, J. M. and Wilhelms, D. E. (2001). Hellas as a possible site of ancient ice-covered lakes on Mars. *Icarus*, **154**, 258−76.

Moore, J. M., Clow, G. D., Davis, W. L., *et al.* (8 authors) (1995). The circum-Chryse region as a possible example of a hydrologic cycle on Mars: geologic observations and theoretical evaluation. *J. Geophys. Res.*, **100**(E3), 5433−47.

Morris, R. V., Klingelhofer, G., Bernhardt, B., *et al.* (17 authors) (2004). Mineralogy at Gusev crater from the Mössbauer spectrometer on the Spirit rover. *Science*, **305**, 833−6.

Mouginis-Mark, P. J. (1990). Recent water release in the Tharsis region of Mars. *Icarus*, **84**, 363−73.

Mouginis-Mark, P. J., Wilson, L. and Head, J. W. (1982). Explosive volcanism on Hecates Tholus, Mars: investigation of eruption conditions. *J. Geophys. Res.*, **87**, 411−14.

Mouginis-Mark, P. J., Wilson, L. and Zimbelman, J. R. (1988). Polygenetic eruptions on Alba Patera, Mars. *Bull. Volc.*, **50**, 361−79.

Murray, J. B., Muller, J-P, Neukum, G., *et al.* (12 authors) (2005). Evidence from the Mars Express High Resolution Stereo Camera for a frozen sea close to the equator. *Nature*, **434**, 352−6.

Musselwhite, D. S., Swindle, T. D. and Lunine, J. I. (2001). Liquid CO_2 breakout and formation of recent small gullies on Mars. *Geophys. Res. Lett.*, **28**, 1283−5.

Mustard, J. F., Cooper, C. D. and Rifkin, M. K. (2001). Evidence for recent climate change on Mars from the identification of youthful near-surface ground ice. *Nature*, **412**, 4211−414.

Mustard, J. F., Poulet, F., Gendrin, A., *et al.* (2005). Olivine and pyroxene diversity in the crust of Mars. *Science*, **307**, 1594−7.

Mutch, T. A., Arvidson, R. A., Binder, A. B., Guiness, E. A. and Morris, E. C. (1977). The geology of the Viking lander 2 site. *J. Geophys. Res.*, **82**, 4452−67.

National Research Council (1990). *The Search for Life's Origins*. Washington, D.C.: National Academy Press.

National Research Council (1992). *Biological Contamination of Mars: Issues and Recommendations*. Washington, D.C.: National Academy Press.

National Research Council (1999). *Size Limits of Very Small Microorganisms*. Washington, D.C.: National Academy Press.

Nedell, S. S., Squyres, S. W. and Anderson, D. W. (1987). Origin and evolution of the layered deposits in the Valles Marineris, Mars. *Icarus*, **70**, 409−41.

Neukum, G. (1983). Meteoritenbombardement und Datierung planetarer Oberflächen. Habilitation Dissertation for Faculty Membership, Ludwig-Maximilians University, Munich, Germany.

Neukum, G. and Hiller, K. (1981). Martian ages. *J. Geophys. Res.*, **86**(B4), 3097−121.

Neukum, G. and Ivanov, B. A. (1994). Crater size distributions and impact probabilities. In *Hazards due to Comets and Asteroids*, ed. T. Gehrels. Tucson: University of Arizona Press, pp. 359−416.

Neukum, G., Konig, B. and Arkani-Hamad, J. (1975). A study of lunar impact crater size distributions. *The Moon*, **12**, 201−29.

Neukum, G., Ivanov, B. A. and Hartmann, W. K. (2001). Cratering record in the inner solar system in relation to the lunar reference system. In *Chronology and Evolution of Mars*, ed. R. Kallenbach *et al.* Dordrecht: Kluwer, pp. 55−86.

Neukum, G., Jaumannn, R., Hoffmann, H., *et al.* (2004). Recent and episodic volcanic and glacial activity on Mars revealed by the High Resolution Stereo Camera. *Nature*, **432**, 971−9.

Neumann, G. A., Zuber, M. T., Wieczorek, M. A., McGovern, P. J., Lemoine, F. G. and Smith, D. E. (2004). Crustal structure of Mars from gravity and topography. *J. Geophys. Res.*, **109**(E8), doi:10.1029/2004JE002262.

Newman, M. J. and Rood, R. T. (1977). Implications of solar evolution for Earth's early atmosphere. *Science*, **198**, 1035−7.

Newsome, H. E. (1980). Hydrothermal alteration of impact melt sheets with implications for Mars. *Icarus*, **44**, 207−16.

Newsome, H. E., Britell, G. E., Hibbets, C. A., Crossey, L. J. and Kudo, A. M. (1996). Impact cratering and the formation of crater lakes on Mars. *J. Geophys. Res.*, **101**, 14,951−5.

Newsome, H. E., Barber, C. A., Hare, T. M., Schelbe, R. T., Sutherland, V. A. and Feldman, W. C. (2003). Paleolakes and impact basins in southern Arabia Terra, including Meridiani Planum: implications for formation of hematite deposits on Mars. *J. Geophys. Res.*, **108**(E12), doi:10.1029/2002JE01993.

Nimmo, F. (2000). Dike intrusion as a possible cause of linear martian magnetic anomalies. *Geology*, **28**, 391−4.

Nimmo, F. and Tanaka, K. (2005). Early crustal evolution of Mars. *Ann. Rev. Earth Planet. Sci.*, **33**, 533−6.

Nisbet, E. G. and Sleep, N. H. (2001). The habitat and nature of early life. *Nature*, **409**, 1083−91.

Nummedal, D. and Prior, D. B. (1981). Generation of martian chaos and channels by debris flows. *Icarus*, **45**, 77−86.

Nyquist, L. E., Bogard, D. D., Shih, C.-Y., Greshake, A., Stoffler, D. and Eugster, O. (2001). Ages and geologic histories of martian meteorites. In *Chronology and Evolution of Mars*, ed. R. Kallenbach *et al.* Dordrecht: Kluwer, pp. 105−64.

Oberbeck, V. R. (1975). The role of ballistic erosion and sedimentation in lunar stratigraphy. *Rev. Geophys. Space Phys.*, **13**, 337−62.

Pace, N. R. (1991). Origin of life − facing up to the physical setting. *Cell*, **65**, 531−3.

Paige, D. A. (1992). The thermal stability of near-surface ground ice on Mars. *Nature*, **356**, 43−5.

Palluconi, F. D. and Kieffer, H. H. (1981). Thermal inertia mapping of Mars from 60°S to 60°N. *Icarus*, **45**, 415−26.

Parker, T. J., Saunders, R. S. and Schneeberger, D. M. (1989). Transitional morphology in the west Deuteronilus Mensae region of Mars: implications for modification of the lowland/upland boundary. *Icarus*, **82**, 111−45.

Parker, T. J., Gorsline, D. S., Saunders, R. S., Pieri, D. and Schneeberger, D. M. (1993). Coastal geomorphology of the martian northern plains. *J. Geophys. Res.*, **98**, 11,061−78.

Parker, T. J., Clifford, S. M. and Banerdt, W. B. (2000). Argyre Planitia and the Mars global hydrologic cycle. LPSC XXXI, Abstract 2033.

Pathare, A. V. and Paige, D. A. (2005). The effects of martian orbital variations upon the sublimation and relaxation of north polar troughs and scarps. *Icarus*, **174**, 419−43.

Pathare, A. V., Paige, D. A. and Tutttle, E. (2005). Viscous relaxation of craters within the martian south polar layered deposits. *Icarus*, **174**, 396−418.

Pechman, J. C. (1980). The origin of polygonal troughs on the northern plains of Mars. *Icarus*, **42**, 185–210.
Pepin, R. O. (1991). On the origin and early evolution of terrestrial planet atmospheres and meteoritic volatiles. *Icarus*, **92**, 2–79.
Pepin, R. O. (1994). Evolution of the martian atmosphere. *Icarus*, **111**, 289–304.
Phillips, R. J., Saunders, R. S. and Conel, J. E. (1973). Mars: crustal structure inferred from gravity anomalies. *J. Geophys. Res.*, **78**, 4815–20.
Phillips, R. J., Zuber, M. T., Solomon, S. C., *et al.* (2001). Ancient geodynamics and global-scale hydrology on Mars. *Science*, **291**, 2587–91.
Picardi, G., Plaut, J. J., Biccari, D., *et al.* (2005). Radar soundings of the subsurface of Mars. *Science*, **310**. 1925–8.
Pieri, D. C. (1980). Martian valleys: morphology, distribution, age and origin. *Science*, **210**, 895–7.
Pike, R. J. (1980a). Control of crater morphology by gravity and target type: Mars, Earth, Moon. LPSC XI, pp. 2159–89.
Pike, R. J. (1980b). Formation of complex impact craters: evidence from Mars and other planets. *Icarus*, **43**, 1–19.
Plescia, J. B. (2000). Geology of the Uranius group volcanic constructs: Uranius Patera, Ceraunius Tholus and Uranius Tholus. *Icarus*, **143**, 376–96.
Plescia, J. B. (2003a). Cerberus Fossae, Elysium, Mars: a source for lava and water. *Icarus*, **164**, 79–95.
Plescia, J. B. (2003b). Tharsis Tholus: an unusual martian volcano. *Icarus*, **165**, 223–41.
Plescia, J. B. (2004). Morphometric properties of martian volcanoes. *J. Geophys. Res.*, **109**, E03003, doi:10.1029.202JE002031.
Plescia, J. B. and Golombek, M. P. (1986). Origin of planetary wrinkle ridges based on the study of terrestrial analogs. *Geol. Soc. Am. Bull.*, **97**, 1289–99.
Plescia, J. B. and Saunders, R. S. (1979). The chronology of martian volcanoes, LPSC XIX, 2841–59.
Plescia, J. B. and Saunders, R. S. (1982). Tectonic history of the Tharsis region of Mars. *J. Geophys. Res.*, **87**, 9775–91.
Pollack, J. B., Colkburn, D. S., Flaser, M., Kahn, R., Carlston, C. E., Pidek, D. (1979). Properties and effects of dust particles suspended in the martian atmosphere. *J. Geophys. Res.*, **84**, 2929–45.
Pollack, J. B., Kasting, J. F., Richardson, S. M., and Poliakoff, K. (1987). The case for a warm, wet climate on early Mars. *Icarus*, **71**, 203–24.
Pollack, J. B., Roush, T., Witteborn, F., *et al.* (1990). Thermal emission spectra of Mars (5.4–10.5 μm): Evidence for sulfates, carbonates and hydrates. *J. Geophys. Res.*, **95**, 14,595–627.
Postawko, S. E. and Kuhn, W. R. (1986). Effect of greenhouse gases on (CO_2, H_2O, SO_2) on martian paleoclimates. *J. Geophys. Res.*, **91**, D431–8.
Prettyman, T. H., Feldman, W. C., Mellon, M. T., *et al.* (13 authors) (2004). Composition and structure of the martian surface at high southern latitudes from neutron spectroscopy. *J. Geophys. Res.*, **109**(E5), doi:10.1029/2003JE002139.
Rabinowitz, D. L., Bowell, E., Shoemaker, E. M. and Muinonem, K. (1994). The population of Earth-crossing asteroids. In *Hazards due to Comets and Asteroids*, ed. T. Gehrels. Tucson: University of Arizona Press, pp. 285–312.
Reese, C. C., Solomatov, V. S. and Baumgardner, J. R. (2002). Survival of impact-induced thermal anomalies in the martian mantle. *J. Geophys. Res.*, **107**(E10), doi:10.1029/2000JE001474.
Reider, R., Gellert, R., Anderson, R. C., *et al.* (2004). Chemistry of rocks and soils at Meridiani Planum from the Alpha Particle X-ray Spectrometer. *Science*, **306**, 1746–9.
Reimers, C. E. and Komar, P. D. (1979). Evidence for explosive volcanic density currents on certain martian volcanoes. *Icarus*, **39**, 88–110.
Rice, J. W., Christensen, P. R., Ruff, S. W. and Harris, J. C. (2003). Martian fluvial landforms: a THEMIS perspective after one year at Mars. LPSC XXXIV, Abstract 2091.
Ringwood, A. E. (1979). *Origin of the Earth and the Moon*. New York: Springer Verlag.
Robers, M. J. (2005). Jökulhlaups: A reassessment of floodwater flow through glaciers. *Rev. Geophys.*, **43**, RG1002.
Robinson, M. S. and Tanaka, K. L. (1990). Magnitude of a catastrophic flood event at Kasei Vallis, Mars. *Geology*, **18**, 902–5.
Roddy, D. J. (1977). Large scale impact and explosion craters: comparison of morphological and structural analogs. In *Impact and Explosion Cratering*, ed. D. J. Roddy. New York: Pergamon, pp. 185–246.
Roddy, D. J. (1979). Structural deformation at the Flynn Creek impact structure, Tennessee: a preliminary report on deep drilling. LPSC XI, pp. 2519–34.
Rossbacher, L. A. and Judson, S. (1981). Ground ice on Mars: inventory, distribution and resulting landforms. *Icarus*, **45**, 35–59.
Rothschild, L. J. and Mancinelli, R. L. (2001). Life in extreme environments. *Nature*, **409**, 1092–101.
Rotto, S. and Tanaka, K. L. (1995). Geologic/geomorphic map of the Chryse Planitia region of Mars. U.S. Geol. Survey Misc. Inv. Map I-2441.
Russell, P. S. and Head, J. W. (2003). Elysium-Utopia flows as mega-lahars: a model of dike intrusion, cryosphere cracking and water-sediment release. *J. Geophys. Res.*, **108**(E6), doi:10.1029/2002JE001995.
Ryan, M. P. (1987). Elasticity and contractancy of Hawaiian olivine tholeiite and its role in the stability and structural evolution of subcaldera magma reservoirs and rift systems. In *Volcanism in Hawaii*, ed. R. W. Decker *et al.* U.S. Geolo. Survey Prof. Paper 1350, pp. 1395–447.
Ryder, G. (2002). Mass flux in the ancient Earth-Moon system and benign implications for origin of life on Earth. *J. Geophys. Res.*, **107**(E4), doi:10.1029/2001JE001583.
Sagan, C. (1977). Reducing greenhouses and the temperature history of Earth and Mars. *Nature*, **269**, 224–6.
Sagan, C. and Chyba, C. (1997). The early faint sun paradox: organic shielding of the ultraviolet-labile greenhouse gases. *Science*, **276**, 1217–21.
Schaeffer, M. W. (1993). Aqueous geochemistry on early Mars. *Geochim. Cosmochim. Acta*, **57**, 4619–25.
Schidlowski, M., Hayes, J. M. and Kaplan, I. R. (1983). Isotopic inferences of ancient biochemistries: carbon, sulfur, hydrogen, and nitrogen. In *Earth's Earliest Biosphere*, ed. J. W. Schopf. Princeton: Princeton University Press, pp. 149–86.
Schmidt, R. M. and Housen, K. R. (1987). Some recent advances in the scaling of impact and explosion cratering. *Int. J. Impact Eng.*, **5**, 543–60.
Schopf, J. W. (1999). *Cradle of Life: The Discovery of Earth's Earliest Fossils*. Princeton: Princeton University Press.
Schopf, J. W. and Walter, M. R. (1983). Archean microfossils: evidence of ancient microbes. In *Earth's Earliest Biosphere*, ed. J. W. Schopf. Princeton: Princeton University Press, pp. 214–39.
Schopf, J. W., Kudtrysvtsev, A. B., Agresti, D. G., *et al.* (2002). Laser-Raman imagery of Earth's earliest fossils. *Nature*, **416**, 73–6.
Schorghofer, N. and Aharonson, O. (2004). Stability and exchange of subsurface ice on Mars. LPSC XXXV, Abstract 1463.
Schubert, G., Solomon, S. C., Turcotte, D. L., Drake, M. J. and Sleep, N. H. (1992). Origin and thermal evolution of Mars. In *Mars*, ed. H. H. Kieffer, B. M. Jakosky, C. W. Snyder and M. S. Matthews. Tucson: University of Arizona Press, pp. 147–83.
Schultz, P. H. (1992). Atmospheric effects on ejecta emplacement and crater formation from Magellan. *J. Geophys. Res.*, **97**, 16,183–248.
Schultz, P. H. and Gault, D. E. (1979). Atmospheric effects on martian ejecta emplacement. *J. Geophys. Res.*, **84**, 7669–87.
Schultz, P. H. and Gault, D. E. (1984). On the formation of contiguous ramparts around martian impact craters. LPSC XV, pp. 732–3.

Schultz, P. H. and Lutz, A. B. (1988). Polar wandering on Mars. *Icarus*, **73**, 91–141.
Schultz, P. H., Schultz, R. A. and Rogers, J. (1982). The structure and evolution of ancient impact basins on Mars. *J. Geophys. Res.*, **87**, 9803–20.
Schultz, R. A. (1991). Structural development of Coprates Chasma and western Ophir Planum, central Marineris rift, Mars. *J. Geophys. Res.*, **96**, 22,777–92.
Schultz, R. A. and Frey, H. V. (1990). A new survey of multiring impact basins on Mars. *J. Geophys. Res.*, **95**, 14,175–289.
Schultz, R. A. and Lin, J. (2001). Three-dimensional normal faulting models of Valles Marineris, Mars, and geodynamical implications. *J. Geophys. Res.*, **106**, 16,549–66.
Sclater, J. G., Jaupart, C. and Galson, D. (1980). The heat flow through oceanic and continental crust and the heat loss of the earth. *Rev. Geophys. Space Phys.*, **18**, 269–311.
Scott, D. H. and Dohm, J. M. (1992). Mars highland channels: an age reassessment. LPSC XXIII, pp. 1251–2.
Scott, D. H. and Tanaka, K. L. (1986). Geologic map of the western equatorial region of Mars. U.S. Geol. Survey Misc. Map I-1802-A.
Scott, E. D. and Wilson, L. (2002). Plinian eruptions and passive collapse events as mechanisms of formation for martian pit chain craters. *J. Geophys. Res.*, **107**(E4), 10.1029/2000JE001432.
Segura, T. L., Toon, O. B., Colaprete, A. and Zahnle, K. (2002). Environmental effects of large impacts. *Science*, **298**, 1977–80.
Seibert, N. M. and Kargel, J. S. (2001). Small-scale martian polygonal terrain: implications for liquid surface water. *Geophys. Res. Lett.*, **28**, 899–902.
Shaller, P. J., Murray, B. C. and Albee, A. L. (1989). Subaqueous landslides on Mars? LPSC XX, pp. 990–1.
Sharp, R. P. (1963). Wind ripples. *J. Geol.*, **71**, 617–36.
Sharp, R. P. (1973a). Mars: troughed terrains. *J. Geophys. Res.*, **78**, 4063–72.
Sharp, R. P. (1973b). Mars: fretted and chaotic terrains. *J. Geophys. Res.*, **78**, 4222–30.
Sharp, R. P. and Malin, M. C. (1975). Channels on Mars. *Geol. Soc. Am. Bull.*, **86**, 593–609.
Shean, D. E., Head, J. W. and Marchant, D. R. (2005). Origin and evolution of cold-based tropical mountain glacier on Mars: the Pavonis Mons fan-shaped deposit. *J. Geophys. Res.*, **110**(E5), 10.1029/2004JR002360.
Shoemaker, E. M. (1966). Preliminary analysis of the fine structure of the lunar surface in Mare Cognitum. In *The Nature of the Lunar Surface*, ed. W. N. Hess *et al.* Baltimore: Johns Hopkins University Press, pp. 23–121.
Shoemaker, E. M. and Wolfe, R. F. (1982). Cratering time scales for the Galilean satellites. In *Satellites of Jupiter*, ed. D. Morrison. Tucson: University of Arizona Press, pp. 277–339.
Shreve, R. L. (1966a). Statistical law of stream numbers. *J. Geol.*, **74**, 17–37.
Shreve, R. L. (1966b). Sherman landslide, Alaska. *Science*, **154**, 1639–43.
Sleep, N. H. (1994). Martian plate tectonics. *J. Geophys. Res.*, **99**, 5639–55.
Sleep, N. H. and Zahnle, K. (1998). Refugia from asteroid impact on early Mars and the early Earth. *J. Geophys. Res.*, **103**(E12), 28,529–44.
Smith, D. E., Zuber, M. T., Frey, H. V., *et al.* (12 authors) (1998). Topography of the northern hemisphere of Mars from the Mars Orbiter Laser Altimeter. *Science*, **279**, 1686–92.
Smith, D. E., Sjogren, W. L., Tyler, G. L., Balmino, G., Lemoine, F. G. and Konopliv, A. S. (1999). The gravity field of Mars: results from Mars Global Surveyor. *Science*, **286**, 94–7.
Smith, D. E., Zuber, M. T., Solomon, S. C., *et al.* (19 authors) (1999). The global topography of Mars and implications for surface evolution, *Science*, **284**, 1495–1503.
Smith, D. E., Zuber, M. T., Frey, H. V., *et al.* (2001). Mars Orbiter Laser Altimeter: experiment summary after the first year of global mapping. *J. Geophys. Res.*, **106**(E10), 23,689–722.
Smith, P. H., Zuber, M. T., Frey, H. V., *et al.* (19 authors) (1997). The imager for Mars Pathfinder experiment. *J. Geophys. Res.*, **102**, 4003–25.
Smrekar, S. E., McGill, G. E., Raymond, C. A. and Dimitriou, A. M. (2004). Geologic evolution of the martian dichotomy in the Ismenius area of Mars and implications for plains magnetization. *J. Geophys. Res.*, **109**(E11), doi:10.1029/2004JE002260
Soderblom, L. A., Kriedler, T. J. and Masursky, H. (1973). Latitudinal distribution of debris mantles on the martian surface. *J. Geophys. Res.*, **78**, 4117–22.
Soderblom, L. A., *et al.* (2004). Soils of Eagle crater and Meridiani Planum at the Opportunity rover landing site. *Science*, **306**, 1723–6.
Solomon, S. C. and Head, J. W. (1982). Evolution of the Tharsis province of Mars: the importance of heterogeneous lithospheric thickness and volcanic construction. *J. Geophys. Res.*, **87**, 9755–74.
Solomon, S. C., *et al.* (17 authors) (2005). New perspectives on ancient Mars. *Science*, **307**, 1214–20.
Spencer, J. R. and Croft, S. K. (1986). Valles Marineris as karst. NASA Tech. Memo 88383, 193–5.
Spencer, J. R. and Fanale, F. P. (1990). New models for the origin of Valles Marineris closed depressions. *J. Geophys. Res.*, **95**, 14,301–13.
Spohn, T., Acuna, M. H., Breuer, D., *et al.* (2001). Geophysical constraints on the evolution of Mars. In *Chronology and Evolution of Mars*, ed. R. Kallenback *et al.* Dordrecht: Kluwer, pp. 231–62.
Squyres, S. W. (1979). The distribution of lobate debris aprons and similar flows on Mars. *J. Geophys. Res.*, **84**, 8087–96.
Squyres, S. W. and Carr, M. H. (1986). Geomorphic evidence for the distribution of ground ice on Mars. *Science*, **231**, 249–52.
Squyres, S. W. and Kasting, J. F. (1994). Early Mars: how warm and how wet? *Science*, **265**, 744–8.
Squyres, S. W. and Knoll, A. H. (2005). Sedimentary rock at Meridiani Planum: origin, diagenesis and implications for life. *Earth Planet. Sci. Lett.*, **240**, 1–10.
Squyres, S. W., Arvidson, R. E., Baumgartner, E. T., *et al.* (12 authors) (2003). Athena Mars rover science investigation. *J. Geophys. Res.*, **108**(E12), doi:10.1029/2003JE002121
Squyres, S. W., *et al.* (50 authors) (2004a). The Opportunity Rover's Athena science investigation at Meridiani Planum, Mars. *Science*, **306**, 1698–1714.
Squyres, S. W., Arvidson, R. E., Bell, J. F., *et al.* (2004b). The Spirit rover's Athena science investigation at Gusev crater, Mars. *Science*, **305**, 794–9.
Squyres, S. W., Grotzinger, J. P., Arvidson, R. E., *et al.* (2004c). In situ evidence for an ancient aqueous environment at Meridiani Planum, Mars. *Science*, **306**, 1709–14.
Squyres, S. W., Arvidon, R. E., Blaney, D. W., *et al.* (14 authors) (2006). The rocks of the Columbia Hills. *J. Geophys. Res.*, **111**, E02S11, doi:10.1029/2005JR002562
Stepinski, T. F. and Coradetti, S., (2004). Systematic differences in topography of martian and terrestrial drainage basins. LPSC XXXV, Abstract 166.
Stepinski, T. F. and O'Hara, W. J. (2003). Vertical analysis of martian drainage basins. LPSC, XXXIV, Abstract 1659.
Stetter, K. O. (1996). Hyperthermophiles in the history of life. In *Evolution of Hydrothermal Ecosystems on Earth* (*and Mars?*), ed. M. Walter. Ciba Foundation Symposium 202. New York: Wiley, pp. 1–18.
Stevens, T. O. and McKinley, J. P. (1995). Lithoautotrophic microbial ecosystems in deep basalt aquifers. *Science*, **270**, 450–4.
Stevenson, D. J. (2001). Mars' core and magnetism. *Nature*, **412**, 214–19.
Stevenson, D. J., Spohn, T. and Schubert, G. (1983). Magnetism and thermal evolution of the terrestrial planets. *Icarus*, **54**, 466–89.
Stewart, E. M. and Head, J. W. (2001). Ancient martian volcanoes in the Aeolis region: new evidence from MOLA data. *J. Geophys. Res.*, **106**, 17,505–13.

Stewart, S. T. and Nimmo, F. (2002). Surface runoff features on Mars: testing of the carbon dioxide hypothesis. *J. Geophys. Res.*, **107**(E9), doi:10.1029/2000JE001465

Stöffler, D. and Ryder, G. (2001). Stratigraphy and isotope ages of lunar geologic units: chronological standard for the inner Solar System. In *Chronology and Evolution of Mars*, ed. R. Kallenbach *et al*. Dordrecht: Kluwer, pp. 9–54.

Strahler, A. N. (1958). Dimensional analysis applied to fluvially eroded landforms. *Geol. Soc. Am. Bull.*, **69**, 279–300.

Strahler, A. N. (1964). Quantitative geomorphology of drainage basins and channel networks. In *Handbook of Applied Hydrology*, ed. V. T. Chow. New York: McGraw Hill.

Tanaka, K. L. (1985). Ice-lubricated gravity spreading of the Olympus Mons aureole deposits. *Icarus*, **62**, 191–206.

Tanaka, K. L. (1986). The stratigraphy of Mars. Proc. 17th Lunar and Planet. Sci. Conf., *J. Geophys. Res.*, **91**, E139–58.

Tanaka, K. L. (1999). Debris-flow origin for the Simud/Tiu deposit on Mars. *J. Geophys. Res.*, **104**, 8637–52.

Tanaka, K. L. and Golombek, M. P. (1989). Martian tension fractures and formation of grabens and collapse features in Valles Marineris. LPSC XIX, pp. 383–96.

Tanaka, K. L. and Leonard, G. J. (1995). Geology and landscape evolution of the Hellas region of Mars. *J. Geophys. Res.*, **100**(E3), 5407–32.

Tanaka, K. L. and Scott, D. H. (1987). Geologic map of the polar regions of Mars. U.S. Geol. Survey, Misc. Inv. Map I-1802C.

Tanaka, K. L., Golombek, N. P. and Banerdt, W. B. (1991). Reconciliation of stress and structural histories of the Tharsis region of Mars. *J. Geophys. Res.*, **96**, 15,617–33.

Tanaka, K. L., Banerdt, W. B., Kargel, J. S. and Hoffman, N. (2001). Huge CO_2 charged debris flow deposit and tectonic sagging in the northern plains of Mars. *Geology*, **29**, 427–30.

Thomas, P. C. and Gierasch, P. J. (1985). Dust devils on Mars. *Science*, **230**, 175–7.

Thomas, P. C. and Veverka, J. (1979). Seasonal and secular variations of wind streaks on Mars: an analysis of Mariner 9 and Viking data. *J. Geophys. Res.*, **84**, 8131–46.

Thomas, P. C., Squyres, S. W. and Carr, M. H. (1990). Flank tectonics of martian volcanoes. *J. Geophys. Res.*, **95**, 14,345–55.

Thomas, P. C., *et al*. (1992). Polar deposits of Mars. In *Mars*, ed. H. H. Kieffer, B. M. Jakosky, C. W. Snyder and M. S. Matthews. Tucson: University of Arizona Press, pp. 767–95.

Thomas, P. C., Malin, M. C., Edgett, K. S., *et al*. (2000). North-south geological differences between the residual polar caps of Mars. *Nature*, **404**, 161–5.

Thomas, P. C., Malin, M. C., James, P. B., Cantor, B. A., Williams, R. M., and Gierasch, P., *et al*. (2005). South polar residual cap of Mars: Features, stratigraphy and changes. *Icarus*, **174**, 535–59.

Thorarinsson, S. (1957). The jökulhlaup from the Katla area in 1955 compared with other jökulhlaups in Iceland. *Reykjavik Mus. Nat. Hist., Misc. Paper* **18**, 21–5.

Toon, O. B., Pollack, J. B., Ward, W., Burns, J. A. and Bilski, K. (1980). The astronomical theory of climate change on Mars. *Icarus*, **44**, 552–607.

Tosca, N. J., McLennan, S. M., Clark, B. C., *et al*. (2005). Geochemical modeling of evaporative processes on Mars: insight from the sedimentary record at Meridiani Planum. *Earth Planet. Sci. Lett.*, **240**, 122–48.

Touma, J. and Wisdom, J. (1993). The chaotic obliquity of Mars. *Science*, **259**, 1294–6.

Treiman, A. H. and Louge, M. Y. (2004). Martian slope streaks and gullies: origins as dry granular flows. LPSC XXXV, Abstract 1323.

Treiman, A. H., Drake, M. J., Janssens, N. J., Wolff, R. and Enihara, M. (1986). Core formation in the Earth and the shergottite parent body. *Geochim. Cosmochim. Acta*, **50**, 1061–70.

Turcotte, D. L., Willeman, R. J., Haxby, W. F. and Norberry, J. (1981). Role of membrane stresses in support of planetary topography. *J. Geophys. Res.*, **86**, 3951–9.

von Engelhardt, W., Bertsch, W., Stoffler, D., Groschopf, P. and Reiff, W. (1967). Anzeichen für den meteoritischen Ursprung des Beckens von Steinheim. *Naturwissenschaften*, **54**, 198–9.

Wahrhaftig, C. and Cox, A. (1959). Rock glaciers in the Alaska Range. *Geol. Soc. Am. Bull.*, **70**, 383–426.

Wallace, D. and Sagan, C. (1979). Evaporation of ice in planetary atmospheres: ice-covered rivers on Mars. *Icarus*, **39**, 385–400.

Walter, M. R. (1983). Archean stromatolites: evidence of the Earth's earliest Benthos. In *Earth's Earliest Biosphere*, ed. J. W. Schopf. Princeton: Princeton University Press, pp. 187–213.

Wänke, H. (1981). Constitution of terrestrial planets. *Phil. Trans. Roy. Soc. London Ser. A*, **303**, 287–303.

Wänke, H. and Dreibus, G. (1988). Chemical composition and accretion history of terrestrial planets. *Phil. Trans. Roy. Soc. London Ser. A*, **325**, 545–57.

Ward, W. R. (1992). Long term orbital and spin dynamics of Mars. In *Mars*, ed. H. H. Kieffer, B. M. Jakosky, C. W. Snyder and M. S. Matthews. Tucson: University of Arizona Press, pp. 298–320.

Washburn, A. L. (1980). *Geocryology*. New York: Wiley.

Watters, T. R. (1991). Origin of periodically spaced wrinkle ridges on the Tharsis plateau of Mars. *J. Geophys. Res.*, **96**, 15,599–616.

Watters, T. R. (1993). Compressional tectonism on Mars. *J. Geophys. Res.*, **98**(E5), 17,049–60.

Weiss, B. P., Vali, H., Baundenbacher, F. J., *et al*. (2002). Records of an ancient magnetic field in ALH84001. *Earth Planet. Sci. Lett.*, **201**, 449–64.

Weitz, C. M. and Parker, T. J. (2000). New evidence that the Valles Marineris interior deposits formed in standing bodies of water. LPSC XXXI, Abstract 1693.

Weitz, C. M., Parker, T. J., Mulmer, M. H., Anderson, F. S. and Grant, J. A. (2003). Geology of the Melas Chasma landing site for the Mars Exploration Rover mission. *J. Geophys. Res.*, **108**(E12), doi:10,1029/2002JE002014

Wenrich, M. L. and Christensen, P. R. (1996). A formational model for the martian polygonal terrains. LSPC XXVII, pp. 1419–20.

Wentworth, C. K. (1922). A scale of grade and class terms for clastic sediments. *J. Geol.*, **30**, 377–92.

Whalley, W. B. and Azizi, F. (2003). Rheological models of active rock glaciers: evaluation, critique and possible test. *Permafrost and Periglacial Processes*, **5**, 37–51.

Wilhelms, D. E. (1987). The geologic history of the Moon. U.S. Geol. Survey, Prof. Paper 1348.

Wilhelms, D. E. and Squyres, S. W. (1984). The martian hemisphere dichotomy may be due to a large impact. *Nature*, **309**, 138–40.

Williams, P. J. and Smith, M. W. (1989). *The frozen Earth*. Cambridge: CUP.

Williams, R. M. and Phillips, R. J. (2001). Morphometric measurements of martian valley networks from Mars Orbiter Laser Altimeter (MOLA) data. *J. Geophys. Res.*, **106**, 23,737–51.

Williams, R. M., Phillips, R. J. and Malin, M. C. (2000). Flow rates and duration within Kasei Vallis, Mars: implications for the formation of a martian ocean. *Geophys. Res. Lett.*, **27**, 1073–6.

Wilshire, H. G., Offield, T. W., Howard, K. A. and Cummings, D. (1972). Geology of the Sierra Madera cryptovolcanic structure, Pecos County, Texas. U.S. Geol. Survey, Prof. Paper 599-H.

Wilson, L. and Head, J. W. (1994). Mars: review and analysis of volcanic eruption theory and relationships to observed landforms. *Rev. Geophys.*, **32**, 221–63.

Wilson, L. and Head, J. W. (2001). Evidence for episodicity in the magma supply to the large Tharsis volcanoes. *J. Geophys. Res.*, **106**, 1423–33.

Wilson, L. and Head, J. W. (2002). Tharsis-radial graben systems as the surface manifestations of plume related dike intrusion complexes: models and implications. *J. Geophys. Res.*, **107**(E8), 10.1029/2001JE001593

Wilson, L. and Mouginis-Mark, P. J. (2003). Phreatomagmatic explosive origin of Hrad Vallis, Mars. *J. Geophys. Res.*, **108**(E8), doi 10.1029/2002JE001927

Wilson, L., Ghatan, G. J., Head, J. W. and Mitchell, K. L. (2004). Mars outflow channels: a reappraisal of the estimation of water flow velocities from water depths, regional slopes and channel floor properties. *J. Geophys. Res.*, **109**(E9), doi:10.1029/2004JE002281

Wilson, M. (1995). *Igneous Petrogenesis*. London: Chapman & Hall.

Wise, D. U., Golombek, M. P. and McGill, G. E. (1979). Tectonic evolution of Mars. *J. Geophys. Res.*, **84**, 7934–9.

Withers, P. and Neumann, G. A. (2001). Enigmatic northern plains of Mars. *Nature*, **410**, 651.

Woese, C. R. (1987). Bacterial evolution. *Microbiol. Rev.*, **51**, 221–71.

Woese, C. R. (1990). Toward a natural system of organisms. *Proc Natl. Acad. Sci. U.S.A.*, **87**, 4576–9.

Wood, C. A. and Ashwal, L. D. (1981). SNC meteorites: igneous rocks from Mars? LPSC XII, pp. 1359–75.

Wood, J. A. (1979). *The Solar System*. Englewood Cliffs, N.J.: Prentice-Hall.

Wu, S. S. C. (1978). Mars synthetic topographic mapping. *Icarus*, **33**, 417–40.

Wyatt, M. B. and McSween, H. Y. (2002). Spectral evidence for weathered basalt as an alternative to andesite in the northern lowlands of Mars. *Nature*, **417**, 263–6.

Wyatt, M. B., McSween, H. Y., Tanaka, K. L. and Head, J. W. (2004). Global geologic context for rock types and surface alteration on Mars. *Geology*, **32**, 645–8.

Yin, G., Jacobsen, S. B., Yamashita, K., Blichert-Toft, J., Tetork, P. and Abarede, F. (2000). A short timescale for terrestrial planet formation from Hf-W chronometry of meteorites. *Nature*, **418**, 949–52.

Yung, Y. L., Nair, H. and Gerstell, M. F. (1997). CO_2 greenhouse in the early martian atmosphere: SO_2 inhibits condensation. *Icarus*, **130**, 222–4.

Zahnle, K. (1998). Origins of atmospheres. In *Origins*, ed. C. E. Woodward *et al. Astron. Soc. Pacific Conf. Series*, **148**, 364–91.

Zhong, S. and Zuber, M. T. (2001). Degree-1 mantle convection and the crustal dichotomy on Mars. *Earth Planet. Sci. Lett.*, **189**, 75–84.

Zimbelman, J. R. and Greeley, R. (1982). Surface properties of ancient cratered terrain in the northern hemisphere of Mars. *J. Geophys. Res.*, **87**, 10,181–9.

Zuber, M. T., Smith, D. E., Solomon, S. C., *et al.* (1998). Observations of the north pole region of Mars from the Mars Orbiter laser altimeter. *Science*, **282**, 2053–60.

Zuber, M. T., Solomon, S. C., Phillips, R. J., *et al.* (15 authors) (2000). Internal structure and early thermal evolution of Mars from Mars Global Surveyor topography and gravity. *Science*, **287**, 1788–92.

Zurek, R. W., Barnes, J. R., Haberle, R. M., Pollack, J. B., Tillman, J. E. & Leovy, C. B. (1992). Introduction to the Mars atmosphere. In *Mars* ed. H. H. Kieffer, B. M. Jakosky, C. W. Snyder and M. S. Matthews. Tucson: University of Arizona Press, pp. 799–817.

Zurek, R. W., *et al.* (1992). Dynamics of the atmosphere of Mars. In *Mars*, ed. H. H. Kieffer, B. M. Jakosky, C. W. Snyder and M. S. Matthews. Tucson: University of Arizona Press, pp. 835–933.

Some useful web sites

http://www.msss.com
http://photojournal.jpl.nasa.gov
http://themis-data.asu.edu/
http://astrogeology.usgs.gov/mdim-bin/dataListPage.pl?lat=15N&lon=113E
http://valles.wr.usgs.gov/mcmolashaded/
http://marsrovers.jpl.nasa.gov/home/index.html
http://marswatch.astro.cornell.edu/pancam_instrument/links.html
http://pds.jpl.nasa.gov/

Index